LIBRARY
Te Tumu Herenga
THE UNIVERSITY OF AUCKLAND

RESEARCHSPACE@AUCKLAND

http://researchspace.auckland.ac.nz

ResearchSpace@Auckland

Copyright Statement

The digital copy of this thesis is protected by the Copyright Act 1994 (New Zealand).

This thesis may be consulted by you, provided you comply with the provisions of the Act and the following conditions of use:

- Any use you make of these documents or images must be for research or private study purposes only, and you may not make them available to any other person.
- Authors control the copyright of their thesis. You will recognise the author's right to be identified as the author of this thesis, and due acknowledgement will be made to the author where appropriate.
- You will obtain the author's permission before publishing any material from their thesis.

To request permissions please use the Feedback form on our webpage.
http://researchspace.auckland.ac.nz/feedback

General copyright and disclaimer

In addition to the above conditions, authors give their consent for the digital copy of their work to be used subject to the conditions specified on the Library Thesis Consent Form and Deposit Licence.

Note : Masters Theses

The digital copy of a masters thesis is as submitted for examination and contains no corrections. The print copy, usually available in the University Library, may contain corrections made by hand, which have been requested by the supervisor.

THE EVOLUTION
OF THE DARAJAT GEOTHERMAL SYSTEM
WEST JAVA - INDONESIA

NINIEK RINA HERDIANITA

A thesis submitted in fulfilment of
the requirements for the degree of Doctor of Philosophy
in Applied Geology, School of Environment, Faculty of Science
The University of Auckland, New Zealand,

2012

ABSTRACT

The Darajat geothermal system is a dry-steam resource, associated with the Quaternary Guntur volcano. Its geology is dominated by andesitic rocks; however the youngest unit is an obsidian flow from Mt. Kiamis. It is a product from a dacitic-rhyolitic parasitic cone in the Kendang caldera having an age younger than 50,000 years. The geothermal system itself is characterized by a ~240°C highly permeable reservoir containing mainly steam with ~2 wt.% non-condensable gases. The occurrence of liquid-formed hydrothermal minerals, such as wairakite, epidote and garnet associated with chlorite, illite and smectite, indicates that the Darajat reservoir was once liquid dominated. Here, the change in reservoir behavior, i.e. from liquid to vapour, was recognized by comparing the characteristics of the hydrothermal minerals, including their compositions and results from fluid-inclusion geothermometry, with present conditions.

The geothermal system started when meteoric derived fluids at temperatures between 350 and 400°C ascended. The fluids were low in CO_2. However, they may have been more saline and enriched in CO_2 and H_2S gasses where magmatic fluids mixed with the meteoric waters. The thermal fluids then boiled at 250-300°C below about +600 m or 1000 m depth in the northern part of the system but were slightly cooler at 200-250°C, when they reached near sea level or about 2000 m depth in the southern part. Boiling and further water-rock interactions caused the fluids to become fully saturated with respect to some calc-silicates and quartz. Consequently, grossular-andradite, actinolite-tremolite, high pistacite epidote, Fe-bearing prehnite and wairakite in association with quartz formed at this stage.

Boiling became more intense, especially in the northern area, as indicated by the occurrence of platy calcite. Vapour that separated from the boiling fluids ascended through fractures and started to fill a reservoir. The residual liquid moved more slowly or even descended and accumulated below this vapour reservoir. Above the reservoir, vapour condensed and formed acid condensate waters. The occurrences of calcite and anhydrite after calc-silicates record these downward percolating condensate waters.

Deposition of calcite and anhydrite decreased the porosity and permeability of rocks above the reservoir. Pressure differences between the reservoir and the surrounding rocks caused hydraulic fracturing to occur, hence increasing the permeability of the reservoir rocks. This lowered the pressure triggering more intense boiling in the reservoir. These events occurred several times. Consequently, more vapour filled the reservoir, until a steam zone formed. In the northern part of the field, the steam zone is 600 m thick but in the southern part it is only 100 m thick. Shallow intrusion of rhyolitic rocks likely accelerated the evolution of the geothermal system since it probably promoted rapid boiling. It is likely that the once liquid-dominated Darajat geothermal system evolved to the vapour-dominated system about 50,000 years ago.

ACKNOWLEDGEMENTS

The study was carried out under the support of NZODA Study Award, provided by the Ministry of Foreign Affairs and Trade (MFAT), New Zealand. Amoseas Indonesia Inc., Pertamina Geothermal Energy and Chevron Geothermal Indonesia Inc. are acknowledged for kindly supplying the drillhole cores studied and all supports.

I sincerely thank my supervisors Assoc. Prof. P.R.L. Browne and Assoc. Prof. S.F. Simmons for their guidance, advice and suggestion throughout this study. I also thank Assoc. Prof. K.A. Rodgers, my former supervisor, and Prof. M.P. Hochstein. Their help in all aspect of my study is very much appreciated.

I would like to express my sincere appreciations to the staff of the Geology Program, School of Environment, the University of Auckland for their help in providing my study needs. Special thanks to Prof. Philippa Black, Dr. Suprijadi Sungkono, Assoc. Prof. Ian Smith and Dr. Kathleen A. Campbell all suggestions, discussions and helps in my work.

I am grateful to all technicians of the Geology Program, School of Environment, the University of Auckland: Dr. Ritchie Sims and John Wilmshurst for their assistance in many laboratory work, Barry Curham for all nice thin sections he made, Louise Cotterall for her help in my drafting, Colin Yong and Elva Leaming. I particularly wish to thank Bothwell Wong, who always solved my computer problems.

I thank Dr. Joe Moore from the Energy and Geoscience Institute, University of Utah, USA, Dr. David Norman and Dr. Nigel Blamey from the New Mexico Tech., USA for their help in the gas analyses. I am grateful to Ed Erb, Jeff Roberts and Julfi Hadi from formerly the Amoseas Indonesia Inc. and all earth scientists of the Amoseas Indonesia Inc. for their help, discussion and suggestions during my study. I particularly thank Brian Lythe from the Counseling Service, Student Services Registry for all his helps during my stay in Auckland. I would like to thank so many friends, especially Ida, Folau, Budi, Luki, Terry, Steve, Yuki and Kyoko. I also appreciate Dan, Marion, Heather, Ghada and others, who keep 'the competition' going. I also appreciate support from my friends and colleagues from Faculty of Earth Science and Technology, and Faculty of Mining and Petroleum Engineering, Institute Technology of Bandung. The warmest stay during my exam in the Institute of Earth Science and Engineering (IESE) of the University of Auckland are also appreciated.

This thesis would not have been possible to make without loving support and continuous encouragement from Adam Priohandono and my family, especially my sisters and my mother in law. For my daughters Diva and Lana - this work is for you! I thank my father for his encouragement even he never had a chance to see me finishing this thesis.

TABLE OF CONTENTS

TABLE OF CONTENTS (Continued).

Chapter 3 (Cont.).

TABLE OF CONTENTS (Continued).

Chapter 6 (Cont.).

TABLE OF CONTENTS (Continued).

Chapter 7 (Cont.).

TABLE OF CONTENTS (Continued).

Chapter 10 (Cont.).

LIST OF TABLES

Chapter 1. INTRODUCTION

Chapter 2. GEOLOGICAL SETTING

Chapter 3. DARAJAT GEOTHERMAL FIELD

Chapter 4. NATURE OF THE HOST ROCK

Chapter 5. HYDROTHERMAL ALTERATION OF THE MATRIX

Chapter 6. VEIN MINERALOGY

Chapter 7. CHEMISTRY OF HYDROTHERMAL MINERALS

LIST OF TABLES (Continued).

Chapter 7 (Cont.).

Chapter 8. PALEOHYDROLOGY

Chapter 9. WATER-ROCK INTERACTIONS

LIST OF TABLES (Continued).

Chapter 9 (Cont.).

Chapter 10. EVOLUTION OF DARAJAT GEOTHERMAL SYSTEM

Chapter 11. CONCLUSIONS AND RECOMMENDATIONS

LIST OF FIGURES

Chapter 1. INTRODUCTION

Chapter 2. GEOLOGICAL SETTING

Chapter 3. DARAJAT GEOTHERMAL FIELD

Chapter 4. NATURE OF THE HOST ROCK

LIST OF FIGURES (Continued).

Chapter 4 (Cont.).

Chapter 5. HYDROTHERMAL ALTERATION OF THE MATRIX

LIST OF FIGURES (Continued).

Chapter 6. VEIN MINERALOGY

Chapter 7. CHEMISTRY OF HYDROTHERMAL MINERALS

LIST OF FIGURES (Continued).

Chapter 7 (Cont.).

Chapter 8. PALEOHYDROLOGY

LIST OF FIGURES (Continued).

Chapter 9. WATER-ROCK INTERACTIONS

Chapter 10. EVOLUTION OF DARAJAT GEOTHERMAL SYSTEM

Chapter 11. CONCLUSIONS AND RECOMMENDATIONS

LIST OF APPENDICES

(Given on CD)

Chapter 1

INTRODUCTION

1.1. LOCATION

The Darajat geothermal system is one of the world's few dry-steam geothermal resources. It is located in West Java, Indonesia, about 150 km southeast of the capital city, Jakarta, 35 km southeast of Bandung and 22 km west of Garut (Figure 1.1). There are several other geothermal fields nearby, including Kamojang (about 10 km to the northeast) and Wayang Windu (about 10 km to the west). These fields lie on a volcanic range nearly 30 km long with several distinguishable eruptive centres. Quaternary volcanoes include Papandayan (2622 m), Cikurai (2821 m), Malabar (2321 m) and Guntur (2249 m). The Darajat field itself is situated on the northern flank of Papandayan.

Darajat is a high priority geothermal project in Java after Kamojang and Awibengkok. Darajat and Kamojang are both vapour-dominated but Darajat has the greater heat output. It is expected to produce up to 430 MWe, compared to Kamojang which supplies 330 MWe.

1.2. PREVIOUS WORK

Hadi (1997) concluded that the Darajat geothermal system was once liquid dominated, as indicated by the occurrence of liquid-formed hydrothermal minerals, such as laumontite, epidote, and adularia associated with chlorite, illite and smectite. Amoseas Indonesia Inc. (1989a) reported that the hydrothermal alteration has generally produced argillic, silicic and propylitic alteration zones.

The occurrence of hydrothermal minerals indicates that the reservoir of Darajat contained liquid or two-phase fluids with neutral pH alkali chloride water at temperatures between 220 and 260°C. A brine is likely present at depth (Kingston Morisson Ltd., 1996 and Hadi, 1997). Nukman (1999) showed that the shallow part of the Darajat system was influenced by acid fluids, as indicated by the occurrence of kaolinite. Acid fluids might also occur at depth (Pramono, 1999).

1.3. AIMS OF STUDY

Understanding the evolution of the Darajat geothermal system is the main aim of this thesis. The system is now vapour dominated under production but it may have been once liquid dominated. If so, some physico chemical conditions must have changed within the reservoir at an unknown timescale. Much geological, geochemical and geophysical data about the Darajat system has been obtained through its exploration. However, there is still uncertainty in understanding its paleohydrology and how this has changed.

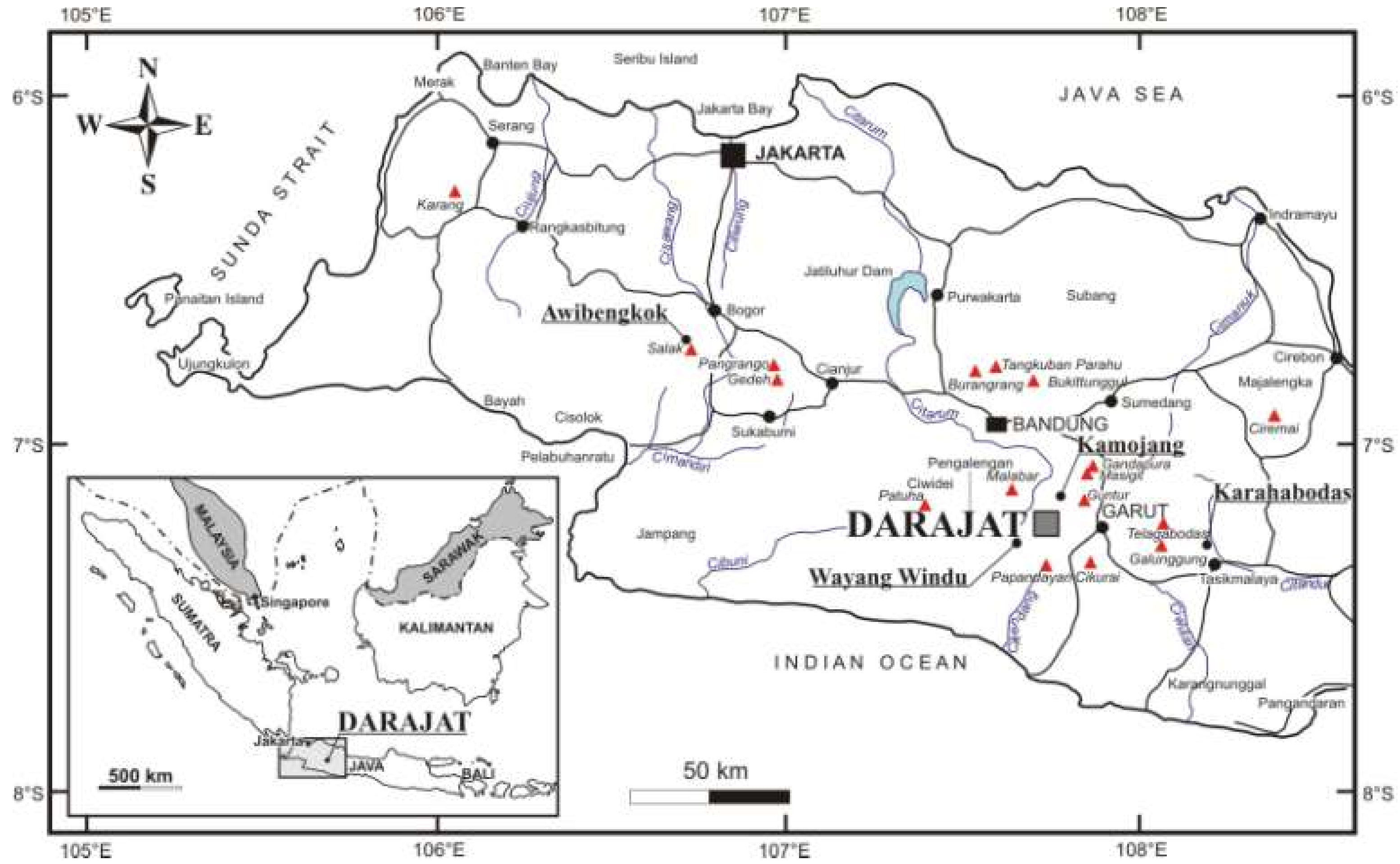

Figure 1.1. West Java, Indonesia showing the locations of the Darajat geothermal system and other places mentioned in this thesis. Mercator projection.

Unlike other well-known vapour-dominated geothermal systems, e.g. the Geysers of California and Larderello of Italy, Darajat is located on the flank of a steep volcano. The geological setting of Darajat also slightly differs from the others being hosted by volcanic rocks. The paleohydrology of Darajat may thus differ from the Geysers and Larderello. Since Darajat is also associated with a young high standing volcanic centre, the system might also be affected by magmatic processes.

The other aim of this study is to examine how the changes in the reservoir conditions affect the composition of hydrothermal minerals and their host rocks. Since one of the wells preserves unaltered host rocks, the nature of the parent rocks of Darajat can be understood and therefore the extent of mass transfer between them and the interacting fluids estimated. Assuming near equilibrium during fluid-rock interactions, the original composition of the thermal fluid can be deduced.

1.4. METHODOLOGY

Darajat is an interesting field to study since continuous cores were recovered from several drillholes. The occurrence of hydrothermal minerals in these cores are expected to record changes that occurred in the geothermal system during its lifetime. This includes fluid inclusions which were trapped during the deposition of hydrothermal minerals in veins. By comparing the results yielded from study of the hydrothermal minerals and the conditions in the present system, the evolution of the geothermal system can be determined. In addition, Darajat started electricity production in 1994, more than 10 years after Kamojang, so changes in the system due to the exploitation are less.

Figure 1.2 summarises the methodology used in this study. The study focussed on determining hydrothermal alteration that has occurred in the matrix of the rocks as a result of their interaction with thermal fluids and the occurrence of minerals in veins and fractures that were produced by processes affecting the circulating thermal fluids. Changes in reservoir conditions may also be revealed by changes in the compositions of hydrothermal minerals, especially those with solid solution, e.g. some calc-silicates and chlorite.

When fluids directly deposit some minerals in veins, they can trap fluid inclusions. These provide insights into the temperatures at the time of trapping and the chemical characteristics of the trapped fluid itself, including gas compositions.

The study also describes the compositions of major and trace elements in the altered rocks. By comparing them with the compositions of the parent unaltered, or least altered, rocks and the chemistry of water, the extent and magnitude of mass transfer as a result of interactions between thermal waters and the surrounding rocks has been estimated.

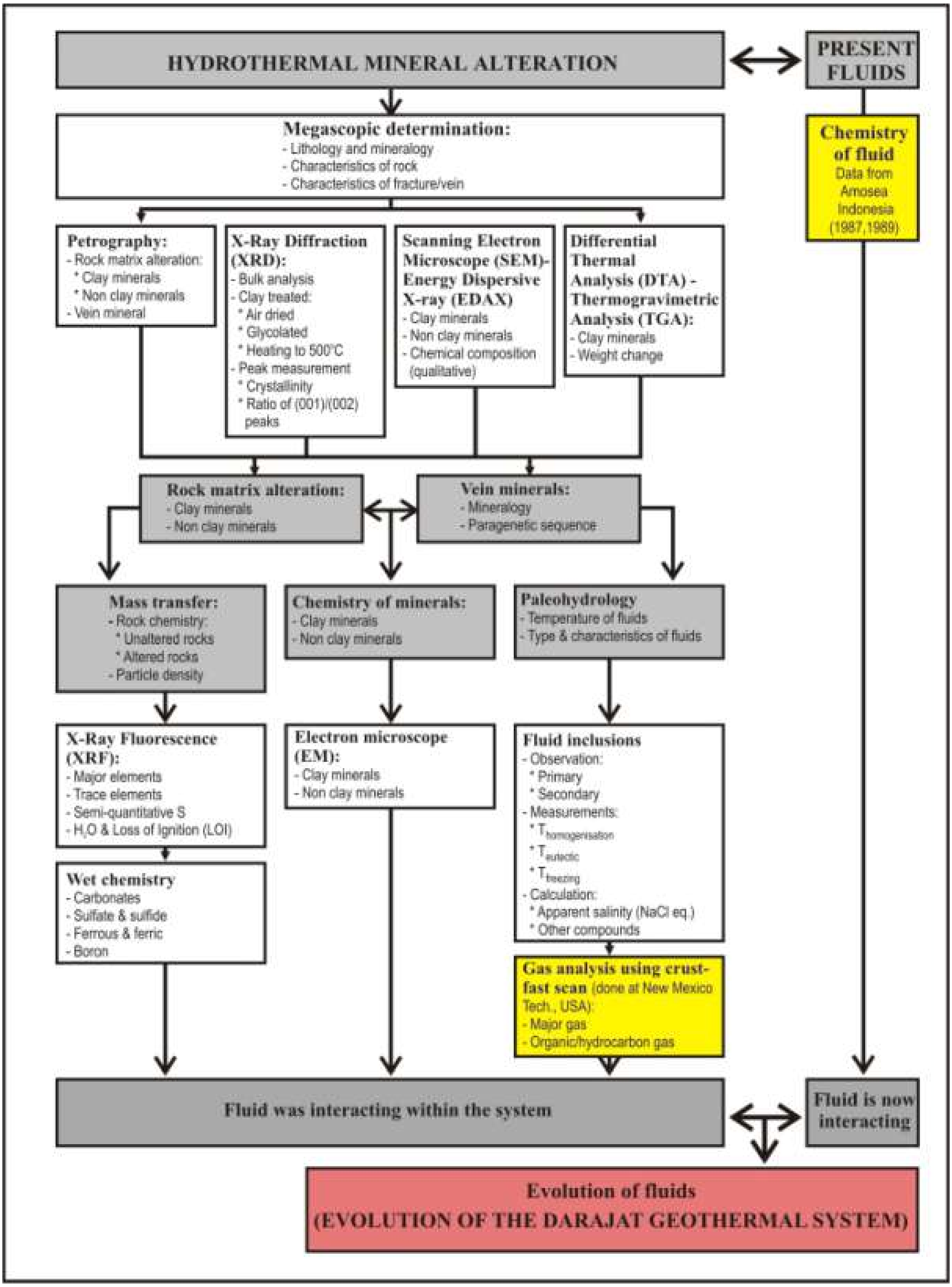

Figure 1.2.Summary of methodology used in this study. The evolution of Darajat, i.e. the change in the reservoir fluid from liquid to vapour dominant, was determined by comparing the results obtained from study of the hydrothermal minerals and present conditions. Yellow box shows analyses not made by the author.

1.5. MODELS OF THE HYDROLOGY OF GEOTHERMAL SYSTEMS

1.5.1. Vapour-dominated Geothermal Systems

Many studies try to explain the nature of vapour-dominated geothermal system, e.g. White et al. (1971), Truesdell and White (1973), Grant (1979a), Pestov (1995) and Young (1996). Their work emphasises well data from a few important vapour-dominated systems, such as The Geysers and Larderello.

In vapour-dominated geothermal systems, vapour, with little or no liquid, fills the reservoir; its saturation can be as high as 40% (Hochstein and Browne, 2000) and it may be enriched in CO_2, H_2S and other non-condensable gases near the top of the reservoir. Vapour is the continuous phase present in open fractures or channels, whereas liquid fills intergranular pore spaces in the host rocks (Goff and Janik, 2000). The phase separation in the reservoir itself occurs at pressures below hydrostatic. The fluid pressure (P_{H_2O}) is usually between 30 and 100 bars (White et al., 1971). Most vapour-dominated systems have reservoirs with permeabilities greater than 10 mD (1 mD = 10^{-15} m^2) (Hochstein and Browne, 2000), porosities greater than 5% (Truesdell and White, 1973) and maximum enthalpy fluids, i.e. at temperatures between 240 and 250°C, and pressures of 32-36 bars.

Ingebritsen and Sorey (1988) summarised three conceptual models in which a vapour-dominated condition can occur (Figure 1.3). Model I was originally proposed by White et al. (1971) and applies to The Geyser, where a large vapour-dominated system occurs within hilly topography. The model consists of a vapour-filled reservoir capped by a steam condensate zone and surrounded by impermeable rocks. This reservoir overlies rocks with deeply circulating water which supply superheated vapour to the reservoir through boiling and is heated by a deeper heat source (Figure 1.3A). The water becomes more saline through concentration by steam loss.

The impermeable rocks act as a barrier for the reservoir and prevent flooding from outside it. The barrier results from self-sealing due to deposition of calcite, anhydrite, quartz and/or clay minerals. The permeability is mostly less than 1-3 mD (Hochstein and Browne, 2000). Steam discharges from fumaroles at temperatures near surface boiling or lower, and forms acid sulfate springs and mud pools. No high Cl springs occur and, consequently, no silica sinter forms at the surface. White et al. (1971) reported that mercury (Hg) might deposit above the vapour reservoir.

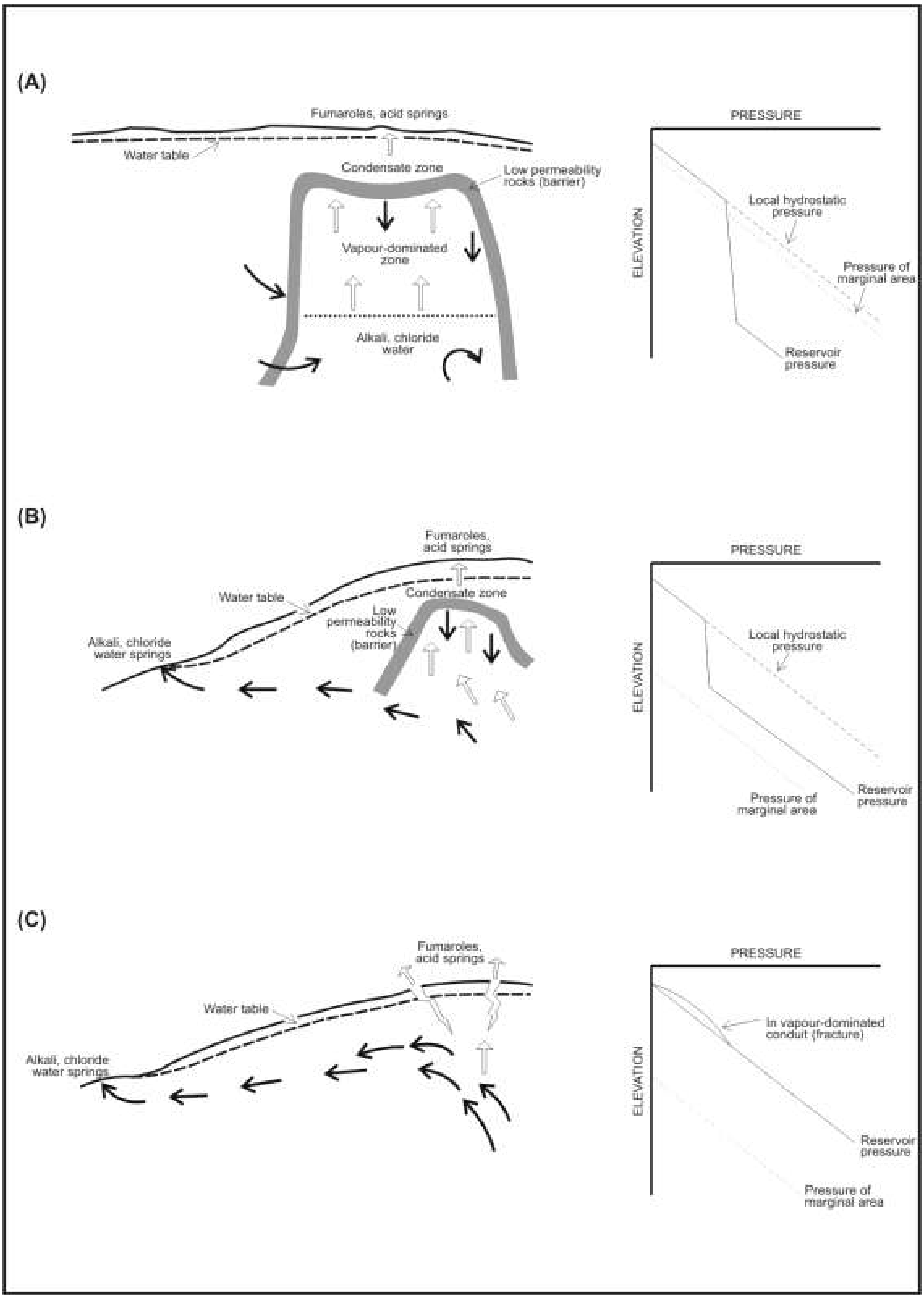

Figure 1.3.Three conceptual models of a vapour-dominated geothermal system; from Ingebritsen and Sorey (1988). Solid arrow (➔) represents liquid and open arrow (⇨) represents steam. Some liquids may descend from the condensate zone into the reservoir. Pressure profiles in the reservoir and marginal area are given. See text for explanation.

Model II is after Grant (1979a) and is generally similar to model I, but it involves a lateral liquid flow (Figure 1.3B). So, instead of discharging vapour or forming acid sulfate waters and fumaroles at high elevations, model II allows discharge of Cl waters at low elevations. The thickness of the vapour zone is controlled by the distance between the caprock and the lateral inflow (Ingebritsen and Sorey, 1988). Model II applies for a small system in moderate to steep topography, such as at Lassen in California where Cl water once discharged, as is indicated by ancient silica sinter (Ingebritsen and Sorey, 1985).

Model III shows that an overlying condensate zone and a barrier of impermeable rocks are unnecessary (Ingebritsen and Sorey, 1988). Indeed, fracture zones must be present to allow vapour to discharge (Figure 1.3C). Unlike models I and II, here the phase separation in the reservoir occurs at pressures near hydrostatic. The vapour reservoir itself is not thick (Ingebritsen and Sorey, 1988); at depth, a liquid-only domain is present. Temperatures of the fluids may be above critical values, i.e. above 400°C, such as in Alto Peak, Philippines (Reyes et al., 1993).

1.5.2. Liquid-dominated Geothermal Systems

Figure 1.4 shows a general model of a liquid-dominated geothermal system, associated with a high standing volcanic centre. The subsurface hydrology of the system is dominated by circulation of neutral pH, alkali chloride water. This water fills the upper reservoir with a deeper heat source of a cooling pluton (Hochstein and Browne, 2000). The water in the reservoir can boil, cool, mix, circulate and ascend. Boiling may produce waters of varying salinities and gas contents. Cool liquid may descend and recharge the reservoir. In the liquid-dominated system, recharge by cool groundwater is not restricted, as is the case in the vapour system (Goff and Janik, 2000).

Temperature and pressure increases steadily with increasing depth, except above the reservoir, where a low-pressure vapour zone may overly the reservoir (Goff and Janik, 2000). The fluid pressure (P_{H_2O}) is usually less than 200 bars (Browne, 1978) and similar to, or slightly above, hydrostatic pressure (Figure 1.4).

Vapour derived from boiling will condense or dissolve into groundwater and form HCO_3^- and SO_4^{2-}-rich waters (Figure 1.4). At higher elevations, fumaroles and steaming ground occur, whereas at lower elevations, neutral pH chloride waters discharge as hot springs, usually accompanied by surficial silica sinter (Figure 1.4). Mixing between chloride rich and steam condensate waters often occurs, so mixed Cl and HCO_3^- waters may discharge several kilometers distant from the upflow zone as warm springs and seeps, some depositing travertine (Hochstein and Browne, 2000).

As boiling continues, it provides additional vapour to the reservoir, so the reservoir then contains both liquid and vapour. Hochstein and Browne (2000) reported that the occurrences of liquid dominated and two-phase geothermal systems result from the overall permeability of the reservoir rocks and their surrounds. If the permeability of the reservoir rocks is high, i.e. greater than 10 mD, but the surrounding rocks have permeabilities of between 3 and 10 mD, then the geothermal system formed is liquid dominated with liquid saturations between 70 and 100%. If both the reservoir and the surrounding rocks have moderate permeabilities, i.e. 3-10 mD, the system will develop as a natural two-phase geothermal system with saturations between 40 and 70% (Hochstein and Browne, 2000).

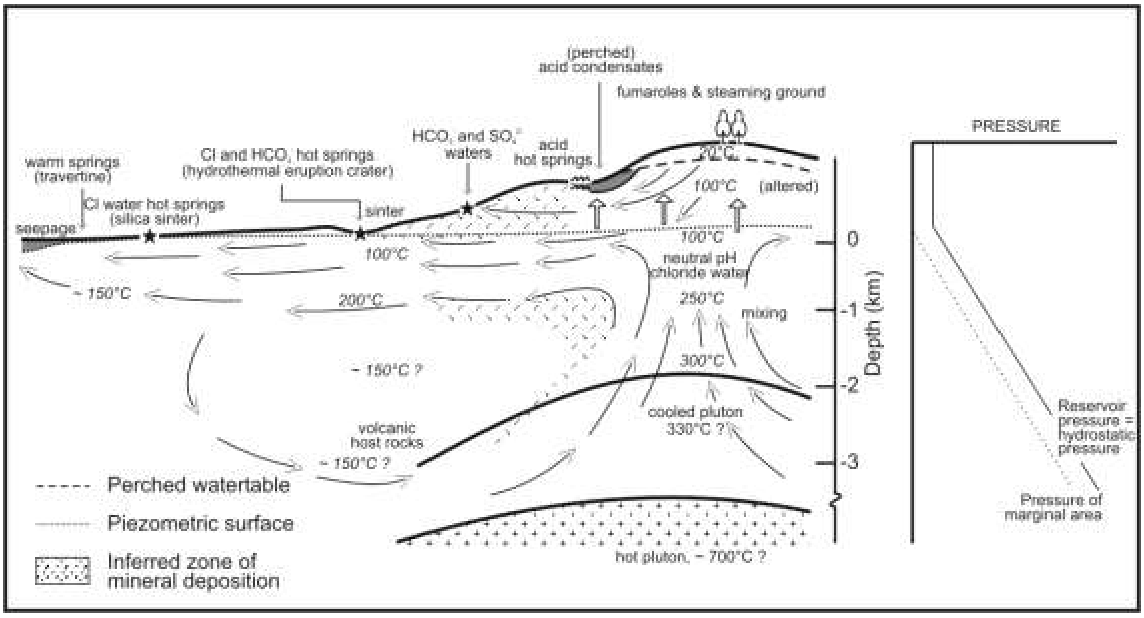

Figure 1.4. General model of a high temperature liquid dominated, volcanic-associated geothermal system (from Hochstein and Browne, 2000). Horizontally unscaled. Solid arrow (➔) represents inferred movement of liquid and open arrow (⇨) represents ascending vapour. Expected pressure profiles in the reservoir and marginal area are shown.

Many studies reveal that a liquid-dominated system precedes development of a vapour-dominated system (e.g. White et al., 1971; Truesdell and White, 1973 and Goguel, 1982). The change in permeability of the reservoir rocks is likely required to allow a vapour-dominated zone to evolve (e.g. Nakamura and Sumi, 1961; Batini et al., 1985, Shook, 1995 and Reyes, 1990). With a potent heat source and a reduced liquid inflow, an initial liquid-dominated system begins to boil off. A vapour-dominated zone will then develop directly below low permeability layers and descend progressively (White et al., 1971). Some steam may condense to liquid and flow downwards (Figure1.3).

1.6. HYDROTHERMAL ALTERATION

Interactions between the circulating fluids and the surrounding rocks will cause hydrothermal alteration of the matrix of the host rocks. By contrast, the hydrothermal minerals deposited in veins and vugs reveal constituents which were once oversaturated in the fluids and the processes that precipitated them. Therefore, it is important to determine and identify the nature and the alteration of the matrix, together with vein and cavity fillings and then use this knowledge to deduce processes that have affected the reservoir of a geothermal system.

Figure 1.5.shows a pattern of hydrothermal alteration in volcanic host rock, given by Giggenbach (1981 and 1988). The hydrothermal minerals formed include clay minerals, e.g. chlorite, illite and smectite, and calc-silicates, e.g. epidote and wairakite. Browne (1978) and Reyes (1990) listed several factors affecting the formation of hydrothermal minerals, i.e. temperature, pressure, the compositions of fluid and rocks, permeability, topography and time.

Temperature. Many studies show that temperature is a primary control on the distribution of hydrothermal minerals. Clays and calc-silicate minerals are thermally sensitive. For example the sequence of illite through interlayered illite-smectite to smectite suggests a retrograde alteration, i.e. cooling from above 220 to less than 140°C. Likewise, the wairakite after actinolite and epidote indicates cooling from above 300 to about 200°C (e.g. Elders et al., 1979 and Reyes, 1990).

Pressure. This has little direct effect. Only a few minerals can be used as geobarometers, e.g. some amphiboles. However, fluid pressure affects the depth of boiling and boiling itself affects gas contents and their distribution, especially CO_2, in the reservoir. In fact, as shown previously, fluid pressure can determine phase separation of the reservoir fluid (Figures 1.3 and 1.4).

Fluid composition is also an important control on the formation of hydrothermal minerals, especially acidity. Acid fluid causes H metasomatism, i.e. argillic alteration zone, whereas a neutral pH fluid commonly causes propylitic Na, Mg, Ca metasomatism (Figure 1.5). Gas contents, especially CO_2 and H_2S, also influence the occurrence of hydrothermal minerals, e.g. calcite and anhydrite.

Type of rock. The original compositions of the host rocks might affect the occurrence of hydrothermal minerals, e.g. illite, adularia and albite are more common in rhyolitic rocks and calc-silicates in andesitic (Browne, 1989). However, at temperatures above 280°C the nature of the parent rocks seem to have little effect (Browne, 1978), compared to its influence on alteration products at lower temperature (e.g. Honda, 1970 and Bargar and Beeson, 1981).

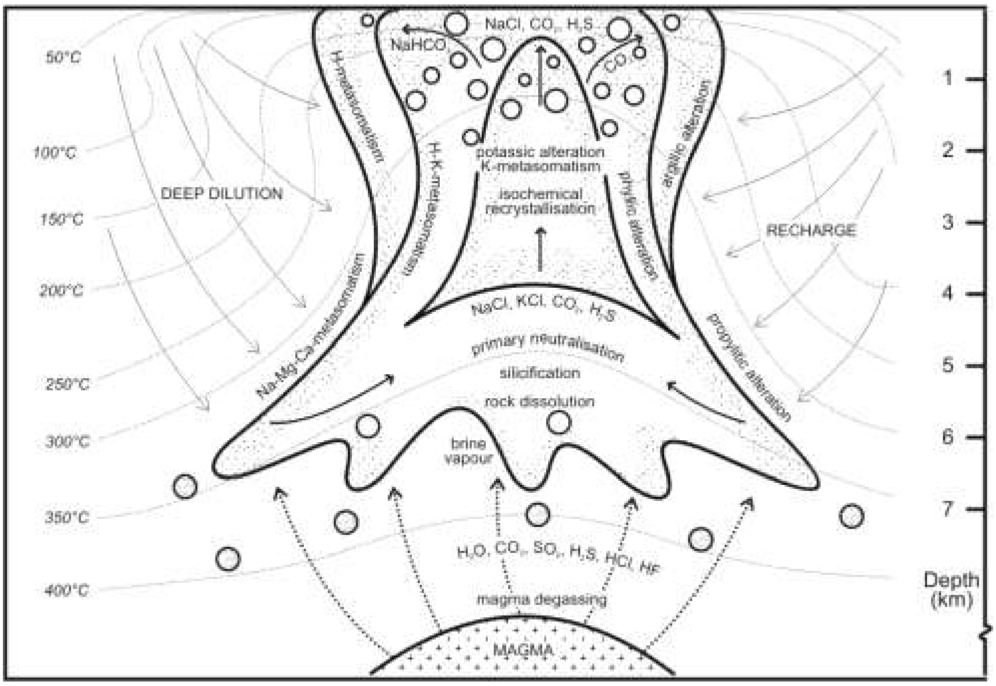

Figure 1.5. Distribution of hydrothermal alteration types, associated with a volcanic system (from Giggenbach, 1988). The magmatic fluid contains high gas contents but it is neutralised during water and rock interactions. Remaining CO_2 and H_2S ascends. Rock dissolution occurs where acid magmatic fluids are dominant; after being neutralised, alteration occurs isochemically. Propylitic alteration and Na-Mg-Ca metasomatism are dominated by the occurrences of calc-silicates, e.g. epidote, and chlorite. Potassium metasomatism forms K-feldspar and K-mica. Propylitic and potassic alteration zones contain minerals which are stable at high temperatures, i.e. above 250-300°C. Phyllic and argillic alteration zones are due to H and/or K metasomatism through the formation of clay minerals at lower temperatures, e.g. smectite and kaolinite. Recharge and dilution by meteoric water occur, resulting in calcite and anhydrite deposition. Note that the temperature gradient near the surface is much steeper than that at depth.

Permeability and porosity of the host rocks, including fluid channels and grain boundaries. In most cases these allow water and rock interactions (Browne, 1978 and Reed, 1997) by the amount of fluid flow through the rocks (Reyes, 1990). Several hydrothermal minerals can be used as permeability indicators, e.g. adularia and albite (Browne, 1978). However, the relationship between hydrothermal mineralogy and permeability of rocks is still arguable, since it is not clear in some geothermal fields (e.g. Tómasson and Kristmannsdóttir, 1972; Elders et al., 1979; Cavarretta et al., 1980 and Reyes, 1990).

Hydrology and topography. The style of hydrothermal alteration differs between geothermal systems in gentle and steep terrains (Browne, 1989). This is clearly due to their different hydrological settings (Reyes 2000). In gentle terrain, the deep fluid reaches the surface whereas in steep terrain, it flows laterally (Figure 1.4). Consequently, the styles of hydrothermal alterations are different.

Duration or time. The residence time of thermal fluids affects the intensity of alteration and therefore the evolution of geothermal system.

1.7. EVOLUTION

During hydrothermal activity, a geothermal system might change in response to internal and external events. Changes may include intensity, location, or thermal processes. The characteristics of thermal fluids can therefore change. These changes are caused by:

Fluid processes, including boiling, steam condensation, mixing with other fluids and cooling. Boiling and cooling are common but heating also occurs in few cases. Hydrothermal minerals in veins reveal fluid processes that have occurred and also record some of the changes in fluid composition. Cross cutting veins also record the chronology of the hydrothermal events and yield information about how a system has changed during its lifetime. Interactions between fluids and rocks also change the thermal fluids.

Mineral deposition. Hydrothermal minerals not only replace the primary minerals but also change the properties of the parent rocks. Commonly, mineral deposition causes self sealing, which decreases the permeability and porosity of the host rocks. As described earlier, where permeability contrasts occur, e.g. between the reservoir rocks and their surrounds, the reservoir fluids change in temperature and pressure or even composition. The occurrence of hydrothermal minerals often increases the density of the host rocks (e.g. Elders et al., 1978 and Browne, 1995).

Magmatic and tectonic activities, including faulting, tilting, caldera collapse, and phreatic and phreato-magmatic eruptions. These processes can change not only the heat source, e.g. at Ngatamariki, New Zealand (Arehart et al., 2002), but also the compositions of thermal fluids, e.g. gas contents in Krafla, Iceland (Gudmundsson and Arnórsson, 2002), fluid pressure, permeability (Shook, 1995 and Allis and Shook, 1999), and hydrological setting, e.g. at Waimangu, New Zealand (e.g. Simmons et al., 1993).

External events, e.g. exploitation, erosion and subsidence. Many studies show that the exploitation of a geothermal system can change its surficial thermal activity, e.g. at Kamojang (Komaruddin and Sujata, 1999), Wairakei, New Zealand (e.g. Brown et al., 1988 and Allis, 1981), Los Humeros, Mexico (D’Amore et al., 1977 and Prol-Ledesma, 1998) and in the Uenotai geothermal system, Japan (Takeno, 2000). In most cases, production causes subsurface pressures to decrease thereby inducing boiling. Other processes like erosion and subsidence change the hydrology of a geothermal system (e.g. Filippo et al., 1985).

1.8. THESIS OUTLINE

The aims, methodology and background of this study are given in Chapter 1. Chapters 2 and 3 summarise the geological setting and the present condition of Darajat respectively. The nature of the host rocks is given in Chapter 4; this chapter gives some ideas about the original conditions of the system before interactions with thermal fluids started.

As thermal fluids interacted, hydrothermal alteration occurred in the matrix of the rocks; this is described in Chapter 5. Chapter 6 describes the occurrence of hydrothermal minerals in veins and fractures as a result of processes affecting the circulating thermal fluids. The variations in the compositions of hydrothermal minerals are reported in Chapter 7.

Study of the fluid inclusions is reported in Chapter 8 which also summarises the paleohydrology of the geothermal system.Chapter 9 describes the compositions of major and trace elements in the altered rocks and explains the extent and magnitude of mass transfer as a result of interactions between thermal waters and the surrounding rocks.

Finally, in Chapter 10, a model of the evolution of the Darajat geothermal system from liquid to vapour domination is presented. This chapter draws upon all previous chapters. In Chapter 11, the conclusions and suggestions for further work are given.

Appendix shows the data that supports this study.

Chapter 2

GEOLOGICALSETTING

2.1. PHYSIOGRAPHY AND TECTONIC SETTING OF WEST JAVA, INDONESIA

Java is dominated by products of an E-W oriented, early Tertiary arc magmatism, continuous with that of Sumatra, and generated by subduction of the Indian-Australian Plate below the Eurasian Plate to the south of Java. The magmatic belt consists of a foreland basin in the north and an outer-arc basin in the south of Java, separated by an intervolcanic basin with a series of Quaternary volcanoes (Hamilton, 1979).

The foreland basin is an analogue of the northern Java alluvial plains and the Bogor zone described by van Bemmelen (1949) (Figure 2.1A). It comprises marine Tertiary sediments, slightly folded and covered by alluvial river deposits, lahars and mud flows derived from volcanoes in the south of the area. Many hypabyssal volcanic necks, stocks and bosses occur in the Bogor zone.

The depression zone of Bandung extends more than 40 km long, trending E-W from the west coast to Sukabumi, Cianjur and Bandung, but then swings to trend NW-SE towards Garut and Tasikmalaya (Figure 2.1A). This zone consists of Oligocene to Miocene rocks, covered mainly by Quaternary volcanic and alluvial deposits (van Bemmelen, 1949). The Bandung zone is likely an intervolcanic basin, identified as such by Hamilton (1979).

The southernmost physiographic zone, considered also to be an outer-arc, early Tertiary tectonic environment, is the southern mountains, which are about 50 km wide (Figure 2.1A). Van Bemmelen (1949) divided this zone into three sections, i.e. Jampang, Pengalengan and Karangnunggal. The Jampang, lying in the western part of the southern mountains, is dominated by Paleogene volcanic rocks, called the Old Andesite Formation. The Jampang section also has some resistant volcanic necks. Upper Cretaceous melange, which are considered to be the basement rocks of Java, is exposed in this section, i.e. in the southwest Java. The central part is the Pengalengan section and the eastern section is the Karangnunggal. The Pengalengan section forms the highest part of the southern mountains and consists of several extinct volcanoes.

The Bogor, Bandung and Southern Mountains zones of van Bemmelen (1949) are located in an intra-arc basin of the Bogor Basin (Martodjojo, 1984). The Bogor Basin is filled by more than 700 m thick sediments, mainly derived from igneous and sedimentary rocks, e.g. andesite, basalt, tuffs and limestone (Martodjojo, 1984). These rocks overlie Paleogene rocks of the fore arc basin (Syahbuddin

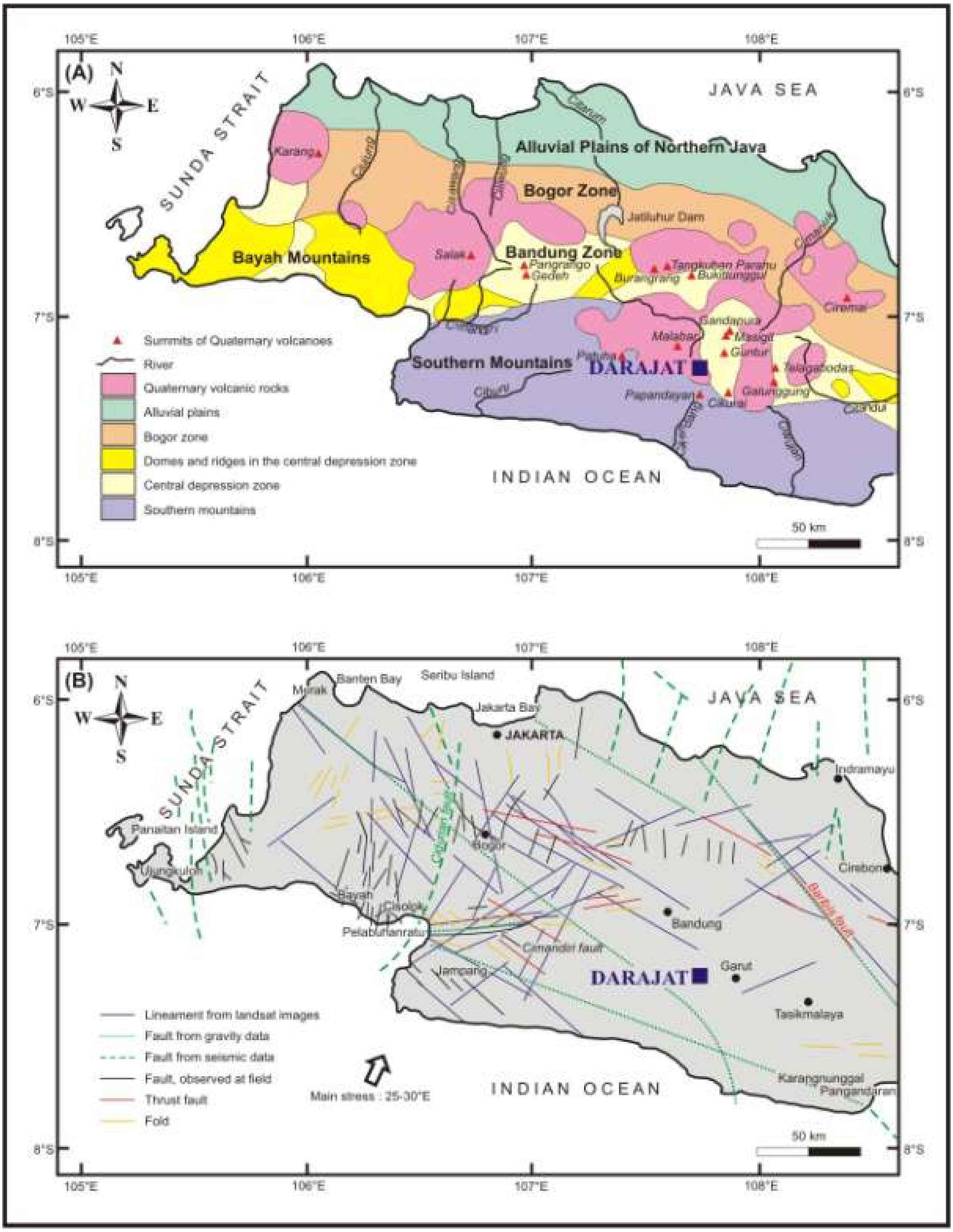

Figure 2.1. Physiography and geology structure of West Java, Indonesia. Mercator projection. **(A)** Physiographic zones, modified from van Bemmelen (1949). **(B)** Geological structure, compiled from Suwijanto (1978) and Martodjojo (1984). The main stress in due to the subduction of the Indian-Australian Plate below the Eurasian Plate at the south of Java, trending about 25°E with a rate of movement of about 7 cm.year^{-1} (e.g. Minster and Jordan, 1978 and Martodjojo, 1984).

et al., 1986). Most of the Quaternary volcanoes are located in the Bogor Basin. The Bogor Basin also contains Miocene volcanic deposits, forming the Jampang and Citarum formations. This volcanism terminated at the end of the early Miocene but sedimentation occurred until the Pliocene. In the late Pliocene, a major uplift of Java began, accompanied by a new period of volcanism that continues until the present time (i.e. Quaternary volcanism).

A series of Quaternary volcanoes are actually present between the Bogor and Bandung zones (Figure 2.1A) and it includes Pangrango, Gedeh and the Sunda Complex with its several peaks, e.g. Burangrang, Tangkuban Parahu and Bukittunggul. South of the Bandung zone are a series of Quaternary volcanoes, including Patuha, Malabar, Papandayan and Cikurai. Compared to Sumatra, the average compositions of the young volcanic rocks in Java are more mafic. They are dominated by pyroxene andesite and calc alkaline, high alumina basalt. Dacite is common, but there are no large masses of silicic rocks. The volcanic belt is superimposed upon older volcanic and volcaniclastic rocks, intercalated with Oligocene and Neogene sediments and intruded by small plutonic masses of similar composition (Hamilton, 1979).

2.2. STRUCTURAL GEOLOGY OF WEST JAVA, INDONESIA

Figure 2.1B shows a geological structure of West Java compiled from Suwijanto (1978) and Martodjojo (1984). Suwijanto (1978) observed that, from the LANDSAT images, West Java contains four lineaments, i.e. 45°, 305°, 330° and 350°E. The structures are concentrated around Bogor and southwest Cirebon areas, and relate to the big structures of the Cimandiri, Baribis and Cidurian Faults (Suwijanto, 1978) (Figure 2.1B). The N-S trend is mostly observed from geophysical study, during oil exploration in the north of Java (Martodjojo, 1984). Katili (1975) revealed that the NE-SW and NW-SE trend structures are mostly of strike slip faults. On the other hand, the N-S structure is mostly normal faults (Padmosukismo and Yahya, 1974), related to subduction during Cretaceous to early Paleogene (Martodjojo, 1984). Numerous folds, mostly trending E-W, occur in the west of Bogor and around the Cimandiri Fault (Figure 2.1B).

2.3. REGIONAL GEOLOGY OF THE GARUT AREA, WEST JAVA

2.3.1. Physiography

Garut lies where the E-W trending Bandung zone changes to a NW-SE trend. Alzwar et al. (1992) included Garut and its surrounding area in a geomorphological unit of volcanic cones, as they are surrounded by three ranges of Quaternary volcanoes. A series of volcanoes, including Malabar, Papandayan and Cikurai, separates the Bandung zone from the southern mountain. A second series of volcanoes lies along the boundary of the Bandung and Bogor zones, including Galunggung and Telagabodas, about 20 km east of Garut. A third series is a range of volcanoes trending E-W separates Garut from the Bandung zone. This range includes Guntur and Gandapura (Figure 2.1A). A plateau geomorphologic unit occurs within the volcanic units and consists of alluvial sediments and young pyroclastic rocks (Alzwar et al., 1992). The volcanic cone unit also separates the drainage pattern in the Garut area with flows to the north, e.g. Citarum and Cimanuk Rivers and the other to the south, e.g. Ciwulan and Cikendang Rivers (Figure 2.1A).

2.3.2. Lithology

Alzwar et al. (1992) demonstrated that the oldest rock in the Garut area consists of andesite lava, andesite breccia and associated tuff, and are exposed about 50 km south of Garut. Fossils from intercalated carbonaceous rock indicate a late Oligocene to early Miocene age. This unit is a part of the Jampang Formation. It is intruded by quartz diorite of middle Miocene age.

The Jampang Formation is unconformably overlain by the late Miocene to early Pliocene Bentang Formation, consisting mainly of conglomerate, tuffaceous sandstone with clay intercalations and lignite lenses. The upper Bentang Formation is dominated by pumiceous vitreous tuff with tuffaceous sandstone. North of Garut, andesite lavas and tuff breccias, containing pumice fragments, gradually become more dominant. This is considered to be the Beser Formation of late Miocene age. The relationship between the Bentang and Beser Formations is unclear.

Figure 2.2 shows that the geology of Garut and its surrounds is dominated by Quaternary volcanic rocks. These volcanic units overlie unconformably the Bentang Formation (Alzwar et al., 1992). They include undifferentiated Pliocene and Plio-Pleistocene volcanic rocks (Qtv), that consist of tuffs, tuff breccia, andesite breccias, breccia and andesite lavas, associated with pyroxene and hornblende andesites (Alzwar et al., 1992). These units are exposed about 10 km southeast of Garut, but their sources are unknown. K-Ar dating indicates an age of 12.0±0.1 Ma (cf. Darman and Sidi, 2000).

The undifferentiated old volcanic rocks are unconformably overlain by products of Pleistocene volcanoes, e.g. Old Malabar and Guntur Complex, and Holocene volcanoes, e.g. Wayang-Windu, Papandayan, Cikurai and Masigit. These deposits formed continuously from 4.4 to 1.3 Ma (cf. Darman and Sidi, 2000).

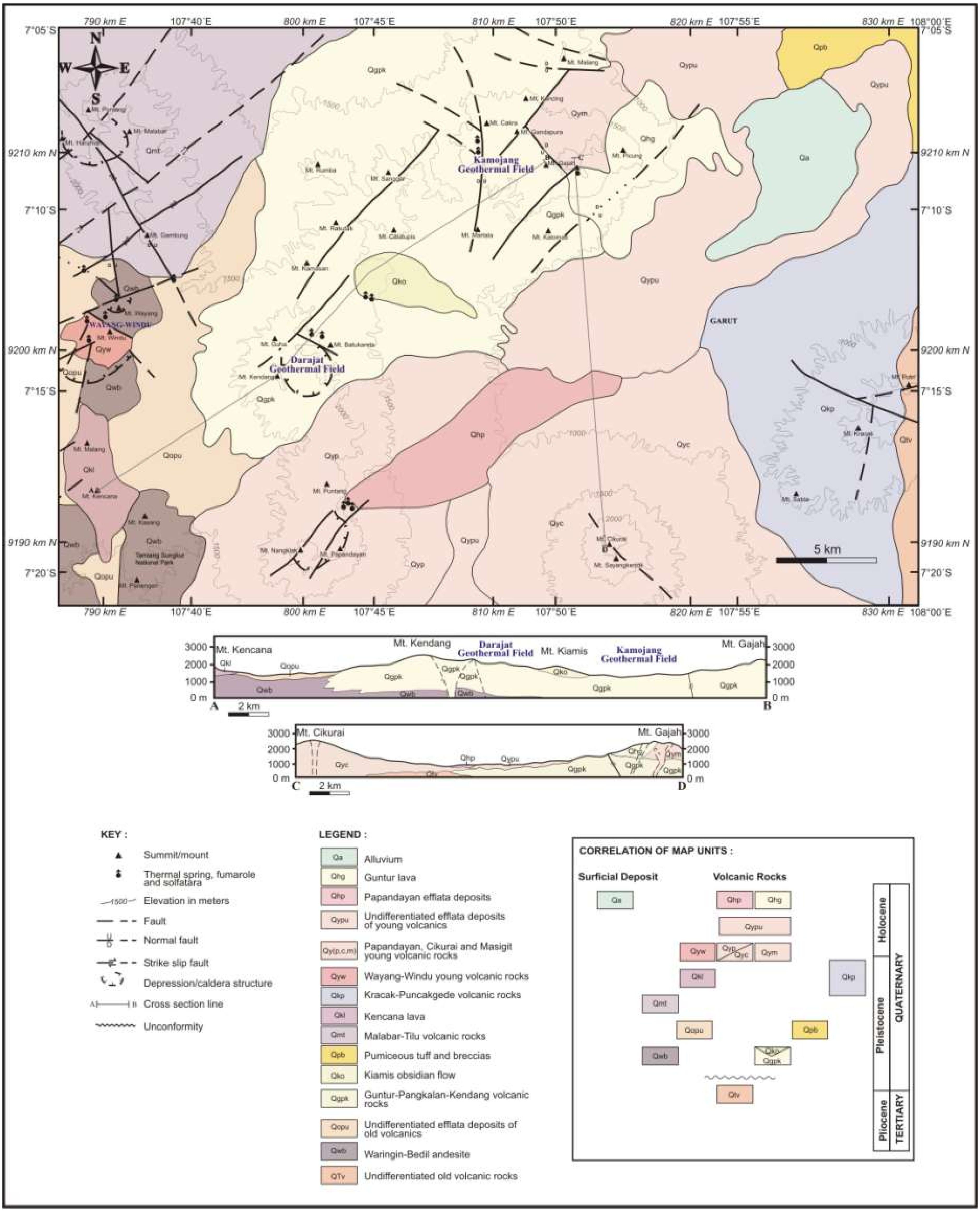

Figure 2.2.Regional geology of the area of Garut. Coordinate grids used are Mercator projection (in degrees) and universal transverse Mercator (UTM) of zone 48 at the southern hemisphere (in km). It also shows the SW-NE cross-sections through the Darajat and Kamojang geothermal systems. Modified from Alzwar et al. (1992).

Old Malabar produced the Waringin-Bedil andesite unit (Qwb), which includes intercalations of pyroxene and hornblende andesite lavas, breccias and tuffs. This unit, exposed about 30 km west of Garut, is overlain by the undifferentiated efflata deposits of the old Malabar (Qopu), which consist of fine to coarse grained dacitic crystalline tuff, tuffaceous breccia, containing pumice and andesitic to basaltic laharic deposits. At Mt. Malabar, the undifferentiated efflata are covered by the Malabar-Tilu rocks (Qmt), which consist of tuff, laharic breccia, with minor pumice and andesitic-basaltic lavas. At the southern flank of old Malabar, the volcanic cone of Mt. Kencana is formed of basaltic to andesitic lavas of the Kencana lava (Qkl) (Alzwar et al., 1992).

In the west of the region, the Pleistocene volcanic rocks are dominated by products of the Guntur Complex and Mt. Kracak. The first, namely the Guntur-Pangkalan-Kendang rocks (Qgpk), consists of efflata and andesitic-basaltic lavas, pyroxene and hornblende, with some olivine andesites. The last is the Kracak-Puncakgede volcanic rocks (Qkp), which consists of fine vitric and lithic tuffs containing lapilli pumice, andesitic lavas and laharic breccia (Alzwar et al., 1992). The units of the Guntur complex include the Kiamis obsidian flow (Qko), which consists of dacitic obsidian with intercalations of vitric tuff, and pumiceous tuff and breccias (Qpb), which consist of dacitic vitric tuffs containing lapilli to bomb sized pumice and andesitic to basaltic breccia. The obsidian flow was produced by a parasitic cone of Mt. Kiamis in the north of Kendang caldera, whereas the sources of the pumiceous tuff and breccia are unknown (Alzwar et al., 1992).

Purbawinata (1988) reported that the Guntur complex has a wide variation of rock composition, i.e. from high Al tholeiitic with low K to calc alkaline series, consisting of dominantly andesites, high Mg basaltic and few dacites. The highest MgO content, reported by Purbawinata (1988), is 8 wt.%. The compositions of Guntur lavas suggest that the Guntur complex likely evolved from heterogeneous parents in multiple processes, involving fractionation and small amounts of crustal contamination (Purbawinata, 1988). K-Ar dating shows that the fractionation might have occurred very recently, i.e. 0.07 to 0.33 Ma.

Quaternary volcanoes of Wayang-Windu, Papandayan, Cikurai and Masigit produced volcanics (Qy[w,p,c,m]) and undifferentiated efflata deposits (Qypu). Those from Wayang-Windu consist of pyroxene and hornblende andesitic lava flows. The Papandayan, Cikurai and Masigit units consist of efflata and pyroxene-hornblende, with few olivine, andesitic-basaltic lava flows. Several volcanic glass deposits occur in Mt. Cikurai and vitric tuffs, pumice and blocks of hornblende andesite are present in Mt. Masigit. The undifferentiated efflata deposits consist of volcanic ash and lapilli, sandy tuff, blocks of andesite-basalt, laharic breccia and efflata (Alzwar et al., 1992).

The youngest rocks in the Garut area are the Papandayan efflata deposits (Qhp), which consist of ash and blocks of andesite and basalt produced in the eruption of 1772 (Taverne, 1926; Alzwar et al., 1992), the Guntur lava (Qhg), which comprises labradorite basaltic lava from the Guntur eruption of 1780-1840 (Alzwar et al., 1992) and alluvium (Qa), which consists of clay, silt, fine to coarse grained sand, gravel and blocks of igneous and sedimentary rocks.

2.3.3. Structural Geology

The geological structure of the Garut area is dominated by folds and normal and strike slip faults generated by compression from the south to north during the late Oligocene and early Miocene. The axis of fold structures is mostly ESE-WNW in the Bentang Formation and NWN-SES in the Jampang Formation. These differences are due to the different intensities of tectonism affecting these two formations (Alzwar et al., 1992).

The Garut area, in the Bandung zone, has normal faults trending E-W. The younger strike-slip faults trend mostly NE-SW, but some have E-W and NW-SE trends. All faults cut Tertiary and Quaternary rocks along re-activated structures (Alzwar et al., 1992). The fault system that affected the Quaternary rocks seems also to control the occurrence of young volcanoes, such as the active Papandayan and Guntur. A detailed study by Bronto (1989) reported that the main lineament in Tasikmalaya and its surrounding is at mainly 315°.

Structures from caldera collapse and eruptive centres are common in the Guntur complex and its surrounding. Guntur itself has 14 main eruptive centres, trending NE-SW; the oldest centres are Mts. Kancing and Gandapura in the north, whereas the younger includes the Kendang caldera in the south.

2.4. GEOLOGICAL HISTORY

Alzwar et al. (1992) revealed that subduction of the Indian-Australian Plate generated andesitic volcanism followed by shallow marine, carbonate sedimentation. Magmatism ended with the intrusion of quartz diorite during the middle Miocene. After marine regression and erosion, the Bentang Formation sediments deposited in the southern area, while volcanism occurred in the north. Both events occurred from the late Miocene to early Pliocene, before another regression, erosion and further magmatism, with injection of andesite dikes, occurred during the Pliocene. Plio-Pleistocene volcanism occurred also and this was followed by activity from the early Quaternary volcanoes until now.

2.5. GEOTHERMAL MANIFESTATIONS IN THE GARUT AREA, WEST JAVA

Numerous fumaroles and solfataras occur on the Papandayan and Guntur volcanoes, including in the Kamojang caldera of Guntur. Acid SO_4^{2-} boiling pools and near neutral HCO_3^- and SO_4^{2-} waters appear in the lower elevations, including Kawah Mas, Kawah Baru and Kawah Nangklak of Papandayan. These manifestations are a common style of liquid-dominated or two-phase geothermal systems, associated with the high topography of volcanic centre (Chapter 1, see Figure 1.3). Several geothermal systems, already under production, include Kamojang and Darajat in Guntur, Wayang Windu in Malabar and Karaha-Talaga Bodas in Galunggung volcano (Figure 1.1).

Chapter 3

DARAJAT GEOTHERMALSYSTEM

The Darajat contract area covers 51 km^2 on the Universal Transverse Mercator (UTM) grid from 9196.5-9205.0 km N to 798-804 km E. The Darajat geothermal project started in 1972 and now has an installed capacity of 260 MWe from the operations of phases I, II and III power plants. Figure 3.1 shows the locations of the power plants and the 31drillholes in the field; the wells are moderate to wide in diameter and from 760 to 2500 m deep mostly sited in the main fumarolic area. Each well can produce 240°C, 35 bars, 15-20 MWe of dry steam. Six drillholes are of slim diameter, i.e. DRJ S-1 to S-6 (Figure 3.1), having 2 3/8 inch liner and 4 1/2 inch casing. These wells provided the continuous cores that are studied here; the samples are listed in Appendix A.

3.1. MORPHOLOGY AND REGIONAL HYDROLOGY

The Darajat geothermal system lies at elevations of 1600-2200 m above sea level on the Quaternary volcanic cone, extending from Mts. Kendang (2611 m), Guha (2414 m) to Kamasan (1514 m) and is dominated by partially collapsed remnants with no obvious cones (Figure 3.1) of an eruptive center of the Kendang Complex.

The Kendang Complex provides the headwaters for streams in the Darajat area, which flow to the east (Figure 3.2). Likely groundwaters in Darajat also move to the east and northeast and discharge as bicarbonate cold springs southeast of Mt. Kiamis. Amoseas Indonesia Inc. (1989a) showed that the level of deep water in the eastern part of Darajat is shallower than it is in the west and south, e.g. in DRJ 1 it occurs at 1500 m, DRJ 5 at 2025 m and DRJ 7 at 1775 m. On the west and south sides of Mt. Kendang, groundwater seems to flow to the southwest and may discharge as cold sulphate springs on the flanks of Mts. Kendang and Jaya (Figure 3.2).

3.2. GEOLOGY

3.2.1. Surface Lithology

Figure 3.3 shows that Darajat and its surrounds are covered by Quaternary volcanic rocks (Healy, 1975). These are dominated by andesitic lavas from Mt. Kendang, which can then be separated into pyroxene (KPA) and hornblende (KHA) rich, Puncak Cae-Ipis (PCIPA) and Tegal Meriuk (TMA) types. Around Mt. Gagak, the volcanic rocks have slightly different compositions and are basaltic (GBA). Pyroclastic breccias and tuffs (BT) around fumarole areas separate the Kendang andesitic lavas. According to Alzwar et al. (1992) all these rocks are Pleistocene in ages.

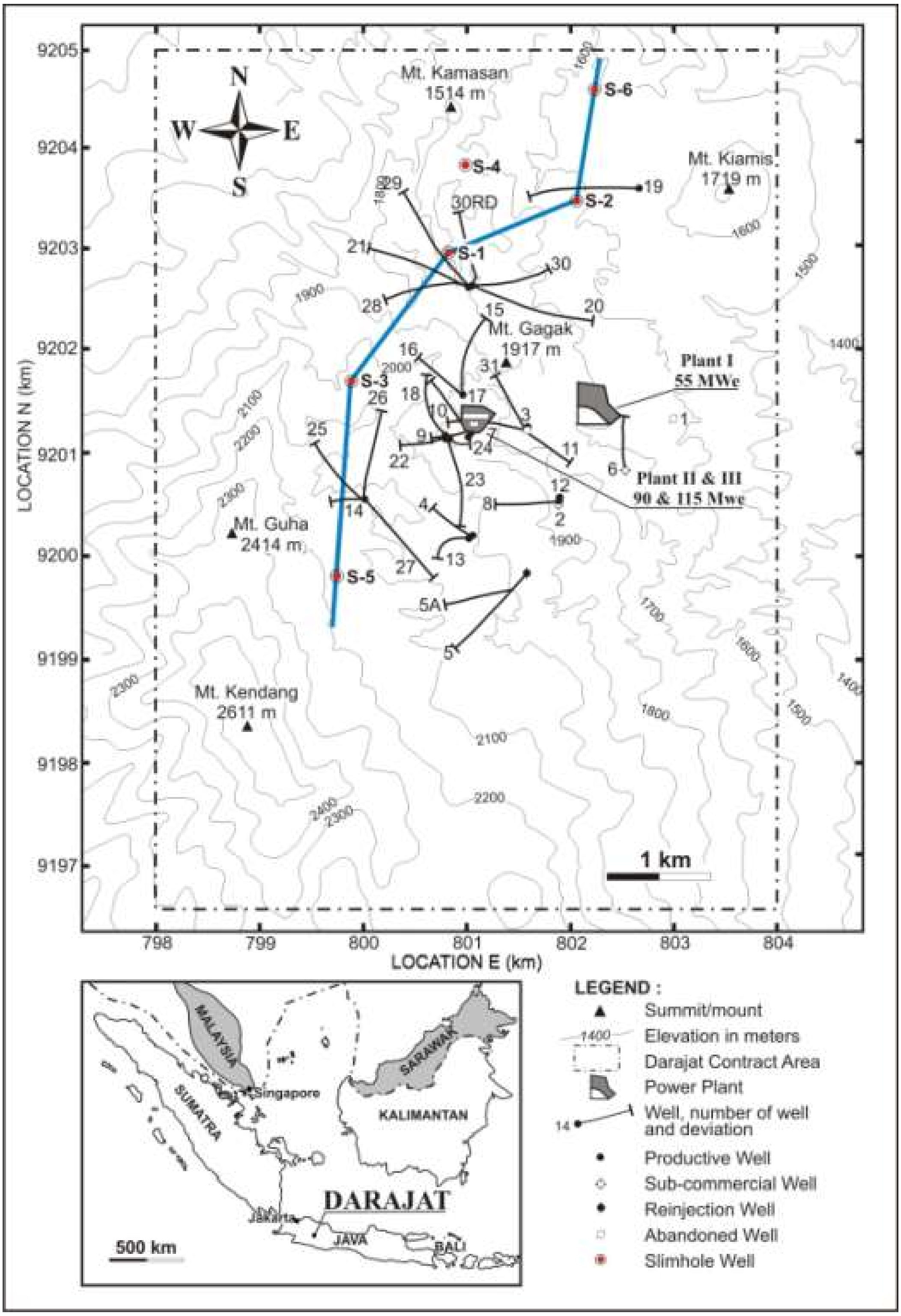

Figure 3.1. Map of Darajat contract area showing locations of wells, slimholes and power plants. Location coordinate is UTM grid of zone 48. Blue line is the south-north section, from DRJ S-5, S-3, S-1, S-2 to S-6, refered in this thesis. Modified from Chevron Geothermal Indonesia Inc. (written com., 2011).

These volcanic rocks are overlain by the youngest magmatic unit, an obsidian flow from Mt. Kiamis (Healy, 1975). The Kiamis obsidian (KO) is dacitic (Alzwar et al., 1992) and contains 76 wt.% SiO_2 (Amoseas Indonesia Inc., 1987). It is a product from a parasitic cone in the Kendang caldera having an age younger than 50,000 years old (Amoseas Indonesia Inc., 1987).

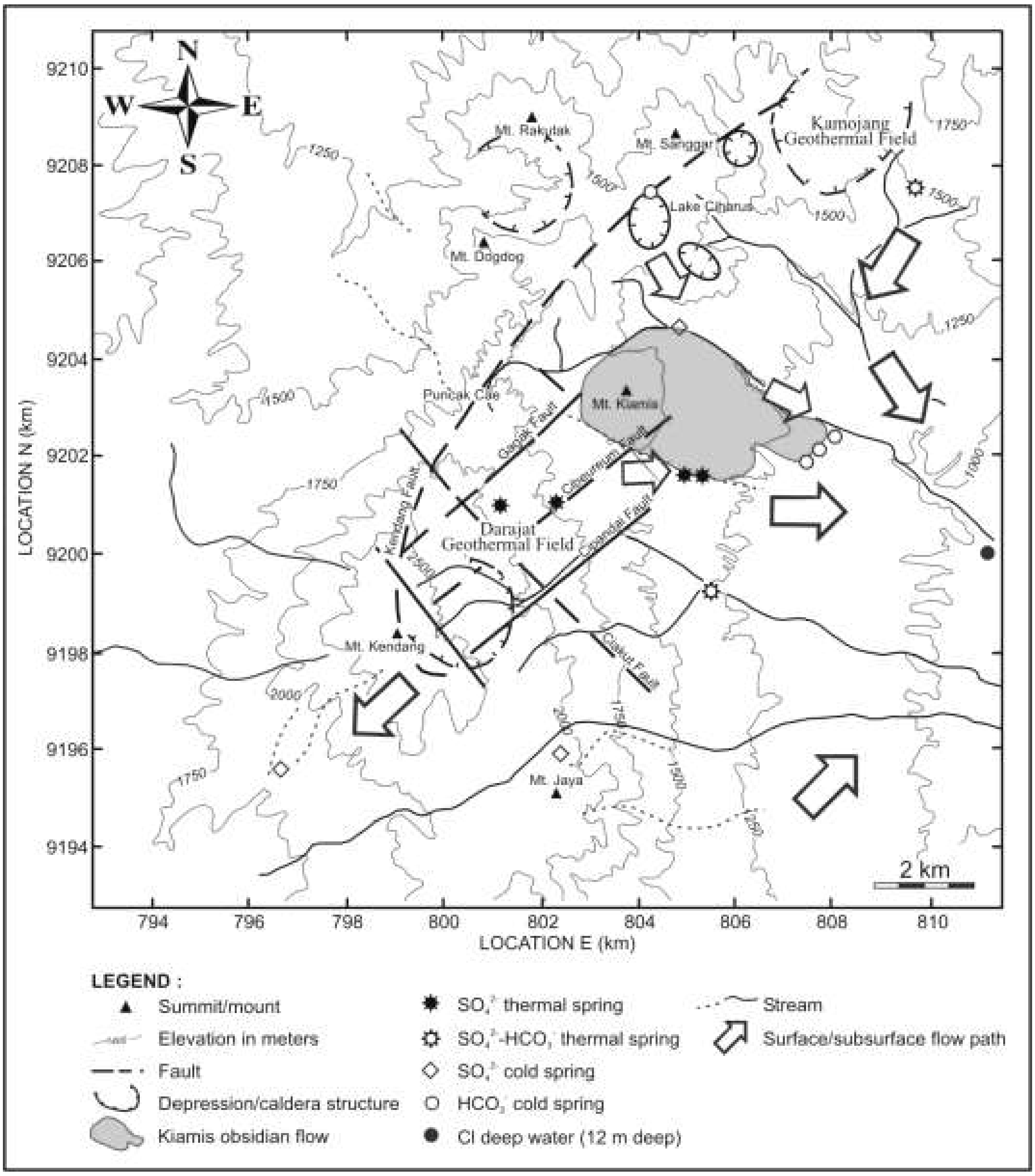

Figure 3.2.Regional hydrology of Darajat and its surrounds showing locations of thermal and non-thermal springs and surface and subsurface flow paths. Location coordinate is UTM grid. Modified from Amoseas Indonesia Inc. (1987).

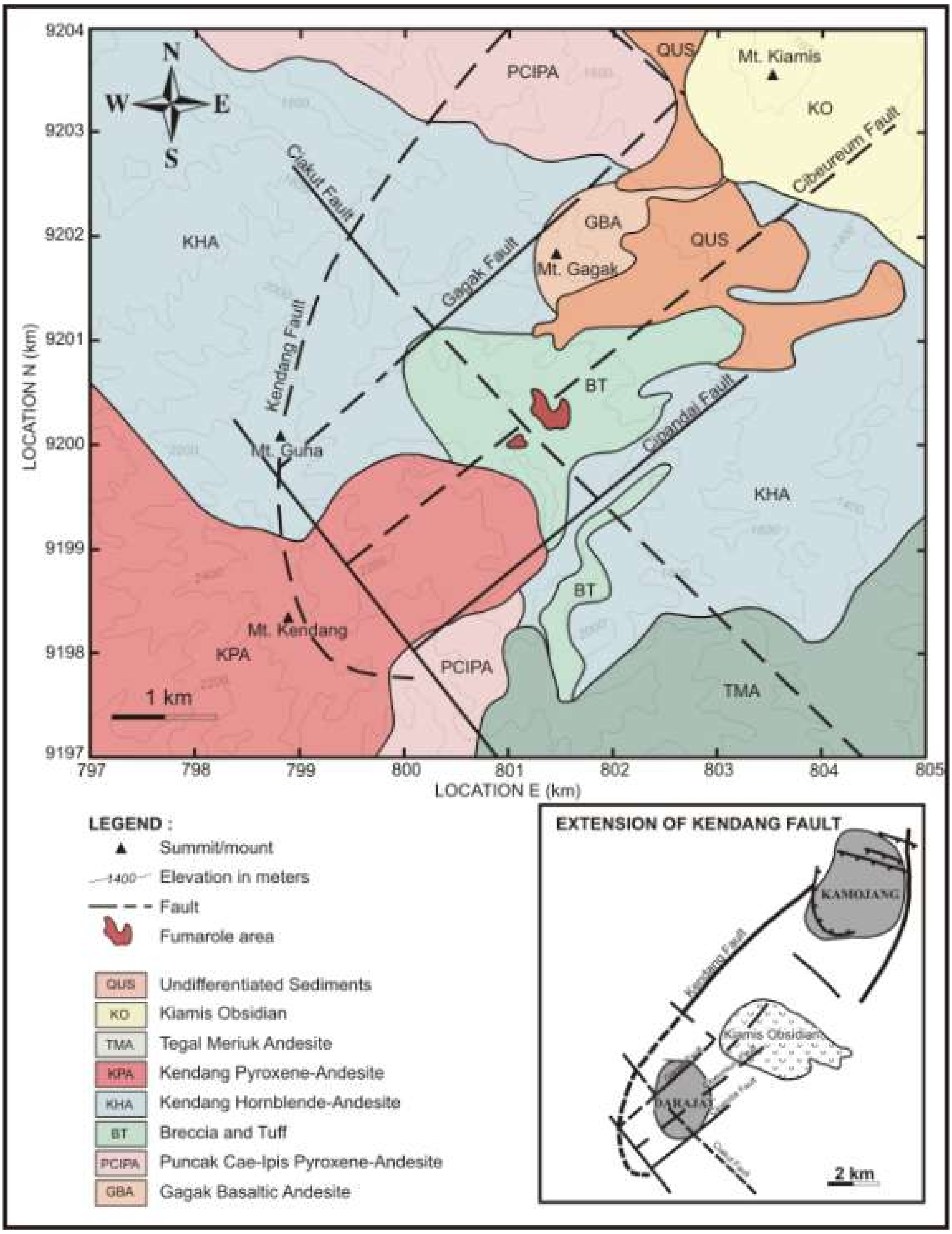

Figure 3.3.Geology of Darajat geothermal system (from Healy, 1975). Location grid is UTM grid. Inset shows the extension of the Kendang Fault through the Kamojang geothermal system.

3.2.2. Subsurface Lithology and Stratigraphy

As shown in the general stratigraphic column (Figure 3.4), the shallower lithological units in Darajat consists of a series of pyroclastic rocks and lava flows. The former consist of breccias, tuffs, lapilli tuffs and tuff breccias. The breccias are dominant; they are light to dark grey, poorly sorted, moderate to well indurated, and composed of fine to medium grained matrix, mostly cryptocrystalline plagioclase, angular to subrounded phenocrysts of plagioclase. Minor broken pyroxene (having fragmental shapes) more than 8 mm in size, tuff and lithic-rich, probably andesite also occur (e.g. Hadi, 1997 and Pramono, 1999). The lavas are basaltic to andesitic, dark grey to black, dense, porphyritic with some glomeroporphyritic and microphorphyritic textures and some are vesicular. They are phenocryst-rich consisting of Ca-plagioclase, i.e. andesine to bytownite, which is euhedral, some 3 mm long, hypersthene and augite. The groundmass is mostly of fine-grained feldspathic type with disseminated iron oxide (Geothermal Energy of New Zealand Ltd. (GENZL), 1990). Individual lava and pyroclastic units range in thickness between 20 and 400 m. The pyroclastic rocks are dominant at the near surface, but are less dominant at the depths where the lavas occur. However, there is no obvious correlation between the pyroclastic rocks and lavas.

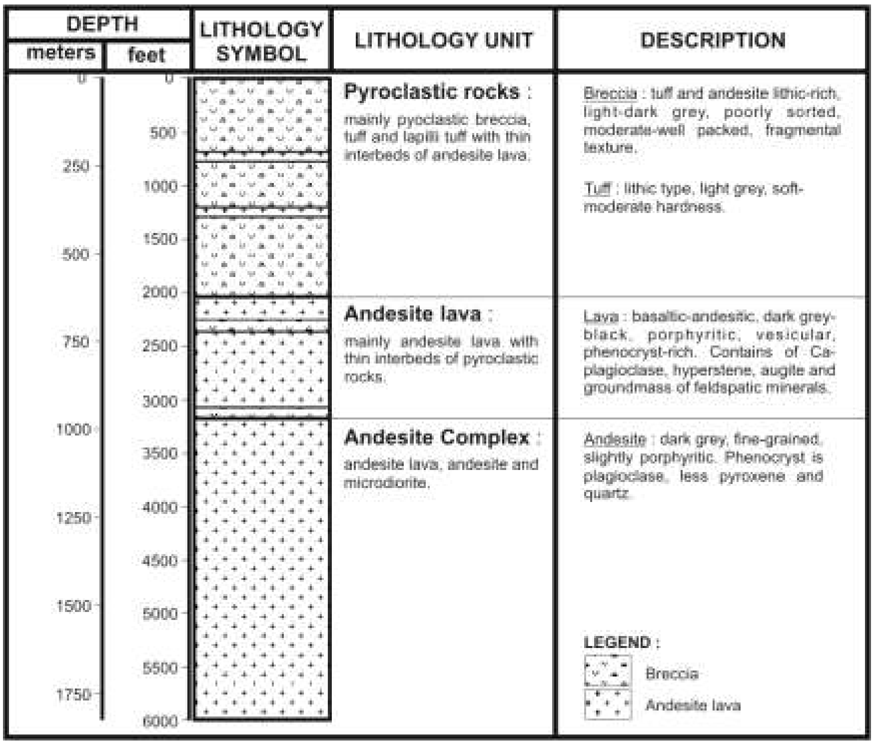

Figure 3.4.General stratigraphy of Darajat geothermal system. Compiled from Healy (1975) and GENZL (1990).

Andesites more than 800 m thick are the deepest rock types recovered from the drill holes. This unit is then referred to as the Andesite Complex, which consists of andesite lavas and microdiorites. Both rock types are typically dark grey, mostly fine-grained, but some are coarse grained and slightly porphyritic. They contain less than 2 mm in size phenocrysts of plagioclase, less pyroxene, some primary quartz, in a fine-grained groundmass (GENZL, 1990).

Until 1990 the Andesite Complex was considered to comprise either lava flows or a series of sills derived from a single microdiorite intrusion. Both models are compatible with the gravity data, which indicates the presence of lava sheets, rather than a dome shaped intrusion (GENZL, 1990). GENZL (1996) suggested that the Andesite Complex is dome shaped with an axis trending approximately N-S. Along the axis, two humps appear, one centered around DRJ 4 and the other about 0.5 km south of DRJ S-1. This structure is close to the top of the reservoir and likely relates to microdiorite intrusives at the eruptive center.

3.2.3. Structural Geology

Most structural features at Darajat seem to result from the main N-S compression of Java. The most prominent structural feature is the Kendang Fault. Figure 3.3 shows that this trends N-S to the west of the field but is a NE-SW lineament toward its northern part extending into the Kamojang region (see inset in Figure 3.3). The Kendang Fault is caldera-like, very old, its trace is deeply eroded and seems to be a fundamental feature that generated a 100-200 m high collapse on the north and east side of the Mt. Kendang (Amoseas Indonesia Inc., 1987). A head-on resistivity survey in 1989 showed this structure dips from 42° to almost vertical. The fault is recognised in cores by the presence of slickensides oblique to their axes.

NE-SW trending structures, striking 40-50°E, are dominant; they mostly dip above 60° to the east or southeast (Whittome and Salveson, 1990). Figure 3.3 also shows other NE-SW trending structures of the Gagak, Cibeureum and Cipandai Faults. No evidence of the Gagak Fault in the Mt. Kiamis area indicates that this fault is older than the Kiamis obsidian flow or that it is only a topographic scarp produced by landslides (Amoseas Indonesia Inc., 1987). However, the Cibeureum and Cipandai Faults, which are parallel to the Gagak Fault to the south, are younger than the Gagak Fault.

Two cross surface lineaments, i.e. striking NE-SW and NW-SE, appear parallel to the Cibeureum and Ciakut Faults. These seem to represent the youngest structural features at Darajat and are interpreted as subsurface fractures (Amoseas Indonesia Inc., written com., 1999). However, they are hard to trace into older deposits to the south and west of the Kendang Fault.

Three distinctive fault zones have been identified based on drilling results, i.e. the Gagak, Kendang and Cibeureum Faults (Rejeki et al., 2010). The Gagak Fault represents a zone of enhanced reservoir permeability and has become an important drilling target for many of the production wells, whereas the Kendang and Cibeureum Faults are structural boundaries of the Darajat geothermal reservoir (Rejeki et al., 2010).

3.3. SURFACE MANIFESTATIONS

The main surface thermal manifestations occur around the area between the Gagak and Cipandai Faults, i.e. Kawah (caldera) Darajat, including Kawah Manuk, Masin, Laher, Cipandai and Laken (Cigupakan) at elevations of 1800-2000 m (Figure 3.5). They are generated by steam rising and consist of steaming ground, steam heated acidic boiling pools and fumaroles with temperatures between 50 and 90°C (Amoseas Indonesia Inc., 1987). Measurements made in 1996 showed that the fumaroles are superheated and have temperatures as high as 118°C (Amoseas Indonesia Inc., written com., 1999). Tables 3.1 and 3.2 show the compositions of steam and water discharged from fumaroles taken from Amoseas Indonesia Inc. (1987). The steam discharges contain about 950 $mmol.mol^{-1}$ CO_2 and 30-40 $mmol.mol^{-1} S_{total}$ in dry gas. They also contain magmatic generated HCl and HF gasses. Average concentrations of He, Ne and Ar in dry gas are respectively $3.2x10^3$, $1.0x10^3$ and 0.05 $mmol.mol^{-1}$, suggesting a mixing between air and magmatic andesitic gases (Figure 3.6).

Surface water in the surface manifestations around Kawah Darajat have pH values of 1.8-2.7 and have SO_4^{2-} as their dominant anion, ranging from 270 $mg.kg^{-1}$ in Kawah Laher to above 3000 $mg.kg^{-1}$ in Kawah Manuk. The water has less than 1.5 $mg.kg^{-1}$Cl but there is no HCO_3^- (Figure 3.7) The average amounts of Na, K and Ca in the surface waters are about 12, 6 and 22 $mg.kg^{-1}$ respectively. The surface waters also contain varying amounts of Fe and Al. The amount of Mg is more uniform at approximately 12 $mg.kg^{-1}$ (Table 3.2). The waters from Kawah Laher and Laken contain high B, i.e. up to 110 $mg.kg^{-1}$, indicating that the steam might derive from a deep high temperature source.

Several thermal water outflows occur at the Toblong, Golangsing and Cibeureum hot springs (Figure 3.5). Toblong is located at about 3 km east of Kawah Darajat, at 1250 m, on the south side of the Kiamis obsidian. About 2.5 km due south is the Golangsing spring at an elevation of about 1350 m. The Cibeureum hot spring is less than 1 km east of well DRJ 3; it appears at an elevation of 1600 m. Table 3.2 and Figure 3.7 show that the Toblong and Cibeureum waters are acid and comprise SO_4^{2-} waters, while the Golangsing spring has a near neutral pH, about 6, and comprises SO_4^{2-}-HCO_3^- water. Table 3.2 also shows that the Golangsing waters have 240 $mg.kg^{-1}$ total dissolved solids but, because of their greater acidity, the other two springs contain more. Golangsing has a temperature below 30°C, while the others are hotter, i.e. 50-60°C. The concentrations of alkalies, Ca, ferromagnesium and Al are significant, but B, F, Cl and Br are low, indicating the absence of a direct magmatic influence. In addition, Amoseas Indonesia Inc. (1987) showed that there is a warm, near neutral pH, SO_4^{2-}-HCO_3^- water seep at Toblong. Its chloride content is slightly higher than that of the Toblong springs themselves (Table 3.2). This seep might result from mixing between SO_4^{2-} and HCO_3^- waters.

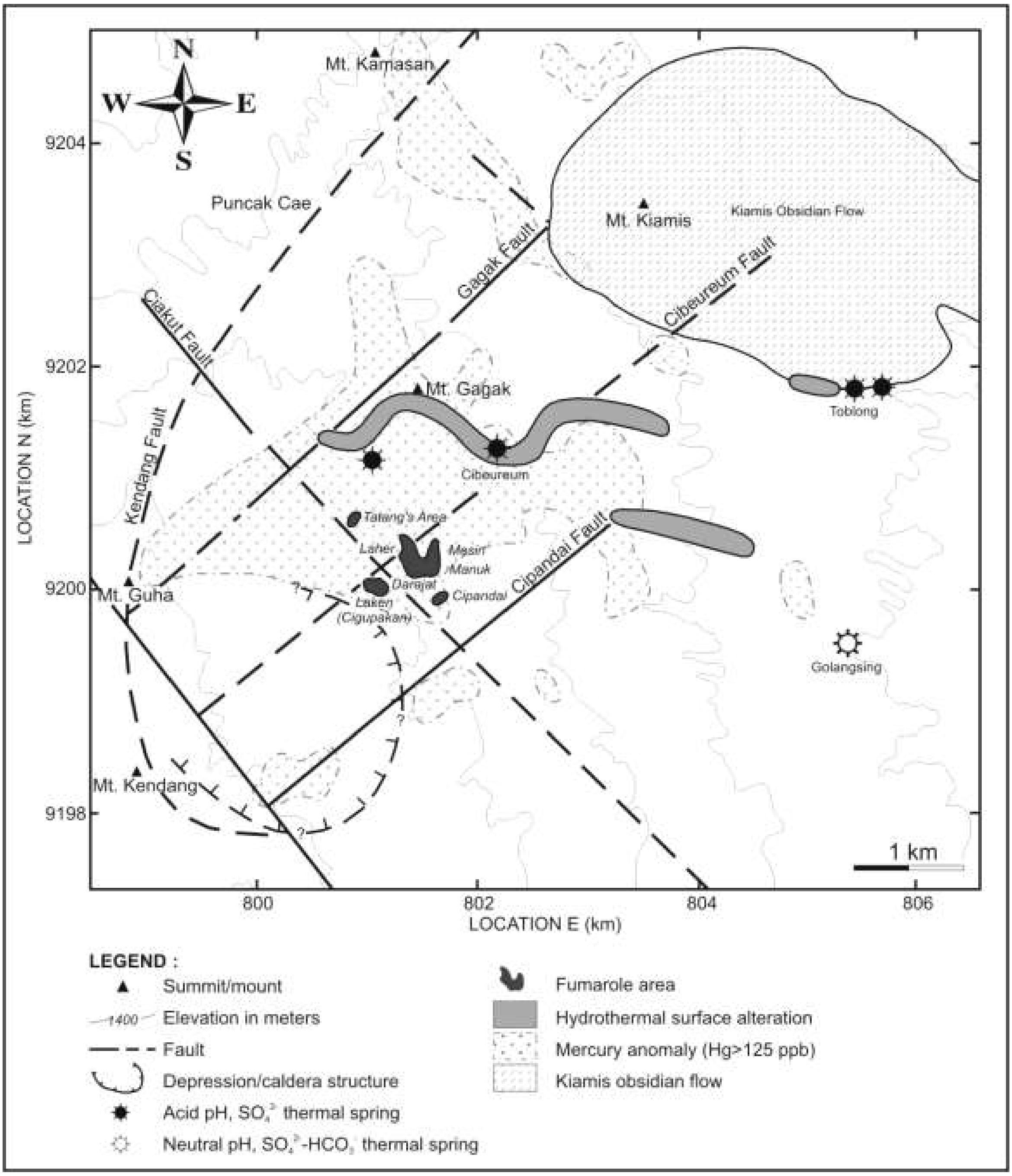

Figure 3.5.Surface manifestation in the Darajat geothermal system showing active fumaroles, hot springs and surface alteration (Amoseas Indonesia Inc., 1987). The extent of the mercury anomaly taken from the survey of 1987 is also shown. Location grid is UTM.

Table 3.1. Composition of steam discharged from fumaroles in the Darajat geothermal system. Locations are given in Figure 3.5. Data from Amoseas Indonesia Inc. (1987).

Concentration (mmol.mol^{-1})	**Kawah Laher**					**Kawah Masin**			**Tatang's Area**
CO_2	960	959	873	952	918	962	952	960	916
S_{total}	24	27	88	30	45	28	31	24	42
HCl	<0.37	<0.64	0.87	0.35	<0.20	<0.58	1.3	<0.37	8.7
HF	0.08	<0.014	0.027	<0.007	<0.009	<0.012	0.037	<0.008	<0.004
NH_3	0.023	0.016	0.03	0.017	0.014	0.08	0.082	0.009	0.013
He (in 10^3)	2.9	2.4	4.3	2.8	5.2	2.7	2.8	2.9	3.5
Ne (in 10^4)	0.21	0.17	2.6	0.2	2.7	0.18	0.16	0.2	1.8
H_2	7.7	7	15.4	9.4	17.1	2.4	6.5	7.7	19.4
Ar	0.014	0.012	0.12	0.015	0.15	0.012	0.013	0.019	0.096
O_2	<0.031	<0.019	<0.10	<0.029	0.22	<0.027	<0.034	<0.031	<0.070
N_2	6.7	5.7	21	7.8	19	6.7	8.7	7.6	12.1
CH_4	0.6	0.55	1.1	0.68	1.1	0.58	0.51	0.57	1.52
CO (in 10^4)	2	<2	<7	<2	<5	<1	<2	<2	<5

Table 3.2.Water chemistry of surface manifestations in the Darajat geothermal system. Locations are given in Figure 3.5. Data from Amoseas Indonesia Inc. (1987).

Water Composition		**Fumaroles**				**Hot springs**					
		Kawah Manuk	Kawah Laken	Kawah Laher	Tatang's area	Cibeureum		Toblong		Warm seep at Toblong	Golangsing
t (°C)		54.0	85.0	77.0	90.0	51.0	48.0	54.0	56.0		29.0
pH		1.8	2.6	2.7	1.9	2.7	2.5	3.3	3.2	6.2	6.3
Concentration (mg.kg^{-1})	TDS*	4260	710	555	-	1175	230	310	240	420	240
	Li	0.013	0.011	<0.005	<0.005	-	<0.05	0.008	<0.005	0.014	-
	Na	15.7	13.6	7.9	10.8	3.8	7.1	16.4	15.7	39	20
	K	6.8	7	3.8	5.8	1.5	3.1	4.9	5	11	7.5
	Mg	19.2	11.1	8.1	11.4	6.8	4.2	4	3.9	13.1	11
	Ca	31	23	14.8	18.5	10.5	11.7	18.4	18.5	37	27
	Fe	100	31	15	125	-	6.5	2.6	0.9	0.3	0.08
	Al	133	43.2	8.8	60.9	-	8	13.7	2.2	<0.1	-
	NH_3	1	11	1.2	1.1	-	0.6	<0.1	<0.1	<0.1	-
	SiO_2	377	187	120	210	560	125	107	109	119	21
	B	1	114	16	<1.0	-	1.6	<1.0	<1.0	<1.0	-
	Fe	0.34	0.25	0.18	0.12	-	0.5	1.7	1.7	1.2	-
	Cl	1.1	2.2	1.6	1	1	1	1	1	1.3	3
	Br	0.09	0.02	<0.02	<0.1	-	<0.01	<0.02	<0.02	<0.02	-
	SO_4^{2-}	3060	330	278	1720	510	189	148	166	680	44
	HCO_3^-	0	0	0	0	0	0	0	0	105	160
	As	0.01	<0.01	0.01	0.01		<0.01	<0.01	<0.01	<0.01	-

* : TDS is total dissolved solids

\- : not analysed

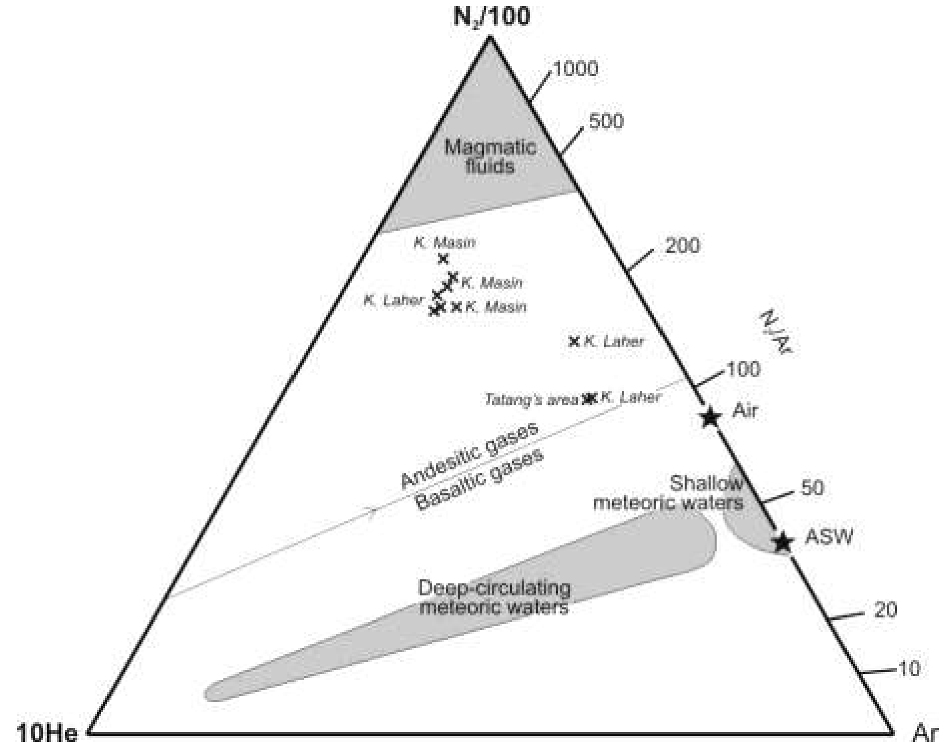

Figure 3.6.Proportions of He, N_2 and Ar contents of fumarole gas. It suggests that the gases result from mixing between shallow meteoric water and magmatic fluids. Data is from Amoseas Indonesia Inc. (1987). Location is given in Figure 3.5. Classification of the origin of water is compiled from Giggenbach, 1992b; Giggenbach et al., 1993; Norman and Musgrave (1994) and Lutz et al. (1999).

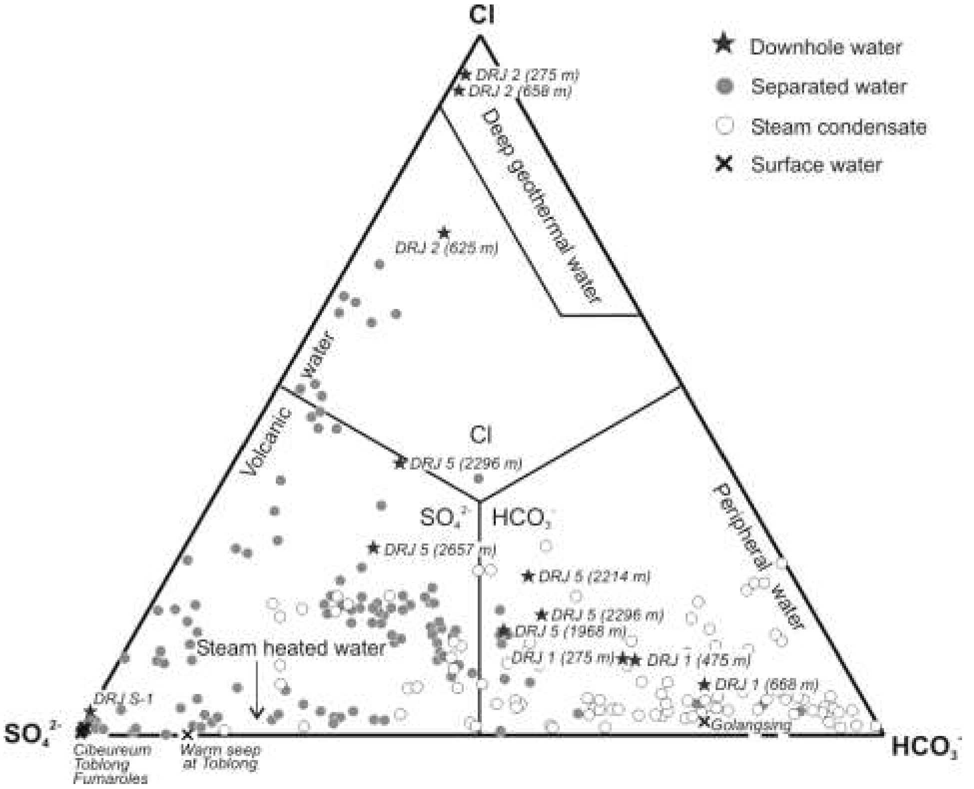

Figure 3.7. Triangular plot of $Cl-HCO_3^--SO_4^{2-}$ for downhole, separated waters, steam condensate and hot spring waters. Data is compiled from Amoseas Indonesia Inc. (1987 and 1989a), except for well DRJ S-1, which is pers. com. (1999). Depths where downhole water collected and compositions of surface water are given. Well location is given in Figure 3.1 and location of hot spring in Figure 3.5.

No neutral pH chloride water outflows in Darajat. However Amoseas Indonesia Inc. (1987) mentioned that deeply derived Cl water occurs 10 km east of Kawah Darajat in a 12 m deep well (Figure 3.2) and possibly at higher altitutes on the west side of Mt. Kendang. However, the origin of these waters is unclear.

Surface hydrothermal alteration is dominated by light coloured, clay altered volcanic rocks and mostly covered by vegetation and/or surficial ash layers. Hadi (1997) pointed out the extensively orange-white altered ground around Puncak Cae (Figure 3.5). He suggested that the alteration is kaolinite and might show either an extension of the reservoir or else it is a relict of former geothermal activity.

3.4. EXTENT OF RESERVOIR

At the present day, the proven area of the Darajat geothermal system is approximately 14 km^2 (Amoseas Indonesia Inc., written com., 1999) with a reservoir thickness of about 1 km (GENZL, 1990). The reservoir has an asymmetric dome-like shape trending NNW-SSE with an axis approximately parallel to the Kendang Fault. It is considered to be vapour dominated having a temperature of 240°C and a pressure of 35 bars. Geophysical surveys carried during 1987-1989 by Amoseas Indonesia Inc., including drilling shallow gradient holes, showed an elongate anomaly occurs in the main fumarolic area indicating the extent of the present reservoir of Darajat. A recent study by Rejeki et al. (2010) showed that the reservoir bottom has a bowl shape extending to approximately -3500 m above sea level.

The reservoir consists of dense intrusive rocks at 700 to 1700 m depth confirmed by the resistivity, gravity and aeromagnetic survey. Several wells (e.g. DRJ 7) encountered the Andesite Complex within the fluid loss zone, several ten meters below the drilling break indicating that the reservoir is actually the highly fractured Andesite Complex (e.g. Amoseas Indonesia Inc., 1989b). Whittome and Salveson (1990) reported that this present reservoir is actually smaller than an earlier developed reservoir.

Amoseas Indonesia Inc. (1987) found that steam present in the deep zone corresponds with a high resistivity anomaly. A condensate zone may overlie the steam reservoir, as is indicated by several geophysical surveys. The existence of the resistivity anomaly at depth over a broader area, mostly in the central area and to the east indicates lateral outflows of condensate fluids away from the central reservoir area (Amoseas Indonesia Inc., 1991). This condensate zone is consistent with a silicification zone. If this is indeed relict alteration from the deep water outflow during earlier stages, then the Darajat system could have once been water dominated.

3.5. COMPOSITION OF DEEP THERMAL FLUIDS

Steam discharged from wells DRJ 3 to 7 contains about 2 wt.% dry gas consisting of about 94 wt.% CO_2, 3 wt.% H_2S and 3 wt.% residual gas. Magmatic gases, such as HF, HCl and SO_2 can be traced in several wells (Amoseas Indonesia Inc., 1989a). The total gas discharge increases from the area of DRJ 7 to the southeast of the field. In the northern part, the total gas discharge is likely to increase to the west. The ratio of CO_2/H_2S increases from the area of DRJ 10 to the southeast. Figure 3.8A shows the variation in the ratio between gas and steam, indicating that the increases in gas contents and CO_2/H_2S ratios of steam compositions indicate a lateral flow and condensation of steam from the center to the margin of the reservoir (e.g. D'Amore et al., 1977; Amoseas Indonesia Inc., 1989a and Bratakusuma, 1996). The increase in gas contents might also relate to the greater degree of boiling in the reservoir.

The Darajat reservoir might contain liquid as indicated by the occurrence of 1-2 wt.% liquid water during the early stages of a well flow test. Using Grant's method (1979b) the water saturation in the reservoir is calculated from non-condensable gases of CO_2 and H_2S and the results show that the reservoir pre-exploitation contained 29 to 36% liquid water (Amoseas Indonesia Inc., 1989b). Table 3.3 and Figure 3.7 show that the compositions of the deep water of Darajat is near neutral Na-HCO_3^--SO_4^{2-}-Cl type (e.g. Amoseas Indonesia 1989a) under partial equilibrium condition (e.g. DRJ 5) and fully equilibrated (e.g. DRJ 2) (Figure 3.9).

The downhole water from well DRJ S-1 is the most immature water, containing low Na. As the downhole waters become fully equilibrated, corresponding to an increase in their Cl contents, the amounts of B and SO_4^{2-}will increase (Figure 3.10). This is likely due to condensation (D'Amore et al., 1977). The water also contains several hundreds mg.kg^{-1}of SiO_2, total dissolved solids of less than 2000 mg.kg^{-1} and several tens mg.kg^{-1} of Fe.

Figure 3.7 and Table 3.3 also show that separated waters are of HCO_3^--SO_4^{2-} type. In fact, the separated waters obtained from wet discharge are similar to that of the downhole waters, but when the discharge is dry, the composition of separated waters becomes very dilute acid SO_4^{2-} with less than 200 mg.kg^{-1} total dissolved solid. As shown in Figure 3.10, increasing the amount of SO_4^{2-} with respect to the Cl contents produces two trends, i.e. with ratios of SO_4^{2-}/Cl of 0.6 and 3.2. When the wells dry out after being initially wet, the waters also change in composition from neutral pH to acid. Amoseas Indonesia Inc. (1989a) concluded that this is likely due to input of SO_2, not CO_2 nor H_2S gases, from the reaction between sulphur species and unlikely derive from a magmatic source.

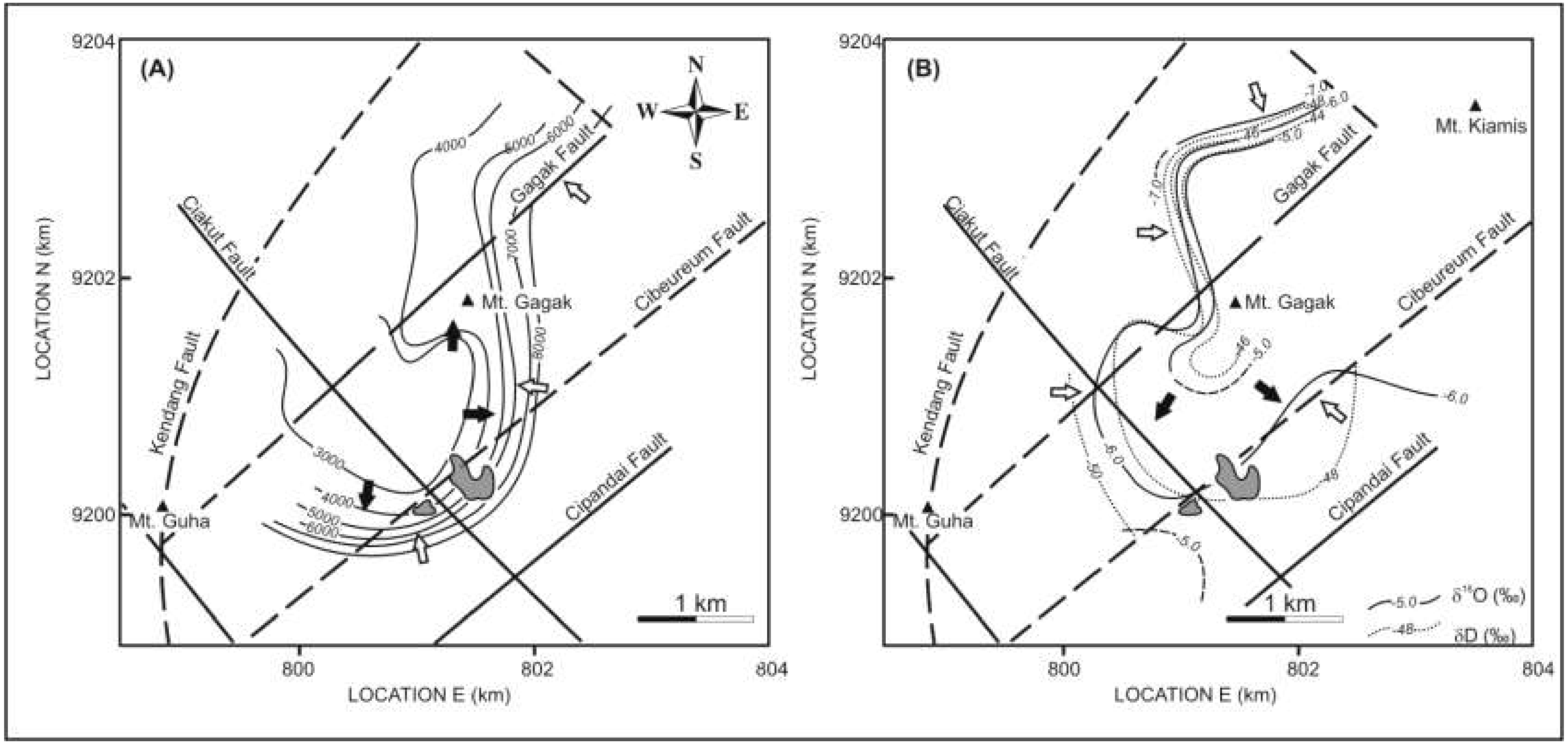

Figure 3.8. **(A)** Distribution of the gas/steam ratios and **(B)** variations in δ^{18}O and δD in Darajat (data from Amoseas Indonesia Inc., 1998). The changes in the gas and isotopic compositions suggest condensation (solid arrow, ➔) and dilution of meteoric waters (open arrow, ⇨) in the center part of the field, i.e. between the Gagak and Cibeureum Faults. Location coordinate is UTM grid.

Table 3.3. Representative compositions of waters in the Darajat geothermal system. Well locations are given in Figure 1.2. Data compiled from Amoseas Indonesia Inc. (1987), (1989a) and written com. (1999).

Type of water		**Downhole water**				**Separated water**						**Steam condensate water**			
Well		DRJ 1	DRJ 2	DRJ 5	DRJ S-1	DRJ 2	DRJ 3		DRJ 4	DRJ 5	DRJ S-1	DRJ 2	DRJ 4	DRJ 5	DRJ 7
Date of measurement		17/07/85	16/07/85	24/02/88	02/07/98	09/07/87	02/01/79	24/08/88	12/09/87	02/12/88	06/04/98	07/09/87	13/01/88	29/02/88	03/10/88
Depth (m)		668	658	2134	-	-	-	-	-	-	-	-	-	-	-
pH		7.1	6.2	6.9	3.5	5.8	8.5	5.5	4.1	8.6	5.0	5.1	5.2	5.4	5.1
Concentration ($mg.kg^{-1}$)	TDS*	4050	-	-	307	-	828	-	-	-	32	-	-	-	-
	TDS* at 105°C	-	6180	1652	-	133	-	230	315	4440	-	30	28	213	38
	TDS* at 180°C	-	-	1592	-	132	-	225	315	4438	-	22	26	193	24
	Li	1.4	1.5	-	-	-	0.4	-	-	0.1	-	-	-	-	-
	Na	1462.0	1950.0	334.6	3.8	3.8	21.0	13.8	32.5	1183.0	1.2	0.3	0.2	0.2	0.1
	K	45.0	80.0	20.6	1.8	1.1	18.7	1.0	4.9	19.3	0.3	0.1	1.4	0.2	0.3
	Mg	4.9	0.5	0.2	1.7	0.2	1.0	0.8	0.1	0.1	0.0	0.2	0.1	0.1	0.1
	Ca	22.3	45.3	24.5	6.6	6.5	15.0	27.2	13.1	74.5	1.8	0.1	0.1	0.1	0.1
	Cl	219	3000	141	4	10	29	3	7	175	1	1	1	1	1
	F	-	4.0	-	0.4	-	0.5	-	-	6.3	0.9	-	-	-	-
	HCO_3^-	2680	70	417	-	11	219	35	6	609	-	15	13	118	17
	SO_4^{2-}	686	194	288	151	30	169	117	180	1946	4	23	12	8	4
	SiO_2	255	380	330	131	20	350	5	15	155	19	4	1	3	2
	B	23.4	638.0	43.2	2.6	37.0	-	0.6	9.9	43.2	706.0	0.9	0.6	2.5	3.5
	As	0.2	12.0	-	0.5	-	0.1	-	-	3.6	0.1	-	-	-	-
	Fe	8.3	1.5	0.5	-	5.0	2.0	16.8	41.9	0.2	0.9	6.9	4.8	35.3	9.8
	NH_4	0.5	2.8	-	-	5.4	1.8	-	-	1.6	0.7	9.0	-	-	-
	Cs	1.7	2.4	-	-	-	-	-	-	0.0	-	-	-	-	-
	Dissolved H_2S	-	-	4	2	2	-	1	43	4	-	7	7	6	41
	Dissolved CO_2	-	-	135	-	40	-	60	368	-	-	144	70	378	124

* TDS = total dissolve solid

Table 3.4. Representative gas contents of waters in the Darajat geothermal system. Well locations are given in Figure 1.2. Data compiled from Amoseas Indonesia Inc. (1987) and (1989a).

Well		**DRJ 2**		**DRJ 3**		**DRJ 4**	**DRJ 5**		**DRJ 7**
Date of measurement		28/09/87	20/10/87	20/03/87	08/07/87	02/09/88	04/04/88	04/08/88	21/09/88
Pressure (psi)	Well Head	55	91	360	210	82	80	81	162
	Separator	53	90	50	180	82	80	81	60
Gas content (wt.%)	Harrison separator	2.26	2.89	1.79	1.75	1.29	2.54	2.18	1.00
	in laboratory	1.70	2.55	-	1.60	1.16	2.05	2.12	0.95
Non-absorbed dry gas (wt.%)	H_2S	0.00	0.00	0.78	0.07	0.01	0.00	0.00	2.64
	O_2+Ar	2.86	2.51	3.73	0.59	9.79	9.81	9.71	0.00
	N_2	10.99	9.63	22.58	2.31	37.79	57.89	51.86	41.25
	CH_4	0.24	0.03	3.41	0.01	0.28	1.05	0.70	0.33
	NH_3	1.35	0.10	0.56	0.87	0.00	0.00	0.00	0.00
	CO	0.00	0.00	4.13	0.00	0.00	0.86	0.73	0.00
Absorbed dry gas (wt.%)	H_2S	13.66	12.18	25.94	29.49	47.32	14.55	14.56	53.03
	CO_2	970.98	974.73	938.77	966.65	897.15	913.97	921.69	793.56
	SO_2	0.00	0.00	0.00	0.00	4.90	0.73	0.00	109.19
	NH_3	1.35	0.91	0.56	0.87	0.96	1.14	0.75	0.00
	HCl	0.00	0.00	0.09	0.00	1.78	0.00	0.00	0.00
	HF	0.01	0.01	0.00	0.02	0.04	0.02	0.01	0.00

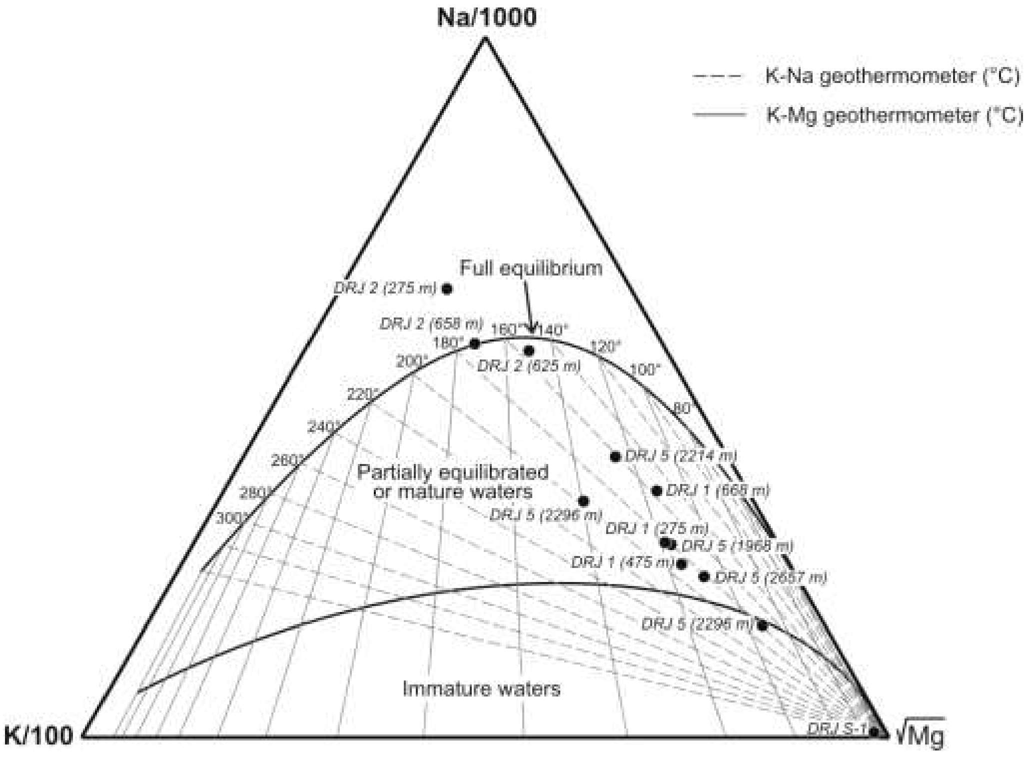

Figure 3.9.Proportions of Na, K and Mg in the downhole waters. Depths where downhole water was collected are given. Data from Amoseas Indonesia Inc. (1989a) and the classification follows Giggenbach (1988).

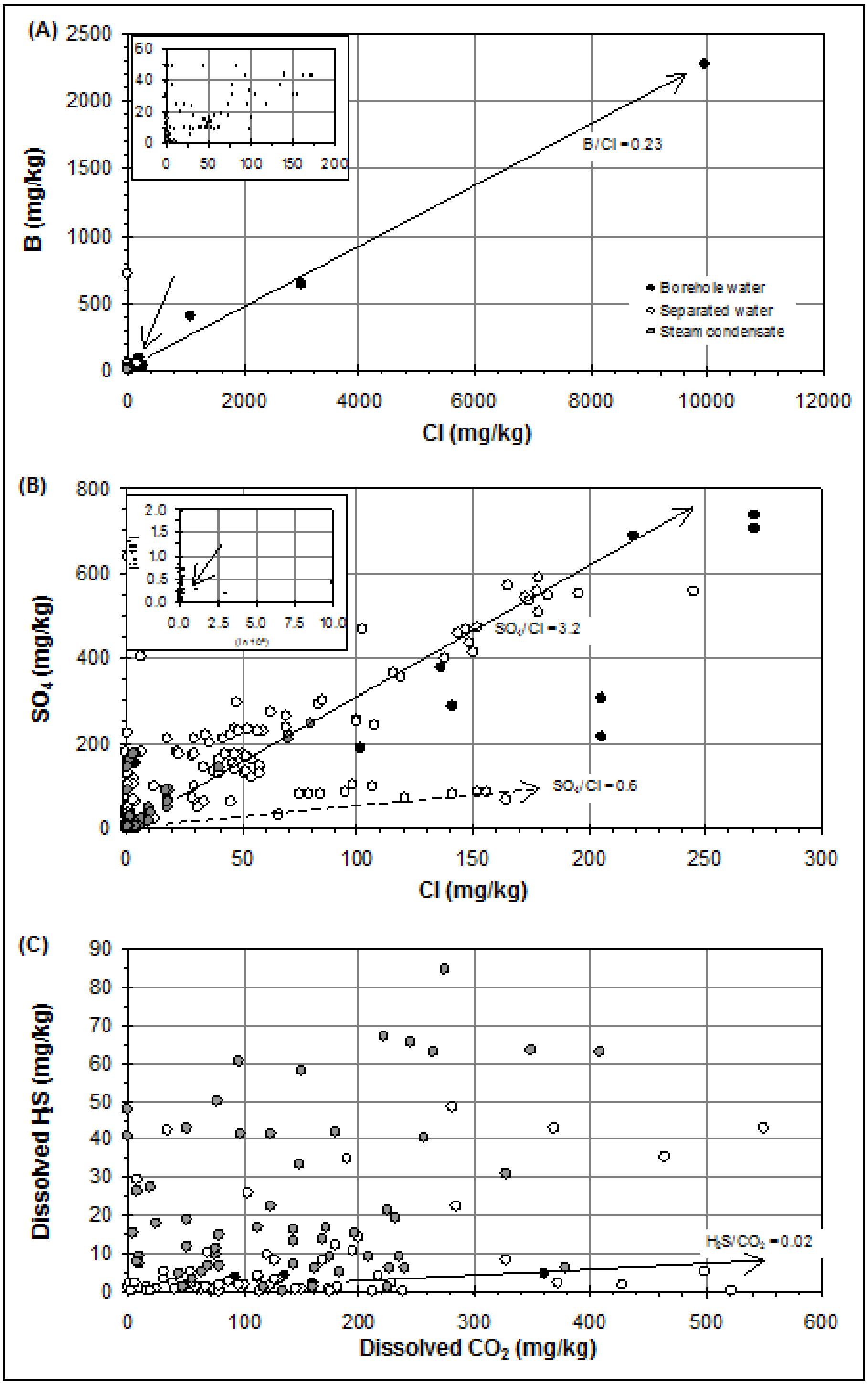

Figure 3.10. Proportions of Cl, B, SO_4^{2-}, dissolved CO_2 and H_2S contents in waters. **(A)** In borehole waters, both Cl and B increase with the ratio of B/Cl of 0.2. Separated and steam condensated waters have very low Cl and B (see inset). D'Amore et al. (1977) reported that B and Cl are carried by steam and can concentrate in liquid due to condensation; but no Cl will be in superheated steam. **(B)** Two trends show an increase in SO_4^{2-} and Cl contents in the separated waters. Inset shows that the amount of Cl in borehole waters could be higher than that in separated waters, whereas that in steam condensates is low. **(C)** Both dissolved CO_2 and H_2S slightly increase in the borehole waters, but the variation is irregular in separated and steam condensated waters. Key for the symbols is given in figure (A).

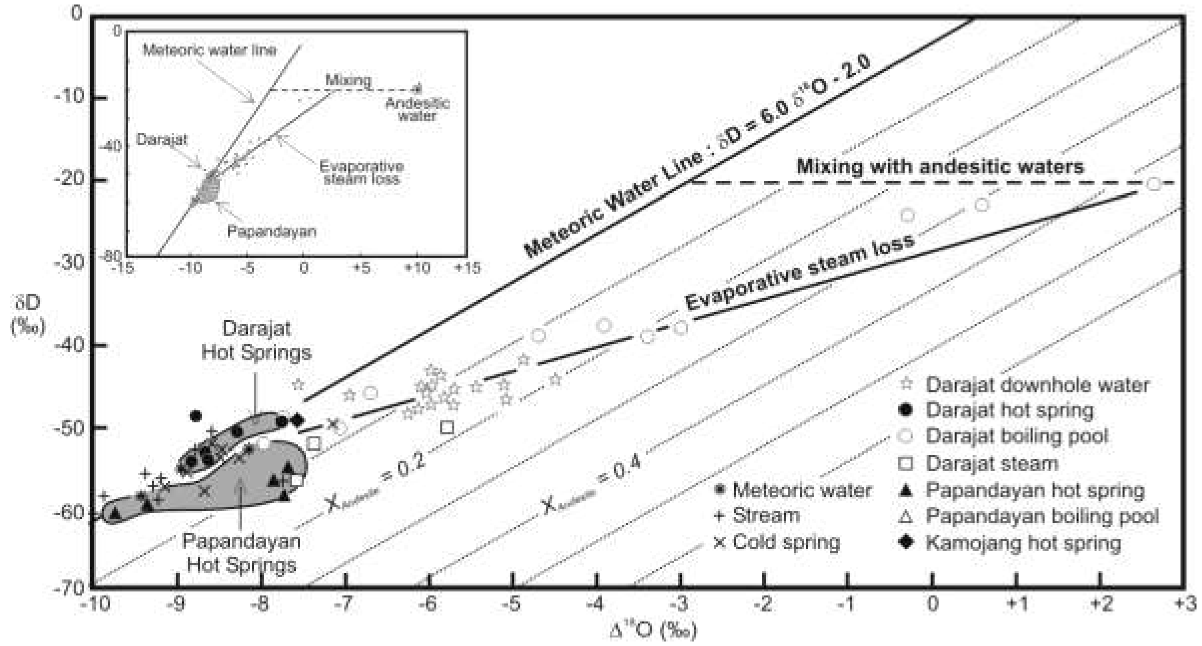

Figure 3.11. Composition of δD and δ^{18}O stable isotopes in the Darajat fluids with some additional Papandayan and Kamojang fluids (compiled from GENZL, 1990 and Amoseas Indonesia Inc, 1998a). The variation in the isotopic composition is likely due to condensation of steam into meteoric waters, followed by heating. Mixing with magmatic andesitic fluids (+10‰ δ^{18}O and -20‰ δD, Giggenbach, 1992a) is likely; the fraction of andesitic water ($X_{Andesite}$) is less than 0.5.

Steam condensates obtained from deep wells are composed of HCO_3^--SO_4^{2-} (Figure 3.7 and Table 3.3) but they have a pH of around 4.8 (Amoseas Indonesia Inc., 1989a). This suggests that the near neutral pH waters derive from the steam reservoir with some condensate dilution by cooler water mixtures above the reservoir.

Stable isotopes show that most Darajat spring water compositions can be distinguished from the local meteoric water (GENZL, 1990). Using a least squares analysis of the cold streams and spring waters to calculate the meteoric water line, the boiling pool and downhole water compositions lie on a clearly defined steam-heating trend originating from the local meteoric water (Figure 3.11). The meteoric waters interact at deeper levels and undergo some processes, such as mixing (Figure 3.8B and 3.11) or an oxygen shift due to water and rock reactions (e.g. Celati et al., 1973).

3.6. THERMAL REGIME

Most productive wells have maximum downhole temperatures of 240-248°C and pressures of 36-38 bars at 1000-1200 m depth. Amoseas Indonesia Inc. (1989b) showed that the downhole pressure/temperatures at Darajat have a profile typical of a vapour-dominated geothermal system. The geothermal gradient is 0.2°C.m^{-1}, until it reaches its maximum temperature at the top of vapour zone. Within the reservoir, i.e. vapour zone, the geothermal gradient reduces to 0.005°C.m^{-1} and the deep temperature is nearly uniform. The top of the vapour zone is likely to be at elevation of about +1100 m (e.g. DRJ 5).

Pressure is constant from near the surface down to 500 m, but it then increases with depth, i.e. to about 35 bars at +1100 m above sea level indicating the top of vapour zone. The pressure within the vapour zone increases only very slightly to about 38 bars at depths of +100 m above sea level. This elevation is suggested as being the probable interface between vapour and underlying liquid (Amoseas Indonesia Inc., 1989b). Below this, the vapour pressure will slightly increase within a vapour zone, but a liquid pressure could increase markedly. However, the temperature and pressure profiles within the 2-phase zone have not been revealed.

3.7. POROSITY AND PERMEABILITY

Reservoir rocks of Darajat have three kinds of porosity: matrix rock, fracture and fault plane. At Darajat, like other geothermal systems, the rock matrix porosity is high at the surface but decreases with depth. In fact, Darajat has a matrix porosity of about 20% at 800 m reducing to 5% at 1500 m depth (Amoseas Indonesia Inc., 1989b). The fracture and fault porosities at the surface are low, but increase to a maximum before they decrease with depth. The maximum fracture porosity of more than 15% occurs at about 1000 m depth. The total porosity of the reservoir decreases from 15% at about 600 m depth to approximately 10% at about 800 m depth. It then increases to a maximum porosity of 15-20% at approximately 1000 m depth but is about 10% below this depth (Amoseas Indonesia Inc., 1989b).Keller et al. (2006) reported that the high fracture density zone occurs between 500 and 1200 m above sea level.

This porosity pattern reflects the permeability regime within the reservoir. Narrow, well-defined zones of high permeability occur and provide conduits for fluids. GENZL (1990) reported rocks having permeabilities of about 150 mD at elevations from 400 to 1200 m comprise the reservoir rocks. Above and beneath these highly permeable zones are regions of medium to low permeability (1.5-15 mD). The high-permeability structure is a dome and has its longer axis oriented E-W. A low permeability zone (0.1-0.2 mD) exists in 1200 to 1400 m above sea level and acts as an aquitard. The area surrounding the reservoir and caprock consists of impermeable rocks of a very low permeability, 0.02-0.04 mD (GENZL, 1990).

The permeability of the Darajat system is mainly provided by interconnected fractures in both vertical and lateral directions. The Amoseas Indonesia Inc. report (1989b) showed that several tens of meters wide fracture zones occur near the reservoir rocks indicating that some joints can transmit steam and gas. Secondary permeability might also occur as a result of dissolving hydrothermal minerals, mainly calcite, by descending acid fluids. Furthermore, Hadi (2001) reported that the major permeability in the reservoir of Darajat is characterized by young, high density fractures where the deposited minerals have been leached by descending steam condensates.

The lateral permeability is indicated by the intense and moderate silicification zone. Generally this zone has a lateral dimension several times its thickness. GENZL (1990) claimed that the lateral permeability is caused by interconnected joints produced by near vertical faulting. Additional joints can occur in more permeable units of lapilli tuffs and tuff-breccias and in contacts within lava blocks or between lava flows and pyroclastic units. Once the joints are sealed by mineral deposition, they are unable to transport further quantities of fluid but more may be created.

3.8. HYDROTHERMAL MODELS

3.8.1. Vapour-dominated Hydrothermal System

Temperature and pressure profiles, water saturation and permeability values, as well as the surface discharges indicate that the Darajat geothermal system is now vapour dominated. Its reservoir, approximately 1 km thick, contains mainly steam having non-condensible gas of about 2%, mainly CO_2 with less H_2S. The initial temperature and pressure reservoir conditions are 255°C and 55 bars at 150 m above sea level but decrease to 243°C and 36.5 bars at 500 m above sea level (Amoseas Indonesia Inc., 1989b). Steam can move along highly permeable zones, while the liquid water is likely an immobile phase. The liquid phase lies at the bottom of the reservoir, as indicated by an increase in water saturation of up to 40%. It can boil, however, and the resulting vapour can move up to replenish the reservoir. The hot water recharge is also indicated by changes in water level, e.g. DRJ 5, and the long activity of most thermal surface features.

3.8.2. Two-phase Hydrothermal System

Many studies concluded that the reservoir of Darajat is dome-like at a temperature of about 240°C and 36 bars (Figure 3.12). It contains coexisting vapour and liquid, but vapour is the continuous, pressure-controlling phase (Amoseas Indonesia Inc., 1987).The reservoir has many fractures filled mostly by steam and minor liquid water. The matrix of the reservoir contains a fluid-steam mixture with water saturation near 30%, whereas the reservoir pores contain a relatively dilute, neutral pH, Na-SO_4^{2-}-HCO_3^--Cl water with abundant silica and very low Mg (Amoseas Indonesia Inc., 1989a). It is still doubtfull whether the reservoir fluid contains also 1-2 wt.% gas contents, mostly CO_2 with CO_2/H_2S mole ratios of 30-90 (Amoseas Indonesia Inc., 1987), or there is a gas envelope in rocks of low permeability surrounding the steam reservoir and producing significant amounts of CO_2, H_2S and H_2 (Amoseas Indonesia Inc., 1989a) (Figure 3.12A). SO_2 gas might occur in the major fracture zones (Amoseas Indonesia Inc., 1989a) and interacts with small water fraction, so the acidity is produced. In the steam-rich fracture zones, the acidity can be neutralised by water and rock.

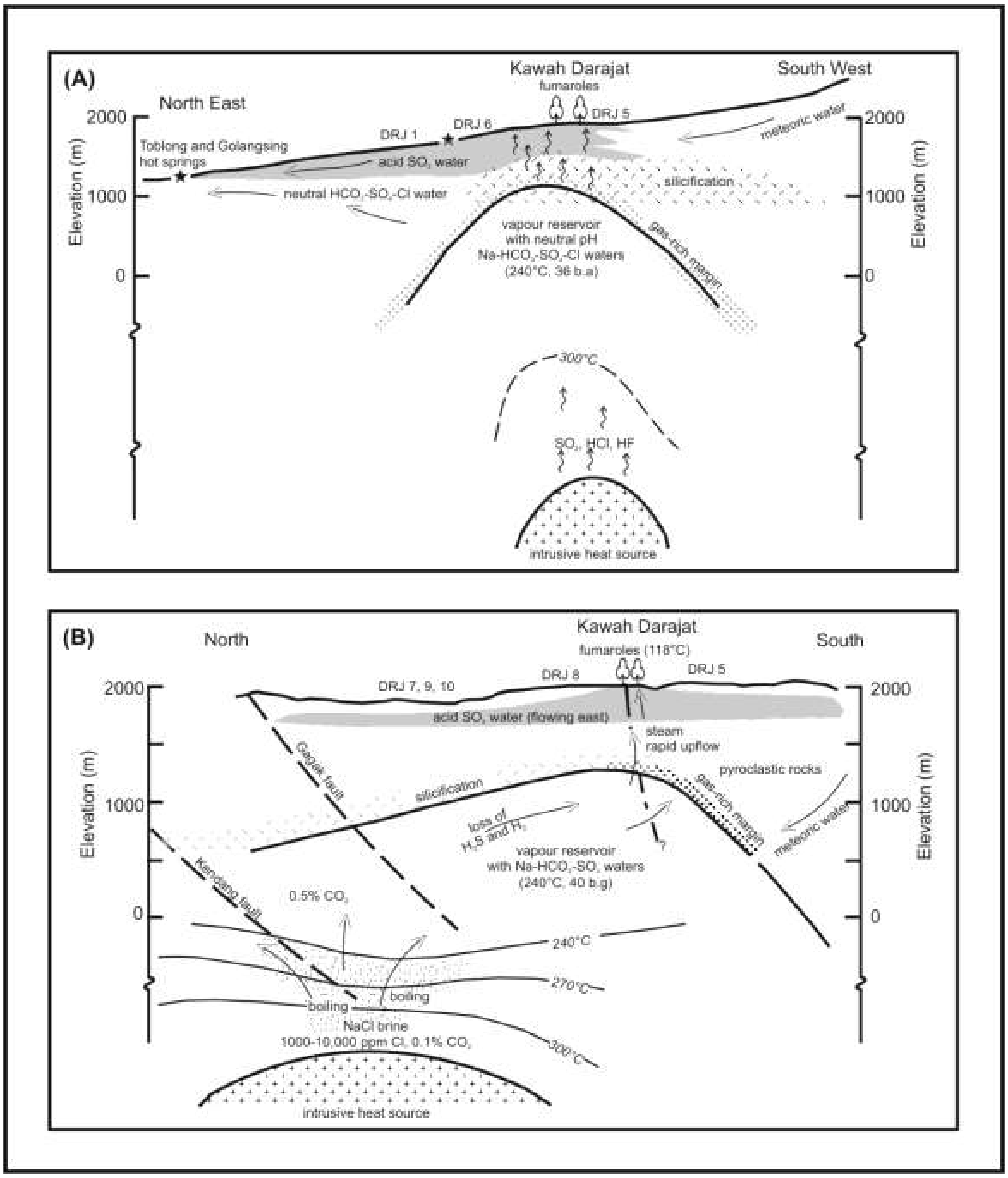

Figure 3.12.Model of andesite hosted geothermal system of Darajat: **(A)** involves two phase reservoir (after Amoseas Indonesia Inc., 1987). **(B)** involves boiling of high NaCl brine below the reservoir. Proposed by Kingston Morisson Ltd. (1996).

A silicification zone might act as a low permeable seal, so it would be over steam pressure (Amoseas Indonesia Inc., 1987). At Kawah Darajat this seal was broken, so steam pressure will then be above the hydrostatic pressure, therefore steam may rise. H_2S gas will oxidise to H_2SO_4 and CO_2 becomes HCO_3. Both form the shallow thermal water, but this could flow downhill and discharge, at elevation of 1250-1400 m, as the thermal features of the Toblong and Golangsing springs.

3.8.3. Andesite-hosted Volcanic Hydrothermal System

The 1990 GENZL report recorded gasses reaching the surface containing components typical of a high temperature magmatic origin (i.e. SO_2, HCl and HF). The Kingston Morrison Ltd. (1996) report revealed an interesting hydrochemical model of Darajat, as shown in Figure 3.12B. The Darajat reservoir is a 240°C and 39 bars vapour-dominated system and is considered to have had a single fluid source. The deep neutral pH NaCl water having 1000-10,000 $mg.kg^{-1}$ Cl, of about 0.1 wt.% dissolved gas and temperature of 300-320°C is inferred to exist beneath the drilled reservoir. The vertical permeability permits steam derived from this deep boiling brine to rise and recharge the steam reservoir. Between the deep brine and the vapour zone there is likely to be a two-phase region but, because of the low gas contents, this is probably not extensive. The center of recharge, i.e. the up flow zone, lies on the west or northwest of the current production area around DRJ 7, 9 and 10 wells.

An acid SO_4^{2-} aquifer exists above the steam reservoir, i.e. at 200-300 m depth. The acid fluid forms from the condensation of steam and oxidation of H_2S in either immobile (stagnant) reservoir liquid or near surface waters originating in the Kawah Darajat area. The gasses and stable isotope compositions of fumarole steam show a remarkable match to the deep reservoir composition, despite having passed through 1000 m of overlying rocks (Kingston Morisson Ltd., 1996). Rapid fault-chanelled up flow can be implied. The acid fluid then outflows to the east and supplies the peripheral surface springs (Figure 3.12B). This is shown by increases in the gas contents and CO_2/H_2S ratios from the west to the south and east indicating the condensation and meteoric water intrusion toward the margin of the field.

The model of the Darajat geothermal system in the report of Kingston Morrison Ltd. (1996) is consistent with the general model of andesite hosted volcanic-hydrothermal systems described by Hochstein and Browne (2000). The deep boiling brine of high salinity (10 to 15 wt.% NaCl) was trapped at about 1220 m depth, as indicated by a freezing measurement of two-phase inclusions on wairakite crystals in DRJ S-1 well (Hadi, 1997). The system might have been mature, so the magmatic fluids become neutralised and diluted. This is indicated by the dominance of SO_4^{2-} over Cl.

3.8.4. Other Models

From his study on the alteration of DRJ S-1 well, Hadi (1997) thought that the area of well DRJ S-1 and its surrounds is associated with a local or different upflow zone separated from that to the south. If so, the geothermal system has two upflow zones, north and south, separated by the Gagak Fault (Amoseas Indonesia Inc., written com., 1999). The north separate upflow zone is associated with a liquid-dominated system but the south upflow zone, now the production field, is a vapour dominated. The north seems to be younger (Amoseas Indonesia Inc., written com., 1999). However, the relationship between the evolution of the two zones remains unanswered.

Chapter 4

NATURE OF THE HOST ROCKS

Well DRJ 1 preserves some unaltered and least altered host rocks of Darajat. This is one of three wells drilled during the first exploration phase of the field in the early 1970’s. It is located about 2 km west of the production area and considered to lie outside the present reservoir (Figure 3.1). To understand the nature of the host rocks of the field, the mineralogy and chemistry of cores from well DRJ 1 were examined in detail. The unaltered rocks were taken as the starting materials before hydrothermal alteration began and used to measure the extent of mass transfer due to geothermal activity.

4.1. CONDITION OF LEAST ALTERED REFERENCE ROCKS

4.1.1. Types of Rocks

The rocks encountered in well DRJ 1 are mostly andesite lavas with intercalated andesite breccias and tuffs. Lavas are mostly grey to black. Tuff is lapilli-rich and reddish brown between 400 and 500 m, but it is light grey at about 550 m depth.

4.1.2. Assessment of Downwell Alteration

Not all the rocks from DRJ 1 are unaltered. The intensity of hydrothermal alteration varies from none to moderate. Figure 4.1 shows the occurrence of hydrothermal minerals in the cores and Table 4.1 shows the pattern and intensity of alteration of phenocryst and groundmass primary minerals. The identifications are based upon petrography and X-ray diffractometry (XRD) (Appendices B and C).

Above 150 m. Andesite lavas here are very little altered. Plagioclase, augite and hypersthene are slightly altered to clays, including smectite, kaolinite, halloysite and possibly zeolite, along cracks. The groundmass, dominated by volcanic glass, is partly altered by cristobalite.

At 100 m, the intensity of alteration is slightly higher. Many cavities, possibly remnants of dissolved phenocrysts, occur, but some plagioclase phenocrysts are survived with a wormy texture. Cristobalite, tridymite and opal-CT, in association with poorly crystalline quartz, are present in cores of some plagioclase. The style of hydrothermal alteration is likely produced by reactions of the rock with gas. This style is more obvious at 130 m depth, where wormy plagioclase with clay and zeolite rims occur together with nearly unaltered augite and hypersthene.

Table 4.1. Pattern and intensity of alteration of primary minerals in cores from well DRJ 1.

No	Depth (m)	Rock Type	Alteration Intensity	Phenocryst	Groundmass
1	70	Andesite lava	None	• Plagioclase → smectite (0-5%) • Augite → smectite (0-5%) • Hypersthene → smectite (0-5%)	• Groundmass → smectite ± cristobalite (5-10%)
2	100	Tuff	High	• Plagioclase → smectite + tridymite + cristobalite ± quartz (100%) → dissolved	• Groundmass → smectite + cristobalite ± quartz (80-100%)
3	130	Andesite lava	Low	• Plagioclase → smectite (5-10%) • Augite → smectite (5-10%) • Hypersthene → smectite (0-5%)	• Groundmass → smectite + cristobalite/tridymite ± opal-CT ± quartz (10-20%)
4	161	Andesite	None	• Plagioclase → smectite ± calcite ± siderite (5%) • Augite → smectite ± calcite ± siderite (5%) • Hypersthene → smectite ± calcite ± siderite (0-5%)	• Groundmass → smectite ± tridymite ± quartz (10-20%)
5	180	Andesite	None	• Plagioclase → smectite (5%) • Augite → smectite (5%) • Hypersthene → smectite (5%)	• Groundmass → smectite ± cristobalite ± quartz (10%)
6	210	Andesite	Moderate	• Plagioclase → smectite + calcite (5-10%) • Pyroxene → calcite ± chlorite (80-100%)	• Groundmass → smectite + quartz + cristobalite + titanite + opaque minerals (80-100%)
7	247	Andesite	Moderate	• Plagioclase → smectite ± calcite (5%) • Augite → smectite ± chlorite (0-5%) • Hypersthene → smectite ± chlorite (0-5%) • Several pyroxene → smectite ± chlorite + calcite + semi-opaque minerals (100%)	• Groundmass → smectite + quartz ± cristobalite ± calcite (80%)
8	309	Andesite	Very low	• Plagioclase → smectite ± calcite (5%) • Hypersthene → smectite (0-5%)	• Groundmass → smectite ± quartz ± cristobalite (5-10%)
9	397	Andesite	Very low	• Plagioclase → chlorite ± calcite (5%) • Augite → chlorite ± calcite (5-10%). • Several augite → calcite + chlorite (80-100%) • Hypersthene → chlorite ± calcite (0-5%)	• Groundmass → chlorite ± quartz ± cristobalite (10%)
10	432	Andesite lava	Intensive	• Plagioclase → chlorite ± smectite (100%)	• Groundmass → chlorite ± smectite (100%)
11	461	Tuff	High	• Phenocryst → smectite + chlorite + quartz (100%)	• Groundmass → smectite + chlorite + quartz + semi-opaque ± tridymite (100%)
12	580	Tuff, lapilli	Moderate	• Plagioclase → chlorite + calcite (5-10%) • Pyroxene → chlorite + calcite (100%)	• Groundmass → quartz ± cristobalite + chlorite + calcite (80%)
13	610	Tuff	Moderate	• Plagioclase → chlorite + calcite (90-100%) • Augite → chlorite ± calcite (100%) • Hypersthene → chlorite (100%)	• Groundmass → chlorite + quartz + titanite + opaque minerals (60%)
14	637	Andesite breccia	Very low	• Plagioclase → chlorite ± smectite (5%) • Augite → calcite (80-100%). • Hypersthene → chlorite (5-10%).	• Groundmass → chlorite ± smectite + quartz ± cristobalite (10%)
15	700	Andesite	Moderate	• Plagioclase → chlorite + smectite + calcite (5-10%) • Some plagioclase → calcite ± chlorite ± smectite (80%) • Pyroxene → chlorite ± illite + calcite (100%)	• Groundmass → chlorite + smectite + quartz ± cristobalite ± calcite (80%)
16	730	Andesite	Moderate	• Plagioclase → chlorite + illite/smectite ± quartz ± calcite (5-10%) • Augite → chlorite ± calcite (100%) • Hypersthene → chlorite (100%)	• Groundmass → chlorite + illite/smectite + quartz (70-80%)
17	732	Andesite	Moderate	• Plagioclase → chlorite + illite/smectite + quartz (5-10%) • Some plagioclase → chlorite + quartz ± calcite (50-60%) • Augite → chlorite ± calcite (100%) • Hypersthene → chlorite (100%)	• Groundmass → chlorite + illite/smectite + quartz (80%)

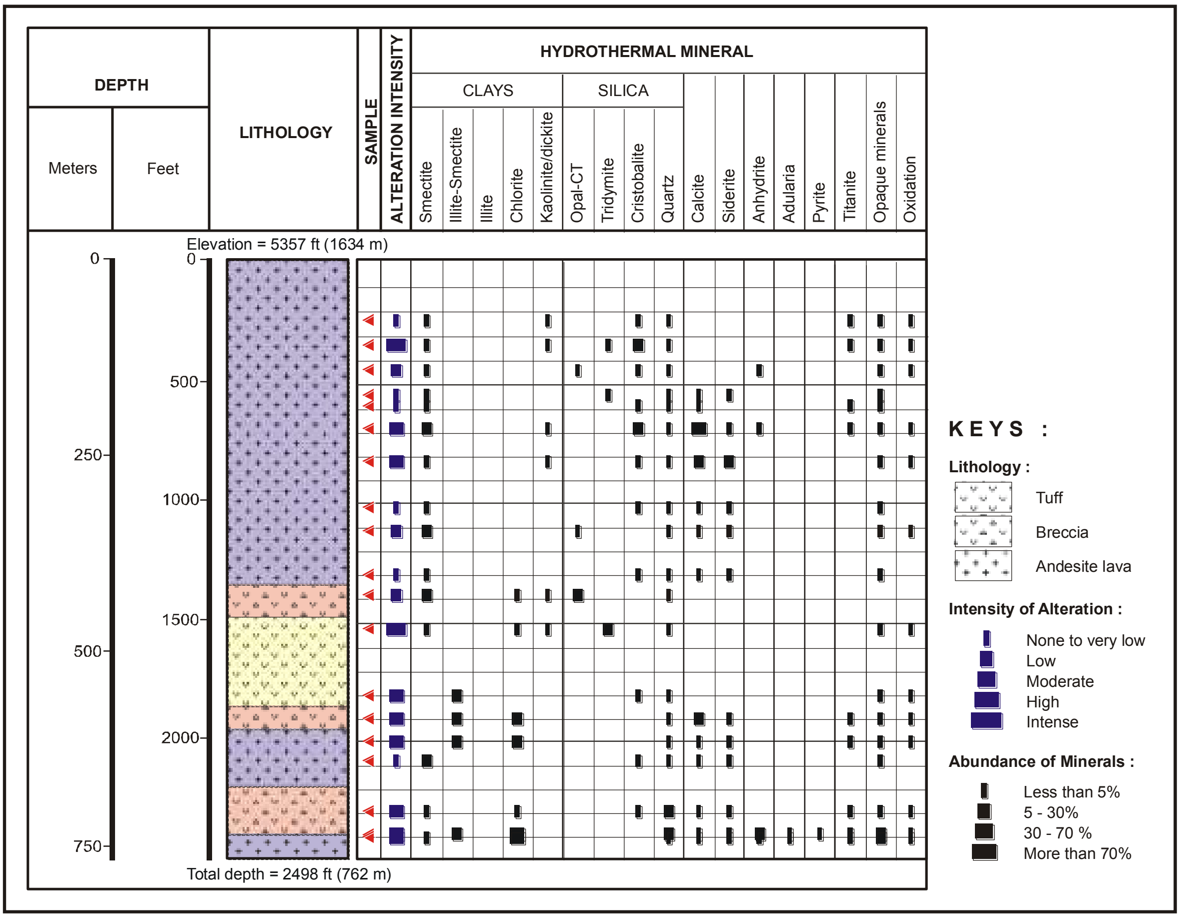

Figure 4.1.Intensity of alteration and occurrence of hydrothermal minerals in the matrix of rocks from DRJ 1.

150-400 m depth. The intensity of alteration of the lava here is low, but it is more moderate between 200 and 250 m. Smectite is still dominant and associated with kaolinite and halloysite. Clay minerals replace 5-10% of the primary minerals, including the groundmass. Cristobalite and tridymite replace up to 20% glass. Opal-CT is present at 340 m depth. All silica phases are commonly associated with poorly crystalline quartz.

Calcite and siderite start to appear at about 160 m depth and become dominant at 200-250 m. Calcite replaces plagioclase, by about 10%, along cracks and within cores, but it almost totally replaces pyroxene. A trace of anhydrite is also present mostly in cavities.

400-600 m depth. Rocks are dominated by altered tuffs. Opal-CT, tridymite, cristobalite, in association with traces of quartz, are present. Carbonates are absent. Chlorite is the dominant hydrothermal mineral at about 420 m depth. It occurs in association with Ca-rich smectite and kaolinite down to 460 m. At 550 m depth, chlorite disappears but smectite is interlayered with illite.

600-700 m depth. The style of alteration here is similar to that between 150 and 400 m. However, the intensity of alteration is higher. Most plagioclase is altered by up to 10%, but at about 600 m depth it has altered almost completely. The alteration of pyroxene is much more intense.

Clay minerals are dominated by illite-smectite and chlorite. The amount of illite in the interlayer is 40-50 %. Quartz is present, but cristobalite and tridymite are rare. Calcite, in association with siderite, replaces primary minerals and fills cavities.

Below 700 m. Andesite lavas and breccias are highly altered. Phenocrysts, especially pyroxene, and groundmass are 80-100% replaced by chlorite, illite, quartz and calcite. However, at about 730 m depth, plagioclase is altered by up to 10% only. Vermiculite or Mg-rich smectite is interlayered with illite. Adularia is present below 700 m and it replaces plagioclase along cracks.

Several veinlets are present near the well bottom, where fractures are rare. Anhydrite is present below 700 m and pyrite appears at 730 m depth. These minerals are mostly associated with calcite. Anhydrite and calcite deposited in cavities after chlorite and quartz, but in veins, they deposited before chlorite.

4.1.3. Unaltered Rocks

Cores from 70, 161, 180, 397 and 637 m depth are least altered andesites with the intensity of alteration from none to very low. The last two samples do contain some calcite; the others are pristine.

4.2. ROCK CHEMISTRY

4.2.1. General

Major and trace element abundances in andesites from well DRJ 1 were determined by X-ray fluorescence (XRF) analysis, as described in Appendix D; the results are summarised in Tables 4.2 and 4.3. As shown in Figure 4.2, their SiO_2 contents confirm that the rocks are mostly andesitic. Three cores, i.e. from 340, 397 and 732 m depth, are andesite-basalt and the sample from 210 m depth is dacitic. Furthermore, their K_2O and Na_2O contents indicate that the rocks are subalkaline and the former indicates a silicic, medium-K suite source.

Figure 4.3 is a Harker diagram showing a correlation between silica and other major elements expressed on an anhydrous wt.% basis. The alkali contents slightly increase with silica content,

Table 4.2. Major elements in cores from well DRJ 1. Oxide contents are expressed on an anhydrous basis.

No	Depth (m)	Major Element Content (wt.%)										
		SiO_2	TiO_2	Al_2O_3	Fe_2O_3	MnO	MgO	CaO	Na_2O	K_2O	P_2O_5	Total
1	70	61.64	0.80	17.17	6.76	0.12	2.74	5.61	3.21	1.71	0.15	99.92
2	161	59.32	0.76	17.13	8.27	0.24	3.00	6.03	3.21	1.53	0.13	99.60
3	180	60.42	0.75	17.41	7.36	0.16	2.52	6.02	3.31	1.60	0.12	99.67
4	210	62.80	0.79	16.97	6.03	0.28	0.94	5.50	3.35	2.28	0.15	99.08
5	247	52.71	0.97	18.46	10.18	0.21	4.12	9.23	2.76	0.74	0.14	99.51
6	340	50.77	1.05	22.48	10.34	0.10	5.49	6.71	2.12	0.33	0.13	99.52
7	397	57.55	0.89	17.82	8.46	0.20	2.79	7.03	3.64	1.16	0.18	99.72
8	580	57.87	0.72	19.94	6.33	0.14	0.99	8.22	3.87	0.69	0.18	98.96
9	610	58.52	0.84	19.81	7.99	0.16	3.09	5.53	2.60	0.54	0.16	99.24
10	637	58.20	0.84	18.29	7.79	0.12	2.68	6.76	3.70	1.14	0.17	99.70
11	700	57.38	0.74	19.26	6.79	0.29	1.74	7.83	3.72	1.06	0.17	98.98
12	730	57.20	0.90	17.60	10.20	0.19	2.70	6.19	2.83	0.72	0.07	98.59
13	732	51.80	1.02	19.35	11.26	0.18	3.59	7.04	3.68	0.19	0.16	98.25

Table 4.3. Trace elements in cores from well DRJ 1 expressed on an anhydrous basis.

No	Depth (m)	Trace Element Content (ppm)																	
		Sc	V	Cr	Ni	Cu	Zn	Ga	Rb	Sr	Y	Zr	Nb	Ba	La	Pb	Ce	Th	U
1	70	20	163	20	9	56	71	17	64	222	34	157	5	268	12	10	39	7	2
2	161	22	165	17	8	30	64	17	55	237	27	130	5	267	11	9	31	5	2
3	180	22	145	17	8	38	59	18	60	246	27	137	4	260	10	10	32	7	2
4	210	26	140	20	6	55	75	16	92	214	66	185	6	469	16	11	39	9	3
5	247	35	271	12	12	90	74	19	23	270	26	85	3	129	6	7	27	3	2
6	340	46	304	27	9	68	82	19	15	230	18	81	3	76	4	8	24	2	1
7	397	28	164	8	4	44	66	18	35	267	34	128	4	216	9	8	24	4	2
8	580	20	133	9	5	64	109	20	23	317	17	101	3	182	10	16	23	4	2
9	610	29	171	23	5	36	76	18	23	286	22	81	2	89	9	12	23	2	2
10	637	27	162	10	4	43	64	20	39	316	23	106	4	201	9	10	26	3	2
11	700	22	157	8	5	33	79	20	34	337	20	93	3	244	9	18	27	4	1
12	730	31	244	51	10	37	70	17	23	252	20	57	3	128	6	5	14	1	1
13	732	44	290	32	12	42	82	18	4	309	23	73	3	79	8	6	24	1	2

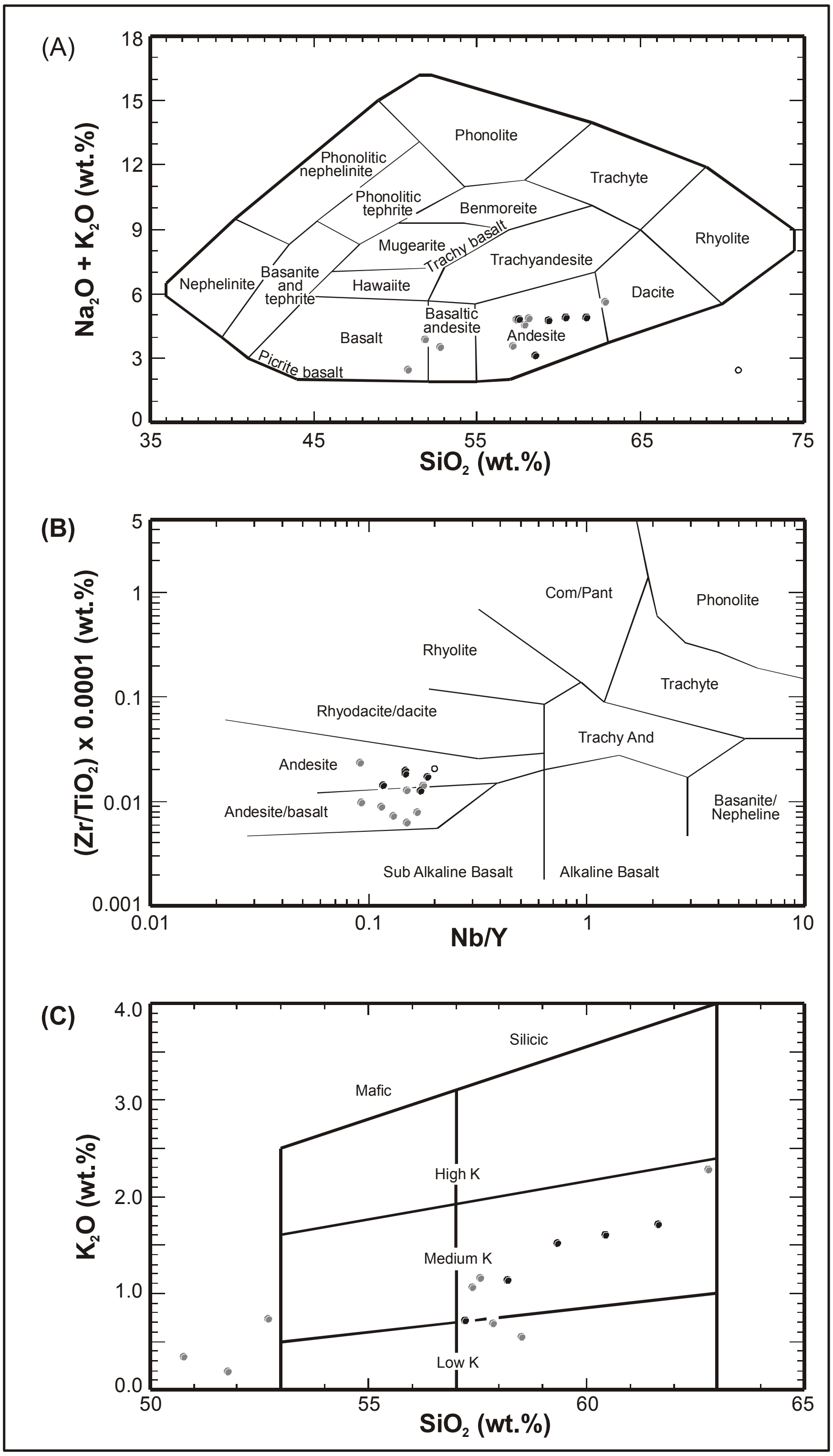

Figure 4.2.Composition of cores from well DRJ 1. **(A)** SiO_2 and alkalies indicate that the rocks are mostly andesites. Classification of Cox et al. (1979). **(B)** Correlation between Nb/Y and Zr/TiO_2 x 0.0001 indicates that the rocks are andesites and andesite-basalts. Axes are logarithmic. Classification of Winchester and Floyd (1977). **(C)** Correlation between SiO_2 and K_2O indicates that andesites are low to medium K, following classification of Gill (1981). Black solid dots represent the unaltered and grey dots represent the least altered cores. A hollow dot represents a rhyolitic core from 2406 m depth of well DRJ 24; it is SiO_2 rich, but Na_2O and K_2O depleted.

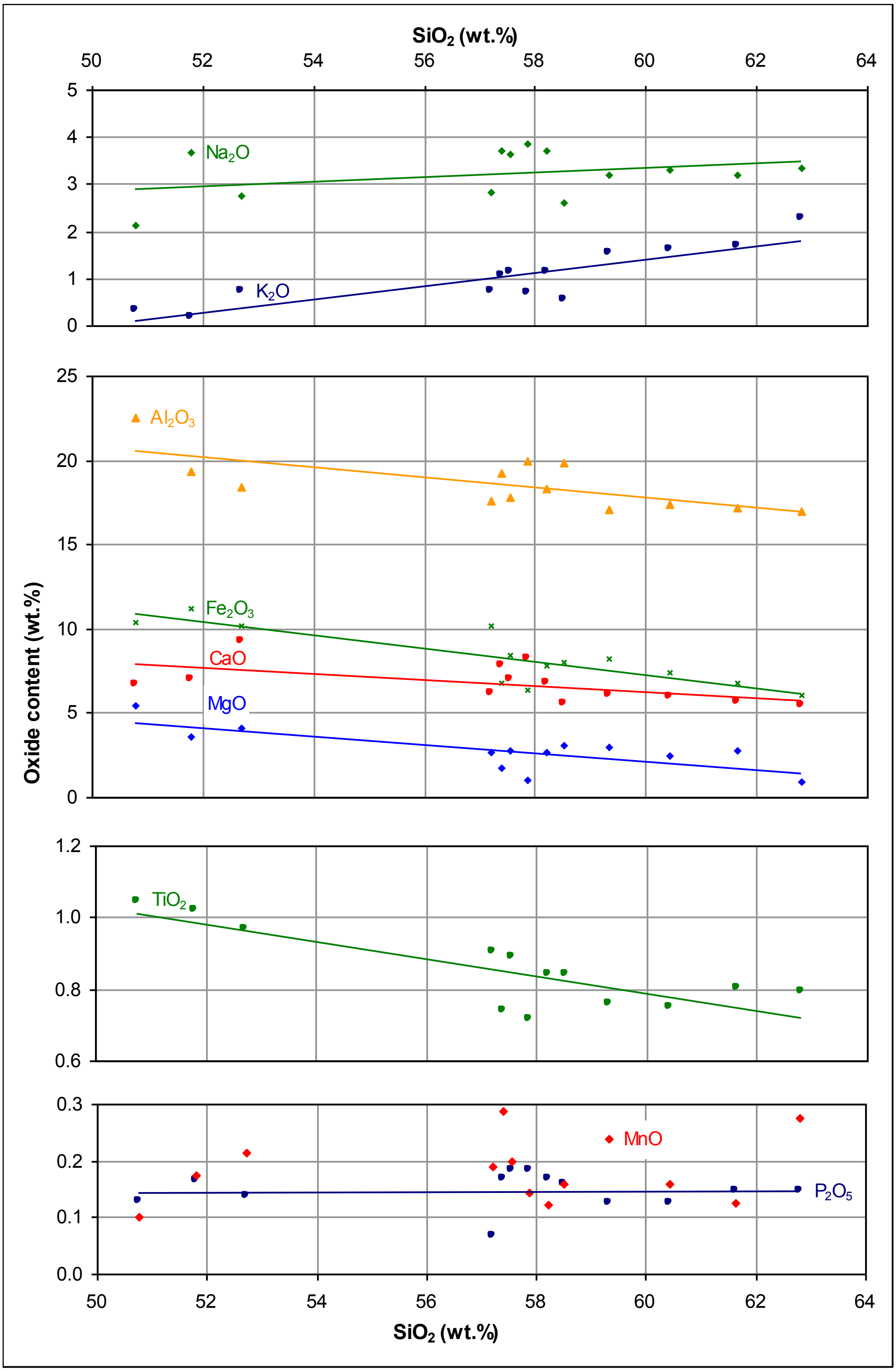

Figure 4.3. Harker Diagram of cores from well DRJ 1, showing variations in SiO_2 with respect to alkalies and other major oxides on an anhydrous wt.% basis. Best-fit linear correlations are given, except for MnO that shows no obvious pattern.

whereas the amount of CaO decreases with increasing SiO_2. The Al_2O_3, Fe_2O_3 and MgO contents also decrease with increasing SiO_2. This negative correlation with respect to SiO_2 is also indicated by TiO_2. P_2O_5 and MnO contents show unsystematic variations.

Correlations between SiO_2 and trace elements are shown on Figure 4.4. The amounts of La, Y, Ce, Ba and Rb increase with increasing SiO_2. The last two elements seem to progressively increase with increasing SiO_2. This correlation is also shown by variations between the trace elements and K_2O contents (Figure 4.5). Sr seems to decrease with increasing SiO_2 and K_2O.

The amounts of Th, U and Pb also increase with respect to SiO_2 (Figure 4.4). There is likely a progressive increase in the amount of Th above 58 wt.% SiO_2 compared to the other Th-group trace elements. In Figure 4.5, this trend is clearly shown, as the amount of K_2O increases. A correlation between K_2O and Pb is unclear. An increase in Zr and Nb with respect to both SiO_2 and K_2O is also shown in Figures 4.4 and 4.5.The amounts of Ga, Sc and V reduce with respect to increasing SiO_2 content, but there is no obvious correlation between SiO_2 and Ni, Cr, Cu, Zn or Pb (Figure 4.4).

4.2.2. Variations in Composition with Depth

Major elements. Figure 4.6A shows the variations in major elements with respect to depth. Generally SiO_2 contents slightly decrease with depth, from 61 wt.% at 70 m to 52 wt.% at 730 m, but at 340 and 732 m the amount is below 50 wt.%. According to Figure 4.3, the alkalis increase with increasing SiO_2, so variations in the alkalis contents with depth are consistent. Unexpectedly, the amount of Na_2O seems to slightly increase with depth. However, at 340, 610 and 730 m depths the Na_2O contents are low. The CaO contents negatively correlate with SiO_2 (Figure 4.3). Consequently, the amount of CaO increases with depth. It is indeed high at 247 and 580 m depths, but decreases at 210 and 610 m. Decreasing the alkali contents is consistent with an increase in CaO

The Al_2O_3 content tends to increase with depth. However, it is slightly lower at 210 m depth, but the core at 340 m depth has the highest. Variations downwell in Fe_2O_3 and MgO with depth are similar (Figure 4.6A). Above 180 m, the Fe_2O_3 and MgO contents seem to increase with depth, but at 210 m depth, the amounts reduce to their lowest. Between 250 and 350 m, the Fe_2O_3 and MgO contents are high, but the amounts decrease below 350 m. However, at about 730 m depth, both Fe_2O_3 and MgO contents are higher. The variations are similar to those of TiO_2. Figure 4.6A also shows variations in MnO and P_2O_5 with respect to depth but the patterns are unclear.

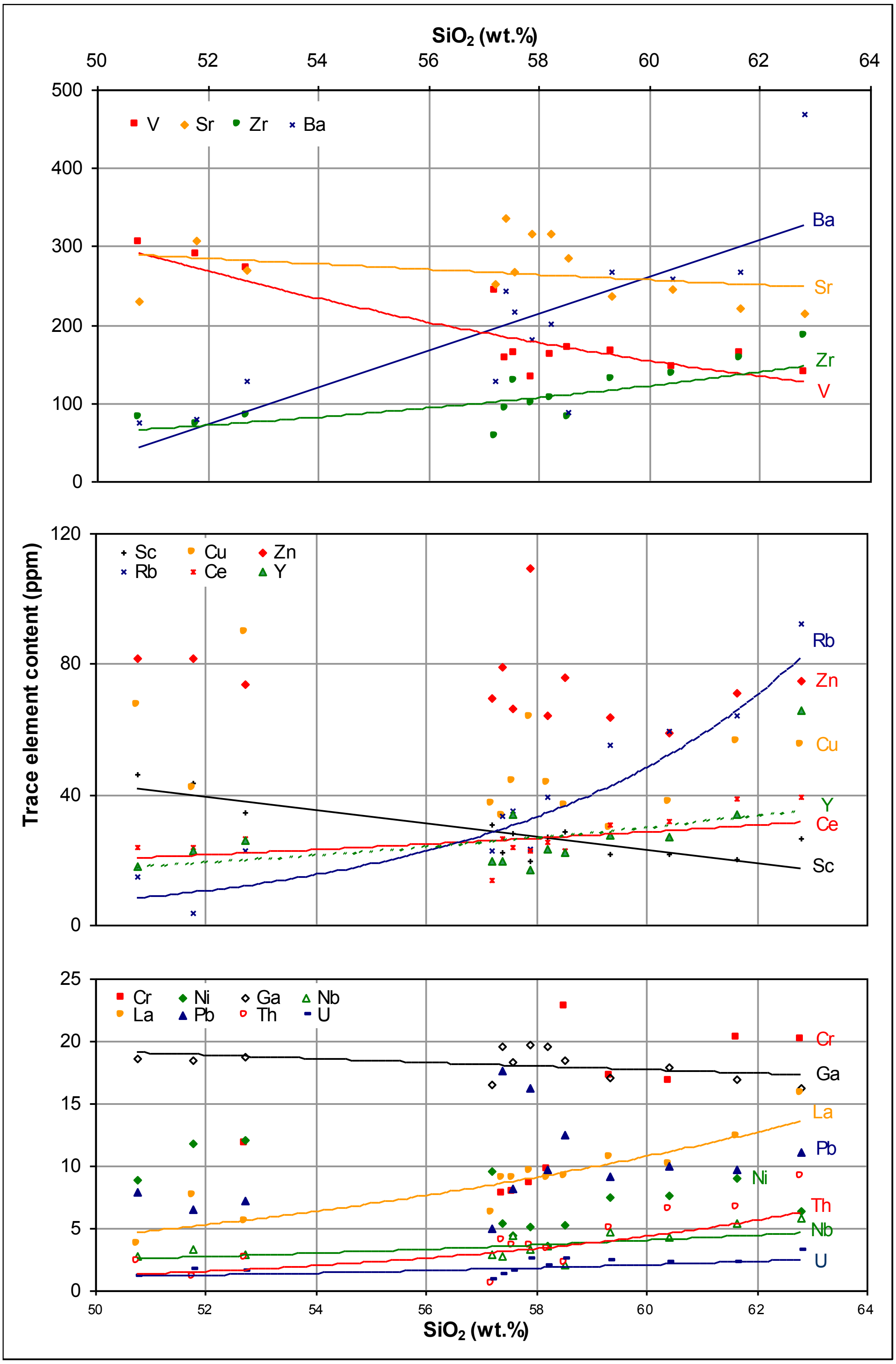

Figure 4.4. Variation in the SiO$_2$ contents with trace elements on an anhydrous basis. Some best-fit correlations are given. Cu, Zn, Cr, Ni and Pb show no obvious correlation with increasing SiO$_2$.

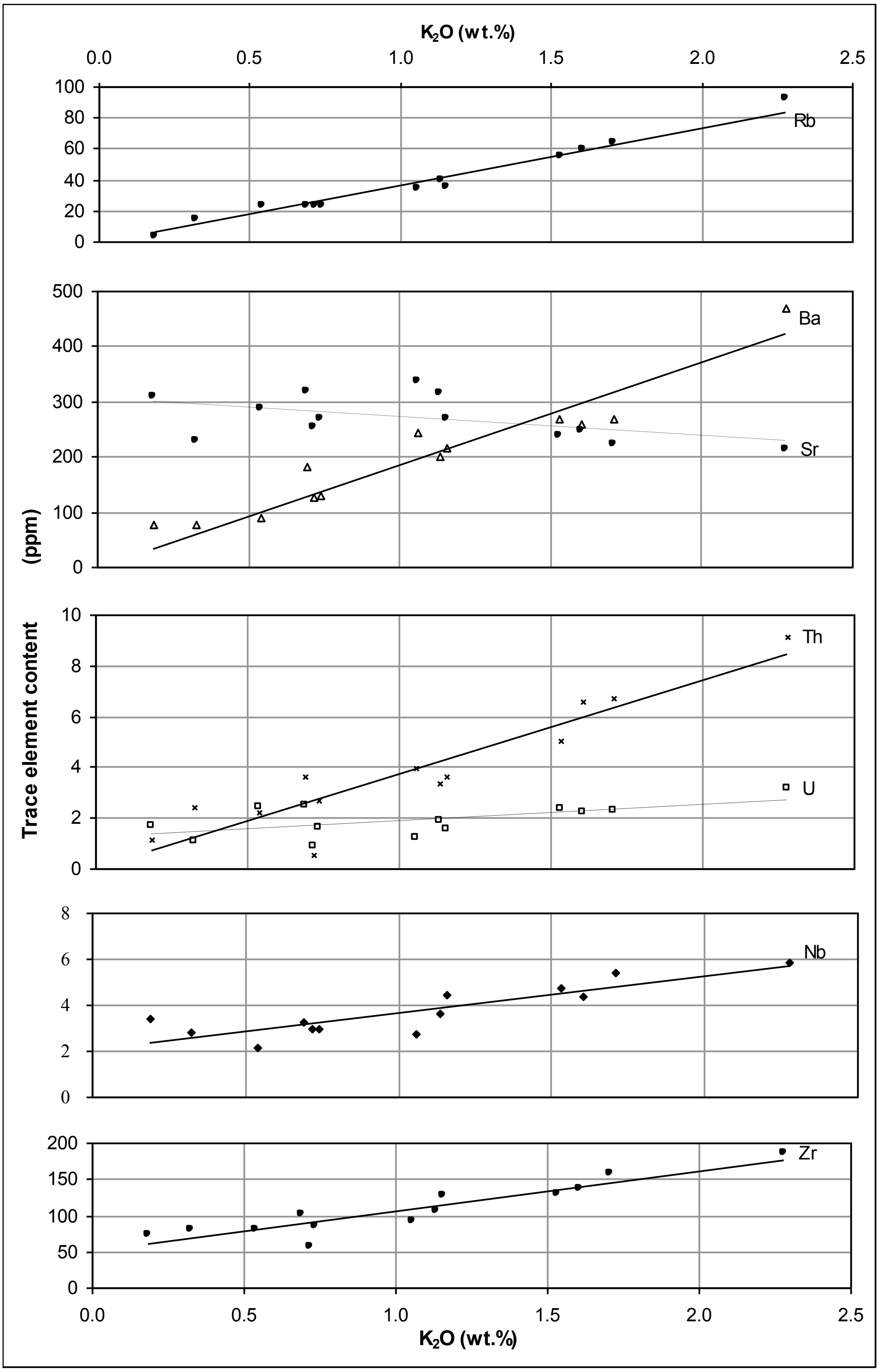

Figure 4.5. Variations between K_2O and selected trace elements. Rb, Sr and Ba are K-group trace elements, Th and U are Th-group trace elements and Nb and Zr are from Ti-group trace elements. Except for Sr, amounts of all trace elements increase with increasing K_2O.

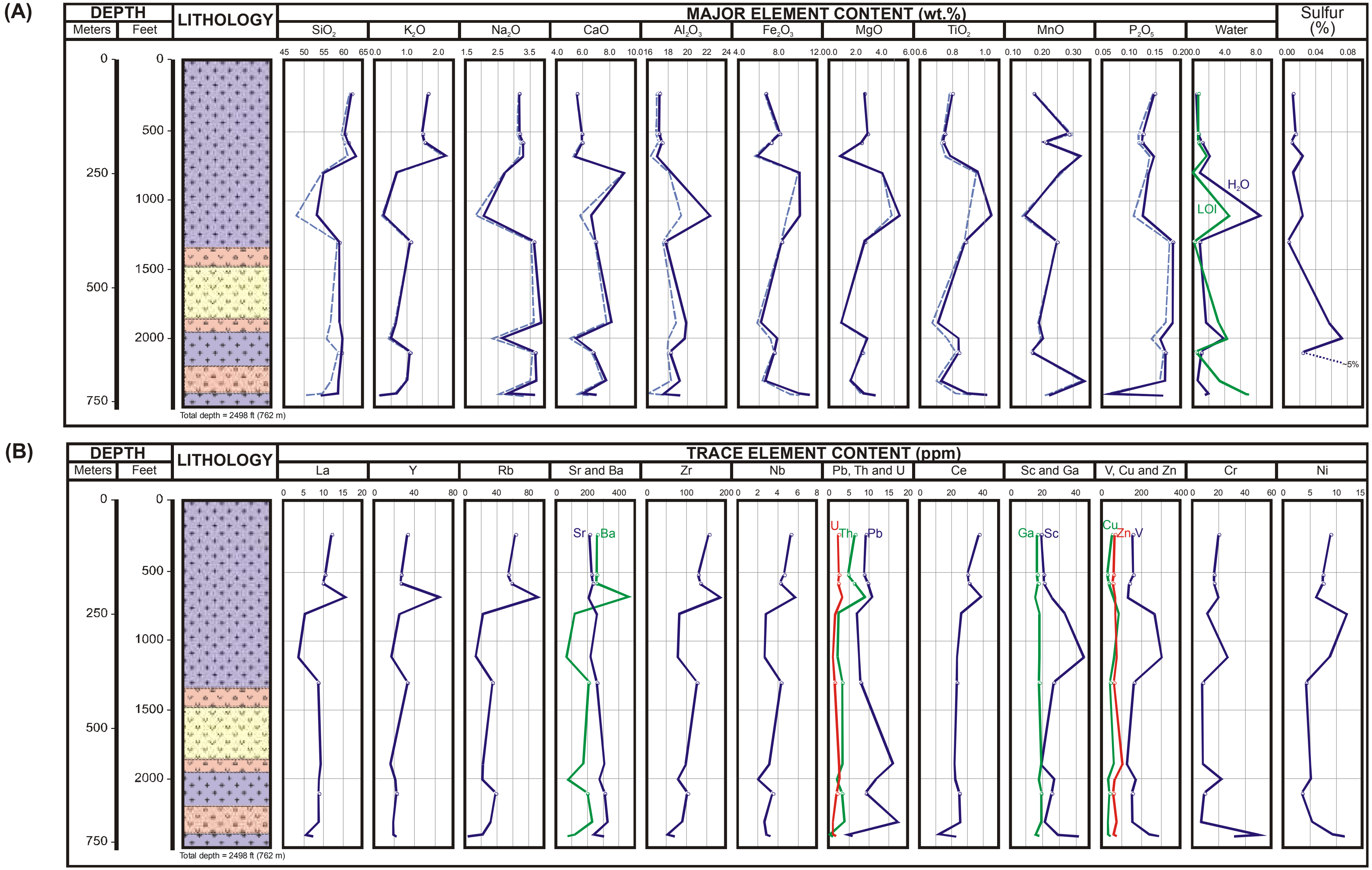

Figure 4.6. Variation in composition of rocks from well DRJ 1 with respect to depth: **(A)** Major elements, expressed as oxides. Solid line represents hydrous and dashed line represents anhydrous wt.% compositions. Water values were determined from the loss of weight after heating to 110°C. Sulfur is semi quantitative. **(B)** Trace elements. White dots represent the unaltered rocks as revealed by petrography.

Trace elements. Variations in trace element contents with depth are given in Table 4.3 and Figure 4.6B. La, Y, Rb, Ba, Zr and Nb show similar trends, i.e. decreasing with depth, but with higher values at about 200 m depth and lower at about 250 m depth. Below 700 m, La, Y, Zr and Nb seem to increase, but the amounts of K-group trace elements, i.e. Rb and Ba, seem to decrease. With increasing depth, the amount of Ce decreases.

The amounts of U and Th are nearly constant with depth. Local enrichment of Th occurs at 210 m depth, where the Th content is the highest. The amount of Pb is also nearly uniform with depth. Between 500 and 700 m, the Pb content is high, whereas below 700 m, it is very low. No variation in contents of Ga, Cu and Zn with depth is indicated. The amounts of Sc, V, Cr and Ni with respect to depth remain at their average values. However, local enrichment is present between 250 and 350 m and below 730 m.

Water and sulfur. The amount of water present in the cores was measured from the loss of weight of a sample after heating. Surface water (H_2O) is measured from the loss of weight after 110°C overnight heating and bonded water (LOI) from the weight loss after ignition to 950°C. The water contents of rocks from well DRJ 1 are given in Table 4.4 and their variations with respect to depth are shown in Figure 4.6A. Generally, the amounts of water vary between 0.6 and 2.2 wt.%. An increase in the surface water content present as a result of hydration occurs at 340 and 610 m depth. The amount of bonded water at both depths is also high and it is very high below 730 m.

Table 4.4. Water and sulfur contents of cores from well DRJ 1.

No	**Depth (m)**	**Content (wt.%)**		
		H_2O	LOI	Sulfur*
1	70	0.62	0.74	0.01
2	161	0.80	0.86	0.02
3	180	1.21	0.81	0.01
4	210	2.15	1.81	0.02
5	247	1.00	0.17	0.01
6	340	8.61	4.64	0.02
7	397	0.98	0.27	0.01
8	580	1.84	3.38	0.06
9	610	4.04	4.42	0.08
10	637	1.20	0.48	0.02
11	700	0.75	3.46	0.18
12	730	2.04	6.67	5.7
13	732	1.63	7.17	5.4

* Sulfur was measured semi-quantitatively on an anhydrous basis.

Sulfur was measured semi-quantitatively by X-ray fluorescence on an anhydrous basis to minimise loss of S during heating (Table 4.4). The amount of S is very low, but higher values occur below 600 m, at the same depths as the bonded water enrichments. The high amount of S might also explain the high amount of loss of weight after ignition at 950°C.

4.2.3. Composition of the Unaltered Rocks

Rock chemistry. Table 4.5 indicates that the unaltered rocks from well DRJ 1, i.e. from 70, 161, 180, 397 and 637 m depth, contain 57-62 wt.% SiO_2, 17-19 wt.% Al_2O_3, about 1.4 wt.% K_2O and 3.4 wt.% Na_2O. The amount of CaO in the unaltered rocks ranges from 5.6 to 7.1 wt.% and it indicates that these are Ca-rich andesites. The ranges of other elements, including water, are given in Table 4.5.

The average values of major elements of the andesites from DRJ 1 are similar to the compositions of andesites from the silicic, medium-K suite in Gill (1981). However, the rocks from DRJ 1 contain higher Fe_2O_3 and lower MgO than the reference andesites. The differences are also shown by the trace element contents.

In addition, a core from 2596 m depth of well DRJ 24 is considered as representative of the unaltered rhyolite. It has low intensity of alteration and contains 72 wt.% SiO_2 and 16 wt.% Al_2O_3, but alkalis and trace elements are low (Figure 4.2). The SiO_2 content is less than that reported by Amoseas Indonesia Inc. (1987), i.e. 76 wt.% (Chapter 3) but higher than that of rhyolite from Galunggung volcano of 71 wt.% SiO_2 (Bronto, 1989).

Normative. The chemical composition of igneous rocks can be expressed as CIPW normative values. The normative mineral of the unaltered rocks from well DRJ 1, calculated using the Minpet Version 2.02 Program from the Geological Software, is summarised in Table 4.6. Unfortunately, the program cannot calculate normative ilmenite nor apatite using the TiO_2 and P_2O_5 contents.

Samples from well DRJ 1 are dominated by normative feldspar, which makes up to 70%, and the remainder is mostly normative quartz and pyroxene. Albite comprises 27-32% and anorthite is 27-30%, but orthoclase is less than 10%. Normative quartz expressing excess SiO_2 is between 14 and 21%. Normative pyroxenes are less than 5% for diopside (Ca-Fe-Mg-pyroxene) and less than 7% for hypersthene (Fe-Mg-pyroxene). Compared to the average normative values of andesites in Gill (1981), these normative pyroxenes are lower.

Table 4.5. Minimum, maximum and average values of major, trace, water and sulfur contents of the unaltered cores from DRJ 1.

Elements		Content*			Average Value by Gill (1981)**
		Minimum	Maximum	Average	
Major elements (wt.%)	SiO_2	57.6	61.6	59.4	59.7
	TiO_2	0.75	0.89	0.81	0.70
	Al_2O_3	17.1	18.3	17.6	17.1
	Fe_2O_3	6.7	8.5	7.7	6.6
	MnO	0.12	0.24	0.17	0.12
	MgO	2.5	3.0	2.7	3.2
	CaO	5.6	7.1	6.3	6.6
	Na_2O	3.2	3.7	3.4	3.3
	K_2O	1.1	1.8	1.4	1.5
	P_2O_5	0.12	0.18	0.15	0.19
Trace elements (ppm)	Sc	19	29	24	16
	V	145	165	160	172
	Cr	7.8	20.3	14.4	39
	Ni	3.6	9.0	6.4	9
	Cu	29	57	42	36
	Zn	58	72	65	-
	Ga	16	20	18	-
	Rb	35	65	51	20
	Sr	222	316	258	490
	Y	23	34	29	18
	Zr	106	157	132	114
	Nb	3.6	5.4	4.5	2
	Ba	200	268	242	522
	La	8.0	12.4	10.2	11
	Pb	8.1	10.0	9.3	3
	Ce	23	39	30	27
	Th	3.3	6.8	5.1	1.8
	U	1.5	2.4	2.1	0.75
H_2O (wt.%)		0.62	1.21	0.96	1.0
LOI (wt.%)		0.27	0.86	0.63	-
Sulfur (wt.%)***		0.01	0.02	0.01	0.02-0.2

* Major elements are in wt.% and that of trace elements in ppm. Major and trace elements are on an anhydrous basis.
** For silicic, medium-K andesites. Trace elements values are taken from a representative calc-alkaline andesite from Fiji.
*** Sulfur was measured semi-quantitatively on an anhydrous basis (wt.%).

Table 4.6.Summary of CIPW normative mineralogy compositions of unaltered cores from DRJ 1.

No	Depth (m)	Quartz (%)	Feldspar* (%)			Pyroxene** (%)		Iron Minerals (%)		Corundum (%)
			Orthoclase	Albite	Anorthite	Diopside	Hypersthene	Magnetite	Hematite	
1	70	20.5	10.1	27.2	27.4	0.4	6.7	0.4	6.5	0.0
2	161	18.0	9.1	27.3	27.9	1.7	6.8	0.8	7.8	0.0
3	180	18.9	9.5	28.1	28.0	1.6	5.6	0.5	7.0	0.0
4	397	14.1	6.9	30.9	29.0	4.8	4.8	0.7	8.1	0.0
5	637	14.7	6.8	31.4	30.0	2.9	5.4	0.4	7.6	0.0

* Orthoclase is expressed as K-feldspar, albite as Na-feldspar and anorthite as Ca-feldspar.
** Diopside is Ca-pyroxene and hypersthene is FeMg-pyroxene.

4.3. POROSITY AND PARTICLE DENSITY

Variation with depth. The porosities and particle densities of rocks from DRJ 1 were measured using a standard method described in Appendix E. The results are summarised in Table 4.7 and their variations with depth are given in Figure 4.7. The porosity and particle density of samples from 550 m depth could not be measured as they completely decomposed when treated with water.

Above 450 m, except at 100, 340 and 423 m, the porosity of the andesite lavas reaches 5% and the particle density ranges between 2.55 and 2.84 g.cm^{-3}. A rock from 100 m depth has a porosity of 28% and a very low particle density of 1.81 g.cm^{-3}. This may be due to the occurrence of gas attack alteration that dissolved the primary minerals, especially plagioclase. Rocks from 340 and 423 m depth also have high porosity, i.e. 13 and 49% respectively, but their particle densities still average 2.59 and 2.54 g.cm^{-3} respectively.

Below 450 m, the porosity of rocks generally increases and ranges from 8 to 30%, except for samples from 637 and 700 m depth, which have less than 1.5%. The particle density here, however, is near uniform. It varies from 2.65 to 2.72 g.cm^{-3}.

Unaltered rocks from well DRJ 1, i.e. from 70, 161, 180, 397 and 637 m depth, have porosities ranging from 0.9 to 3.2%. In fact, the cores from shallow depths tend to have higher porosities than those from deeper. The particle density, however, is uniform at about 2.70 g.cm^{-3}, which is in the range of the densities of andesites, i.e. 2.4 to 2.9 g.cm^{-3} (Gill, 1981).

4.4. MINERALOGY OF THE UNALTERED ROCKS

4.4.1. Modal Composition

The modal compositions were measured by point counting, i.e. 1000 points per sample and the results are summarised in Table 4.8. Similar to the calculation of normative mineralogy, plagioclase is dominant in the unaltered rocks from well DRJ 1. It comprises 29-37% as phenocrysts and 18-43% as groundmass. Quartz, glass and other silica minerals make the groundmass up to 34%. Pyroxene includes phenocryst phases, i.e. up to 4% augite and up to 11% hypersthene, and up to 3% groundmass. The amount of opaque minerals is 1.5-3.0%, which is lower than the normative hematite and magnetite values calculated from the chemical compositions. In addition, the porosity of the unaltered rocks varies 0.9-3.2% compared with the amount of vesicles of 1.3-3.3% (Table 4.8).

Table 4.7. Porosity and density values of cores from well DRJ 1.

No	Depth (m)	Porosity (%)	Particle Density ($g.cm^{-3}$)
1	70	3.0	2.67
2	100	28.0	1.81
3	130	5.1	2.55
4	161	2.2	2.72
5	180	3.2	2.67
6	210	2.7	2.57
7	247	1.0	2.84
8	309	2.8	2.75
9	340	13.1	2.59
10	397	0.9	2.74
11	423	49.4	2.54
12	461	33.8	2.65
13	580	21.5	2.68
14	610	8.5	2.69
15	637	1.2	2.70
16	700	1.5	2.69
17	730	29.3	2.72
18	732	9.0	2.72

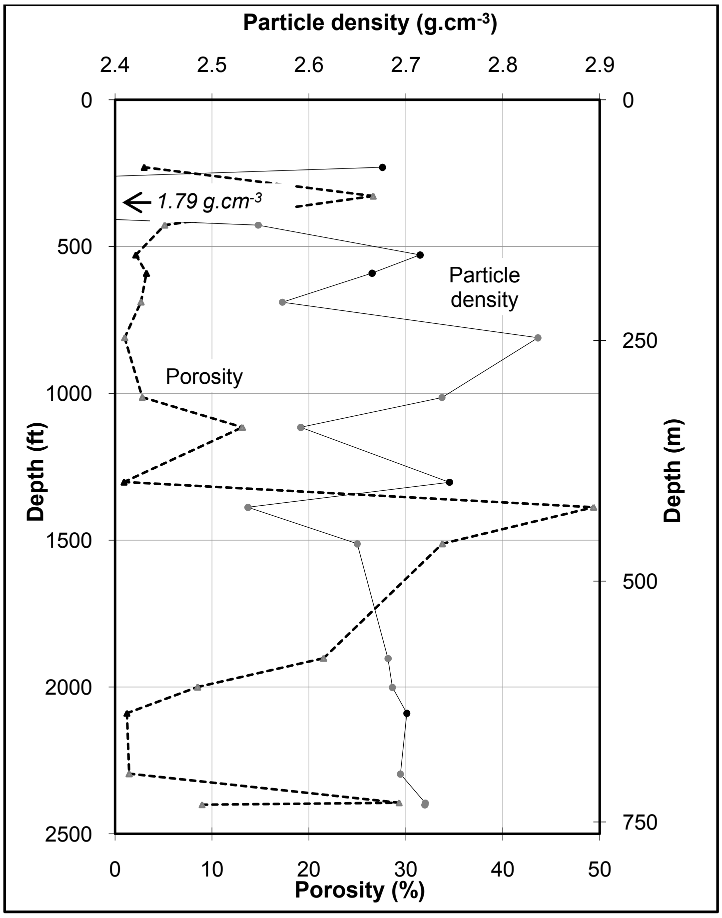

Figure 4.7.Variation in porosity and particle density of rocks from well DRJ 1 with respect to depth. Dots represent particle densities, black for the unaltered rocks and grey for the least altered rocks. Triangles show porosity, black for unaltered and grey for least altered.

Table 4.8.Modal composition of unaltered cores from well DRJ 1.

No	Depth (m)	Phenocryst (%)			Groundmass (%)			Opaque Minerals (%)	Vesicles (%)
		Plagioclase	Augite	Hypersthene	Glass and Quartz	Plagioclase	Pyroxene		
1	70	30.7	2.4	10.3	31.0	18.3	2.6	2.8	1.9
2	161	36.2	2.1	6.1	19.0	30.8	2.7	1.8	1.3
3	180	29.0	3.9	2.6	33.2	24.5	2.7	2.5	1.6
4	397	32.8	1.6	2.5	20.8	38.6	0.9	1.5	1.3
5	637	32.7	0.3	0.9	16.3	42.5	1.8	2.2	3.3

Percentage calculation is based on 1000 counts per sample.

4.4.2. Stability of Primary Minerals

Andesite from the Darajat geothermal system is mainly composed of a glassy to microcrystalline groundmass plus phenocrysts of plagioclase, pyroxene, minor primary quartz and rare hornblende and biotite. Most primary minerals described here were encountered in well DRJ 1, but some are from other wells. The primary minerals hydrothermally alter in different style and intensity, according their stability and ambient conditions.

4.4.2.1. Groundmass

Volcanic glass is the most readily altered component being replaced, at low temperatures, by smectite, chlorite, illite, calcite and quartz. Cores from well DRJ 1 indicate that the first alteration products of volcanic glass are cristobalite, tridymite and opal-CT with a trace of quartz.

Microcrystalline plagioclase occurring in the groundmass generally has a flow texture (Figure 4.8). The composition of the plagioclase groundmass was determined by electron microprobe (Appendix F) and representative analyses are given in Table 4.10. This shows that microcrystalline plagioclase contains 49-56% SiO_2, 26-31% Al_2O_3, 9-15% CaO, 2-6% Na_2O and up to 0.3% K_2O. Figure 4.9 is a summary of plagioclase compositions and it shows that the microcrystalline plagioclase is mainly sodic labradorite ($An_{\sim 50}$). Microcrystalline plagioclase is more resistant to hydrothermal alteration than is volcanic glass.

4.4.2.2. Phenocrysts

Plagioclase. Figure 4.8 shows that plagioclase phenocrysts are usually subhedral and range from 0.02 to 2.5 mm. Their compositions were determined on unaltered andesites from well DRJ 1. Table 4.9 present representative results and shows that the plagioclase phenocrysts consist of 45-62% SiO_2,

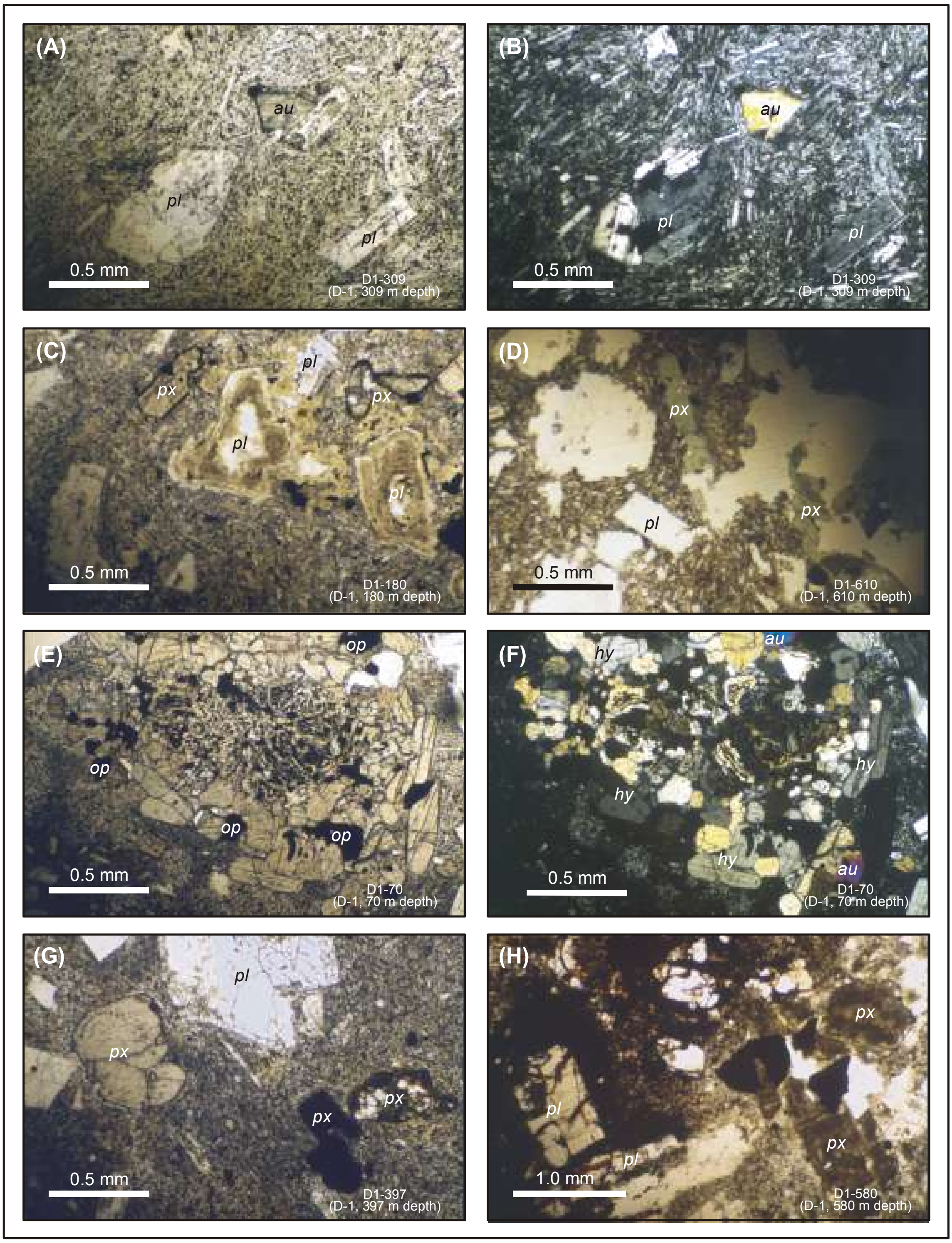

Figure 4.8. Primary plagioclase and pyroxene in well DRJ 1. **(A)** Plane polars. **(B)** Cross polars showing microcrystalline and phenocryst plagioclase (*pl*) and a crystal of augite (*au*). Note flow texture of andesite lava. **(C)** Plagioclase (*pl*) with a wormy texture is mainly altered, whereas pyroxene (*px*) remains unaltered. It indicates a style of gas alteration. Plane polars. **(D)** Secondary porosity due to dissolution of plagioclase (*pl*). Pyroxene (*px*) altered totally to chlorite. Plane polars. **(E)** Glomeroporphyritic pyroxene showing augite and hypersthene in association with opaque minerals (*op*). Plane polarised light. **(F)** Augite (*au*) has higher interference colours than hypersthene. Cross polars. **(G)** When pyroxene (*px*) is altered, it still has a euhedral habit and high relief. Plane polars. **(H)** Pyroxene (*px*) totally altered to chlorite and plagioclase (*pl*) partly altered along cracks to chlorite. Plane polars. Sample number and depth are given.

22-35% Al_2O_3, 8-19% CaO, up to 6.5% Na_2O and up to 1.5% K_2O. The compositions of plagioclase are summarised in Figure 4.9 showing that the plagioclase phenocrysts are mainly labradorite-bytownite (An_{60}-An_{90}) but some are as sodic as andesine. The plagioclase cores are mostly more calcic than their rims but some have rims more calcic than their cores.

Plagioclase alters to a variety of hydrothermal minerals. Calcite, quartz and chlorite are its most common products. Calcite can dominantly replace plagioclase, but this is usually absent when quartz and chlorite occur. Chlorite and quartz replace plagioclase along cracks and can be closely intergrowth with it. Plagioclase seems to be more resistant, but alters to quartz and chlorite rather than to calcite.

At shallow depths, i.e. at low temperatures, plagioclase may alter to smectite. Anhydrite may appear along cracks or in cavities within plagioclase. At higher temperatures, plagioclase can partly be replaced by several calc-silicate minerals, e.g. pumpellyite, prehnite and epidote. Pumpellyite and prehnite usually appear in the cores of plagioclase or along twin boundaries indicating that they preferentially occur along cracks. Epidote can replace plagioclase along cracks and also form from the surface inward. Laumontite replaces plagioclase in cores. Adularia commonly alters plagioclase along cracks. Illite appears along cracks, mostly associated with chlorite.

Olivine forms crystals 0.6 mm in diameter, is present at 1980 m depth in DRJ S-3, where andesite lava is moderately altered. It alters to chlorite and calcite.

Augite is mostly euhedral to subhedral, 0.05 to 0.5 mm, but some phenocrysts are 1.5 mm long. Figure 4.8 shows that small crystals locally form glomerophorphyritic textures with plagioclase. Some have inclusions of glass. The occurrence of this clinopyroxene is confirmed by its composition, i.e. between Wo_{37-43} En_{38-45} Fs_{15-22} (Table 4.10 and Figure 4.10).

When augite is fresh as in well DRJ 1, it contains 50-54% SiO_2, 9-13% FeO, 13-16% MgO and 18-21% CaO. The amount of Fe_2O_3, calculated using the stoichiometric criteria of Droop (1987), is up to 2.6%. Augite also contains 0.8-4.0% Al_2O_3 and traces of TiO_2, Na_2O and K_2O of up to 1.0, 0.5 and 0.2% respectively.

Augite can alter to calcite and anhydrite or to chlorite, opaque minerals, epidote and quartz. Calcite, anhydrite and chlorite, in association with smectite or illite, generally replace augite in cavities or along cracks, whereas the others occur at the surface of augite and may form reaction rims. If the intensity of alteration is high, augite has reaction rims of opaque minerals. Although the mineralogy has changed, cleavages can often be recognised.

Table 4.9. Electron microprobe analyses and structural formulae of representative plagioclase of the unaltered cores from well DRJ 1.

	Phenocryst rim				Phenocryst core				Microphenocrysts				Groundmass			
Run no.	5669	5683	5747	5796	5682	5741	5790	5848	5724	5725	5826	5862	2838	2891	5851	5862
wt.%																
SiO_2	50.58	54.53	54.20	48.35	54.65	53.78	51.40	45.32	53.25	49.35	57.41	53.01	54.28	54.62	58.02	53.01
TiO_2	< 0.18	< 0.18	< 0.18	< 0.15	< 0.18	<0.15	< 0.18	< 0.18	< 0.18	< 0.18	< 0.18	< 0.18	< 0.14	< 0.14	< 0.15	< 0.18
Al_2O_3	30.97	28.34	28.24	32.98	28.42	28.77	30.24	34.46	28.39	30.74	25.31	28.76	28.04	28.03	26.81	28.76
FeO	0.57	0.58	0.53	0.51	0.53	0.50	1.04	0.40	0.50	0.59	1.28	0.92	0.49	0.73	0.93	0.92
MnO	< 0.14	< 0.14	< 0.17	< 0.14	< 0.17	< 0.14	< 0.14	< 0.14	< 0.17	< 0.14	< 0.17	< 0.14	< 0.11	< 0.11	< 0.14	< 0.14
MgO	< 0.24	< 0.15	< 0.15	< 0.24	< 0.24	< 0.15	< 0.24	< 0.17	< 0.24	< 0.24	0.38	< 0.24	< 0.06	< 0.06	< 0.24	<0.24
CaO	14.17	11.18	11.34	16.37	11.13	11.50	14.01	18.69	11.66	14.77	7.89	12.11	11.24	11.11	9.47	12.11
Na_2O	3.12	4.74	4.71	1.84	4.77	4.41	3.07	0.78	4.41	2.80	6.29	4.52	4.85	5.09	5.95	4.52
K_2O	0.21	0.26	0.24	0.13	0.35	0.23	0.22	< 0.11	0.31	0.16	0.53	0.18	0.35	0.31	0.49	0.18
Cl	< 0.08	< 0.08	< 0.06	< 0.06	< 0.06	< 0.08	< 0.06	< 0.06	< 0.06	< 0.06	< 0.08	< 0.06	< 0.06	< 0.06	< 0.05	< 0.06
P_2O_5	< 0.15	< 0.15	< 0.15	< 0.15	< 0.15	< 0.15	< 0.15	< 0.15	< 0.15	< 0.15	< 0.15	< 0.15	< 0.10	< 0.10	< 0.15	< 0.15
SO_3	< 0.18	< 0.14	< 0.14	< 0.14	< 0.14	< 0.14	< 0.14	< 0.18	< 0.14	< 0.14	< 0.18	< 0.18	< 0.04	< 0.04	< 0.18	< 0.18
Cr_2O_3	< 0.18	< 0.18	< 0.15	< 0.20	< 0.18	< 0.15	< 0.15	< 0.15	< 0.18	< 0.18	< 0.15	< 0.18	< 0.15	< 0.15	< 0.15	< 0.18
NiO	< 0.21	< 0.20	< 0.20	< 0.20	< 0.24	< 0.24	< 0.24	< 0.21	< 0.24	< 0.21	< 0.24	< 0.24	< 0.21	< 0.21	< 0.20	< 0.24
Total	99.62	99.63	99.26	100.18	99.85	99.49	99.98	99.65	98.52	98.41	99.09	99.50	99.47	100.03	99.67	99.50
Number of ions on the basis of 32(O)																
Si	9.166	9.803	9.786	8.763	9.794	9.079	9.292	8.313	9.862	9.755	10.344	9.584	9.883	9.894	10.059	9.584
Al	6.609	6.000	6.004	7.039	5.998	6.660	6.438	7.444	5.922	6.053	5.370	6.124	6.012	5.979	5.669	6.124
Ti	0.025	0.024	0.024	0.020	0.024	0.025	0.024	0.025	0.024	0.025	0.024	0.024	0.005	0.000	0.020	0.024
Fe^{2+}	0.086	0.087	0.080	0.077	0.079	0.091	0.157	0.061	0.068	0.076	0.193	0.139	0.075	0.111	0.140	0.139
Mn	0.021	0.021	0.025	0.021	0.025	0.021	0.021	0.021	0.021	0.021	0.025	0.021	0.000	0.014	0.021	0.021
Mg	0.065	0.040	0.040	0.065	0.064	0.066	0.065	0.045	0.064	0.041	0.102	0.065	0.000	0.016	0.064	0.065
Ca	2.751	2.153	2.194	3.179	2.137	2.911	2.714	3.673	2.110	2.214	1.523	2.346	2.193	2.156	1.822	2.346
Na	1.096	1.652	1.649	0.647	1.657	0.999	1.076	0.277	1.682	1.603	2.197	1.585	1.715	1.788	2.072	1.585
K	0.049	0.060	0.055	0.030	0.080	0.038	0.051	0.025	0.057	0.053	0.122	0.042	0.081	0.072	0.112	0.042
End member																
Albite	28.1	42.7	42.3	16.8	42.8	25.3	28.0	7.0	43.7	41.4	57.2	39.9	43.0	44.5	51.7	39.9
Anorthite	70.6	55.7	56.3	82.4	55.2	73.7	70.7	92.4	54.8	57.2	39.6	59.0	55.0	53.7	45.5	59.0
Orthoclase	1.3	1.6	1.4	0.8	2.1	1.0	1.3	0.6	1.5	1.4	3.2	1.1	2.0	1.8	2.8	1.1

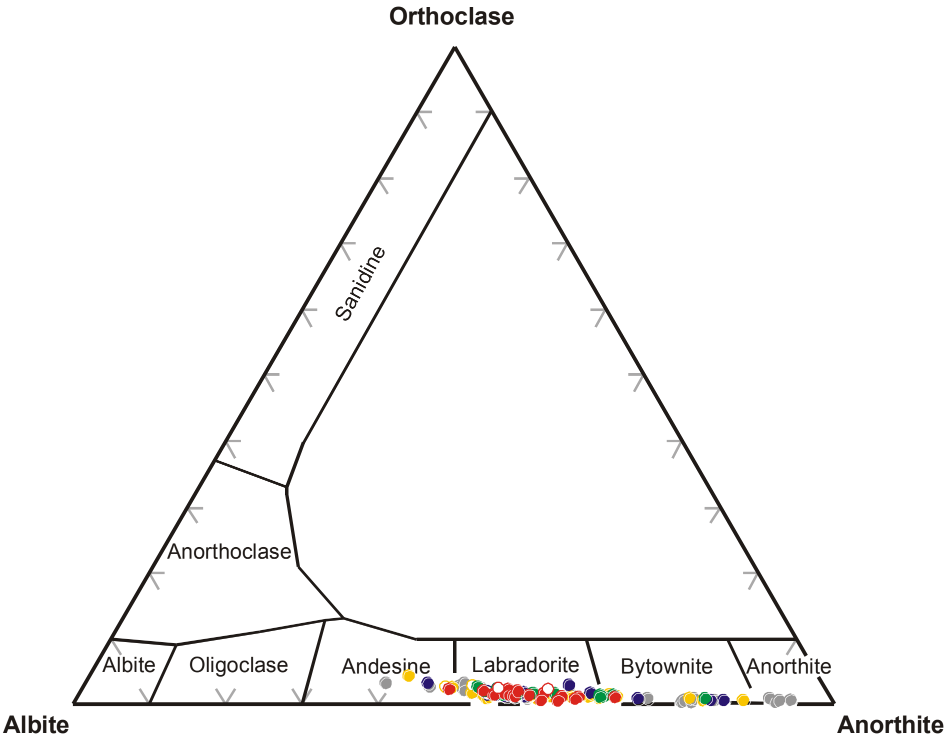

Figure 4.9. Variation in compositions of primary plagioclase showing that phenocrysts (solid dots) range from andesine to anorthite but the groundmass (circles) is mainly labradorite. Analyses were made on unaltered rocks from DRJ 1. Red dots (●) represent samples from 70 m depth, green dots (●) are plagioclase from 161 m depth, blue (●), yellow (●) and grey (●) dots represent plagioclase of samples from 180, 397 and 637 m depth respectively.

Hypersthene. Table 4.10 and Figure 4.10 summarises orthopyroxene compositions and shows they are enstatite (Wo_{2-5} En_{57-72} Fs_{25-40}), containing 51-55% SiO_2, 15-24% FeO and 19-27% MgO. The amount of Fe_2O_3, calculated using Droop (1987), is less than 1.4%. Al_2O_3 ranges from 0.2 to 2.2% and the amounts of TiO_2, CaO and K_2O are generally low, i.e. about 0.3%, less than 2.2 and about 0.1% respectively. Some orthopyroxene also contains traces of Cl and P_2O_5 with up to 0.1 and 0.3% respectively.

Like augite, hypersthene can alter to chlorite, sometimes in association with smectite and illite, and opaque minerals. Reaction rims of chlorite and opaque minerals usually have wide dark brown to black edges. However, hypersthene is not as readily altered as augite, especially by carbonate.

Hornblende. Two euhedral hornblende crystals are in a thin section from 1000 m depth of DRJ S-3. They are about 2 mm long, pale yellow to yellowish brown, slightly pleochroic and yellow to reddish brown. One has a cleavage, which is partly filled by opaque minerals. The compositions of hornblende are hard to be determined due to their extensive alteration. Table 4.11 represents the composition of hornblende, showing that the primary amphibole already alters to actinolite and tremolite, containing 51-54 wt.% SiO_2, up to 4 wt.% Al_2O_3 and 19-21 wt.% CaO. It is Mg rich,

Table 4.10. Electron microprobe analyses and structural formulae of representative pyroxenes in the unaltered cores from well DRJ 1.

	Augite rim		Augite Core		Micro-augite	Hypersthene rim		Hypersthene core		Micro-hypersthene	
Run no.	5685	5847	5684	5782	5808	5762	5688	5630	5769	5698	5837
wt.%											
SiO_2	52.88	52.29	53.08	50.87	51.47	53.26	55.02	52.47	52.78	53.86	53.51
TiO_2	0.43	0.45	0.27	0.89	0.41	0.31	< 0.18	0.25	0.40	0.30	0.27
Al_2O_3	1.26	1.55	1.00	3.52	1.90	1.17	0.71	0.64	1.00	1.13	1.14
FeO	10.22	11.87	10.85	9.33	12.40	19.64	16.00	23.38	21.18	17.97	19.13
Fe_2O_3	0.00	0.00	0.00	1.31	0.36	0.00	0.00	0.00	0.00	0.00	0.00
MnO	0.43	0.36	0.43	0.37	0.55	0.53	0.43	0.80	0.70	0.53	0.47
MgO	14.17	14.74	14.09	14.44	13.47	23.24	26.37	20.17	21.71	24.17	23.96
CaO	20.55	18.39	20.52	19.30	18.55	1.42	1.61	1.52	1.79	1.73	1.48
Na_2O	< 0.45	< 0.53	< 0.45	< 0.45	< 0.45	< 0.21	< 0.23	< 0.21	< 0.21	< 0.23	< 0.50
K_2O	< 0.11	< 0.12	< 0.11	0.11	< 0.11	< 0.09	< 0.09	0.10	< 0.09	< 0.09	< 0.09
Cl	< 0.06	< 0.06	< 0.08	< 0.06	< 0.08	< 0.08	< 0.08	< 0.08	< 0.08	< 0.06	< 0.06
P_2O_5	< 0.17	< 0.18	< 0.17	< 0.15	< 0.17	< 0.15	< 0.15	< 0.15	< 0.23	< 0.15	< 0.15
SO_3	< 0.15	< 0.17	< 0.15	< 0.20	< 0.15	< 0.18	< 0.20	< 0.15	< 0.20	< 0.14	< 0.20
Cr_2O_3	< 0.20	< 0.23	< 0.20	< 0.17	< 0.17	< 0.17	< 0.15	< 0.17	< 0.17	< 0.18	< 0.18
NiO	< 0.27	< 0.26	< 0.26	< 0.26	< 0.27	< 0.26	< 0.26	< 0.26	< 0.21	< 0.26	< 0.26
Total	99.94	99.65	100.24	100.01	99.08	99.57	100.14	99.33	99.56	99.69	99.96
Number of ions on the basis of 6(O)											
T Si	1.956	1.938	1.961	1.878	1.934	1.959	1.971	1.976	1.961	1.964	1.943
T Al	0.044	0.062	0.039	0.122	0.066	0.041	0.029	0.024	0.039	0.036	0.049
T Fe^{3+}	0.000	0.000	0.000	0.000	0.000	0.000	0.000	0.000	0.000	0.000	0.000
M1 Al	0.011	0.006	0.005	0.031	0.018	0.009	0.001	0.004	0.005	0.013	0.000
M1 Ti	0.012	0.013	0.008	0.025	0.012	0.009	0.005	0.007	0.011	0.008	0.007
M1 Fe^{3+}	0.000	0.000	0.000	0.036	0.010	0.000	0.000	0.000	0.000	0.000	0.000
M1 Fe^{2+}	0.182	0.153	0.198	0.101	0.192	0.000	0.000	0.000	0.000	0.000	0.000
M1 Cr	0.006	0.007	0.006	0.005	0.005	0.005	0.004	0.005	0.005	0.005	0.005
M1 Mg	0.782	0.814	0.776	0.795	0.755	0.970	0.982	0.976	0.973	0.966	0.980
M1 Ni	0.008	0.008	0.008	0.008	0.008	0.008	0.007	0.008	0.006	0.007	0.007
M2 Mg	0.000	0.000	0.000	0.000	0.000	0.304	0.426	0.157	0.229	0.348	0.317
M2 Fe^{2+}	0.135	0.215	0.137	0.188	0.198	0.604	0.479	0.736	0.658	0.548	0.581
M2 Mn	0.013	0.011	0.013	0.012	0.018	0.017	0.013	0.026	0.022	0.016	0.014
M2 Ca	0.815	0.730	0.812	0.763	0.747	0.056	0.062	0.061	0.071	0.068	0.058
M2 Na	0.032	0.038	0.032	0.032	0.033	0.015	0.016	0.015	0.015	0.016	0.035
M2 K	0.005	0.006	0.005	0.005	0.005	0.004	0.004	0.005	0.004	0.004	0.004
Sum cat	3.995	3.994	3.995	3.995	3.995	3.996	3.996	3.995	3.996	3.996	3.996
Ca	42.299	37.958	41.934	41.093	39.130	2.868	3.149	3.136	3.647	3.474	2.953
Mg	40.582	42.331	40.064	42.779	39.535	65.319	71.761	57.905	61.544	67.523	66.514
Fe^{2+}- Mn	17.119	19.711	18.002	16.128	21.334	31.813	25.091	38.959	34.81	29.004	30.533
*End member**											
WO	42.3	38.0	41.9	40.3	39.0	2.9	3.1	3.1	3.6	3.5	3.0
EN	40.6	42.3	40.1	42.0	39.3	65.3	71.8	57.9	61.6	67.5	66.5
FS	17.1	19.7	18.0	17.7	21.7	31.8	25.1	39.0	34.8	29.0	30.5
WEF	96.8	96.2	96.8	96.6	96.7	98.5	98.4	98.5	98.5	98.4	100.0
JD	3.2	3.8	3.2	1.6	2.1	1.5	1.6	1.5	1.5	1.6	0.0
AE	0.0	0.0	0.0	1.8	1.2	0.0	0.0	0.0	0.0	0.0	0.0

* End member: WO = wollastonite, EN = enstatite, FS = ferrosilite, WEF = wollastonite enstatite ferrosilite, JD = jadeite and AE = aegirine.

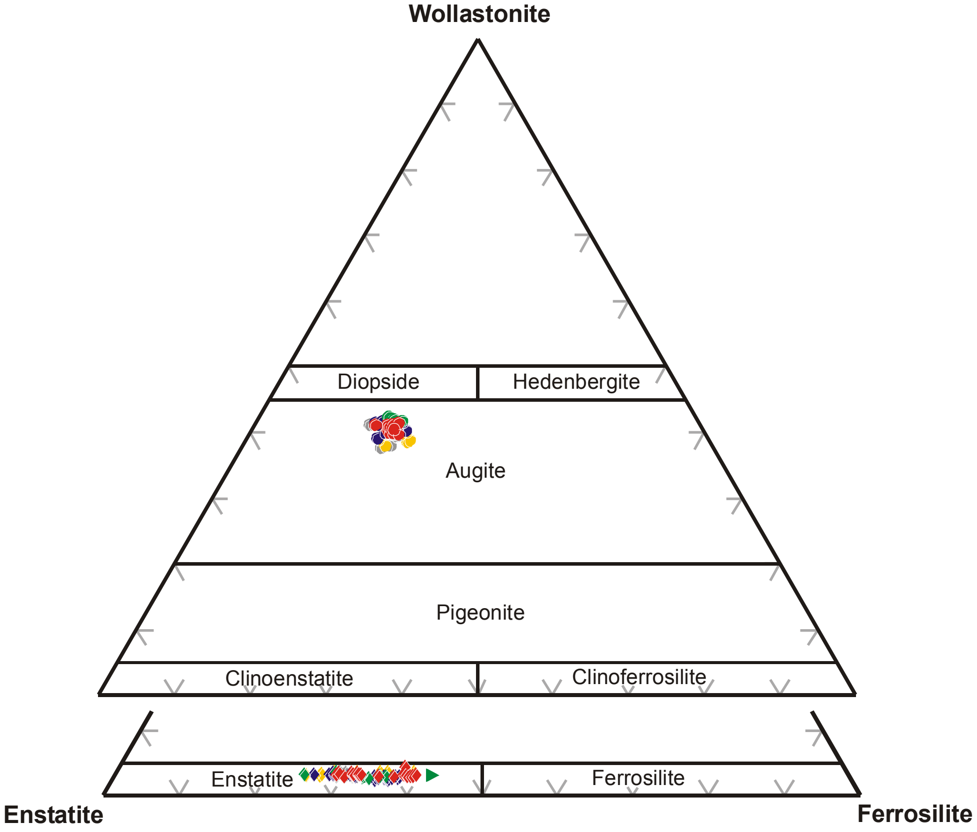

Figure 4.10.Variation in compositions of pyroxenes showing that augite and enstatite dominate. Analyses were made on unaltered cores from DRJ 1. Red (●), green (●) and blue (●) dots represent pyroxene in samples from 70, 161 and 180 m depth respectively. Yellow (●) and grey (●) dots are pyroxene in samples from 397 and 637 m depth respectively.

having Mg and Mg+Fe ratios of 0.8-1.0. The amounts of MgO range from 13 to 18 wt.% and the FeO and Fe_2O_3 are less than 4 and 6-9 wt.% respectively. TiO_2 is present only up to 2 wt.%. Chlorite also replaces hornblende along cracks.

Biotite is rare at 1202 and 1351 m depth at DRJ S-3. It occurs in low to moderately altered porphyritic andesite. It alters totally to chlorite, but preserves its euhedral and elongate habit. A euhedral and elongate biotite crystal from 1009 m depth of DRJ S-1 is totally altered to calcite in association with quartz and opaque minerals.

Quartz. Primary quartz is unaffected during hydrothermal alteration. This is indicated by the occurrence of anhedral quartz in intensely altered pyroclastic rocks from 1460 m depth in DRJ S-3. However, at 2596 m depth of DRJ 24, primary quartz in rhyolitic core is partly altered along cracks to illite and chlorite.

Apatite rarely occurs as a primary mineral but forms phenocrysts above 161 m in well DRJ 1. It is about 0.1 mm long and is euhedral. The apatite contains 52-55% CaO and 40-43% P_2O_5 (Table 4.12).

It is likely to be chlorapatite, since up to 1.0% Cl is present. Primary apatite also contains up to 0.4% SiO_2, 0.2-1.6% FeO, up to 0.4 MgO and up to 0.3% Al_2O_3.

Opaque minerals from well DRJ 1 are euhedral to anhedral and 0.05-0.30 mm in diameter. These are mostly titanomagnetite with 32-47% FeO, 25-53% Fe_2O_3 and 5-19% TiO_2 (Table 4.13). The amounts of MnO and MgO vary up to 2% and that of Cr_2O_3 and NiO are up to 0.4%.

Table 4.11.Electron microprobe analyses and structural formulae of representative hornblendes in a core from 1000 m depth of well DRJ S-3.

	Phenocryst rim				Phenocryst core	
Run no.	4429		4450		4469	
wt.%						
SiO_2	53.87		52.77		51.03	
TiO_2	0.64		1.51		1.73	
Al_2O_3	1.25		1.04		3.34	
FeO*	-		3.22		-	
Fe_2O_3*	8.05		8.44		6.99	
MnO	0.29		0.66		0.37	
MgO	17.83		13.68		15.84	
CaO	19.22		19.87		20.52	
Na_2O	0.50		0.27		0.88	
K_2O	0.07		0.07		0.02	
Cl	0.02		-		< 0.01	
P_2O_5	0.07		0.10		< 0.12	
Cr_2O_3	0.06		0.14		0.13	
NiO	< 0.01		< 0.02		0.01	
Total	101.84		101.58		100.75	
Number of ions on the basis of 24 (O, OH)						
T Si	7.64	7.83	7.74	7.91	7.44	7.92
T Al	0.16		0.09		0.40	
T Fe^{3+}	-		-		-	
T Ti	0.03		0.08		0.09	
C Al	0.05	5.00	0.09	5.00	0.18	5.00
C Cr	0.01		0.02		0.02	
C Fe^{3+}	-		-		-	
C Ti	0.04		0.09		0.10	
C Mg	3.77		2.99		3.44	
C Fe^{2+}	-		0.40		-	
C Mn	0.04		0.08		0.05	
C Ca	1.10		1.34		1.22	
B Mg	-	1.82	-	1.71	-	1.83
B Fe^{2+}	-		-		-	
B Mn	-		-		-	
B Ca	1.76		1.67		1.71	
B Na	0.07		0.04		0.12	
A Ca	0.07	0.15	0.12	0.17	0.27	0.41
A Na	0.07		0.04		0.13	
A K	0.01		0.01		-	
Sum Cat	15		15		15	
Ratio Mg:(Mg+Fe^{2+})						
	1.00		0.88		1.00	

* Amounts of FeO and Fe_2O_3 are calculated from the amount of $FeO_{equivalent}$ following Droop (1987).

Table 4.12. Electron microprobe analyses and structural formulae of representative primary apatites from well DRJ 1.

	Phenocryst rim			Phenocryst core			Cracks	
Run no.	2841	2909	6490	2851	2883	6496	6495	6499
wt.%								
SiO_2	0.34	0.36	0.36	< 0.08	0.13	< 0.23	< 0.23	0.25
TiO_2	< 0.14	< 0.14	< 0.21	< 0.14	< 0.14	< 0.21	< 0.17	< 0.17
Al_2O_3	0.09	< 0.05	0.22	< 0.05	< 0.05	< 0.15	< 0.15	< 0.21
FeO	1.60	0.40	0.85	0.85	1.21	0.88	0.29	0.56
MnO	< 0.11	< 0.11	< 0.17	< 0.11	< 0.11	< 0.17	< 0.17	< 0.17
MgO	0.19	0.24	< 0.26	0.34	0.23	< 0.24	< 0.24	0.29
CaO	52.11	53.65	54.22	52.90	52.90	54.27	54.33	54.47
Na_2O	0.11	< 0.06	< 0.18	0.11	0.14	< 0.18	< 0.18	< 0.17
K_2O	< 0.04	< 0.04	< 0.11	< 0.04	< 0.04	< 0.12	< 0.11	< 0.12
Cl	0.74	0.96	0.48	0.78	0.67	0.70	0.81	0.43
P_2O_5	40.64	42.74	41.41	41.13	41.42	41.01	41.06	41.35
SO_3	< 0.04	< 0.04	< 0.18	< 0.04	< 0.04	< 0.18	< 0.18	< 0.18
Cr_2O_3	< 0.15	0.23	< 0.18	< 0.15	< 0.15	< 0.17	< 0.18	< 0.18
NiO	0.33	< 0.21	< 0.30	< 0.21	< 0.21	0.31	0.30	< 0.30
Total	96.32	98.62	97.54	96.35	96.64	97.17	96.72	97.35
Number of ions on the basis of 12(O) and 0(OH)								
Fe^{2+}	0.11	0.03	0.06	0.06	0.08	0.06	0.02	0.04
Mn	-	-	0.01	-	-	0.01	0.01	0.01
Mg	0.02	0.03	0.03	0.04	0.03	0.03	0.03	0.04
Ca	4.63	4.61	4.66	4.68	4.65	4.70	4.72	4.70
Na	0.02	-	0.03	0.02	0.02	0.03	0.03	0.03
K	-	-	0.01	-	-	0.01	0.01	0.01
Si	0.03	0.03	0.03	-	0.01	0.02	0.02	0.02
P	2.85	2.90	2.81	2.88	2.88	2.81	2.82	2.82
S	-	-	0.01	-	-	0.01	0.01	0.01
CF	-	-	-	-	-	-	-	-
CCl	0.21	0.26	0.13	0.22	0.19	0.19	0.22	0.12

Table 4.13. Electron microprobe analyses of representative opaque minerals from well DRJ 1.

	Opaque core			Opaque rim			Microcrystalline opaque		
Run no.	5751	2831	3077	5734	5752	5692	5679	5708	5811
wt.%									
SiO_2	< 0.20	0.34	0.15	< 0.20	< 0.20	< 0.14	< 0.20	< 0.20	0.27
TiO_2	9.32	14.23	16.69	15.69	5.57	12.82	15.41	10.84	16.30
Al_2O_3	2.77	2.28	2.41	2.21	2.84	1.97	2.04	3.05	2.67
FeO*	76.55	73.57	71.87	71.56	79.79	75.52	73.19	75.39	71.68
Fe_2O_3*	-	-	-	-	-	-	-	-	-
MnO	0.31	0.58	1.25	0.46	0.39	0.45	0.44	0.26	0.93
MgO	1.39	1.54	0.16	0.97	1.45	0.74	0.71	1.72	0.54
CaO	< 0.12	< 0.06	0.01	< 0.12	< 0.12	< 0.12	< 0.12	0.17	< 0.15
Na_2O	< 0.50	0.13	< 0.06	< 0.14	< 0.15	< 0.50	< 0.14	< 0.14	< 0.17
K_2O	< 0.11	0.02	< 0.03	< 0.11	< 0.11	< 0.11	< 0.11	< 0.11	< 0.12
Cl	< 0.08	< 0.02	0.04	< 0.08	< 0.08	< 0.08	< 0.08	< 0.08	< 0.09
P_2O_5	< 0.17	0.06	0.03	< 0.21	< 0.17	< 0.23	< 0.17	< 0.17	< 0.20
SO_3	< 0.21	< 0.04	< 0.08	< 0.21	< 0.21	< 0.21	< 0.17	< 0.21	< 0.26
Cr_2O_3	< 0.20	0.13	0.11	< 0.20	< 0.20	< 0.20	< 0.21	< 0.21	< 0.26
NiO	< 0.30	< 0.21	0.05	< 0.30	< 0.30	0.38	< 0.30	< 0.26	< 0.33
Total	90.34	92.90	92.66	90.89	90.04	91.88	91.79	91.43	92.39
Number of ions on the basis of 10(O)									
Si	-	0.04	0.02	-	0.02	-	0.02	-	0.03
Ti	0.82	1.18	1.38	1.31	0.50	1.09	1.29	0.93	1.34
Al	0.38	0.30	0.31	0.29	0.40	0.26	0.27	0.41	0.34
Fe^{2+}	7.48	6.77	6.60	6.67	8.00	7.14	6.79	7.19	6.57
Fe^{3+}	-	-	-	-	-	-	-	-	-
Mn	0.03	0.05	0.12	0.04	0.04	0.04	0.04	0.03	0.09
Mg	0.24	0.25	0.03	0.16	0.26	0.12	0.12	0.29	0.09
Ca	0.01	-	-	-	0.01	-	-	0.02	-
Na	-	0.03	-	-	-	-	-	-	-
K	-	-	-	-	0.01	-	-	-	-
Cl	-	-	0.01	-	-	-	-	-	-
P	-	0.01	-	-	-	-	-	-	-
S	-	-	-	-	-	-	0.01	-	-
Cr	-	0.01	-	-	-	-	-	-	-
Ni	-	-	-	-	0.02	0.03	-	-	-

* Amounts of FeO and Fe_2O_3 are calculated from the amount of $FeO_{equivalent}$ following Droop (1987).

Chapter 5

HYDROTHERMAL ALTERATION OF THE MATRIX

As thermal fluids interacted, hydrothermal alteration occurred in the matrix of the rocks. The occurrence of hydrothermal minerals, therefore, record changes that occurred in the geothermal system during its lifetime. The identifications of hydrothermal alteration are based upon petrography and X-ray diffractometry (XRD), described in the Appendices B and C respectively.

5.1. INTENSITY OF HYDROTHERMAL ALTERATION

The intensity of alteration indicates how far a rock has altered to new hydrothermal minerals (Browne, 1995). It is independent to the identities and abundances of the hydrothermal minerals. In this thesis, the intensity is reported semi-quantitative from petrographic examination and Table 5.1 defines the intensity of hydrothermal alteration, as applied here.

Andesite lavas mostly have an intensity of alteration ranging from low to moderate. Pyroclastic rocks are altered more intensely than the lavas. Tuff is usually completely altered, even at shallow depths. Rhyolite encountered at 2600 m depth in well DRJ 24 has a low intensity of alteration. The intensity of alteration of intrusive rocks, e.g. microdiorite, diorite, tonalite and gabbro encountered in well DRJ S-1, ranges from low to moderate. The alteration of the groundmass is usually more intense than that of the accompanying phenocrysts. The alteration intensity can also vary, even on a millimeter scale, because thermal fluids move through joints, not pervasively via interconnected pores, as in many rhyolitic pyroclastic rocks (Browne, 1989).

5.2. OCCURRENCE AND DISTRIBUTION OF HYDROTHERMAL MINERALS

Table 5.2 shows a common style of hydrothermal alteration of the primary minerals. Compared to the other primary minerals, plagioclase can alter readily to a wide variety of hydrothermal minerals, e.g. calc-silicates and clays. However, groundmass plagioclase is replaced only by calcite and clays.

Figures 5.1 and 5.2 are cross sections from south to north across the field, i.e. from wells DRJ S-5, through S-3, S-1 and S-2, to S-6, showing the occurrence of clay minerals and several other hydrothermal minerals. The occurrence and distribution of hydrothermal minerals in individual wells, i.e. wells DRJ S-1, S-2, S-3, S-5 and S-6, are shown in Figures 5.3 to 5.7. Figures 5.8 to 5.12 show variations in the characteristics of clay minerals, as indicated by their XRD patterns.

Table 5.1.Definition of the intensity of hydrothermal alteration.

Intensity of Alteration	Definition
Very low	Neither groundmass nor phenocrysts are altered.
Low	Groundmass is partly altered, but phenocrysts are usually unaltered.
Moderate	Both groundmass and phenocryst are partly altered. The original texture of the rock is still clearly seen.
High	Both groundmass and phenocryst are almost totally altered and the original texture of rock is hardly recognisable.
Intense	Both groundmass and phenocryst are completely altered. The original texture of the rock has gone.

Table 5.2.Common replacement alteration products of primary minerals.

Primary Mineral		Intensity	Replacement	Occurrence
Groundmass	Volcanic glass	0-100%	Cristobalite, tridymite, opal-CT, quartz	-
			Calcite	-
			Smectite, chlorite, illite	-
	Microcrystalline plagioclase	0-60%	Calcite	-
			Smectite, chlorite, illite	-
Phenocrysts	Plagioclase	0-100%	Quartz	Cracks
			Laumontite, pumpellyite, prehnite, epidote	Core, cavity, cracks
			Calcite, anhydrite	Cracks, cavity
			Adularia	Cracks
			Smectite, chlorite, illite	Cracks
	Olivine	100%	Calcite	Cracks
			Chlorite	Cracks
	Augite	0-100%	Quartz	Cracks, cavity
			Prehnite, epidote	Core, surface
			Calcite, anhydrite	Cracks, cavity
			Smectite, chlorite, illite	Cracks
			Opaque minerals	Surface
	Hypersthene	0-100%	Smectite, chlorite, illite	Cracks
			Opaque minerals	Surface
	Hornblende	80-100%	Chlorite	Cracks, cavity
			Opaque minerals	Surface
	Biotite	100%	Quartz	Cracks, cavity
			Calcite	Cracks
			Chlorite	Cracks
			Opaque minerals	Surface
	Quartz	0-10%	Chlorite, illite	Cracks

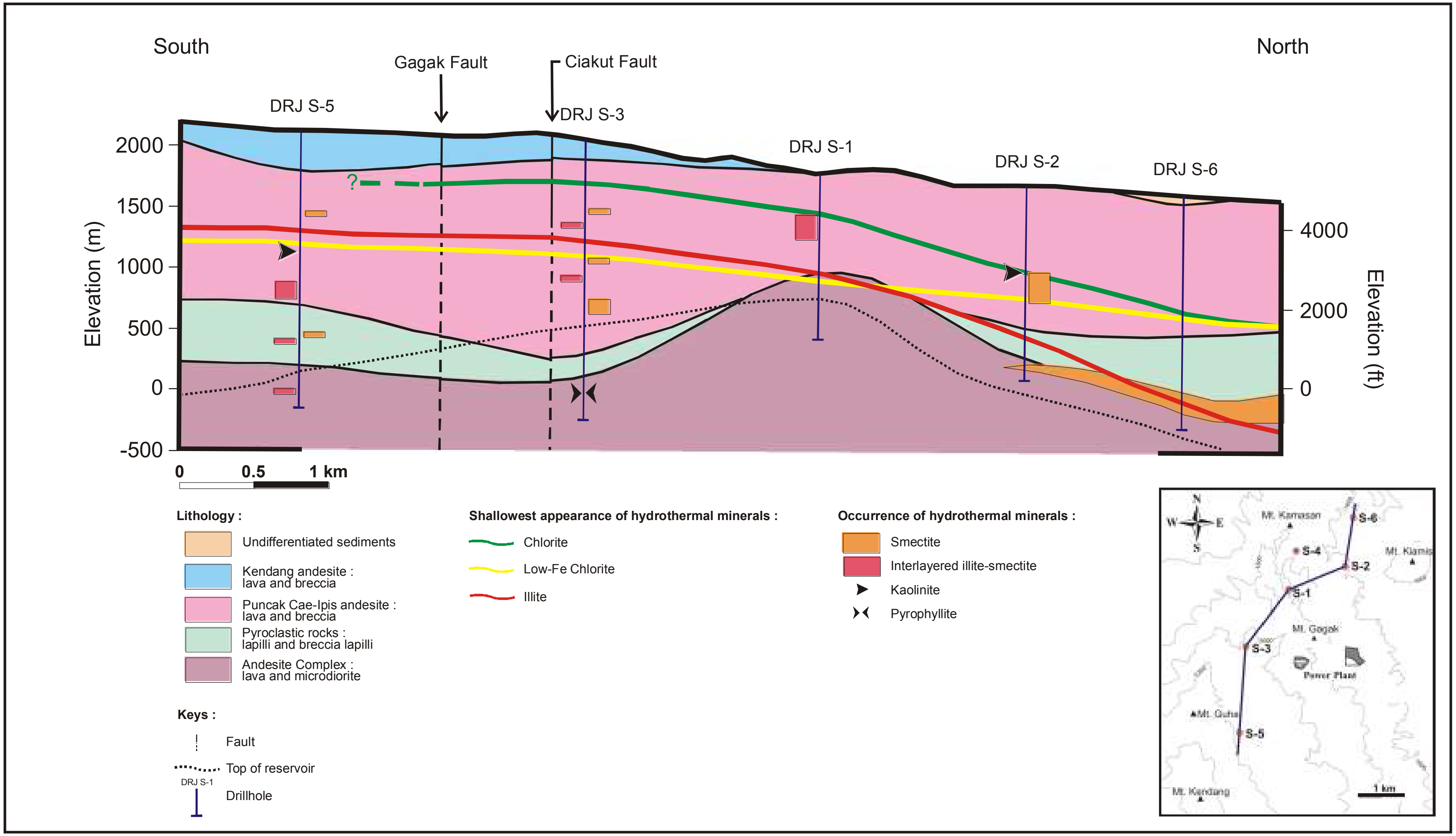

Figure 5.1. South-north cross-section, from DRJ S-5, S-3, S-1, S-2 to S-6, showing the distribution of clay minerals present in the matrix of the rocks.

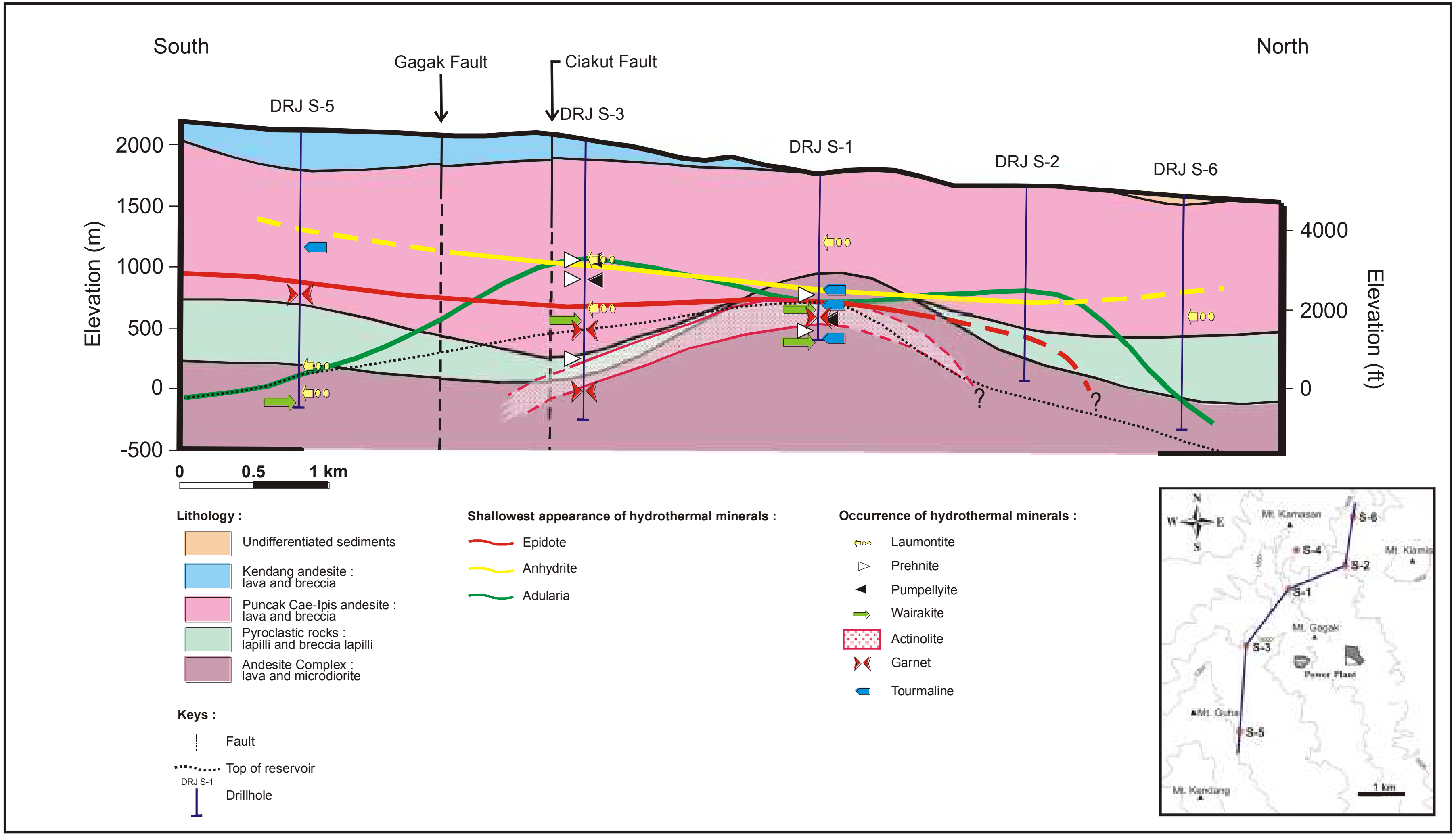

Figure 5.2. South-north cross-section, from DRJ S-5, S-3, S-1, S-2 to S-6, showing the distribution of hydrothermal minerals present in the matrix of the rocks.

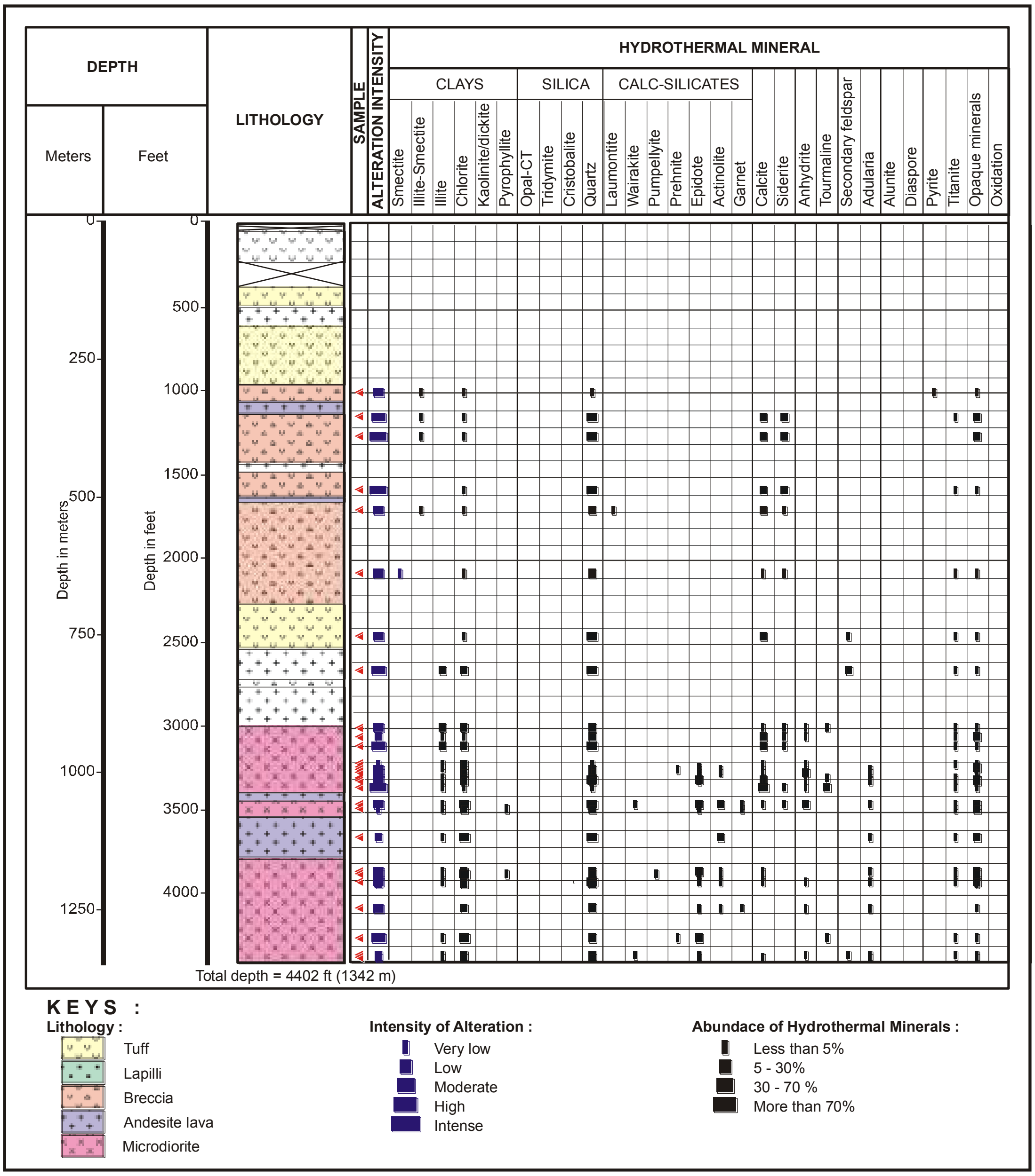

Figure 5.3.Intensity of hydrothermal alteration and occurrence of hydrothermal minerals in the matrix of rocks from well DRJ S-1.

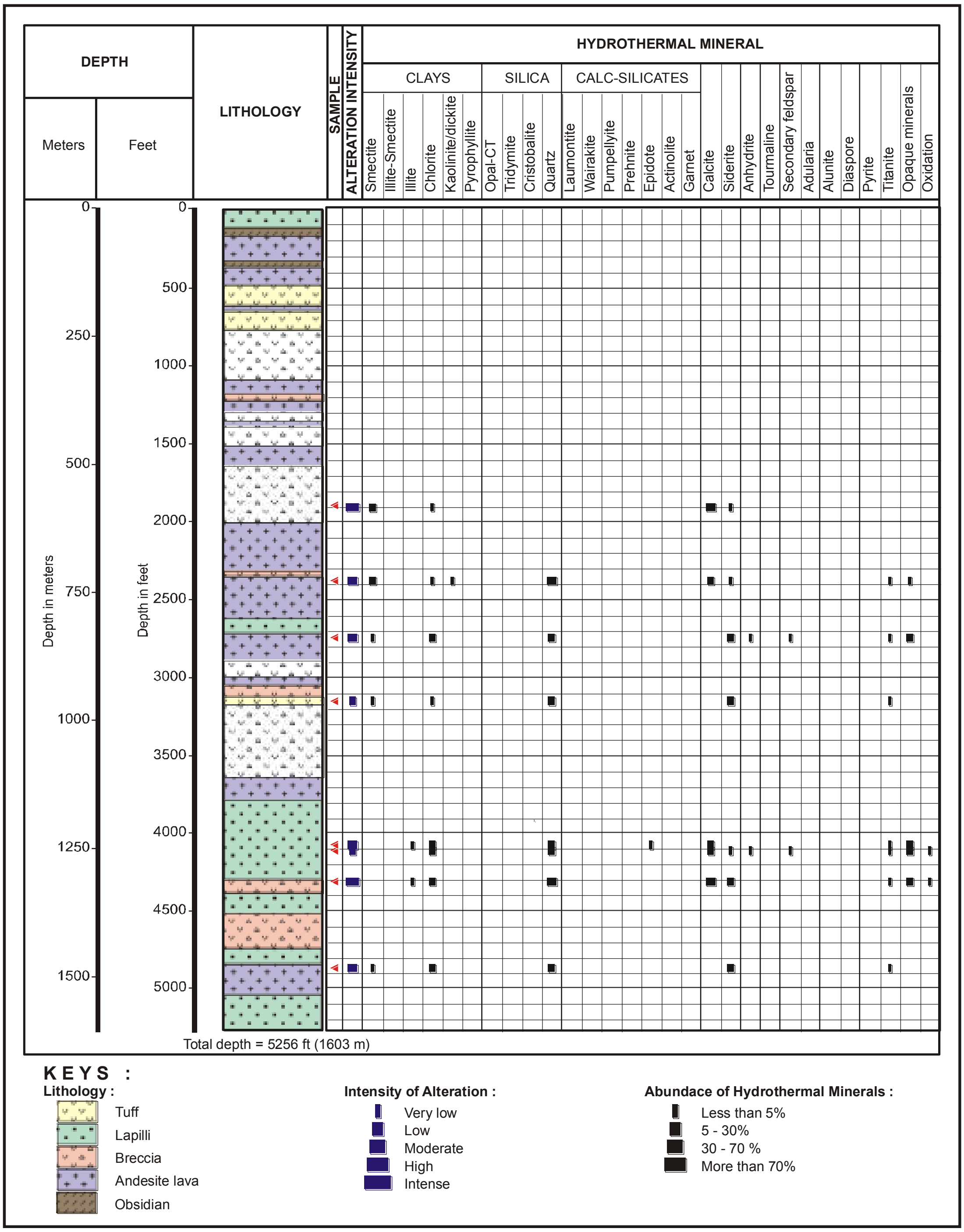

Figure 5.4.Intensity of hydrothermal alteration and occurrence of hydrothermal minerals in the matrix of rocks from well DRJ S-2.

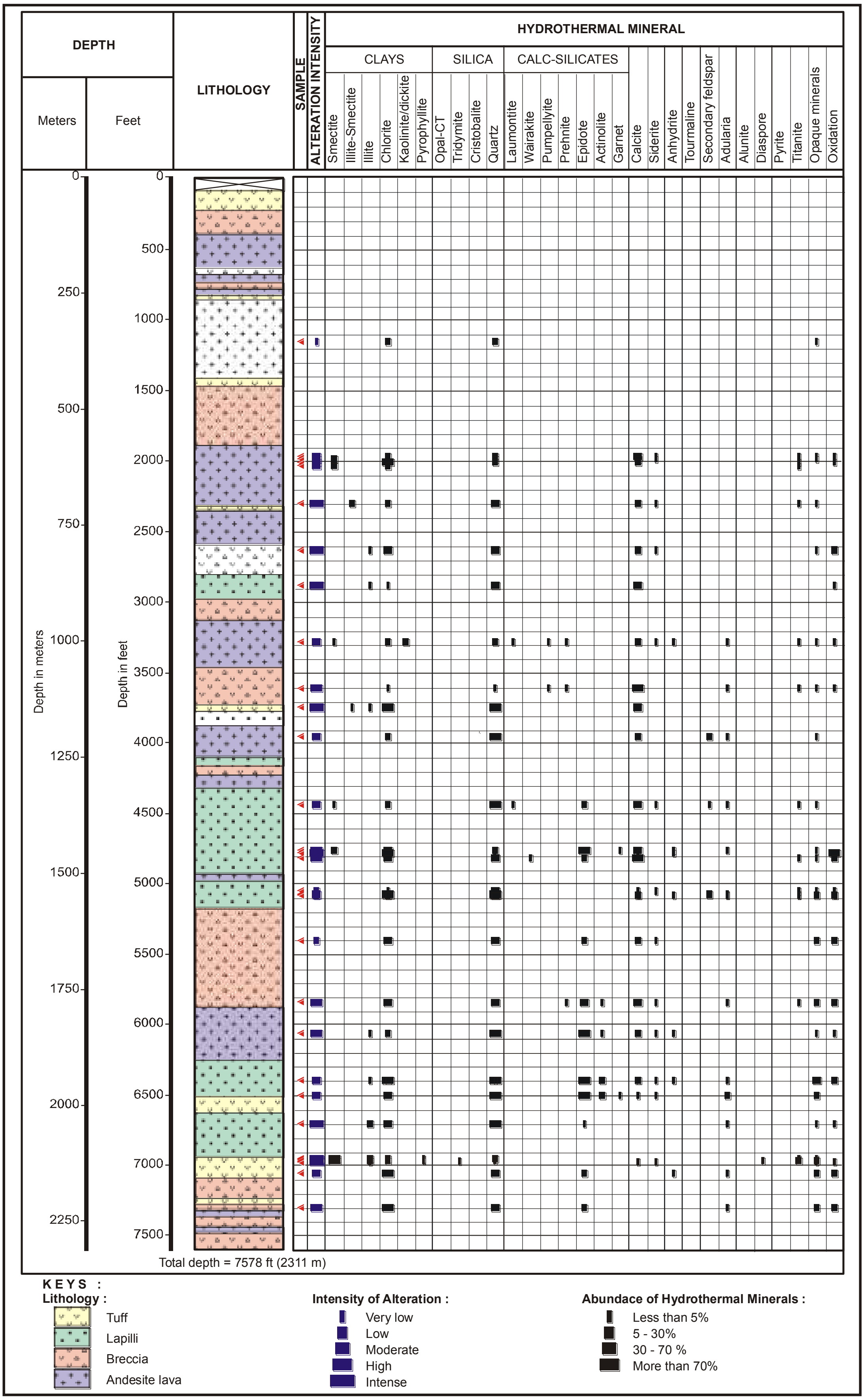

Figure 5.5.Intensity of hydrothermal alteration and occurrence of hydrothermal minerals in the matrix of rocks from well DRJ S-3.

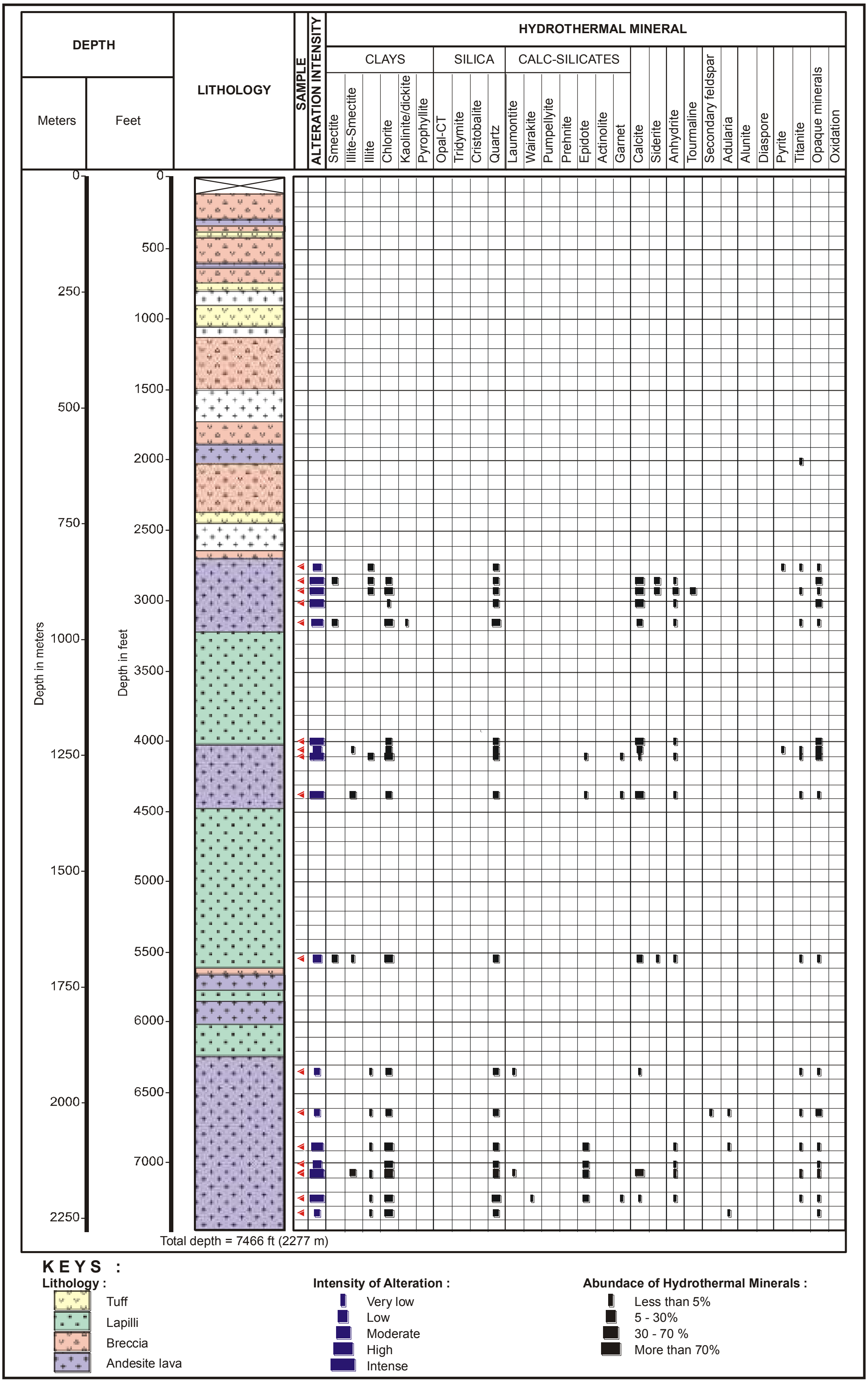

Figure 5.6.Intensity of hydrothermal alteration and occurrence of hydrothermal minerals in the matrix of rocks from well DRJ S-5.

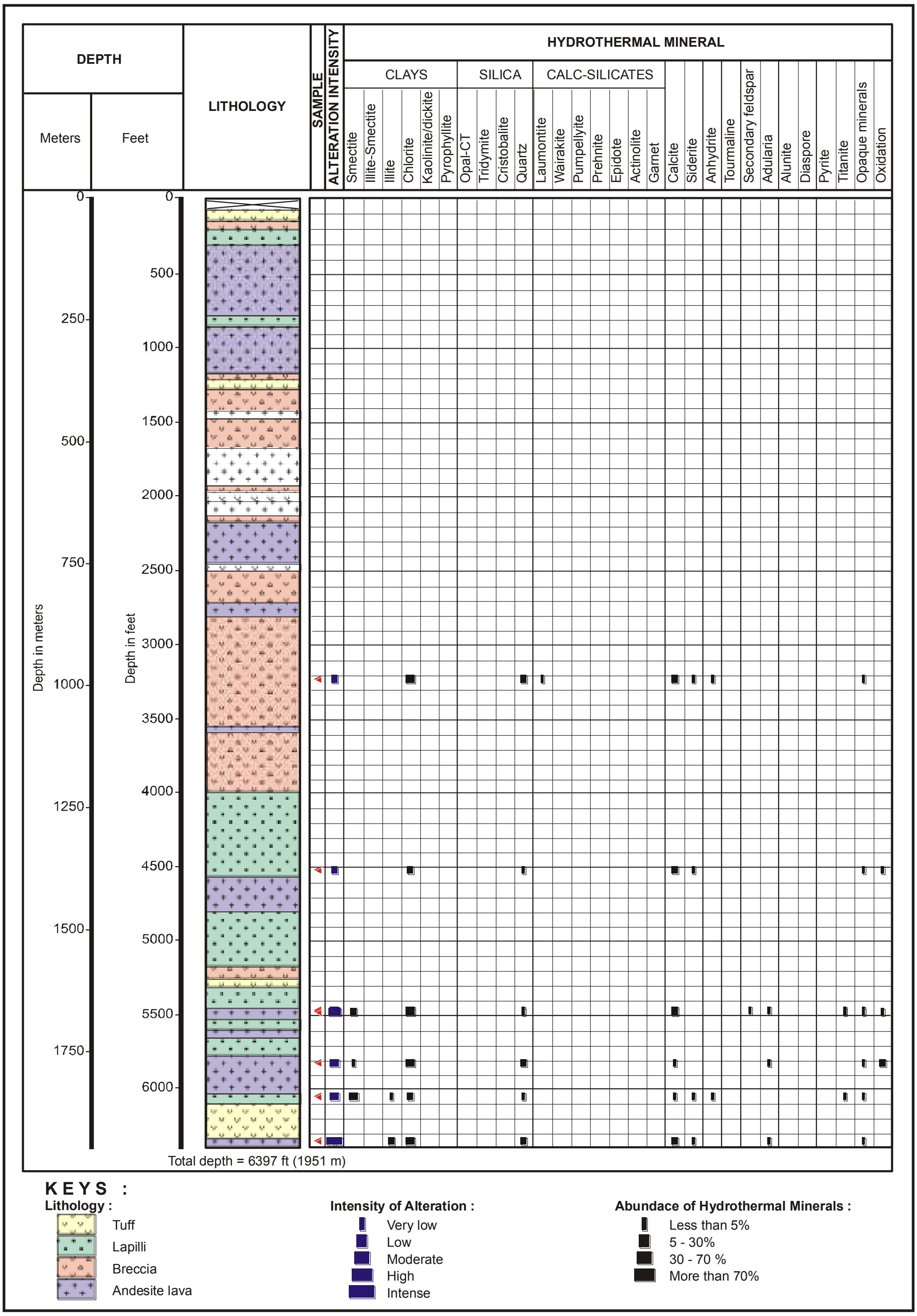

Figure 5.7.Intensity of hydrothermal alteration and occurrence of hydrothermal minerals in the matrix of rocks from well DRJ S-6.

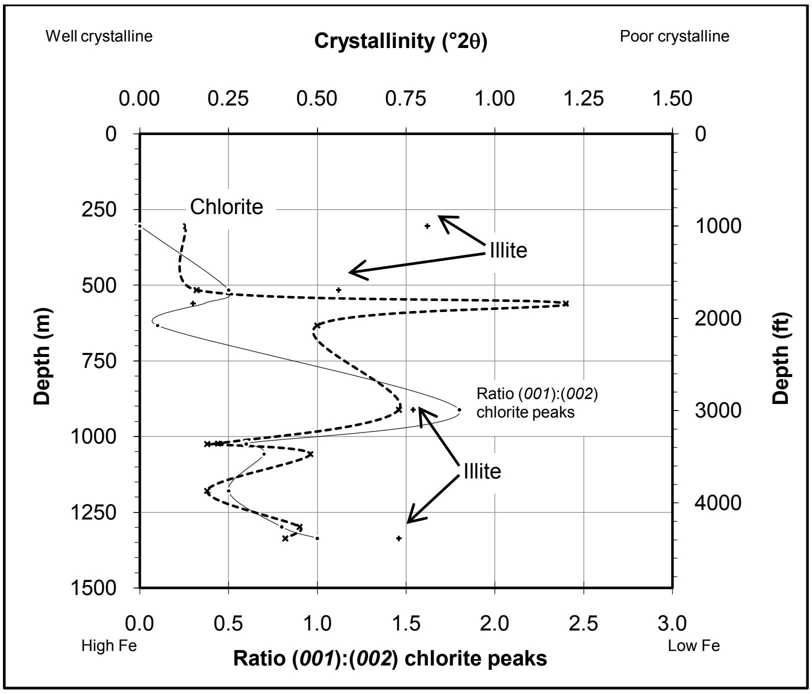

Figure 5.8. Variation in crystallinity of chlorite and illite, and ratio of (*001*) and (*002*) chlorite peaks in cores from well DRJ S-1. Increasing the degree of crystallinity 2θ indicates that the crystals become poorly crystalline and increasing the ratio of (*001*):(*002*) indicates a decrease in Fe content in chlorite.

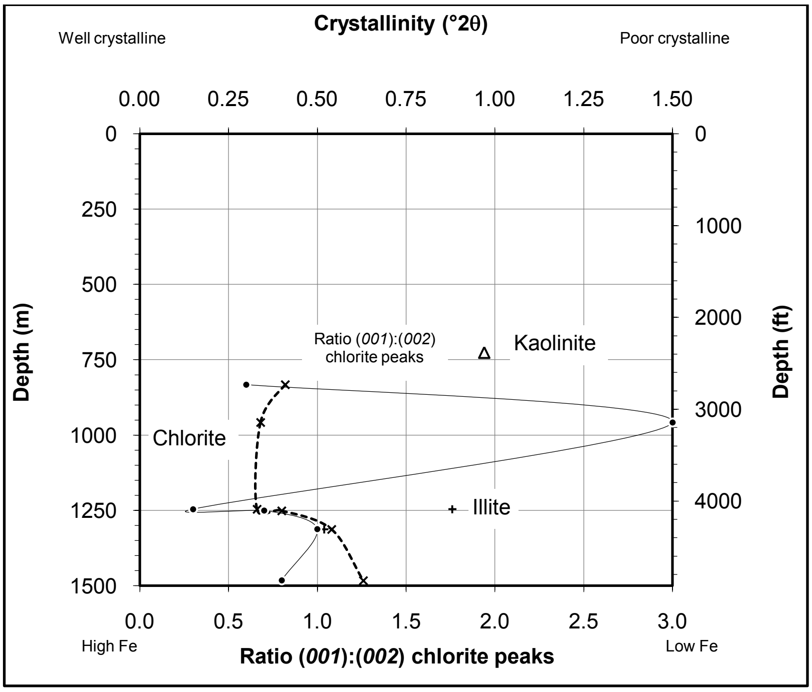

Figure 5.9. Variation in crystallinity of chlorite and illite, and ratio of (*001*) and (*002*) chlorite peaks in cores from well DRJ S-2. Kaolinite occurs at 730 m depth.

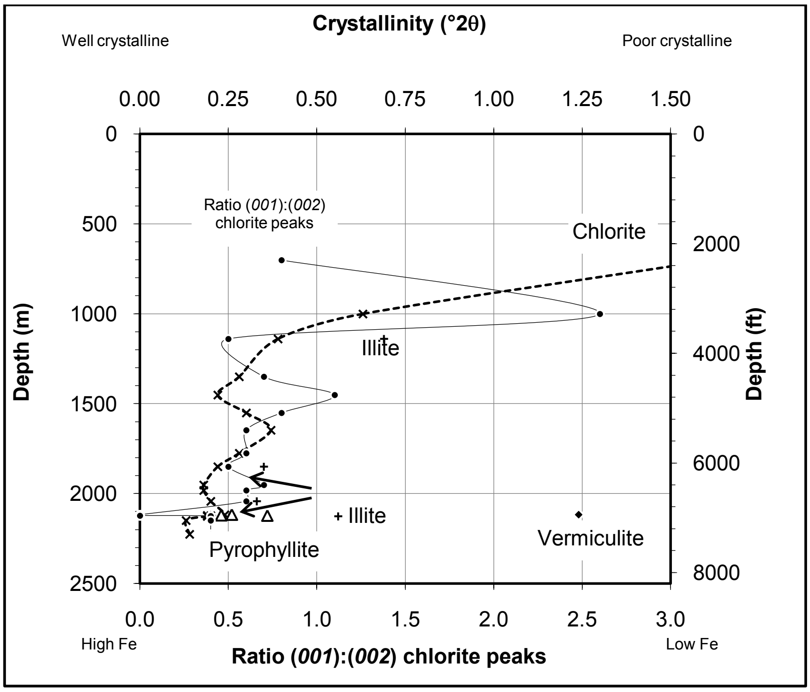

Figure 5.10. Variation in crystallinity of chlorite and illite, and ratio of (*001*) and (*002*) chlorite peaks in cores from well DRJ S-3. Pyrophyllite and vermiculite may occur at about 2100 m depth.

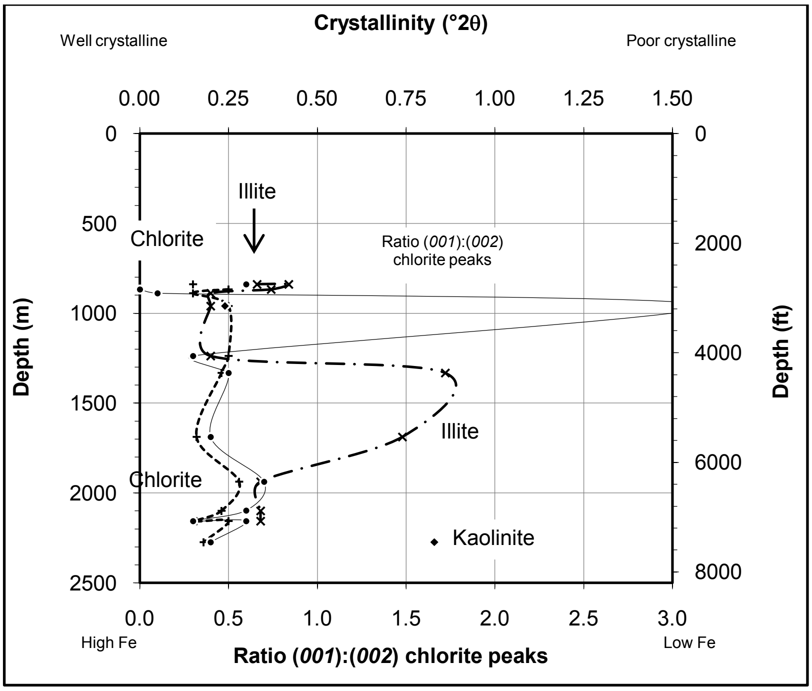

Figure 5.11. Variation in crystallinity of chlorite and illite, and ratio of (*001*) and (*002*) chlorite peaks in cores from well DRJ S-5. Kaolinite occurs at 960 and 2274 m depth.

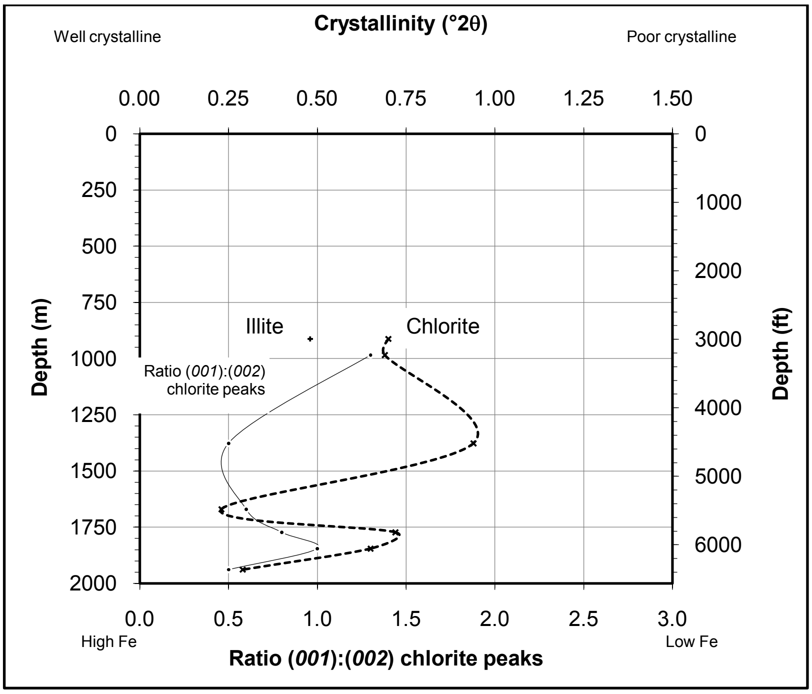

Figure 5.12. Variation in crystallinity of chlorite and illite, and ratio of (*001*) and (*002*) chlorite peaks in cores from well DRJ S-6.

5.2.1. Clay Minerals

Chlorite is the most common hydrothermal clay mineral at Darajat. It occurs in samples from all wells and at most depths. It occurs over a wide range of temperatures, i.e. from 120 to 330°C (Reyes, 1990) and replaces almost all primary minerals. Chlorite is usually pale green to dark green, slightly pleochroic, with low birefringence. Figures 5.13A and B show chlorite as disc-like platelets with round edges, 2-4 μm in diameter and about 0.2 μm thick. The platelets usually cluster together face-to-face or occur in a rosette pattern.

Chlorite is indicated by the appearance of peaks at about 14, 7.1, 4.7 and 3.55 Å identified as chlorite (001), (002), (003) and (004) reflections respectively. These are unaffected by ethylene glycol treatment, but the intensity of the peak at 7.1 Å may increase after being heated to 500°C for 1 hour. In some cases, the odd chlorite peaks are weak, or absent, and this probably reflects the amount of Fe in the chlorite (Moore and Reynolds, 1989). Therefore, the intensity ratio between the (001) and (002) peaks can be used to determine the relative amounts of Fe in the chlorite. If the ratio is high, the amount of Fe in the chlorite is low. However, a higher amount of Fe in chlorite is also suggested by a difference in its colour in thin section, from green to brownish green.

The degree of disordering of the chlorite lattice is indicated by the degree of crystallinity expressed as °2θ, measured on the half width of its (002) peak at 7.1 Å after ethylene glycol treatment. The higher the 2θ value, the more disordered the chlorite. Measuring the (001) peak at ~14 Å is not suggested since it is affected by the amount of Fe present.

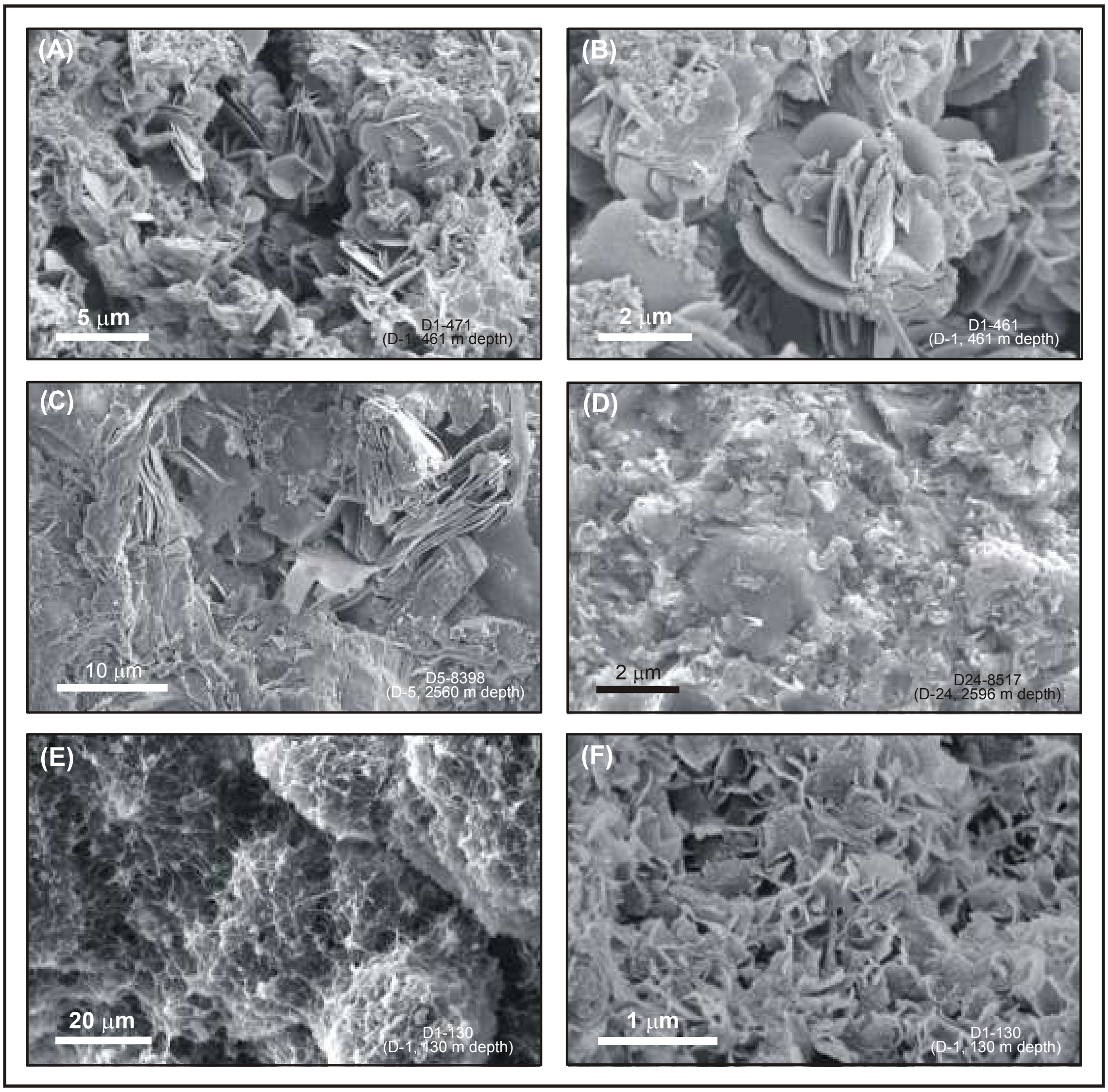

Figure 5.13.Microtextures of common clay minerals viewed under scanning electron microscope. **(A)** Chlorite has platelets. **(B)** Chlorite platelets forming rosette like assemblages. **(C)** Illite is present as irregular platelets within plagioclase (see Figure 5.14). **(D)** Illite also occurs as flakes covering quartz (see Figure 5.14). **(E)** Smectite as thin, ribbon-like crystals coating primary minerals. **(F)** Smectite flakes. The occurrences of clay minerals are confirmed by X-ray diffraction. Sample numbers and locations are given.

The shallowest appearance of chlorite in well S-3 is at an elevation of +1700 to +1800 m (Figure 5.1). It is deeper in the north, in well DRJ S-1, and is first present at about +1500 m. In DRJ S-2 and S-6, chlorite occurs at about +1000 and +700 m respectively. In well DRJ S5, chlorite is present together with illite at +1200 m elevation. However, it may also occur at higher elevations, but no shallower cores are available.

Figure 5.1 shows that low-Fe chlorite is present at elevations of +800 to +1200 m, i.e. 100-200 m below the shallowest occurrence of illite. The well crystallised chlorite is Fe rich but poorly crystallised chlorite contains less Fe. The degree of crystallinity,°2θ, of chlorite in well DRJ S-3 decreases with depth, indicating that it becomes more crystalline with increasing depth (Figure 5.10). Here the amount of Fe in chlorite also increases with depth. Chlorite in well DRJ S-1 is mostly well crystallised and Fe-rich, except at about +800 m (i.e. 915 m depth in DRJ S-1), where it is poorly crystallised and contains little Fe (Figure 5.8). The presence of smectite might be associated with this increased disorder in the chlorite. However, the crystallinity of chlorite in DRJ S-5 is uniform but the amount of Fe in it seems to increase with depth (Figure 5.11). In DRJ S-2 at shallow depth, chlorite is well crystallised and contains little Fe, but at depth it is poorly crystalline and Fe rich (Figure 5.9). Chlorite is mostly poorly crystalline in well DRJ S-6, except at -100 m elevation, where illite is also present (Figure 5.12). The amount of Fe tends to increase with depth. Low-Fe chlorite in DRJ S-2 and S-6 is present at elevations of +600 to +800 m, i.e. above the shallowest appearance of illite.

The amount of Fe in chlorite will decrease with an increase in temperature of chlorite formation (e.g. Curtis, et al., 1985; Cathelineau and Nieva, 1985). However, the compositions of chlorite are compared with direct analyses of their chemistry, as in Chapter 7.

Illite forms about 2 μm diameter flakes replacing plagioclase along cracks (Figure 5.13C-D and 5.14). It is mostly colourless, but some is slightly yellow, very pale green or brown. Illite is mostly associated with chlorite. The shallowest appearance of illite is at +1000 to +1400 m, except in the northern area (i.e. wells DRJ S-2 and S-6), where it is first present at -100 to +500 m, i.e. about 800 m below the shallowest occurrence of chlorite.

The crystallinity of illite can be measured from the half-width (001) peak at ~10 Å. The measurement was made on a glycol-solvated specimen to minimise the effect of any expandable mixed layers present. Illite from well DRJ S-5 is well crystallised, except it is poorly crystallised between +400 and +800 m (Figure 5.11). In DRJ S-3, illite is poorly crystalline at shallow depths but it seems to be well crystallised at depth (Figure 5.10). However, at about sea level, illite is poorly crystalline, possibly connected to some occurrences of pyrophyllite and vermiculite. The crystallinity of illite in well DRJ S-1 seems to be low and uniform with increasing depth (Figure 5.8). In well DRJ S-2, illite is well crystallised (Figure 5.9), whereas in DRJ S-6, it is poorly crystalline (Figure 5.12). Several studies show that illite crystallinity relates to the temperature of its formation. Illite generally occurs between 220 and 330°C (Reyes, 1990) but may be as high as 360°C (Rosenberg, 2002). A decrease in a crystallinity value indicates that the degree of its disordering decreases with increasing depth perhaps as a result of an increase in temperature (e.g. Ji and Browne, 2000). Illite also contains more Fe with an increase in temperature (Cathelineau, 1988; and Yates and Rosenberg, 1996).

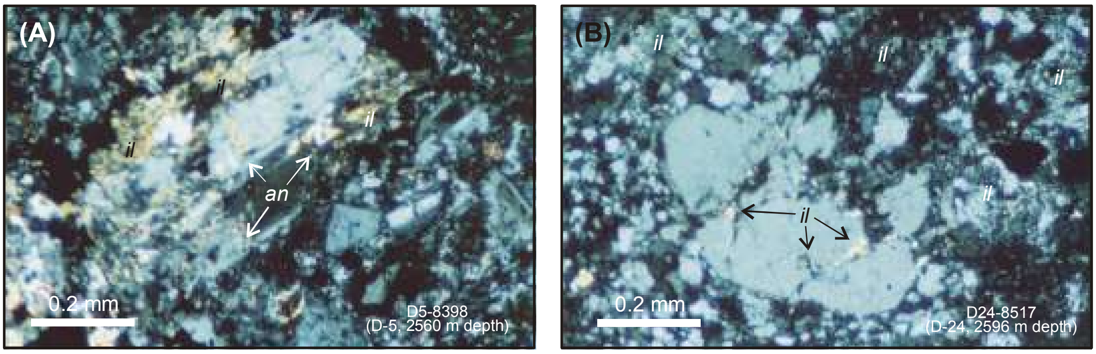

Figure 5.14.Illite as replacement mineral. **(A)** Illite (*il*) replaces plagioclase and is associated with anhydrite (*an*). Cross polars. **(B)** Illite (*il*) is also present along cracks of primary quartz (*qz*) in a rhyolitic rock from well DRJ 24. It also alters the groundmass. Cross polars. This illite viewed under Scanning Electron Microscope is given in Figures 4.13C and D. Sample number and location are given.

Smectite and vermiculite. Smectite mostly replaces the groundmass and forms brown, sometimes yellowish brown, fine-grained aggregates. It also replaces plagioclase and forms brown to dark brown flakes. Figures 5.13E-F show that, under the Scanning Electron Microscope, smectite has a thin and webby morphology crusting primary minerals. It can also occur as irregular and wavy flakes up to about 0.5 μm diameter.

The XRD pattern of smectite shows an intense, but rather broad (001) peak at 12-15.5 Å, which expands to 17-18 Å after ethylene glycol treatment but shifts to about 10 Å after heating for 1 hour at 500°C. A d-spacing of about 12.5 Å indicates that the smectite is the Na^+ variety but a spacing between 14.5 and 15.5 Å indicates that the cation is Ca^{2+} (Grim, 1968). Prol-Ledesma (1998) showed that the Ca^{2+} rich smectite is more stable at high temperature than the Na^+ rich variety. The other peaks of smectite are at about 8.5 and 5.64 Å, identified as smectite (002) and (003) respectively, but yielded by the glycol-solvated samples only. The presence of other cations, e.g. Fe and Mg, can affect the d-spacing of the (002) peak; Fe rich smectite has the peak at 9.0-9.1 Å but Mg smectite at about 9.2 Å (Deer et al., 1962a). The concentration of Fe in smectite may be indicated by higher (002) peaks, but a decrease in the (003) peak (Moore and Reynolds, 1997). Therefore, the amount of Fe in smectite affects the ratio of the (002) to (003) peaks.

The amount of Fe in smectite also affects dehydration processes and phase changes recorded on the DTA patterns. Smectite shows 2-4 endothermic reactions due to dehydration at temperatures below 900°C and an exothermic reaction due to phase change at temperatures about 1000°C but this can be as high as 1200°C with increasing the amount of Fe in smectite (Grim, 1968). All smectite in Darajat seems to be the Ca^{2+} variety and contains low Fe.

Smectite is usually absent where illite is present. This indicates that smectite is unstable at high temperatures, i.e. above 220°C. Smectite is widespread in the northern area. It occurs at elevations of +700 to +1000 m in well DRJ S-2 and deepens to 0 to -200 m in DRJ S-6. Smectite is deep in DRJ S-2, i.e. at +200 m elevation but in well DRJ S-1, it is absent. In the south, smectite is present locally at about +500 and +1500 m in DRJ S-5 and at elevations of +1500, +1100 and +600 to +700 m in DRJ S-3. Some local smectite might be due to overprinting, since it appears in the illite zone and, indeed, also below the shallowest appearance of epidote.

Vermiculite has optically similar characteristics to smectite. It can be distinguished from smectite by its XRD reflection at 10.6-14.5 Å, which expands to 13.5-15.8 Å after ethylene glycol treatment but shifts to 10.6 Å after heating (Grim, 1968). Vermiculite and smectite can also be distinguished by an addition of glycerol (Moore and Reynolds, 1997); after this, the d-spacing of vermiculite remains at 14.5 Å, whereas that of the smectite will shift to 17.7 Å. In the samples studied, vermiculite is only present, associated with pyrophyllite and chlorite, at about sea level in well DRJ S-3. Vermiculite and Fe-Mg rich smectite may be stable up to 450°C (Deer et al., 1962a)

Interlayered illite-smectite. This clay is hard to identify in thin section, although its birefringence is an indication, but it is readily identified by XRD (see Appendix C). The portion of illite in the interlayered illite-smectite can be estimated from the positions of the interlayer peak at about 10 Å on the ethylene glycol treated specimen (Moore and Reynolds, 1989). Basically, the greater the portion of illite, the closer the reflection position is to 10 Å.

At Darajat, interlayered illite-smectite is present in all cores from wells DRJ S-1 and S-5 at elevations of +1200 to +1500 and +800 to +900 m respectively. Below +500 m in well DRJ S-5, the interlayer clay is locally present at +400 m and about sea level. The amount of illite in well DRJ S-1 ranges from 40 to 70% but in well DRJ S-5 it is generally more than 80%. In DRJ S-3, the interlayer clay is present at +1300 and +900 m. Reyes (1990) reported that interlayered illite-smectite usually occurs between 180 and 260°C, but this may extend to higher temperatures under condition of poor permeability.

Kaolinite is present at +1100 to +1200 m in well DRJ S-5 and about +1000 m in well DRJ S-2. It is identified by the appearance of strong X-ray peaks at about 7.1 and 3.6 Å. These peaks are destroyed after one hour heating at 500°C; this distinguishes it from chlorite (Moore and Reynolds, 1989). The degree of crystallinity, indicating degree of disordering of kaolinite, can be measured from the half-width (001) peak at 7.1 Å and the Hinckley Index (HI) of (020), (110) and (111) peaks at about 4 Å

(Hinckley, 1963). Kaolinites from well DRJ S-3 and S-5 are well crystallised (Figure 5.11), but those from well DRJ S-2 are poorly crystallised (Figure 5.9). Kaolinite is absent in wells DRJ S-1 and S-6.

Kaolinite can also be identified by its DTA pattern. It shows dehydration endothermic peaks at temperatures below 500°C and an exothermic reaction due to phase change at about 1010°C.

Metahalloysite gives XRD peaks and DTA patterns identical to kaolinite (see Appendix C). However, they can be distinguished by their shapes; kaolinite has sharp and intense peaks whereas metahalloysite has a broad and very weak peaks. Kaolinite and metahalloysite are also distinguished by using formamide as described by Churchman et al. (1984). Other methods sometime used to differentiate them, e.g. Miller and Keller (1963) and Keller and Haenni (1978), cannot be applied to hydrothermal clays due to their heterogeneity. Most metahalloysite can hydrate, so halloysite can form (e.g. in sample from 43 m depth of well DRJ 2). Therefore, the d-spacing of about 7 Å may shift to about 10 Å with introduction of an additional 2.9 Å thick water layer (Moore and Reynolds, 1989).

Kaolinite viewed with a Scanning Electron Microscope totally differs from halloysite. Figure 5.15A shows kaolinite from DRJ 1 with pseudo hexagonal plates about 5 μm a cross and up to 1 μm thick. The platelets are face-to-face and book-shaped. Halloysite, as shown in Figure 5.16A-B, has tubular-shaped crystals. A sample from 100 m depth from well DRJ 1 shows that the tubular crystals of halloysite present can be longer than 2 μm, are parallel to one another and crust primary minerals. Some are also unoriented, up to 2 μm long with diameters of 0.1-0.2 μm. Figure 5.16C-D shows halloysite as spheroids with diameters ranging from 1 to 4 μm. The core of the spheroid seems to be a hollow and its surface is irregular. EDAX analysis confirm that the spheroid is a clay that consists mainly of Si, Al and O. Dixon and McKee (1974), who described tubular and spheroidal halloysite from Colorado and Minnesota respectively, revealed that the tubular crystal may form from rolled kaolinite plates and the spheroidal form has a patchy exterior of kaolinite plates. They also reported that spheroidal halloysite may be more structurally disordered than the tubular variety. However, since kaolinite can hydrate and form halloysite, these two minerals can appear together (Figure 5.15B).

According to Deer et al. (1962a), kaolinite occurs at temperatures below 200°C, at ambient pressures and in acid conditions. Mas et al. (2003) reported that disordered kaolinite can occur at temperatures between 50 and 70°C. Halloysite can form as an alteration product of kaolinite due to interaction of sulfur-bearing solutions, but it can also form directly from solution and usually accompanied by allophane and alunite, such as occurs at DRJ 2. At higher temperatures, structurally ordered dickite is the stable kaolin phase.

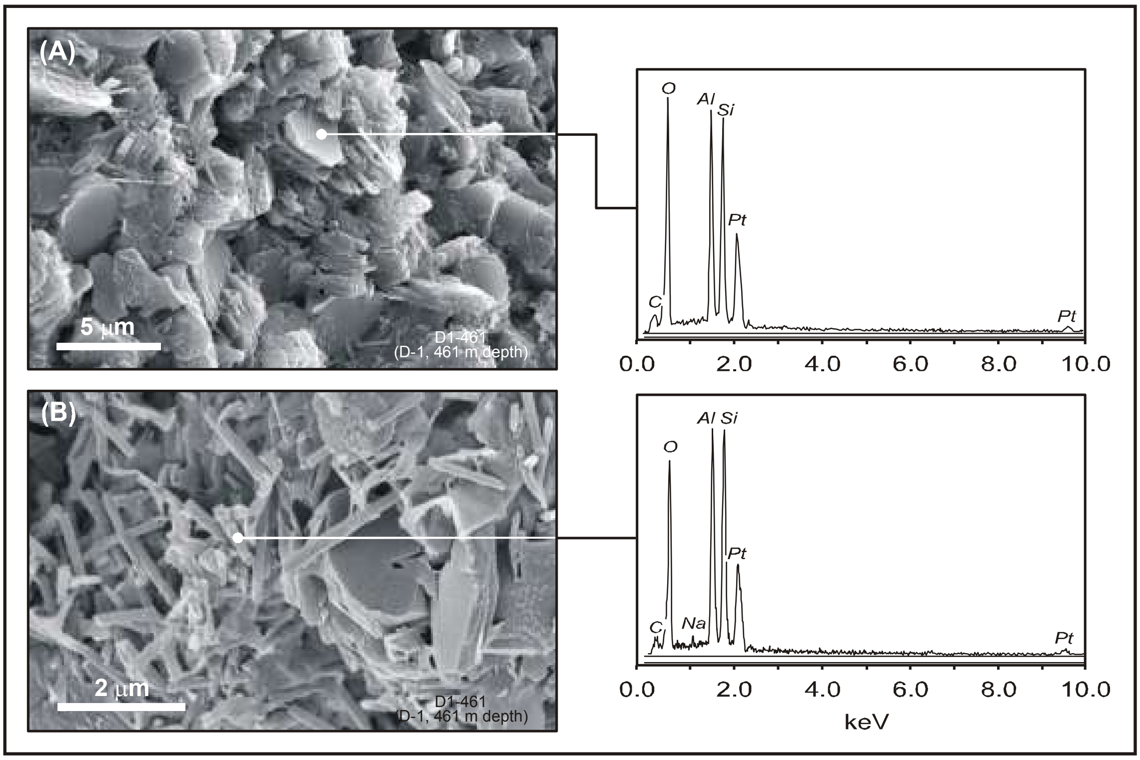

Figure 5.15.Kaolinite in sample from 461 m depth in well DRJ 1. **(A)** Kaolinite pseudo hexagonal platelets. **(B)** Kaolinite occurs together with unoriented tubular crystals of halloysite as a product of kaolinite hydration. The EDAX analyses show that the platy crystals are kaolinite, not chlorite, consisting of Al, Si and O. The tubular crystals are also composed of Al, Si, O and trace Na. The presences of Pt and C on the EDAX spectrum are due to the coating used. The vertical axis of the spectrum is unscaled. The occurrence of kaolinite is also confirmed by X-ray diffraction.

Pyrophyllite occurs at about sea level in well DRJ S-3. It appears mostly in cavities as a colourless mineral. It sometimes forms radiating clusters. A trace of pyrophyllite, associated with chlorite and smectite, also occurs at an elevation about +900 m in well DRJ S-1, as indicated from weak X-ray reflections. Pyrophyllite is mostly identified by the occurrence of XRD peaks at 9.2, 4.6 and 3.1 Å, which are not affected by ethylene glycol or heating for 1 hour at 500°C. The Darajat pyrophyllite has peaks 9.2-9.4, 4.9-5.0 and 3.3 Å. These slightly higher values may be due to its greater amount of Fe (Brindley and Brown, 1980). In addition, its high Fe content is also indicated by chlorite that is present and associated with pyrophyllite. The degree of crystallinity of pyrophyllite is measured on the (001) peak at about 9 Å. In well DRJ S-3, pyrophyllite is well crystallised (Figure 5.10).

Swindale and Hughes (1968) reported that pyrophyllite gives 3 endothermic reactions, i.e. below 150°C due to dehydration, 500-600 and 800-850°C due to phase changes. The Darajat pyrophyllite shows the last phase change at temperatures between 730 and 780°C. These lower temperatures may indicate that the pyrophyllite is Fe rich. In addition, some pyrophyllites also show an exothermic reaction at temperatures about 1060°C, suggesting the occurrence of kaolinite.

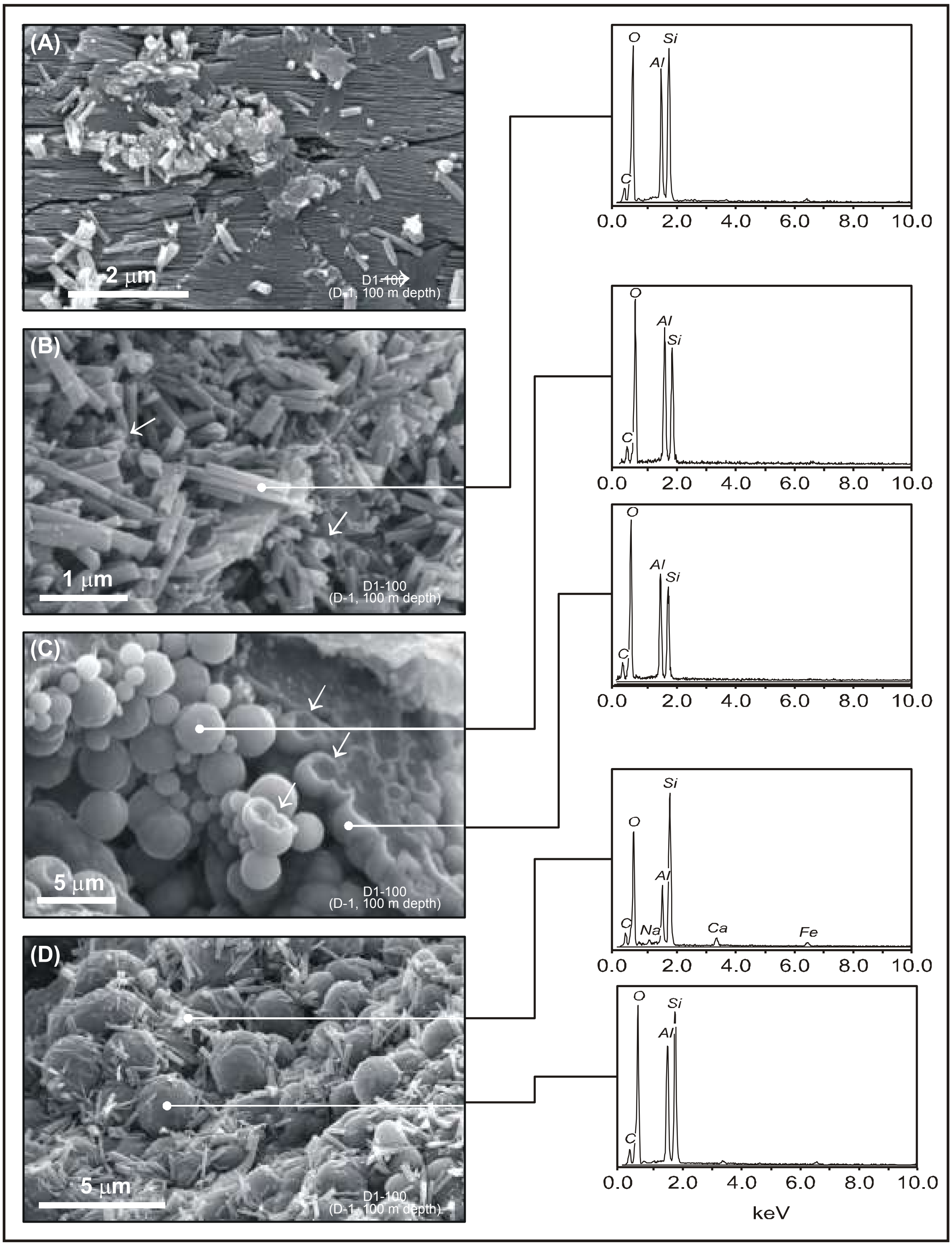

Figure 5.16.Halloysite in sample from 100 m depth in well DRJ 1. **(A)** Halloysite occurring as oriented, parallel tubular crystals partly covering a primary mineral (see arrow). **(B)** Halloysite occurring as unoriented tubular, unrolled crystals (see arrows). **(C)** Halloysite occurring as spheres. The core seems to be a hollow (see arrows). **(D)** Halloysite tubular and spherical forms. The occurrence of clay minerals is confirmed by the X-ray diffraction and EDAX analyses. The EDAX analyses indicate that both tubular and spherical halloysites consist mainly of Al, Si and O; C on the spectrum is coating. The vertical axis of the spectrum is unscaled.

Figure 5.17 shows that samples from about 2120 m depth of well DRJ S-3 contain flakes less than 2 µm cross. EDAX analyses indicate that these are composed of Si, Al and O with traces of Ca, K and Fe. Swindale and Hughes (1968) showed that pyrophyllite can form by the transformation of kaolinite at high temperatures and at low silica activity. However, in geothermal systems, pyrophyllite usually forms at pH between 2 and 4 (Reed, 1974), probably affected by magmatic fluids (cf. Reyes, 2000) at temperatures as high as 500°C (Kalinin and Shapovalova, 1975).

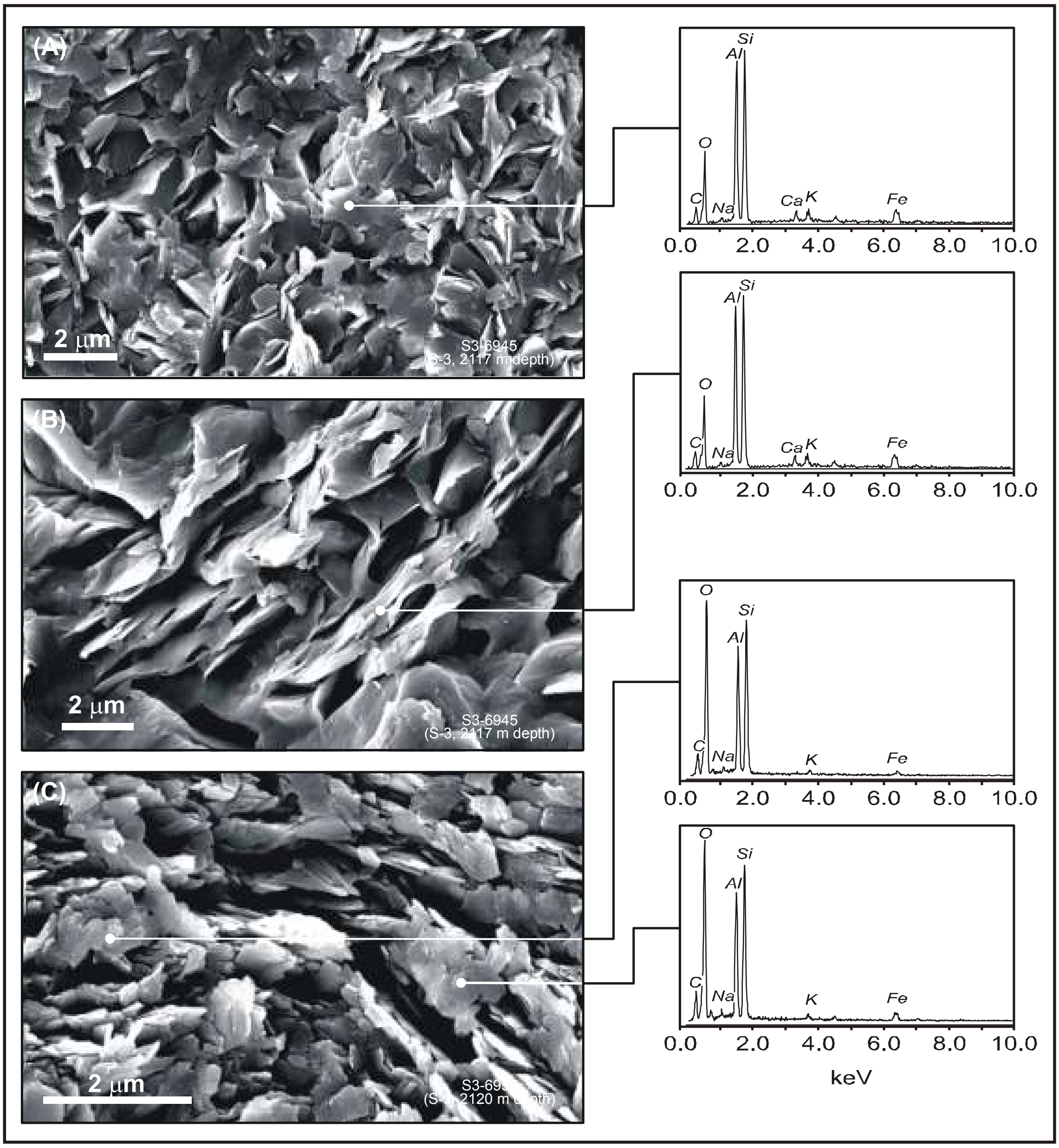

Figure 5.17. Pyrophyllite in samples from well DRJ S-3: **(A)** 2117 m depth. **(B)** 2117 m depth.**(C)** 2120 m depth. The occurrence of clay was confirmed by X-ray diffraction. The EDAX analyses confirm that pyrophyllite consists of Al, Si, O and traces of Fe, Na and K. The C on the EDAX spectra is due to the coating.

5.2.2. Silica

Quartz is the most common hydrothermal mineral at Darajat occurring in all wells and at all depths. It replaces primary plagioclase and pyroxene along cracks from the crystals surfaces inward. Quartz also alters groundmass, mostly volcanic glass.

Other silica phases, including opal-CT, cristobalite and tridymite, are common at shallow depths (e.g. in well DRJ 1). They mostly replace volcanic glass. In thin section cristobalite shows a (cracked) tile-like texture and tridymite has wedge-shapes, but both are colourless and have low interference colours. Opal-CT is easily seen under SEM; it occurs as spherical particles of about 2 μm with thin-bladed, lepispheres, and sometimes in botryoidal aggregates (Figure 5.18). Opal-CT, cristobalite and tridymite can be readily identified by XRD. Opal-CT has a weakly developed X-ray pattern with peaks at 4.04, 4.34 and 4.42 Å. Cristobalite is identified from its X-ray reflections at 4.03-4.04 Å and increased ordering of tridymite is indicated by the appearance of a reflection at 4.42-4.44 Å, usually followed by disappearance of the cristobalite reflection.

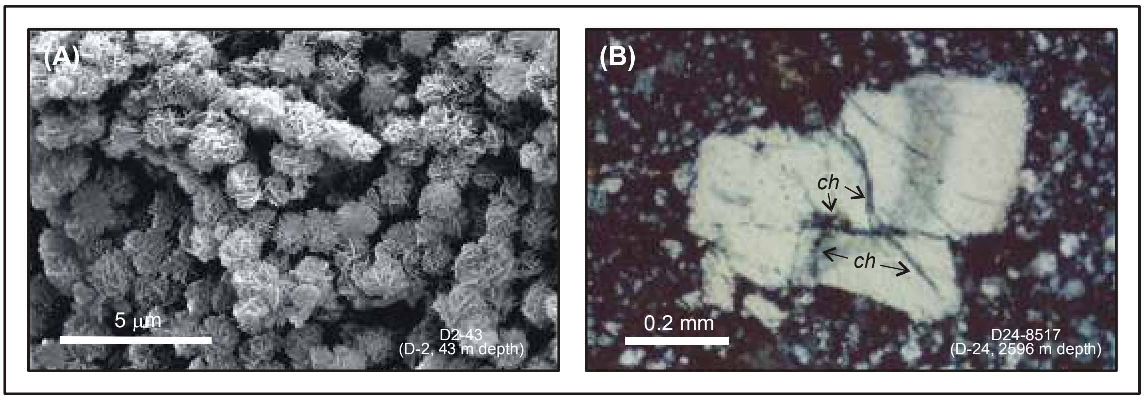

Figure 5.18.Quartz and silica minerals. **(A)** Opal-CT is the first alteration products of volcanic glass. The SEM image is taken from groundmass of a core from well DRJ 2. **(B)** Primary quartz is unaffected during hydrothermal alteration, but in a rhyolitic rock, it can be replaced by chlorite (*ch*) along cracks. Cross polars. Sample numbers and locations are given.

5.2.3. Calc-silicates

Laumontite is rare as a replacement mineral. It occurs in wells DRJ S-1, S-3, S-5 and S-6 at elevations of +1250, +700 to +1100, 0 to +200 and about +600 m respectively. Laumontite is mostly present in cores of plagioclase phenocrysts (Figure 5.19A). In well DRJ S-3, it is associated with prehnite and pumpellyite and in wells DRJ S-1 and S-5, in association with calcite. Laumontite is stable at temperature below 220°C (Bird et at., 1984).

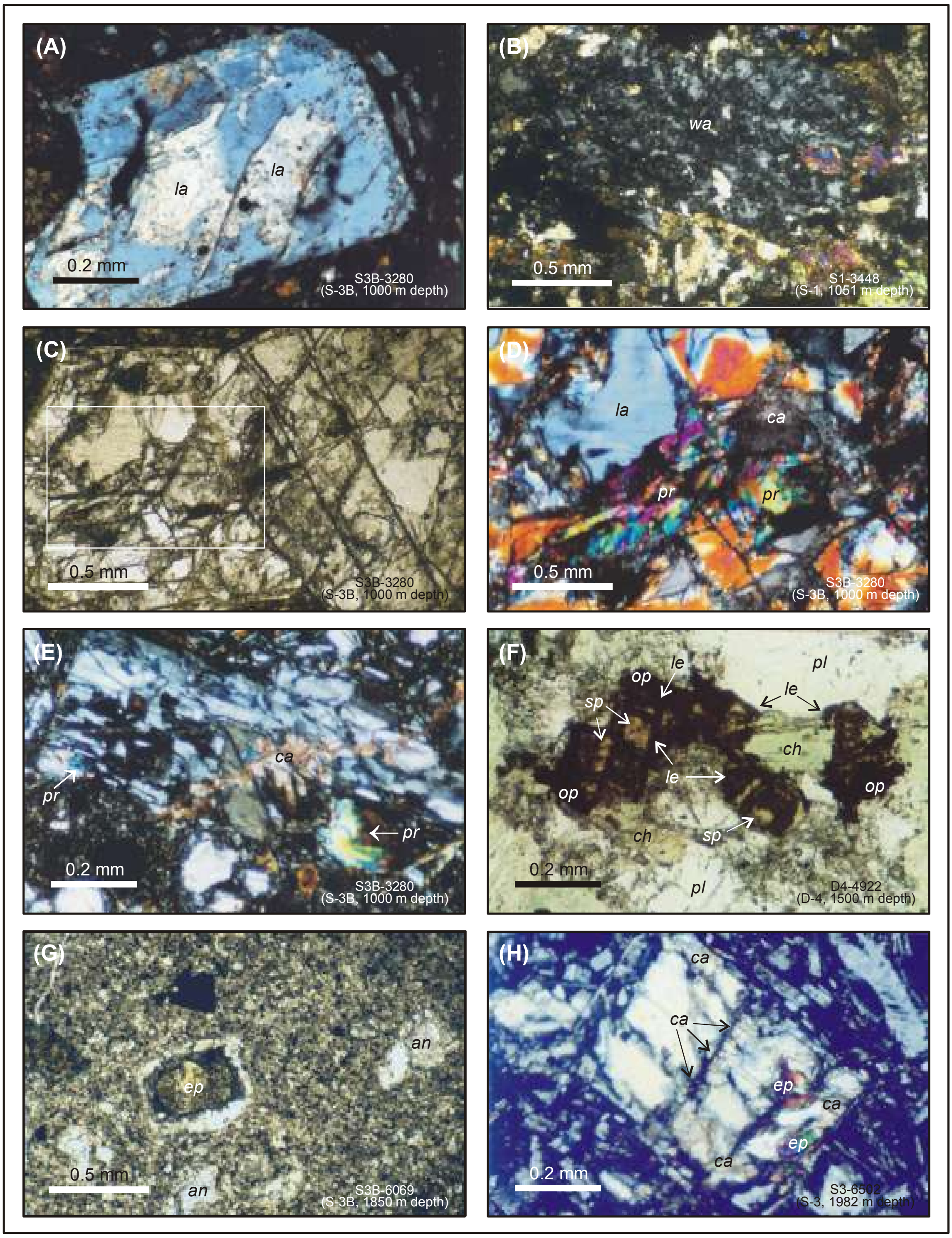

Figure 5.19.Calc-silicate minerals. **(A)** Laumontite (*la*) replacing plagioclase at the core. Laumontite is colourless, has low birefringence with a good cleavage. Cross polars. **(B)** Wairakite (*wa*) replacing plagioclase. Cross polars. **(C)** Prehnite replacing augite. Plane polars. **(D)** Cross polars of an area marked on (C) showing prehnite (*pr*) along cracks. Laumontite (*la*) seems to replace at the core and calcite (*ca*) also occurs. **(E)** Prehnite (*pr*) and calcite (*ca*) replace plagioclase along cavities and cracks. Cross polars. **(F)** Titanite (*sp*) and opaque minerals (*op*) are disseminated in the matrix; titaniteis intergrowth with leucoxene (*le*). Plagioclase (*pl*) phenocryst is altered to chlorite (*ch*). Plane polars. **(G)** Plane polarised light appearance of epidote (*ep*) that replaces core of plagioclase phenocryst. The colourless, low relief mineral is anhydrite (*an*). **(H)** Epidote (*ep*) replaces plagioclase and predates calcite (*ca*) that occurs along cracks of plagioclase. Cross polars. Sample number and location are given.

Wairakite is stable at higher temperatures than laumontite, i.e. between 200 and 300°C (Bird et al., 1984). In Darajat, wairakite rarely replaces plagioclase (Figure 5.19B), from the crystal surface inward. It is present at an elevation of -100 m in well DRJ S-5. To the north, the occurrence of replacement wairakite is shallower; in well DRJ S-3, it appears at +600 m and in DRJ S-1, it is present at +400 and +700 m.

Pumpellyite. In thin section, pumpellyite is green, pleochroic and forms fan shaped aggregates. Pumpellyite replaces plagioclase but mostly occurs in cavities in plagioclase. It is present mostly associated with chlorite at an elevation of about +600 m in well DRJ S-1. In well DRJ S-3, pumpellyite occurs together with prehnite along twin planes in plagioclase at an elevation of +900 m. Pumpellyite is replaced by prehnite or epidote in the presence of chlorite (Liou, 1971) and excess Fe (Schiffman and Liou, 1983).

Prehnite tends to form radiating crystals. It replaces plagioclase along cracks and occurs in cavities and also replaces pyroxene (Figure 5.19C-E). Prehnite is present at elevations of +500 and +800 m in well DRJ S-1 and at +300, +900 and +1100 m in well DRJ S-3. It is also recorded by Amoseas Indonesia Inc. (1989) at +1000 and +800 in wells DRJ 4 and 5 (about 2 km east DRJ S-5) respectively. Prehnite is mostly associated with calcite.

Prehnite and pumpellyite are stable at temperature of 260-350°C (Bird et al., 1984) and at high pressure, where the stability of wairakite is restricted (Liou, 1971). Prehnite also can occur, when excess CaO is present, but it will be limited, and wairakite will occur, when the ratio of CaO to Al_2O_3 is less than unity (Liou, 1971).

Titanite (Figure 5.19F) is mostly associated with opaque minerals and occurs as small grains disseminated in the groundmass. It is also intergrowth with rutile and leucoxene, and occurs on the surfaces and along cracks in plagioclase. Titanite forms between 150 and 220°C (Bird et al., 1984 and Reyes, 2000).

Epidote can replace plagioclase and pyroxene at the crystal surfaces and also occurs in cavities within primary minerals. In intensely altered rocks, epidote is disseminated in the groundmass but mostly it forms clusters together with chlorite and titanite. Epidote is also commonly associated with quartz and illite. As shown in Figures 5.19G-H, replacement epidote is mostly euhedral to subhedral with rims of opaques.

Epidote is first present between +700 and +900 m in wells DRJ S-1, S-3 and S-5; in the production area, i.e. around wells DRJ 4, 7, 9 and 13, it appears between +1000 and +1400 m. The abundance of epidote increases with depth, especially where actinolite and garnet coexist. However, in well DRJ

S-3, the amount of epidote decreases with depth between –100 and –200 m. Epidote abundance also decreases to the north, as in wells DRJ S-2 and S-6 it is absent. To the east, Amoseas Indonesia Inc. (1987 and 1989) reported that the shallowest occurrence of epidote is at elevations +1300 and +1400 m in wells DRJ 2, 3, and 5 (more than 2 km east DRJ S-5) but lower at +500 m in well DRJ 6 (1.5 km SW DRJ 1). At Darajat, epidote is commonly overprinted by calcite, such as at 1051 m depth in well DRJ S-1, where euhedral epidotes are present within calcite.

This mineral is stable above 250°C and up to 320-350°C (e.g. Elders et al., 1979 and Keith et al., 1968). Reyes (2000) reported that the crystal size and abundance of epidote might increase with increasing temperatures. Lithology seems to have an effect on the presence of epidote. About 1450 m depth, well DRJ S-3 penetrated andesite lava, lapilli tuff and andesite breccia; all are intensively altered to chlorite and quartz and epidote is dominant in the lavas and breccia but it is absent from pyroclastic tuff.

Actinolite and hornblende. Actinolite (Figures 5.20A-B) is mostly anhedral, dark green with high blue maximum interference colours. It is disseminated in the groundmass, replaces plagioclase from the crystal surfaces inward and fills vugs. Actinolite is usually associated with epidote, chlorite and opaque minerals. In well DRJ S-1 it occurs with prehnite.

Some amphiboles, like that in well DRJ S-1 at 1189 m depth, seem to be hornblende. This is subhedral to anhedral, but other crystals are prismatic, euhedral and green to brown or brownish-green with high interference colours. It can be distinguished from actinolite by its stronger pleochroism. Like actinolite, hornblende is also associated with chlorite and epidote and has rims of opaque minerals.

Actinolite is present mostly in the northern part of the field. It occurs between +500 and +750 m in well DRJ S-1 and 0 and +250 m in well DRJ S-3. Below these depths, actinolite is absent, eventhough epidote is still present. Actinolite is absent in well DRJ S-5. The distribution of actinolite forms a dome with a thickness of about 200 m (Figure 5.2). Actinolite is present at elevations about +1000 m in DRJ 5 and +600 m in production wells DRJ 4 and 7 (Amoseas Indonesia Inc., 1989).

Garnet is present in the epidote-rich zone, i.e. at the sea level and at an elevation of about +500 m in well DRJ S-3, and +800 m in well DRJ S-5. It is colourless to dark brown with opaque rims (Figure 5.20C). Actinolite and epidote are associated minerals (Figure 5.20D). Garnet and actinolite are stable above 260-280°C (Reyes, 2000).

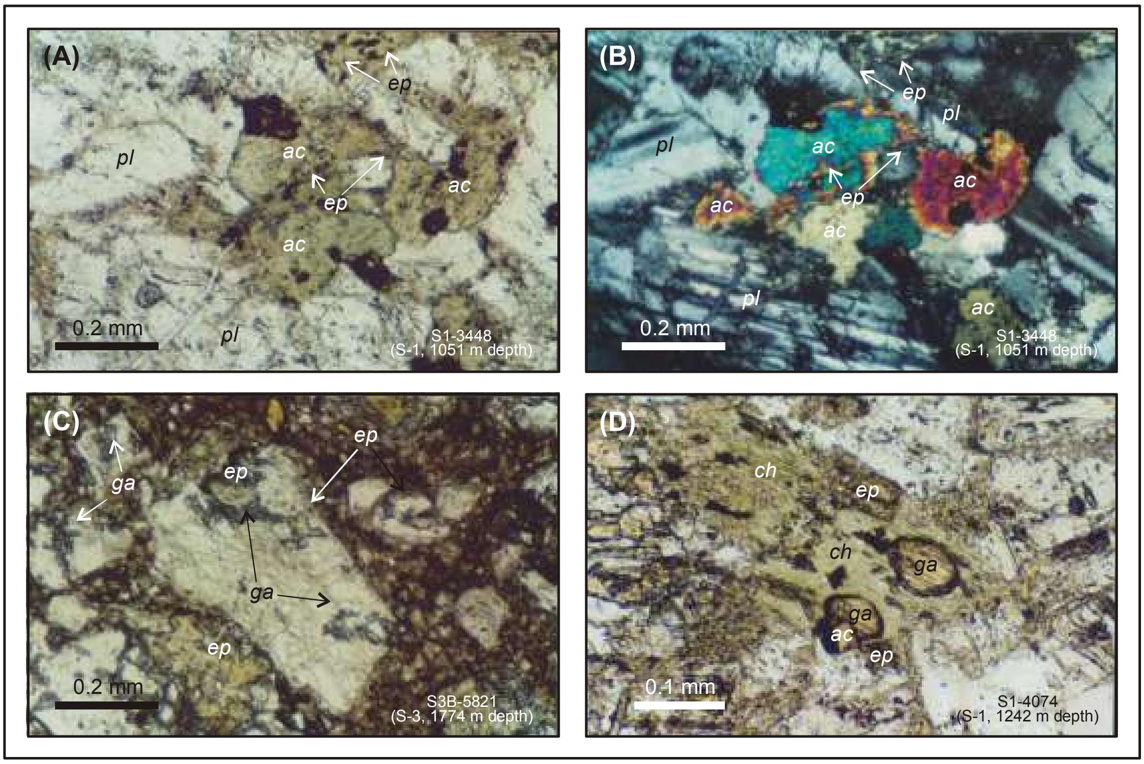

Figure 5.20.Actinolite and garnet. **(A)** Actinolite (*ac*) mostly replaces augite and hypersthene. Plane polars. **(B)** Cross polars view of figure (A). Actinolite is mostly associated with epidote (*ep*), which also replaces plagioclase (*pl*). **(C)** Anhedral and granular garnet in association with epidote (*ep*) replaces plagioclase. Plane polars. **(D)** Euhedral garnet and predating chlorite (*ch*) totally replace plagioclase and are associated with epidote (*ep*) and actinolite (*ac*). Plane polars. Sample numbers and locations are given.

5.2.4. Carbonates and anhydrite

Calcite. Replacement calcite forms through hydrolysis reaction involving calcium alumino-silicates and CO_2saturated water (Browne and Ellis, 1970, and Simmons and Christenson, 1994). It is the most common replacement hydrothermal mineral at Darajat. It is present mostly at shallow depths and its abundance decreases with increasing depth. Calcite replaces plagioclase, pyroxene and the groundmass (Figure 5.21A-B). Calcite may replace plagioclase crystals by up to 60% but it will usually completely replace pyroxene (e.g. at 350 to 900 m depth in well DRJ S-3). Calcite is more abundant in phenocrysts than in the groundmass. It is also more abundant in andesite lavas than in tuff (e.g. 1140 m depth of well DRJ S-3). Likewise, calcite is usually absent in the fine grained andesite lavas (e.g. at 1250 m depth in well DRJ S-5). Calcite replaces primary minerals, but secondary cavities form when it dissolves (e.g. ~250 m depth in well DRJ 1). Calcite is overprinted by quartz, chlorite and smectite but elsewhere, such as at 1007 m depth in well DRJ S-1, it postdates epidote, chlorite and quartz.

Anhydrite is also a common hydrothermal mineral in Darajat. It replaces plagioclase (Figure 5.21A) and pyroxene along cracks and from the crystal surfaces inward. It is also present as cavity filling, commonly associated with calcite. Anhydrite is present as shallow as +700 to +800 m in wells DRJ S-1, S-2 and S-6, and +1000 m in well DRJ S-3, but its distribution becomes shallower to the south, i.e. about +1400 m in well DRJ S-5 (Figure 5.2).

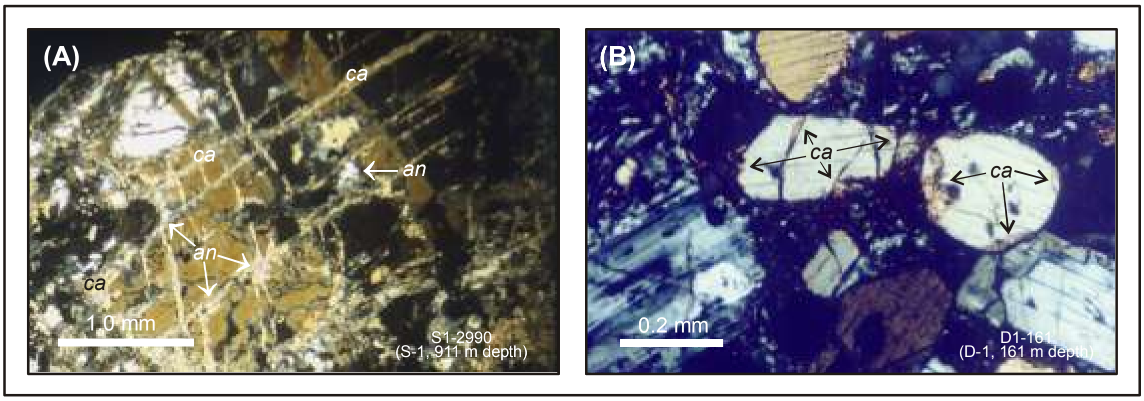

Figure 5.21.The occurrences of calcite and anhydrite. **(A)** Calcite (*ca*) and anhydrite (*an*) replacing plagioclase along cracks. Cross polars. **(B)** Calcite (*ca*) also replacing augite along cracks and at the surface of crystal. Cross polarised light. Sample numbers and locations are given.

5.2.5. Feldspars

Adularia occurs mostly as a plagioclase replacement. Figure 5.22 shows it forms diamond shape crystals clustering along cracks in plagioclase (e.g. below +950 m in well DRJ S-1). It also occurs as big, euhedral, diamond shaped crystals in places within the groundmass, e.g. at about 1980 m depth in well DRJ S-3. However, adularia is likely overprinted along cracks by chlorite, illite and, sometimes, calcite. About 1350 m depth in well DRJ S-3, adularia is present with epidote and laumontite replacing plagioclase along cracks (Figures 5.22C-D).

Adularia indicates good permeability (Browne, 1978). The distribution of its shallowest occurrence is in the form of a broad dome (Figure 5.2). Adularia occurs in shallowest depth in wells DRJ S-1 and S-5 at +700 and +100 m respectively, i.e. at the same depth of the top reservoir condition reported by Amoseas Indonesia Inc. (1989a). In well DRJ S-3, its shallowest appearance is at about +1100 m and in wells DRJ S-2 at +900 m. It is between 600 and 800 m above the top of reservoir. The shallowest occurrence of adularia in well DRJ S-6 is at -100 m.

Albite (Na-feldspar) replaces plagioclase phenocrysts along cracks but also occurs in the microcrystalline groundmass, e.g. at 1201 m depth in well DRJ S-3. Albite is likely to occur where adularia is abundant.

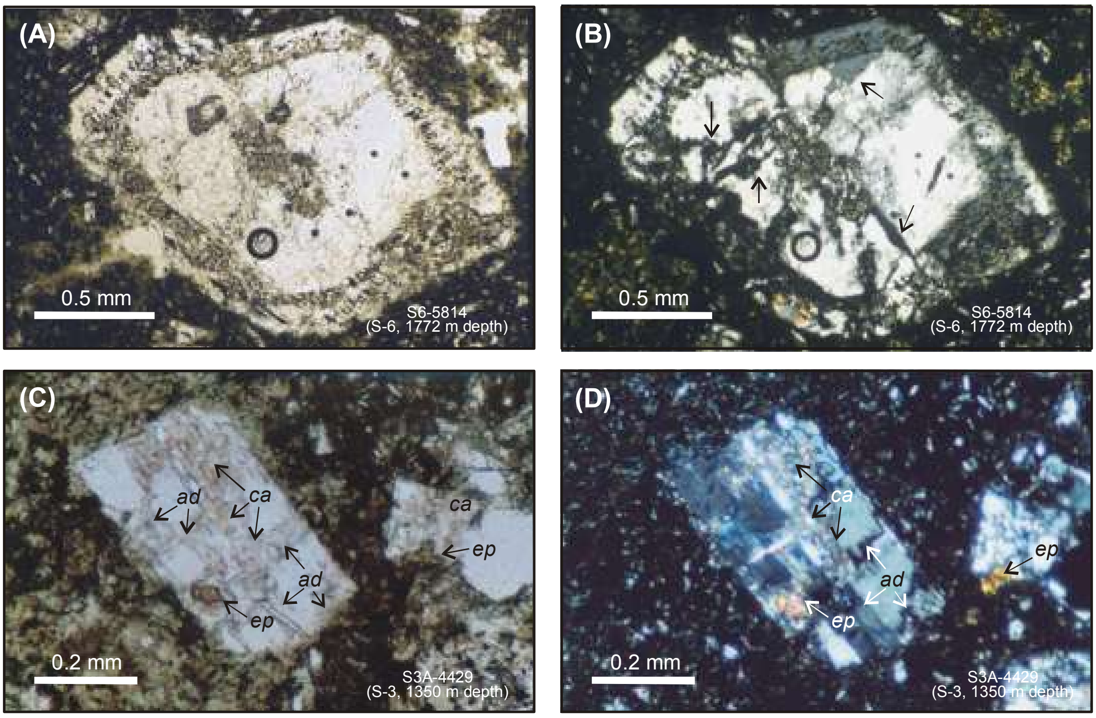

Figure 5.22.Adularia as replacement in plagioclase. **(A)** It mostly occurs along cracks of plagioclase (see arrows). Plane polars. **(B)** Cross polars view of (A). **(C)** Adularia (*ad*) is present with calcite (*ca*) along cracks of plagioclase. It is also associated with epidote (*ep*). Plane polars. **(D)** Cross polars of (C). Sample numbers and locations are given.

5.2.6. Other minerals

Alunite (Figures 5.23A-B) forms subhedral, elongate, mostly radiating crystals, replacing plagioclase at shallow depths, e.g. at 43 m depth in well DRJ 2. Amoseas Indonesia Inc. (1989) recorded that alunite in association with kaolinite is present above 400 m in a production well DRJ 7. Alunite commonly forms due to oxidation of H_2S to sulfate in a steam condensate layer, i.e. in acid conditions (pH about 1.5; Reed, 1974) and temperatures between 60 and 180°C (Ebert and Rye, 1997); at high temperatures, anhydrite is more common (Reyes, 2000).

Alunite is indicated by the appearance of peaks at 2.89-2.99, 2.29, 1.93 and 4.96 Å. The d-spacing of the first reflection will be higher with greater K and Fe contents, which substitute for Na and Al respectively (Alpers et al., 1992).

Diaspore occurs as less than 0.025 mm long, diamond shaped crystals. Diaspore appears only at about +100 m in well DRJ S-3, where pyrophyllite is also present. Diaspore generally occurs at temperatures above 120°C (Reyes, 1990) and at a pH of about 2.2 (Africano and Bernard, 2000).

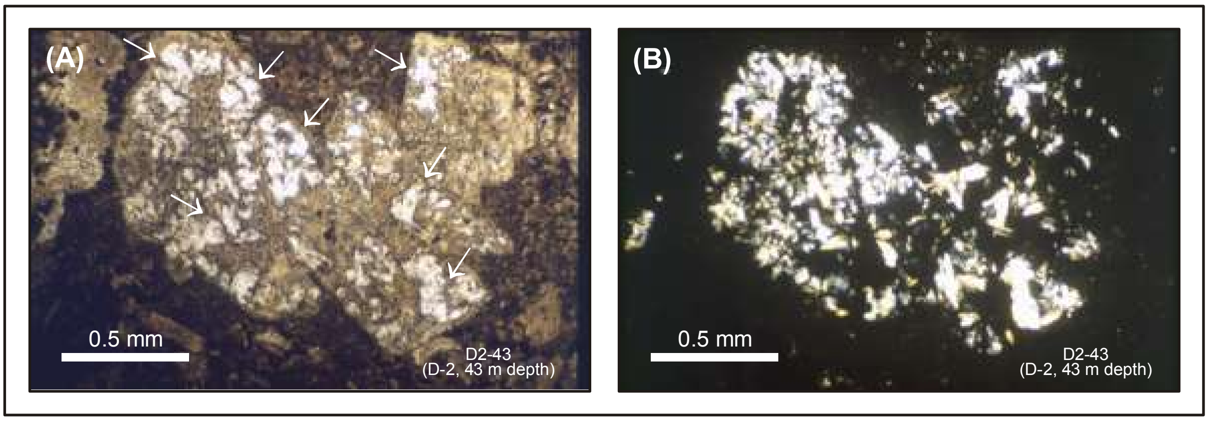

Figure 5.23.Alunite (see arrows) as replacement in plagioclase. **(A)** Plane polarised light. **(B)** Cross polarised light of (A) showing alunite with low birefringence. Sample numbers and locations are given.

Tourmaline is characterised in thin section as euhedral, elongate, 0.1-0.6 mm long crystals with green to blue pleochroism. It forms radiating clusters and replaces plagioclase on crystal surfaces. It is associated with calcite and anhydrite at elevations of +400 to +800 m in well DRJ S-1 and about +1200 m in well DRJ S-5. Tourmaline is absent in cores from other wells.

Biotite (Figure 5.24) is rare. It replaces plagioclase and pyroxene along cracks and on crystal surfaces in about –500 m in production well DRJ 17 and +150 m in DRJ 13. It is also disseminated in groundmass and fills vugs. Amoseas Indonesia Inc. (1989) also recorded that biotite occurs at about sea level in well DRJ 5.

Biotite is mostly associated with illite and amphiboles. Biotite is stable at a minimum temperature of 400°C (Gianelli and Ruggieri, 2002) under reduction condition (D'Amore and Gianelli, 1984) but it could also form at lower temperatures.

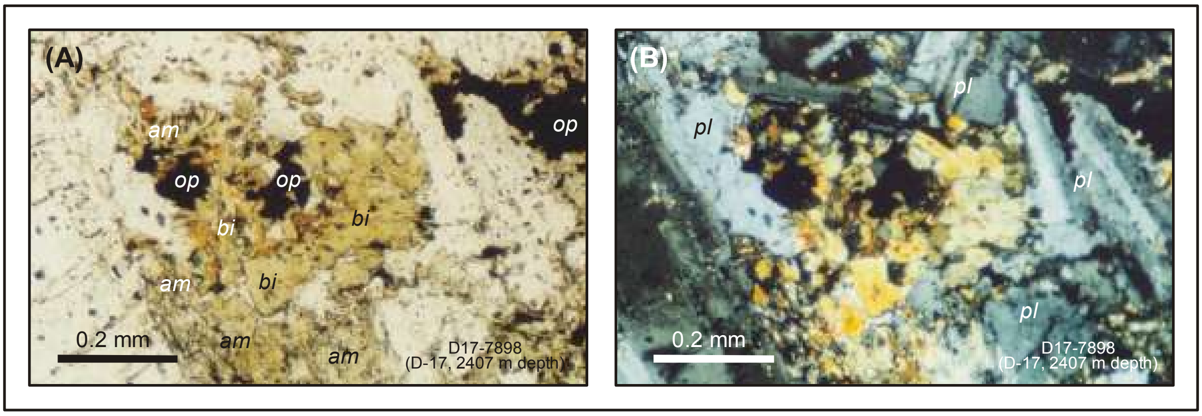

Figure 5.24.Hydrothermal biotite. **(A)** Biotite (*bi*) with strong pleocroism present with amphiboles (*am*) and opaque minerals (*op*). Plane polars. **(B)** Cross polars view of (A) shows that biotite and amphiboles replace plagioclase (*pl*).

Apatite, disseminated in groundmass, is very rare. It mostly fills vugs (see Chapter 5) and associated with rutile, titanite and chlorite, e.g. 1058 m depth of well DRJ S-1 and 960 m depth of DRJ S-5 (Figure 5.25). Many studies showed that apatite can form from two types of fluid, i.e. high temperature (hotter than 450°C), volatile rich magmatic fluid (e.g. Mark and Foster, 2000; and Pollard, 2001) and 250-350°C, high CO_2, boiling water (e.g. Sheets et al., 1997). Reyes et al. (1993) reported that apatite commonly forms in association with anhydrite in vapour-dominated magmatic-hydrothermal systems.

Pyrite, rutile and leucoxene. Pyrite is common, disseminated in the groundmass and rims the surface of plagioclase crystals. Rutile and leucoxene are reddish brown and commonly associated with pyrite and other opaque minerals. Figure 5.25 shows that they can be easily distinguished from pyrite and other opaque minerals by using back scattered X-ray image. Pyrite, rutile and leucoxene are associated with other hydrothermal minerals, e.g. titanite, epidote and chlorite (Figure 5.25). They also seem to replace primary titanomagnetite and be an oxidation product of glass, smectite and chlorite. In addition, pyrite is abundant in well DRJ S-3, i.e. at ~2120 m depth, where pyrophyllite also occurs.

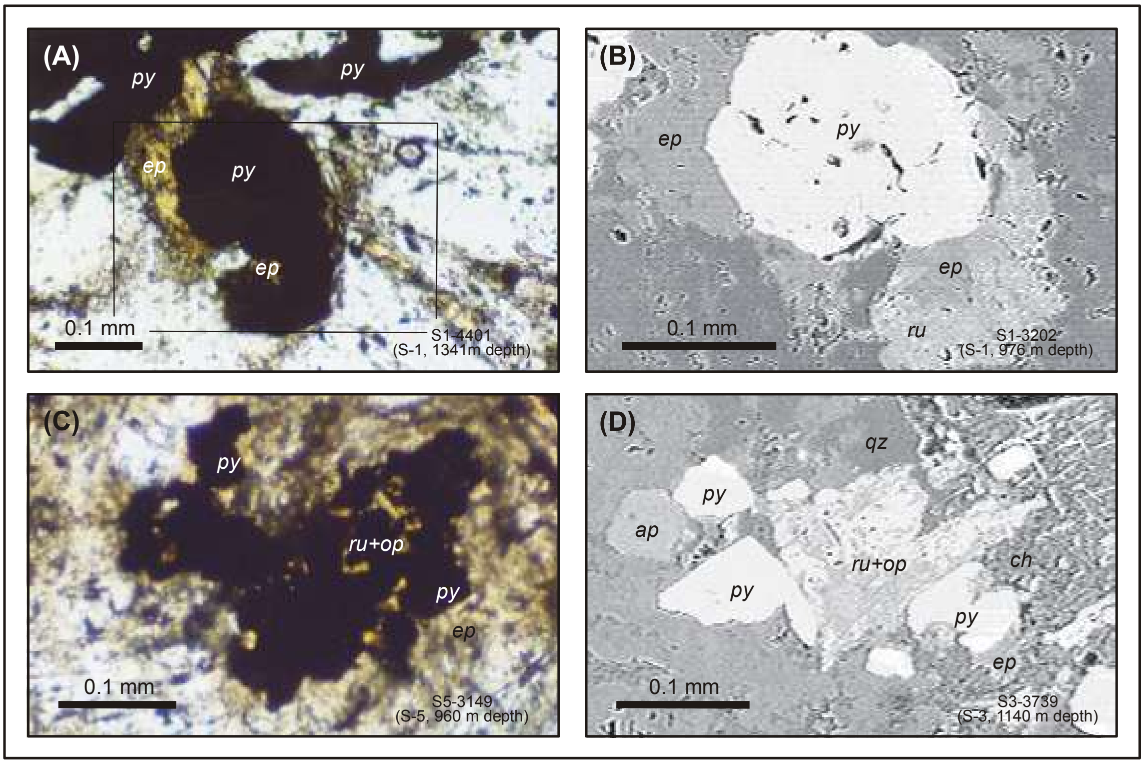

Figure 5.25.Secondary rutile. **(A)** Rutile is red brown to dark brown in plane polars, hardly distinguished with pyrite (*py*) and other opaque minerals, but it differs from epidote (*ep*). **(B)** Back scattered image of the area in figure (A) can distinguish rutile (*ru*) and pyrite (*py*), present in association with epidote (*ep*). **(C)** Rutile (*ru*) in association with pyrite (*py*) and opaque minerals (*op*) is present in the groundmass. Epidote (*ep*) also occurs in the matrix. **(D)** Back scattered image of figure (C) showing intergrown rutile (*ru*) and opaque minerals (*op*). Apatite (*ap*) is commonly associated with rutile. Chlorite (*ch*) replaces plagioclase phenocrysts and quartz (*qz*) is present in the matrix. Sample numbers and locations are given.

5.3. DISCUSSION

The occurrence of hydrothermal minerals in the matrix of the rocks records the types of circulating fluids that interacted with the surrounding rocks and their presence can be used to estimate changes in the fluid characteristics. In general, the deep fluid of the Darajat geothermal system had neutral pH. This fluid boiled, followed by cooling from above 300 to about 200°C and allowed calc-silicates, e.g. garnet, actinolite, epidote and wairakite, to form in association with adularia and chlorite (Figures 5.1 and 5.2).

Steam resulting from deeper boiling condenses into groundwater and produces high X_{CO_2} condensate above the boiling zone. Mixing between the deeper fluid and steam condensate water occurred in a transitional zone. In the marginal wells DRJ S-2 and S-6, steam condensate also occurs separately as well as mixing with cold water. There is also evidence that a hot acid magmatic fluid is present in well DRJ S-3 indicated by the occurrence of pyrophyllite and diaspore.

Well DRJ S-1 is divided into 3 zones with different styles of hydrothermal alteration. Below 1250 m depth, the hydrothermal minerals present are wairakite, prehnite and epidote in association with chlorite and illite (Figure 5.3). Calcite and anhydrite are minor. This indicates the occurrence of neutral pH with very low dissolved CO_2 (X_{CO_2}).

Between 1000 and 1250 m, the appearance of garnet and actinolite suggests less X_{CO_2}in the water. However, at about 1000 m depth there is an increase in the abundance of calcite (Figure 5.3). Calcite becomes dominant above 1000 m, as calc-silicates and adularia disappear(Figure 5.3). This indicates that the thermal fluid contained high X_{CO_2} as steam condenses into groundwater. Chlorite becomes Mg rich and poorly crystalline (Figure 5.8). Smectite and interlayered illite and smectite are present above 700 m, whereas illite is present below it. This suggests heating descending fluid from below 220 to about 300°C. Since anhydrite has a reverse solubility, the occurrence of this mineral below 900 m suggests that the water is descending and heating (Moore and Adams, 1988). At about 1000 m depth, the steam condensate water, containing high X_{CO_2} that mixes with the lower X_{CO_2} deep fluid, resulting an increase in abundance of calcite, as mentioned before.

Well DRJ S-2 has the simplest hydrothermal alteration pattern. The minerals present include calcite and Fe rich chlorite (Figures 5.4 and 5.9). Anhydrite and illite are minor; the latter only appears below 1200 m. The occurrence of hydrothermal minerals indicates that the thermal fluid had high X_{CO_2} due to steam condensation. The occurrence of kaolinite suggests that the fluid was slightly acid. Mixing and cooling might occur above 1200 m, indicated by the appearance of smectite and poorly crystalline chlorite (Figure 5.9).

Well DRJ S-3. Below 2100 m depth, the hydrothermal minerals present are epidote, adularia and chlorite. Anhydrite is minor. Neither calcite nor illite appears (Figure 5.5). The occurrence of hydrothermal minerals suggests boiling of neutral pH, low X_{CO_2} deep fluid. Between 1400 and 2100 m depth, the occurrences of actinolite, prehnite and secondary feldspars (Figure 5.5) confirm a decrease in X_{CO_2} and an increase in pH respectively as a result of boiling.

However, illite and calcite are also present and suggest mixing of low pH, high X_{CO_2} fluid. The acid fluid is likely of magmatic origin with temperatures as high as 500°C, as indicated by the occurrence of pyrophyllite at about 2100 m depth (Figure 5.5). When the hot acid magmatic fluid mixed with the deep fluid and interacted with the surrounding rocks, the temperatures and the acidities of the mixed fluid were still high and neutral enough to allow calc silicates, e.g. garnet and actinolite, to form.

Between 900 and 1400 m depth, cooling occurs, indicated by the appearance of smectite and laumontite but the disappearance of epidote (Figure 5.5). Above 900 m, all calc silicates and adularia are absent. Calcite and Mg rich chlorite are dominant (Figures 5.5 and 5.10). Steam condensate increases the amount of CO_2 in the thermal fluid and thus calc silicates cannot form. A decrease in the proportion of smectite but an increase in illite in the interlayered illite and smectite from 600 to 900 m depth suggest that the CO_2 rich steam condensated water is heated downward.

Well DRJ S-5. The occurrences of epidote, wairakite and adularia suggest boiling of neutral pH, low X_{CO_2} fluid below 2000 m (Figure 5.6). Calcite and anhydrite are minor but become dominant between 1400 and 2000 m. This indicates that the deep fluid becomes CO_2 rich causing calc silicates to disappear. Heating likely occurs downward, indicated by an increase in the proportion of illite in the interlayered illite and smectite with depth.

Between 1200 and 1400 m depth, epidote and garnet occur in association with calcite, anhydrite and chlorite (Figure 5.6). This suggests boiling. A decrease in X_{CO_2}, following boiling, allows calc silicate to form after calcite. High X_{CO_2} steam condensate occurs above 1200 m indicated by the dominance of calcite and anhydrite in association with chlorite, smectite and illite.

Well DRJ S-6 is the northernmost well. However, the occurrence of adularia below 1600 m (Figure 5.7) suggests that boiling still occurs. The occurrence of calcite indicates that the thermal fluid was high X_{CO_2}. Above 1600 m, the absence of adularia but the dominance of Fe rich chlorite and calcite in association with laumontite at low-intensity altered rocks (Figures 5.7 and 5.12) suggest cooling.

Chapter 6

VEIN MINERALOGY

The occurrence of hydrothermal minerals in veins and fractures records changes in the fluid characteristics, likely related to changes in the reservoir conditions and processes affecting the circulating thermal fluids. The identifications of hydrothermal alteration are mainly based upon petrography analyses as described in the Appendix B.

6.1. CHARACTERISTIC OF VEINS

6.1.1. Veins and veinlets

Most veins and veinlets dip 80° to almost vertical with respect to the core axes but some dip0-10°. In well DRJ S-1, as indicated by the cross cutting veins, the horizontal veins are older than the vertical ones. Other old veins include cross cutting 30-60° and 40-50° dipping veins. These veins are older than almost all the vertical veins, as indicated by their cross cutting relationship, e.g. below 1300 m in well DRJ S-1.

Veins filled by calcite, anhydrite, quartz, chlorite and epidote are mostly up to 5 mm wide. Opaque minerals, such as pyrite and chalcopyrite, may fill veins less than 0.5 mm wide, but zeolites, such as laumontite and wairakite, occurs in wider veins, mostly 5 to 20 mm wide. Most hydrothermal minerals show a sequence of deposition presumed to be from oldest at the margin to youngest in the middle of the vein.

Brecciated veins are present at about 600 m depths in well DRJ S-2 and 700 m depth in DRJ S-3. They contain rock fragments and hydrothermal minerals, mostly calcite and quartz, filling inter-fragment pores. At about 950 m depth in DRJ S-2, laumontite is present as inter-fragment filling. In well DRJ S-3 at 1550 m depth, a micro scale brecciated vein is present, with altered andesite lavas present as fragments in a calcite-filled vein. Browne and Lawless (2001) suggested that subsurface brecciatiation, i.e. brecciated veins, can form by the forceful disruption of the host rocks by lowering the pressure to promote boiling to produce steam.

Discontinuous veins are common, e.g. at about 950 m depth in well DRJ S-2, where veinlets are up to 8 mm wide and up to 2 cm long. They are usually filled by calcite in association with laumontite.

6.1.2. Fractures

Fracture surfaces are coated by mm to cm thick layers of hydrothermal minerals, mostly dipping at 80-90°, but about 70° dip fractures are also common, e.g. at about 1200 and 2300 m depths in well DRJ S-5. Gentler fractures include those with 20-30° dips (e.g. at about 1600 m depth in well DRJ S-6), 30-40° dip (e.g. at about 1000 m depth in well DRJ S-1) and 60° dip fractures (e.g. at about 2100 m depth in well DRJ S-5). In well DRJ S-5, an almost horizontal fracture is present at 950 m depth.

Some fractures have striae on their surfaces, which indicate movement. A normal (or reverse) fault is likely present at about 1550 and 750 m depths in wells DRJ S-3 and S-5 respectively. A fault with strike slip movement dips at 20-30° with respect to core axis in well DRJ S-6, i.e. at 1600 m depth.

6.2. OCCURRENCE AND DISTRIBUTION OF HYDROTHERMAL MINERALS

Figure 6.1 shows the distribution of minerals present in veins in wells DRJ S-5 through S-3, S-1 and S-2, to S-6, i.e. from south to north in the field. The occurrence of minerals in individual wells is summarised in Figures 6.2 to 6.6.

6.2.1. Silica

Quartz is very common in fractures, veins and vugs. It is usually anhedral, massive and compact, but some are euhedral with crystals up to 2 mm long. In the open spaces, euhedral quartz can be up to 5 mm long. Less than 0.5 mm long, euhedral quartz crystals are rare on the surface of other minerals, e.g. calcite and wairakite (Figure 6.7). Unlike anhedral quartz, which forms lamellar and band textures, euhedral quartz in veins, especially in open space, commonly has comb textures. Quartz is mostly white or clear, but it is also milky, rose coloured and smoky. Quartz from about 2100 m depth in well DRJ S-5 is light green and transluent. This might be due to micro inclusions of epidote or actinolite.

Other silica phases. Chalcedonic quartz is present in well DRJ S-3 at about 617 and 1982 m depths. It forms spherical masses in the margins of veins, is associated with chlorite and overprinted by milky quartz. Quartz clusters, as rosettes, at about 930 m depth in well DRJ S-1, might be a relict botyroidal of chalcedony. Here, chalcedonic quartz is associated with anhydrite and calcite (Figure 6.8).

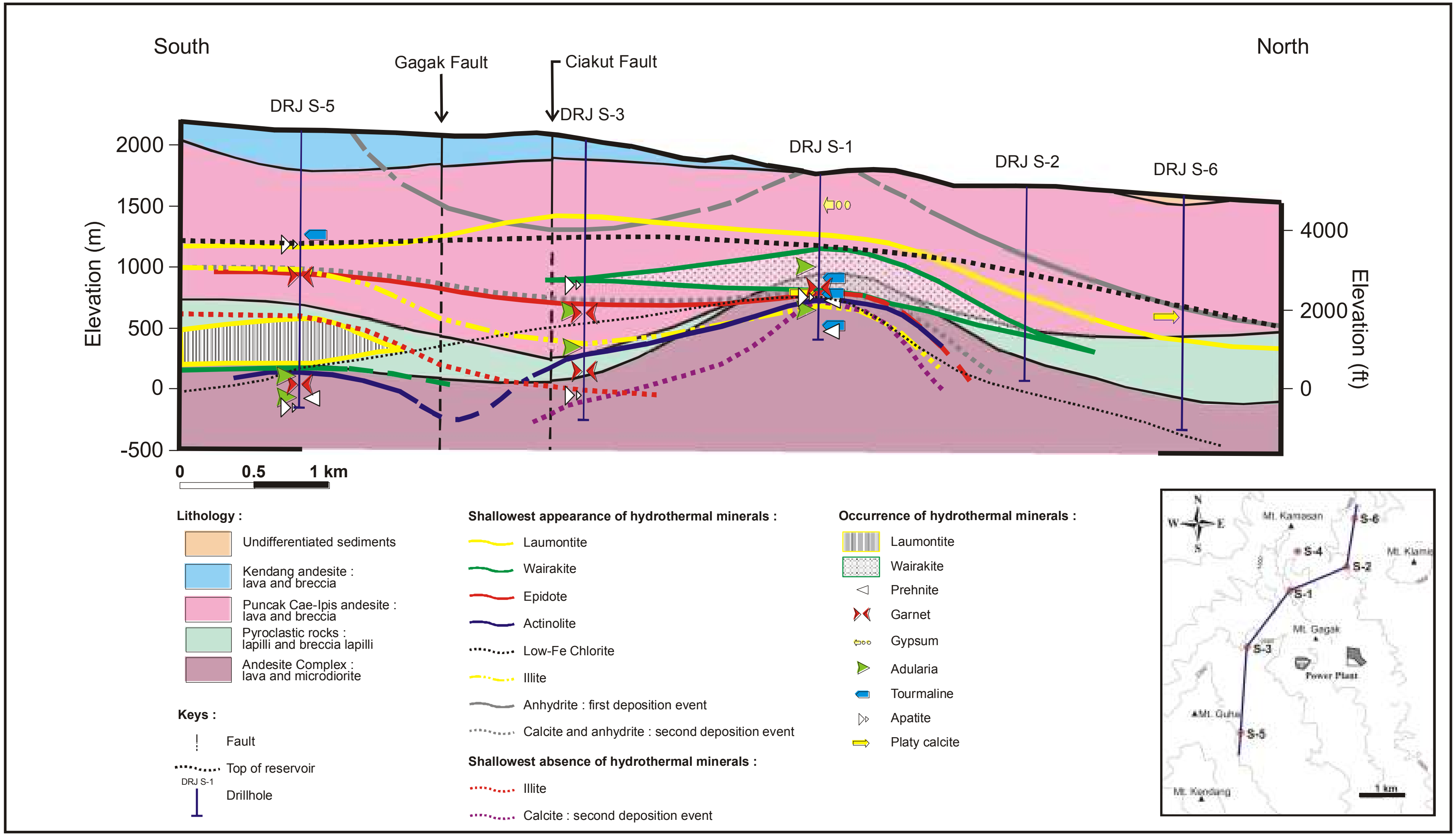

Figure 6.1. South-north cross-section, from DRJ S-5, S-3, S-1, S-2 to S-6, showing the distribution of hydrothermal minerals present in veins.

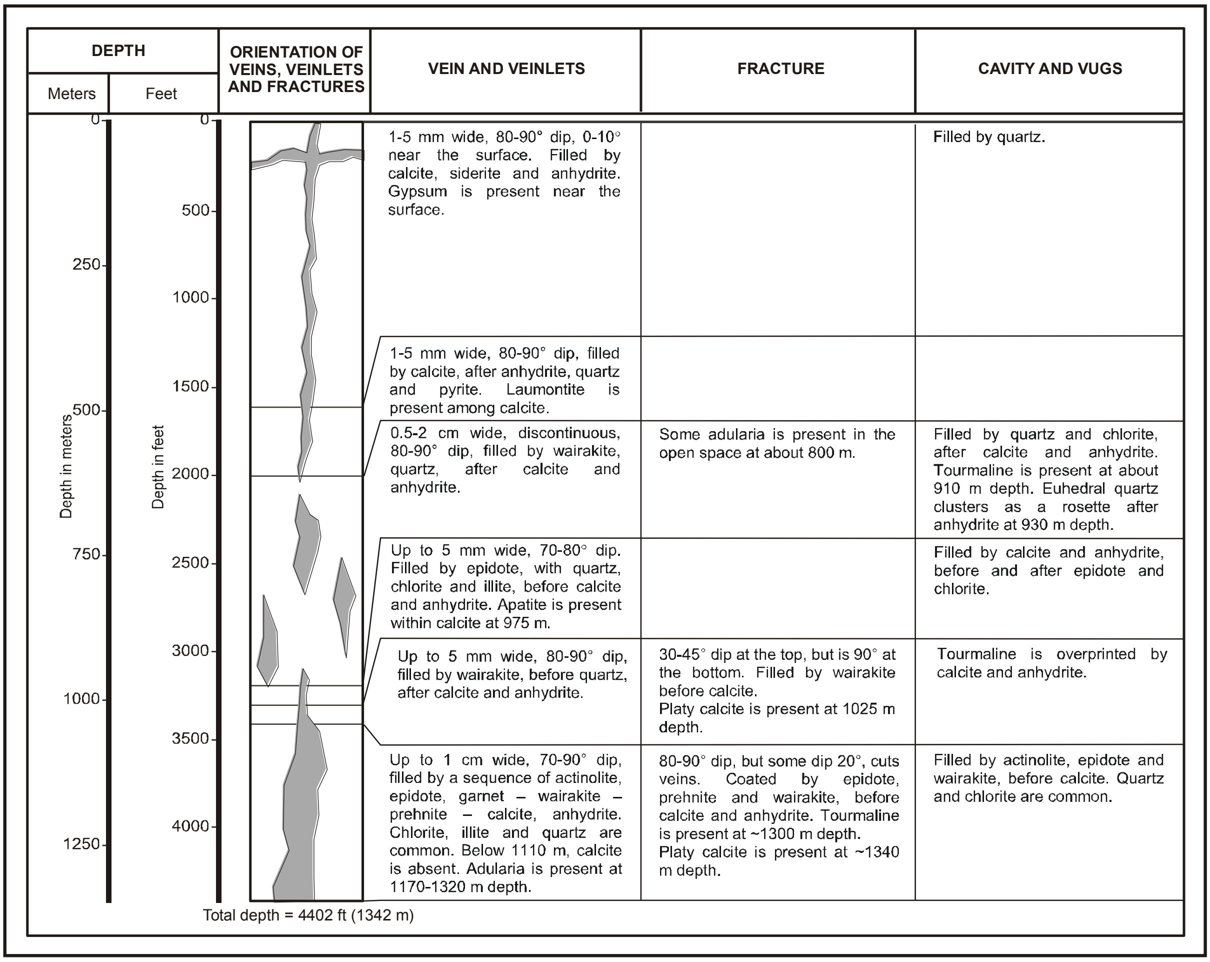

VEIN AND VEINLETS	FRACTURE	CAVITY AND VUGS
1-5 mm wide, 80-90° dip, 0-10° near the surface. Filled by calcite, siderite and anhydrite. Gypsum is present near the surface.		Filled by quartz.
1-5 mm wide, 80-90° dip, filled by calcite, after anhydrite, quartz and pyrite. Laumontite is present among calcite.		
0.5-2 cm wide, discontinuous, 80-90° dip, filled by wairakite, quartz, after calcite and anhydrite.	Some adularia is present in the open space at about 800 m.	Filled by quartz and chlorite, after calcite and anhydrite. Tourmaline is present at about 910 m depth. Euhedral quartz clusters as a rosette after anhydrite at 930 m depth.
Up to 5 mm wide, 70-80° dip. Filled by epidote, with quartz, chlorite and illite, before calcite and anhydrite. Apatite is present within calcite at 975 m.		Filled by calcite and anhydrite, before and after epidote and chlorite.
Up to 5 mm wide, 80-90° dip, filled by wairakite, before quartz, after calcite and anhydrite.	30-45° dip at the top, but is 90° at the bottom. Filled by wairakite before calcite. Platy calcite is present at 1025 m depth.	Tourmaline is overprinted by calcite and anhydrite.
Up to 1 cm wide, 70-90° dip, filled by a sequence of actinolite, epidote, garnet – wairakite – prehnite – calcite, anhydrite. Chlorite, illite and quartz are common. Below 1110 m, calcite is absent. Adularia is present at 1170-1320 m depth.	80-90° dip, but some dip 20°, cuts veins. Coated by epidote, prehnite and wairakite, before calcite and anhydrite. Tourmaline is present at ~1300 m depth. Platy calcite is present at ~1340 m depth.	Filled by actinolite, epidote and wairakite, before calcite. Quartz and chlorite are common.

Total depth = 4402 ft (1342 m)

Figure 6.2.Occurrence of hydrothermal minerals in veins, on fracture surfaces and in cavities in well DRJ S-1.

6.2.2. Calc-silicates

Laumontite(Figures 6.9A-B and 6.10A-C) is mostly present in wide veins and open fractures. It is rare in vugs and cavities. Its shallowest occurrences are at elevations of +1100 to +1400 m in the south and +800 to +1200 m in the north. Laumontite is present at elevations of about +400 m in well DRJ -6 but absent below +600 to +800 m. In well DRJ S-5, it is present between elevations of +200 and +600 m.

Laumontite usually deposited after calcite and anhydrite as white, euhedral, 2-3 mm long, soft, prismatic and radiating crystals. In some places, it is platy and fan shaped. In open spaces at several depths in well DRJ S-5, laumontite crystals reach 8 mm long, but are up to 0.5 mm long only in a vein in well DRJ S-6. Laumontite hydrate to form stilbite, which is dendritic, about 0.5 mm long and present in open space at about 840 m depth in well DRJ S-5.

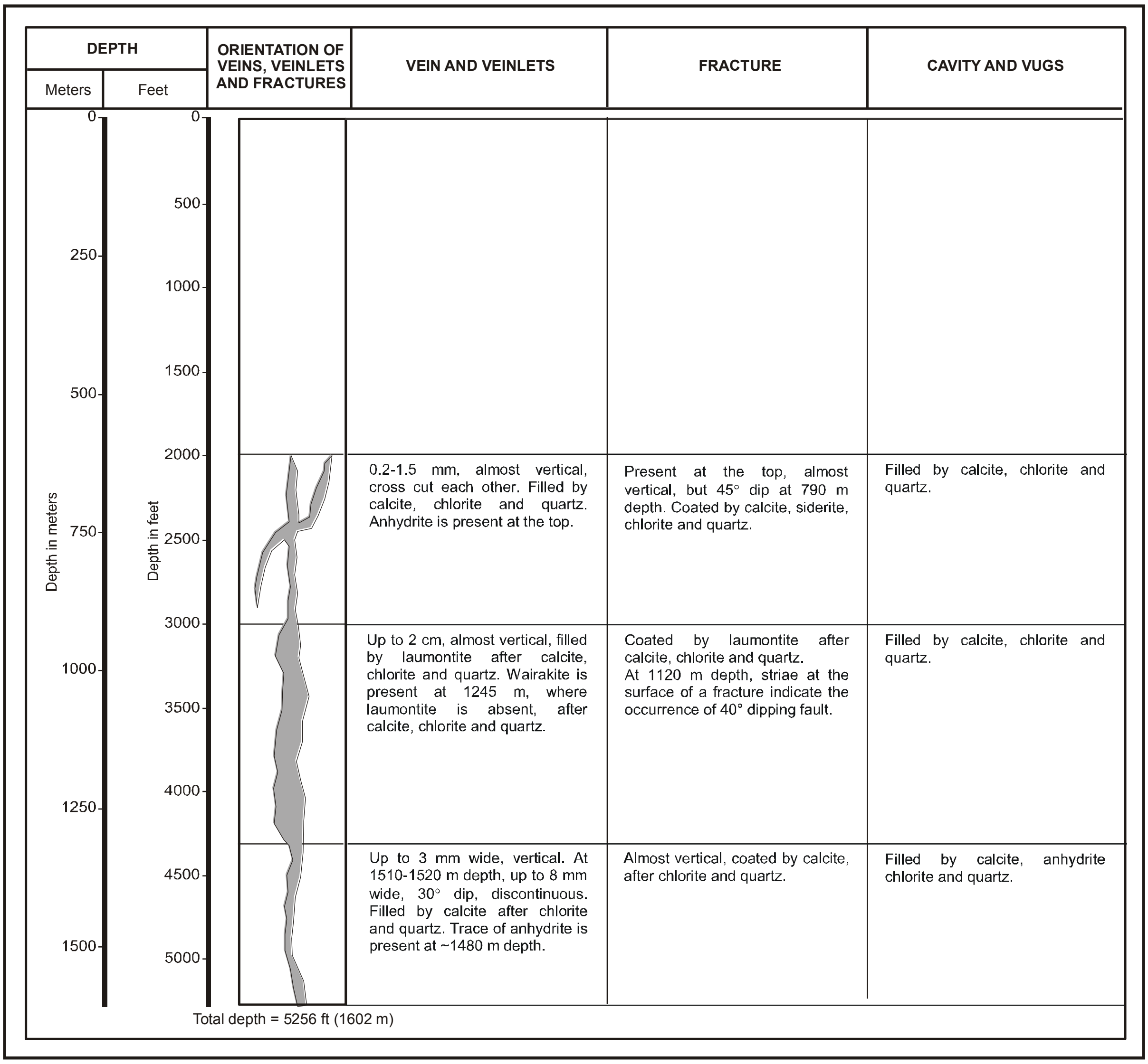

DEPTH	ORIENTATION OF VEINS, VEINLETS AND FRACTURES	VEIN AND VEINLETS	FRACTURE	CAVITY AND VUGS
		0.2-1.5 mm, almost vertical, cross cut each other. Filled by calcite, chlorite and quartz. Anhydrite is present at the top.	Present at the top, almost vertical, but 45° dip at 790 m depth. Coated by calcite, siderite, chlorite and quartz.	Filled by calcite, chlorite and quartz.
		Up to 2 cm, almost vertical, filled by laumontite after calcite, chlorite and quartz. Wairakite is present at 1245 m, where laumontite is absent, after calcite, chlorite and quartz.	Coated by laumontite after calcite, chlorite and quartz. At 1120 m depth, striae at the surface of a fracture indicate the occurrence of 40° dipping fault.	Filled by calcite, chlorite and quartz.
		Up to 3 mm wide, vertical. At 1510-1520 m depth, up to 8 mm wide, 30° dip, discontinuous. Filled by calcite after chlorite and quartz. Trace of anhydrite is present at ~1480 m depth.	Almost vertical, coated by calcite, after chlorite and quartz.	Filled by calcite, anhydrite chlorite and quartz.

Figure 6.3.Occurrence of hydrothermal minerals in veins, on fracture surfaces and in cavities in well DRJ S-2.

Wairakite is mostly present in open fractures as euhedral, dodecahedral, clear, shiny crystals, up to 2 mm in diameter. They may be bigger, i.e. 3-5 mm across, in open space (e.g. in well DRJ S-1 at 1058 m depth) or anhedral (Figures 6.9C-D and 6.10D).

Wairakite mostly occurs deeper than laumontite, but it can also coexist with it. Wairakite is dominant in well DRJ S-1 from +800 to +1200 m. At shallow depths, like laumontite, wairakite deposited after both calcite and anhydrite, but at depth, it is overprinted by them. In wells DRJ S-3 and S-2, wairakite occurs locally at elevations of about +900 and +500 m respectively, where it deposited after calcite and anhydrite. In well DRJ S-5, wairakite, in association with traces of laumontite, deposited below +200 m before calcite and anhydrite.

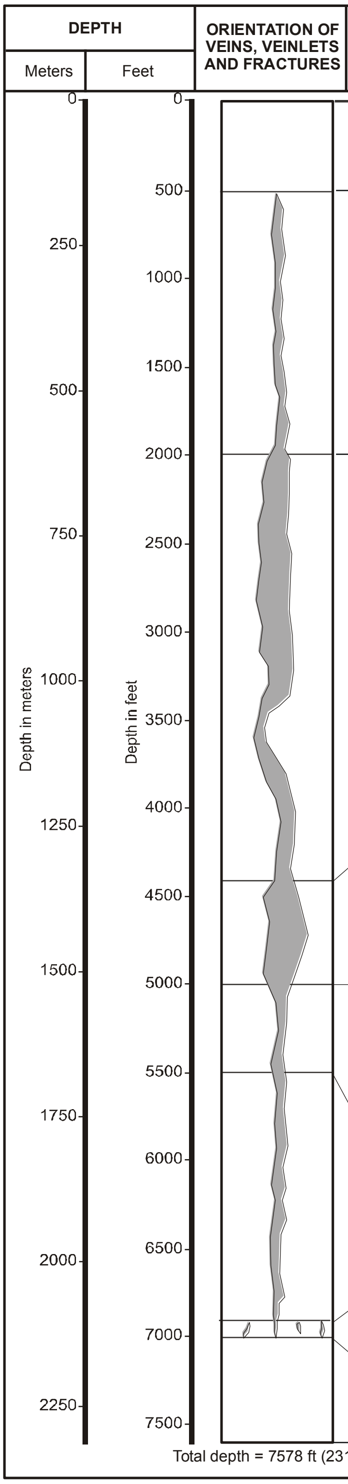

VEIN AND VEINLETS	FRACTURE	CAVITY AND VUGS
Up to 4 mm wide, 90° dip, filled by calcite, siderite, chlorite, quartz and opaque minerals. Laumontite and trace of wairakite are deposited after calcite and quartz.	70-80° dip, filled by a sequence of chlorite – calcite – laumontite.	Filled by a sequence of chlorite – calcite, siderite – laumontite. Quartz is common.
Up to 4 mm, can be 1-2 cm at ~900 m depth, almost vertical, but between 1050-1200 m depth is 40-70° dip. Filled by calcite and anhydrite after chlorite, quartz and pyrite. Laumontite and wairakite are present at 930 and 1140 m depths respectively, deposited after calcite.	Vertical at 900 m depth, filled by calcite and pyrite. Euhedral quartz is present on the surface of calcite at 1140 m depth.	Filled by calcite, anhydrite, chlorite and quartz. Wairakite is present at ~1140 m depth. Apatite is present among calcite at 1140 m depth.
More than 2 cm wide, vertical, filled by epidote, chlorite and quartz, before calcite and anhydrite. Wairakite is present at some depths and adularia is present at ~1460 m depth.	70-80° dip, coated by calcite and anhydrite after chlorite and quartz.	~1 cm across, filled by chlorite, quartz, calcite and anhydrite. Epidote is deposited before calcite.
Up to 4 mm wide, 80-90° dip, filled by chlorite, before calcite and anhydrite. Quartz is common. Euhedral quartz is present at ~1600 m depth. Trace epidote appears at ~1460 m depth, but absent below.	40-50° dip and coated by chlorite, quartz and calcite. The presence of striae in the surface indicate a fault at 1540 m depth.	Filled by chlorite and quartz.
Up to 7 mm wide, 80-90° dip, but 40-50° at ~1855 m depth. Filled by a sequence of chlorite, quartz – epidote, actinolite, garnet – calcite, siderite, anhydrite. Trace of prehnite is present among euhedral epidote at 1775 m depth. Adularia is present at 1780 m depth. Apatite is likely present at ~1980 m depth.		Filled by actinolite and epidote. Chlorite, quartz, calcite and anhydrite deposited before and after epidote. Illite and opaque minerals are common.
~1 mm wide, filled by pyrite, chlorite and quartz. Calcite and anhydrite are absent.		Filled by pyrite and chlorite.
	70-80° dip and coated by a sequence of chlorite – wairakite, epidote, quartz – calcite.	Filled by a sequence of chlorite – epidote, quartz – anhydrite. Calcite is absent.

Total depth = 7578 ft (2310 m)

Figure 6.4.Occurrence of hydrothermal minerals in veins, on fracture surfaces and in cavities in well DRJ S-3.

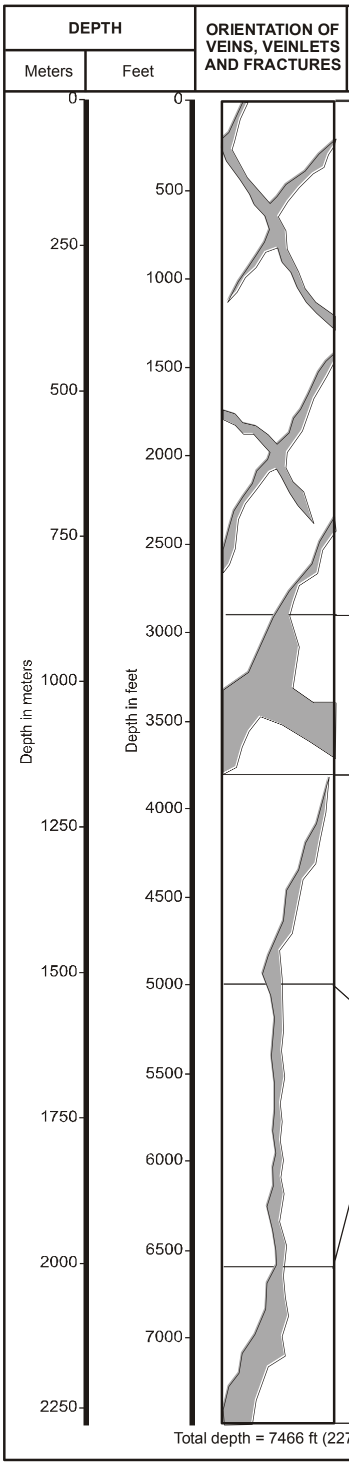

VEIN AND VEINLETS	FRACTURE	CAVITY AND VUGS
Up to 5 mm wide, 40-60° and 130° dips, cross cut each other. Filled by calcite and anhydrite, after chlorite, quartz and pyrite. Natron and stilbite are present at ~840 m depth.	45° dip at ~750 m depth. Striae in the surface indicates a fault at ~840 m depth.	
0.5-2 cm wide, 40-50° and 130-140° dips. Filled by laumontite, after chlorite, quartz, calcite and anhydrite. Tourmaline is present at 890 m depth, deposited before calcite and anhydrite.	70-80° and 0-10° dip. Coated by chlorite, quartz, calcite, anhydrite and pyrite.	Filled by chlorite, quartz, opaque minerals, calcite and anhydrite. Apatite is present at 890 m depth. Laumontite is present in <2 cm diameter cavities at 940 m depth, deposited after quartz, calcite and anhydrite.
Up to 5 mm wide, 60-80° dip and filled by a sequence of chlorite, illite, quartz – calcite, anhydrite – epidote – calcite, anhydrite. Laumontite deposited before calcite and anhydrite in <3 cm wide veins between 1240 and 1370 m depth. At 1370 m depth, epidote and quartz deposited after laumontite, calcite and anhydrite.	70-80° dip and coated by chlorite, quartz, pyrite and chalcopyrite, before calcite and anhydrite. Laumontite is present among calcite at ~1370 m depth, where trace epidote also deposited before calcite and anhydrite.	Filled by a sequence of chlorite, quartz – epidote, opaque minerals – calcite, anhydrite. Illite and titanite are rare. Laumontite is present at ~1370 m depth. Apatite is present before chlorite at 1250 m depth.
Up to 5 mm wide, the vertical veins cut 0-10° dipping veins. Filled by chlorite and quartz, before calcite and anhydrite. Laumontite deposited after calcite. Epidote is absent.	Coated by laumontite, calcite, anhydrite and pyrite, after chlorite, quartz and chalcopyrite.	Filled by chlorite and quartz, after calcite and anhydrite. Laumontite is present at ~1690 m depth.
Up to 1.5 cm wide, 70-90° dip, cut 40-50° dip and almost horizontal veinlets at 2100-2270 m depth. Filled by a sequence of chlorite, quartz, opaque minerals, calcite, anhydrite – epidote, titanite, ±garnet – wairakite, ±laumontite – prehnite – calcite, anhydrite. Adularia is first present at ~2100 and 2250 m depth. Apatite is present with opaque minerals at ~2160 m depth.	60-90° dip, coated by a sequence of chlorite, quartz – epidote – laumontite, anhydrite, ±calcite. Wairakite is present at ~2210 m depth.	Filled by chlorite, quartz, calcite, anhydrite and opaque minerals. Epidote is present at 2155 m depth. Wairakite and prehnite are present at ~2210 m depth.

Figure 6.5.Occurrence of hydrothermal minerals in veins, on fracture surfaces and in cavities in well DRJ S-5.

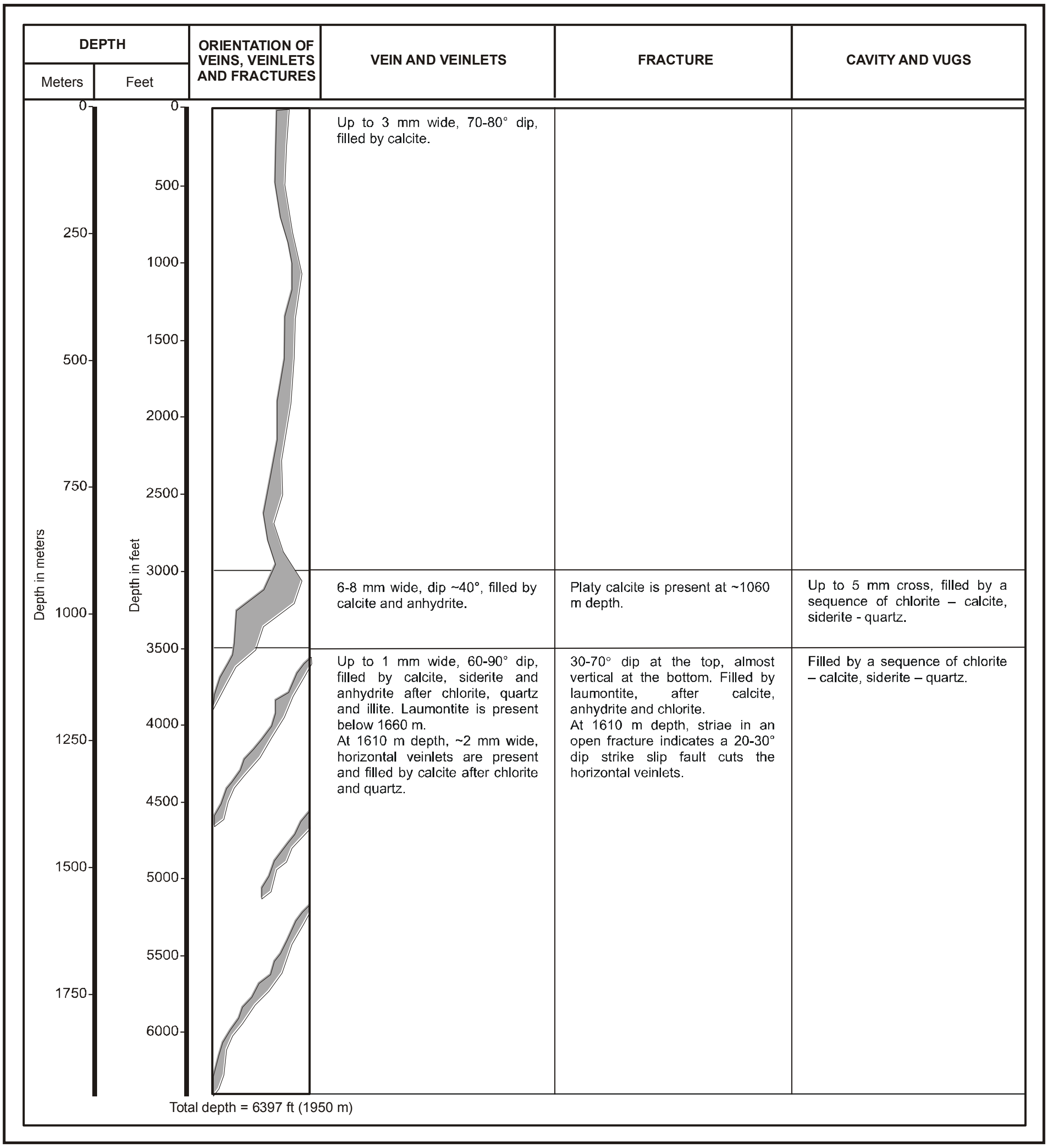

VEIN AND VEINLETS	FRACTURE	CAVITY AND VUGS
Up to 3 mm wide, 70-80° dip, filled by calcite.		
6-8 mm wide, dip ~40°, filled by calcite and anhydrite.	Platy calcite is present at ~1060 m depth.	Up to 5 mm cross, filled by a sequence of chlorite – calcite, siderite - quartz.
Up to 1 mm wide, 60-90° dip, filled by calcite, siderite and anhydrite after chlorite, quartz and illite. Laumontite is present below 1660 m. At 1610 m depth, ~2 mm wide, horizontal veinlets are present and filled by calcite after chlorite and quartz.	30-70° dip at the top, almost vertical at the bottom. Filled by laumontite, after calcite, anhydrite and chlorite. At 1610 m depth, striae in an open fracture indicates a 20-30° dip strike slip fault cuts the horizontal veinlets.	Filled by a sequence of chlorite – calcite, siderite – quartz.

Figure 6.6.Occurrence of hydrothermal minerals in veins, on fracture surfaces and in cavities in well DRJ S-6.

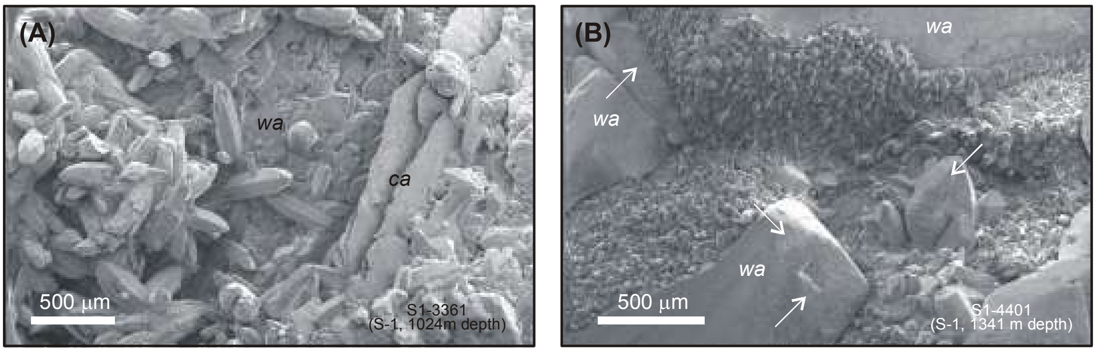

Figure 6.7.Quartz under Scanning Electron Microscope. **(A)** Radiating, euhedral quartz is present in an open fracture after wairakite (*wa*) and platy calcite (*ca*). **(B)** Minute euhedral quartz postdates wairakite (*wa*) in an open fracture. Note also dissolution of the surface of wairakite (arrows). Sample numbers and locations are given.

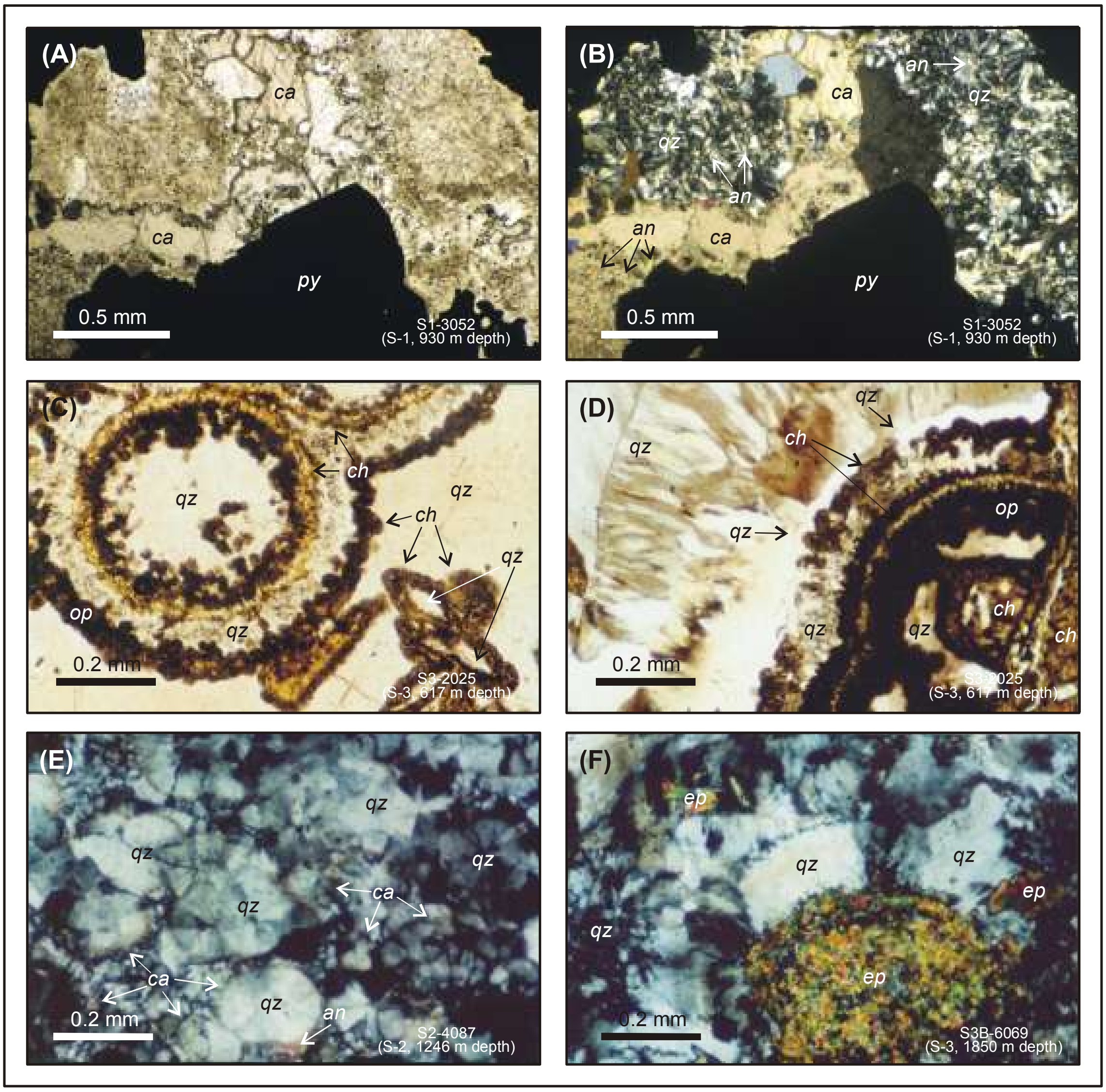

Figure 6.8.Chalcedonic quartz. **(A)** Plane polars view showing the occurrence of chalcedonic quartz in association with calcite (*ca*) and pyrite (*py*). **(B)** Cross polars view of (A) showing that chalcedonic quartz occurs as rosette-like assemblages of quartz (*qz*) crystals. Anhydrite (*an*) occurs as a core of rosette quartz. **(C)** Spherical texture of chalcedony, intercalated with chlorite (*ch*) and opaque minerals (*op*), is present in the margin of a vein. Chalcedonic quartz also occurs as micro-amygdaloidal texture. Plane polars. **(D)** Quartz (*qz*) replaces chalcedony while retaining its spherical form. Chalcedonic quartz is intercalated with chlorite (*ch*) and opaque minerals (*op*). Cross polars. **(E)** Chalcedonic quartz (*qz*) predates calcite (*ca*) and anhydrite (*an*), coating spheres. Cross polars. **(F)** Chalcedonic quartz (*qz*) also postdates epidote (*ep*). Cross polars. Sample numbers and locations are given.

<u>Prehnite</u> is mostly present in fractures. It is white, transluent, tabular, about 1 mm diameter and always occurs in clusters that are fan shaped (Figures 6.9E-F and 6.10E-F). Minute prehnite crystals are also present in vugs and cavities. They are usually less than 0.5 mm long.

Prehnite deposited after wairakite at elevations of about +500 and -50 m in wells DRJ S-1 and S-5 respectively. Trace of prehnite also occurs with epidote at elevations of about +300 m in well DRJ

S-3. Prehnite is absent in cavities, except at about 2208 m depth in well DRJ S-5, where it deposited onto the surfaces of epidote crystals

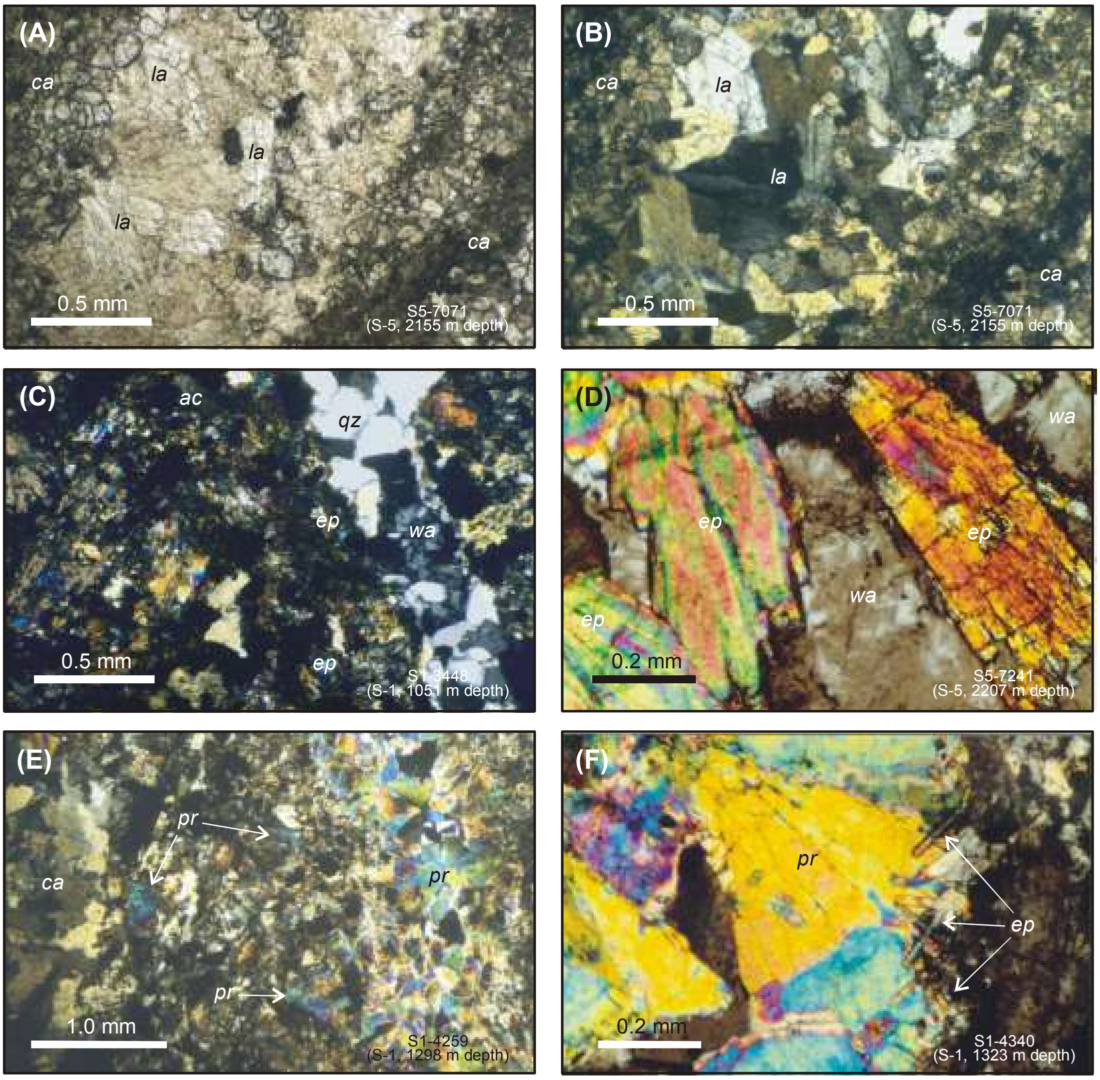

Figure 6.9.The occurrences of laumontite, wairakite and prehnite in veins, fractures and cavities. **(A)** Laumontite (*la*) fills a vein in association with calcite (*ca*). Plane polars. **(B)** Cross polars view of (A). **(C)** Wairakite (*wa*) occurs in a vein and is associated with quartz (*qz*). Cross polars. The matrix shows replacement epidote (*ep*) and actinolite (*ac*). **(D)** Wairakite (*wa*) is mostly present after epidote (*ep*), indicated by its occurrence within euhedral epidote. Cross polars. **(E)** Prehnite (*pr*) in a vein. Cross polars. Calcite (*ca*) may have predated prehnite as indicated by the occurrence of calcite in the margin of the vein. **(F)** Prehnite (*pr*) mostly postdates epidote (*ep*), indicated by its occurrence after euhedral epidote in the margin of a vein. Cross polars. Sample numbers and locations are given.

Epidote is yellowish green, acicular, up to 1 mm long and in some places is needle-like and radiating, but it is also anhedral and granular in cavities and compact and massive at the margins of veins (Figure 6.11). In open fractures, euhedral epidote crystals can be 2-3 mm long and up to 0.5 wide.

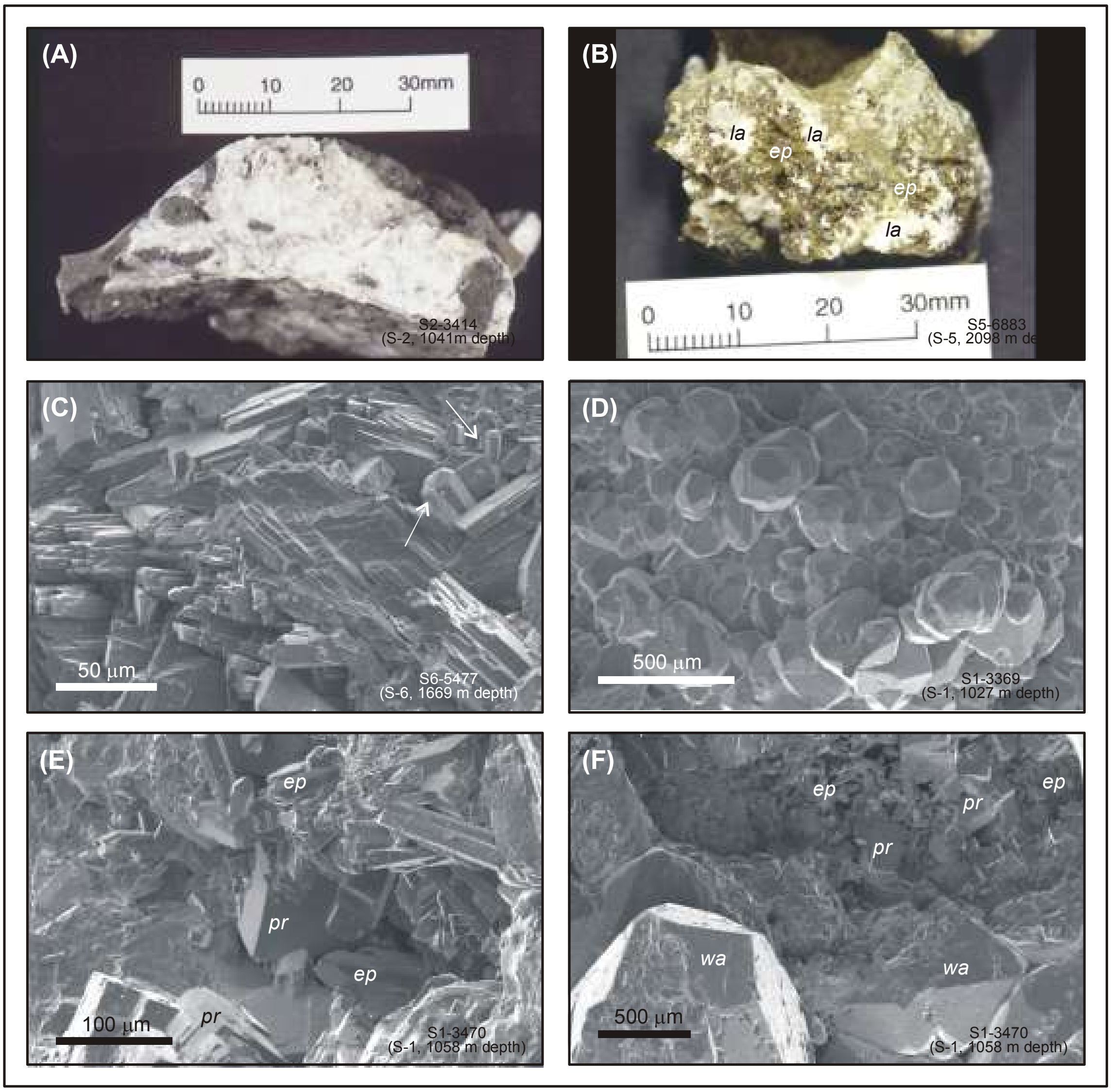

Figure 6.10.Occurrences of calc-silicate minerals in veins, fractures and cavities. **(A)** Laumontite occurs as white, radiating, friable crystals filling a cavity. **(B)** White, radiating laumontite (*la*) fill fractures with green, elongated, radiating epidote (*ep*) crystals. **(C)** Laumontite under scanning electron microscope is mostly radiating and broken, but can also be euhedral (arrows). **(D)** Fan-shaped of prehnite (*pr*) and euhedral, tubular epidote (*ep*) in cavity. **(E)** Euhedral, dodecahedral wairakite coating a fracture. **(F)** Wairakite (*wa*) mostly occurs in association with epidote (*ep*) and prehnite (*pr*). Note different shapes and sizes of the calc-silicates. Sample numbers and locations are given.

Vein epidote occurs as shallow as +1000 m in well DRJ S-5 and +700 to +800 m in wells DRJ S-3 and S-1, but it is absent in wells DRJ S-2 and S-6. At shallow depths, epidote is associated with wairakite and quartz, but deeper, it is also associated with prehnite and actinolite. Usually epidote is absent where laumontite occurs (e.g. between 1520 and 2010 m depth in well DRJ S-5). However, at about 1367 m depth in well DRJ S-5, epidote deposited after laumontite.

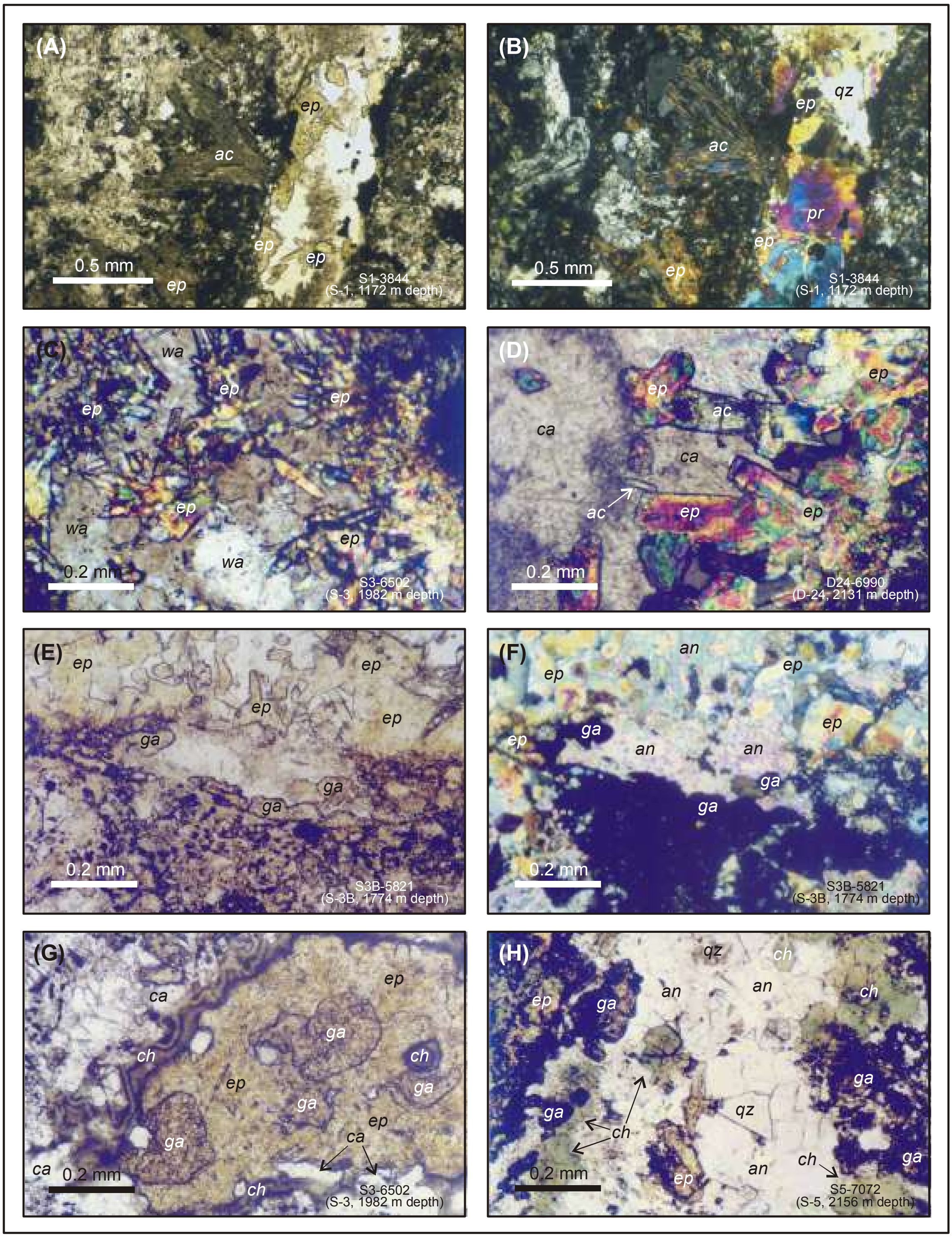

Figure 6.11.Epidote, actinolite and garnet in veins. **(A)** Epidote (*ep*) in a vein and as a replacement product in the matrix. Plane polars. **(B)** Cross polarised light view of (A) showing that quartz (*qz*) and prehnite (*pr*) also occur with epidote in the vein. The coloured, high birefringence mineral with a good cleavage in the matrix is actinolite (*ac*). **(C)** Some euhedral crystals of epidote (*ep*) associated with actinolite (*ac*) predate calcite (*ca*). In someplaces, actinolite is present as needle like crystals. Cross polars. **(D)** Some epidote (*ep*) crystals also predate wairakite (*wa*). Cross polars. **(E)** Euhedral garnet (*ga*) is present in the margin of a vein indicating its early deposition, i.e. before epidote (*ep*). Plane polars. **(F)** Cross polarised light view of (E) showing that anhydrite (*an*) postdates garnet and epidote. **(G)** Euhedral garnet (*ga*) also occurs associated with epidote (*ep*) in cavity. Chlorite (*ch*) and calcite (*ca*) formed earlier in the margin of cavity. Plane polars. **(H)** Garnet (*ga*) also occurs as anhedral, minute crystals surrounding epidote (*ep*). Garnet and epidote are associated with chlorite (*ch*) and deposited before anhydrite (*an*) and quartz (*qz*). Plane polars. Sample numbers and locations are given.

Epidote mostly deposited before wairakite and prehnite (Figures 6.9D and F, 6.10E-F and 6.11A-C). At depth, it is also overprinted by calcite and anhydrite (Figure 6.11D), but in DRJ S-5, epidote is present after calcite and anhydrite. Quartz, chlorite and illite are commonly associated with epidote. At 1983 m depth of well DRJ S-3, epidote occurs with actinolite and garnet in association with chalcedonic quartz.

Actinolite is present as needle-like and radiating crystals, associated with epidote (Figure 6.11D) in wells DRJ S-1, S-3 and S-5. Like epidote, in wells DRJ S-2 and S-6, actinolite is absent. The shallowest appearance of actinolite in well DRJ S-1 is at about +700 m and that in wells DRJ S-3 and S-5 is at about +250 m, i.e. far below the shallowest appearance of epidote.

Garnet is locally present in wells DRJ S-1, i.e. at elevations of about +800 m, S-3 (about +100 and +600 m) and S-5 (about +50 and +950 m). It is mostly euhedral, 0.1-0.2 mm diameter and associated with epidote and actinolite. In well DRJ S-3, garnet is also present in cavities as granular, tiny, 0.02-0.05 mm diameter crystals, associated with epidote (Figures 6.11E-H). However, it is rare in fractures.

6.2.3. Carbonates and Anhydrite

Calcite and other carbonates. Calcite is very common in veins, vugs and fractures. It is mostly clear, up to 5 mm across, anhedral and massive. In open spaces, calcite crystals can be euhedral, clear and up to 4 mm long (Figure 6.12). Euhedral, white, prismatic crystals, up to 2 mm long and radiating are present in open fracture, e.g. in wells DRJ S-2 and S-5.

Calcite occurs at most depths and in all wells, commonly with anhydrite. At shallow depths, it is present at the margin of veins and vugs. This indicates that it deposited, before other hydrothermal minerals, e.g. calc-silicates. In some places early calcite occurs after chlorite and quartz (Figure 6.12C). After calcite deposited, it can be dissolved creating secondary pores. At depth, late calcite overprints calc-silicates (Figure 6.11D). Therefore, at depth, calcite usually deposited in 2 periods. Below +700 m in well DRJ S-1 and -100 of well DRJ S-3, calcite is absent.

Platy calcite up to 1 mm long is present in open fractures at an elevation of about +800 m in well DRJ S-1 (Figure 6.13). It also occurs in well DRJ S-6 at about +650 m. Another carbonate associated with calcite is siderite, which is present at shallow depths in wells DRJ S-1, S-2 and S-3. Siderite also occurs between 1645 and 2150 m depth in well DRJ S-3. In well DRJ S-6, siderite is present below 1060 m. Natron is present at 838 m depth in DRJ S-5 as platy, clear crystals with a good cleavage and up to 1 mm long, possibly formed as a result of hydration of calcite.

Calcite forms through hydrolysis reaction involving CO_2 rich fluid:

$$Ca^{2+} + CO_2 + H_2O \rightarrow CaCO_3 + 2H^+ \tag{6.1}$$

and due to boiling:

$$Ca^{2+} + 2HCO_3^- \rightarrow CaCO_3 + CO_2 + H_2O \tag{6.2}$$

The first process decreases the amount of dissolved CO_2 and the later releases CO_2 gas (e.g. Browne and Ellis, 1970, and Simmons and Christenson, 1994). Platy calcite is formed in the later process (Simmons and Christenson, 1994).

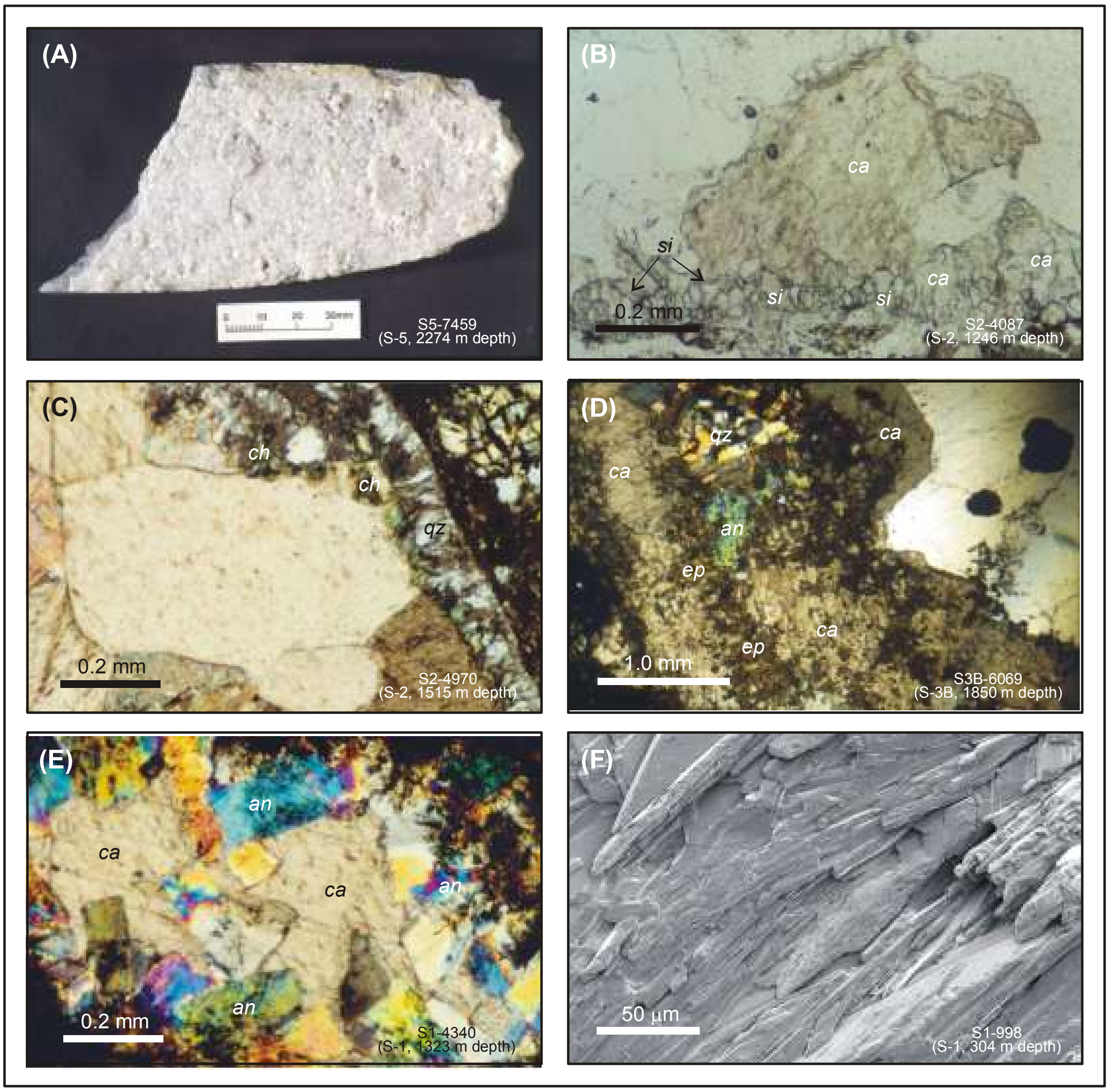

Figure 6.12.Calcite and anhydrite in veins and fractures. **(A)** Sugary grains of calcite on the surface of an open fracture. **(B)** In someplaces, siderite (*si*) is associated with calcite (*ca*). It can be distinguished by its black edges. Plane polars. **(C)** First deposited calcite in a vein occurs mostly after quartz (*qz*) and chlorite (*ch*). Note that quartz has a chalcedonic texture. Cross polars. **(D)** Calcite (*ca*) is commonly associated with, and deposited after, anhydrite (*an*). Cross polarised light. **(E)** Calcite (*ca*) and anhydrite (*an*) also occur in a vein after epidote (*ep*) as the second deposition event, associated with quartz (*qz*). Cross polars. **(F)** Gypsum with fibrous texture resulted from hydration of anhydrite is present at shallow depths in well DRJ S-1. The mineralogy is confirmed by X-ray diffraction. Sample numbers and locations are given.

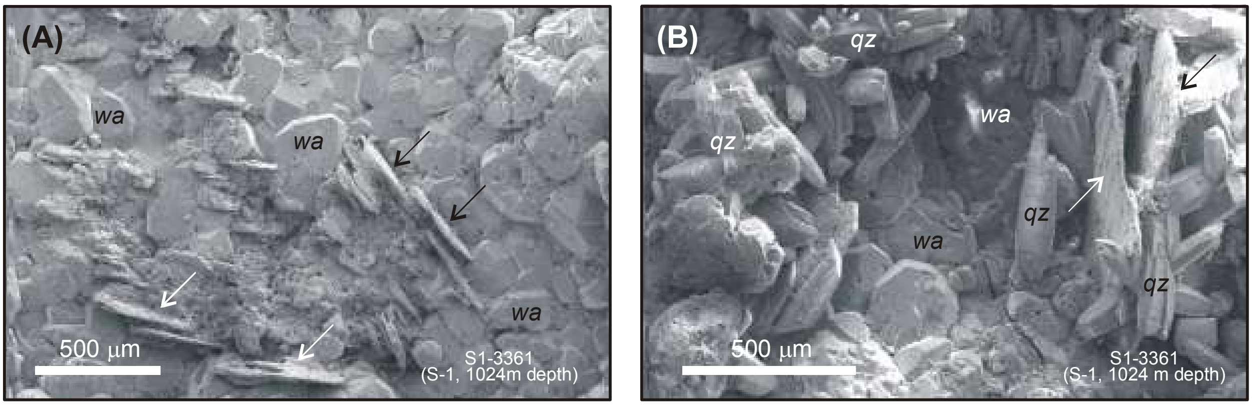

Figure 6.13.Platy calcite. **(A)** It (arrows) is present in an open fracture and postdates wairakite (*wa*). Dissolution might occur after calcite deposition. **(B)** Euhedral quartz (*qz*) occurs after or in association with platy calcite (arrows). Both postdate wairakite (*wa*). Sample numbers and locations are given.

Anhydrite is present in association with calcite (Figure 6.12E). It is typically euhedral, about 1 mm long, but some crystals are platy. In some places, anhydrite crystals are 8 mm long and 0.5 mm wide, e.g. at 2207 m depth in well DRJ S-5. However, anhedral, granular and fine-grained anhydrite is also common. Anhydrite crystals also tend to be radiating.

Anhydrite is absent above +1300 m in well DRJ S-3 and above +1100 and +700 m in wells DRJ S-2 and S-6 respectively. Above +1000 m in well DRJ S-5 and +750 to +800 m in wells DRJ S-1 and S-3 anhydrite deposited early as it is present at the margins of veins and vugs; but below these depths, anhydrite in association with calcite deposited later, encapsulating other hydrothermal minerals, such as calc-silicates. In wells DRJ S-2 and S-6, there is no record of late deposition of anhydrite. Here, anhydrite and calcite deposited early but after chlorite and quartz.

Hydration can transform anhydrite to gypsum (e.g. Groves, 1958; Hawthorne and Ferguson, 1975). This occurs only where anhydrite forms at temperatures between 130 and 200°C as a semi-hydrate state; anhydrite formed above 300°C will not convert to gypsum (Azam et al., 1998). Gypsum may be fibrous (Figure 6.12F) and grows perpendicular to the surface of the vein or granule. In Darajat, the gypsum conversion occurred at shallow depths, i.e. about 300 m depth, in well DRJ S-1.

6.2.4. Clay Minerals

Chlorite is very common in veins, fractures and vugs. It occurs at almost all depths and in all wells. It is also associated with all other hydrothermal minerals. Chlorite, which is present at the margins of cavities and associated with quartz, is mostly green to dark green, anhedral and fine-grained. Light green chlorite usually occurs with epidote and is present in the middle of a vein. This difference in colour might indicate a difference in Fe content.

Some chlorite is also subhedral, elongated and fibrous. Hexagonal plates of chlorite are present in cavities at about 940 m depth in well DRJ S-5. Low Fe chlorite is likely present at +1200 to 1300 m in wells DRJ S-1, S-3 and S-5, and between +600 and +900 m in the marginal area.

Illite (Figure 6.14) is rare as a vein mineral. It is usually associated with chlorite, quartz and epidote. It is present below +700 m in well DRJ S-1 and in wells DRJ S-3 and S-5 occurs at 0 to +400 and +600 to +1000 m respectively. In wells DRJ S-2 and S-6, where no epidote occurs, illite is absent.

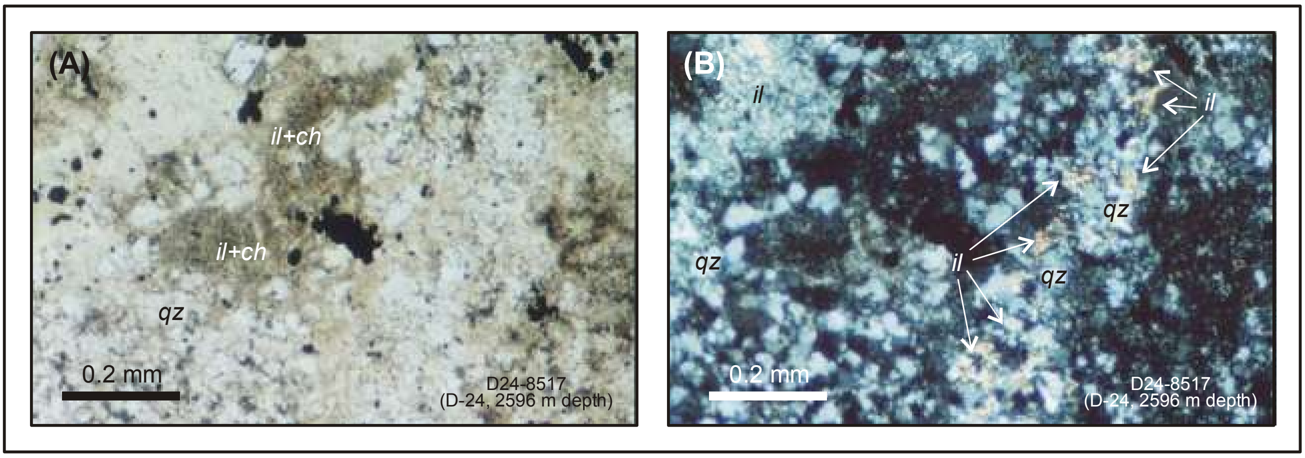

Figure 6.14.Vein illite. **(A)** Illite (*il*) in association with quartz (*qz*) is present in a vein. Plane polars. **(B)** Cross polars view of figure (A). Illite (*il*) is also associated with chlorite (*ch*) replacing the groundmass. Quartz (*qz*) in the groundmass is primary in a rhyolitic rock. Sample numbers and locations are given.

6.2.5. Other Minerals

Adularia is rare. It forms white, diamond shaped crystals in veinlets (Figure 6.15). It is associated with quartz and chlorite in veins at elevations of about +650 m in well DRJ S-1, at +400 and +600 m in DRJ S-3 and at 0 to +100 m in DRJ S-5. Adularia also occurs in open fractures at about +1000 m in well DRJ S-1.

Adularia indicates good permeability (Browne, 1978) and its occurrence usually reflects reservoir conditions. In Darajat, adularia occurs at about the top of the present reservoir, but varies by up to ±100 m. Vein adularia also indicates boiling (e.g. Browne, 1995 and Reyes, 2000).

Tourmaline is green-blue, acicular, up to 1 mm long and forms radiating crystals (Figure 6.16). It mostly fills vugs in wells DRJ S-1, i.e. at elevations of +750 and +900 m, and overprinted by calcite and anhydrite. Tourmaline is also present in fractures at +500 m in well DRJ S-1 and in veins, where it deposited before calcite and anhydrite, at +1300 m in well DRJ S-5.

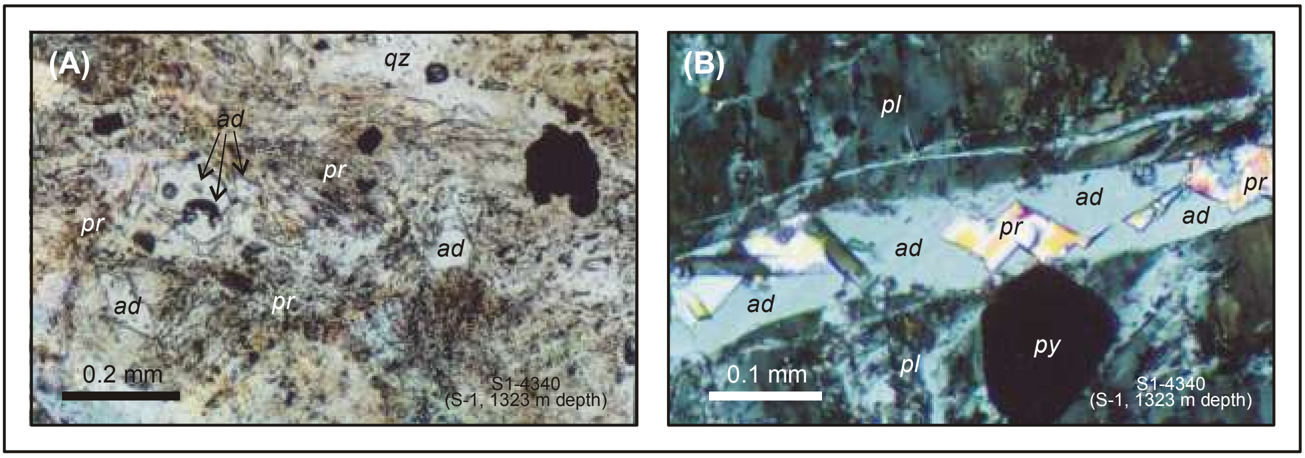

Figure 6.15. Adularia in veins is rare. It can be distinguished from quartz by its diamond shape. **(A)** Adularia (*ad*) as euhedral crystals is disseminated among prehnite (*pr*) and quartz (*qz*) in a vein. Plane polars. **(B)** Adularia (*ad*) is present in the margin of a veinlet and predates prehnite (*pr*). The veinlet cross-cuts plagioclase (*pl*) phenocryst. Cross polars. Sample numbers and locations are given.

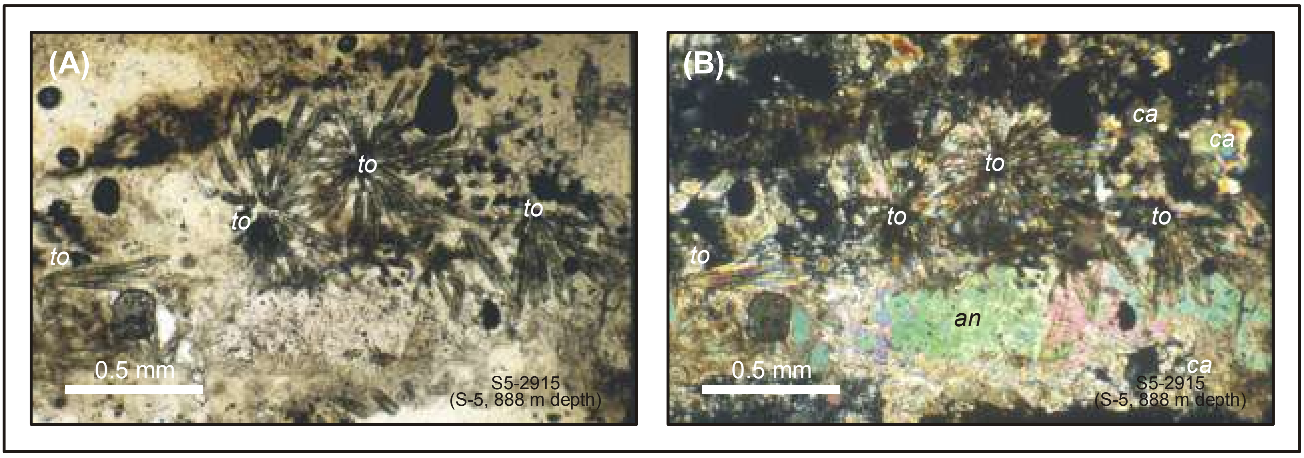

Figure 6.16.Vein tourmaline. **(A)** Plane polars radiating crystals of tourmaline (*to*) with green-blue pleocroism. **(B)** Calcite (*ca*) and anhydrite (*an*) likely postdate tourmaline (*to*). Cross polars.

Apatite is present in veins at elevations of about +750 m in well DRJ S-1 and -50 to -100 m in wells DRJ S-3 and S-5. It is euhedral to subhedral, up to 0.1 mm long and is associated mostly with calcite and chlorite (Figure 6.17). Apatite also fills cavities with opaque minerals at +850 and +1150 m in wells DRJ S-3 and S-5 respectively and is present as inclusions in wairakite (Figure 6.17E-F).

Pyrite, chalcopyrite and other iron bearing minerals. Pyrite is usually euhedral, up to 1 mm wide and disseminated in veins and fractures. Anhedral and fine-grained pyrite are usually compact and present in vugs. In some places, pyrite can also be 2 mm long. Chalcopyrite is fine-grained and anhedral. It usually forms 1-2 mm across nodules. Pyrite and chalcopyrite mostly occur in wells DRJ S-3 and S-5 and are associated with chlorite and quartz. Both are also present with anhydrite and calcite.

Other opaque minerals include goethite, which is present in well DRJ S-5 at about 2130 m depth. The other is an unknown platy, 0.5-1 mm cross, subhedral opaque mineral, which occurs at 1332 m depth in well DRJ S-5.

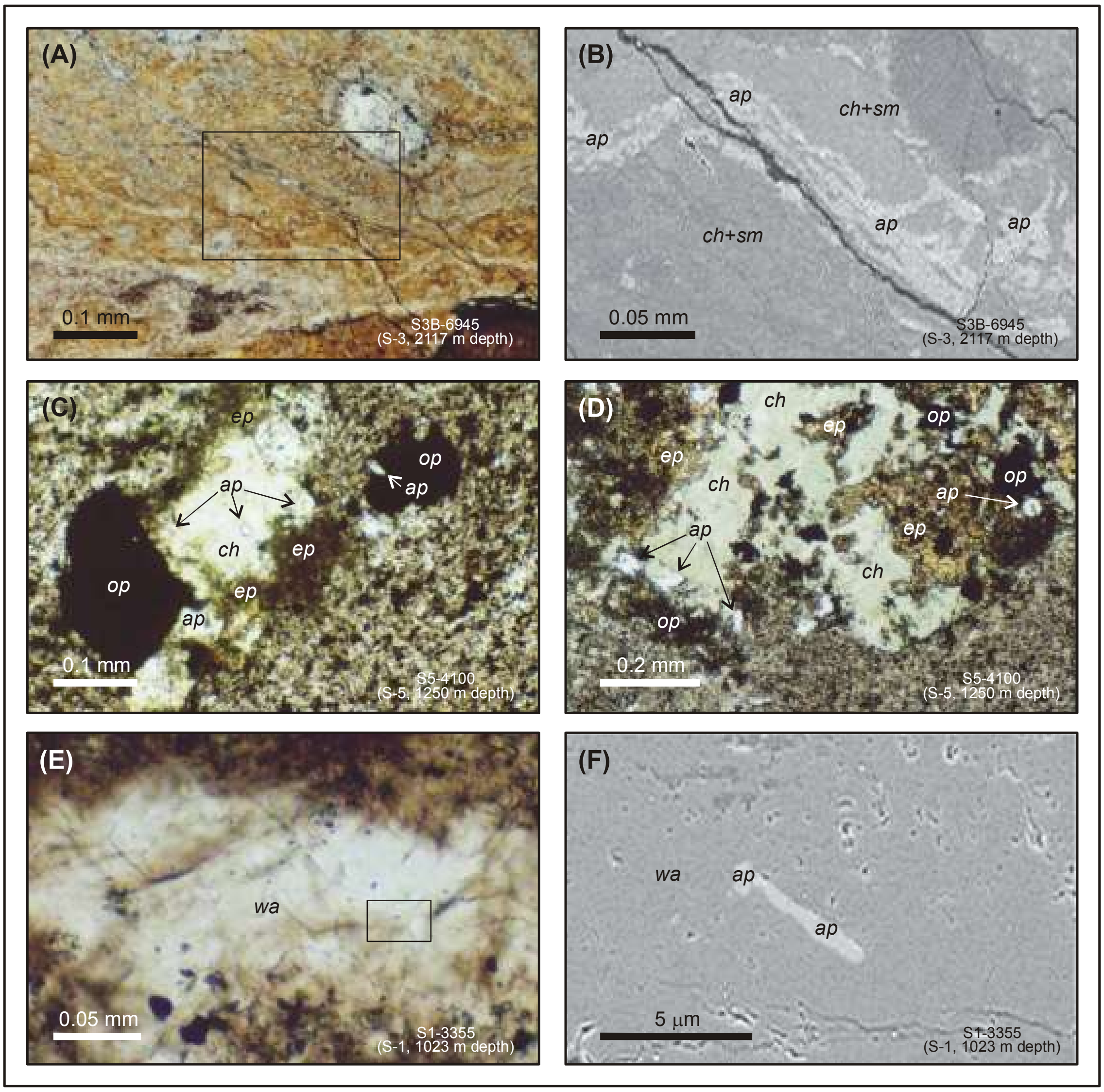

Figure 6.17.Secondary apatite. **(A)** Apatite is present in a vein of an acid altered rock from well DRJ S-3. Plane polars. **(B)** Back scattered image of an area in figure (A) showing that apatite (*ap*) occurs along cracks and is associated with chlorite and smectite (*ch+sm*). **(C)** Apatite (*ap*) is present as euhedral crystals within chlorite (*ch*) in a cavity. It is also associated with opaque minerals (*op*). Epidote (*ep*) is present in the margin of the cavity. Plane polars. **(D)** Apatite (*ap*) is associated with epidote (*ep*) and opaque minerals (*op*) present in the margin of cavity. They are postdated by chlorite (*ch*). **(E)** Apatite is also present as inclusions in wairakite (*wa*). Plane polars. **(F)** High magnification and back scattered image of area in figure (E) showing apatite (*ap*) inclusions in wairakite (*wa*) crystals. Sample numbers and locations are given.

6.3. RELATIONSHIPS OF HYDROTHERMAL MINERALS

Based on their cross-cutting relationships and infilling sequences, at least 7 episodes of vein mineralisation can be recognised. The petrogenetic sequence is summarised in Table 6.1.

The earliest episode (1) was dominated by alternating deposition of chlorite, quartz and opaque minerals. Chlorite is mostly the high Fe type and predated quartz. Chalcedony is (likely) associated with this quartz. Although calcite and anhydrite are also present in veins, they are minor phases. Tourmaline and apatite might also occur at this episode. Calcite, siderite and anhydrite become dominant during episode 2. In Figure 6.1, they are represented as the first deposition of calcite and anhydrite; they occur near the surface and at the margin of the field, i.e. at wells DRJ S-2 and S-6 but they are absent at some depth in well DRJ S-3.

Table 6.1.Petrogenetic sequence of mineralisation in veins and fractures.

Hydrothermal Minerals	Episode Older → Younger						
	1	2	3	4	5	6	7
Tourmaline	■						
Apatite	■						
Quartz	■	■	■	■	■	■	■
Chlorite, high Fe	■	■	■	■	■		
Calcite	■	■ Fe-rich				■	
Anhydrite	■	■				■	■
Chlorite, low Fe			■	■	■	■	■
Adularia			■				
Titanite			■				
Actinolite			■				
Garnet			■				
Epidote			■	■	■		
Illite			■	■	■		
Prehnite				■	■		
Wairakite				■	■		
Laumontite				■	■		

The most complex of the vein mineralisation started at episode 3, as calc-silicate minerals deposited then. Episode 3 is well developed in the deepest part of the field. It is characterised by epidote, actinolite and garnet infillings. Quartz, chlorite, illite and opaque minerals are present alternating with the calc-silicates. Chlorite is mostly low Fe. Titanite is present as a trace. Chalcedonic quartz and adularia might also occur locally. Episode 4 is dominated by the occurrence of prehnite, alternating with quartz, chlorite and opaque minerals. Wairakite and laumontite formed during episode 5. Wairakite is dominant at the northern area, i.e. about well DRJ S-1, whereas laumontite dominates in the south, i.e. well DRJ S-5 and its surrounds (Figure 6.1). In this episode, the calc-silicate minerals are associated with quartz, chlorite and opaque minerals. Illite is minor. If veins episode 5 are developed continuously to elevations of +1300 to +1400 m, minerals episode 4 are present locally in only the deeper part of the field. At depth, deposition of epidote, wairakite and prehnite occurred in several cycles. The sequence of calc-silicates indicates boiling (Giggenbach, 1981). Association with adularia also suggests an increase in pH due to boiling (e.g. Browne, 1978 and Cavarretta et al., 1980). Episode 5 was the last episode of deposition of calc-silicate minerals.

Calcite and anhydrite deposited in episode 6, as shown in Figure 6.1. This was the second deposition episode of calcite and anhydrite, and these postdate all the calc-silicates. Since calcite and anhydrite have reverse solubilities with temperature, their occurrence may be due to heating of downward percolating bicarbonate and sulfate rich steam condensate from the overlying aquifer (Moore et al., 2000a). Platy calcite is present at some depths but it is a minor phase resulting from CO_2 loss during boiling. However, calcite after calc-silicate minerals at depth also indicates a progressive loss of $CO_2$from the deep thermal fluid (Browne and Ellis, 1970). Calcite is absent in veins of the last episode, episode 7, but anhydrite is still dominant. Chlorite and quartz are common. The occurrence of anhydrite after calcite suggests heating (Reyes, 2000) and/or decreasing pressure (Blount and Dickson, 1969, and Sasada, 1986).

Chapter 7

COMPOSITION OF HYDROTHERMAL MINERALS

The compositions of hydrothermal minerals record information about the physicochemical conditions and processes prevailing during their formation, sometimes including temperature, pressure and fluid composition. In this chapter, the mineral compositions are used to predict the characteristics of the geothermal fluids. Detailed chemical analyses are given in AppendicesF and G; only representative analyses are reported here.

7.1. CLAY MINERALS

7.1.1. Chlorite: $(Mg,Al,Fe)_{12}[(Si,Al)_8O_{20}](OH)_{16}$

Chlorite is the most common clay mineral present; it occurs as a replacement of phenocrysts and groundmass and in veins. Tables 7.1 and 7.2 show the compositions of replacement and vein chlorites respectively. Figure 7.1 classifies the chlorites in terms of Si and Fe^{2+}, following Hey (1954) and Foster (1962) and Figure 7.2 shows variations in their ratios of Mg and Fe+Mg.

Figure 7.1 shows that the compositions of some replacement and vein chlorites are the same. Between 800 and 980 m depth in well DRJ S-1, chlorite is Mg rich, clinochlore and penninite (Figure 7.1A). It contains 10-30 wt.% MgO and 3-14 wt.% FeO; the ratio of Mg to Mg+Fe is above 0.7 (Figure 7.2A). The amounts of SiO_2 and Al_2O_3 in cavity fill and vein chlorites are 29-33 and 16-22 wt.% respectively; they are higher in chlorite replacing plagioclase, i.e. up to 38 wt.% SiO_2 and 25 wt.% Al_2O_3. Traces of TiO_2 are present but less than 0.5 wt.%, and MnO is up to 1 wt.%.

Below 1020 m in well DRJ S-1, chlorite becomes more Fe rich and has slightly less Mg (Figure 7.2A); the FeO and MgO contents are 10-22 and 18-27 wt.% respectively. Figure 7.1A shows that the end member chlorite lies between pycnochlorite, diabantite and penninite. However, between 1300 and 1325 m depth, chlorite is slightly Si rich and becomes talc-chlorite with 30-38 wt.% SiO_2 and 14-18 wt.% Al_2O_3; the amount of FeO can be as low as 6 wt.% and the ratio between Mg and Mg+Fe is between 0.7 and 0.9 (Figure 7.2A).

Chlorite from well DRJ S-3 at about 1000 m depth is diabantite and pycnochlorite below 1200 m (Figure 7.1B). Diabantite contains 29-34 wt.% SiO_2 and 14-17 wt.% Al_2O_3; the other contains slightly less SiO_2 but more Al_2O_3. The amounts of FeO and MgO are 18-23 and 17-20 wt.% respectively for diabantite, and 16-24 and 15-21 wt.% respectively for pycnochlorite. However, at about 1140 m depth, the FeO content becomes dominant, whereas MgO is reduced (Figure 7.2B),

Table 7.1. Compositions and structural formulae of representative chlorites present in the matrix of rocks.

Well	DRJ 1		DRJ 17		DRJ S-1		DRJ S-2		DRJ S-3		DRJ S-5		DRJ S-3		DRJ 1		DRJ S-2	
Depth (m)	637		2407		976		1251		1000		2207		1000		580		1251	
Sample	D1-637		D17-7898		S1-3202		S2-4103		S3-3280		S5-7241		S3-3280		D1-580		S2-4103	
Analysis no.	3133		2271		6173		3555		4424		4590		4780		4865		3720	
Precursor	Plagioclase		Plagioclase, with amphibole		Plagioclase		Plagioclase		Plagioclase, core		Plagioclase, core		Pyroxene, crack		Groundmass		Groundmass	
Name	Diabantite		Pycnochlore		Penninite		Pycnochlore		Diabantite		Pycnochlore		Diabantite		Brunsvigite		Daphnite	
Oxide (wt.%)																		
SiO_2	36.71		29.18		33.82		29.88		32.04		28.76		31.11		33.94		22.78	
TiO_2	< 0.01		0.08		0.06		< 0.05		0.09		< 0.04		0.06		< 0.03		0.49	
Al_2O_3	10.59		17.73		18.71		17.31		15.34		18.94		15.34		17.93		11.08	
FeO	24.29		19.56		6.91		20.02		20.71		20.30		20.79		23.86		38.55	
MnO	0.13		0.25		0.37		0.46		0.33		0.64		0.41		0.17		0.45	
MgO	15.68		20.58		25.10		19.29		19.11		19.57		18.05		8.66		13.47	
CaO	0.48		0.17		0.07		0.12		0.52		0.13		0.65		0.56		0.30	
Na_2O	0.28		< 0.14		0.11		0.09		< 0.01		0.03		0.06		0.27		< 0.04	
K_2O	0.32		0.03		0.95		0.08		0.04		0.03		0.01		0.33		0.04	
Cl	0.05		0.03		-		-		< 0.03		0.03		< 0.01		0.11		0.02	
NiO	0.06		< 0.14		0.12		0.10		< 0.09		< 0.04		< 0.01		0.01		< 0.07	
Cr_2O_3	-		0.05		0.02		0.08		0.09		0.01		0.01		< 0.01		0.01	
P_2O_5	< 0.09		< 0.08		0.04		< 0.08		0.10		< 0.08		0.09		< 0.04		0.05	
Total	88.59		87.35		86.85		87.30		88.32		88.43		86.60		85.79		87.19	
Number of ions on the basis of 36 (O, OH)																		
Si	7.505	8.00	5.967	8.00	6.516	8.00	6.132	8.00	6.489	8.00	5.851	8.00	6.451	8.00	7.117	8.00	5.356	8.00
Al^{IV}	0.495		2.033		1.484		1.868		1.511		2.149		1.549		0.883		2.644	
Al^{VI}	2.055	11.01	2.237	11.92	2.762	11.16	2.316	11.75	2.148	11.51	2.388	11.89	2.197	11.47	3.545	10.46	0.424	12.90
Fe^{2+}	4.153		3.345		1.113		3.436		3.508		3.454		3.605		4.184		7.580	
Mg	4.779		6.274		7.210		5.902		5.770		5.935		5.580		2.707		4.721	
Ti	-		0.012		0.009		-		0.014		-		0.009		-		0.087	
Cr	-		0.008		0.003		0.013		0.014		0.002		0.002		-		0.002	
Mn	0.023		0.043		0.060		0.080		0.057		0.110		0.072		0.030		0.090	
Ca	0.105	0.30	0.037	0.05	0.014	2.89	0.026	0.08	0.113	0.12	0.028	0.05	0.144	0.17	0.126	0.32	0.076	0.12
Na	0.111		-		0.041		0.036		-		0.012		0.024		0.110		0.018	
K	0.083		0.008		0.234		0.021		0.010		0.008		0.003		0.088		0.012	
CCl	0.035		0.021		-		-		-		0.021		-		0.078		0.016	
Ratio																		
Fe:(Fe+Mg)	0.46		0.35		0.13		0.37		0.38		0.37		0.39		0.61		0.62	
Mg:(Fe+Mg)	0.54		0.65		0.87		0.63		0.62		0.63		0.61		0.39		0.38	

Table 7.2. Compositions and structural formulae of representative chlorites present in veins and vugs.

Well	DRJ 24		DRJ S-1		DRJ S-1		DRJ S-3		DRJ S-5		DRJ 24		DRJ S-1		DRJ S-3		DRJ S-5	
Depth (m)	2596		976		1023		1000		2207		2596		976		1000		2207	
Sample	D24-8517		S1-3202		S1-3355		S3-3280		S5-7241		D24-8517		S1-3202		S3-3280		S5-7241	
Analysis no.	1272		6195		3095		4495		4605		1233		6184		4754		4693	
Occurrence	Vein		Vein		Vein, middle		Vein, margin		Vein		Vugs		Vugs		Vugs, rim		Vugs, middle	
Name	Talc-chlorite		Clinochlore		Pycnochlore		Diabantite		Pycnochlore		Brunsvigite		Penninite		Diabantite		Pycnochlore	
Oxide (wt.%)																		
SiO_2	47.64		32.99		29.24		30.66		31.54		25.68		32.46		31.13		29.33	
TiO_2	0.17		0.06		0.10		-		0.10		0.11		< 0.06		0.13		< 0.08	
Al_2O_3	31.86		18.93		18.00		13.88		20.57		20.20		18.25		15.19		18.74	
FeO	9.84		8.18		15.79		20.49		15.26		30.39		8.98		22.18		18.85	
MnO	0.15		0.53		1.15		0.46		0.33		0.09		0.51		0.23		0.74	
MgO	7.23		28.37		21.93		18.02		24.76		9.03		27.67		18.72		20.73	
CaO	0.03		0.02		0.12		0.62		0.12		0.32		0.21		0.29		0.07	
Na_2O	< 0.05		< 0.03		< 0.04		0.12		0.24		-		0.25		0.06		< 0.01	
K_2O	0.16		0.17		0.00		0.08		-		0.61		0.07		0.07		0.07	
Cl	0.07		0.03		0.05		0.02		0.01		0.06		0.01		0.03		0.01	
NiO	< 0.12		0.14		< 0.14		0.25		-		0.11		< 0.15		0.07		0.14	
Cr_2O_3	< 0.08		0.07		< 0.01		0.16		0.15		0.06		< 0.05		0.11		0.03	
P_2O_5	< 0.08		0.04		< 0.02		< 0.09		< 0.03		< 0.09		< 0.09		< 0.03		< 0.11	
Total	96.74		89.48		86.47		84.67		93.06		86.66		88.24		88.18		88.45	
Number of ions on the basis of 36 (O, OH)																		
Si	7.813	8.00	6.178	8.00	5.965	8.00	6.539	8.00	5.886	8.00	5.666	8.00	6.207	8.00	6.385	8.00	5.908	8.00
Al^{IV}	0.187		1.822		2.035		1.461		2.114		2.334		1.793		1.615		2.092	
Al^{VI}	5.966	9.12	2.353	11.66	2.289	11.86	2.025	11.52	2.407	11.77	2.915	11.54	2.317	11.72	2.054	11.66	2.354	11.89
Fe^{2+}	1.350		1.281		2.694		3.655		2.382		5.608		1.436		3.805		3.176	
Mg	1.768		7.921		6.669		5.729		6.889		2.970		7.887		5.724		6.225	
Ti	0.021		0.008		0.015		-		0.014		0.018		-		0.020		-	
Cr	-		0.010		-		0.027		0.022		0.010		-		0.018		0.005	
Mn	0.021		0.084		0.199		0.083		0.052		0.017		0.083		0.040		0.126	
Ca	0.005	0.04	0.004	0.05	0.026	0.03	0.142	0.21	0.024	0.11	0.076	0.25	0.043	0.15	0.064	0.11	0.015	0.03
Na	-		-		-		0.050		0.087		-		0.093		0.024		-	
K	0.033		0.041		-		0.022		-		0.172		0.017		0.018		0.018	
CCl	0.039		0.019		0.035		0.014		0.006		0.045		0.006		0.021		0.007	
Ratio																		
Fe:(Fe+Mg)	0.43		0.14		0.29		0.39		0.26		0.65		0.15		0.40		0.34	
Mg:(Fe+Mg)	0.57		0.86		0.71		0.61		0.74		0.35		0.85		0.60		0.66	

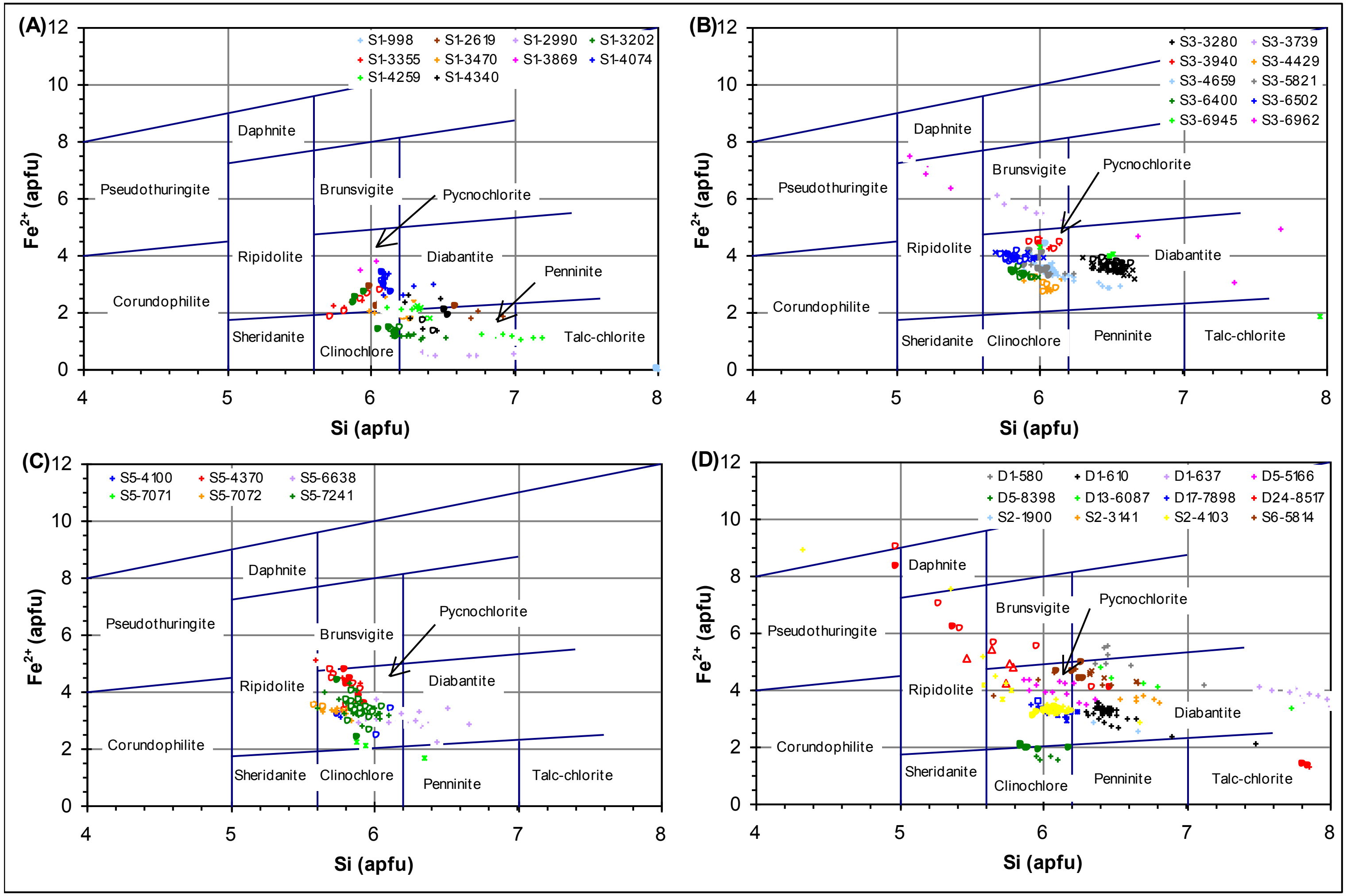

Figure 7.1. Classification of chlorites based on the amounts of Si and Fe (apfu = atoms per formulae unit) in the 36 oxygen structure formulae: **(A)** DRJ S-1, **(B)** DRJ S-3, **(C)** DRJ S-5 and **(D)** other wells, i.e. DRJ 1, 5, 13, 17, 24, S-2 and S-6. Sample numbers are given; precursor: (+) plagioclase, (×) pyroxene, (□) amphibole and (∗) groundmass replacements; (–) present in cracks in opaque minerals and (△) in cracks in quartz; (○) represent chlorite in cavities and (●) represent vein chlorite.

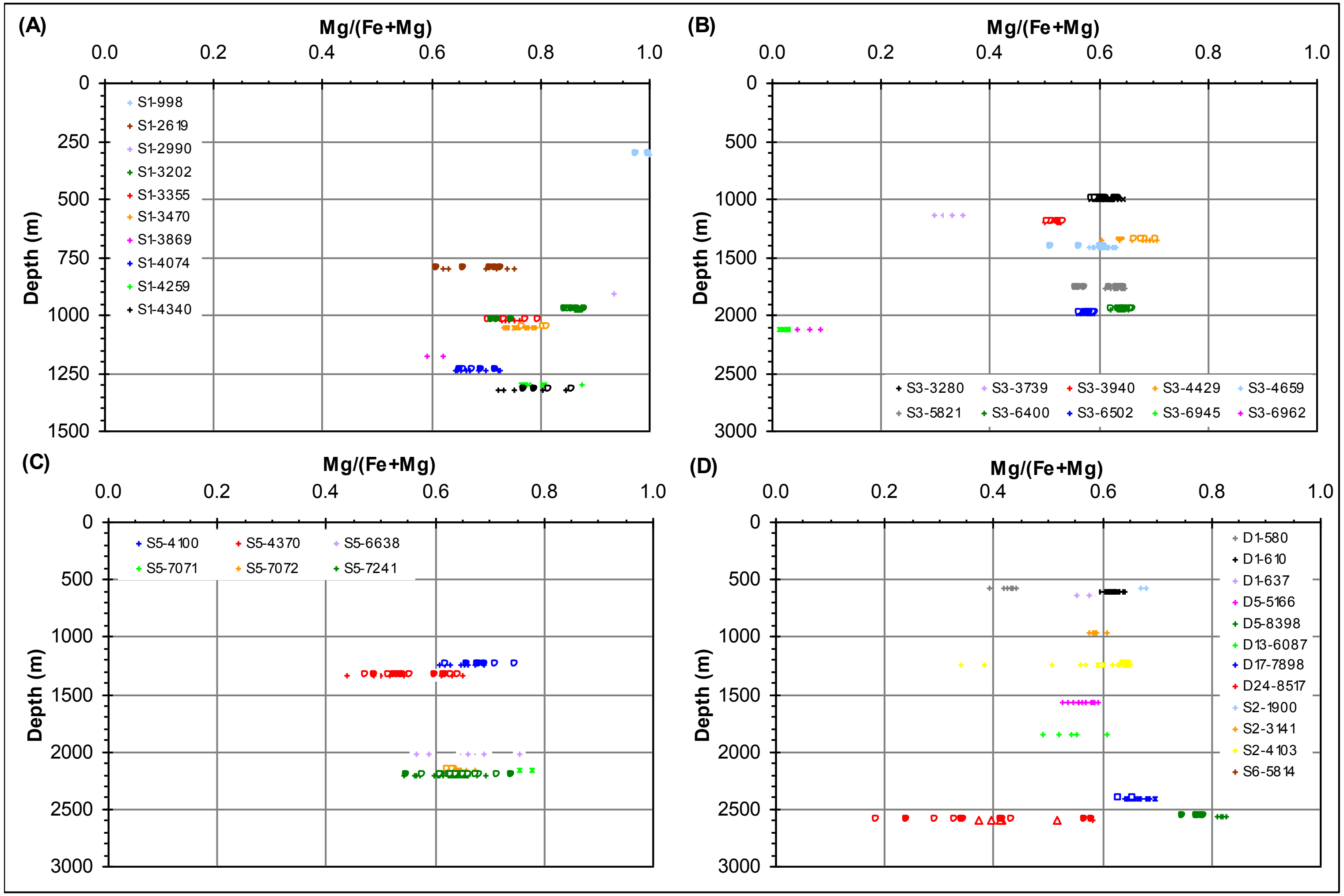

Figure 7.2. Variations in the ratios between Mg and Fe+Mg of chlorites with respect to depth in wells: **(A)** DRJ S-1, **(B)** DRJ S-3, **(C)** DRJ S-5 and **(D)** other wells, i.e. DRJ 1, 5, 13, 17, 24, S-2 and S-6. Sample numbers are given; precursor: (+) plagioclase, (×) pyroxene, (□) amphibole and (∗) groundmass replacements; (–) present in cracks in opaque minerals and (△) in cracks in quartz; (○) represent chlorite in cavities and (●) represent vein chlorite.

where brunsvigite occurs; it is present at 27-29 and 6-9 wt.% respectively. Brunsvigite also contains 26-28 wt.% SiO_2 and 18-20 wt.% Al_2O_3.

Chlorite present in an acid alteration zone at about 2120 m depth of DRJ S-3 is Fe rich (Figure 7.2B), containing 23-40 wt.% SiO_2, 24-30 wt.% Al_2O_3 and 19-38 wt.% FeO. The MgO is about 2 wt.% only, but TiO_2 can be up to 6 wt.%. Figure 7.1B shows that the end member chlorite is between daphnite and diabantite, but may be talc-chlorite.

Figure 7.1C shows that well DRJ S-5 contains more homogeneous chlorite, i.e. pycnochlorite. The SiO_2 ranges from 25 to 32 wt.% and Al_2O_3 varies between 16 and 21 wt.%. The amounts of FeO and MgO are identical, i.e. 12-27 and 13-25 wt.% respectively. However, chlorite replacing plagioclase at 2023 m depth may contain SiO_2 as high as 34 wt.%, while Al_2O_3 is present as low as 15 wt.%, as the end member of this chlorite shifts to diabantite.

The marginal wells DRJ 1, S-2 and S-6 also contain diabantite with 30-35 wt.% SiO_2, 14-23 wt.% Al_2O_3, 15-25 wt.% FeO, 14-21 wt.% MgO and traces of TiO_2 and MnO of less than 2 and up to 1 wt.% respectively. However, SiO_2 can be as high as 41 wt.% and FeO can be as high as 30 wt.%, while MgO is as low as 8 wt.%, as brunsvigite is associated with diabantite. Pycnochlorite is present at 1251 m depth in well DRJ S-2. As shown in Figure 7.1D, it contains less SiO_2 than diabantite. The SiO_2 and Al_2O_3 contents are 27-30 and about 17 wt.% respectively, but SiO_2 can be as low as 23 wt.%. In well DRJ S-6, pycnochlorite and diabantite occur together at 1772 m depth.

Pycnochlorite and diabantite also occur in the production wells DRJ 5 and 17, i.e. at 1575 and 2407 m depth respectively (Figure 7.1D). They contain 27-32 wt.% SiO_2, 15-19 wt.% Al_2O_3, 16-25 wt.% FeO and 15-22 wt.% MgO. At 2560 m depth in well DRJ 5, the chlorite present is clinochlore, containing less FeO, but more MgO, i.e. 9-12 and 19-27 wt.% respectively. The MnO can be up to 2 wt.%. Here, chlorite replacing plagioclase contains less Al_2O_3 and FeO but more MgO. At 1855 m depth in well DRJ 13, diabantite is Si rich; SiO_2 may be as high as 38 wt.%, but Al_2O_3 can be as low as 10 wt.%. The FeO and MgO contents are 20-26 and 13-18 wt.% respectively.

Rhyolite from 2596 m depth in well DRJ 24 contains chlorite with slightly less replacement Si. Figure 7.1D shows that the end member composition of chlorite is between ripidolite, pycnochlorite and brunsvigite with 25-28 wt.% SiO_2 and 20-22 wt.% Al_2O_3. Its FeO and MgO contents vary from 23 to 30 and 9 to 15 wt.% respectively. However, chlorite present in vugs and veins can contain SiO_2 from 20 to 48 wt.% and Al_2O_3 from 15 to 32 wt.%. The FeO can be as low as 9 wt.% with about 12 wt.% MgO, but can also be as high as 44 wt.%, followed by MgO of about 5 wt.%. The end member chlorite present in cavities and veins varies from daphnite, brunsvigite, diabantite and talc-chlorite. This variation in chlorite compositions likely reflects the type of host rock, i.e. rhyolite.

Fe-Mg compositional zoning occurs. The core of replacement and cavity fill chlorites, e.g. those from 580 m depth in DRJ S-1 and 2207 m depth in DRJ S-5, tends to contain more Mg, whereas the rim contains more Fe, but less Mg. However, chlorites present in veins have more Mg, or less Fe, from core to rim, e.g. chlorites from 1000 and 1332 m depth in DRJ S-3 and S-5 respectively. Zoning of replacement chlorite might indicate an equilibrium process during interactions between fluids and rocks, as suggested by Pattison (1994), and this zoning of vein minerals may suggest cooling circulating fluids (see later). The amount of H_2O in chlorites is approximately 8 to 15 wt.%; chlorites present in the rim and cracks of precursor minerals and the margin of veins are more hydrous.

7.1.2. Illite: $KAl_4[Si_7AlO_{20}](OH)_4$

Illite is present in cavities and veins in wells DRJ S-1, S-5 and DRJ 5. The compositions of illite are represented in Table 7.3 and variations in their amounts of Al, Fe and Mg are shown in Figure 7.3. Illite contains 40-52 wt.% SiO_2, 26-35 wt.% Al_2O_3 and up to 10 wt.% K_2O. Illite from well DRJ 1 may contain less Al_2O_3. Illite filling cavities and veins contains phengitic component; its FeO and MgO vary up to 4 and 5 wt.% respectively. Some chlorite is interlayered with illite or mixed else the two occur as separate phases, e.g. in samples from wells DRJ 1 and from 2550-2600 m depth in well DRJ 5 and 24. Illites then belong to phengite and sericite (Figure 7.3). Phengite is also found in other geothermal systems, e.g. Broadland-Ohaaki, New Zealand (Peacor et al., 2002).

Interlayered phases between illite and smectite are more common altering plagioclase and pyroxene, e.g. at 2155 m depth in DRJ S-5. They contain up to 3 wt.% CaO and Na_2O.

End member composition illite has 0.60 to 0.85 interlayer (alkali) cations per half cell. Illites from well DRJ 1 and 798 m depth in DRJ S-1 have interlayer cations of less than 0.6, suggesting cooler formation condition (Rosenberg, 2002).

7.1.3. Smectite: $(\frac{1}{2}Ca,Na)_{0.7}(Al,Mg,Fe)_4(Si,Al)_8O_{20}(OH)_4.nH_2O$

Smectite replaces plagioclase and pyroxene, and is also present as vug and vein minerals. Table 7.4 represents the composition of smectite. Figure 7.4 shows its variations in Si, Al, Fe, Ca and Na contents and Figure 7.5 shows the proportions of Al, Fe and Mg. The compositions of the smectite, plotted in Figures 7.4 and 7.5, indicate their heterogeneity. Christidis and Dunham (1993) suggested that this is due to the varying proportions of tetrahedral and octahedral charges and substitution by Fe and Mg for exchangeable Ca, Na and K.

Table 7.3.Compositions and structural formulae of representative illites.

Well	DRJ 5		DRJ S-1		DRJ S-1		DRJ S-5		DRJ 5		DRJ S-1		DRJ S-5		DRJ S-1		DRJ S-5	
Depth (m)	2560		798		1023		2155		2560		976		2207		976		890	
Sample	D5-8398		S1-2619		S1-3355		S5-7071		D5-8398		S1-3202		S5-7241		S1-3202		S5-2919	
Analysis no.	2673		1116		3122		3742		3265		6176		4735		6155		5078	
Precursor	Groundmass		Plagioclase		Plagioclase, cracks		Plagioclase		Vein		Vein		Vein, cracks		Vugs		Vugs	
Name*	Mg-Fe Sericite		Phengite		Illite		Phengite		Phengite		Phengite		Illite		Phengite		Phengite	
Oxide (wt.%)																		
SiO_2	44.61		47.79		45.56		49.65		49.44		48.75		43.33		48.21		48.24	
TiO_2	0.10		-		0.24		-		0.18		0.14		0.09		0.06		0.09	
Al_2O_3	29.36		30.85		33.01		31.58		31.38		29.75		33.07		28.78		31.10	
FeO	2.05		1.77		0.26		0.57		0.88		0.74		0.27		0.78		0.86	
MnO	0.11		0.07		0.07		0.11		< 0.08		< 0.02		0.10		0.08		0.19	
MgO	4.22		1.60		0.73		1.34		1.23		1.93		0.47		2.05		2.17	
CaO	0.52		0.74		0.20		0.65		0.89		0.35		0.28		0.58		0.16	
Na_2O	0.27		0.08		0.07		0.06		0.17		0.19		< 0.06		0.15		0.20	
K_2O	7.30		6.60		9.44		7.96		8.69		9.04		10.35		8.33		9.97	
Cl	0.02		0.11		0.07		0.03		0.02		0.07		0.05		0.08		0.05	
NiO	-		< 0.03		0.02		0.01		0.16		< 0.06		0.01		0.04		< 0.01	
Cr_2O_3	< 0.01		-		< 0.06		0.03		0.04		< 0.05		-		< 0.07		< 0.03	
P_2O_5	< 0.03		-		< 0.13		-		< 0.13		< 0.07		< 0.04		0.12		< 0.07	
Total	88.70		89.99		89.69		92.07		93.25		90.86		87.95		89.86		93.02	
Number of ions on the basis of 22 (O)																		
Si	6.314	8.00	6.179	8.00	6.358	8.00	6.666	8.00	6.622	8.00	6.710	8.00	6.226	8.00	6.666	8.00	6.534	8.00
Al^{IV}	1.686		1.821		1.642		1.334		1.378		1.290		1.774		1.334		1.466	
Al^{VI}	3.220	4.39	2.880	3.34	3.792	3.99	3.660	4.01	3.572	3.92	3.528	4.03	3.836	3.99	3.352	3.86	3.506	4.06
Fe^{2+}	0.242		0.159		0.022		0.066		0.088		0.088		0.022		0.088		0.088	
Mg	0.902		0.300		0.154		0.264		0.242		0.396		0.110		0.418		0.440	
Ti	-		-		0.022		-		0.022		0.022		-		-		-	
Mn	0.022		-		-		0.022		-		-		0.022		-		0.022	
Ca	0.088	1.47	0.083	1.18	0.022	1.72	0.088	1.47	0.132	1.65	0.044	1.67	0.044	1.91	0.088	1.61	0.022	1.78
Na	0.066		0.022		0.022		0.022		0.044		0.044		-		0.044		0.044	
K	1.320		1.079		1.672		1.364		1.474		1.584		1.892		1.474		1.716	
Cl	-		-		0.022		-		-		0.022		-		0.022		-	
Ratio																		
K:(K+Na+Ca)	0.90		0.81		0.97		0.93		0.89		0.95		0.99		0.92		0.96	

* Name follows Deer et al. (1962a).

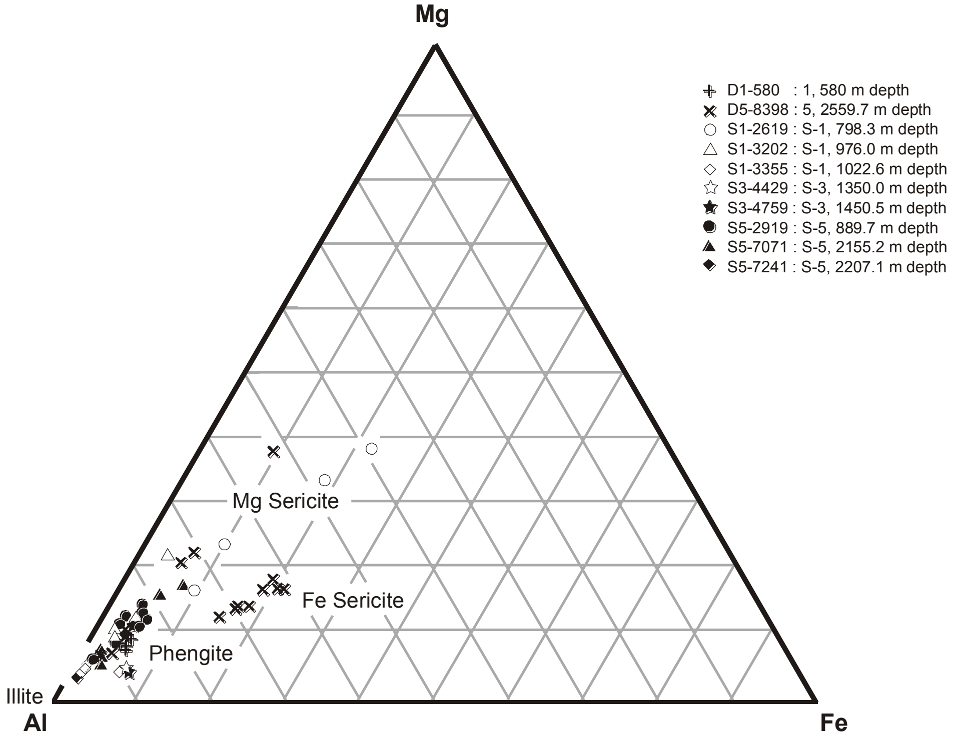

Figure 7.3.Proportions of Al, Fe and Mg in the octahedral site of illite. Most illites are Mg and Fe bearing phengite, some are sericite (classification follows Deer et al., 1962a). Illite is present as a replacement and cavity fillings, except that from samples D5-8398, S1-3202 and S5-7241 which is also a vein mineral. Sample numbers are given.

The compositions of smectite are mostly between montmorillonite and biedellite, containing 44-56 wt.% SiO_2 and 28-37 wt.% Al_2O_3. As shown in Figure 7.4A, there is a negative correlation between total Al and Si. The amounts of CaO vary up to 4 wt.% but can be as high as 10 wt.% in wells DRJ S-2 and S-5. The Na_2O and K_2O contents range up to 3 and 2 wt.% respectively. The ratio values of Ca to Ca+K+Na are greater than 0.5, but at 1350 m depth in DRJ S-3, the ratio of Ca to Ca+alkalis is between 0.2 and 0.4, as the ratio of Na to Ca+alkalis is up to 0.6.

Smectite is typically Fe poor (Figure 7.5), containing less than 3 wt.% FeO and only traces of MgO and MnO. However, smectite from an acid alteration zone at about 2120 m depth in well DRJ S-3 contains up to 17 wt.% FeO and that from 400-600 m depth in DRJ 1, S-2 and S-3 contains up to 15 wt.% MgO. The smectites are classified into nontronite and saponite (Figure 7.5), likely to be associated with chlorite, pyrophyllite or vermiculite. Velde and Brusewitz (1986) reported that the composition of smectite is controlled by the type of host rocks and temperature condition.

Table 7.4.Compositions and structural formulae of representative smectites.

Well	DRJ S-2		DRJ S-3		DRJ S-3		DRJ S-3		DRJ S-3		DRJ S-5		DRJ S-5		DRJ S-3		DRJ S-3	
Depth (m)	579		617		1350		2120		2122		2207		2207		617		617	
Sample	S2-1900		S3-2025		S3-4429		S3-6956		S3-6962		S5-7241		S5-7241		S3-2025		S3-2025	
Analysis no.	5876		3866		3382		1054		3614		4687		4688		3868		3861	
Precursor	Plagioclase		Pyroxene		(Plagioclase)		Plagioclase		Groundmass		Plagioclase		Plagioclase		Vein		Vugs, middle	
Name*	Mg Biedelite		Nontronite-Saponite		Montmorillonite-Hectorite		Biedelite-Hectorite		Biedelite-Hectorite		Montmorillonite		Montmorillonite		Nontronite-Saponite		Nontronite-Saponite	
Oxide (wt.%)																		
SiO_2	55.63		41.79		49.04		46.67		50.29		53.55		53.18		39.25		40.35	
TiO_2	< 0.03		< 0.02		0.01		0.42		0.46		< 0.09		< 0.07		0.02		0.06	
Al_2O_3	21.49		9.87		35.88		33.51		33.07		21.48		21.03		9.58		10.24	
FeO	4.15		17.17		0.50		9.05		3.25		0.42		0.46		16.80		16.62	
MnO	0.01		0.20		< 0.09		< 0.01		< 0.04		< 0.08		0.04		0.39		0.39	
MgO	5.19		15.73		< 0.07		0.26		< 0.08		0.05		0.19		14.66		15.36	
CaO	2.36		2.11		2.32		2.23		2.25		11.38		11.02		2.58		2.10	
Na_2O	0.64		0.31		3.03		1.77		1.67		0.24		0.16		0.32		0.08	
K_2O	0.92		0.31		1.44		0.57		0.53		0.16		0.08		0.16		0.19	
Cl	0.04		0.05		-		0.02		0.01		< 0.02		0.01		0.03		0.10	
NiO	0.11		0.08		< 0.10		< 0.05		0.04		0.06		< 0.01		< 0.02		< 0.16	
Cr_2O_3	0.04		0.14		0.05		0.02		0.01		0.05		0.06		0.09		0.12	
P_2O_5	< 0.01		< 0.06		< 0.14		0.05		< 0.10		< 0.05		< 0.05		< 0.10		0.01	
Total	90.50		87.65		91.84		94.51		91.38		87.10		86.03		83.81		85.44	
Number of ions on the basis of 22 (O)																		
Si	7.458	8.00	6.490	8.00	6.424	8.00	6.204	8.00	6.644	8.00	7.480	8.00	7.502	8.00	6.402	8.00	6.402	8.00
Al^{IV}	0.452		1.510		1.576		1.796		1.356		0.520		0.498		1.598		1.598	
Al^{VI}	2.846	4.34	0.294	6.17	3.968	4.01	3.440	4.50	3.792	4.17	3.022	3.09	3.000	3.09	0.250	6.15	0.316	6.19
Fe^{2+}	0.462		2.222		0.044		1.012		0.352		0.044		0.044		2.288		2.200	
Mg	1.034		3.630		-		0.044		-		0.022		0.044		3.564		3.630	
Ti	-		-		-		0.044		0.044		-		-		-		-	
Mn	-		0.022		-		-		-		-		-		0.044		0.044	
Ca	0.330	0.66	0.352	0.51	0.330	1.34	0.308	0.86	0.308	0.81	1.694	1.78	1.672	1.74	0.440	0.57	0.352	0.42
Na	0.176		0.088		0.770		0.462		0.418		0.066		0.044		0.110		0.022	
K	0.154		0.066		0.242		0.088		0.088		0.022		0.022		0.022		0.044	
Cl	-		0.022		-		-		-		-		-		-		0.022	
Ratio																		
Ca:(Ca+K+Na)	0.50		0.69		0.25		0.36		0.38		0.95		0.96		0.77		0.84	
Na:(Ca+K+Na)	0.27		0.17		0.57		0.54		0.52		0.04		0.03		0.19		0.05	

* Name follows Deer et al. (1962a) and Grim (1968).

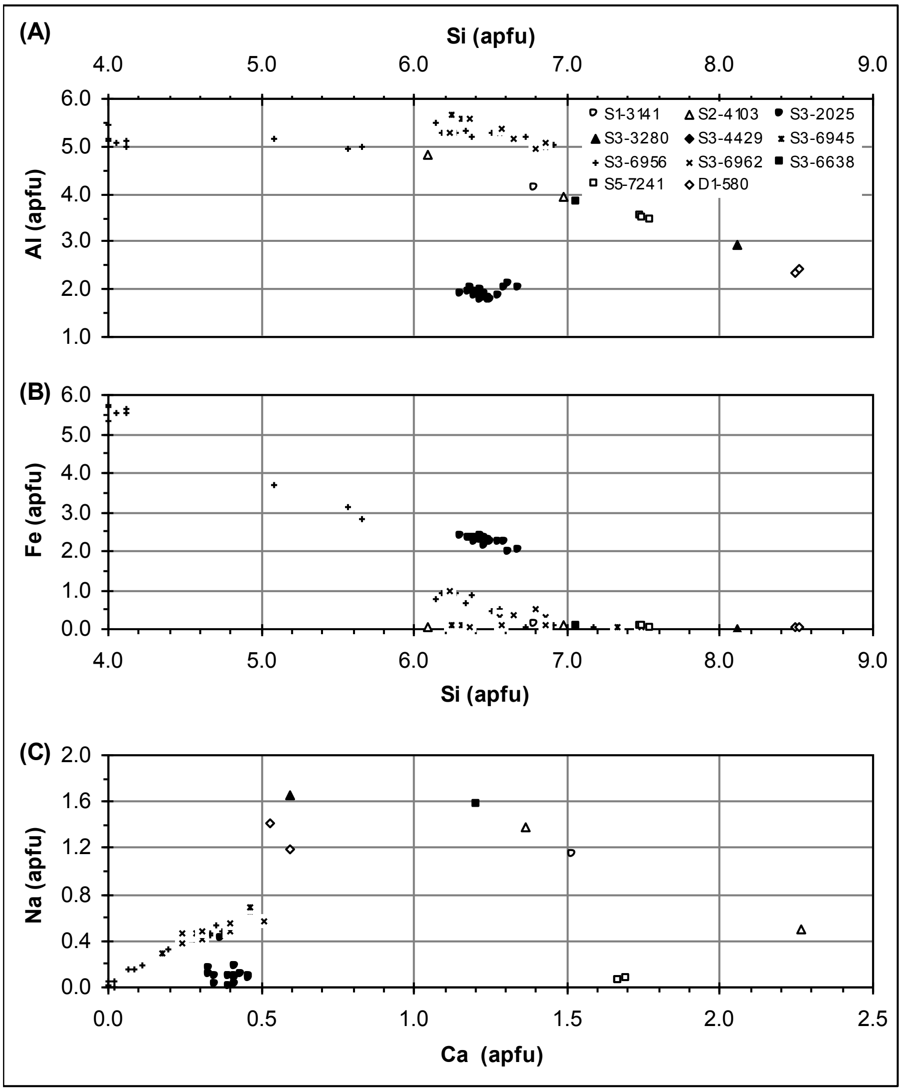

Figure 7.4. Variations in the amounts of Si and: **(A)** Al, **(B)** Fe and **(C)** Ca and Na (apfu = atoms per formulae unit) in smectite, calculated on the basis of 22 oxygens. Sample numbers are given.

7.1.4. Kaolinite: $Al_4(Si_4O_{10})(OH)_8$

Kaolinite is present at several depths in well DRJ 1, 2, S-1 and S-5. Table 7.5 represents its composition and this replaces plagioclase and fills veins containing 45-53 wt.% SiO_2 and 32-40 wt.% Al_2O_3. End member kaolinite can be expressed as $Al_{2.3\text{-}2.8}(Si_{2.9\text{-}3.2}O_{10})(OH)_8$. However, kaolinite replacing plagioclase at 43 m depth in well DRJ 2 may contain more SiO_2 but less Al_2O_3, i.e. about 70 and 14-16 wt.% respectively. This kaolinite also contains less than 1.6 wt.% FeO and about 2 wt.% SO_3; it probably contains a trace of pyrite.

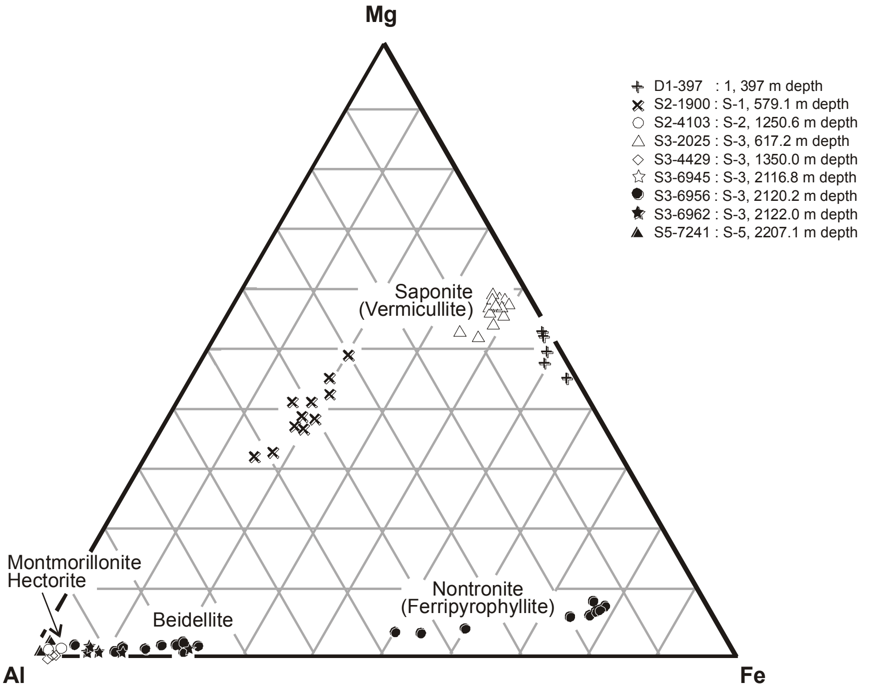

Figure 7.5.Proportions of Al, Fe and Mg in the octahedral site of smectite. The diagram follows Velde (1985) and Güven (1988); the smectite classification is after Deer et al. (1962a). All smectites are likely expandable, according to the classification of Christidis and Dunham (1993) and they are mostly between montmorillonite-hectorite and beidellite, but some smectites are Mg rich saponite and Fe rich nontronite. Saponite is chemically similar to vermiculite and nontronite is structurally identical with pyrophyllite (Deer et al., 1962a). Sample numbers are given. All smectites are present as replacement and in vugs, except that from 617 m in DRJ S-3, which is also a vein mineral.

7.1.5. Pyrophyllite: $Al_2(Si,Al)_4O_{10}(OH)_2$

Pyrophyllite is present in well DRJ S-3 at about 2120 m depth and representative analyses are shown in Table 7.6. At 2117 m depth in DRJ S-3, pyrophyllite that occurs in groundmass contains about 64 wt.% SiO_2, 29 wt.% Al_2O_3 and less than 2 wt.% FeO. Traces of TiO_2 are present, but MgO and MnO are absent. No CaO and alkalis are present in groundmass pyrophyllite. However, pyrophyllite in cavities and veins contains up to 2 wt.% CaO and alkalis, with slightly less SiO_2 (50 to 60 wt.%) and more Al_2O_3 and FeO (34 and 7 wt.% respectively). This might be due to the occurrence of interlayered smectite and chlorite in the interstratified phases (Evans and Guggenheim, 1988). According to Rosenberg and Cliff (1980), end member pyrophyllite can be expressed as $Al_{1.0\text{-}1.4}(Si_{3.0\text{-}3.5},Al_{1.0\text{-}0.5})O_{10}(OH)_n$.

At 2120 m depth, pyrophyllite replacing plagioclase and filling cavities has a significantly different composition. This pyrophyllite contains 20-38 wt.% SiO_2, 23-29 wt.% Al_2O_3, 22-39 wt.% FeO and up to 3 wt.% MgO. This suggests that both Fe and Mg have substituted for Al in the octahedral structure, therefore the end member composition is likely to be ferripyrophyllite,

Table 7.5.Compositions and structural formulae of representative kaolinite.

Well	DRJ 1		DRJ S-5		DRJ 2		DRJ S-1		DRJ S-5	
Depth (m)	580		890		43		304		890	
Sample	D1-580		S5-2919		D2-43		S1-998		S5-2919	
Analysis no.	4854		5100		1024		5835		5083	
Precursor	Plagioclase		Plagioclase		Groundmass		Vein, margin		Vugs	
Oxide (wt.%)										
SiO_2	45.87		46.84		52.41		45.81		45.45	
TiO_2	< 0.02		0.08		0.01		0.12		0.09	
Al_2O_3	37.79		38.48		32.26		38.29		37.40	
FeO	0.14		< 0.03		0.37		< 0.03		0.17	
MnO	0.05		< 0.04		0.02		< 0.03		< 0.03	
MgO	0.12		0.01		< 0.01		0.21		0.14	
CaO	0.17		0.01		0.02		0.23		0.14	
Na_2O	0.01		-		0.09		0.01		0.01	
K_2O	0.06		0.05		0.09		0.02		0.04	
Cl	0.01		-		0.01		0.02		0.02	
NiO	0.02		< 0.06		< 0.07		0.03		-	
Cr_2O_3	0.19		< 0.06		< 0.01		0.14		0.06	
SO_3	< 0.03		< 0.09		0.59		0.02		-	
P_2O_5	< 0.05		< 0.02		< 0.08		0.07		< 0.05	
Total	84.32		85.18		85.71		84.90		83.45	
Number of ions on the basis of 10 (O)										
Si	2.880	4.00	2.920	4.00	3.210	4.00	2.860	4.00	2.880	4.00
Al^{IV}	1.120		1.080		0.790		1.140		1.120	
Al^{VI}	1.680	1.69	0.670	0.68	1.540	1.56	1.670	1.70	1.680	1.70
Ti	-		-		-		0.010		-	
Fe^{2+}	0.010		-		0.020		-		0.010	
Mn	-		-		-		-		-	
Mg	0.010		0.010		-		0.020		0.010	
Ca	0.010	0.02	0.010	0.03	-	0.02	0.020		0.010	
Na	-		0.010		0.010		-		-	
K	0.010		0.010		0.010		-		-	

$(Al_{0.1-0.8},Fe_{2.6-1.3},Mg_{0.0-0.3})$ $(Si_{1.7-2.6},Al_{2.3-1.4})O_{10}(OH)_n$. In addition, an increase in the amount of Fe is also reflected by the XRD pattern (see Appendix C).

Takagi et al. (2000) reported that the amount of Al_2O_3 in pyrophyllite relates to the temperature of its formation; the decrease in Al_2O_3 contents from 29 to 23 wt.% suggests a slight decrease in the formation temperatures from 300 to 250°C.

Table 7.6.Compositions and structural formulae of representative pyrophyllite.

Well	DRJ S-3	DRJ S-3	DRJ S-3	DRJ S-3	DRJ S-3	DRJ S-3	DRJ S-3	DRJ S-3	DRJ S-3
Depth (m)	2117	2117	2120	2117	2120	2117	2117	2120	2120
Sample	S3-6945	S3-6945	S3-6956	S3-6945	S3-6956	S3-6945	S3-6945	S3-6956	S3-6956
Analysis no.	3370	3373	1033	3367	1039	3389	3393	1035	1051
Precursor/ Occurrence	Groundmass	Groundmass, with laths	Groundmass	Plagioclase, crack, smectite	Plagioclase*	Vein, with apatite, smectite	Vugs, middle, with smectite	Vugs*	Vugs, with quartz*
Oxide (wt.%)									
SiO_2	64.20	63.89	63.30	52.35	35.67	50.91	55.20	23.26	22.36
TiO_2	0.10	0.17	< 0.01	1.93	< 0.05	3.14	0.13	0.07	0.02
Al_2O_3	29.16	28.96	30.46	30.90	27.01	30.76	33.73	26.92	24.38
FeO	1.43	0.57	1.31	6.49	23.91	6.47	0.46	37.25	38.17
MnO	0.07	< 0.04	< 0.13	0.10	0.25	0.11	< 0.08	0.26	0.29
MgO	< 0.05	< 0.07	0.06	0.13	0.73	0.08	< 0.03	1.63	1.88
CaO	0.28	0.34	0.32	1.40	0.55	1.53	1.87	0.03	< 0.02
Na_2O	0.68	0.59	0.66	0.98	0.49	1.09	1.34	0.09	0.01
K_2O	0.09	0.14	0.57	0.28	0.26	0.32	1.13	0.02	< 0.01
Cl	0.03	0.04	0.06	0.01	< 0.06	-	< 0.04	< 0.04	0.00
NiO	0.04	-	0.12	0.02	0.00	< 0.04	0.04	< 0.18	< 0.06
Cr_2O_3	-	0.04	0.03	< 0.1	< 0.10	< 0.08	0.02	0.01	0.09
Total	96.07	94.56	96.75	94.34	88.57	94.33	93.88	89.34	87.20

Number of ions on the basis of 10 (O)

	3370		3373		1033		3367		1039		3389		3393		1035		1051	
Si	3.520	4.00	3.540	4.00	3.460	4.00	3.080	4.00	2.530	4.00	3.000	4.00	3.160	4.00	1.820	4.00	1.820	4.00
Al^{IV}	0.480		0.460		0.540		0.920		1.470		1.000		0.840		2.180		2.180	
Al^{VI}	1.400	1.47	1.430	1.47	1.420	1.48	1.220	1.65	0.780	2.30	1.140	1.62	1.430	1.46	0.300	2.94	0.150	2.99
Ti	-		0.010		-		0.090		-		0.140		0.010		-		-	
Fe^{2+}	0.070		0.030		0.060		0.320		1.420		0.320		0.020		2.430		2.590	
Mn	-		-		< 0.010		0.010		0.020		0.010		-		0.020		0.020	
Mg	-		-		-		0.010		0.080		0.010		-		0.190		0.230	
Ca	0.020	0.10	0.020	0.09	0.020	0.13	0.090	0.22	0.040	0.13	0.100	0.24	0.110	0.34	-	0.01	-	
Na	0.070		0.060		0.070		0.110		0.070		0.120		0.150		0.010		-	
K	0.010		0.010		0.040		0.020		0.020		0.020		0.080		-		-	

* Ferripyrophyllite (Evans and Guggenheim, 1988) or, probably, nontronite (Deer et al., 1962a).

7.2. CALC-SILICATES

7.2.1. Laumontite: $Ca[Al_2Si_4O_{12}].nH_2O$

Laumontite replaces plagioclase below 1000 m depth in well DRJ S-3 and fills veins at 2155 m depth in DRJ S-5. The composition of laumontite is representatively given in Table 7.7. Where laumontite replaces plagioclase, it contains 52-58 wt.% SiO_2, 16-22 wt.% Al_2O_3 and 8-12 wt.% CaO. The amount of SiO_2 is less and both Al_2O_3 and CaO are greater in laumontite veins. The SiO_2 values range from 51 to 54 wt.% and Al_2O_3 and CaO vary from 20 to 22 and 10 to 12 wt.% respectively. Alkalis are present as traces, i.e. less than 0.6 wt.%. The ratio of Ca to Ca plus alkalis is above 0.89.

The composition of end member laumontite replacing plagioclase can then be expressed as $Ca_{0.7\text{-}1.0}[Al_{1.5\text{-}2.0}Si_{4.0\text{-}4.5}O_{12}].nH_2O$ and that in veins as $Ca_{0.6\text{-}1.0}[Al_{1.6\text{-}2.0}Si_{3.7\text{-}4.3}O_{12}].nH_2O$. Analysis totals of 82-86 wt.% indicate that the amount of H_2O present is between 14 and 18 wt.% in replacement laumontite and between 14 and 16 wt.% in vein laumontite.

Table 7.7.Compositions and structural formulae of representative laumontites.

Well	DRJ S-3	DRJ S-3	DRJ S-3	DRJ S-5	DRJ S-5	DRJ S-5
Depth (m)	1000	1000	1350	2155	2155	2155
Sample	S3-3280	S3-3280	S3-4429	S5-7071	S5-7071	S5-7071
Analysis no.	4511	4512	2711	3707	3709	3720
Precursor/ Occurrence	Plagioclase	Plagioclase	Plagioclase, crack	Vein	Vein	Vein
Oxide (wt.%)						
SiO_2	56.17	57.29	52.16	53.02	51.96	52.96
TiO_2	0.09	< 0.01	-	0.13	0.02	0.04
Al_2O_3	16.44	16.38	21.86	21.19	20.69	20.96
FeO	< 0.02	< 0.02	0.03	0.05	0.02	< 0.03
MnO	0.01	0.04	0.12	0.03	< 0.08	0.11
MgO	< 0.01	< 0.03	< 0.05	0.01	-	< 0.05
CaO	8.89	8.44	11.79	11.23	11.07	10.85
Na_2O	0.35	0.31	< 0.01	0.16	0.17	0.27
K_2O	0.16	0.12	0.07	0.13	0.14	0.26
Cl	0.01	< 0.04	< 0.05	< 0.01	< 0.02	0.01
NiO	0.03	0.15	0.09	0.05	< 0.01	< 0.03
Cr_2O_3	0.17	0.04	< 0.01	0.14	0.17	0.04
SO_3	< 0.01	< 0.02	< 0.04	< 0.03	0.08	0.04
P_2O_5	< 0.01	< 0.08	< 0.06	< 0.01	< 0.04	< 0.03
Total	82.27	82.58	85.91	86.10	84.18	85.39
Number of ions on the basis of 48 (O)						
Si	17.760	18.000	16.080	16.320	16.320	16.368
Al	6.144	6.048	7.968	7.680	7.632	7.632
Ti	-	-	-	0.048	-	-
Fe^{2+}	-	-	-	-	-	-
Mn	-	-	0.048	-	-	0.048
Mg	-	-	-	-	-	-
Ca	3.024	2.832	3.888	3.696	3.744	3.600
Na	0.240	0.192	-	0.096	0.096	0.144
K	0.048	0.048	0.048	0.048	0.048	0.096
Ratio						
Ca:(Ca+K+Na)	0.91	0.92	0.99	0.96	0.96	0.94

7.2.2. Wairakite: $Ca[AlSi_2O_6].nH_2O$

Wairakite replaces plagioclase and fills cavities, veins and fractures at 1020-1060 m in well DRJ S-1 and 1332 and 2207 m in well DRJ S-5. In DRJ 5, wairakite occurs in veins overprinted by anhydrite. Table 7.8 shows some selected analyses of wairakite. Wairakite replacing plagioclase in phenocrysts and the groundmass is composed of 52-55 wt.% SiO_2, 21-23 wt.% Al_2O_3 and 10-13 wt.% CaO. Alkalis are low, i.e. less than 1 wt.% Na_2O and 0.1 wt.% K_2O; the ratio of Ca to Ca+K+Na is above 0.86. Wairakite is also present in veins as a product of direct fluid deposition. This has slightly more SiO_2, Al_2O_3 and CaO (Table 7.8).

The end member composition of wairakite, in replacement and vein minerals, can be expressed as $Ca_{0.7\text{-}1.1}[Al_{1.9\text{-}2.0}Si_{4.0\text{-}4.2}O_{12}].nH_2O$. Low total oxides indicate that its H_2O content is between approximately 10 and 16 wt.% as a replacement, but slightly less in veins, where wairakite may contain 9 to 15 wt.% H_2O.

7.2.3. Prehnite: $Ca_2Al[AlSi_3O_{10}](OH)_2$

Prehnite occurs between 1050 and 1300 m depth in DRJ S-1 as replacement, cavity and vein filling minerals, and at 1000 m depth in DRJ S-3 as plagioclase replacement. Selected compositions of prehnite are given in Table 7.9. As replacement and vein minerals, prehnite contains 42-44 wt.% SiO_2, 18-24 wt.% Al_2O_3 and 22-27 wt.% CaO. The wide variation in Al_2O_3 relates to the amount of FeO present. The pistacite content, expressed as the ratio of Fe to Fe+Al in the tetrahedral site, is shown in Figure 7.6. Both MnO and MgO are less than 1 wt.%.

Prehnite commonly replaces plagioclase but also pyroxene. In DRJ S-1, the Al_2O_3 and FeO contents of the replacement prehnite are 21-22 and up to 6 wt.% respectively, yielding pistacite values of up to 0.2. In DRJ S-3, the Al_2O_3 and FeO contents are more uniform, i.e. averaging 20 and 8 wt.% respectively, and the pistacite values vary between only 0.1 and 0.2. Prehnite present in the groundmass at 1058 m depth in DRJ S-1 has about 23 wt.% Al_2O_3 but FeO is about 1.2 wt.%. Consequently, its pistacite content is only about 0.05.

Vein prehnite varies widely in its Al_2O_3 and FeO contents, i.e. 18-24 and up to 10 wt.% respectively, so its pistacite content is up to 0.3. Prehnite is also present in cavities between 1240 and 1300 m depth in well DRJ S-1. The variations in Al_2O_3 and FeO are 21-23 and 1-3 wt.% respectively and the pistacite is less than 0.1. Zoning is hardly evident, however, some prehnites, e.g. a crystal from 1323 m depth in well DRJ S-1, has a rim with less FeO than in its core.

Table 7.8.Compositions and structural formulae of representative wairakites.

Well	DRJ S-1	DRJ S-1	DRJ S-5	DRJ S-5	DRJ S-1	DRJ S-1	DRJ S-1	DRJ S-5	DRJ 5	DRJ 5	DRJ S-1	DRJ S-1
Depth (m)	1058	1023	1332	2207	1023	1058	1058	2207	2560	2560	1023	1023
Sample	S1-3470	S1-3355	S5-4370	S5-7241	S1-3355	S1-3470	S1-3470	S5-7241	D5-8398	D5-8398	S1-3355	S1-3355
Analysis no.	3033	3126	2200	4567	3107	3006	3007	4736	3247	3252	3141	3148
Precursor/ Occurrence	Plagioclase	Plagioclase	Plagioclase	Plagioclase	Groundmass, with epidote	Vein	Vein	Vein	Vein, with anhydrite	Vein	Vugs	Vugs
Oxide (wt.%)												
SiO_2	52.11	53.16	52.85	55.82	53.54	52.32	53.64	55.21	54.13	52.38	54.75	52.77
TiO_2	0.03	0.12	0.16	-	0.06	< 0.02	0.01	0.10	0.13	< 0.12	0.01	0.03
Al_2O_3	21.75	22.62	20.65	21.39	22.28	22.04	22.63	22.90	22.06	21.39	22.42	22.47
FeO	0.09	0.07	0.09	0.07	0.45	< 0.12	0.09	0.04	0.02	0.03	0.21	0.54
MnO	0.01	0.03	0.10	0.13	< 0.03	< 0.02	0.04	0.11	< 0.07	0.06	0.07	0.06
MgO	< 0.07	< 0.08	< 0.03	< 0.07	< 0.03	0.09	-	< 0.01	< 0.05	0.01	0.05	< 0.02
CaO	12.24	12.41	10.83	11.00	12.21	11.88	12.35	12.16	11.92	11.70	12.22	12.45
Na_2O	0.21	0.07	0.22	0.21	0.14	0.07	0.09	0.43	0.45	0.46	0.34	0.07
K_2O	0.06	0.03	0.20	0.17	0.03	0.04	0.01	0.10	0.10	0.02	-	0.03
Cl	0.04	< 0.02	0.04	0.01	-	< 0.03	0.05	0.03	0.02	0.03	< 0.03	0.08
NiO	0.15	0.12	0.09	0.05	-	0.13	0.03	< 0.14	< 0.03	< 0.02	0.04	0.18
Cr_2O_3	0.06	0.18	< 0.04	0.02	< 0.01	0.01	< 0.01	0.08	0.15	0.02	0.04	0.12
SO_3	0.01	< 0.11	0.14	< 0.03	< 0.05	0.07	< 0.05	0.06	0.06	0.17	0.09	< 0.02
P_2O_5	< 0.13	< 0.14	< 0.03	0.01	< 0.16	< 0.08	< 0.07	< 0.08	< 0.05	0.06	< 0.02	0.02
Total	86.56	88.45	85.26	88.76	88.43	86.39	88.81	90.99	88.84	86.19	90.21	88.79
Number of ions on the basis of 6 (O)												
Si	2.004	1.998	2.052	2.070	2.010	2.004	2.004	2.010	2.022	2.016	2.016	1.986
Al	0.984	1.002	0.942	0.936	0.984	0.996	0.996	0.984	0.972	0.972	0.972	0.996
Ti	-	0.006	0.006	-	-	-	-	-	0.006	-	-	-
Fe^{2+}	0.006	-	-	-	0.012	-	-	-	-	-	0.006	0.018
Mn	-	-	0.006	0.006	-	-	-	0.006	-	-	-	-
Mg	-	-	-	-	-	0.006	-	-	-	-	-	-
Ca	0.504	0.498	0.450	0.438	0.492	0.486	0.492	0.474	0.474	0.480	0.480	0.504
Na	0.018	0.006	0.018	0.018	0.012	-	0.006	0.030	0.030	0.036	0.024	0.006
K	-	-	0.012	0.006	-	-	-	0.006	0.006	-	-	-
Ratio												
Ca:(Ca+K+Na)	0.97	0.99	0.94	0.95	0.98	1.00	0.99	0.93	0.93	0.93	0.95	0.99

Table 7.9.Compositions and structural formulae of representative prehnites.

Well	DRJ S-1	DRJ S-1	DRJ S-3	DRJ S-1	DRJ S-1	DRJ S-1	DRJ S-1	DRJ S-1	DRJ S-1
Depth (m)	1179	1298	1000	1298	1058	1058	1179	1298	1242
Sample	S1-3869	S1-4259	S3-3280	S1-4259	S1-3470	S1-3470	S1-3869	S1-4259	S1-4074
Analysis no.	1877	3871	4523	3882	3048	3013	1874	3773	3694
Precursor	Plagioclase	Plagioclase	Plagioclase	Pyroxene?	Groundmass	Vein	Vein	Vein	Vugs
Oxide (wt.%)									
SiO_2	42.34	43.71	43.80	43.18	44.10	43.83	42.14	43.36	43.33
TiO_2	0.19	0.08	0.04	0.10	0.09	0.21	< 0.03	< 0.01	< 0.02
Al_2O_3	19.16	23.31	19.80	21.43	23.24	23.26	19.88	22.87	22.27
FeO	5.69	1.23	5.44	3.60	1.47	0.68	5.07	1.20	2.29
MnO	0.05	< 0.08	0.01	0.05	0.15	0.27	0.01	0.06	< 0.07
MgO	< 0.03	0.07	0.08	0.07	0.03	-	< 0.01	< 0.01	0.03
CaO	26.19	26.51	25.73	26.27	25.90	26.20	26.04	26.27	25.83
Na_2O	0.07	0.12	0.08	-	0.26	< 0.03	0.01	< 0.04	0.10
K_2O	0.07	0.01	0.04	-	0.02	0.04	0.05	0.16	0.04
Cl	0.05	< 0.01	0.01	0.02	0.03	< 0.04	< 0.03	< 0.04	0.04
NiO	< 0.06	0.05	< 0.03	0.05	-	-	< 0.05	0.05	0.07
Cr_2O_3	< 0.01	0.16	0.11	0.05	< 0.06	0.14	0.05	0.13	0.08
SO_3	-	0.03	< 0.04	0.04	0.04	0.01	< 0.09	0.11	< 0.08
P_2O_5	< 0.14	< 0.03	< 0.04	-	< 0.04	< 0.14	< 0.07	0.11	< 0.05
Total	93.57	95.16	95.06	94.87	95.24	94.45	92.97	94.22	93.87

Number of ions on the basis of 24 (O, OH)

Si	6.160		6.072		6.226		6.094		6.116		6.116		6.138		6.072		6.138	
Al^{IV}	-		-		-		-		-		-		-		-		-	
Al^{VI}	3.278	3.98	3.806	3.96	3.322	3.98	3.564	4.00	3.784	3.98	3.828	3.96	3.410	4.03	3.784	3.92	3.856	4.12
Ti	0.022		-		-		-		-		0.022		-		-		-	
Fe^{2+}	0.682		0.132		0.638		0.418		0.176		0.088		0.616		0.132		0.264	
Mn	-		-		-		-		0.022		0.022		-		-		-	
Mg	-		0.022		0.022		0.022		-		-		-		-		-	
Ca	4.070	4.11	3.938	3.96	3.916	3.94	3.960	3.96	3.850	3.92	3.916	3.92	4.048	4.05	3.938	3.66	3.916	3.94
Na	0.022		0.022		0.022		-		0.066		-		-		-		0.022	
K	0.022		-		-		-		-		-		-		-		-	
Pistacite $Fe^{2+}:(Fe^{2+}+Al^{IV})$	0.17		0.03		0.15		0.10		0.04		0.02		0.15		0.03		0.06	

The end member composition of prehnite can be expressed as $Ca_{1.4-1.7}Al_{1.3-1.7}[Al_{0.2-0.0}Si_{2.2-2.6}O_{10}](OH)_n$. The amount of H_2O in prehnite (estimated by difference) is approximately 4 to 8 wt.%. Vein prehnite mostly has more Fe but less H_2O. Figure 7.6 shows that the pistacite values of prehnite from well DRJ S-1 tend to increase with increasing depth.

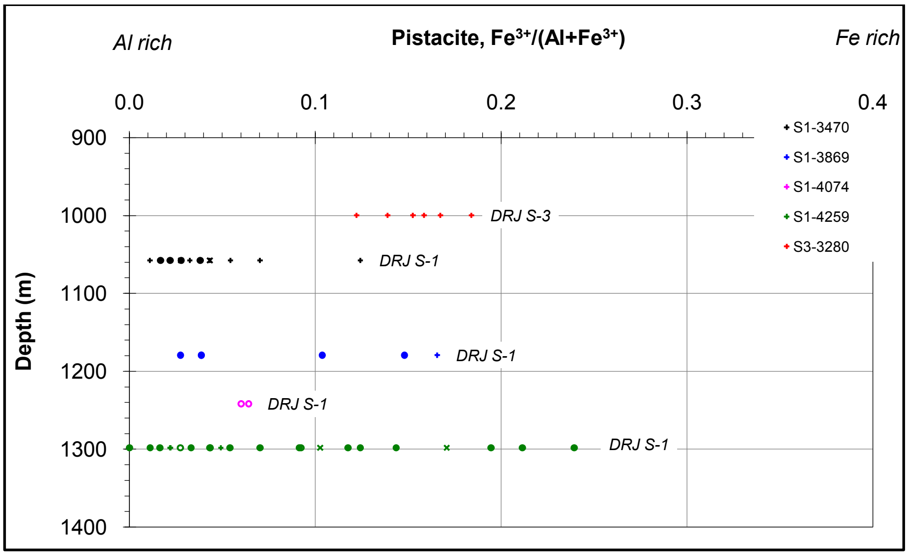

Figure 7.6. Variations in the pistacite values, i.e. ratio between Fe^{3+} and Fe^{3+} plus Al, in prehnite (on the basis of 24 oxygens) and depth (m) from wells DRJ S-1 and S-3. High pistacite values indicate Fe rich prehnite, whereas low values indicate Al rich prehnite. Sample numbers are given; precursor symbols (+) plagioclase, (×) pyroxene and (∗) groundmass; (○) prehnite in cavities and (●) vein prehnite.

7.2.4. Titanite: $CaTi[SiO_4](O,OH,F)$

Titanite replaces plagioclase and pyroxene; it also occurs in veins and vugs. Table 7.10 reports the compositions of titanite and shows it contains 25-36 wt.% SiO_2, 26-46 wt.% TiO_2 and 23-29 wt.% CaO. Aluminium oxide (Al_2O_3) varies up to 9 wt.%; the FeO content is less than 2.5 wt.%. Titanite replacing the groundmass contains less SiO_2, TiO_2, CaO and FeO. The Al_2O_3 content of vein and vug titanites is less than 5 wt.%.

End member titanite can be expressed as $Ca_{3.3-4.0}[Ti_{2.8-4.7}Al_{1.2-0.0}]Si_{3.3-4.6}O_{20}$, where it replaces phenocrysts and the groundmass, and $Ca_{3.8-4.0}[Ti_{2.6-3.8}Al_{1.4-0.1}][Si_{4.0-4.3}]O_{20}$ and $Ca_{3.5-4.0}Ti_{3.1-4.0}Al_{0.7-0.2}]Si_{3.9-4.6}O_{20}$, when it is present in veins and as a cavity mineral respectively.

The compositional zoning shows that the rims of titanite seem to contain more TiO_2, e.g. titanites from 1982 and 2156 m depth in DRJ S-3 and S-5 respectively, whereas the cores have more FeO and MgO.

Table 7.10.Compositions and structural formulae of representative titanites.

Well	DRJ S-3		DRJ S-5		DRJ S-5		DRJ S-3		DRJ S-1		DRJ 5		DRJ S-5		DRJ S-3		DRJ S-5	
Depth	1201		1250		2207		1982		1023		2560		2207		1350		1332	
Sample	S3-3940		S5-4100		S5-7241		S3-6502		S1-3355		D5-8398		S5-7241		S3-4429		S5-4370	
Analysis no.	2317		3558		4600		5574		3099		2662		4608		2741		2122	
Precursor/ Occurrence	Plagioclase, with epidote		Plagioclase		Plagioclase, with epidote		Pyroxene		Groundmass, with opaque		Vein		Vein, with epidote		Vugs, with chlorite		Vugs	
Oxide (wt.%)																		
SiO_2	31.45		30.24		29.85		30.73		29.92		31.66		30.30		32.04		29.91	
TiO_2	32.39		35.94		36.69		33.33		37.10		31.55		38.64		31.68		37.72	
Al_2O_3	3.69		2.83		2.57		3.85		1.21		6.42		1.26		3.86		1.32	
FeO	1.51		0.92		1.02		1.23		1.49		0.48		1.01		1.85		0.92	
MnO	< 0.08		0.10		< 0.10		< 0.04		0.22		0.19		0.16		< 0.02		0.05	
MgO	0.10		0.03		0.09		0.01		< 0.07		0.12		0.10		0.09		0.03	
CaO	26.70		27.22		27.54		28.15		27.44		27.42		27.74		27.18		27.95	
Na_2O	0.08		< 0.02		0.01		0.01		< 0.06		0.01		0.03		-		-	
K_2O	0.05		0.02		0.05		< 0.02		< 0.03		0.27		< 0.02		0.02		< 0.01	
Cl	-		0.05		< 0.04		-		< 0.02		< 0.03		< 0.02		< 0.01		0.07	
NiO	< 0.03		0.11		0.02		0.02		0.09		0.04		0.10		< 0.09		0.15	
Cr_2O_3	0.18		0.09		0.21		0.23		0.37		0.16		0.11		0.38		0.25	
P_2O_5	0.07		0.02		0.11		< 0.06		0.07		0.29		< 0.04		0.09		< 0.07	
Total	96.09		97.53		98.03		97.47		97.68		98.80		99.26		97.04		98.48	
Number of ions on the basis of 20 (O)																		
Si	4.234		4.036		3.970	4.00	4.104		4.013		4.131		3.988	4.00	4.274		3.989	4.00
Al^{IV}	-		-		0.030		-		-		-		0.012		-		0.011	
Al^{VI}	0.585	4.07	0.445	4.18	0.372	4.20	0.606	4.12	0.191	4.17	0.987	4.20	0.183	4.17	0.606	4.05	0.196	4.12
Ti	3.280		3.608		3.670		3.349		3.743		3.097		3.826		3.179		3.784	
Cr	0.019		0.009		0.022		0.024		0.039		0.016		0.011		0.040		0.026	
Mg	0.020		0.006		0.018		0.002		-		0.023		0.020		0.018		0.006	
Fe^{2+}	0.170		0.103		0.113		0.137		0.167		0.052		0.111		0.206		0.103	
Mn	-		0.011		-		-		0.025		0.021		0.018		-		0.006	
Na	0.021	3.88	-	3.90	0.003	3.94	0.003	4.03	-	3.94	0.003	3.88	0.008	3.92	-	3.89	-	3.99
Ca	3.851		3.893		3.924		4.028		3.944		3.833		3.912		3.885		3.994	
K	0.009		0.003		0.008		-		-		0.045		-		0.003		-	

7.2.5. Epidote: $Ca_2Fe^{2+}Al_2O.OH[Si_2O_7][SiO_4]$

Epidote is the most common calc-silicate mineral present, replacing plagioclase, pyroxene, the groundmass and occurring as a vein mineral. However, its composition, as shown in Table 7.11, is not controlled by its occurrence. The SiO_2 of replacement epidote varies from 32 to 40 wt.%, but as a vein and vug mineral it can be as high as 43 wt.%. The Al_2O_3 and CaO contents vary from 18 to 27 and 18 to 24 wt.% for the replacement and 18 to 29 and 22 to 26 wt.% respectively for vein and vug epidotes. The amounts of FeO and MgO are mostly 6-18 and less than 3 wt.% respectively.

Figure 7.7 shows variations in the pistacite content of epidote, i.e. the ratio between Fe and Fe+Al in the tetragonal structure. Replacement and vein epidote have pistacite values of mostly between 0.1 and 0.5. Figure 7.7B also shows that epidote from well DRJ S-3 contains slightly more pistacite than that from the other wells. End member epidote can be expressed as $Ca_{1.6-2.1}Al_{1.7-2.5}Fe_{0.4-1.2}[Si_{2.9-3.2}Al_{0.1-0.0}]O_{12}(OH)$ for replacement of phenocryst and groundmass, and $Ca_{1.9-2.3}Al_{1.8-2.6}Fe_{0.2-1.1}[Si_{2.7-3.5}Al_{0.3-0.0}]O_{12}(OH)$ and $Ca_{1.5-3.1}Al_{1.1-2.5}Fe_{0.5-1.1}[Si_{2.6-3.5}Al_{0.4-0.1}]O_{12}(OH)$ for vein and vug epidotes respectively.

Figure 7.7 also shows that there are no systematic variations in the compositions of epidote with increasing depth. There is no compositional difference between euhedral, radiating and granular epidotes, e.g. epidote from 1575 m depth in well DRJ 14 and 1023 m depth in DRJ S-1, but compositional zoning is likely present. The core of replacement epidote contains more Al, whereas the rim contains more Fe. Epidote present in cavities and veins contains less pistacite values toward their rims, e.g. vein epidote from 2207 m depth in well DRJ S-5. The variations in composition of vug and vein epidotes depend also on the associated minerals; epidote associated with garnet and pyrite usually has high pistacite values, whereas that in association with calcite and anhydrite contains low pistacite (Table 7.11). Vug and vein epidotes present at the margin of the cavities or veins contain more Fe than those deposited latter in the middle of the cavities or veins, e.g. vein epidote from 1174 m depth in well DRJ S-3.

7.2.6. Amphiboles: $(Ca,Na,K,Mn)_{2-3}(Mg,Fe^{2+},Fe^{3+},Al,Ti,Mn,Cr)_5(Si,Al)_8O_{22}(OH)_2$

Amphibole replaces plagioclase and is also present in cavities and veins. Table 7.12 represents its composition and structural formulae; the amount of Fe_2O_3 was calculated from the FeO content using the stoichiometric formulae of Droop (1987). The amphiboles, shown on Figure 7.8, are mostly actinolite and tremolite. Figure 7.9 shows variations in the amounts of Al^{IV}, Al present in the tetragonal structure, and total Al.

Table 7.11.Compositions and structural formulae of representative epidotes.

Well	DRJ 14	DRJ S-1	DRJ S-3	DRJ S-1	DRJ S-1	DRJ S-5	DRJ S-5	DRJ S-1	DRJ S-3
Depth	1575	1023	1951	1058	1058	2207	2207	1023	1951
Sample	D14-5166	S1-3355	S3-6400	S1-3470	S1-3470	S5-7241	S5-7241	S1-3355	S3-6400
Analysis no.	4285	3129	3889	3041	3015	5019	5042	3145	3897
Precursor/ Occurrence	Plagioclase, granular	Plagioclase, core	Pyroxene	Groundmass, granular	Vein, with prehnite	Vein, after calcite	Vein, after garnet	Vugs, with pyrite	Vugs, radiating
Oxide (wt.%)									
SiO_2	38.74	38.19	37.37	38.24	37.78	38.52	37.62	37.25	37.52
TiO_2	< 0.01	0.00	0.05	0.04	0.11	< 0.08	0.04	0.15	0.06
Al_2O_3	22.12	22.54	21.97	23.51	23.11	27.46	23.49	22.46	23.95
FeO	13.48	12.57	13.07	11.16	11.26	6.80	11.57	12.88	10.53
MnO	0.06	< 0.01	0.17	0.51	0.32	0.47	1.12	0.24	0.13
MgO	0.13	0.06	0.10	0.32	0.14	0.06	0.06	0.11	< 0.02
CaO	23.11	22.89	22.70	23.36	23.25	23.30	21.83	22.64	22.74
Na_2O	-	0.07	< 0.07	-0.03	< 0.02	0.07	< 0.03	0.09	-
K_2O	< 0.05	0.04	0.04	0.04	-	0.01	-	0.02	< 0.04
Cl	< 0.02	< 0.06	0.04	-0.04	< 0.02	0.06	0.02	< 0.02	0.06
NiO	0.04	< 0.02	0.02	0.14	0.02	0.05	< 0.01	0.03	0.06
Cr_2O_3	0.12	0.16	0.02	0.14	0.13	0.18	0.18	0.03	0.05
P_2O_5	< 0.06	< 0.14	< 0.03	-0.18	< 0.05	< 0.03	< 0.01	< 0.1	< 0.08
Total	97.58	96.39	95.53	97.28	95.89	96.88	95.82	95.82	94.95

Number of ions on the basis of 13 (O, OH)

Si	3.055		3.049		3.021		3.026		3.024		3.015		3.016		3.001		3.025	
Al^{IV}	-		-		-		-		-		-		-		-		-	
Al^{VI}	2.054	2.97	2.119	2.98	2.092	3.00	2.191	3.01	2.179	2.98	2.531	3.02	2.218	3.08	2.131	3.04	2.274	3.00
Ti	-		-		0.003		0.002		0.007		-		0.002		0.009		0.004	
Cr	0.007		0.010		0.001		0.009		0.008		0.011		0.011		0.002		0.003	
Fe^{3+}	0.890		0.840		0.880		0.740		0.750		0.440		0.770		0.870		0.710	
Mn	0.004		-		0.012		0.034		0.022		0.031		0.076		0.016		0.009	
Mg	0.015		0.007		0.012		0.038		0.017		0.007		0.007		0.013		-	
Ca	1.953	1.95	1.958	1.97	1.966	1.97	1.981	1.99	1.994	1.99	1.954	1.97	1.875	1.88	1.954	1.97	1.964	1.96
Na	-		0.011		-		-		-		0.011		-		0.014		-	
K	-		0.004		0.004		0.004		-		0.001		-		0.002		-	
Pistacite $Fe^{3+}:(Fe^{3+}+Al^{IV})$	0.30		0.28		0.30		0.25		0.26		0.15		0.26		0.29		0.24	

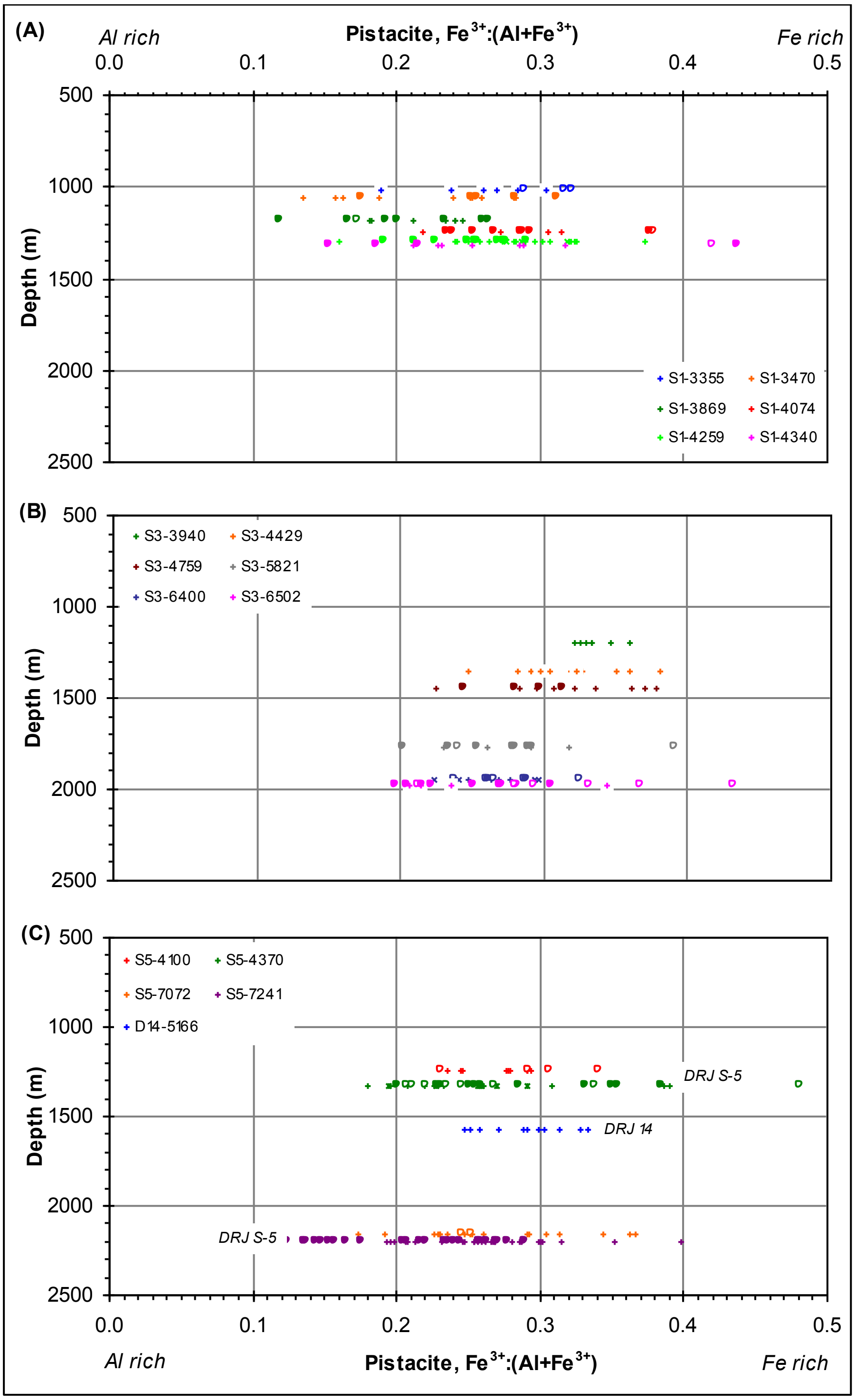

Figure 7.7. Variations in the pistacite values, i.e. ratios of Fe^{3+} to Fe^{3+} plus Al, of epidote and depth (m) from wells: **(A)** DRJ S-1, **(B)** DRJ S-3 and **(C)** DRJ S-5 and DRJ 14. The number of ions are calculated on the basis of 13 oxygens. Sample numbers are given; precursor symbols (+) plagioclase, (×) pyroxene and (∗) groundmass; (○) epidote in cavities and (●) vein epidote.

Replacement amphibole contains 39-56 wt.% SiO_2, 7-13 wt.% CaO, up to 10 wt.% Al_2O_3, 5-22 wt.% FeO, less than 2 wt.% Fe_2O_3, 13-18 wt.% MgO and less than 3 wt.% TiO_2. The amounts of MnO, NiO and Cr_2O_3 are very low, i.e. less than 0.5 wt.%. In wells DRJ 13 and 17, Na_2O can be present up to 1.5 wt.%. End member amphibole is $Ca_{0.0-2.8}[Mg_{3.1-5.9}Fe^{2+}_{0.4-3.4}Fe^{3+}_{0.0-1.8}Al_{0.0-1.1}][Si_{6.0-8.5}Al_{1.8-0.0}Fe_{0.0-0.3}]O_{22}(OH)_n$ and, as shown in Figure 7.8, is between actinolite and tremolite with Mg to $Mg+Fe^{2+}$ ratios above 0.6. There is likely an increase in Fe content from the rim to core of replacement actinolite and tremolite, e.g. those from 2407 m depth in DRJ 17. Some amphiboles are magnesio-hornblende and contain less SiO_2, e.g. from well DRJ 13. In well DRJ S-3, the replacement amphibole contains more FeO and Fe_2O_3, i.e. 19-21 and 4-7 wt.% respectively, but less than 1 wt.% MgO and MnO.

Amphibole occurring in cavities contains 52-54 wt.% SiO_2, less Al_2O_3, i.e. only up to 2 wt.%, about 12 wt.% CaO, 11-13 wt.% MgO, 15-18 wt.% FeO, traces of Fe_2O_3 and MnO, i.e. less than 2 and 1 wt.% respectively. End member amphibole present in cavities is $Ca_{1.7-2.0}[Mg_{2.6-2.8}Fe^{2+}_{1.8-2.1}Fe^{3+}_{0.0-0.1}Al_{0.2-0.0}][Si_{7.7-7.9}Al_{0.3-0.1}]O_{22}(OH)_n$. This composition is identical to that of amphibole in veins, which contains 48-56 wt.% SiO_2, 1-5 wt.% Al_2O_3 and 11-13 wt.% CaO. However, vein amphibole can contain more MgO, up to 21 wt.% and 6-18 wt.% FeO, but no Fe_2O_3. End member vein amphibole can be expressed as $Ca_{1.6-2.2}[Mg_{2.5-4.5}Fe^{2+}_{0.2-2.9}Fe^{3+}_{0.0-0.1}Al_{0.6-0.1}][Si_{7.6-8.3}Al_{0.4-0.0}]O_{22}(OH)_n$. Zoning shows more MgO but less FeO towards the rim of vein amphiboles, e.g. those from 1179 m depth in well DRJ S-1 and 1982 m depth in well DRJ S-3.

At 1774 m in well DRJ S-3, amphibole contains less SiO_2, i.e. about 35 wt.%, but more CaO, i.e. about 32 wt.%, expressed as tschermakite, i.e. $Ca_{5.3-5.7}[Mg_{0.0-0.1}Fe^{3+}_{0.7-0.9}][Si_{5.6-5.7}Al_{0.6-0.2}Fe_{1.6-2.2}]O_{22}(OH)_n$, is likely present (Figure 7.8).

7.2.7. Garnet: $(Ca,Fe,Mg,Mn)_3(Al,Fe^{3+},Ti,Cr)_2Si_3O_{12}$

Table 7.13 represents the composition and structural formulae of garnet at Darajat. End member garnet is summarised on Figure 7.10 and was calculated after Rickwood (1968) and Deer et al. (1992).

Garnet replaces plagioclase. In wells DRJ S-1 and S-5, it contains 34-38 wt.% SiO_2, 8-12 wt.% Al_2O_3 and 31-35 wt.% CaO. Using Droop (1987), the amounts of FeO and Fe_2O_3 present are similar, i.e. 5-10 wt.%. However, garnet in well DRJ S-3 contains between 8 and 16 wt.% FeO and Fe_2O_3, as Al_2O_3 is only up to 8 wt.%. Garnet also contains less than 2 wt.% MgO but up to 4 wt.% TiO_2. The compositions are $Ca_{2.8-3.0}Al_{0.0-1.1}Fe^{3+}_{0.8-2.0}[Fe^{2+}_{0.0-0.2}Mg_{0.0-0.2}][Si_{2.9-3.1}Al_{0.1-0.0}]O_{12}$, i.e. andradite

Table 7.12.Compositions and structural formulae of representative amphiboles.

Well	DRJ 17		DRJ 17		DRJ S-1		DRJ S-5		DRJ S-1		DRJ S-3		DRJ S-3		DRJ S-1		DRJ S-3	
Depth	2407		1855		1179		1250		1179		1774		1982		1179		1982	
Sample	D17-7898		D17-7898		S1-3869		S5-4100		S1-3869		S3-5821		S3-6502		S1-3869		S3-6502	
Analysis no.	2228		2254		1859		3555		1881		2818		5466		1849		5448	
Precursor/ Occurrence	Plagioclase, euhedral		Plagioclase		Plagioclase		Plagioclase, with opaque, epidote		Vein, margin		Vein, euhedral		Vein, with calcite		Vugs at plagioclase		Vugs, middle	
Name	Mg Hornblende		Tremolite		Actinolite		Actinolite		Actinolite		Tschermakite		Actinolite		Actinolite		Actinolite	
Oxide (wt.%)																		
SiO_2	45.82		54.19		55.18		53.89		51.62		35.43		53.73		51.53		53.30	
TiO_2	0.54		0.24		0.18		0.20		0.13		0.12		0.08		0.22		< 0.01	
Al_2O_3	7.08		2.30		1.67		1.58		4.26		1.60		0.50		3.66		2.09	
FeO*	13.79		6.83		11.33		12.44		15.90		21.02		18.18		14.67		15.23	
Fe_2O_3*	-		-		-		-		-		5.68		0.53		-		1.80	
MnO	0.28		0.26		0.44		1.04		0.45		0.31		0.95		0.78		0.66	
MgO	16.61		19.65		16.94		16.81		12.49		0.07		11.81		13.84		12.51	
CaO	9.14		12.50		12.29		10.37		12.39		32.39		12.71		12.07		12.33	
Na_2O	0.33		0.14		0.05		< 0.04		< 0.06		< 0.07		< 0.01		0.30		0.11	
K_2O	0.31		0.08		0.12		0.06		0.20		< 0.04		0.08		0.10		0.10	
Cl	0.09		0.16		0.11		0.07		0.01		0.04		0.02		0.03		< 0.01	
NiO	< 0.04		< 0.03		0.05		0.01		0.01		< 0.08		0.10		0.08		< 0.09	
Cr_2O_3	0.30		0.07		0.15		0.09		0.04		0.15		0.09		0.13		0.14	
P_2O_5	< 0.04		< 0.03		< 0.09		< 0.05		< 0.11		0.03		< 0.11		< 0.06		< 0.02	
Total	94.18		96.40		98.47		96.58		97.38		96.75		98.65		97.39		98.24	
*Number of ions on the basis of 24 (O, OH)***																		
T Si^{IV}	7.173	8.00	8.181		8.149		8.030		7.607	8.00	5.635	8.00	7.896	8.00	7.641	8.00	7.790	8.00
T Al^{IV}	0.827		-		-		-		0.393		0.300		0.087		0.359		0.210	
T Fe^{3+IV}	-		-		-		-		-		2.065		0.018		-		-	
T Ti^{IV}	-		-		-		-		-		-		-		-		-	
C Al	0.479	5.00	0.409	5.00	0.290	5.00	0.277	5.00	0.346	5.00	-	5.00	-	5.00	0.280	5.00	0.150	5.00
C Cr	0.037		0.008		0.017		0.011		0.005		0.019		0.010		0.015		0.016	
C Fe^{3+}	-		-		-		-		-		0.731		0.004		-		-	
C Ti	0.064		0.027		0.020		0.022		0.014		0.014		0.009		0.025		-	
C Mg	3.877		4.422		3.730		3.734		2.744		0.017		2.587		3.059		2.726	
C Fe^{2+}	0.544		0.133		0.942		0.955		1.891		-		2.212		1.621		1.862	
C Mn	-		-		-		-		-		0.042		0.118		-		0.082	
C Ca	-		-		-		-		-		4.177		0.059		-		0.166	
B Mg	-	2.00	-	2.00	-	2.00	-	2.00	-	2.00	-	1.34	-	1.94	-	2.00	-	1.80
B Fe^{2+}	1.261		0.729		0.457		0.595		0.069		-		-		0.198		-	
B Mn	0.037		0.033		0.055		0.131		0.056		-		-		0.098		-	
B Ca	0.702		1.238		1.488		1.274		1.875		1.342		1.942		1.704		1.765	
B Na	-		-		-		-		-		-		-		-		0.031	
A Ca	0.832	0.24	0.784	0.84	0.457	0.49	0.382	0.39	0.081	0.12	-	-	-	0.02	0.214	0.32	-	0.02
A Na	0.100		0.041		0.014		-		-		-		-		0.086		-	
A K	0.062		0.015		0.023		0.011		0.038		-		0.015		0.019		0.019	
Ratio Mg:(Mg+Fe^{2+})	0.80		0.97		0.80		0.80		0.59		1.00		0.54		0.65		0.59	

* Calculated after Droop (1987).

** Based on the formulae of Leake (1978): $A_{0-1}B_2C^{VI}_5T^{IV}_8O_{22}(OH,F,Cl)_2$

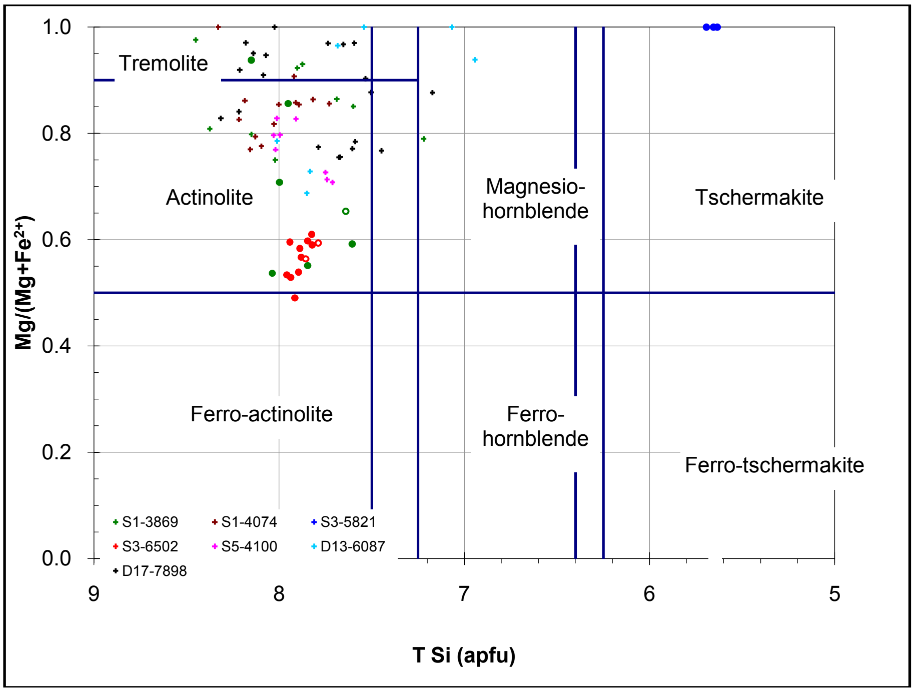

Figure 7.8. Classification of amphiboles based on the amounts of T Si (apfu = atoms per formulae unit) and ferromagnesians on the basis of 24 oxygens. Sample numbers are given; (+) represents plagioclase replacement, (O) and (●) represent amphiboles present in vugs and veins respectively.

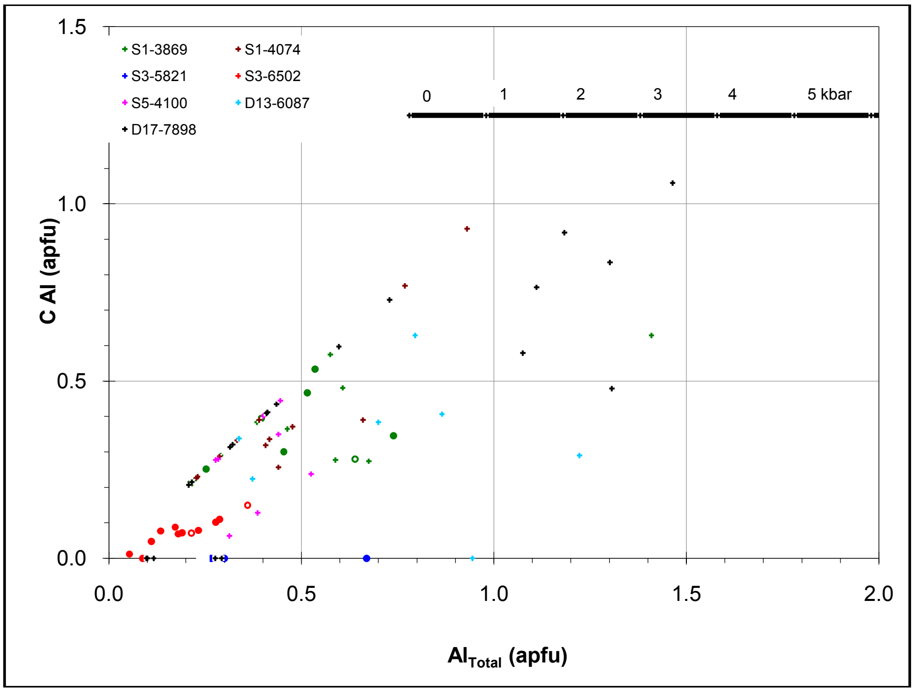

Figure 7.9. Variations in the amounts of total Al and C Al (apfu = atoms per formulae unit) in the tetragonal sites of amphiboles, calculated on the basis of 24 oxygens. Sample numbers are given; precursor symbols (+) plagioclase; (O) amphiboles in vugs and (●) vein amphiboles. An increase in the amount of Al indicates an increase in pressure of amphibole formation; the approximate 5 kbar pressure after Hammarstrom and Zen (1986), given in a black line, applies to igneous rocks; for a geothermal condition, the number is away too high (much more than 50 times).

Table 7.13.Compositions and structural formulae of representative garnets.

Well	DRJ S-1		DRJ S-3		DRJ S-3		DRJ S-3		DRJ S-5		DRJ S-5		DRJ S-5		DRJ S-5		DRJ S-1	
Depth	1242		1774		1451		1774		1250		1250		1332		1250		1242	
Sample	S1-4074		S3-5821		S3-4759		S3-5821		S5-4100		S5-4100		S5-4370		S5-4100		S1-4074	
Analysis no.	3652		2851		4382		2815		3566		3575		2145		3588		3689	
Precursor/ Occurrence	Plagioclase, with actinolite		Groundmass		Vein		Vein, with epidote		Vein, euhedral		Vein, granular		Vein, margin		Vugs, margin		Vugs, inclusion at chlorite	
Oxide (wt.%)																		
SiO_2	37.24		35.41		35.03		36.23		35.64		36.84		33.77		35.70		35.84	
TiO_2	0.22		0.08		< 0.01		1.41		< 0.01		0.47		21.20		0.07		0.25	
Al_2O_3	9.41		0.20		0.55		8.57		< 0.1		10.78		10.52		0.01		11.72	
FeO*	7.53		14.17		0.31		8.74		13.43		6.31		5.59		14.45		5.68	
Fe_2O_3*	7.63		15.92		29.52		8.78		15.78		8.34		-		14.85		7.61	
MnO	0.37		0.65		0.53		0.26		0.59		1.48		0.06		0.53		0.22	
MgO	1.53		0.14		0.09		0.20		0.01		0.01		0.15		0.08		0.35	
CaO	31.76		31.88		32.24		33.24		32.06		33.31		25.95		31.72		33.52	
Na_2O	-		0.10		< 0.05		0.01		< 0.02		0.12		0.05		< 0.02		0.11	
K_2O	0.06		< 0.01		0.07		0.03		< 0.02		< 0.04		0.09		0.11		0.04	
Cl	0.01		0.05		0.03		0.03		0.06		0.02		-		< 0.03		-	
NiO	< 0.01		0.07		0.13		< 0.01		0.14		0.18		0.05		0.14		0.02	
Cr_2O_3	0.18		< 0.01		0.12		< 0.03		0.16		0.25		< 0.05		0.34		0.31	
P_2O_5	< 0.09		< 0.01		0.18		0.12		< 0.17		< 0.08		-		0.02		0.01	
Total	95.89		98.65		98.77		97.91		97.48		97.92		97.37		97.95		95.72	
Number of ions on the basis of 12 (O)																		
Tsi	3.062		2.993	3.00	3.005		2.975	3.00	3.047		2.982	3.00	2.846	3.00	3.045		2.944	3.00
Tal	-		0.007		-		0.025		-		0.018		0.154		-		0.056	
Al^{VI}	0.911	1.86	0.013	2.00	0.056	1.98	0.804	1.93	-	1.90	1.010	1.99	0.891	2.23	0.001	1.91	1.078	1.97
Fe^{3+}	0.920		1.986		1.911		1.040		1.886		0.935		-		1.883		0.861	
Ti	0.014		0.005		-		0.087		-		0.029		1.344		0.004		0.015	
Cr	0.012		-		0.008		-		0.011		0.016		-		0.023		0.020	
Fe^{2+}	0.070	3.08	0.028	3.00	0.017	3.03	0.103	3.07	0.090	3.07	-	3.01	0.394	2.77	0.100	3.05	-	3.03
Mg	0.188		0.018		0.012		0.024		0.001		0.001		0.019		0.010		0.043	
Mn	0.026		0.047		0.039		0.018		0.043		0.101		0.004		0.038		0.015	
Ca	2.798		2.887		2.963		2.924		2.937		2.889		2.343		2.898		2.950	
Na	-		0.016		-		0.002		-		0.019		0.008		-		0.018	
*End member***																		
Almandine	2.3		0.9		0.6		3.4		2.9		-		14.2		3.3		-	
Andradite	49.5		99.2		96.8		53.9		100.0		47.0		-		98.5		43.6	
Grosssular	40.6		-		0.8		41.4		-		48.2		84.8		-		52.9	
Pyrope	6.1		0.6		0.4		0.8		-		-		0.7		0.3		1.4	
Spessartine	0.8		1.6		1.3		0.6		1.4		3.4		0.1		1.2		0.5	
Uvarovite	0.6		-		0.4		-		0.6		0.8		-		1.2		1.0	
Pistacite $Fe^{3+}:(Fe^{3+}+Al^{IV})$	0.50		0.99		0.97		0.96		1.00		0.48		-		1.00		0.44	

* Calculated based on Droop (1987).

** Calculated after Rickwood (1968) or Deer et al. (1992).

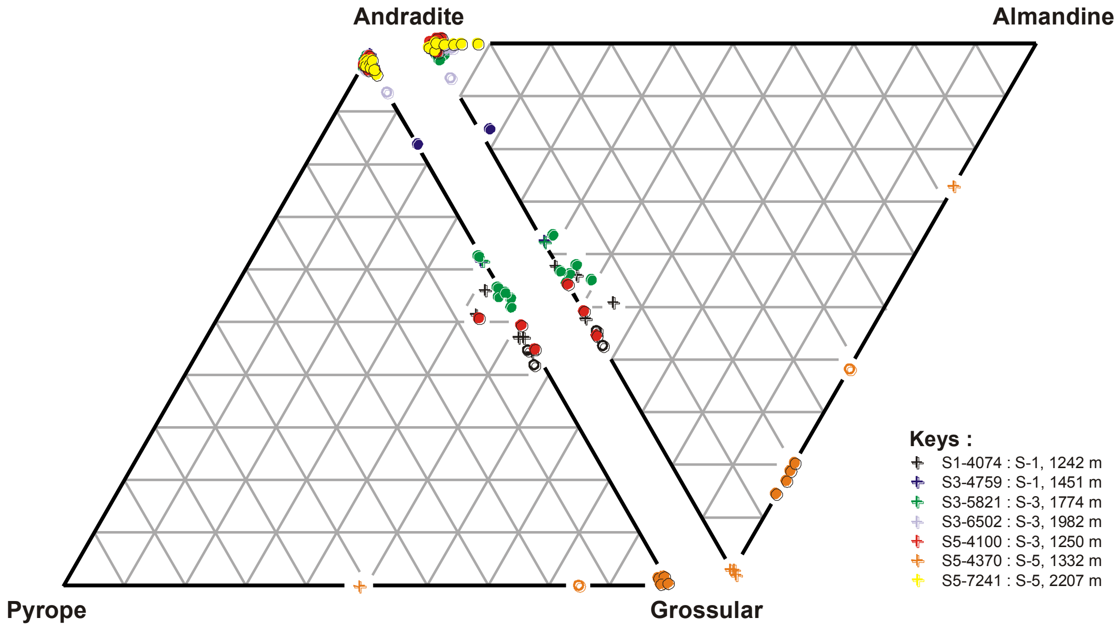

Figure 7.10.Proportions of the end member compositions of garnet. Sample numbers are given; precursor: (+) plagioclase; occurrence: (○) cavities and (●) vein. Most garnets belong to grossular-andradite (grandite) solid solution. Almandine, present at 1332 m depth in DRJ S-5, also contains Ti.

($And_{97-100}Alm_{0-2}Pyr_{0-1}Spess_{0-2}Uvaro_{0-1}$) in well DRJ S-3, grossular ($Gros_{71-97}Alm_{0-1}Spess_{0-1}Uvaro_{0-1}$) in well DRJ S-5 and grandite, coexisting grossular and andradite, ($And_{43-56}Gro_{40-54}Alm_{0-6}Pyr_{0-6}$ $Spess_{0-1}Uvaro_{0-2}$) in well DRJ S-1 (Figure 7.10).

Figure 7.11 shows variations in the ratios between Fe and Al+Fe in the tetrahedral structure of garnet. The values are mostly between 0.4 and 0.6 with andradite having more than 0.9, whereas grossular less than 0.1 pistacite. In addition, grossular is likely hydrogrossular, containing up to 5 wt.% H_2O as indicated by sub 100% totals.

Garnet also occurs in cavities and veins. Vug garnet contains 34-36 wt.% SiO_2 and 31-34 wt.% CaO. Garnet in well DRJ S-1 has about 12 wt.% Al_2O_3, 6 wt.% FeO and 8 wt.% Fe_2O_3. Garnets in wells DRJ S-3 and S-5 have lower Al_2O_3, i.e. only up to 2 wt.%. The amount of FeO varies from less than 1 to about 14 wt.%, as the Fe_2O_3 contents also vary from about 15 to 28 and 32 wt.% in wells DRJ S-5 and S-3 respectively. Figure 7.10 shows that vug garnet is mostly andradite ($And_{91-100}Gro_{0-7}$ $Alm_{0-4}Pyr_{0-2}Spess_{0-4}Uvaro_{0-2}$), having the composition $Ca_{2.8-3.1}Al_{1.0-1.2}Fe^{3}_{0.8-1.2}[Fe^{2}_{0.0-0.2}Mg_{0.0-0.1}]$ $[Si_{2.9-3.1}Al_{0.1-0.0}]O_{12}$. However, garnet in vugs of cores from well DRJ S-1 is also andradite-grossular ($And_{41-43}Gro_{52-56}Pyr_{1-2}Spess_{0-1}Uvaro_{0-1}$) with formulae of $Ca_{2.8-3.1}Al_{0.0-0.4}Fe^{3+}_{1.5-2.1}[Fe^{2+}_{0.0-0.2}$ $Mg_{0.0-0.2}][Si_{2.9-3.1}Al_{0.1-0.0}]O_{12}$.

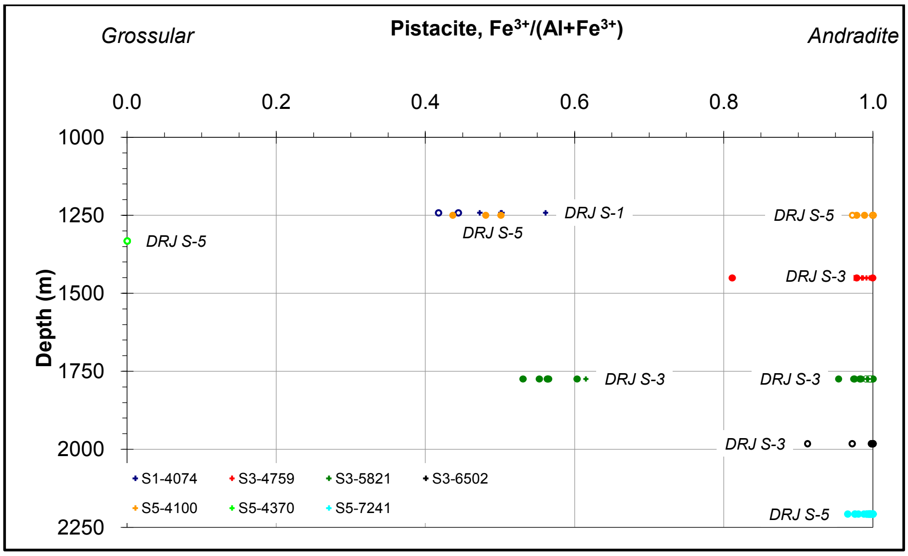

Figure 7.11. Variation in pistacite values, i.e. ratio between Fe^{3+} and Fe^{3+} plus Al, of garnet (on the basis of 12 oxygens) and depth (m) from wells DRJ S-1, S-3 and S-5. Sample numbers are given; precursor symbols (+) plagioclase, (○) garnet in cavities and (●) vein garnet. Andradite is rich in Fe_2O_3, whereas grossular is Al_2O_3 rich. Garnet from about 1300 m depth in DRJ S-5 contains no Fe_2O_3, but 12-22 wt.% TiO_2; almandine and pyrope are associated with grossular.

Variations in Al_2O_3, FeO and Fe_2O_3 also occur in vein garnet. As shown in Figure 7.10, well DRJ S-5 has 3 types of vein garnet. One from 1332 m depth contains 10-17 wt.% Al_2O_3, 5-12 wt.% FeO and less than 2 wt.% MgO. This is likely grossular-almandine ($Gross_{79-85}Alm_{14-21}Pyr_{0-1}Spess_{0-1}$), i.e. $Ca_{1.4-2.4}Al_{0.8-1.5}Ti_{0.7-1.4}[Fe^{2+}_{0.3-1.0}Mg_{0.0-0.1}][Si_{2.8-2.9}Al_{0.2-0.1}]O_{12}$, as TiO_2 is present between 12 and 22 wt.% and CaO is between 14 and 26 wt.%. The others contain less than 0.6 wt.% Al_2O_3 and either about 14 wt.% FeO and Fe_2O_3 or are more oxidised with less than 2 wt.% FeO and 26-32 wt.% Fe_2O_3. The Fe_2O_3 rich garnet is likely to be andradite ($And_{95-100}Alm_{0-9}Pyr_{0-2}Spess_{0-5}Uvaro_{0-2}$) and is present in the deeper part of the well, i.e. about 2210 m, whereas the other is andradite-grossular, i.e. $And_{43-50}Gro_{41-54}Pyr_{0-7}Spess_{0-4}Uvaro_{0-1}$, present above 1250 m.

Garnet present in veins between 1450 and 1775 m depth in well DRJ S-3 contains low Al_2O_3, i.e. less than 4 wt.%, 12-15 wt.% FeO, about 15 wt.% Fe_2O_5 and less than 2 wt.% TiO_2. Figure 7.10 shows that this garnet is andradite ($And_{96-100}Gro_{0-2}Alm_{0-4}Pyr_{0-1}Spess_{0-2}Uvaro_{0-1}$). At 1460 m, garnet is more oxidised, containing 25-30 wt.% Fe_2O_3 and only up to 2 wt.% FeO. However, where garnet is associated with epidote, it is andradite-grossular ($And_{50-60}Gro_{35-45}Alm_{0-5}Pyr_{0-1}Spess_{0-2}$). The Al_2O_3 contents are higher and range between 7 and 10 wt.%; the amounts of FeO and Fe_2O_3 are slightly lower, i.e. between 6 and 11 wt.% respectively.

Garnet replacing plagioclase is not zoned but garnet in vugs is, e.g. garnet between 1770 and 1980 m in well DRJ S-3, and at about 2200 m in DRJ S-5, where a rim of garnet contains more Fe_2O_3 but less FeO. Where grossular is present, the proportion of its end member increases toward the rim of the garnet vein, e.g. at about 1330 m depth in well DRJ S-5.

7.3. CARBONATES AND ANHYDRITE

7.3.1. Carbonates: Calcite ($CaCO_3$), Siderite ($FeCO_3$), etc

Calcite is the most common hydrothermal mineral at Darajat. It replaces plagioclase and pyroxenes, and also fills cavities and veins. Representative compositions of calcite are given in Tables 7.14 and 7.15. The amount of CO_2 was calculated from stoichiometry and the classification of calcite follows Deer et al. (1962b). The composition of the carbonates is likely controlled by the mineralogy of the host rocks (e.g. Deer et al., 1962b; Morad, 1998 and White et al., 2003); where chlorite is dominant, calcite is commonly Mg rich but where pyrite is abundant, the calcite is more Fe rich.

Calcite from wells DRJ S-1 and S-5 is manganoan, containing 50-56 wt.% CaO, 39-44 wt.% CO_2 and up to 3 wt.% MnO. The amount of FeO is less than 1 wt.% and MgO is up to 1.5 wt.%. Calcite from well DRJ S-3 is slightly different. It contains 46-57 wt.% CaO and it is ferroan manganoan calcite with up to 5 wt.% FeO and MnO. In general, the compositions of calcite present in cavities are between that of calcite formed as a replacement, which is ferroan, and that deposited in veins, which is more manganoan.

Calcite in cavities from marginal area, wells DRJ S-2 and S-6, contains more magnesium, i.e. up to 3 wt.% MgO. The FeO and MnO are also up to 5 wt.%. Calcite in well DRJ 1 is mostly a plagioclase replacement. Its FeO, MnO and MgO contents are less than 7, 8 and 4 wt.% respectively.

Siderite is present in veins from well DRJ 1. It contains 40-52 wt.% FeO and less than 11 wt.% CaO (Table 7.16). The amount of MnO ranges from 2 to 8 wt.% and MgO is present up to 2 wt.%. Cavities in a core from well DRJ S-3 contain coexisting calcite and siderite, i.e. ankerite. Table 7.16 shows that the carbonates contain wide variations in FeO, i.e. 14-36 wt.%, and 31-44 wt.% CaO. Traces of MnO and MgO occur but are less than 0.5 wt.%. End member compositions are $Ca_{1.0-1.3}Fe_{0.4-0.9}(CO_3)_2$.

Table 7.14.Compositions and structural formulae of representative calcite in the matrix.

Well	DRJ S-1		DRJ S-2		DRJ S-3		DRJ S-3		DRJ S-5		DRJ 1	
Depth (m)	911		579		1000		1451		2155		397	
Sample	S1-2990		S2-1900		S3-3280		S3-4759		S5-7071		D1-397	
Analysis no.	3597		5844		4434		4354		3755		3093	
Precursor	-		Plagioclase		Pyroxene		Plagioclase, surface		Plagioclase		-	
Oxide (wt.%)												
FeO	0.06		0.51		0.33		2.23		0.12		1.55	
MnO	2.41		3.91		1.77		0.16		0.70		7.35	
MgO	0.30		0.71		0.12		0.98		0.05		1.80	
CaO	52.09		49.51		50.52		48.78		51.92		44.79	
CO_2*	40.88		38.85		39.65		38.28		40.75		35.15	
Total	96.02		94.44		92.69		90.49		94.54		91.57	
Number of ions on the basis of 6 (O)												
Fe^{2+}	0.002	1.99	0.014	1.95	0.010	1.98	0.066	1.99	0.004	1.94	0.044	1.94
Mn	0.070		0.112		0.054		0.004		0.020		0.206	
Mg	0.016		0.036		0.006		0.052		0.002		0.090	
Ca	1.906		1.784		1.912		1.872		1.910		1.596	

* Calculated stoichiometrically using reactions: $CaO + CO_2 \leftrightarrow CaCO_3$

Table 7.15. Compositions and structural formulae of representative calcite present in veins and vugs.

Well	DRJ S-1		DRJ S-3		DRJ S-1		DRJ S-2		DRJ S-3		DRJ 1	
Depth (m)	976		1201		976		579		1000		280	
Sample	S1-3202		S3-3940		S1-3202		S2-1900		S3-3280		D1-580	
Analysis no.	6191		2314		6158		5880		4755		4823	
Occurrence	Vein		Vein, margin, with chlorite		Vugs		Vugs, middle		Vugs		Vugs in plagioclase	
Oxide (wt.%)												
FeO	0.07		1.39		0.17		4.91		0.02		2.16	
MnO	0.28		4.28		0.24		1.36		1.02		1.23	
MgO	0.57		0.16		< 0.02		2.73		0.04		0.84	
CaO	51.88		47.83		53.80		46.50		51.45		48.02	
CO_2*	40.71		37.54		42.22		36.49		40.38		37.68	
Total	94.10		91.83		97.01		91.98		93.17		90.23	
Number of ions on the basis of 6 (O)												
Fe^{2+}	0.002	1.96	0.040	1.95	0.004	1.96	0.138	2.00	-	1.98	0.064	1.98
Mn	0.008		0.126		0.006		0.038		0.030		0.038	
Mg	0.030		0.008		-		0.138		0.002		0.044	
Ca	1.916		1.780		1.956		1.684		1.944		1.836	

* Calculated stoichiometrically using reactions: $CaO + CO_2 \leftrightarrow CaCO_3$

Table 7.16.Compositions and structural formulae of representative Fe rich carbonates.

Well	DRJ 1		DRJ 1		DRJ 1		DRJ S-3		DRJ S-3		DRJ S-3	
Depth (m)	180		397		397		1350		1350		1350	
Sample	D1-180		D1-397		D1-397		S3-4429		S3-4429		S3-4429	
Analysis no.	2863		3101		3107		2690		2724		2725	
Precursor	Vein		-		-		With opaque		With opaque		With opaque	
Name	Siderite		Siderite		Siderite		Ankerite		Ankerite		Ankerite	
Oxide (wt.%)												
FeO	45.54		44.45		40.93		23.16		16.96		35.81	
MnO	7.59		3.67		2.85		0.22		0.27		0.31	
MgO	1.33		1.74		1.59		-		0.07		< 0.01	
CaO	3.84		7.43		8.44		39.10		43.07		31.42	
CO_2*	27.89		27.23		25.07		28.37		20.78		21.93	
Total	86.46		84.88		81.69		92.05		81.95		91.18	
Number of ions on the basis of 6 (O)												
Fe^{2+}	1.730	2.00	1.436	1.96	1.286	1.81	0.610	1.94	0.456	1.95	0.894	1.91
Mn	0.176		0.120		0.090		0.006		0.008		0.008	
Mg	0.046		0.100		0.090		-		0.004		-	
Ca	0.050		0.308		0.340		1.320		1.484		1.004	

* Calculated stoichiometrically using reactions: $FeO + CO_2 \leftrightarrow FeCO_3$, $CaO + FeO + 2CO_2 \leftrightarrow CaFe(CO_3)_2$

7.3.2. Anhydrite: $CaSO_4$

Anhydrite replaces plagioclase and is present in vugs and veins. Its composition as given in Table 7.17, shows it contains 40-42 wt.% CaO and 58-60 wt.% SO_3. FeO occurs up to 0.5 wt.%. At 300 m depth in well DRJ S-1, gypsum is also present. Table 7.17 shows that the CaO and SO_3 contents of gypsum are slightly lower than those of anhydrite. Consequently, the totals range between 95 and 98 wt.% and the remaining includes 2-5 wt.% H_2O, which is much less than the H_2O content of gypsum cited by Deer et al. (1962b).

Table 7.17.Compositions and structural formulae of representative anhydrite and gypsum.

Well	DRJ S-5	DRJ S-1	DRJ S-5	DRJ S-1	DRJ S-1
Depth (m)	2207	304	890	304	304
Sample	S5-7241	S1-998	S5-2919	S1-998	S1-998
Analysis no.	5010	5830	5056	5831	5838
Precursor	Plagioclase	Vein	Vugs	Vein	Vein
Name	Anhydrite	Anhydrite	Anhydrite	Gypsum	Gypsum
Oxide (wt.%)					
FeO	0.19	0.08	0.35	< 0.03	< 0.01
MnO	< 0.10	< 0.10	0.11	0.02	< 0.06
MgO	< 0.03	-	0.06	0.07	< 0.06
CaO	40.01	41.97	39.68	38.30	39.70
SO_3	59.69	58.22	59.03	56.68	57.80
Total	100.09	100.13	99.63	95.39	97.56
Number of ions on the basis of 4 (O)					
Fe^{2+}	0.004	-	0.008	-	-
Mn	-	-	0.004	-	-
Mg	-	-	0.004	0.004	-
Ca	0.968	1.024	0.964	0.972	0.988
S	1.008	0.996	1.008	1.008	1.008
Ratio					
$CaO:SO_3$*	0.96	1.03	0.96	0.96	0.98

* Calculated on the basis of mol.%.

7.4. SECONDARY FELDSPARS

7.4.1. Adularia: (½Ca,K,Na)[$AlSi_3O_8$]

Adularia is present along cracks within plagioclase in samples from wells DRJ S-1, S-3 and S-5. It is rare in veins in DRJ S-5. Table 7.18 represents the composition of adularia.

Adularia contains 63-67 wt.% SiO_2, 17-19 wt.% Al_2O_3 and 13-17 wt.% K_2O. Adularia replacing plagioclase has up to 2 wt.% CaO and Na_2O, whereas as a vein mineral, e.g. at 1323 m depth in DRJ S-1 and 2207 m depth in DRJ S-5, it contains no CaO and Na_2O. Figure 7.12 shows that the most potassic adularia has the formulae $Ab_{0-15}An_{0-5}Or_{82-99}$.

Table 7.18.Compositions and structural formulae of representative adularia and secondary feldspars of albite and sanidine.

Well	DRJ 14	DRJ S-3	DRJ S-5	DRJ S-5	DRJ S-1	DRJ S-1	DRJ S-3	DRJ S-3	DRJ S-5	DRJ S-5	DRJ S-5	DRJ 24	DRJ S-2	DRJ S-2
Depth (m)	1575	1201	2207	2207	1323	1179	1000	1201	1332	2156	2207	2596	579	579
Sample	D14-5166	S3-3940	S5-7241	S5-7241	S1-4340	S1-3869	S3-3280	S3-3940	S5-4370	S5-7072	S5-7241	D24-8517	S2-1900	S2-1900
Analysis no.	4308	2282	4711	4610	3952	1844	4785	2323	2142	5612	4673	1280	5843	5847
Precursor/ Occurrence	Plagioclase crack	Plagioclase	Plagioclase with opaque	Vein	Vein, with prehnite	Plagioclase	Plagioclase crack	Plagioclase	Plagioclase	Plagioclase	Plagioclase	Quartz	Plagioclase	Plagioclase
Name	Adularia	Adularia	Adularia	Adularia	Adularia	Albite	Albite	Albite	Oligoclase	Oligoclase	Albite	Sanidine	Sanidine	Sanidine
Oxide (wt.%)														
SiO_2	64.51	64.27	64.28	65.22	64.61	67.11	66.42	65.31	61.98	65.16	67.26	64.83	65.04	64.30
TiO_2	0.09	< 0.01	0.13	0.18	0.13	< 0.04	0.01	0.07	< 0.06	< 0.04	< 0.04	0.11	0.11	0.03
Al_2O_3	18.26	17.92	17.91	17.53	18.01	19.91	20.95	20.63	22.70	21.32	20.12	18.44	18.13	18.02
FeO	0.16	0.16	0.29	0.18	0.03	< 0.09	< 0.05	< 0.01	0.55	0.16	0.14	0.04	0.01	0.15
MnO	< 0.06	< 0.05	< 0.04	0.04	0.06	< 0.02	< 0.09	< 0.06	< 0.02	-	0.07	0.08	0.03	-
MgO	0.08	0.01	0.07	0.01	< 0.01	< 0.04	0.03	< 0.01	< 0.07	< 0.03	0.05	< 0.04	0.14	< 0.03
CaO	0.11	0.27	0.42	0.09	0.14	1.24	1.85	2.17	5.36	2.74	1.16	0.37	0.18	0.13
Na_2O	0.22	0.16	0.24	0.09	0.30	11.01	10.59	10.85	8.63	9.92	10.92	1.63	< 0.03	< 0.06
K_2O	16.94	16.26	15.94	16.65	16.27	0.08	0.08	0.07	0.19	0.55	0.11	13.80	16.66	16.76
Cl	< 0.02	< 0.02	0.01	-	< 0.02	0.04	-	-	0.01	0.03	< 0.01	0.05	< 0.01	0.05
NiO	< 0.03	< 0.02	0.06	0.04	0.15	0.19	0.03	< 0.07	0.04	< 0.09	< 0.08	0.17	0.01	0.10
Cr_2O_3	0.05	< 0.05	0.08	-	< 0.03	0.03	0.01	< 0.03	0.10	< 0.02	0.12	0.07	0.03	0.04
SO_3	< 0.04	0.02	0.22	0.05	0.05	0.02	< 0.01	-	0.02	< 0.03	0.04	0.10	< 0.02	0.02
P_2O_5	< 0.07	0.06	0.07	< 0.03	0.06	< 0.03	< 0.02	0.17	0.01	< 0.1	< 0.04	0.08	-	< 0.03
Total	100.22	99.00	99.68	100.08	99.74	99.41	99.81	99.09	99.44	99.55	99.80	99.73	100.27	99.47
Number of ions on the basis of 32 (O)														
Si	11.955	12.014	11.967	11.993	12.084	11.839	11.671	11.612	11.096	11.543	11.814	11.947	12.004	12.003
Al	3.985	3.945	3.927	3.961	3.897	4.136	4.335	4.320	4.786	4.448	4.162	4.002	3.941	3.961
Ti	0.013	-	0.018	0.025	-	-	0.001	0.009	-	-	-	0.015	0.015	0.004
Fe^{2+}	0.025	0.025	0.045	0.027	-	-	-	-	0.082	0.024	0.021	0.006	0.002	0.023
Mn	-	-	-	0.006	-	-	-	-	-	-	0.010	0.012	0.005	-
Mg	0.022	0.003	0.019	0.003	-	-	0.008	-	-	-	0.013	-	0.039	-
Ca	0.022	0.054	0.084	0.018	0.04	0.234	0.348	0.413	1.028	0.520	0.218	0.073	0.036	0.026
Na	0.079	0.058	0.087	0.057	0.043	3.766	3.608	3.741	2.996	3.407	3.719	0.582		
K	4.005	3.878	3.786	3.881	3.767	0.018	0.018	0.016	0.043	0.124	0.025	3.244	3.923	3.991
End member														
Albite	1.9	1.5	2.2	1.4	1.1	93.7	90.8	89.7	73.7	84.1	93.9	14.9	0.0	0.0
Anorthite	0.5	1.4	2.1	0.5	1.0	5.8	8.8	9.9	25.3	12.8	5.5	1.9	0.6	0.3
Orthoclase	97.5	97.2	95.7	98.1	97.8	0.4	0.5	0.4	1.1	3.1	0.6	83.2	99.4	99.9

7.4.2. Albite and Sanidine: (½Ca,K,Na)[$AlSi_3O_8$]

Other secondary feldspars, i.e. albite and sanidine, alter plagioclase along cracks but neither occurs in veins. Albite is more common and is mostly associated with adularia, except at shallow depths in well DRJ S-2, where it is present with sanidine. Rhyolite from about 2600 m depth in well DRJ 24 contains sanidine along cracks in quartz.

The compositions of secondary feldspars are reported in Table 7.18 and summarised in Figure 7.12. The amounts of SiO_2 and Al_2O_3 are 62-70 and 18-24 wt.% respectively. Albite contains 8-12 wt.% Na_2O, up to 6 wt.% CaO and less than 2 wt.% K_2O. By contrast, the K_2O content of sanidine, like adularia, varies between 13 and 17 wt.% and CaO and Na_2O are both less than 2 wt.%. Albite has the composition of $Ab_{73\text{-}98}An_{1\text{-}26}Or_{0\text{-}12}$, i.e. ranging between oligoclase and albite (Figure 7.12). Sanidine formulae can be expressed as $Ab_{0\text{-}17}An_{0\text{-}5}Or_{80\text{-}100}$.

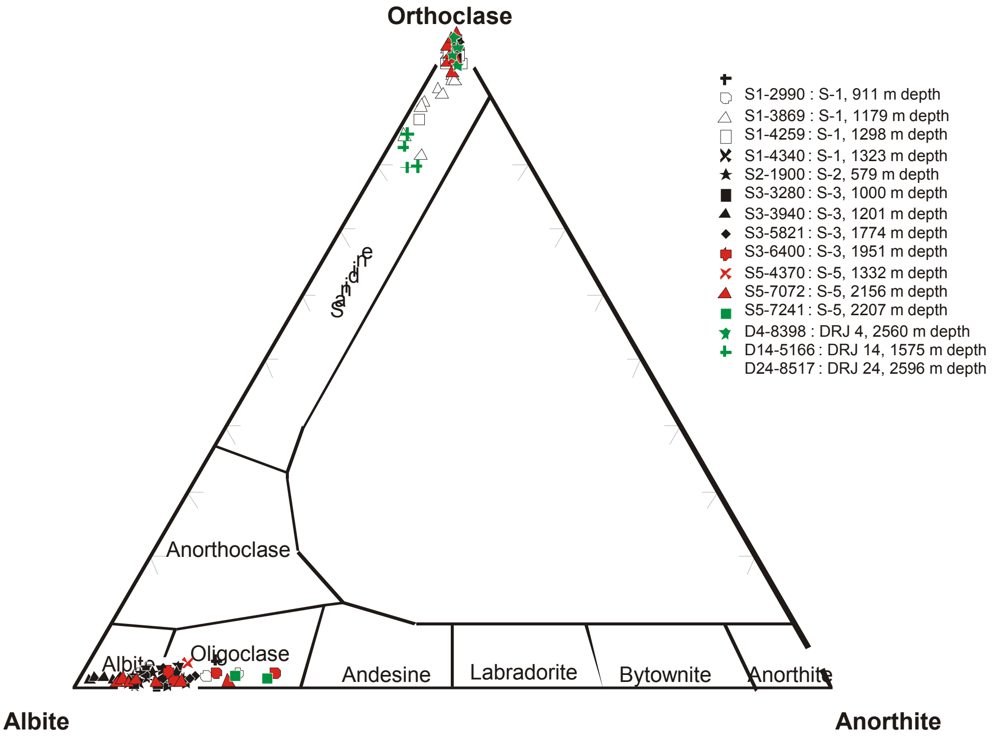

Figure 7.12.Compositions of hydrothermal mineral of feldspars. Sample numbers are given; few adularia vein minerals are present at 1323 m depth in wellDRJ S-1 (sample S1-4340), the other secondary feldspars are plagioclase replacements.

7.5. OTHER MINERALS

7.5.1. Alunite: $(Na,K)Al_3(SO_4)_2(OH)_n$

Alunite replaces plagioclase and the groundmass, and fills cavities and veins at 43 m depth in well DRJ 2. The compositions, as shown in Table 7.20, are identical. Alunite contains 34-45 wt.% Al_2O_3, 36-41 wt.% SO_3, up to 1.2 wt.% Na_2O and 2-6 wt.% K_2O. SiO_2 is present at less than 2.5 wt.%, mostly in the groundmass and is likely to be a contaminant. The other oxides include up to 1.5 wt.% FeO, mostly present in vein alunite, and less than 1.5 wt.% P_2O_5 (Table 7.19). The alunite composition can be expressed as $(Na_{0.0\text{-}0.2},K_{0.5\text{-}0.2})Al_{2.5\text{-}3.0}(SO_4)_{1.7\text{-}1.8}(OH)_n$ and Fe can substitute Al (Alpers et al., 1992).

Table 7.19.Compositions and structural formulae of alunites.

Well	DRJ 2		DRJ 2		DRJ 2		DRJ 2		DRJ 2		DRJ 2	
Depth (m)	43		43		43		43		43		43	
Sample	D2-43		D2-43		D2-43		D2-43		D2-43		D2-43	
Analysis no.	1006		1020		1014		1025		1003		1005	
Precursor	Plagioclase		Plagioclase		Groundmass		Groundmass		Vein, middle		Vein	
Oxide (wt.%)												
SiO_2	0.08		0.12		0.22		0.46		0.57		0.02	
TiO_2	0.04		0.26		0.01		-		0.08		0.16	
Al_2O_3	43.16		41.70		41.17		42.55		41.64		42.36	
FeO	0.12		0.28		0.19		0.09		0.09		0.08	
MnO	< 0.06		0.09		0.03		< 0.04		< 0.08		-	
MgO	0.05		< 0.05		-		0.05		0.09		0.01	
CaO	0.21		0.61		0.44		0.08		0.11		0.26	
Na_2O	0.80		1.10		0.93		1.17		0.43		1.14	
K_2O	4.26		3.27		4.53		3.77		5.36		3.88	
Cl	0.17		0.12		0.12		0.16		0.04		0.14	
NiO	0.03		0.02		< 0.01		0.08		0.01		< 0.04	
Cr_2O_3	-		< 0.11		< 0.03		< 0.05		< 0.05		0.01	
SO_3	40.42		38.48		37.75		38.77		38.27		39.83	
P_2O_5	0.46		1.30		1.00		0.08		0.53		0.63	
Total	89.76		87.18		86.36		87.16		87.09		88.47	
Number of ions on the basis of 10 (O)												
Si	-		0.010		0.010		0.030		0.030		-	
Al	2.950		2.930		2.950		3.000		2.950		2.940	
Ti	-		0.010		-		-		-		0.010	
Fe^{2+}	0.010		0.010	0.02	0.010		-		-		-	
Mn	-		-		-		-		-		-	
Mg	-		-		-		-		0.010		-	
Ca	0.010		0.040		0.030		-		0.010		0.020	
Na	0.090	0.42	0.130	0.42	0.110	0.49	0.140	0.43	0.050	0.47	0.130	0.44
K	0.320		0.250		0.350		0.290		0.410		0.290	
Cl	0.020		0.010		0.010		0.020		-		0.010	
S	1.760		1.720		1.720		1.740		1.730		1.760	
P	0.020		0.070		0.050		-		0.030		0.030	
Ratio												
Na:K	0.28		0.52		0.31		0.48		0.12		0.45	

7.5.2. Biotite:$K_2(Mg,Fe^{2+})_{6-4}(Fe^{3+},Al,Ti)_{0-2}[Si_{6-5}Al_{2-3}O_{20}]O_{0-2}(OH,F)_{4-2}$

Biotite replaces plagioclase at 1855 m depth in DRJ 13 and 2407 m depth in DRJ 17. The composition of biotite, as given representatively in Table 7.20 and Figure 7.13, shows that Mg is dominant, relative to Fe. The amount of MgO is from 16 to 22 wt.% and FeO varies from 10 to 15 wt.%; the FeO content is 2 wt.% higher than that reported by Foster (1961). This confirms that biotite is present as phlogopite with the end member of $K_{1.0-2.0}(Mg_{3.7-4.8},Fe^{2+}_{2.0-1.4})(Al_{0.2-0.5}, Ti_{0.6-0.1})[Si_{5.5-6.8}Al_{1.2-2.5}O_{20}](OH,F)_n$. The amounts of SiO_2 and Al_2O_3 are 33-46 and 9-15 wt.% respectively; the K_2O contents range between 4 and 10 wt.%. TiO_2 is up to 6 wt.%, almost double the TiO_2 content of hydrothermal phlogopite reported by Jacobs and Parry (1976).

Phlogopite is less SiO_2 in cores from wells DRJ 13 to DRJ 17, but there is more Al_2O_3. The amounts of FeO and TiO_2 tend to increase, whereas MgO decreases. Compositional zoning is also evident; the core of phlogopite usually contains less MgO but more K_2O and TiO_2 than the rim.

Table 7.20.Compositions and structural formulae of representative hydrothermal biotites.

Well	DRJ 13		DRJ 13		DRJ 17		DRJ 17		DRJ 17	
Depth (m)	1855		1855		2407		2407		2407	
Sample	D13-6087		D13-6087		D17-7898		D17-7898		D17-7898	
Analysis no.	1907		1921		2209		2220		2268	
Precursor	Plagioclase, crack		Plagioclase		Plagioclase, vug, middle		Plagioclase, granular		Plagioclase, euhedral	
Name	Phlogopite		Phlogopite		Phlogopite		Phlogopite		Phlogopite	
Oxide (wt.%)										
SiO_2	41.40		45.24		40.17		37.35		35.21	
TiO_2	2.59		1.53		4.42		5.33		3.53	
Al_2O_3	11.22		9.46		12.11		12.96		13.45	
FeO	10.94		11.65		11.38		11.87		14.29	
MnO	0.13		0.09		0.16		0.03		0.23	
MgO	19.45		21.34		17.94		16.18		16.87	
CaO	0.17		0.09		0.06		0.11		0.35	
Na_2O	< 0.06		< 0.06		< 0.06		< 0.06		< 0.06	
K_2O	8.23		5.45		9.18		9.72		6.55	
Total	94.39		95.30		95.91		93.97		90.52	
Number of ions on the basis of 24 (O, OH, F)										
Si	6.341	8.00	6.724	8.00	6.128	8.00	5.880	8.00	5.743	8.00
Al^{IV}	1.659		1.276		1.872		2.120		2.257	
Al^{VI}	0.365		0.380		0.304		0.283		0.327	
Ti	0.298		0.171		0.507		0.631		0.433	
Fe^{+2}	1.401	6.52	1.448	6.74	1.452	6.36	1.563	6.28	1.949	6.84
Mn	0.017		0.011		0.021		0.004		0.032	
Mg	4.441		4.729		4.080		3.797		4.102	
Ca	0.028		0.014		0.010		0.019		0.061	
Na	-	1.64	-	1.05	-	1.80	-	1.97	-	1.42
K	1.608		1.033		1.787		1.952		1.363	
Ratio										
Fe:(Fe+Mg)	0.24		0.23		0.26		0.29		0.32	
Mg:(Fe+Mg)	0.76		0.77		0.74		0.71		0.68	

7.5.3. Apatite: $Ca_5(PO_4)_3(OH,F,Cl)$

Secondary apatite is present in cavities and veins in DRJ S-1, S-3 and S-5 and in the production area. Apatite also occurs at the margin of veins in hot acid altered rocks from 2117 m depth in DRJ S-3.

Table 7.21 represents the compositions of several apatites and shows that they are composed of 50-55 wt.% CaO and 35-43 wt.% P_2O_5. They contain up to 1.5 wt.% SiO_2 and 1.2 wt.% Al_2O_3. The amount of FeO varies up to 2 wt.%; traces of MnO and MgO are usually present but less than 2 wt.%. Substitution of Ca by Na may also occur and reaches up to 2 wt.% Na_2O.

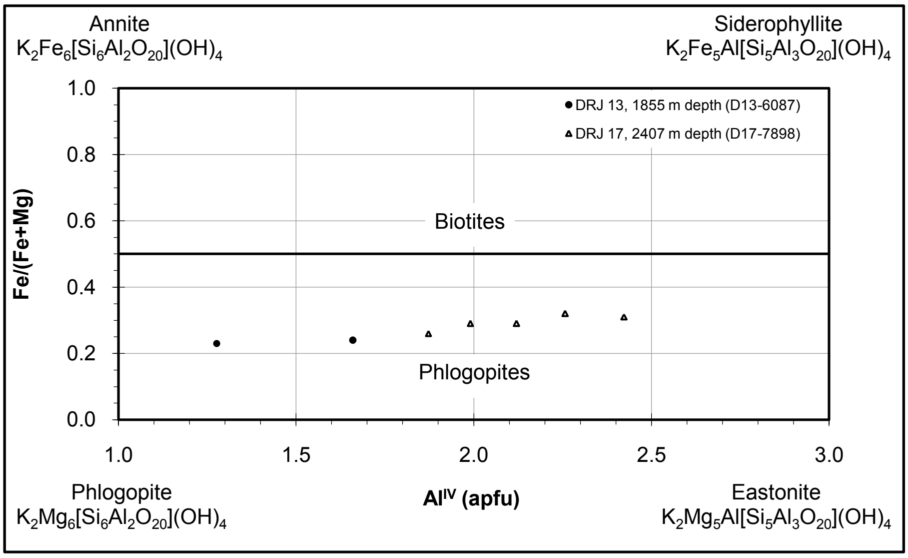

Figure 7.13. Classification of biotite from wells DRJ 13 and 17, based on the number of Al (apfu = atoms per formulae unit) in the tetragonal site and the ratio of ferromagnesian end members. The number of ions is calculated on the basis of 24 oxygens.

Chlorine (Cl) and F are commonly present. The former is up to 3 wt.%, but the latter unfortunately cannot be determined. Substitution of SO_4 may occur (Deer et al., 1962b), as is indicated by the presence of up to 10 wt.% SO_3 in DRJ S-1 and S-5, while in other wells it is less than 1 wt.% only.

The apatite formulae based on 12 oxygens (Table 7.21) has an end member composition of $(Ca_{4.5\text{-}5.1},Na_{0.2\text{-}0.0},Fe_{0.2\text{-}0.0},Mg_{0.1\text{-}0.0},Mn_{0.2\text{-}0.0})P_{2.6\text{-}3.0}O_{12}(OH,F,Cl)$. The analyses show that the total oxide is about 95 wt.%; the remainder may include F, H_2O and possibly CO_2. No compositional zoning within a crystal was detected.

Table 7.21.Compositions and structural formulae of representative hydrothermal apatites.

Well	DRJ S-1	DRJ S-3	DRJ S-5	DRJ S-3	DRJ S-3	DRJ S-5	DRJ S-5	DRJ 5
Depth (m)	798	1140	2156	1000	2117	890	2207	2560
Sample	S1-2616	S3-3739	S5-7072	S3-3280	S3-6945	S5-2919	S5-7241	D5-8398
Analysis no.	1109	855	6188	4403	3388	5107	4712	2682
Occurrence	Vein	Vein	Vein	-	Vein	Vugs	Vugs, with opaque	Vugs, euhedral
Oxide (wt.%)								
SiO_2	0.12	0.14	0.27	< 0.06	0.91	0.05	0.20	0.27
TiO_2	< 0.01	0.23	< 0.02	< 0.02	-	0.10	0.20	< 0.09
Al_2O_3	-	0.14	0.18	0.08	0.74	-	< 0.06	0.17
FeO	0.50	0.46	0.36	0.61	1.39	< 0.11	0.75	0.22
MnO	0.45	< 0.09	0.07	< 0.02	< 0.15	1.19	-	0.28
MgO	< 0.04	0.21	0.13	0.19	0.15	0.07	< 0.04	0.35
CaO	52.55	53.74	53.79	52.82	51.61	50.66	50.38	53.65
Na_2O	< 0.11	< 0.07	0.36	0.09	< 0.04	0.05	-	< 0.03
K_2O	-	0.07	0.09	< 0.05	-	-	0.02	0.05
Cl	3.10	0.79	0.11	1.32	< 0.01	0.51	1.46	1.17
NiO	0.12	< 0.20	< 0.01	0.15	0.25	-	0.08	0.23
Cr_2O_3	0.07	< 0.05	< 0.14	< 0.11	0.06	0.08	0.08	< 0.04
SO_3	0.27	0.10	0.70	0.07	0.98	9.26	5.58	0.16
P_2O_5	41.29	41.04	41.86	42.33	36.06	35.31	37.50	39.19
Total	98.33	96.30	97.77	97.41	91.95	97.18	96.15	95.58

Number of ions on the basis of 12 (O)

Fe^{2+}	0.035		0.032		0.024		0.042		0.102		-		0.056		0.016	
Mn	0.032		-		0.005		-		-		0.093		-		0.020	
Mg	-		0.026		0.016		0.023		0.020		0.010		-		0.044	
Ca	4.652	4.73	4.742	4.82	4.678	4.81	4.620	4.70	4.870	5.07	4.994	5.11	4.809	4.89	4.850	4.96
Na	-		-		0.057		0.014		-		0.009		-		-	
K	-		0.007		0.009		-		-		-		0.002		0.005	
Si	0.010		0.012		0.022		-		0.080		0.005		0.018		0.023	
P	2.889		2.862		2.876		2.926		2.689		2.750		2.829		2.800	
S	0.017		0.006		0.043		0.009		0.061		0.388		0.346		0.010	
CCl	0.043		0.221		0.030		0.365		-		0.159		0.441		0.335	

7.5.4. Rutile: TiO_2

Secondary rutile occurs in many cavities and vugs in wells DRJ S-1, S-3, S-5 and in the production area. It is intergrown with other opaque minerals and is associated with pyrite. It is rarely present as inclusions in quartz veins. Some selected compositions are given in Table 7.22, showing that the TiO_2 content ranges from 93 to 100 wt.%. Some vugs in plagioclase also contain up to 2 wt.% SiO_2, 0.5 wt.% Al_2O_3 and 2 wt.% CaO, but are likely contaminants. Rutile can also have less than 1 wt.% FeO but may be as high as 6 wt.%. This may be due to being intergrown with ilmenite (Deer, et al., 1962b). However, rutile compositions can be expressed as $Ti_{0.9\text{-}1.0}O_2$.

Table 7.22.Compositions and structural formulae of representative rutiles.

Well	DRJ S-1	DRJ S-1	DRJ 24	DRJ 24	DRJ 24	DRJ S-5
Depth (m)	911	911	2596	2596	890	890
Sample	S1-2990	S1-2990	D24-8517	D24-8517	S5-2919	S5-2919
Analysis no.	3612	3031	1263	1227	1256	5063
Precursor/ Occurrence	-	Plagioclase	Inclusion at quartz	Vugs	Vugs	Vugs, with pyrite
Oxide (wt.%)						
SiO_2	0.25	1.29	< 0.01	0.16	0.17	0.48
TiO_2	97.19	96.76	98.20	98.85	98.48	95.41
Al_2O_3	0.16	0.49	< 0.02	0.01	0.07	1.25
FeO	0.22	0.31	0.46	1.11	0.74	0.39
MnO	-	0.05	0.07	< 0.04	0.04	0.09
MgO	0.06	0.16	< 0.04	0.17	0.05	-
CaO	0.92	0.76	0.06	0.08	0.02	0.44
Na_2O	0.01	-	< 0.05	0.14	-	0.01
K_2O	< 0.05	0.03	0.02	< 0.01	0.05	-
Cl	< 0.07	0.01	< 0.02	-0.05	< 0.01	< 0.01
NiO	0.01	0.09	0.21	0.01	0.06	-
Cr_2O_3	0.08	< 0.04	0.14	0.11	0.30	0.05
SO_3	0.23	< 0.17	0.02	< 0.15	< 0.14	0.30
P_2O_5	0.15	0.01	0.10	0.29	0.09	0.15
Total	99.17	99.75	99.14	100.67	99.92	98.55
Number of ions on the basis of 2 (O)						
Ti	0.98	0.97	0.99	0.99	0.99	0.97
Fe^{2+}	-	-	0.01	0.01	0.01	-
Si	- } 0.99	0.02 } 1.01	- } 1.00	- } 1.00	- } 1.00	0.01 } 1.00
Al	-	0.01	-	-	-	0.02
Ca	0.01	0.01	-	-	-	0.01

7.5.5. Tourmaline: $Na(Mg,Fe,Mn,Li,Al)_3Al_6[Si_6O_{18}](BO_3)_3(OH,F,Cl)_4$

Tourmaline is present in cavities at 911 m depth in well DRJ S-1 and 890 m depth in DRJ S-5. Table 7.23 represents its composition and Figure 7.14 shows the proportions of Al, Ca, Fe and Mg. Tourmaline occurs as Mg-rich (dravite) and Fe-rich (schorl) crystals as indicated by the MgO and FeO contents of up to 11 and 13 wt.% respectively. The ratio between Mg and Fe+Mg varies from 0.5 to 1.0. The amount of SiO_2 ranges from 34 to 38 wt.% and Al_2O_3 varies between 25 and 38 wt.%;

CaO and alkalis are very low, i.e. less than 3 wt.%. Tourmaline also contains 10-12 wt.% B_2O_3 and up to 0.7 wt.% Li_2O, calculated following Dutrow and Henry (2000). The end member composition of tourmaline is $Na_{0.5-0.8}Ca_{0.0-0.4}(Mg_{1.5-2.6},Fe_{0.0-1.8},Mn_{0.0-0.1},Li_{0.0-0.3},Al_{0.0-0.8})Al_{5.0-6.0}[Si_{5.5-6.0}O_{18}](BO_3)_3(OH,F,Cl)_4$.

Table 7.23.Compositions and structural formulae of representativetourmaline.

Well	DRJ S-1	DRJ S-1	DRJ S-1	DRJ S-5	DRJ S-5	DRJ S-5
Depth (m)	911	911	911	890	890	890
Sample	S1-2990	S1-2990	S1-2990	S5-2919	S5-2919	S5-2919
Analysis no.	3571	3618	3619	5055	5072	5081
Occurrence	Vugs, core	Vugs, (rim)	Vugs, core	Vugs	Vugs, (rim)	Vugs, (rim)
Name°	Dravite	Schorl-dravite (±uvite)	Schorl-dravite (±uvite)	Schorl-dravite	Dravite	Dravite
Oxide (wt.%)						
SiO_2	36.60	36.23	35.21	35.89	36.40	36.35
TiO_2	0.07	0.22	0.20	0.22	0.21	0.22
Al_2O_3	35.68	29.46	28.59	30.07	33.08	32.87
FeO	0.53	7.88	9.71	9.37	1.95	1.35
MnO	0.38	0.25	0.19	0.18	0.04	0.09
MgO	8.81	8.30	8.03	6.46	9.72	10.55
CaO	0.06	1.72	2.06	0.42	0.11	0.06
Na_2O	2.03	1.53	1.92	2.16	2.50	2.52
K_2O	0.03	0.10	0.05	0.12	0.08	0.08
Cl	0.04	< 0.01	0.07	0.10	-	0.01
Total$^{1)}$	84.37	85.75	85.90	84.89	84.64	84.84
Li_2O*	0.35	-	-	0.17	0.37	0.28
B_2O_3**	11.05	10.66	10.55	10.56	10.93	10.96
H_2O***	3.80	3.68	3.62	3.61	3.77	3.78
Total$^{2)}$	99.56	99.93	99.57	99.23	99.72	99.85

Number of ions on the basis of 31 (O, OH, F)												
Si	5.760		5.905		5.804		5.909		5.786		5.765	
Al^{IV}	6.000		5.659		5.554		5.835		6.000		6.000	
Al^{VI}	0.117	2.788	-	3.135	-	3.350	-	2.915	0.197	2.788	0.144	2.849
Ti	0.008		0.027		0.025		0.027		0.025		0.026	
Fe^{2+}	0.070		1.074		1.338		1.290		0.259		0.179	
Mn	0.025		0.017		0.013		0.013		0.003		0.006	
Mg	2.067		2.017		1.973		1.586		2.303		2.494	
Ca	0.005	0.627	0.150	0.644	0.182	0.801	0.037	0.739	0.009	0.788	0.005	0.788
Na	0.619		0.483		0.614		0.689		0.770		0.775	
K	0.003		0.010		0.005		0.013		0.008		0.008	
Vacancy$^{3)}$	0.373		0.356		0.199		0.261		0.212		0.212	
Li*	0.212		-		-		0.085		0.212		0.151	
B**	3.000		3.000		3.000		3.000		3.000		3.000	
Cl	0.011	4.000	-		0.020	4.000	0.028	4.000	-		0.003	4.000
OH***	3.989		4.000		3.980		3.972		4.000		3.997	

Ratio						
Mg:(Mg+Fe)	0.97	0.65	0.60	0.55	0.90	0.93
Al:(Al+Mg)	0.76	0.74	0.74	0.79	0.73	0.71
Ca:(Ca+Na)	0.01	0.24	0.23	0.05	0.01	0.01

° Based on Deer et al. (1978).

* Li was estimated by subtracting the sum of Al^{IV}, Ti, Fe^{2+}, Mn and Mg cations from 3; the Li_2O was then calculated stoichiometrically (Dutrow and Henry, 2000).

** B in the structure containing 6 ions of Si was equivalent to 3 (Dutrow and Henry, 2000); the B_2O_3 was then calculated stoichiometrically.

*** Calculated with assumption of 4 total ions of OH, Cl and F. Since F was not determined, the sum of OH and Cl ions is 4; the H_2O was then calculated stoichiometrically.

1) Total oxide before calculations of Li_2O, B_2O_3 and H_2O, i.e. the total analysis.

2) Total oxide after calculations of Li_2O, B_2O_3 and H_2O.

3) Amount of vacancy, i.e. in the X site, was calculated by subtracting the sum of Ca, Na and K cations from 1.

The composition of tourmaline is strongly affected by substitutions between Na, Ca, Mg, Fe and Al (Deer et al., 1978). The relationships between Fe and Mg, Ca and Na are given in Figure 7.15. Zoning occurs, as the core of tourmaline is more FeO and CaO rich but less Al_2O_3, SiO_2 and Na_2O poor than the rim. As shown in Figures 7.14 and 7.15, tourmaline from well DRJ S-5 contains less Fe and Mg than that from DRJ S-1; it also has less Ca but more Na.

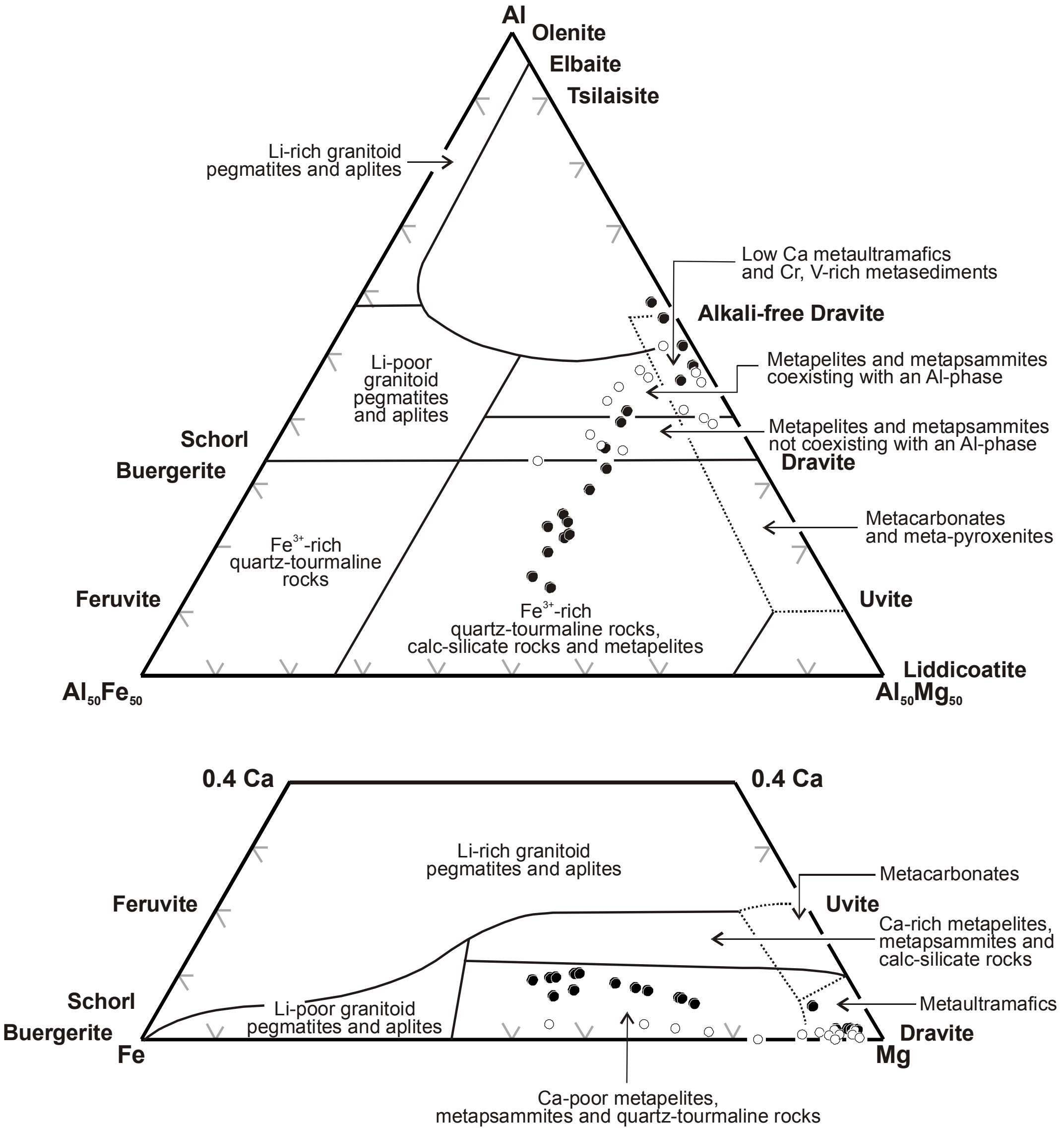

Figure 7.14. Proportions of Al, Fe, Mg and Ca in the structure of tourmaline, calculated on the basis of 24 oxygens. According to Deer et al. (1978 and 1992), dravite, schorl and buergerite are Na tourmaline, and uvite and feruvite are Ca tourmaline; dravite and uvite are Mg rich, schorl and feruvite are Fe^{2+} rich and buergerite is Fe^{3+} rich; other tourmalines include olenite (Na rich), elbaite (Li bearing), tsilaisite (Mn bearing) and liddicoatite (Li-Mg rich). Symbol (●) represents tourmaline from about 900 m depth in well DRJ S-1 and (○) represents tourmaline from DRJ S-5. All tourmalines are present in cavities. Typical host rocks containing tourmaline as shown by Henry and Guidotti (1985).

Tourmaline is an indicator mineral for a change in the composition of the depositing fluids (e.g. Dutrow and Henry, 2000; von Goerne and Franz, 2000 and 2001). Sodium, Fe and Mg rich tourmaline is usually associated with silicate and sulfide reactions, as reported by Jiang et al. (2002), at temperatures above 300°C (von Goerne and Franz, 2001). Higher Ca contents might suggest an increase in the temperature of tourmaline formation, i.e. above 500°C (von Goerne and Franz, 2000), e.g. in well DRJ S-1. Boron itself can be deposit from the hydrothermal fluid but can also come from a magma or be released by dehydration of muscovite or illite (Kawakami, 2001). Tourmaline occurs in other geothermal systems, e.g. Larderello, as a relict metamorphic mineral; the geothermometer suggests the formation temperatures of 400-625°C (Gianelli and Ruggieri, 2002).

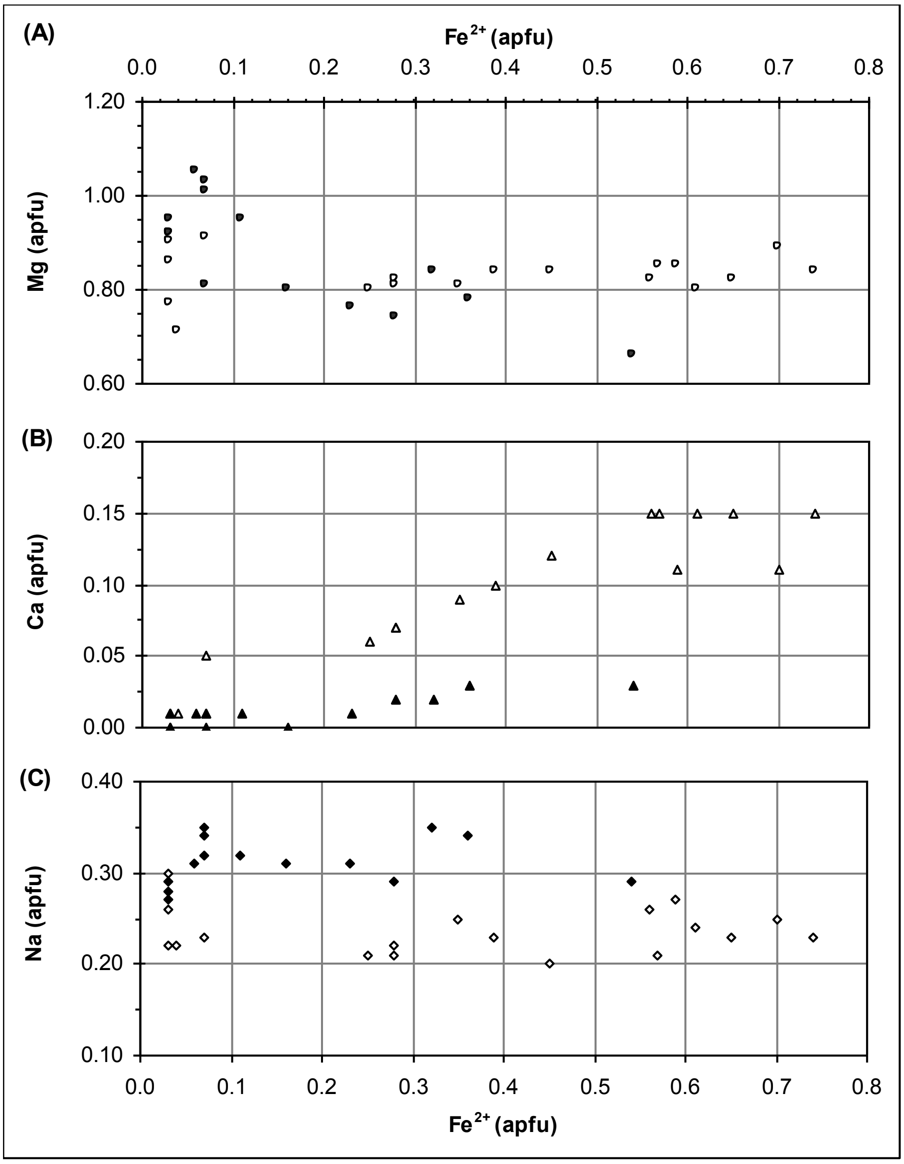

Figure 7.15. Relationship between the amounts of Fe and: **(A)** Mg, **(B)** Ca and **(C)** Na (apfu = atoms per formulae unit) in the structure of tourmaline, calculated on the basis of 24 oxygens. The compositions were determined on 2 samples only, i.e. from 911 m depth in well DRJ S-1 (hollow symbols) and 890 m depth in DRJ S-5 (solid symbols).

7.5.6. Opaque Minerals

Opaque minerals are present in veins, vugs and along cracks. They are mostly magnetite and hematite. Table 7.24 shows the composition of several opaque minerals. The total iron is expressed as FeO and Fe_2O_3, based on an assumption that hematite is Fe_2O_3, whereas magnetite contains FeO about 0.3 of the total iron. Differentiation between hematite and magnetite is given in Appendix F.

Magnetite is more common than hematite; it is present in all wells, including DRJ 13 and 17, below 1250 m. It contains 26-30 wt.% FeO and 59-66 wt.% Fe_2O_3. However, at about 1250 m depth in well DRJ S-2, hematite is associated with magnetite and, at 900-1000 m depth in wells DRJ S-1 and S-3, hematite becomes dominant. It contains between 77 and 89 wt.% Fe_2O_3. Hematite also replaces the groundmass at about 2120 m depth in well DRJ S-3. Up to 10 wt.% TiO_2 and less than 4 wt.% MnO, MgO and Cr_2O_3 are present in hematite.

At about 1240 m depth in well DRJ S-1 and 2400 m in DRJ 17, ilmenite is intergrown with rutile and titanite. It contains 25-52 wt.% TiO_2 and 38-66 wt.% FeO. Magnesium can substitute for Fe and is present up to 14 wt.% MgO. However, ilmenite may become hydrous, as indicated by its total oxide as low as 92 wt.%. Oxidation of FeO to Fe_2O_3 is unlikely, indicated by the Fe^{2+} and Fe^{3+} calculation after Droop (1987) and Mücke and Chaudhuri (1991). At about 1020 m depth in well DRJ S-1, ilmenite is Mn rich, containing about 30 wt.% MnO; FeO and TiO_2 are about 18 and 53 wt.% respectively. Jiang et al. (1996) reported that Mn rich ilmenite is due to the remobilisation of Mn at high temperatures. In contrast, ilmenite from 3280-3940 m depth in well DRJ S-3 and below 1980 m in wells DRJ S-3 and S-5 is rich in Fe. The FeO contents range from 70 to 74 wt.%, as TiO_2 and MnO are only present at 11-17 and up to 3 wt.% respectively. Oxidation is likely, as suggested by Mücke and Chaudhuri (1991).

Pyrite is present in cavities and veins and its composition is represented in Table 7.25. Pyrite contains 56 to 62 wt.% FeO and 50 to 56 wt.% S. The ratio of S to Fe varies between 1.8 and 2.1. Leucoxene is associated with pyrite and other opaque minerals. It replaces primary opaque minerals and other hydrothermal minerals. Its composition seems to be intermediate (Morad and Aldahan, 1985) or mixture between SiO_2, Al_2O_3, FeO, MgO and TiO_2.

Table 7.24.Compositions of representative opaque minerals. Names of opaque minerals are given.

Well	DRJ S-3	DRJ S-3	DRJ 17	DRJ S-5	DRJ 14	DRJ S-2	DRJ S-1	DRJ S-1
Depth (m)	1951	1000	2407	1332	1575	1251	1023	1242
Sample	S3-6502	S3-3280	D17-7898	S5-4370	D14-5166	S2-4103	S1-3355	S1-4074
Analysis no.	5573	4415	2242	2123	4295	3486	3117	3681
Precursor/ Occurrence	Pyroxene	Plagioclase	Plagioclase, cracks	Vugs	Vugs at plagioclase	Vugs	Vugs, with epidote	Vugs, with rutile, epidote
Name	Magnetite	Hematite	llmenite	Magnetite	Magnetite	Hematite	Ilmenite	llmenite
Oxide (wt.%)								
SiO_2	0.76	1.41	0.09	0.45	0.17	0.84	0.14	0.01
TiO_2	4.32	1.01	44.59	0.15	0.35	1.41	52.21	48.21
Al_2O_3	0.39	0.60	0.04	0.36	0.23	0.50	< 0.03	< 0.02
FeO*	27.82	-	48.27	28.60	29.52	-	15.07	42.87
Fe_2O_3*	61.84	87.67	-	63.56	65.61	88.07	-	-
MnO	0.56	< 0.04	3.17	0.19	0.37	0.57	30.61	6.69
MgO	-	< 0.08	0.08	0.16	< 0.06	0.64	0.12	0.09
CaO	0.36	0.13	0.16	0.35	0.43	0.08	0.99	0.01
Na_2O	0.11	0.13	< 0.01	< 0.04	-	< 0.02	< 0.07	0.08
K_2O	< 0.02	-	< 0.01	0.03	0.09	0.05	< 0.04	0.02
Cl	< 0.02	0.02	< 0.08	< 0.01	0.04	< 0.01	< 0.01	< 0.01
NiO	< 0.14	< 0.13	< 0.03	-	0.03	< 0.03	< 0.04	0.10
Cr_2O_3	< 0.01	0.13	0.12	0.13	< 0.01	-	-	0.20
SO_3	0.15	< 0.03	< 0.05	< 0.07	0.02	< 0.05	< 0.05	< 0.09
P_2O_5	< 0.09	0.04	0.01	< 0.12	< 0.15	0.02	< 0.06	< 0.07
Total	96.04	90.87	96.34	93.75	96.64	92.06	98.85	98.09

* Recalculated from the total iron analysis (FeO) using assumptions that magnetite could contain 0.3 of the total iron present as FeO and 0.7 of the iron as Fe_2O_3 (Deer et al., 1962b), and all iron in hematite is Fe_2O_3. The amount of Fe_2O_3 in ilmenite was calculated after Droop (1987) and Mücke and Chaudhuri (1991); no excess FeO can be calculated as Fe_2O_3.

Table 7.25.Compositions of representative pyrites.

Well	DRJ S-1	DRJ S-5	DRJ 24	DRJ S-1	DRJ S-5
Depth (m)	1298	2207	2596	304	2023
Sample	S1-4259	S5-7241	D24-8517	S1-998	S5-6638
Analysis no.	3786	4622	1225	5819	3673
Occurrence	Vein	Vein, with anhydrite	Vein, with quartz	Vugs	Vugs
Name	Pyrite	Pyrite	Pyrite	Pyrite	Pyrite
Oxide (wt.%)					
SiO_2	< 0.13	0.13	0.19	< 0.05	0.46
TiO_2	< 0.03	0.01	< 0.19	0.06	0.02
Al_2O_3	< 0.07	< 0.03	< 0.05	< 0.12	< 0.05
FeO	60.12	61.33	61.64	59.96	58.70
MnO	0.16	-	0.07	0.08	0.13
MgO	< 0.02	0.21	0.01	0.01	0.14
CaO	0.19	0.16	0.08	0.16	0.11
Na_2O	0.24	0.53	0.30	0.01	0.21
K_2O	0.07	0.25	0.12	0.01	0.20
Cl	0.05	< 0.06	< 0.08	< 0.08	< 0.02
NiO	< 0.09	0.08	< 0.1	0.09	< 0.08
Cr_2O_3	0.01	< 0.19	0.06	0.03	0.01
SO_3	135.93	139.21	127.34	140.23	131.69
P_2O_5	0.02	0.16	< 0.21	0.01	0.15
Total	196.48	201.77	189.18	200.40	191.68
Fe	46.73	47.67	47.91	46.61	45.63
S	54.43	55.75	50.99	56.16	52.74
Oxide (mol.%)					
TiO_2	-	-	-	-	-
FeO	0.84	0.85	0.86	0.83	0.82
MnO	-	-	-	-	-
MgO	-	0.01	-	-	-
NiO	-	-	-	-	-
Cr_2O_3	-	-	-	-	-
SO_3	1.70	1.74	1.59	1.75	1.64
Ratio					
S:Fe	2.03	2.04	1.85	2.10	2.01

7.6. DISCUSSION

7.6.1. Zoning

Compositional zoning of hydrothermal minerals is mostly shown by variations in Fe and Mg. Non ferromagnesian minerals, e.g. laumontite and wairakite, are not zoned. Table 7.26 summarises the compositional zoning of chlorites and some calc-silicates. The cores of replacement minerals tend to contain more Mg and/or Al, whereas the rims contain more Fe. In contrast, zoning of vein minerals shows that the core has more Fe but less Mg.

Table 7.26.Comparison of the compositional zoning between replacement and cavity and/or vein minerals.

Mineral	Replacement	Cavity and vein
Chlorites	Core has more Mg, whereas rim is more Fe rich.	Core has more Fe, whereas rim is more Mg rich.
Prehnite	-	Core contains more Fe.
Titanite	-	Core contains more Fe and Mg, and the rim contains more Ti.
Epidote	Core has less Fe but more Al (lower pistacite) than the rim.	Core has more Fe than the rim.
Amphiboles	Core is more Mg but the rim contains more Fe.	Core has more Fe, whereas the rim is more Mg rich.
Garnet	-	Core contains more Fe (andradite), whereas the rim has more Al (grossular). The rim also contains more Fe^{3+} due to oxidation.

Zoning, especially of epidote, is also reported in other geothermal systems such as Larderello (Cavarretta et al., 1980 and 1982), Cerro Prieto of Mexico (Bird et al., 1984) and Salton Sea in California (McDowell and Elders, 1983). However, these authors did not distinguish between the zoning of replacement and that vein minerals. The compositional zoning of epidote in those geothermal systems is similar to that of the replacement minerals at Darajat.

Partitioning of Mg before Fe in the replacement minerals suggests equilibrium processes during interactions between thermal fluids and surrounding rocks. Pattison (1994) and Huertas et al. (1995) claimed that the partitioning between Mg and Fe is not directly controlled by pressures and temperatures, but by thermodynamic properties, e.g. Gibbs free energy, enthalpy and entropy. Size or radius (r) of cations is a major control; Mg^{2+} is smaller ($r_{Mg}{}^{2+}$= 0.66Å) than Fe^{2+} ($r_{Fe}{}^{2+}$= 0.78Å), thus Mg is easier to nucleate in minerals than Fe.

The distribution of cations in clay minerals, e.g. in chlorite, also depends on the charge balance. The substitution of Al^{3+} for Si^{4+} in the tetrahedral structure causes the octahedral site to be unbalanced. Furthermore, Mg^{2+} can first replace Al^{3+} in the octahedral site. Since Mg, together with Ca, K and Na, are exchangeable cations in the clay structure, they can be replaced by Fe^{2+} and Mn^{2+} (Grim, 1968). The remaining Al^{3+} in the octahedral structure can then be replaced by Fe^{3+} or Cr^{3+}. Ca^{2+} can replace Na^+ in smectite, then Mg^{2+} is more likely to replace Ca^{2+} first than Fe^{2+} and Fe^{3+} (Grim, 1968 and Huertas et al., 1995). This likely occurred in calc-silicate minerals, e.g. epidote and amphiboles, where their rims contain more Fe than the cores (Table 7.26).

The distribution of Mg and Fe is different in cavity and vein minerals. The rims of have more Mg but less Fe than the core. The rim also contains more Ti in titanite and Al in epidote and garnet (Table 7.26). This is likely to be due to changes in fluid compositions, temperatures and/or pressures. Changes in fluid composition thus affect the compositions of replacement and vein minerals.

7.6.2. Replacement and Vein Minerals

The variations in compositions of the hydrothermal minerals formed as replacements and those present in veins are summarised in Table 7.27. Generally, there are no differences. This indicates that the fluids in the matrix channels had the same compositions as the circulating fluids. However, Fe and Si seem to concentrate in vein minerals, whereas replacement minerals contain more Mg and Al. This indicates that the thermal fluid, that interacted with the reservoir rocks, was once Mg rich, but the fluid circulating in fractures was Fe rich and saturated with silica.

Table 7.27. Comparison between the compositions of hydrothermal minerals formed as replacement and those present in cavities and veins.

Mineral	Replacement	Cavity and vein
Chlorites	More Mg but less Fe, Al and H_2O	More H_2O
Laumontite	More H_2O	More Ca, less H_2O
Wairakite	More H_2O -	More Si, Ca and Al but less H_2O
Prehnite	More Al but less Fe	More Fe but less H_2O
Titanite	-	More Fe but less Al and Ti
Epidote	More Al (lower pistacite)	More Si and Fe (maximum in vein)
Amphiboles	More Al but less Fe	Generally more Fe but less Al, Mg
Garnet	More Al	More Fe^{2+} and Fe^{3+}

Cavity and vein filling clay minerals, e.g. chlorite, are more hydrous than the replacement ones. In contrast, calc-silicates, e.g. laumontite and wairakite, present in cavities and veins are less H_2O rich than the replacement minerals. The variation in compositions of vug and vein epidotes depends also on the associated minerals present and the infilling sequence. This is a signature that, instead of fluid and rock interactions, fluid affecting processes, e.g. cooling and boiling, can change in fluid characteristics and hence mineral compositions. This is discussed for each well below.

7.6.3. Variation in the Compositions of Hydrothermal Minerals between Wells

Variations in the compositions of hydrothermal minerals between wells suggest that the conditions in which the minerals formed slightly differ.

Wells DRJ S-1 and S-5. Table 7.28 compares the variations in the compositions of hydrothermal minerals present in wells DRJ S-1 and S-5.

Table 7.28. Comparison between the compositions of chlorite, illite and calc-silicates present in wells DRJ S-1 and S-5.

Mineral	DRJ S-1	DRJ S-5
Chlorites	More Si and Mg	More Fe but less Mg
Illite	More Si and Mg	More Fe
Laumontite	Absent	-
Wairakite	Similar	Similar
Prehnite	-	Absent
Epidote	More Al (lower pistacite)	More Fe (higher pistacite)
Amphiboles	More Fe but less Mg	More Mg
Garnet	More Al but less Fe	More Fe (andradite)

The compositions of garnet and epidote indicate that temperature of the circulating fluids reached about 400°C. More andradite rich garnets and higher pistacite values of epidotes from well DRJ S-5 suggest that rocks in this well were once hottest (Holdaway, 1972; Ferry and Spear, 1978; and Heuss-Aβbichler and Fehr, 1997). A slight colder fluid in well DRJ S-1 is consistent with an association with prehnite (Bird and Helgeson, 1981; Bird et al., 1984), a more Mn rich ilmenite (Ghiorso and Sack, 1991) and by decreases in the Fe and Al contents in the tetrahedral structure, but an increase in Mg of chlorites (e.g. Cathelineau and Nieva, 1985; Cathelineau, 1988; de Caritat et al., 1993; and Aja and Dyar, 2002).

Almandine from 1332 m depth in well DRJ S-5 also indicates hot temperatures but lower P_{H_2O} conditions in this well than DRJ S-1 (James, 1977). Liou (1971) reported that prehnite could form at higher fluid pressures (P_{H_2O}) than wairakite. Since prehnite is absent in well DRJ S-5, the other well may have had higher P_{H_2O}. High P_{H_2O} in well DRJ S-1 is also suggested by the occurrences of Al rich amphiboles (Figure 7.9, Hammarstrom and Zen, 1986) and low pistacite epidote and garnet (Holdaway, 1972 and Brown, 1977). The occurrences of wairakite and laumontite in well DRJ S-5 suggest that a decrease in P_{H_2O} likely relates to temperatures of fluid about 210°C. In well DRJ S-1, cooling as fluid ascends is indicated by a decrease in the pistacite values of prehnite (Liou et al., 1983) from up to 0.3 at 1300 m to less than 0.1 at about 1000 m depth (Figure 7.6).

If temperatures and pressure remain constant, the variations in the compositions of calc-silicates then suggest changes in the fluid compositions. An increase in the Fe content of vein minerals, e.g. epidote, amphibole and prehnite, indicates that the circulating fluid contains more Fe than the fluid that interacted with the rocks. This is consistent with Liou et al. (1983) that epidote and garnet can form under high activity of Fe^{2+} ($a_{Fe^{2+}}$). There is also an increase in $a_{Ca^{2+}}$ of the fluid that allows prehnite to postdate epidote and garnet. Furthermore, the formation of prehnite can decrease $a_{Fe^{2+}}$ of the remaining liquid, but increase the a_{SiO_2} of the fluid (Browne et al., 1989). The $a_{Ca^{2+}}$ was still high enough to form wairakite after prehnite and epidote.

The occurrences of garnet, epidote and prehnite indicate that the amount of dissolved CO_2 (X_{CO_2}) was very low (Cavarreta et al., 1982 and Wheeler et al., 2001). Almandine present in well DRJ S-5 suggests that the X_{CO_2} was up to 0.2 (Gianelli and Ruggieri, 2002). Wairakite and laumontite that postdate epidote and prehnite suggest a decrease in X_{CO_2} due to boiling; the X_{CO_2} seems to decrease from 0.2 to below 0.05 (Bird and Helgeson, 1981; and Schiffman et al., 1984). Consequently, the amount of CO_2 in the vapour phase (f_{CO_2}) increased, i.e. from less than 10 bars to above 100 bars (Cavarreta et al., 1982 and Giggenbach, 1997a). In addition, the X_{CO_2} in well DRJ S-1 was likely higher than that in DRJ S-5, as indicated by the occurrence of Mg chlorite, e.g. clinochlore and penninite, and reported by Hutcheon et al., (1974). Either the rate of boiling or the compositions of the initial altering fluids in wells DRJ S-1 and S-5 was different. Reed (1974) reported that the sequence of calc silicates from garnet, epidote, prehnite to wairakite and laumontite, instead of decreasing X_{CO_2}, also indicates a decrease in the amount of SO_4 in the liquid phase (X_{SO_4}).

According to the pistacite values of garnet, epidote and prehnite, wells DRJ S-1 and S-5 are likely to have had oxygen fugacities (f_{O_2}) between 10^{-34} and 10^{-24} atm (Bird and Helgeson, 1981). However, the f_{O_2} then increased, as suggested by the later wairakite and laumontite (Cavarreta et al., 1982). The occurrence of almandine with TiO_2 at 1332 m depth in well DRJ S-5 suggests that the fluid here was more reducing (Green and Ringwood, 1968; and Liou, 1972) or drier(Green and Ringwood, 1972). Chlorites from well DRJ S-5 are also less Mg rich (Table 7.28), indicating less oxidising conditions than in well DRJ S-1 (Hutcheon et al., 1974).

Well DRJ S-3. High temperature and reducing conditions due to the interactions of acid fluids occurred about 2120 m depth in well DRJ S-3. These conditions permitted Fe rich chlorite, e.g. daphnite and brunsvigite, in association with pyrophyllite and nontronite to form (Bryndzia and Scott, 1987; Porter et al., 2000; and Martínez-Serrano, 2002). The association of these clays suggests that the pH fluid was less than 4 (Reed, 1974 and Tsuzuki, 1976). The acid fluid was likely of magmatic origin, as also suggested by the occurrence of Fe rich garnet, i.e. andradite (Crowne et al., 2001) and apatite (Takagi et al., 2000) at about 1980 m depth. Rare occurrence of diaspore suggests that the fluids were still saturated in silica with respect to quartz (Bowers et al., 1984 and Reed, 1997). The occurrences of Fe-rich epidote and garnet in association with hematite suggest past temperatures as high as 450°C (Liou et al., 1983). The presence of grossular above 1830 m depth suggests a mixing and neutralisation by meteoric water (Crowne et al., 2001). Increases in the amounts of hematite about 1000 m depth confirm an increase in oxidising conditions by mixing with meteoric waters (Reed, 1974). The mixing was then followed by cooling, as indicated by the disappearance of garnet but the presence of prehnite at about 1370 m depth.

Since the ratio between Mg and Mg+Fe of amphiboles is pressure dependent (Pe-Piper, 1988), amphiboles from 1982 m depth likely formed at highest pressures. The occurrence of pyrophyllite confirms that the P_{H_2O} was very high (Bird and Helgeson, 1981), i.e. higher than that elsewhere. However, the occurrence of tschermakite at about 1770 m suggests a sudden decrease in P_{H_2O} (Liou, 1973). This probably results from a decrease in X_{CO_2} due to boiling and/or mixing. Oxidation conditions as a result of fluid mixing is indicated by the higher pistacite values of epidotes and higher Fe_2O_3 of the garnets from well DRJ S-3 compared to those from DRJ S-1 and S-5 (Liou et al., 1983) and the abundance of hematite (Helgeson et al., 1978).

Marginal wells. Wells DRJ S-1, S-3 and S-5 were hotter than the marginal wells DRJ 1, DRJ S-2 and S-6. This is suggested by the abundances of Na relative to Ca rich smectites (Martínez-Serrano, 2002), saponite (Mg rich smectite) instead of chlorite (Fulignati et al., 1997) and Mg relative to Mn and Fe rich calcites (Veizer, 1983 and Gemmell et al., 2002). In well DRJ 2, the Fe bearing kaolinite also indicates that the formation temperatures were low (de Ligny and Navrotsky, 1999).

The occurrences of Mg rich calcite and siderite in the marginal area indicate a mixing of cold, surface, meteoric water (Reed, 1974; Essene, 1983; and Morad, 1998) and deep thermal water. The mixed fluid was likely CO_2 and SO_4^{2-} rich (Elder et al., 1981). Some oxidation occurred, as indicated by the presence of saponite in DRJ 1 and S-2 (Porter et al., 2000).

Below 1500 m in the present production area. The composition of amphiboles from wells DRJ 13 and 17 suggests low P_{H_2O} (Hammarstrom and Zen, 1986), i.e. lower than elsewhere in the field. Oxidation is indicated by the occurrences of Mn rich ilmenite (Grey et al., 1994) with associated rutile and titanite (Pe-Piper, 1988).

Phlogopite with ratios of Mg to Mg+Fe between 0.7 and 0.8 suggests that the altering thermal fluid contained high SO_2, CO_2 and other volatiles (Helgeson et al., 1978; Cavarretta and Tecce, 1987; and Belkin et al., 1988). The fluid had temperatures up to 350°C (Beane, 1974) and pressures as low as 20 bars (Jacobs and Parry, 1979) and as high as 220 bars (Belkin et al., 1988). Beane (1974) also reported that phlogopite can form under slightly acid conditions (pH < 5), reducing ($f_{O_2} \approx 10^{-27}$ and $f_{S_2} \approx 10^{-7}$ atm). High Ti contents of phlogopite suggest the influence of magmatic fluid (Wendland and Eggler, 1980). Since phlogopite can form due to an increase in a_{Mg}^{2+}, followed by increasing pH (Jacobs and Parry, 1979), and a decrease in P_{H_2O} but increase in f_{CO_2} (Helgeson et al., 1978), boiling might occur.

Chapter 8

PALEOHYDROLOGY

Fluids trapped in inclusions within minerals can record paleohydrological conditions and thus be used to help deduce the origin and evolution of fluids at Darajat. Figure 8.1 shows several types of fluid inclusions present in different minerals that deposited in veins. Methodology and detailed results are given in Appendix H.

8.1. FLUID PHASES AND TEMPERATURES

The identification of the fluid phases in the inclusions was estimated from the ratio of vapour to liquid volume (V/L). They can also be distinguished from the changes in gas composition at different crushing events, as the first crush will open the bigger inclusions but further crushing will open smaller ones. The paleotemperatures were determined from the temperature of homogenisation (Th). These are equivalent to be within 10°C of the trapping temperature, since pressure corrections are not deemed necessary. The downhole paleotemperatures of wells DRJ S-1, S-3 and S-5, and those in the marginal area, i.e. wells DRJ S-2 and S-6, are shows in Figures 8.2 to 8.5.

Well DRJ S-1. Analyses of gases in fluid inclusions in laumontite from a vein at about 500 m depth indicate the occurrence of 2 phase fluids, i.e. liquid rich, occurring in very small inclusions, but gas rich, in bigger inclusions. Unfortunately, laumontite is too soft and fragile for its microthermometry to be studied.

Between 500 and 1000 m depth, anhydrite contains secondary fluid inclusions, trapped at 2 different temperatures (Figure 8.2). At 200-210°C, the fluids are liquid rich with V/L ratios of 0.2, whereas those trapped between 300-310°C are mostly vapour rich. However, about 1000 m depth, secondary inclusions were trapped in calcite at 300-310°C, but at lower temperature of 230-240°C in anhydrite.

Below 1000 m, calc-silicates, e.g. prehnite, wairakite and epidote, are present in association with quartz. Primary inclusions in prehnite, present between 1000 and 1300 m depth, are liquid and vapour rich, homogenising at 250-260°C and 310-340°C respectively. The secondary inclusions are smaller, liquid rich and trapped at 280-290°C. Several inclusions also have unknown solid phases, still present at temperatures above 320°C.

Quartz, which predates prehnite, hosts primary and secondary fluid inclusions. The primary inclusions homogenise at 300-310°C and the secondary ones at 250-260°C. About 1300 m depth, the secondary fluid inclusions are present along 2 partly sealed cracks in quartz, cross cutting each other. The inclusions in the older crack were trapped at 250-260°C and those in the younger one at 290-300°C.

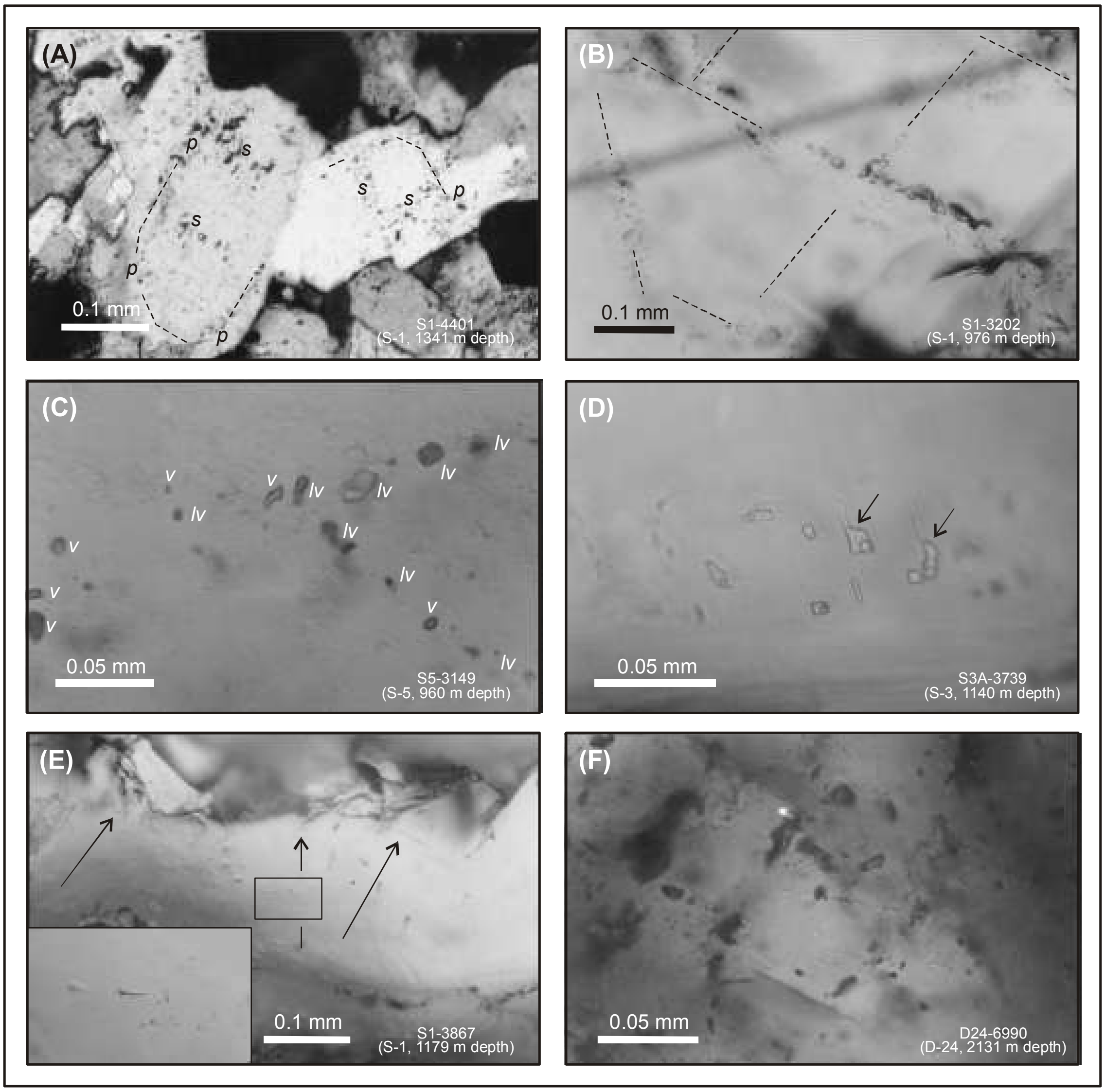

Figure 8.1.Occurrences of fluid inclusions.**(A)** Primary fluid inclusions (*p*) are subparallel to the crystal growth direction (dashed lines), while secondary fluid inclusions (*s*) occur along healed fractures. Most inclusions in quartz are up to 30 μm long, but may be > 100 μm. **(B)** Up to 20 μm diameter, secondary fluid inclusions are present along separate, cross-cutting cracks within calcite (dashed lines). **(C)** Two phase, liquid and vapour (*lv*), and vapour rich (*v*) indicate boiling in a quartz crystal. Liquid rich inclusions usually have a ratio of vapour and liquid (V/L) of 0.2-0.5 and the V/L of vapour rich ones ranges from 0.8-1.0. **(D)** Anhydrite hosting faceted hexagonal fluid inclusions from 2 to 20 μm. Some inclusions are necked (arrows). **(E)** Prehnite with 4-20 μm, faceted tetragonal, secondary fluid inclusions. Inset is a black square area and show primary fluid inclusions, present in fan shape, crystal growth zones (arrows). The size of primary inclusions in prehnite can be as small as 1 μm, but some are also as big as 60 μm. **(F)** Fluid inclusions in wairakite crystals are irregular and 4-20 μm in size; they readily leak during heating and hence temperatures of homogenization can hardly be determined. However, the ice melting temperature can be determined.

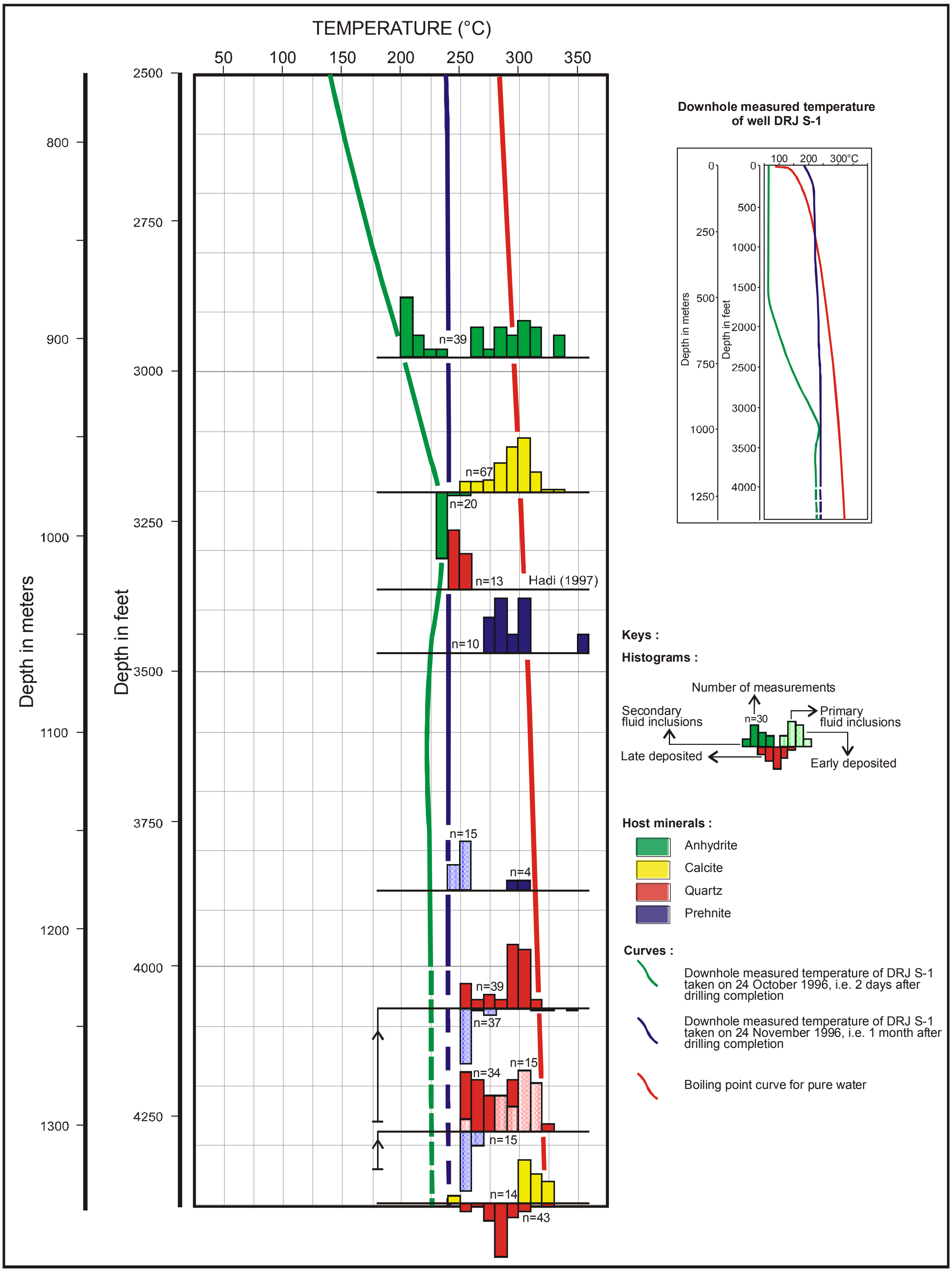

Figure 8.2. Temperature of homogenization (Th) of fluid inclusions present in samples from well DRJ S-1. Data at about 1025 m depth is taken from Hadi (1997), i.e. samples S1-3356 and 3377. Cooling is indicated by the Th's of different sequences of minerals. The results are compared to the present downhole temperatures and indicate cooling from the time of vein minerals deposited to the present conditions. The boiling point curve pure H_2O is also shown.

Quartz deposited after calcite at 1344 m depth. Both minerals contain secondary and liquid rich inclusions with V/L ratios of 0.2-0.5. The Th's of inclusions in quartz are 280-290°C and those in calcite are at 300-310°C. Wairakite is also present and hosts liquid rich, primary and secondary inclusions, which are mostly necked. The few Th values obtained were between 300 and 310°C.

Well DRJ S-3. At about 1100 m depth, calcite deposited before quartz but both host secondary, liquid rich inclusions. The Th's indicate that the liquid was trapped at 220-230°C in calcite but at 210-220°C in quartz (Figure 8.3). At about 1500 m depth, the trapping temperatures were slightly higher, i.e. at 230 to 240°C and 270 to 280°C respectively. Secondary vapour rich fluid inclusions are also present along cracks and were trapped at 280-290°C in calcite and above 300°C in quartz.

Fluid inclusions in calcite from 1800-2000 m depth are mostly secondary, liquid rich and were trapped at 250-260°C. Quartz is associated with calcite and its inclusions were trapped at 270-280°C. Calcite and quartz also contain some tiny primary fluid inclusions, homogenising at temperature above 300°C. Some secondary vapour rich inclusions are also present; they homogenise above 350°C.

Since well DRJ 24 is about 2 km SE well DRJ S-3 (see Figure 3.1), the results of fluid inclusions study can be compared. A sample from 2131 m depth has a vein filled with anhydrite with many secondary liquid rich inclusions. The fluid inclusions homogenise at 250-260°C (Figure 8.3).

Well DRJ S-5. The paleotemperatures are summarised in Figure 8.4. At about 1000 m depth, quartz deposited in a vein before calcite. This quartz contains many secondary fluid inclusions; some are vapour rich, but most are liquid rich. These inclusions were trapped at temperatures of 370 to 380°C. On the other hand, the secondary fluid inclusions were trapped in calcite at much lower temperatures, i.e. at 130-140°C.

Several hydrothermal minerals, including anhydrite, calcite and calc-silicates, fill veins from 2000 to 2300 m depth. Anhydrite deposited first; it contains many secondary, liquid and vapour rich inclusions, homogenising at 230-240°C and 280-330°C respectively. Some vapour rich inclusions homogenise at the critical point. Calcite, which postdates anhydrite, is host to secondary and liquid rich inclusions, trapped at 200-230°C. Some secondary liquid rich inclusions in calcite contain an unknown solid phase. Some inclusions in calcite and anhydrite are also (single) liquid rich phase inclusions.

Epidote, wairakite and prehnite, which deposited after calcite and anhydrite, contain secondary fluid inclusions along cracks and cleavage planes. The inclusions are mostly liquid rich, but some are

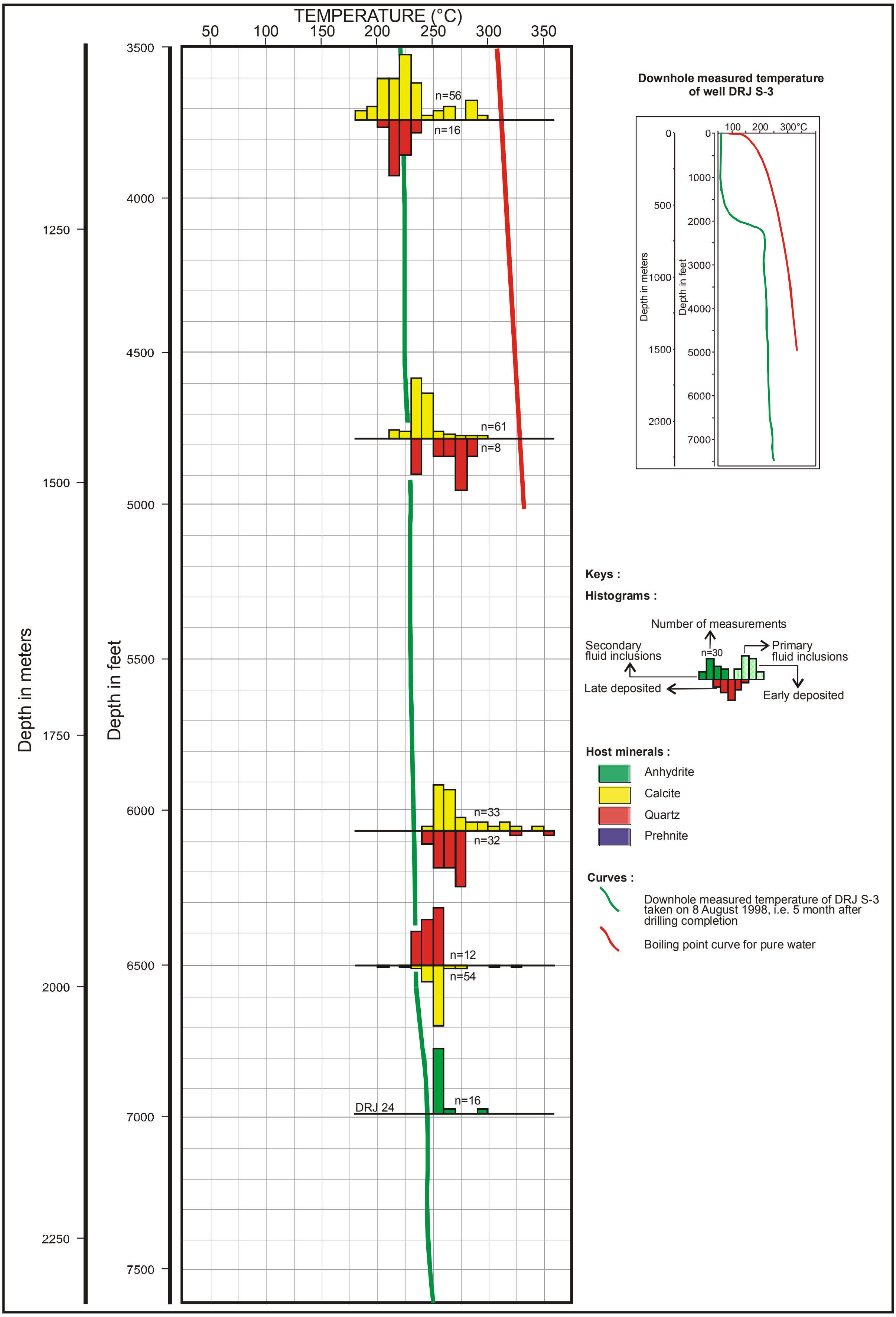

Figure 8.3. Temperatures of homogenisation of fluid inclusions from well DRJ S-3, compared with the well temperature measured on 8 August 1998. The temperatures are close. The boiling point curve for pure H_2O is also given. Data at about 2130 m depth is from well DRJ 24 (about 1 km south-east well DRJ S-3), i.e. measured on a sample of D24-6990.

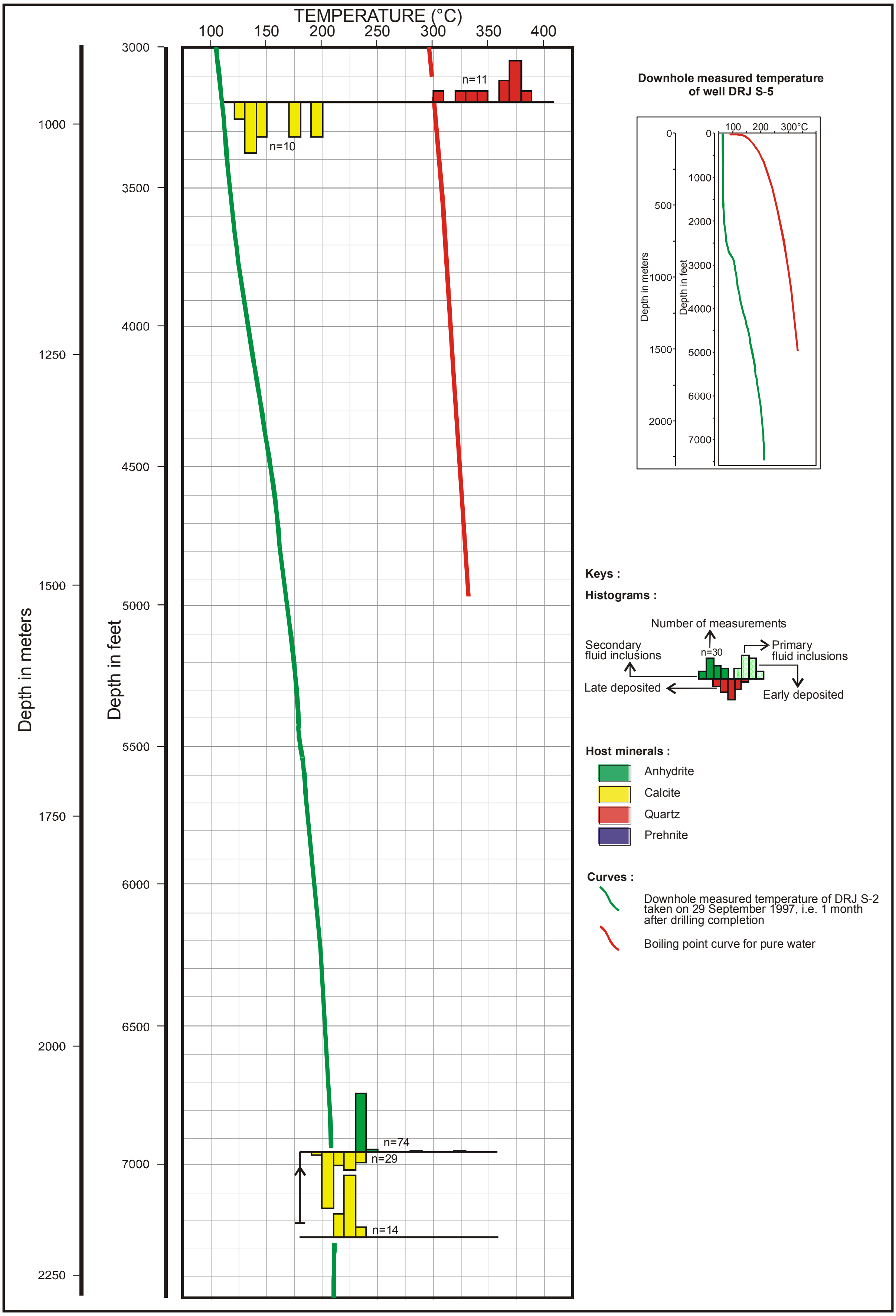

Figure 8.4. Temperatures of homogenisation of fluid inclusions in well DRJ S-5, compared to the downhole temperatures, measured on 29 September 1997 and the pure H_2O boiling point curve. Cooling is indicated at about 900 m depths, but the deeper part the downhole temperatures are the same as those when the inclusions formed.

vapour rich and single liquid phase inclusions. However, most inclusions are necked. Gas analyses indicate that laumontite from about 2100 m depth contains liquid and gas rich inclusions. The liquid rich inclusions are mostly small, whereas those that are vapour rich are mostly bigger. The Th values of inclusions in calc-silicate minerals could not be measured due to decrepitation. However, one inclusion trapped at 142°C in prehnite. Some inclusions in prehnite also homogenise to vapour between 180 and 310°C.

Marginal area. Calcite from a vein at 1062 m depth of well DRJ S-6 contains abundant secondary fluid inclusions that homogenise at 240-250°C. Some inclusions homogenise to vapour at temperatures above 270°C. However, some may have leaked. The results of the heating measurements are compared with the present temperature for well DRJ S-2 in Figure 8.5.

In DRJ S-2 itself, primary and secondary fluid inclusions were trapped in calcite at 1515 m depth. The primary inclusions are liquid rich and homogenise above 320°C. The secondary inclusions are smaller and also liquid rich; they homogenise at 2 different temperatures, i.e. at 220-240 and 280-290°C.

8.2. FLUID COMPOSITIONS

8.2.1. Apparent Salinity

The compositions of liquid in inclusions were determined by measuring the temperature of last ice melting (Tm). Pure water has Tm of 0.0°C, but this is lowered by the presence of other components. The temperature of the eutectic (Te) can be used to help recognise the presence of other components. Liquids containing NaCl have Te values ranging from -20.8 to about -28°C (Roedder, 1984). Concentration of dissolved constituents can then be expressed as the amount of NaCl equivalent (NaCl eq.) using the formulae giving Potter II et al. (1978). If CO_2 is present, the Te will be about -56°C (Roedder, 1984) and sulfate (SO_4^{2-}) bearing waters will have Te of about -75°C (Moore et al., 2002a). Results of the freezing measurements, i.e. Te and Tm, and the calculation of NaCl equivalent are given in Appendix H. Salinity, calculated as NaCl eq., is summarised in Figures 8.6 to 8.9.

Well DRJ S-1. Fluids inclusions, present in anhydrite from 500 to 900 m depth, have very low salinity, i.e. equivalent to 0.0-0.4 wt.% NaCl. However, the amount of NaCl is as high as 1.1 wt.% (Figure 8.6).

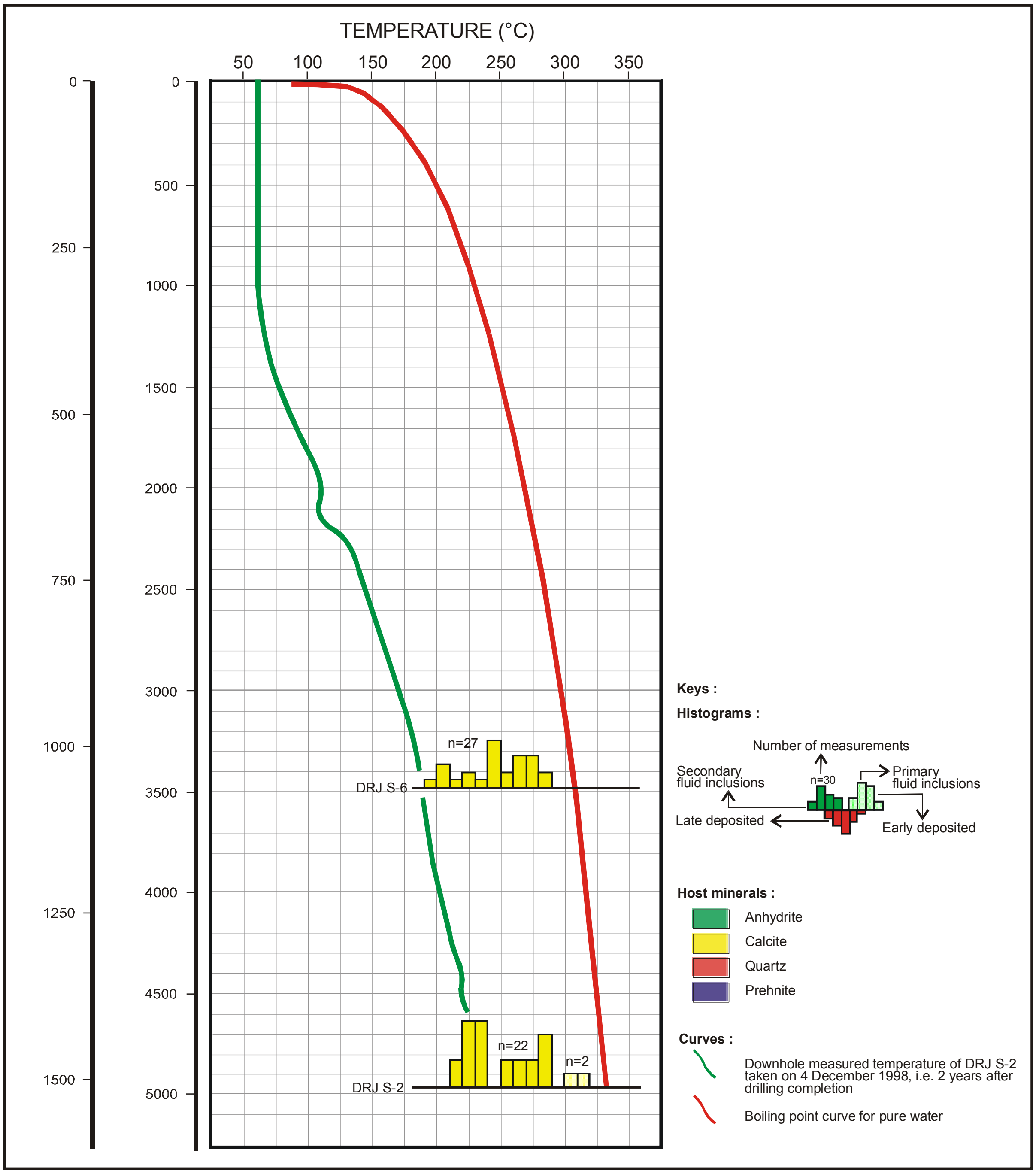

Figure 8.5. Temperatures of homogenisation of fluid inclusions present in marginal wells, including DRJ S-2 and S-6. The results are compared to the downhole temperature of well DRJ S-2, measured on 4 December 1998, and the boiling point curve for pure H_2O. Cooling has occurred.

About 980 m depth, wairakite hosts inclusions with pure H_2O. Calcite and anhydrite contain H_2O with less than 0.5 wt.% NaCl eq. However, some inclusions in calcite and anhydrite may contain SO_4^{2-}, as indicated by their Te of -30 to -70°C. As the Tm's range from 0.0 to -0.4°C only, the concentration of $H_2SO_4$is likely up to 0.4 mol.% (Weast, 1974).

Below 1000 m, inclusions with salinities up to 0.4 wt.% NaCl eq. still dominate in calcite, quartz, prehnite and wairakite. Hadi (1997), who studied inclusions present in quartz, found that the fluids from about 1025 m depth contain 10-15 wt.% NaCl eq.

Some inclusions in prehnite from 1058 m depth have ice melting points from 0.0 to 0.3°C. These higher Tm might indicate that the inclusions contain metastable supercooled fluids, which commonly occur in low salinity fluids (Roedder, 1984). However, this can also happen, if the partial pressure of the gases trapped is high (Moore et al., 2000b) or the inclusion contains high CO_2 (Gonzáles-Partida et al., 2000).

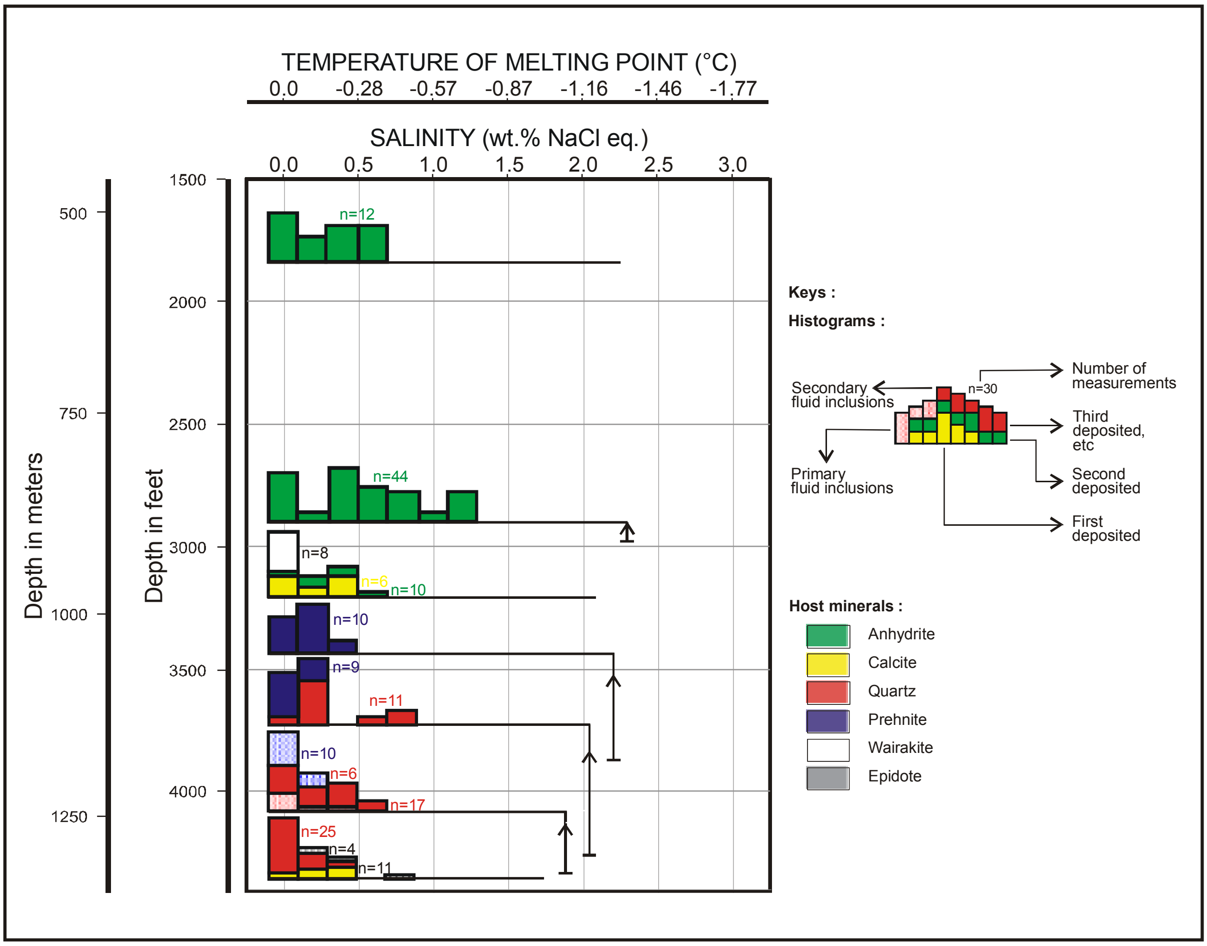

Figure 8.6. Salinity of fluid inclusions present in well DRJ S-1, calculated as wt.% NaCl eq. using the formulae given in Potter II et al. (1978). The calculation is only made if the temperature of the eutectic point, i.e. when the ice first melts, is about -30°C.

Well DRJ S-3. As shown in Figure 8.7, fluid inclusions in calcite and quartz from between 1100-1500 m depth contain dilute H_2O with up to 1.0 wt.% NaCl eq. However, at about 1100 m depth, the apparent salinities of inclusions in calcite are as high as 2.9 wt.% NaCl eq.

Below 1800 m, most fluid inclusions in quartz contain pure H_2O. However, some are as saline as 1.8 wt.% NaCl eq. Calcite hosts slightly more saline inclusions with NaCl contents of 1.2-1.4 wt.%. Some inclusions, however, can contain as much as 2.4 wt.% NaCl eq., e.g. at 1850 m depth, but others are pure H_2O, i.e. those at about 1980 m depth.

At 2131 m depth in well DRJ 24, anhydrite hosts inclusions with pure H_2O. However, some may be metastable, as indicated by the persistence of ice up to 0.3°C.

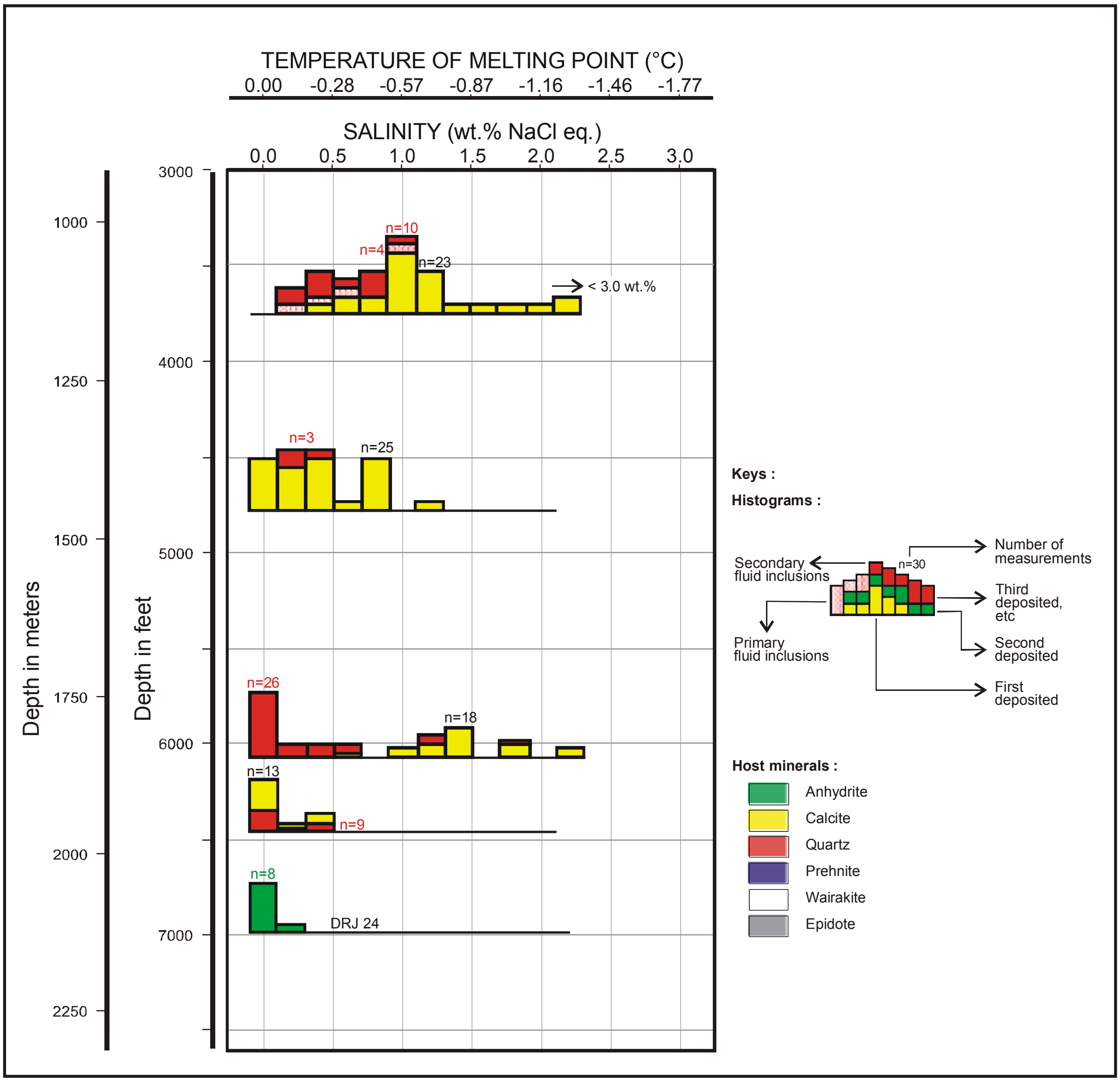

Figure 8.7. Salinity of fluid inclusions in well DRJ S-3, calculated as wt.% NaCl eq. Salinity of liquid trapped in calcite at about 1100 depth can be up to 3.0 wt.% NaCl eq. Data from inclusions at about 2130 m depth were measured on a sample from DRJ 24, i.e. D24-6990. Well DRJ 24 is about 1 km south-east well DRJ S-3.

Well DRJ S-5. The Te's of fluids in inclusions present in quartz, calcite and anhydrite are about -20°C and the Tm's indicate that the inclusions are H_2O rich without NaCl nor CO_2 (Figure 8.8). However, some inclusions in calcite, which deposited after quartz at 960 m depth, contain up to 0.4 wt.% NaCl and those in epidote from about 2200 m depth have NaCl equivalents of 0.2 to 0.4 wt.%.

Marginal area. At 1062 m depth in well DRJ S-6, secondary fluid inclusions in calcite are pure H_2O (Figure 8.9). Those from 1515 m depth in well DRJ S-2 contain 0.6-0.8 wt.% NaCl eq., but the NaCl eq. some are as low as 0.1 wt.% and others as high as 2.4 wt.%.

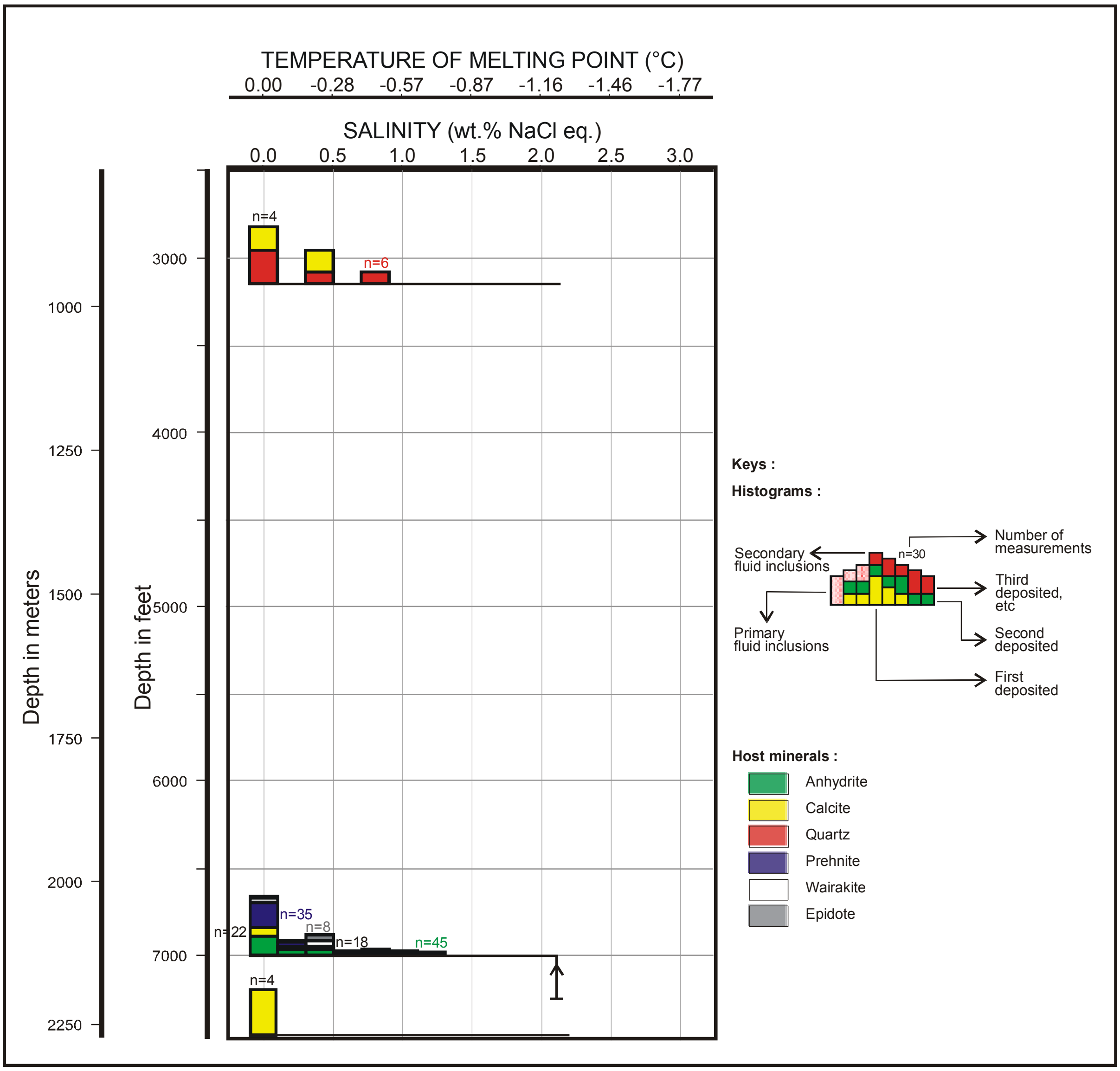

Figure 8.8. Salinity of fluid inclusions in well DRJ S-5, calculated as wt.% NaCl eq. Temperatures of melting point (Tm) and eutectic point (Te) of fluids, present in inclusions of calc silicate minerals, can be easily determined, unlike the temperature of homogenization (Th), as the inclusions will readily leak due to overheating.

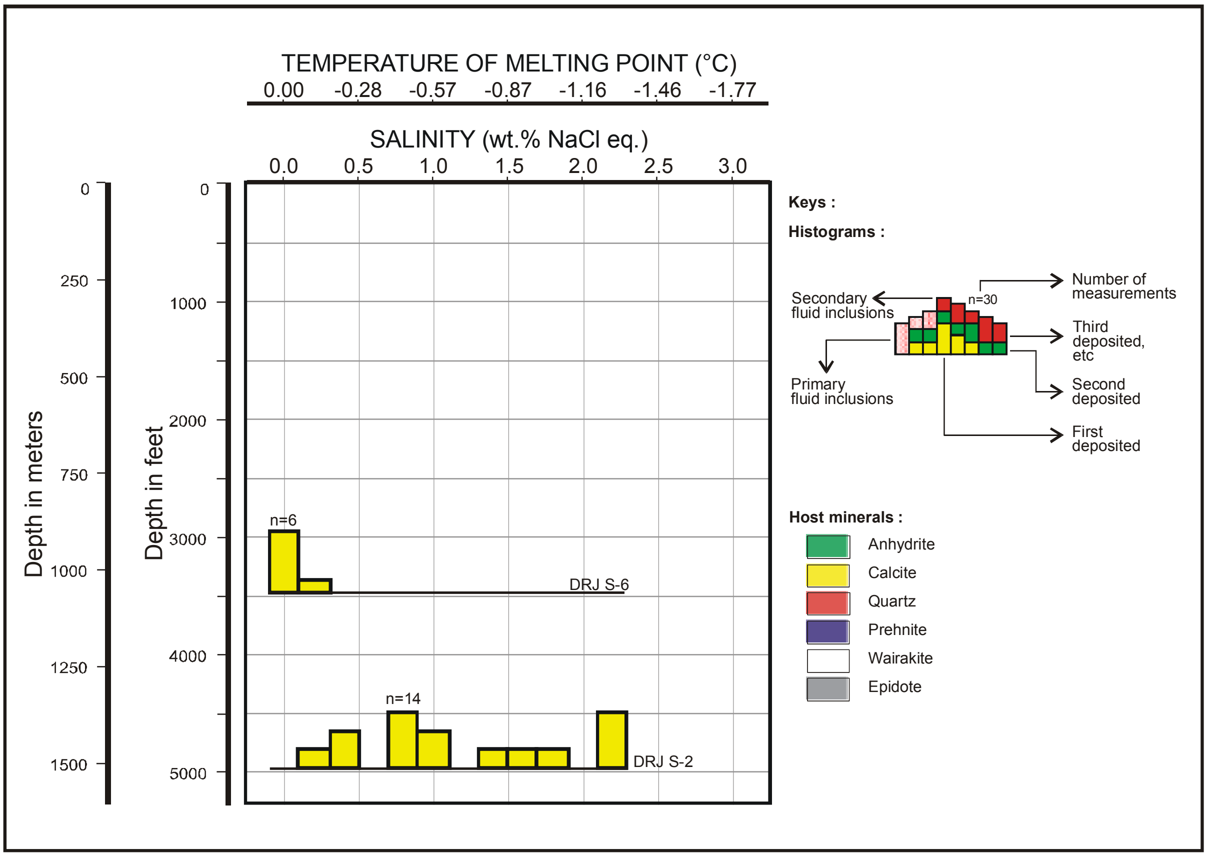

Figure 8.9. Salinity of fluid inclusions present in the margin area, i.e. surrounding wells DRJ S-2 and S-6, calculated as wt.% NaCl eq.

8.2.2. Gas Contents and Organic Volatiles

The compositions of gas, including H_2O, CO_2, N_2, He, Ar and $C_{2\text{-}7}$ organic volatiles present in fluid inclusions, were measured on 12 hand picked vein minerals using the crush-fast scan (CFS) method. Analyses were made by opening the inclusions, in 4 to 12 crushes, in a vacuum chamber and the gases released were analysed in a mass spectrometer. Representative analyses are given in Table 8.1. This shows that the gas contents in the inclusions vary with respect to the number of crushes. The method of making the gas analyses is described in detail by Norman and Sawkins, 1987, Norman et al., 1996 and Norman et al., 1997.

Table 8.1 shows that H_2O dominates almost all fluid inclusions and, as shown in Figure 8.10, mostly exceed 95 mol.% and increase with the amount of total gas up to almost 100 mol.% total gas. Carbon dioxide (CO_2) and N_2 are the second and third most dominant gases; these range from 0.02 to 3.4 and 0.005 to 2.2 mol.% respectively and tend to increase with respect to the total gas of above 99 mol.%.

Table 8.1. Representative gas analyses released from crushed fluid inclusions.

Well	DRJ S-1						DRJ S-3	
Sample	S1-1693		S1-3470		S1-4259		S3-4786	
Depth (m)	516		1058		1298		1459	
Mineral	Laumontite		Prehnite*	Wairakite	Prehnite		Wairakite	
Crushing no.	3	4	3	9	3	4	1	6
Gas contents (mol.% for major and ppm.vol^{-1} for organic gas)								
H_2	0.365	0.107	0.000	0.001	0.017	0.000	0.000	0.000
He	0.001	0.000	0.000	0.000	0.000	0.000	0.000	0.000
CH_4	1.354	1.933	0.002	0.006	0.093	0.007	0.022	0.025
H_2O	95.589	97.026	42.445	99.815	96.184	99.804	98.739	96.106
N_2	0.952	0.303	0.078	0.032	2.194	0.157	0.253	0.262
H_2S	0.001	0.001	0.002	0.005	0.001	0.001	0.002	0.001
Ar	0.012	0.005	0.001	0.000	0.004	0.001	0.002	0.002
CO_2	1.493	0.513	0.171	0.091	1.465	0.027	0.932	3.365
SO_2	0.003	0.004	n.a	0.000	0.000	0.000	0.001	0.001
O_2	0.040	0.012	n.a	0.047	0.023	0.002	0.039	0.174
Ethene (C_2H_4)	0.0	0.0	n.a	1.6	18.8	0.0	0.0	0.0
Ethane (C_2H_6)	299.1	266.6	n.a	10.0	119.1	0.0	48.5	583.8
Propene (C_3H_6)	36.6	5.5	n.a	0.1	1.1	0.0	0.0	8.2
Propane (C_3H_8)	60.8	54.8	n.a	2.1	25.4	6.9	29.0	22.3
Butene (C_4H_8)	391.2	318.8	n.a	2.3	2.0	0.3	5.1	3.1
Butane (C_4H_{10})	44.5	2.1	n.a	2.5	0.0	0.0	0.0	0.8
Pentene (C_5H_{10})	75.7	0.0	n.a	1.9	2.5	1.4	0.0	1.5
Benzene (C_6H_6)	1000.5	313.5	n.a	10.1	24.6	3.6	21.8	11.2
Heptene (C_7H_{10})	0.0	0.0	n.a	0.2	0.2	0.0	0.8	0.0

Well	DRJ S-3		DRJ S-5				DRJ S-2	DRJ S-6
Sample	S3-6069		S5-6883		S5-7241		S2-4087	S6-5477
Depth (m)	1850		2098		2207		1246	1669
Mineral	Epidote	Quartz	Laumontite		Epidote	Wairakite	Wairakite	Laumontite
Crushing no.	5	7	1	8	12	7	8	1
Gas contents (mol.% for major and ppm.vol^{-1} for organic gas)								
H_2	0.026	0.001	0.000	0.029	0.000	0.000	0.000	0.006
He	0.000	0.000	0.000	0.000	0.000	0.000	0.000	0.000
CH_4	0.071	0.016	0.028	0.395	0.004	0.009	0.008	0.038
H_2O	95.125	99.027	99.732	97.556	99.748	99.891	99.903	99.485
N_2	1.613	0.166	0.097	1.020	0.081	0.052	0.029	0.188
H_2S	0.001	0.000	0.000	0.001	0.000	0.000	0.000	0.000
Ar	0.005	0.001	0.001	0.010	0.001	0.000	0.000	0.003
CO_2	3.095	0.773	0.125	0.842	0.034	0.034	0.059	0.234
SO_2	0.001	0.000	0.000	0.001	0.000	0.000	0.000	0.000
O_2	0.045	0.011	0.006	0.081	0.000	0.009	0.000	0.030
Ethene (C_2H_4)	15.0	0.0	26.0	75.0	20.0	23.2	0.0	14.9
Ethane (C_2H_6)	94.8	22.5	0.0	44.6	0.0	0.0	0.0	3.5
Propene (C_3H_6)	0.8	0.0	0.0	0.0	0.0	0.0	0.0	0.0
Propane (C_3H_8)	20.2	20.4	12.8	77.7	0.0	13.9	2.9	16.7
Butene (C_4H_8)	6.1	0.5	14.4	77.2	3.2	0.9	0.9	54.3
Butane (C_4H_{10})	0.0	1.0	0.0	0.0	2.9	4.6	0.0	0.0
Pentene (C_5H_{10})	2.9	0.0	5.1	16.6	0.0	4.8	0.0	4.9
Benzene (C_6H_6)	37.8	7.6	57.5	362.5	6.9	9.5	8.5	76.1
Heptene (C_7H_{10})	0.0	0.0	0.0	0.0	0.4	0.6	0.0	0.0

* Analysed using the old Utah parameter; analyses of the organic volatiles are not available (n.a).

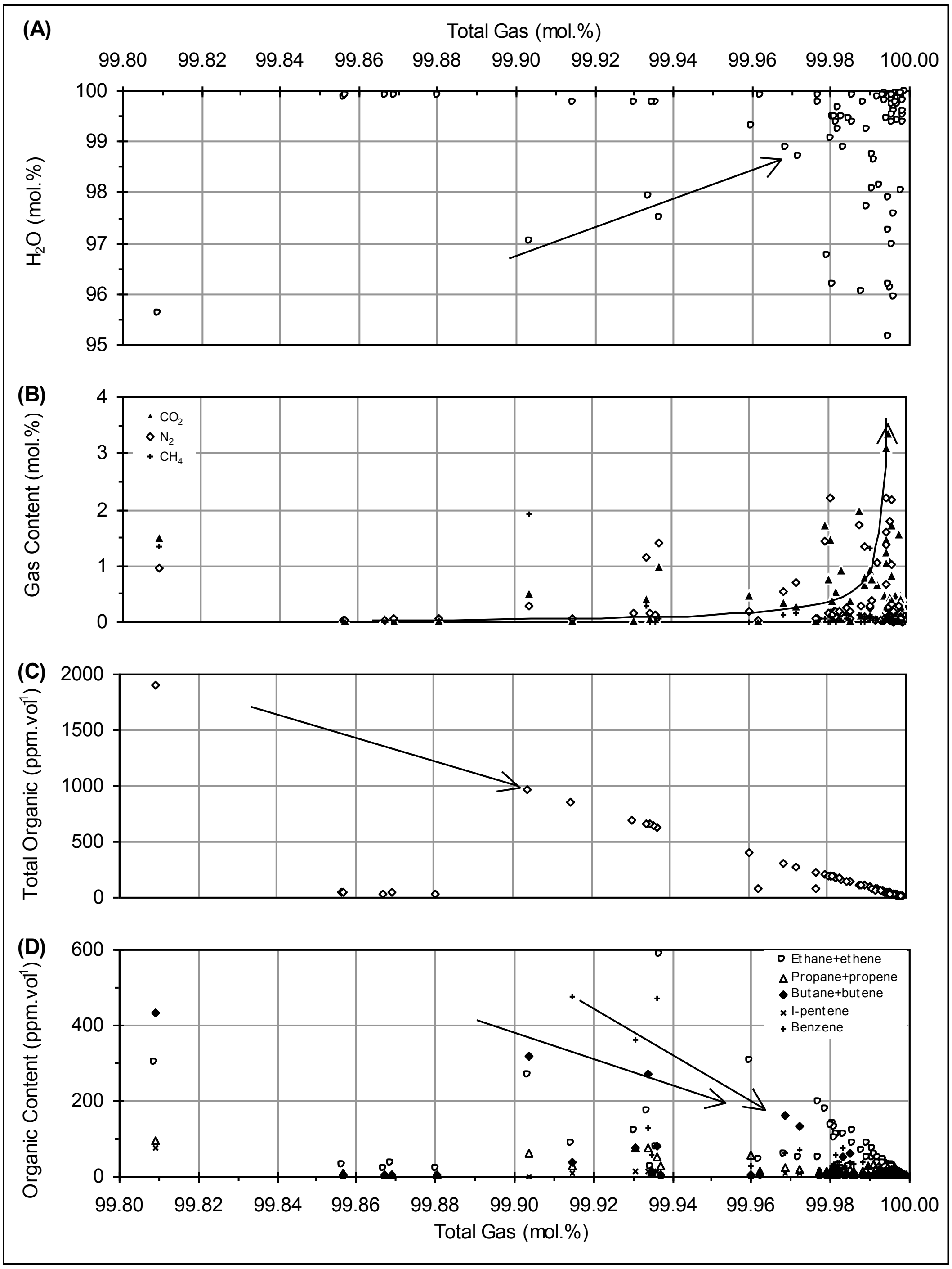

Figure 8.10.Comparison between total gas and major and organic gas contents. **(A)** H_2O is dominant in fluid inclusions and inset shows that H_2O increase with an increase in the total gas contents. However, inclusions have loss H_2O at a total gas of about 100 mol.%. **(B)** The amounts of CO_2, N_2 and CH_4 relative to the amount of total gas showing that CO_2 and N_2 increase with a decrease in H_2O, as in figure (A). **(C)** Total of organic gases decreases with increasing total gas. **(D)** Variations in the amount of C_{2-6} volatiles present with respect to the total gas shows that C_2 compounds (ethane and ethene) and benzene are dominant.

Benzene, ethene and ethane dominate the organic volatiles, whereas concentration of the heavy organic compounds, e.g. pentene and heptene, is low. Figure 8.10 shows that the amount of total organic gases has a negative correlation with the amount of total gas present. This might relate to the dominance of benzene. Further, variations in the amount of organic volatiles in fluid inclusions present in different samples in wells DRJ S-1 to S-6 are given in Figure 8.11.

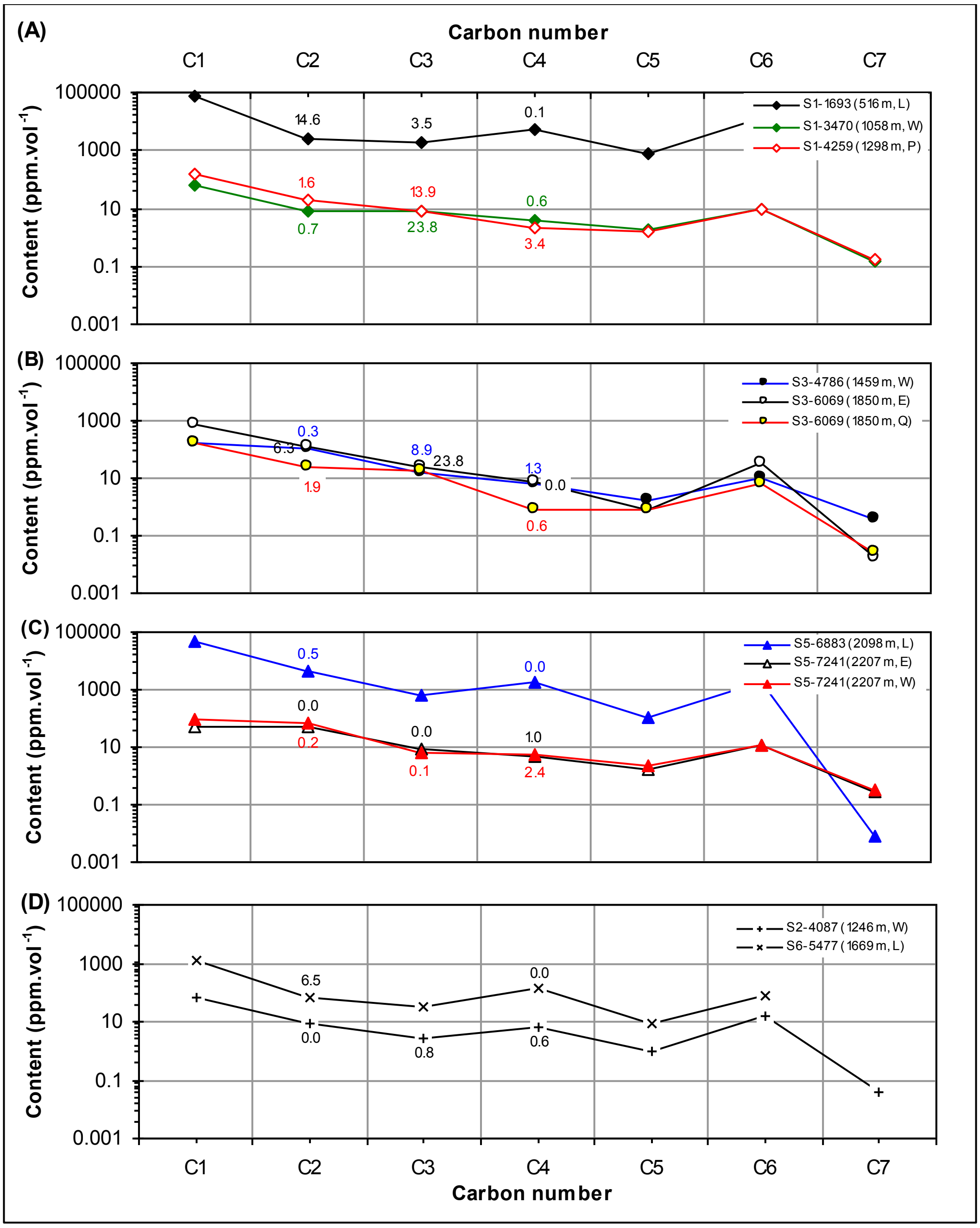

Figure 8.11. Variations in the average amount of $C_{1\text{-}7}$ organic gases present in inclusions: **(A)** DRJ S-1, **(B)** DRJ S-3, **(C)** DRJ S-5 and in **(D)** the marginal wells DRJ S-2 and S-6. Label shows the ratios of alkanes/alkenes; label in C_2 is the ratio of ethane/ethene, C_3 is the propane/propene and C_4 is the butane/butene ratio. Sample number and depth are given; character in bracket represents host mineral: (L) laumontite, (W) wairakite, (P) prehnite, (E) epidote and (Q) quartz. The y-axis is logarithmic.

Well DRJ S-1. Laumontite, present together with calcite in a vein at 516 m depth, yielded about 96 mol.% H_2O after 3 crushes. Gases of CO_2, N_2 and CH_4 are 0.5-1.5, up to 1.0 and 1.3-2.0 mol.% respectively (Table 8.1). The inclusions are organic rich, dominated by benzene and butene.

Prehnite from about 1060 m depth contains vapour rich fluid inclusions, with up to 54 mol.% H_2O, 0.1-0.5 mol.% CO_2 and up to 0.6 mol.% N_2. It differs from wairakite at the same depth, which postdates prehnite and contains liquid rich inclusions with about 99.8 mol.% H_2O but only 0.1 mol.% CO_2. Oxygen ranges up to 0.02 mol.%; it may derive from adsorbed water released from minor cracks during crushing (Moore et al., 2001). In addition, the high gas content in prehnite might also explain the persistence of ice up to 0.3°C at 1058 m depth.

The occurrences of liquid and vapour rich inclusions in prehnite from about 1300 m depth are indicated by the gases released after 3 and 4 crushes (Table 8.1). After 3 crushes, the inclusions, possibly those vapour rich, release 96.2 mol.% H_2O, 2.2 mol.% N_2 and 1.5 mol.% CO_2. The proportion of H_2O increases to 99.8 mol.% and the other gasses were slightly depleted after 4 crushes, where liquid rich inclusions are dominant. Liquid rich inclusions in wairakite and prehnite contain up to 35 $ppm.vol^{-1}$ ethane, 2-16 $ppm.vol^{-1}$ propane and 5-14 $ppm.vol^{-1}$ benzene. In vapour rich inclusions, these organic contents are higher.

Well DRJ S-3. Wairakite from about 1460 m depth postdates calcite and contains inclusions having H_2O of 96.1 to 99.6 mol.% (Table 8.1). The amount of CO_2 ranges from 0.2 to 1.6 mol.%, but was as high as 3.4 mol.% after 6 crushes. The other gases include N_2, CH_4, traces of H_2S and SO_2, ethane and benzene.

A vein in core from 1851 m depth is filled by epidote, postdating quartz. Fluid inclusions in this epidote contains about 97 mol.% H_2O and those in quartz contains about 99 mol.% H_2O. Consequently, the amount of gas in the inclusions in epidote is higher than that of quartz; the CO_2 contents are 0.6-3.1 and 0.2-1.0 mol.% and the amount of N_2 is 1.0-2.2 and 0.1-0.2 mol.% respectively. Ethane comprises about 110 $ppm.vol^{-1}$ in epidote and 20 $ppm.vol^{-1}$ in quartz. Propane and benzene are about 55 $ppm.vol^{-1}$ in epidote and 32 and 11 $ppm.vol^{-1}$ respectively in quartz.

Well DRJ S-5. The gas analyses indicate that laumontite, postdating epidote, from about 2100 m depth contains liquid rich fluid inclusions. The inclusions consist of about 98 mol.% H_2O, 0.7 mol.% CO_2, 0.6 mol.% N_2 and 0.2 mol.% CH_4. These components are mostly released after 5-6 crushes (Table 8.1).

Benzene is the most dominant organic gas in the inclusions in laumontite; it is present up to 400 $ppm.vol^{-1}$. Other common organic gases include ethene, propane and butene, which are present up to 80 $ppm.vol^{-1}$.

In a vein at about 2210 m depth, epidote predates wairakite. Both minerals contain liquid rich fluid inclusions, which have about 99.8 mol.% H_2O (Table 8.1). Other gases include N_2, CO_2 and CH_4. Organic volatiles in epidote include ethene and benzene but in wairakite, the C_2 organic species is present as ethane.

Marginal area is characterised by wairakite from 1247 m depth of well DRJ S-2 and laumontite from 1671 m depth of DRJ S-6 (Table 8.1). Both minerals are associated with calcite and contain fluid inclusions with more than 97 mol.% H_2O. The remaining components include CO_2 and N_2, which are almost nil in wairakite, but vary from 0.2-0.4 and 0.2-1.2 mol.% respectively in laumontite.

Benzene is dominant in the inclusions present in wairakite and laumontite, and varies 7-40 and 39-128 $ppm.vol^{-1}$ respectively. The other organic constituents in laumontite include less than 95 $ppm.vol^{-1}$ ethene and 274 $ppm.vol^{-1}$ butene, which are present only as traces in wairakite.

8.3. FLUID PRESSURES

Assuming that the fluids contain H_2O and CO_2 gas but no NaCl and other gases, the fluid pressures (P_{Total}) of inclusions can be estimated from the Th values and the amount of CO_2. The P_{Total} is then equivalent to the hydrostatic pressure of pure H_2O (P_{H_2O}), when the liquid trapped at Th, and the partial pressure of CO_2 (P_{CO_2}):

$$P_{Total} = P_{H_2O} + P_{CO_2} \qquad (8.1)$$

P_{H_2O} was calculated using the thermal profile for pure H_2O liquid (after Haas, 1971) and P_{CO_2} was calculated using the relationship between Henry's Law coefficient and the fraction of CO_2 in the fluids obtained from the gas analyses (Ellis and Golding, 1963). The results of the calculation are given in Table 8.2.

Fluid inclusions trapped in samples from wells DRJ S-1, S-3 and S-5 seem to have P_{Total}'s between 30 and 80 bars. Those from DRJ S-2 and S-6 are slightly low, i.e. from 20 to 50 bars. However, the P_{Total} can be as high as 120 bars above 500 m in DRJ S-1 and about 1850 m depth in DRJ S-3.

Table 8.2.Estimation of fluid pressure (P_{Total}) in inclusions.

Well	DRJ S-1				DRJ S-2	DRJ S-3			DRJ S-5			DRJ S-6
Sample no	S1-1693	S1-3470		S1-4259	S2-4087	S3-4786	S3-6069		S5-6883	S5-7241		S6-5477
Depth (m)	516	1058		1298	1246	1459	1850		2098	2207		1669
Mineralogy*	Laumontite^3	Prehnite^7	Wairakite^7	Prehnite^1	Wairakite^{10}	Wairakite^1	Epidote^3	Quartz^2	Laumontite^6	Epidote^4	Wairakite^5	Laumontite^4
CO_2 (mol.%)	1.4930	0.2586	0.1227	0.0423	0.0510	0.9317	1.4646	0.4909	0.7696	0.0536	0.0363	0.3029
X_{CO_2}	0.0149	0.0026	0.0012	0.0004	0.0005	0.0093	0.0146	0.0049	0.0077	0.0005	0.0004	0.0030
Th (°C)**	200$^{1)}$	280	280$^{2)}$	250	220$^{3)}$	230$^{4)}$	250$^{5)}$	270	200$^{6)}$	200$^{7)}$	200$^{8)}$	240$^{9)}$
Tm (°C)***	0.3$^{1)}$	0.3$^{a)}$	0.3$^{2)}$	0.1	1.4$^{3)}$	1.7$^{4)}$	0.8$^{5)}$	0.6	0.5$^{6)}$	0.4	0.5	4$^{a), 7)}$
P_{CO_2} (bars)	98.45	12.01	5.70	2.32	3.16	55.65	80.35	24.25	50.75	3.53	2.39	17.38
P_{H_2O} (bars)	15.91	63.86	63.86	39.99	23.59	28.34	39.99	54.96	15.91	15.91	15.91	33.79
$P_{Total}^{(i)}$ (bars)	114.36	75.87	69.56	42.31	26.75	84.00	120.34	79.21	66.66	19.45	18.31	51.17
$P_{CO_2}^{(ii)}$ (bars)	19.09	13.45	13.45	5.30	82.82	96.69	42.15	28.52	31.76	25.43	31.76	213.83
$P_{Total}^{(ii)}$ (bars)	35.00	77.31	77.31	45.30	106.41	125.03	82.14	83.48	47.67	41.34	47.67	247.62
$P_{CO_2}^{(iii)}$ (bars)	0.05	11.74	11.74	1.80	0.22	0.46	1.80	6.44	0.05	0.05	0.05	0.92
$P_{Total}^{(iii)}$ (bars)	15.96	75.61	75.61	41.80	23.81	28.80	41.80	61.39	15.96	15.96	15.96	34.71
$\log f_{O_2}$ $^{(iv)}$	-37.2	-32.3	-32.3	-34.0	-35.8	-35.2	-34.0	-32.9	-37.2	-37.2	-37.2	-34.6
$\log f_{S_2}$ $^{(iv)}$	-12.8	-11.1	-11.1	-11.7	-12.3	-12.1	-11.7	-11.3	-12.8	-12.8	-12.8	-11.9

* Superscript number is crushing number on gas analyses.

** Taken from microthermometry on samples: $^{1)}$ anhydrite from 560 m depth, $^{2)}$ prehnite, $^{3)}$ calcite from 1515 m depth, $^{4)}$ calcite, $^{5)}$ calcite, $^{6)}$ calcite from 2207 m depth, $^{7)}$ calcite, $^{8)}$ calcite,$^{9)}$ calcite from 1063 m depth.

*** Maximum Tm depression: $^{a)}$ increasing Tm, $^{1)}$ anhydrite from 560 m depth, $^{2)}$ prehnite, $^{3)}$ calcite from 1515 m depth, $^{4)}$ calcite, $^{5)}$ calcite, $^{6)}$ calcite from 2207 m depth, $^{7)}$ calcite from 1063 m depth.

(i) Calculated using equation (*8.1*).

(ii) Calculated using Tm values following Hedenquist and Henley (1985):
$C_{CO_2} = |\, Tm/1.86 \,|$
the fraction of CO2 in the fluid = $X_{CO_2} = C_{CO_2}/(C_{CO_2}+C_{H_2O}) = C_{CO_2}/(C_{CO_2}+55.56)$.

(iii) Calculated using a van't Hoff formulae (Giggenbach, 1981):
$\log P_{CO_2} = 15.26 - 7850/(t+272.2)$ and t = Tm.

(iv) Calculated following D'Amore and Gianelli (1984):
$\log f_{O_2} = -3.81 - 13.71[10^3/(t+272.2)] - 2.07[10^3/(t+272.2)]^2$
$\log f_{S_2} = -18.68 + 14.73[10^3/(t+272.2)] - 6.14[10^3/(t+272.2)]^2$ and t = Tm

8.4. SOURCES OF FLUIDS

8.4.1. Meteoric and Magmatic Waters

Inclusions with very low salinity fluids indicate that the source of their liquids is meteoric water and that variations in salinity are due to processes that affect the fluids. No magmatic fluids are present, since these would be hypersaline, having more than 6 wt.% NaCl eq. (Burnham, 1997).

The origin of fluids is also be indicated by the gases present in the inclusions, especially CO_2, CH_4, N_2, Ar and He. Meteoric waters typically have N_2/Ar gas ratios ranging from 38 to 84, i.e. derived from air saturated water at 20°C or air (e.g. Giggenbach, 1992b; Giggenbach, 1997b and Norman et al., 1997), but they can circulate deeply and accumulate radiogenic He in the subsurface (Giggenbach et al., 1993 and Norman and Musgrave, 1994). Crustal fluids, i.e. fluids that are not involved in the meteorological cycle (Moore et al., 2000c), and fluids of magmatic origin are characterised by N_2/Ar ratios exceeding 100; the crustal fluids will have the CO_2/CH_4 ratios of less than 4, i.e. less than magmatic (Norman and Moore, 1999), and may contain high He (Norman and Musgrave, 1994).

Figures 8.12 and 8.13 show that the source of the Darajat fluids is mostly meteoric, having N_2/Ar ratios of about the air. Variations in radiogenic He indicates that the waters have circulated deeply. Mixing of crustal and magmatic derived fluids is indicated by ratios of N_2/Ar of up to 600 and CO_2/CH_4 from 0.1 to 132. The presence of C_{2-7} organic species in crustal originated gases (Table 8.1), as suggested by Moore et al. (2001), confirms that the mixed fluids were trapped in inclusions from wells DRJ S-1 and S-5.

A magmatic, i.e. andesitic gas, input into well DRJ S-3 is indicated by the negative correlation between the N_2/Ar and CO_2/CH_4 ratios (Norman et al., 2001; Figure 8.12B) and low He contents (Figure 8.13C). It is also indicated by the dominance of benzene as the most stable organic volatile, after CH_4, at high temperature, i.e. close to magmatic temperature (Giggenbach, 1995).

8.4.2. Steam Condensate Waters

Meteoric fluids and steam derived waters at the Geysers geothermal system, USA have identical patterns in N_2/Ar and CO_2/CH_4 (Moore et at., 2001), but they can be distinguished by the relative amounts of H_2S, CO_2, CH_4 and SO_2. The relationship of H_2S-CO_2-CH_4 (Figure 8.14) suggests that steam condensate derived waters are likely present below 1060 m of well DRJ S-1, as is indicated by relatively high amounts of trapped H_2S. However, the fluids contain very little SO_2 (Table 8.1).

In addition, the presence of steam condensate at about 1000 m depth in well DRJ S-1 is consistent with the measured eutectic temperature of fluid inclusions here at -30 to -70°C. The trapped liquid then cannot lie in the NaCl-H_2O system but more likely the H_2SO_4-H_2O system (Moore et al., 2002a).

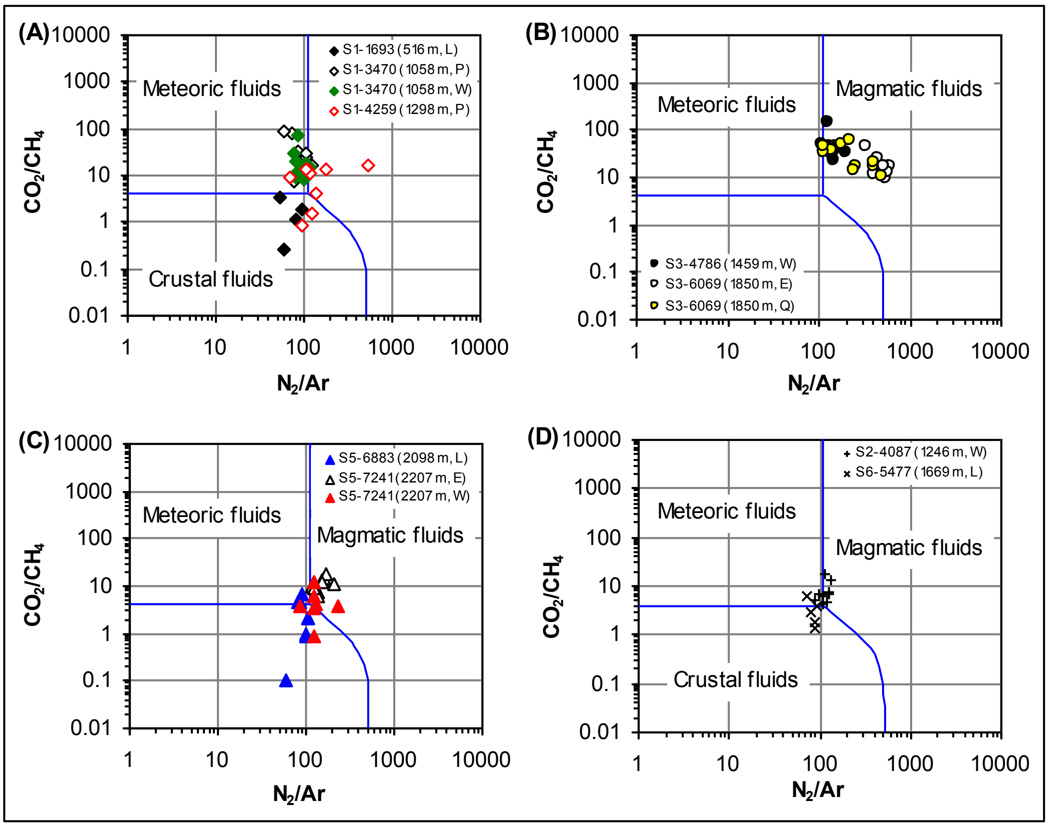

Figure 8.12. Relationship between N_2/Ar and CO_2/CH_4 ratios in fluid inclusions present in: **(A)** well DRJ S-1, **(B)** DRJ S-3, **(C)** DRJ S-5 and **(D)** the marginal area, i.e. wells DRJ S-2 and S-6, indicating the origin of fluids. Sample number and depth are given; character in brackets indicates the host mineral: (L) laumontite, (P) prehnite, (W) wairakite, (E) epidote and (Q) quartz. Both axes are logarithmic.

8.4.3. Degradation of Organic Components

Organic volatiles present in the fluid inclusions are mostly light compounds with low molecular weight, e.g. C_{2-3} species. A positive correlation between methane and the C_3 compounds may indicate their organic origin (Moore et al., 2000c), i.e. from either sedimentary rocks or groundwaters. Figure 8.15 shows that organic gases may contribute at about 1300 m depths in well DRJ S-1, at about 2100 m depth in DRJ S-5 and at 1670 m depth in DRJ S-6.

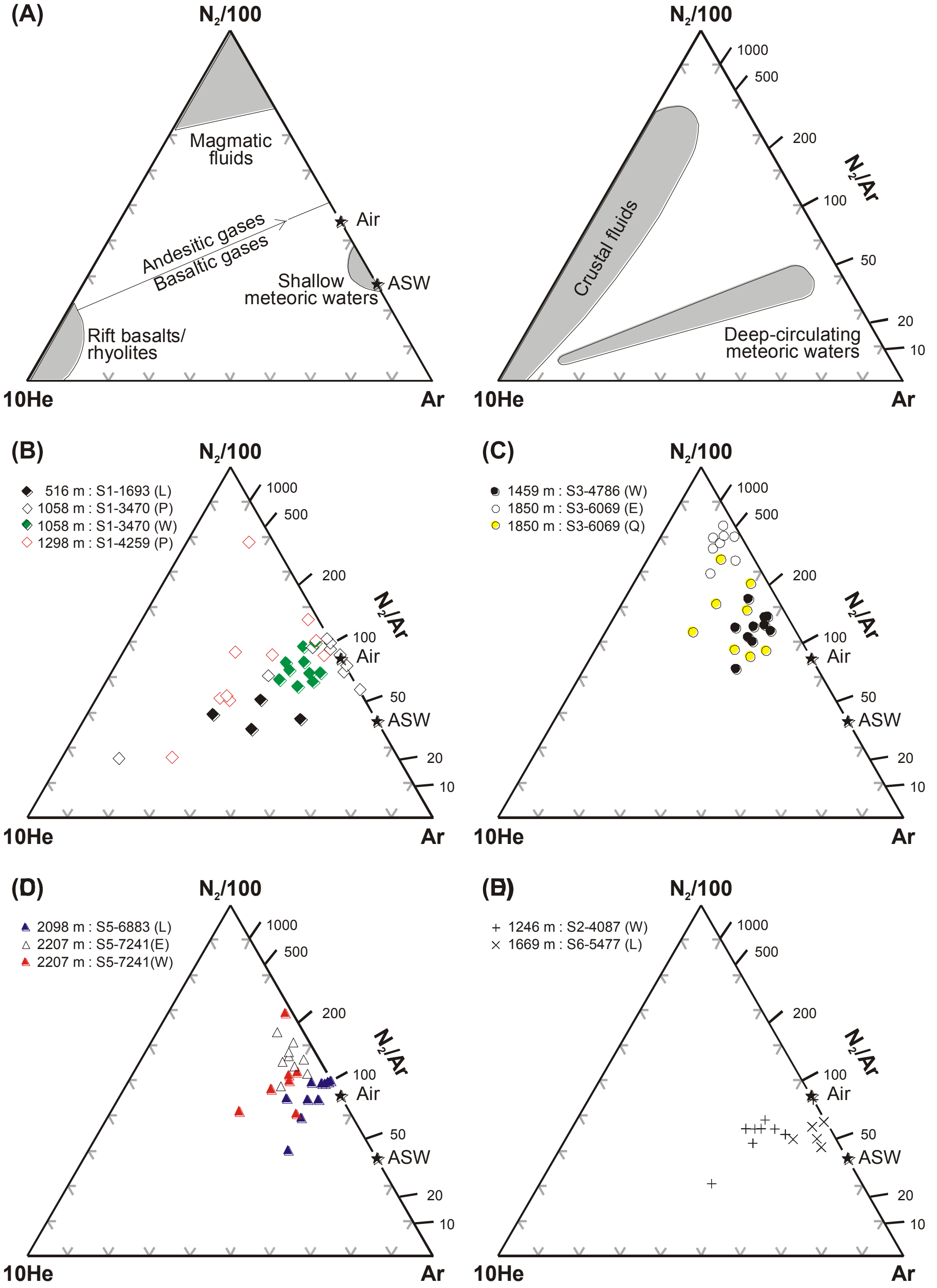

Figure 8.13.He-N_2-Ar relationship of gases.**(A)** Relative gas contents of magmatic, rift basalts/rhyolites, crustal, shallow and deep circulating meteoric waters (Giggenbach, 1992b; Giggenbach et al., 1993 and Norman and Musgrave, 1994). A line separates the compositions of andesitic and basaltic gases, following Lutz et al. (1999). The compositions of air and air saturated water at 20°C (ASW), and the ratio of N_2/Ar are also shown. The other ternary diagrams include the relative gas contents in: **(B)** well DRJ S-1, **(C)** DRJ S-3, **(D)** DRJ S-5 and **(E)** the marginal area, including wells DRJ S-2 and S-6. They indicate the presence of deep circulating meteoric fluids, except in DRJ S-3, where magmatic fluids likely contribute. Sample number and depth are given and character in bracket represents the host mineral: (L) laumontite, (P) prehnite, (W) wairakite, (E) epidote and (Q) quartz.

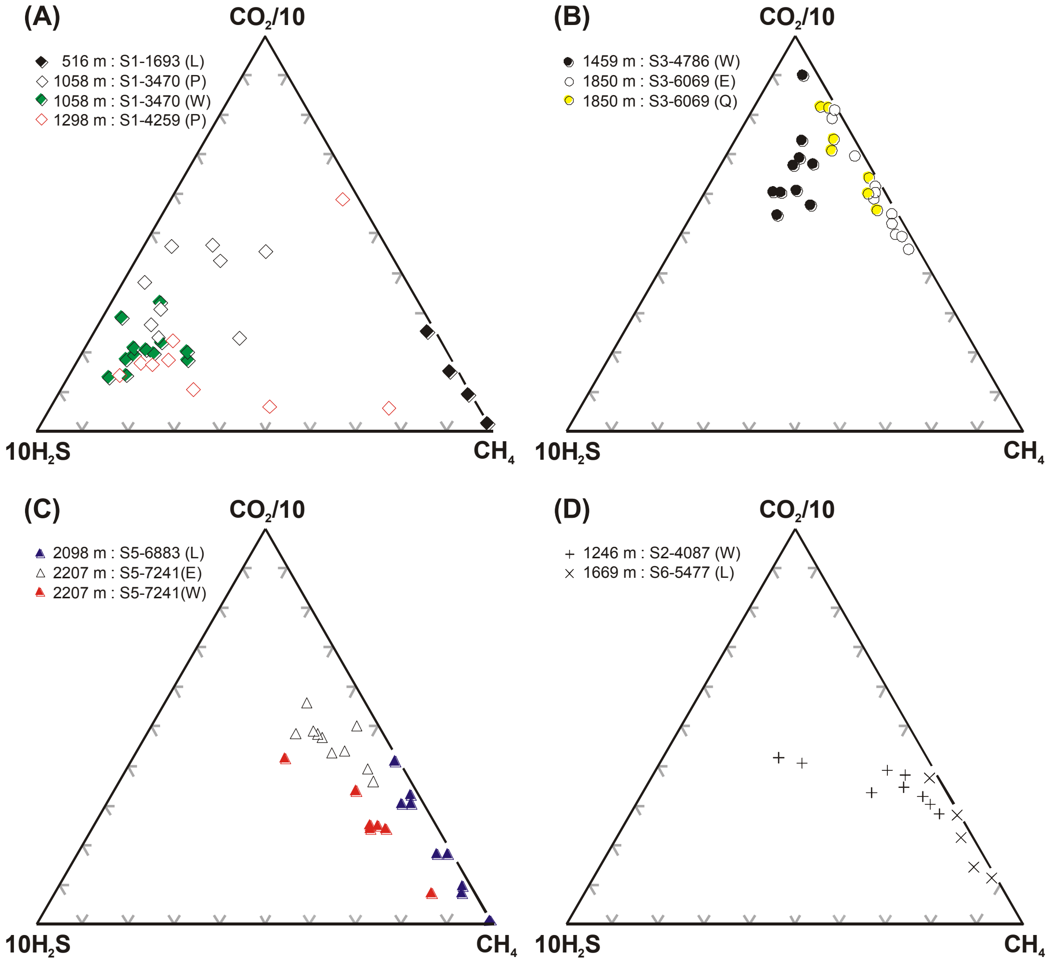

Figure 8.14. Proportions of H_2S, CO_2 and CH_4 in fluid inclusions from: **(A)** well DRJ S-1, **(B)** DRJ S-3, **(C)** DRJ S-5 **(D)** and the marginal area, including wells DRJ S-2 and S-6. Well DRJ S-1 likely has high H_2S, steam derived fluids; fluids in DRJ S-3 are CO_2 rich, with an influx of magmatic gas and those from DRJ S-5 and the marginal area are rich in CH_4. Sample number and depth are given; host minerals are given in brackets: (L) laumontite, (P) prehnite, (W) wairakite, (E) epidote and (Q) quartz.

The presence of methane, benzene and N_2(Yoshida, 1984) confirms that a biogenic process was involved. In DRJ S-6, where alkenes are more common than alkanes, interaction between organic rich fluids and wall rocks may have also occurred (Norman et al., 2002). However, the organic rich fluids were only trapped in laumontite, where their proportion vary widely. It might indicate that organic volatiles are produced by chemical equilibrium at temperature about 200°C (e.g. Giggenbach et al., 1993 and Sugisaki and Nagamine, 1995).

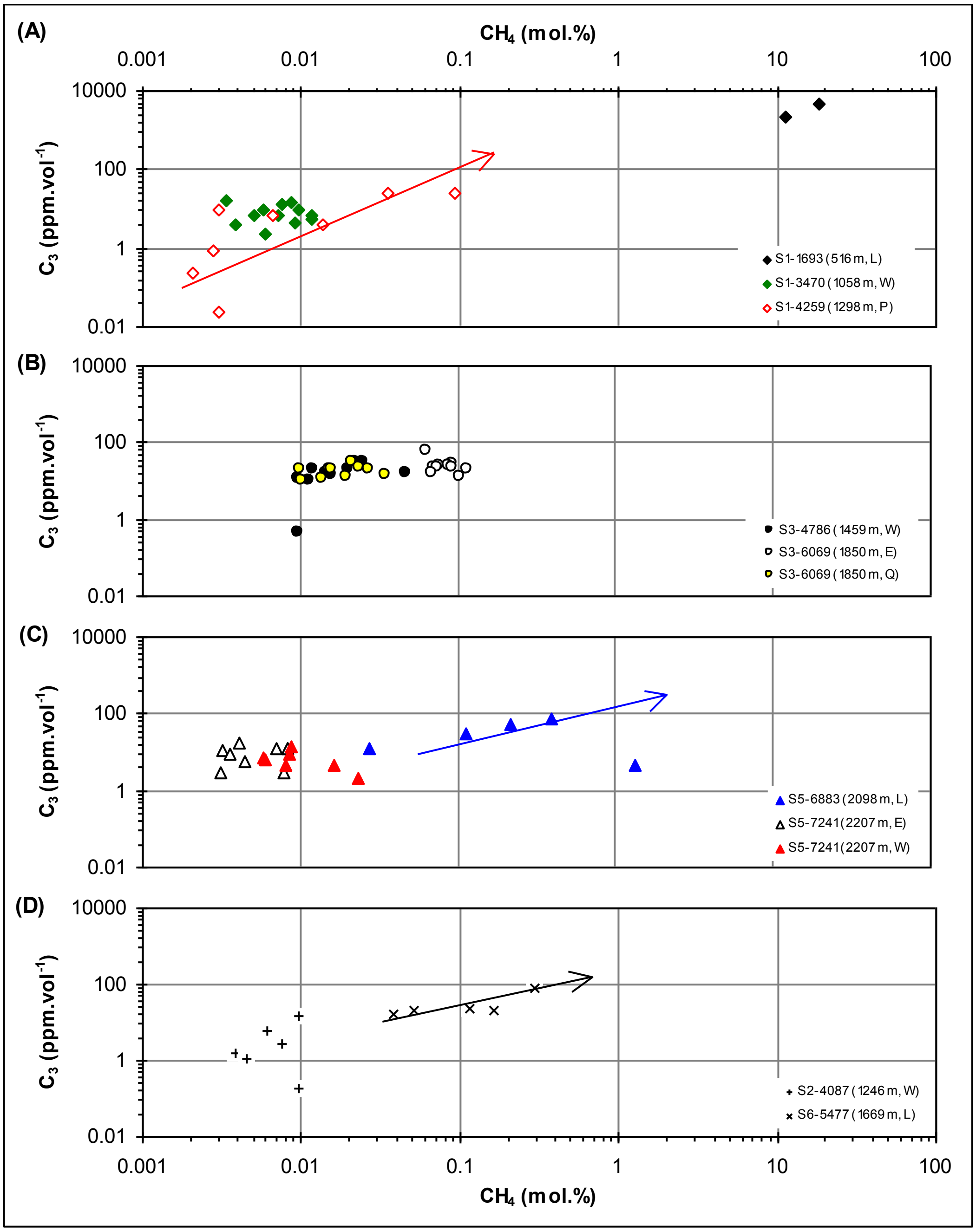

Figure 8.15. Relations between CH$_4$ and C$_3$ organic (propane+propene) contents in inclusion gases: **(A)** DRJ S-1, **(B)** DRJ S-3, **(C)** DRJ S-5 and in **(D)** the marginal area, including wells DRJ S-2 and S-6. Arrows show positive correlations, indicating the components organic origin. Negative correlations were not recognised. Sample number and depth are given, and character in bracket represents host mineral: (L) laumontite, (W) wairakite, (P) prehnite, (E) epidote and (Q) quartz. Both x- and y-axes are in logarithmic.

8.5. PROCESSES AFFECTING THE THERMAL FLUIDS

8.5.1. Boiling

Coexisting liquid and vapour rich fluid inclusions indicates that boiling occurred at about 910 m depth and below 1300 m in well DRJ S-1, below 1150 m in well DRJ S-3 and at 960 and 2200-2300 m depth in DRJ S-5.

Figure 8.16 shows the relationship between Th and Tm of the fluid inclusions, following Hedenquist and Henley (1985). It confirms boiling occurred in wells DRJ S-1, S-3 and S-5 at temperatures between 200 and 320°C. The primary fluid with low salinity (0.1 wt.% NaCl eq.) and low gas at 330-340°C and likely meteoric origin, was the source of the boiling fluids. However, both hotter and more saline fluids were trapped in DRJ S-1 and S-5 (Figure 8.16). They indicate a prolonged boiling of a thermal fluid of lower salinity and higher gas content.

Since the gases analysed were mixtures of liquid and vapour rich fluid inclusions, boiling is indicated by progressive changes in gas content of the inclusions over several crushings. Progressive boiling will cause an increase in CO_2 in the released gases relative to CH_4 and H_2, which are less soluble and will preferentially move into the vapour phase, according to the reaction:

$$CH_4 + 2H_2O \leftrightarrow 4H_2 + CO_2 \quad \text{.......} \quad (8.2)$$

Moore et al. (2000c) demonstrated that due to boiling, the proportion of CO_2 will increase but the CH_4/H_2 ratio will remain nearly constant as the steam fraction increases. They also recognised that boiling in an open system will produce gases which have low H_2/CH_4 ratios, while in an adiabatic closed system boiling is characterised by gases with high H_2/CH_4 ratios.

Figure 8.17 shows the relationships between CO_2, CH_4 and H_2 in the fluids trapped in the inclusions. The results suggest that boiling occurs in an open system. Loss of steam would increase H_2/CH_4 ratios (Moore et al., 2000c). This occurs in DRJ S-1 and S-5, as fluids ascend (Figures 8.17A and C).

Norman et al. (2002) showed that boiling would also increase CO_2 relative to N_2, accompanied by a decrease in the amount of total gas. This relationship is shown in Figure 8.18 and indicates that boiling occurs about 1060 and 1300 m depth in well DRJ S-1, between 1450 and 1850 m depth in DRJ S-3 and about 2210 m depth in DRJ S-5. In fact, at about 1850 m depth in DRJ S-3, the excess gas due to boiling, determined by Norman et al. (2002), is mostly present in epidote rather than in quartz. As epidote deposited first, degassing due to boiling might occur and decrease the total gas and the ratio of CO_2/N_2. Boiling likely also occurs in the marginal area at about 1250 m depth in DRJ S-2 and 1670 m depth in DRJ S-6.

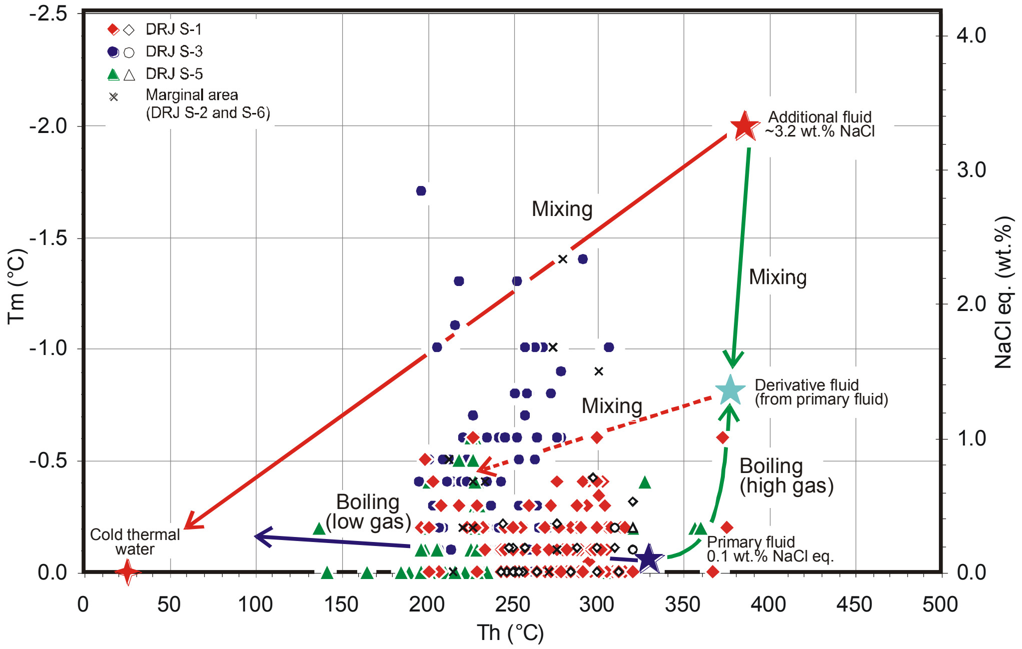

Figure 8.16.Relationship between Th and Tm of fluid inclusions showing trends of boiling (blue line) and mixing (red line). Solid symbols represent secondary inclusions and the open ones primary. Symbols ★ and ★represent the composition of the initial and evolved primary fluids, ★an additional fluid, i.e. magmatic, and ✦ cold thermal water. The green curve shows the evolution of primary fluids involved in boiling and mixing (see text).

8.5.2. Condensation

Condensation is indicated by the very low ratio of CO_2/N_2 (J.N. Moore, personal com., 2002). The relationship between the ratios of CO_2/N_2 and total gas (Figure 8.18) also record condensation effects which will also increase the ratio of CO_2/N_2, but in this case, the total gas increases (Norman et al., 2002). Condensation is likely indicated at 516 m depth in well DRJ S-1. The gas contents lie in the area of the gas cap, described by Norman et al. (2002). Some inclusions in calcite and anhydrite also show the presence of SO_4^{2-} bearing fluids, derived from steam condensate, at about 980 m depth, indicated by their Te values. In DRJ S-5, condensate occurs at about 2100 m depth, where boiling occurred about 100 m deeper. The steam condensation likely also occurs in the marginal well of DRJ S-6, indicated by the high ratio of H_2/H_2S of about 40 (D'Amore et al., 1977). No condensate is recognised in DRJ S-3.

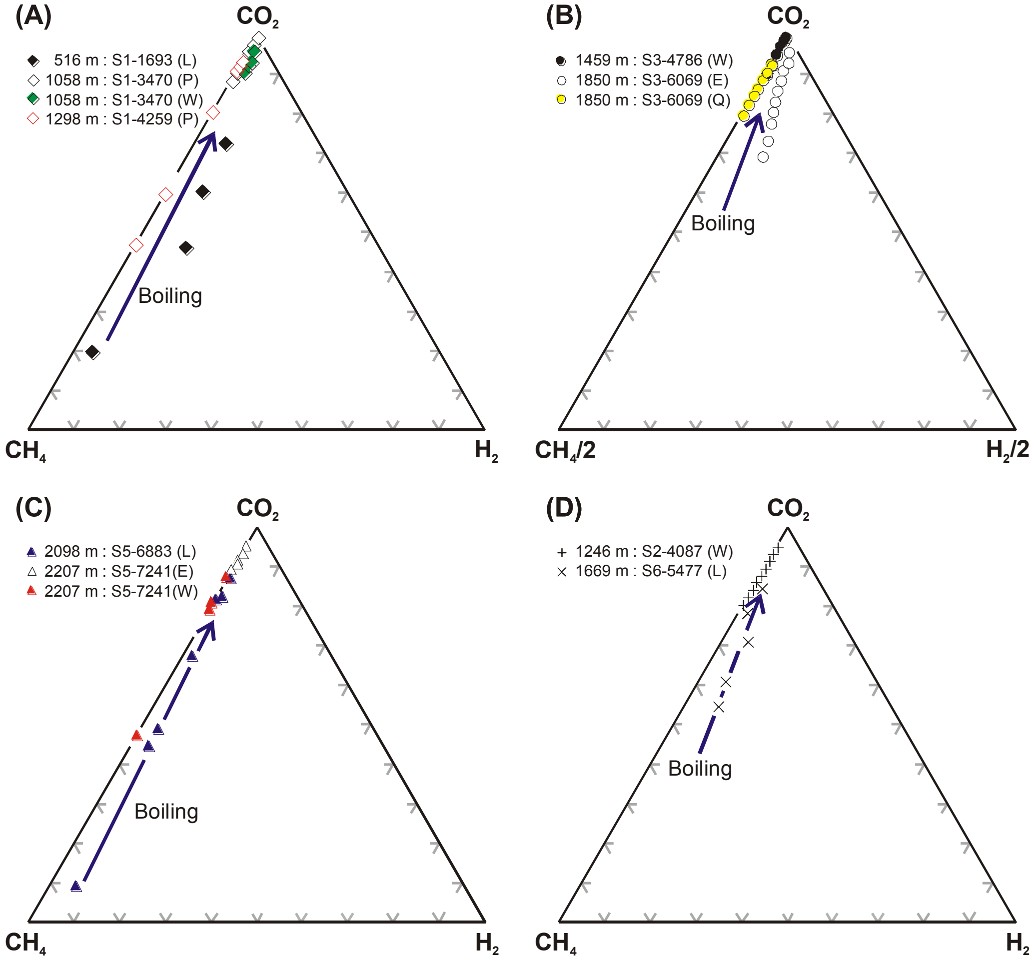

Figure 8.17. CH_4-CO_2-H_2 relationship of gas compositions showing the effect of boiling in: **(A)** well DRJ S-1, **(B)** DRJ S-3, **(C)** DRJ S-5 **(D)** and in the marginal area, including wells DRJ S-2 and S-6. Note different scale for figure (B). Boiling will increase the proportion of CO_2 with the CH_4/H_2 ratio remaining nearly constant. This might occur in an open system. Sample number and depth are given and character in bracket represents host mineral: (L) laumontite, (P) prehnite, (W) wairakite, (E) epidote and (Q) quartz.

8.5.3. Mixing

The gas compositions of the fluid inclusions, as described earlier, indicate that meteoric and magmatic waters were trapped and mixing may have occurred. Mixing can also be recognised from the microthermometry data, i.e. from the relationship between Th and Tm. Figure 8.16 shows another source fluid in well DRJ S-3, which has temperature of about 390°C and, as indicated by its Tm values of about -1.9°C, was gas rich and saline. It may be magmatic and could mix with the derivative fluid. There is also another end member cold meteoric thermal water and mixing occurs between this and either the magmatic fluid, e.g. that trapped in well DRJ S-3, or the derivative primary fluid, e.g. that trapped in wells DRJ S-1 and S-5. Mixing is also indicated by the relative amount of organic compounds, i.e. ratios of CH_4/C_2H_6 and C_2H_6/C_3H_8. Giggenbach (1997a) reported that methane could form by the equilibrium decarboxylation reaction of CO_2 from magmatic fluids, whereas the other organic compounds, i.e. C_2H_6 and C_3H_8, are introduced by meteoric water recharge. As shown in Figure 8.19, mixing occurs in well DRJ S-3 and likely in wells DRJ S-1 and S-5.

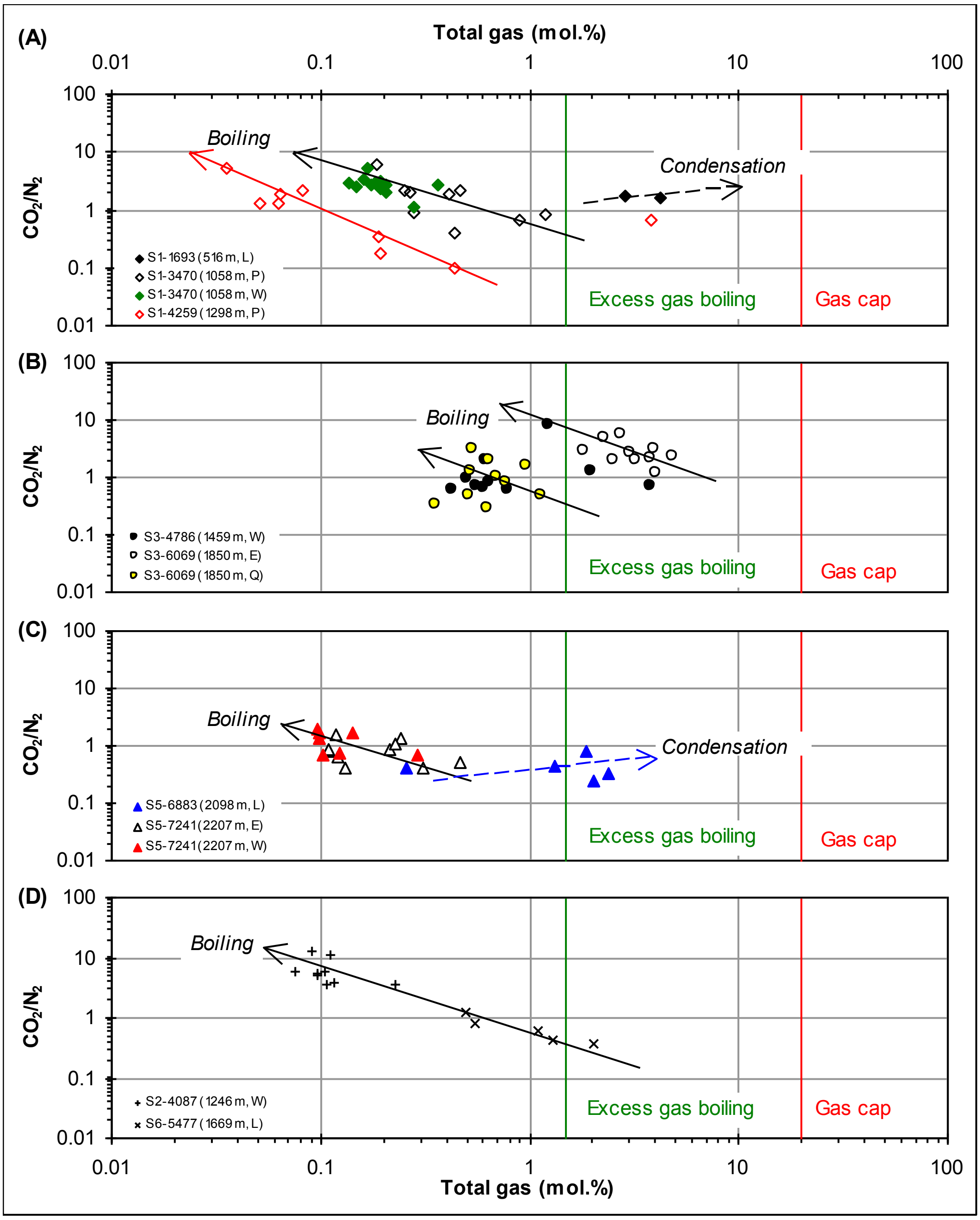

Figure 8.18. Boiling and condensation processes, indicated by plotting the amount of total gas and the ratio of CO_2/N_2: **(A)** DRJ S-1, **(B)** DRJ S-3, **(C)** DRJ S-5 and in **(D)** the marginal wells DRJ S-2 and S-6. Boiling trend is shown as a solid arrow and the condensation trend is represented by a dashed arrow. Sample number and depth are given, and character in bracket represents host mineral: (L) laumontite, (P) prehnite, (W) wairakite, (E) epidote and (Q) quartz. The amount of total gas excludes H_2O. The amount of excess gas due to boiling and amount of total gas in a gas cap (Norman et al., 2002) is shown by the green and red lines respectively. Both x- and y-axes are logarithmic.

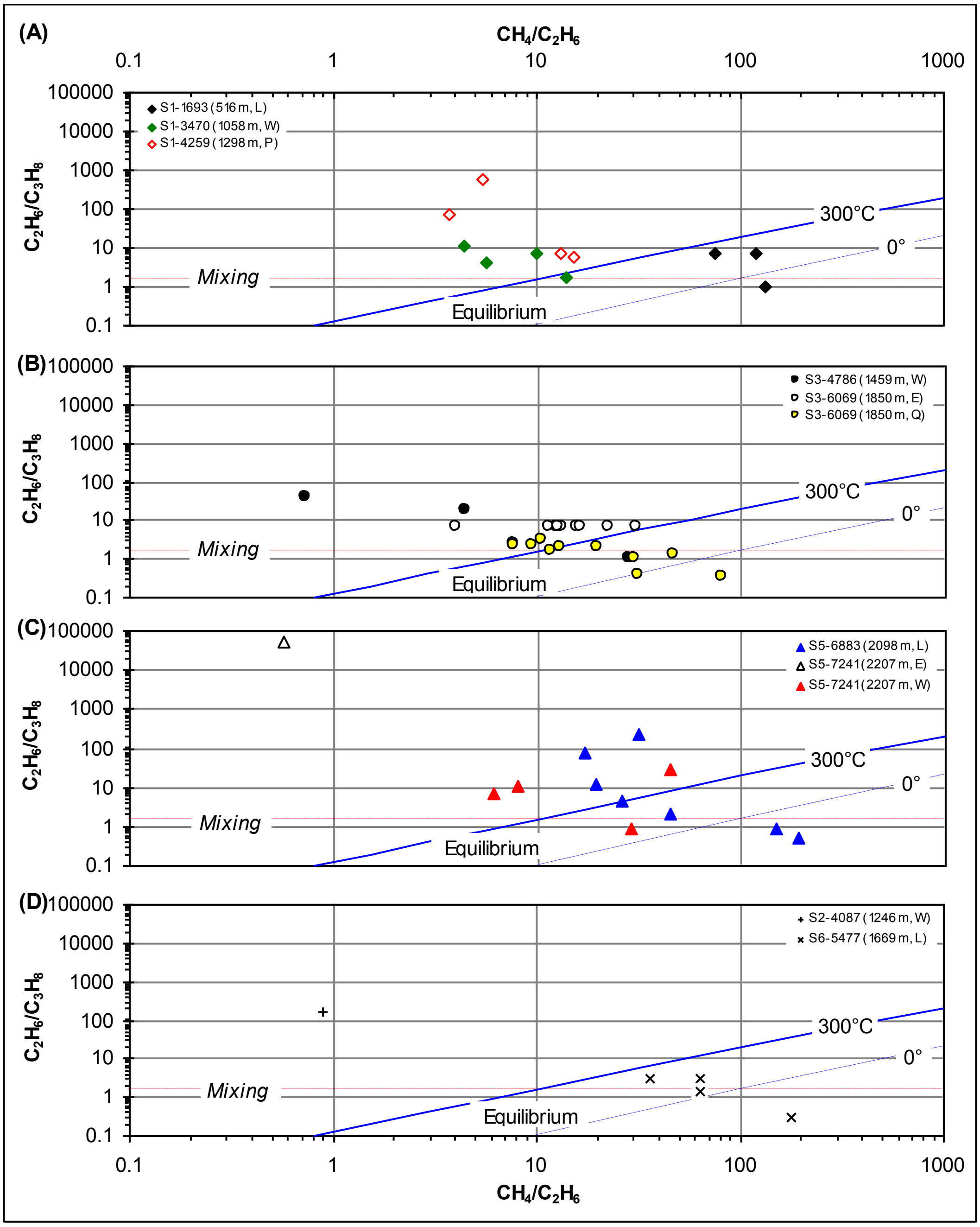

Figure 8.19. Plotting between ratios of CH_2/C_2H_6 and C_2H_8/C_3H_8: **(A)** DRJ S-1, **(B)** DRJ S-3, **(C)** DRJ S-5 and in **(D)** the marginal area, surrounding wells DRJ S-2 and S-6. Both x- and y-axes are logarithmic. Blue lines represent the proportion of gas contents in equilibrium condition at 300°C (solid line) and 0°C (dashed line) and red line represents a mixing given in Giggenbach (1997a). Mixing likely occurs in wells DRJ S-1, S-3 and S-5. Organic compounds from wells DRJ S-2 and S-6 occur due to internal equilibrium process at low temperature. Sample number and depth are given; character in bracket represents host mineral: (L) laumontite, (P) prehnite, (W) wairakite, (E) epidote and (Q) quartz.

Mixing might change the oxidation state of the fluids. Norman et al. (1996) shows that oxidation may be indicated by the ratio of alkanes to alkenes:

$$C_nH_{2n+2} + \tfrac{1}{2} O_2 \leftrightarrow C_nH_{2n} + H_2O \quad \ldots\ldots \tag{8.3}$$

Figure 8.20 shows the amounts of butane and butene, relative to the C_2 organic compounds, i.e. ethane and ethane. This indicates that in well DRJ S-1, oxidation occurs above 1060 m, whereas reduction affects deeper fluids. This is also indicated by the ratio of alkanes to alkenes in Figure 8.11A. The presence of the reduced fluids might result from boiling and the oxidised fluids, which are also present in DRJ S-2 and S-6 (Figure 8.20D), might reflect dilution by more oxidising meteoric waters (Moore et al., 2000c).

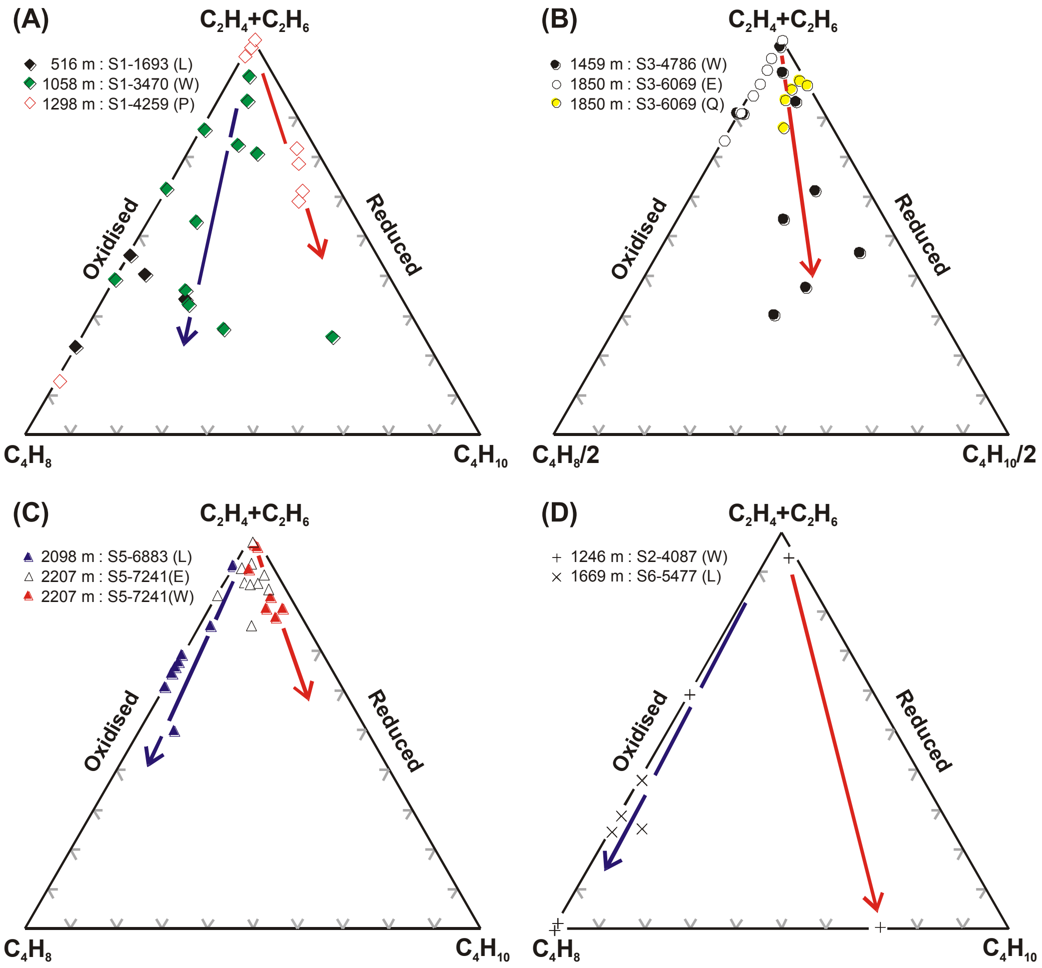

Figure 8.20. Relative compositions of butene (C_4H_8), butane (C_4H_{10}) and lighter organic species of ethane (C_2H_4) and ethane (C_2H_6) in: **(A)** well DRJ S-1, **(B)** DRJ S-3, **(C)** DRJ S-5 **(D)** and in the margin area surrounding wells DRJ S-2 and S-6. Oxidation of alkanes to alkenes, indicated by the relative amounts of C_4H_8 and C_4H_{10}, will determine the effect of oxidation (blue line) and reduction (red line) in fluids. Sample number is given and character in bracket represents mineral where analysis was done; (L) represents laumontite, (W) is for wairakite, (P) represents prehnite, (E) is epidote and (Q) is quartz.

Reduced fluids were also trapped at about 1460 m depth in well DRJ S-3, where light organic species are dominant (Figure 8.20B). They might result from upwelling fluids, originated from deeper or magmatic or both (Moore et al., 2000c), that is in equilibration with CO_2 at temperatures of 400-500°C (Kiyosu et al., 1992). However, a ratio of alkanes to alkenes of less than 1 (Figure 8.11B) indicates oxidation, which may be due to a contribution of more oxidised CO_2 rich magmatic fluids (Moore et al., 2000c).

8.5.4. Cooling and Heating

Comparison between the present downhole temperatures and those of the paleofluids, determined from fluid inclusion geothermometry, suggests that cooling has occurred in the DRJ S-1 (Figure 8.2). Below 1300 m, cooling from 280 to 250°C has occurred, and then to the present 200-225°C. However, heating also occurred since inclusions were trapped in DRJ S-1, i.e. at about 1150 m depth, as indicated by fluid inclusions present in prehnite. The temperature of the paleofluids was 250-260°C, before the fluids heated to 290-310°C (Figure 8.2).

Thermal decomposition is a temperature dependent non equilibrium process, which can breakdown the C-C bond in the organic compound, regarding reaction:

$$C_{n-1}H_{2n} + CO_2 + 3H_2 = C_nH_{2n+2} + 2H_2O \quad \text{........................} \quad (8.4)$$

Figure 8.21 shows that the organic decomposition might occur at high temperature, indicated by low ratio of CH_4/C_2H_6 and C_2H_6/C_3H_8 (Giggenbach, 1997a). At 1850 m depth in well DRJ S-3, the thermal decomposition indicates an increase in temperature from the deposition of epidote to that of quartz. On the other hand, cooling is indicated at about 2210 m depth in well DRJ S-5, where epidote predates wairakite.

8.6. SUMMARY

Figure 8.22 models the paleohydrology condition of Darajat, from wells DRJ S-5, through S-3 and S-1, to the marginal area of DRJ S-2 and S-6 on the northern part.

Feeding fluid zones were likely trapped by the deep part of wells DRJ S-1 and S-5. The fluids are of meteoric origin, contain up to 0.4 wt.% NaCl eq. and were hotter than 320°C. This high temperature is also indicated by the occurrence of garnet and actinolite in veins. The ascending fluids boiled off below an elevation of about +600 m in DRJ S-1 at 250-290°C, but were slightly cooler at 200-240°C at about the sea level near DRJ S-5. Boiling depth and temperature varied the amount of CO_2 of up to 1.5 mol.%. Consequently, the fluid pressures varied from 30 to 80 bars. The fugacities of O_2 (f_{O_2}) and

S_2 (fs_2), calculated after D'Amore and Gianelli (1984) are 10^{-37} to 10^{-31} atm and about 10^{-12} atm respectively. Gas rich, saline fluids formed in the upper part of the boiling zone in DRJ S-1; the amount of gas is up to 4 mol.%. Slow cooling is then a result of boiling. In DRJ S-5, as the boiled and degassed fluids ascended, they cooled to 130-140°C.

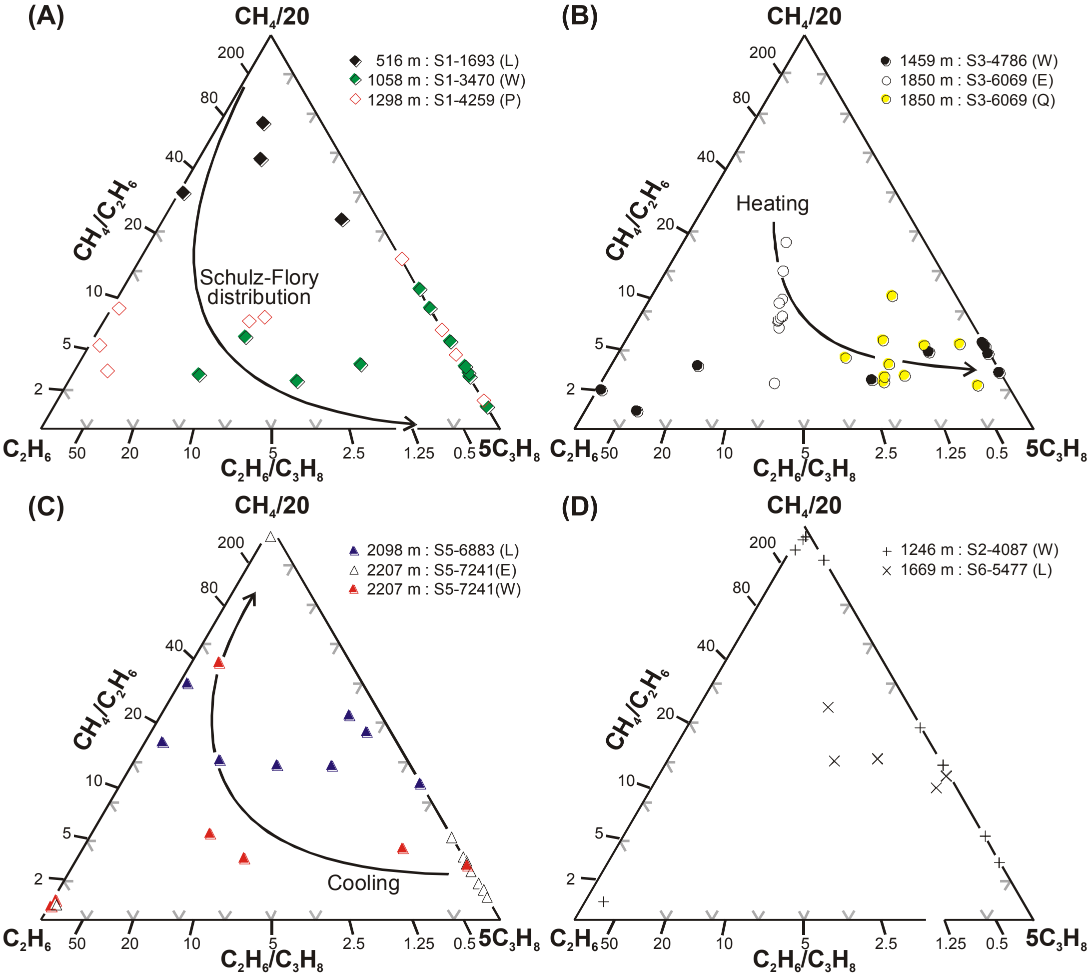

Figure 8.21. Relative CH_4, C_2H_6 and C_3H_8 in fluid inclusions from: **(A)** well DRJ S-1, **(B)** DRJ S-3, **(C)** DRJ S-5 **(D)** and the marginal wells of DRJ S-2 and S-6. The ratios of CH_4/C_2H_6 and C_2H_6/C_3H_8 are given. The solid curve in Figure (A) represents the equilibrium Schulz-Flory distribution process with an increase in temperature (Giggenbach, 1997a). Heating likely occurs in well DRJ S-3, whereas cooling is indicated in well DRJ S-5. In wells DRJ S-2 and S-6, high ratio CH_4/C_2H_6 indicates an equilibrium condition at low temperature. Sample number and depth are given; host minerals are given in brackets: (L) laumontite, (P) prehnite, (W) wairakite, (E) epidote and (Q) quartz.

A steam condensate zone is present above the boiling zone. In DRJ S-1, this is 600 m thick, i.e. from +700 to +1300 m. It is also characterised by the occurrence of anhydrite and calcite; the paleotemperature was 200-210°C at shallow depth but increased to boiling temperature (about 250°C) at about +800 m elevation. Mixing between boiled fluids and steam condensates was followed by cooling, most likely in the upper part of boiling zone. Well DRJ S-5 has a thin

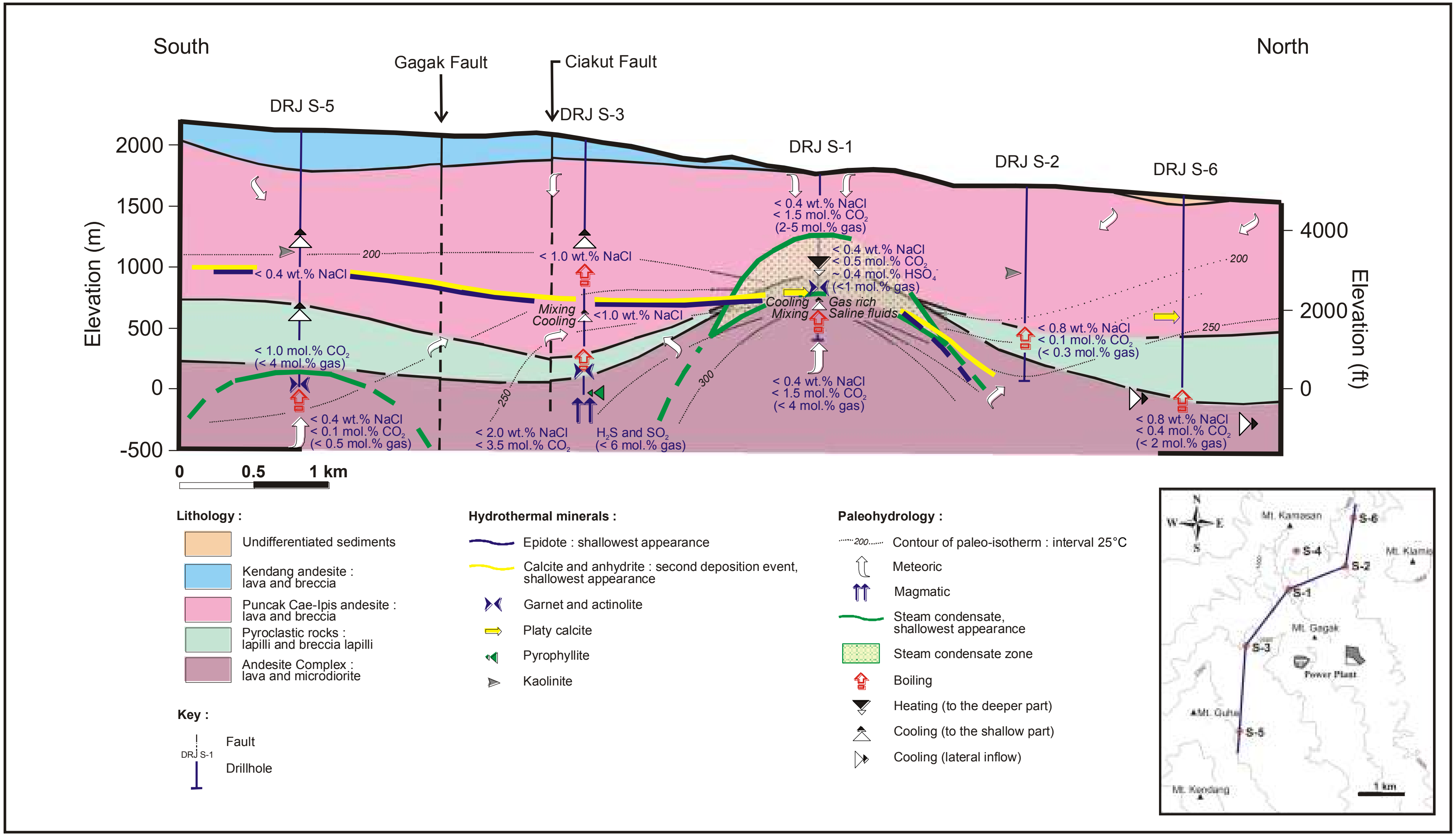

Figure 8.22. South-north cross section showing paleohydrology conditions, i.e. from DRJ S-5, S-3, S-1, S-2 to S-6, based on the fluid inclusion study. The occurrences of some hydrothermal minerals, described in the previous chapters, are also given here; epidote, garnet, actinolite, calcite and anhydrite are present in veins and fractures, whereas pyrophyllite and kaolinite replaced the matrix of the rocks.

condensate zone at an elevation of +100 to +200 m only. Condensate waters in DRJ S-1 are very dilute and contain up to 0.5 mol.% CO_2 and about 0.4 mol.% H_2SO_4. The gas content is below 1 mol.%. However, above the condensate zone, fluids could be gas rich with 2 to 5 mol.% gas, containing up to 1.5 mol.% CO_2. The pressure of the condensate waters is likely below the hydrostatic pressure, i.e. about 50 bars.

Boiling is the main process occurring in Darajat. It is also present in the marginal wells DRJ S-2 and S-6, i.e. at elevations between sea level and +600 m, and at temperatures of 280-290°C. Boiling in well DRJ S-6 is also indicated by the appearance of platy calcite. In the marginal area, cooling of the fluids to 220-250°C followed boiling, as the fluids ascended to the north. Cooling may also be due to mixing between thermal water and colder, surface water, probably was steam condensate, as indicated by the occurrence of kaolinite. The mixing of cold water is also confirmed by the occurrences of Mg rich calcite, siderite and bimodal Th's variation in the marginal wells (Reyes, 2000).

The paleohydrology of the area surrounding well DRJ S-3 differed from that elsewhere. Magmatic fluids likely penetrated into the deep part of DRJ S-3, as is indicated by the composition of gas in fluid inclusions. These fluids contain 1.2-1.8 wt.% NaCl eq., up to 6 mol.% gas, mainly CO_2 of less than 3.5 mol.% and traces of H_2S and SO_2, and have temperature of above 300°C, consistent with the presence of garnet and actinolite in veins. The magmatic input might also form pyrophyllite in the matrix of the rocks. These magmatic fluids then boiled off at 250-280°C at elevation of about +100 m. Mixing with meteoric waters occurred at about +600 m elevation and caused the fluids to cool down to 230-240°C and become less saline. Meteoric waters at temperatures of 210-230°C become dominant above an elevation of +800 m, where magmatic fluids are absent. The origin of the meteoric waters is likely from well DRJ S-1. However, it can also be from either well DRJ S-5 or the surface waters, which flow through the faults.

Furthermore, from the time the vein minerals formed, cooling has occurred. The present downhole temperatures show that near the surface, the temperature is nearly constant at 60-70°C, but at 600-1000 m depth, it increases progressively to 240-250°C, before remaining constant downwell (Amoseas Indonesia Inc., 1989b). The maximum temperature likely occurs at the top of boiling zone. However, the downhole temperature in DRJ S-3 is relatively constant at about 250°C.

Depressurisation has also occurred. The fluid pressures have decreased from about, or above, to below the hydrostatic pressure, i.e. from up to 80 bars, when the fluids trapped in inclusions to the present reservoir pressure condition of 36 bars.

Chapter 9

WATER-ROCK INTERACTIONS

Interactions between water and rocks commonly change the mass and chemical compositions of the host rocks, as well as the fluids. The change in rock composition was calculated using the Gresens metasomatic equation (Gresens, 1967), based on the volume change between the unaltered and altered rocks. The method used and the calculations are given in Appendix I.

It was first necessary to determine the chemical compositions of the unaltered and least altered rocks and how they vary in three dimensions. The values would then be used as a reference with which to compare the compositions of the rocks which have been more intensively altered. Theoriginal compositions of the host rocks are taken as the unaltered andesite lavas, encountered in well DRJ 1.Their mineralogy and chemistry are described in detail in Chapter 4. Here, their compositions are expressed in usable mass exchange units, i.e. g.100 g^{-1} for major elements and $g.tonne^{-1}$ for trace elements, and given in Table 9.1. In addition, the composition of a least altered rhyolite from 2596 m depth in well DRJ 24 is also given.

9.1. RECOGNITION OF IMMOBILE AND LEAST MOBILE ELEMENTS

Calculation of the mass exchange requires one or more immobile elements were not lost or gained during alteration. Appleyard (1991) reported that these elements could readily be recognised from rocks with low intensity alteration. Cores from other than the five unaltered rocks from well DRJ 1 were considered; their mineralogy and chemical compositions, given in Chapter 4, still reflect the presence of primary minerals, but are also influenced by the occurrence of some common secondary minerals, e.g. calcite, anhydrite, smectite and chlorite. Table 9.2 and Figure 9.1 represent variations in their changes in volume (FV^0) and mass compared to unaltered rocks from the same well. Table 9.2 shows that Al and Ga are immobile, with FV^0 between 0.8 and 1.2, equivalent to a 20% volume loss and a 20% volume increase respectively. In contrast, K, Mg and Rb were mobile during alteration, as is indicated by their wide range of FV^0 values.

The immobility of Al and Ga, recognised from the clustering pattern of FV^0 values (e.g. Taylor and Appleyard, 1983; Elliott-Meadows and Appleyard, 1991), is also assessed using the immobile-immobile-element plots following MacLean and Kranidiotis (1987). Figure 9.2 shows that Al_2O_3 and Ga were likely constant during alteration, but values decreased slightly with gain of mass.

Other immobile elements commonly used in mass transfer study are Ti, Zr, Y and Sr (e.g. MacLean, 1990; Leitch and Lentz, 1994). However, their amounts vary both with alteration intensity and to original fractionation of the igneous rocks (MacLean and Barrett, 1993) (Figure 9.2). As indicated by their FV^0 (Table 9.2), they are slightly mobile. In several cases, Zr and Sr can be mobile during carbonate and sulfate deposition (MacLean and Kranidiotis, 1987; Shriver and MacLean, 1993; Leitch and Lentz, 1994).

Table 9.1. Composition of the unaltered rocks from well DRJ 1, expressed in relative weight units.

Sample no. **Depth (m)**	D1-70 70	D1-161 161	D1-180 180	D1-397 397	D1-637 637	D24-8517* 2596
Elements (g.100g^{-1} for major and g.tonne^{-1} for trace elements)						
Si	28.80	27.70	28.20	26.90	27.20	33.60
Ti	0.48	0.46	0.45	0.53	0.50	0.35
Al	9.09	9.07	9.21	9.43	9.68	8.53
Fe_{total}^{+3}	4.73	5.78	5.15	5.92	5.45	3.90
Mn	0.09	0.19	0.12	0.16	0.09	0.02
Mg	1.65	1.81	1.52	1.68	1.62	1.14
Ca	4.01	4.31	4.30	5.02	4.83	0.64
Na	2.38	2.38	2.46	2.70	2.74	0.27
K	1.42	1.27	1.33	0.96	0.95	1.72
P	0.07	0.06	0.05	0.08	0.07	0.05
S	0.01	0.02	0.01	0.01	0.02	0.34
Sc	20.0	21.6	21.7	28.1	27.3	18.9
V	163.0	165.0	145.0	164.0	162.0	113.0
Cr	20.2	17.2	16.9	7.9	9.8	48.7
Ni	9.0	7.6	7.6	4.4	3.6	2.2
Cu	56.4	29.6	37.7	43.9	43.4	10.9
Zn	71.1	63.6	58.9	66.1	64.3	17.7
Ga	17.0	17.1	17.9	18.3	19.6	14.2
Rb	64.1	55.3	59.6	35.0	39.2	63.9
Sr	222.0	237.0	246.0	267.0	316.0	63.0
Y	33.9	27.5	27.2	34.0	23.3	21.9
Zr	157.0	130.0	137.0	128.0	106.0	113.0
Nb	5.4	4.7	4.3	4.5	3.6	4.2
Ba	268.0	267.0	260.0	216.0	201.0	233.0
La	12.4	10.7	10.1	9.0	9.1	9.3
Ce	38.7	30.9	31.7	24.0	25.6	24.3
Pb	9.7	9.2	10.0	8.2	9.7	5.2
Th	6.7	5.1	6.6	3.6	3.4	4.3
U	2.3	2.3	2.2	1.6	1.9	1.6

* Slightly altered rhyolite from 2596 m depth, well DRJ 24.

9.2. WHOLE ROCK COMPOSITIONS

Representative compositions of the altered rocks, recalculated for no volume change, are given in Table 9.3 and summarised for each well in Figures 9.3 to 9.6. Water contents and the amounts of S and CO_2 are listed in Table 9.4.

Wells DRJ S-1 and S-5. Silica contents range from 18 to 29 g.100g^{-1}. At 516 and 1298 m depth in well DRJ S-1 and 868 and 2274 m in DRJ S-5, there was an increase in Si of up to 38 g.100g^{-1} during alteration (Figures 9.3 and 9.4).

Calcium ranges from 4.4 to 7.2 g.100g^{-1} and the Na and K contents are up to 2.7 and 1.6 g.100g^{-1} respectively. However, at shallower than 560 m in DRJ S-1 and between 860 and 890 m in DRJ S-5, K can be as high as 4.8 $g.100g^{-1}$ and Na is up to 1.6 $g.100g^{-1}$, but Ca is only 1.8 $g.100g^{-1}$. In deeper parts, K contents reach 3.5 $g.100g^{-1}$ at 1298 m depth of DRJ S-1 and Na is about 3.0 $g.100g^{-1}$ at 2274 m in DRJ S-5 but Ca is low, i.e. about 2.8 $g.100g^{-1}$. In addition, both K and Na are very low at 1023 m in DRJ S-1, i.e. less than 0.2 $g.100g^{-1}$ in a very intensely altered rock.

Table 9.2. Zero change volume factors (FV^0) for the least altered rocks from well DRJ 1. $FV^0$of above 1 suggests an increase in volume, while below 1 represents a loss of volume.

Altered Rocks	D1-210		D1-247	D1-340	D1-580	D1-700	D1-730		D1-732
Depth (m)	210		247	340	580	700	730		732
Compared to	D1-70	D1-637	D1-161	D1-180	D1-397	D1-637	D1-70	D1-637	D1-637
FV^0 for elements:									
Si	1.020	0.974	1.080	1.220	1.020	1.020	1.060	1.010	1.130
Ti	1.050	1.120	0.751	0.734	1.270	1.140	0.872	0.927	0.810
Al	1.050	1.130	0.889	0.796	0.915	0.953	0.957	1.030	1.000
Fe_{total}^{+3}	1.160	1.360	0.778	0.732	1.370	1.150	0.650	0.759	0.686
Mn	0.445	0.450	1.090	1.650	1.460	0.415	0.620	0.628	0.628
Mg	3.020	3.000	0.698	0.472	2.880	1.550	0.995	0.986	0.726
Ca	1.060	1.290	0.626	0.922	0.875	0.866	0.889	1.090	0.971
Na	0.994	1.160	1.110	1.610	0.963	0.998	1.110	1.300	1.300
K	0.778	0.525	1.980	4.990	1.720	1.080	2.330	1.570	7.080
P	1.040	1.190	0.890	0.949	1.020	1.000	2.100	2.410	1.060
S	0.519	1.050	1.920	0.514	0.171	0.111	0.002	0.003	0.004
Sc	0.78	1.08	0.60	0.48	1.45	1.23	0.64	0.88	0.62
V	1.21	1.22	0.58	0.49	1.26	1.03	0.65	0.66	0.55
Cr	1.04	0.51	1.40	0.63	0.93	1.26	0.39	0.19	0.31
Ni	1.47	0.60	0.60	0.87	0.88	0.68	0.93	0.38	0.31
Cu	1.06	0.83	0.32	0.57	0.71	1.31	1.49	1.16	1.03
Zn	0.99	0.90	0.83	0.74	0.62	0.82	1.00	0.92	0.78
Ga	1.08	1.27	0.88	0.99	0.95	1.00	1.00	1.17	1.05
Rb	0.72	0.45	2.29	4.14	1.55	1.17	2.73	1.69	10.90
Sr	1.08	1.55	0.84	1.10	0.86	0.94	0.87	1.25	1.02
Y	0.53	0.37	1.01	1.53	2.04	1.18	1.67	1.17	1.01
Zr	0.88	0.60	1.47	1.74	1.30	1.15	2.69	1.84	1.44
Nb	0.96	0.65	1.54	1.59	1.38	1.32	1.77	1.21	1.06
Ba	0.59	0.45	1.98	3.51	1.21	0.83	2.05	1.56	2.54
La	0.81	0.60	1.83	2.77	0.96	1.01	1.94	1.44	1.17
Ce	1.03	0.69	1.11	1.36	1.08	0.97	2.76	1.85	1.06
Pb	0.90	0.91	1.23	1.29	0.52	0.55	1.90	1.93	1.48
Th	0.77	0.39	1.82	2.81	1.02	0.85	12.90	6.53	2.89
U	0.75	0.63	1.40	2.10	0.65	1.59	2.47	2.08	1.09

Total Fe varies up to 7 $g.100g^{-1}$, except at 1023 and 1299 m depth in well DRJ S-1, where Fe exceeds 8.6 $g.100g^{-1}$. In DRJ S-1, the amount of Mg ranges from 2.2 to 3.6 $g.100g^{-1}$, except at 560 m depth, where it is as high as 6.3 $g.100g^{-1}$. The Mg content in the altered rocks in DRJ S-5 is less than that in DRJ S-1; it varies between 0.8 and 2.6 $g.100g^{-1}$. Variations of Ti in the altered rocks from DRJ S-1 and S-5 also differ. In DRJ S-1, the Ti contents range from 0.4 to 0.9 $g.100g^{-1}$, but in DRJ S-5 they are only about 0.4 $g.100g^{-1}$. No change in Mn content usually occurs due to alteration, as indicated by their same amounts in the unaltered and altered rocks of 0.2 $g.100g^{-1}$. However, at about 550 and 1020 m in DRJ S-1 and 840 m in DRJ S-5, Mn reaches 0.3-0.5 $g.100g^{-1}$ (Figures 9.3 and 9.4). The amount of Fe in DRJ S-1 seems to increase with depth. The amount of Fe^{2+} is usually higher than Fe^{3+}. However, above 910 m and at 1200 m depth in DRJ S-1 and at 2275 m in DRJ S-5, oxidation has caused Fe^{3+} to exceed Fe^{2+}.

Variations in trace element contents in the altered rocks are summarised in Figures 9.3 and 9.4. They generally vary sympathetically with the major elements, e.g. Rb and Ba with K, Sc and Ni with Fe. Most trace elements in rocks of well DRJ S-1 tend to increase as the rocks altered, whereas in well DRJ S-5, most decrease. Some traces, e.g. Ba, Cu, Cr and Th, vary widely but others, e.g. U and Zr, are immobile.

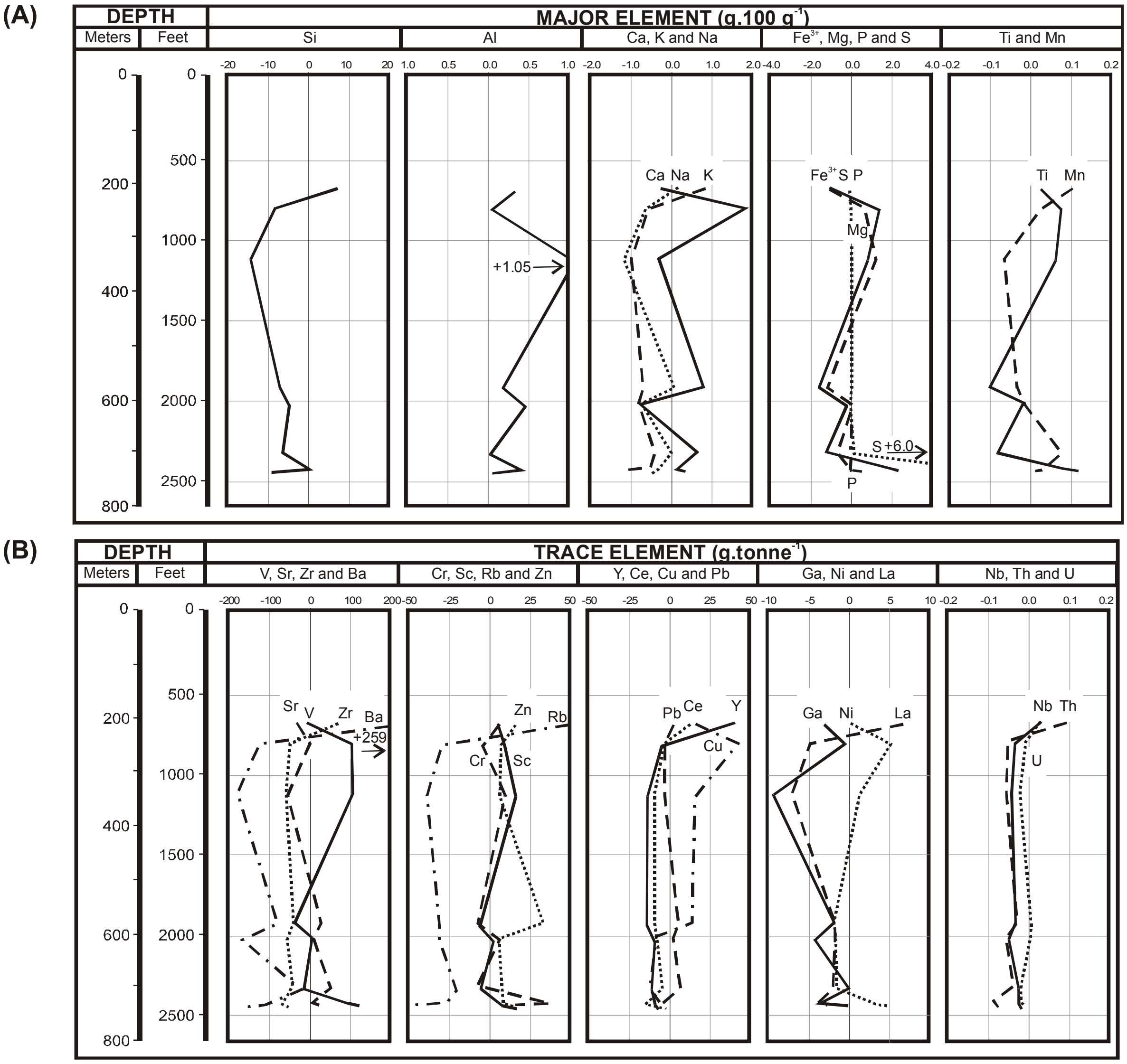

Figure 9.1. Variations in mass exchange of the least altered rocks from well DRJ 1, compared to unaltered rocks from the same well, for: **(A)** major and **(B)** trace elements. Positive values plot right of 0.0, indicating a gain, whereas a negative value indicates a loss. Immobile elements are Al and Ga; Si, K and Na tend to decrease; Ca, Fe, Mg, Ti and Mn vary with type of alteration. Most trace elements, e.g. Zr, Ba, Rb and Th, decrease, some, e.g. Pb and U, show no change, but Zn and Cu usually increase with alteration intensity.

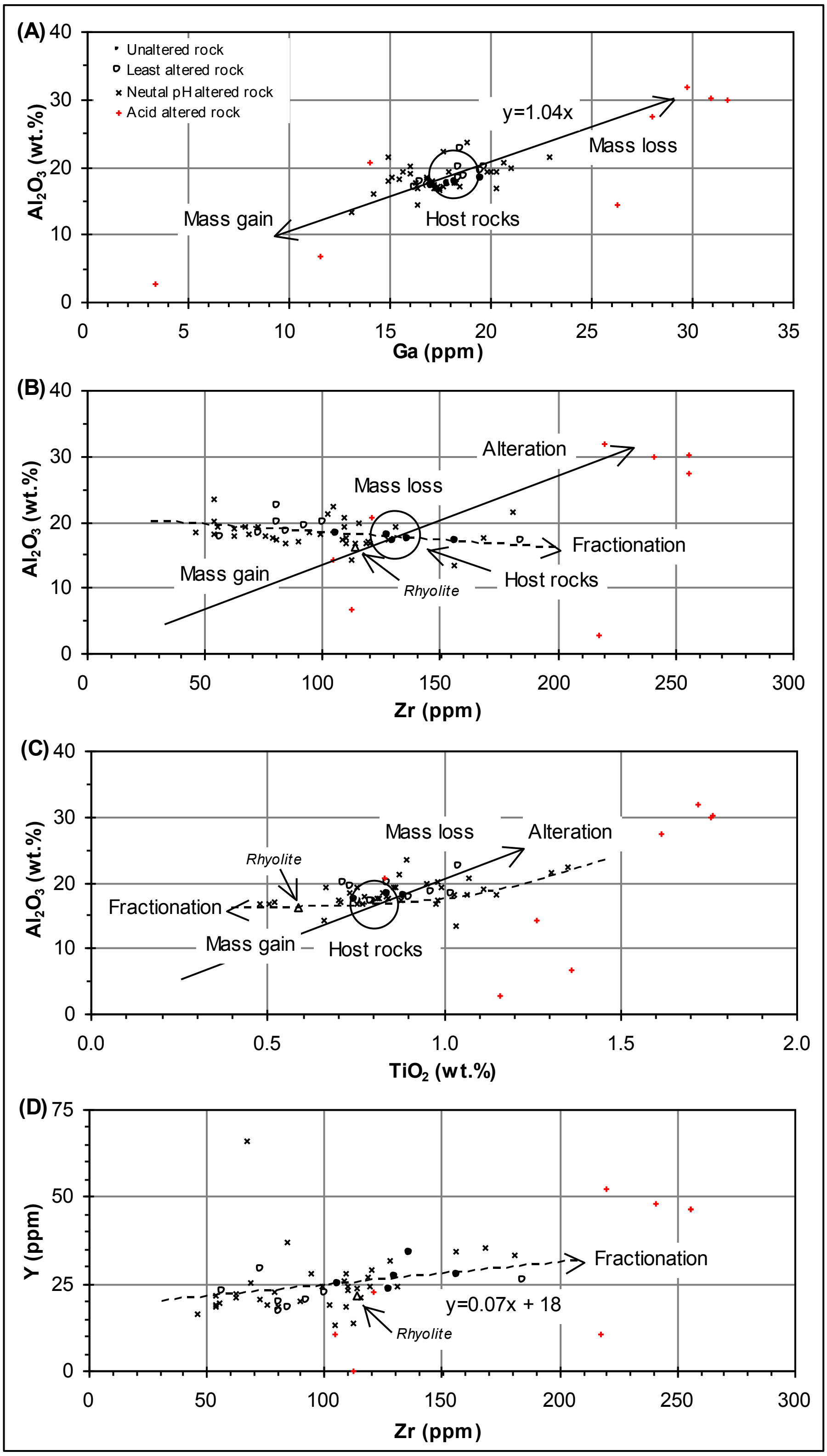

Figure 9.2. Plots of immobile elements with respect to Al_2O_3 for: **(A)** Ga, **(B)** Zr, **(C)** TiO_2 and **(D)** between Zr and Y of the unaltered and least altered rocks from well DRJ 1, and altered rocks from other wells, including those altered by acid fluids. Aluminium and Ga are immobile, as determined from volume factors; gains of mass or volume are slight. Ti, Zr and Y are considered immobile in many mass transfer studies; their amounts vary with alteration and fractionation. The host rocks lie at the intersection between the alteration (solid line) and fractionation (dashed line) trends and are close to the unaltered rocks from DRJ 1. The plots follow MacLean and Kranidiotis (1987) and MacLean and Barrett (1993).

Table 9.3. Representative compositions of altered rocks compared with the unaltered rocks. Type of rocks and intensity of alteration are given.

Well	DRJ S-1			DRJ S-3			DRJ S-5			DRJ S-2		DRJ S-6	
Depth (m)	561	1023	1299	618	1000	1775	888	1938	2243	958	1247	912	1938
Sample no.	S1-1838	S1-3355	S1-4259	S3-2025	S3-3280	S3-5821	S5-2915	S5-6353	S5-7355	S2-3141	S2-4087	S6-2991	S6-6359
Derived from	D1-70	D1-161	D1-397	D1-70	D1-397	D1-397	D1-161	D1-637	D1-180	D1-180	D1-161	D1-637	D1-70
Rock type*	Tuff	Microdiorite	Micro(diorite)	Andesite(tuff)	Andesite	Tuff	Tuff	Tuff	Andesite	Andesite	Andesite	Andesite	Andesite
Alteration	Moderate	Intense	Intense	Moderate	Moderate	Intense	Intense	Intense	Low	Low	Moderate	Moderate	Intense
Elements ($g.100g^{-1}$ for major and $g.tonne^{-1}$ for trace elements)													
Si	17.50	20.90	38.10	18.40	27.90	25.00	24.10	29.80	21.50	20.20	23.80	24.10	24.70
Ti	0.53	0.75	0.85	0.40	0.44	0.66	0.34	0.34	0.46	0.49	0.58	0.72	0.51
Al	9.04	10.90	9.69	8.72	9.64	10.40	8.81	9.82	9.22	9.07	10.10	10.90	9.42
Fe_{total}^{+3}	3.49	8.28	9.27	4.77	5.98	7.91	4.93	4.76	6.46	6.05	6.57	8.80	7.69
Mn	0.29	0.30	0.20	0.08	0.14	0.16	0.05	0.13	0.19	0.13	0.12	0.17	0.17
Mg	6.02	3.01	3.55	1.85	1.88	3.45	1.30	1.00	2.41	2.38	2.18	2.78	2.34
Ca	1.72	6.91	4.51	4.76	5.04	7.44	2.12	5.38	6.28	5.58	5.21	8.17	5.09
Na	0.04	0.07	2.20	1.97	2.98	2.04	0.10	2.78	1.67	2.63	0.86	1.87	2.58
K	4.62	0.18	3.60	0.25	0.71	0.38	1.19	1.62	0.24	0.32	1.93	0.70	0.38
P	0.06	0.10	0.10	0.05	0.06	0.07	0.07	0.10	0.06	0.06	0.06	0.06	0.09
Sc	25.8	29.4	53.0	25.7	19.5	37.3	19.2	12.8	23.9	31.2	32.5	43.6	18.6
V	252.0	253.0	369.0	168.0	175.0	276.0	95.7	38.9	203.0	241.0	269.0	275.0	127.0
Cr	12.3	41.0	60.5	29.4	8.2	24.7	137.0	10.7	8.3	32.0	19.1	57.4	0.0
Ni	3.9	8.9	17.3	6.8	5.9	14.5	4.0	2.2	7.0	13.0	13.0	18.5	2.0
Cu	8.6	66.2	10.4	38.5	52.3	39.4	16.7	4.6	123.0	67.6	48.5	41.6	17.9
Zn	184.0	75.1	72.4	67.7	68.2	69.5	44.6	54.0	77.4	62.4	59.0	67.8	79.5
Ga	17.0	14.2	17.8	17.7	17.9	16.6	17.6	19.3	17.9	18.2	15.3	17.4	16.3
Rb	290.0	8.3	145.0	11.7	24.8	8.5	60.0	71.5	7.8	7.8	63.4	23.1	9.8
Sr	28.8	94.1	307.0	343.0	353.0	287.0	58.4	234.0	276.0	334.0	157.0	228.0	296.0
Y	15.4	31.9	47.1	14.8	19.3	23.1	24.5	25.7	18.5	21.7	19.2	23.8	22.7
Zr	90.3	173.0	212.0	78.5	83.6	57.5	94.4	121.0	65.7	99.6	54.5	67.2	79.1
Nb	3.5	5.4	6.4	2.6	3.0	2.7	3.1	4.2	2.4	3.5	2.4	3.4	3.5
Ba	782.0	67.0	502.0	90.5	192.0	121.0	258.0	210.0	88.3	179.0	253.0	93.6	72.3
La	8.7	14.0	19.7	10.1	8.2	3.9	6.7	8.9	2.5	7.8	1.2	1.7	1.5
Ce	16.8	28.0	50.8	26.2	22.4	15.1	18.8	24.5	13.0	30.3	10.6	14.2	16.4
Pb	30.6	8.8	12.0	9.5	10.7	3.2	4.4	11.9	6.8	6.9	3.5	3.6	5.3
Th	3.1	8.2	10.5	2.7	1.9	0.4	1.5	4.5	1.4	3.5	0.0	0.7	0.9
U	0.0	2.1	2.4	2.0	2.1	0.7	1.6	1.3	1.5	1.7	2.0	0.2	2.5

* Tuff = andesitic, andesite = lava.

Table 9.4.Representative water, CO_2, S contents, particle density and porosity of altered rocks.

Sample no.	Water (wt.%)[(i)]		CO_2[(ii)] (wt.%)	S[(iii)] ($g.100g^{-1}$)	Particle Density ($g.cm^{-3}$)	Porosity (%)
	H_2O	LOI				
Unaltered*	0.62-1.21	0.27-0.86	n.d	<0.01	2.67-2.74	1-3
S1-1838	4.49	9.64	0.9	0.63	2.74	8.2
S1-3355	0.72	11.33	0.1	3.04	2.53	3.3
S1-4259	0.82	4.12	n.d	2.68	2.79	5.8
S3B-2025	4.37	6.10	0.4	0.18	2.60	14
S3A-3280	0.76	2.49	n.d	0.02	2.68	3.5
S3B-5821	0.36	2.88	n.d	0.05	2.84	5.6
S5-2915	1.66	10.21	n.d	4.47	2.44	6.7
S5-6353**	0.50	6.16	0.2	6.16	1.54	-
S5-7355	0.22	1.01	0.3	0.12	2.84	1.7
S2-3141	1.44	1.95	0.6	0.03	2.70	11.2
S2-4087	1.50	6.80	3.4	0.03	2.66	7.5
S6-2991	3.07	10.21	2.1	0.07	2.64	3.9
S6-6359	0.56	5.12	2.7	0.08	2.73	2.1

(i) H_2O is surface water and was measured from the loss of weight for 110°C overnight heating. LOI is bonded water and was measured from the weight loss after ignition to 950°C

(ii) CO_2 was measured using colorimetry/titration; n.d, not determined.

(iii) After mass transfer calculation.

* Range in value of the unaltered andesites from 70, 161, 180, 397 and 637 m depth of well DRJ 1.

** Density was measured using a picnometer, so porosity cannot be determined.

The altered rocks from well DRJ S-1 and S-5 mostly have low adsorbed surface water, i.e. less than 1 wt.%, except those between 500 and 900 m depth, where H_2O ranges up to 4 wt.% (Figures 9.3 and 9.4). Bonded structure water (LOI) is mostly between 1 and 7 wt.% but it can be up to 15 wt.%. The amounts of S and CO_2 vary up to 6 $g.100g^{-1}$ and 5 wt.% respectively. The particle densities of the altered rocks in wells DRJ S-1 and S-5 varies from 2.34 to 2.84 $g.cm^{-3}$, almost similar to the density of the unaltered rocks.

However, samples from 838 and 1938 m depth in DRJ S-5, i.e. S5-2749 and S5-6353 respectively, have very low particle densities, i.e. about 1.50 $g.cm^{-3}$. The porosities of the altered rocks vary from 1 to 7%, except at about 550 m depth in DRJ S-1, where the porosity can exceed 50%.

Well DRJ S-3 altered rocks contain 19 to 28 $g.100g^{-1}$ Si (Figure 9.5). The amount of Ca ranges between 4 and 5 $g.100g^{-1}$ and the Na and K contents are about 2 and up to 1 $g.100g^{-1}$ respectively. Between 1770 and 1950 m depth, Ca reaches 7.4 $g.100g^{-1}$.

Figure 9.5 also shows that the Fe and Mg contents mostly vary about 5 and 2 $g.100g^{-1}$ respectively, except between 1350 and 1950 m depth, where the rocks contain up to 8.7 $g.100g^{-1}$ Fe and 3.5 $g.100g^{-1}$ Mg. Below 1775 m, the amount of Fe^{2+} is slightly higher than Fe^{3+}, i.e. about 4 and up to 3.4 wt.% respectively. Above that depth, the Fe^{2+} is between 1 and 4 wt.% and the Fe^{3+} is mostly higher and varies from 3 to 6 wt.%.

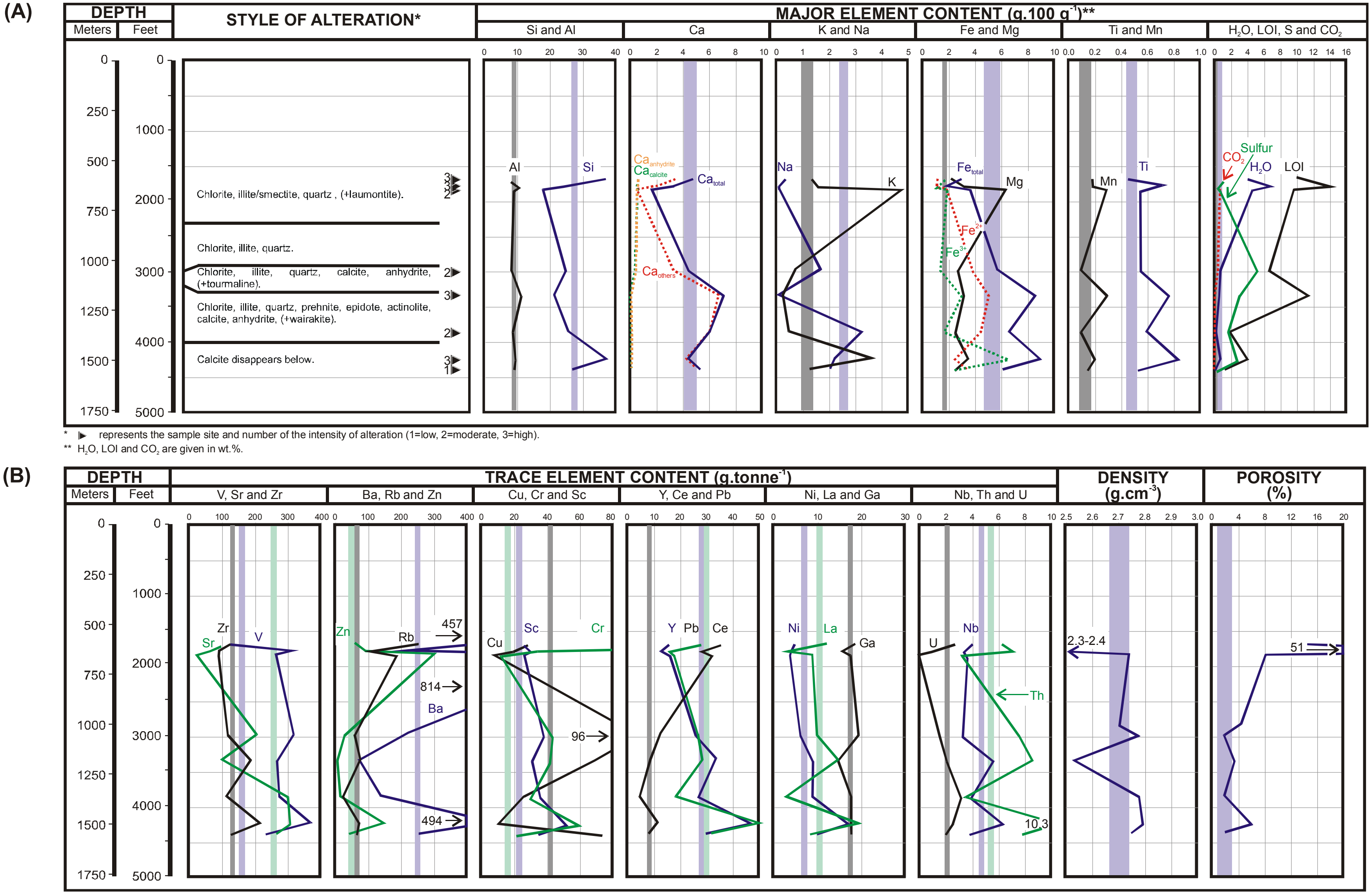

* ▶ represents the sample site and number of the intensity of alteration (1=low, 2=moderate, 3=high).

** H_2O, LOI and CO_2 are given in wt.%.

Figure 9.3. Variations in chemical compositions and densities of altered rocks from well DRJ S-1. **(A)** Major elements. **(B)** Trace elements, particle density and porosity. The style and intensity of alteration from petrography are also given. Background lines represent the average values of each element in unaltered rocks.

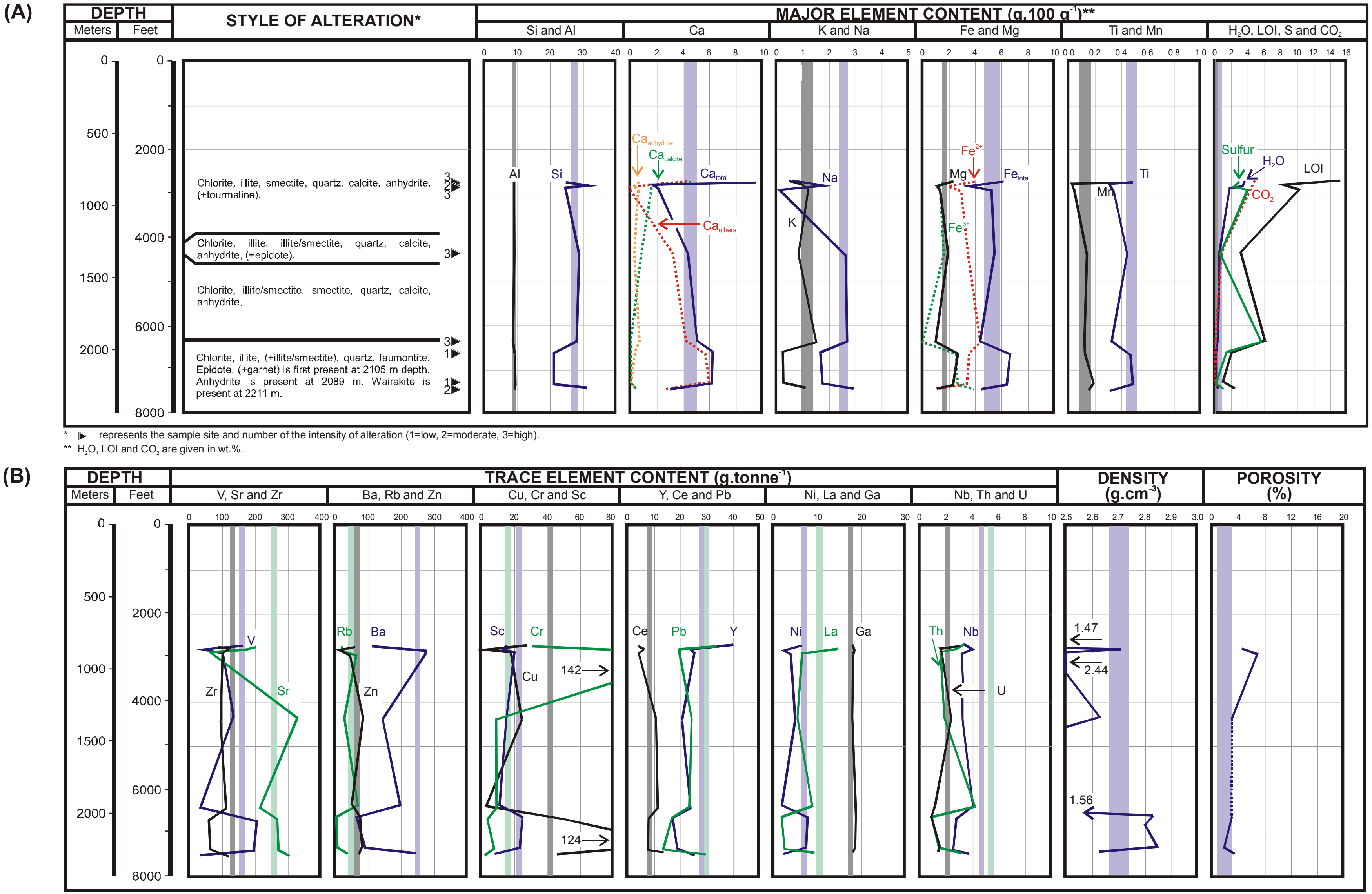

Figure 9.4. Variations in chemical composition and density of altered rocks from well DRJ S-5 with respect to depth. **(A)** Major elements. **(B)** Trace elements, particle density and porosity. The style and intensity of alterations from petrography are also given. Background lines represent the average value of the element in unaltered rocks. Some density values were obtained using picnometer and, hence, have no porosity values.

Most trace elements in cores from well DRJ S-3 are depleted, compared to the unaltered rocks from DRJ 1. This includes Zr, Ba, Rb, Pb and Th, however, Ni, V and Cr have increased but Zn and U have remained constant (Figure 9.5).

Figure 9.5 shows that the amount of water present is up to 0.8 wt.% for the absorbed surface water (H_2O) and less than 4 wt.% for the bonded structure water (LOI). At about 620 m depth, the water contents are about 4 and 6 wt.% for H_2O and LOI respectively. Unlike in other wells, the variations in LOI present in the altered rocks from well DRJ S-3 are not identical to changes in the amounts of S and CO_2. Sulfur is up to 0.3 $g.100g^{-1}$ and the CO_2 is less than 2 wt.%. The particle densities of the altered rocks from DRJ S-3 vary at about 2.7 $g.cm^{-3}$ and porosities vary between 2 and 6%, except at 617, 1351 and 2227 m depth, where it exceeds 10%.

Marginal area. The altered rocks from wells DRJ S-2 and S-6 contain 20-26 $g.100g^{-1}$ Si and are characterised by high amounts of Fe and Ca, which vary from 6.0-8.4 and 4.7-7.7 $g.100g^{-1}$ respectively (Figure 9.6). The amount of Fe^{2+} is about 3 wt.% and Fe^{3+} ranges from 3 to 5.5 wt.%. Figure 9.6 also shows that the Mg contents vary to about 2.5 $g.100g^{-1}$. However, at 1482 m depth in DRJ S-2 and 1730 m in DRJ S-6, Mg reaches 4.7 and 1.7 $g.100g^{-1}$ respectively. In addition, compared to the unaltered rocks from well DRJ 1, the altered rocks in the marginal area show no difference in their Mn contents, but have had a slight increase in Ti.

The amount of Na varies between 1.7 and 2.7 $g.100g^{-1}$ and that of K is up to 1 $g.100g^{-1}$. However, at 1247 m depth in DRJ S-2, the Na content is very low, i.e. 0.9 $g.100g^{-1}$, with its corresponding K content of about 2 $g.100g^{-1}$ (Figure 9.6).The amounts of Cu and Ba vary widely in the marginal wells. The other trace elements tend to decrease with alteration intensity, except V, Cr, Sc and Ni.

In the marginal wells, water is up to 1.5 wt.% adsorbed and 7 wt.% bonded but above 910 m, both may be more than 3 and 10 wt.% respectively. The CO_2 contents range from 0.5 to 3.5 wt.% and S is very low, i.e. up to 0.01 $g.100g^{-1}$ only. The particle densities of the altered rocks are about 2.7 $g.cm^{-3}$ and porosity varies from 2 to 4%, but between 958 and 1251 m depth they range from 7 to 12%.

9.3. MASS EXCHANGES

Knowledge of the compositions of the reservoir rocks before they interacted with thermal fluids allows the extent of mass transfer between fluids and rocks to be quantified. This follows the Gresens method (Gresens, 1967).

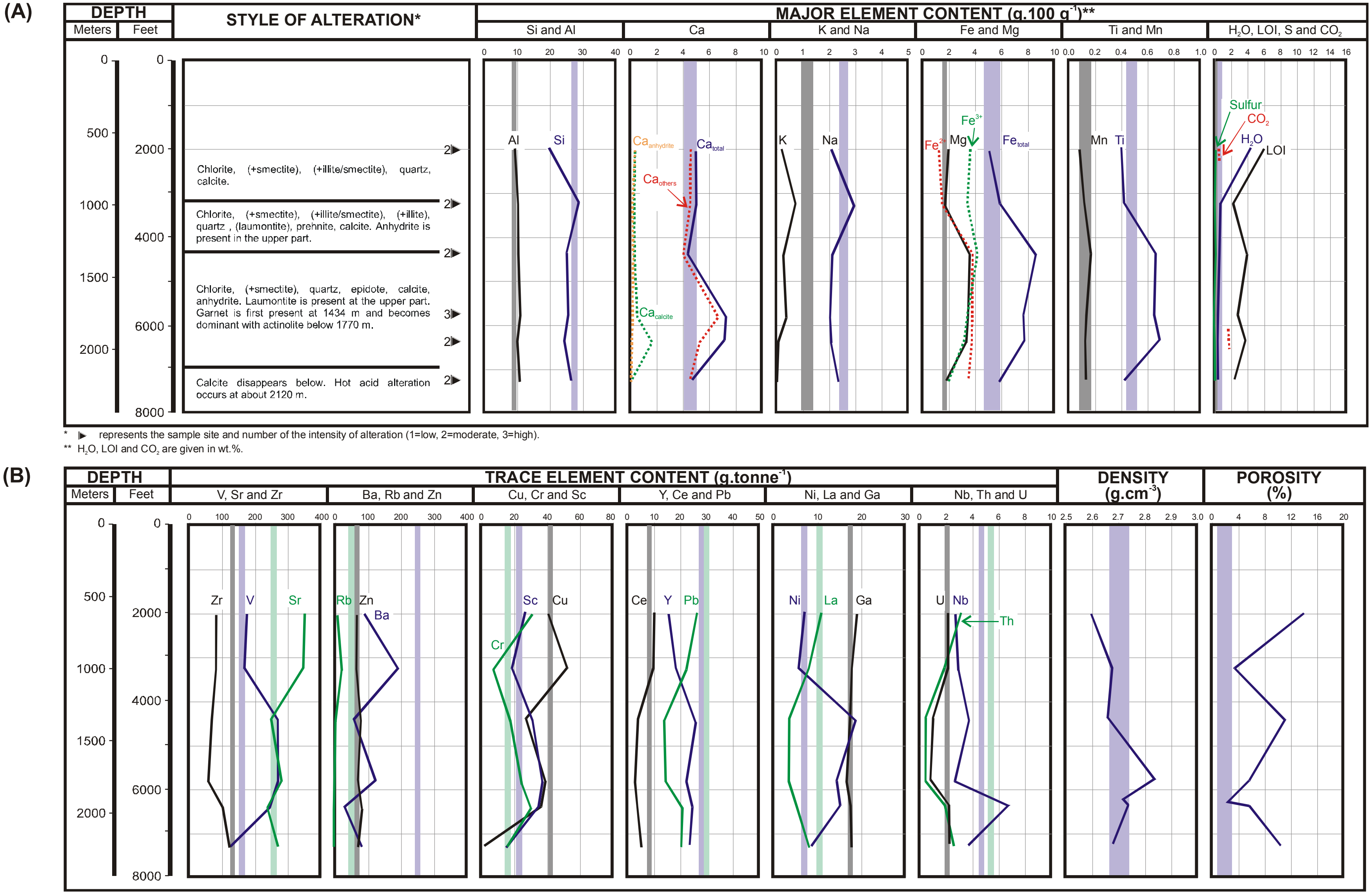

Chlorite, (+smectite), (+illite/smectite), quartz, calcite.

Chlorite, (+smectite), (+illite/smectite), (+illite), quartz , (laumontite), prehnite, calcite. Anhydrite is present in the upper part.

Chlorite, (+smectite), quartz, epidote, calcite, anhydrite. Laumontite is present at the upper part. Garnet is first present at 1434 m and becomes dominant with actinolite below 1770 m.

Calcite disappears below. Hot acid alteration occurs at about 2120 m.

* ▶ represents the sample site and number of the intensity of alteration (1=low, 2=moderate, 3=high).

** H_2O, LOI and CO_2 are given in wt.%.

Figure 9.5. Variations in chemical compositions and densities of altered rocks from well DRJ S-3. **(A)** Major elements. **(B)** Trace elements, particle density and porosity. The style and intensity of alterations from petrography are also given. Background lines represent the average value of the element in the unaltered rocks. At about 2120 m depth, an acid alteration occurs; it is described separately in detail later.

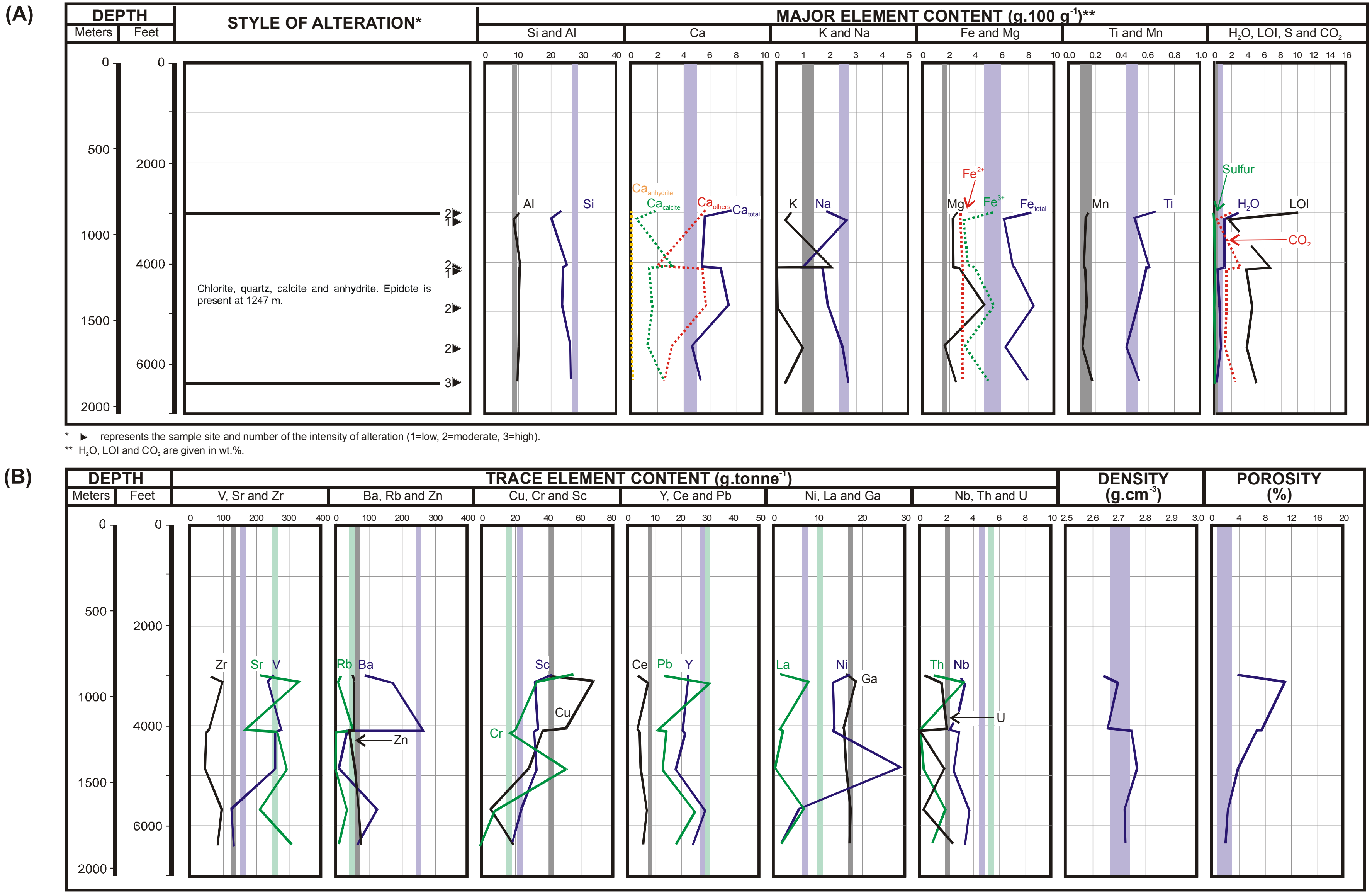

* ▶ represents the sample site and number of the intensity of alteration (1=low, 2=moderate, 3=high).

** H_2O, LOI and CO_2 are given in wt.%.

Figure 9.6. Variations in chemical compositions and densities of altered rocks from margin, compiled from wells DRJ S-2 and S-6. **(A)** Major elements. **(B)** Trace elements, particle density and porosity. The style and intensity of alteration from petrography are also given. Background lines represent the average value of the element in the unaltered rocks.

Figure 9.7 shows the proportions of the Al, Fe, Ca and the alkali contents of the altered compared to the unaltered rocks. Figures 9.8 to 9.11 show the variations in the mass exchanges of major elements and Figure 9.12 the variations in the mass exchange of Si and Ca compared to their water contents. The figures suggest that the intensity of alteration has little effect on changes in chemical composition, but the mass exchange is consistent with the hydrothermal minerals present. Certainly, the different types of fluids that have interacted with rocks will cause different styles of alteration and hence different elements will exchange.

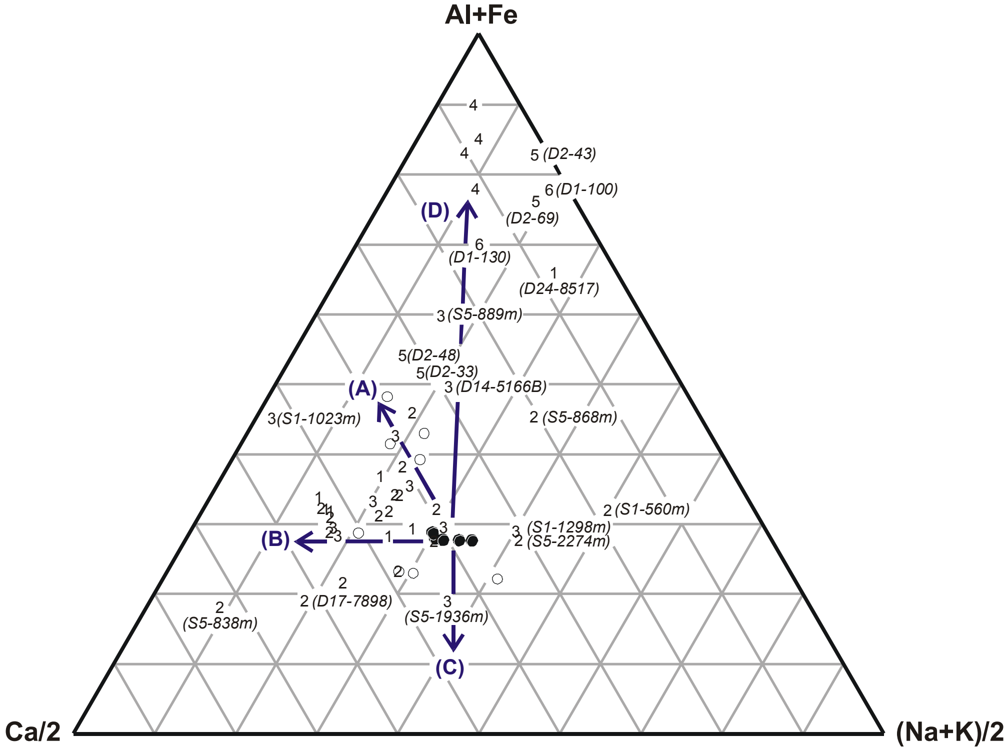

Figure 9.7. Variations in the amounts of Al+Fe, Ca and Na+K in the altered rocks, compared to the unaltered (●) and least altered rocks (○) from well DRJ 1. Numbers represent the intensity of alteration, where 1=low; 2=moderate; 3=intense; 4 represents hot acid alteration of rocks from well DRJ S-3; 5 is acid altered cores from DRJ 2; 6 represents vapour attacked cores from well DRJ 1. Values are after mass exchange. Interactions between waters and rocks likely follows 4 trends; their interactions with neutral pH water will cause the rocks to: (A) gain Al+Fe, lose Na+K, but with no change in Ca, where chlorite occurs; (B) gain Ca, loss of Na+K but constant Al+Fe when calc-silicate minerals are present; (C) less commonly gain of Ca, Na+K, but loss of Al+Fe, as smectite is present. Interactions with acid water will enrich rocks in Al+Fe but Ca, Na+K will be depleted (trend D), due to dissolution of plagioclase.

Si-Mg-Fe. Although quartz is the most common hydrothermal mineral, the rocks tend to lose Si during alteration. Figure 9.8 shows a relationship between mass exchanges of Si, Mg and Fe. It shows that the altered rocks mostly gain Mg and Fe, as Si is depleted due to the formation of chlorite and calc-silicate minerals, e.g. epidote and actinolite. However, Fe and Mg decrease with an increase in Si from smectite and illite.

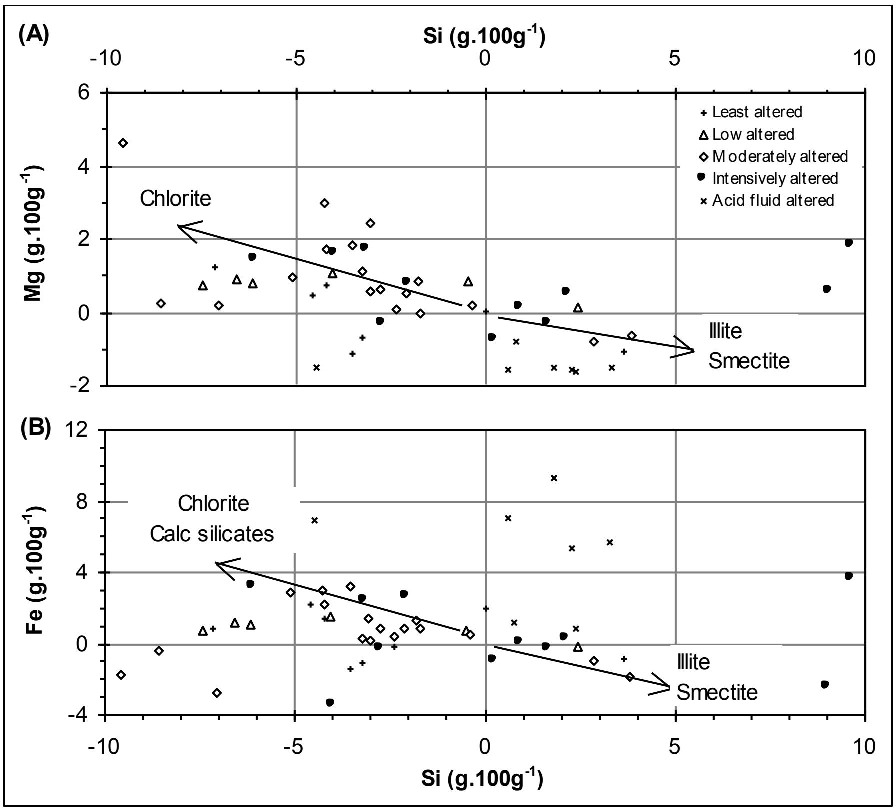

Figure 9.8. Relationship between mass exchanges of Si and: **(A)** Mg and **(B)** Fe. The occurrence of chlorite and calc-silicates gains Mg and Fe, but decreases Si. In contrast, the formation of illite and smectite reduces Mg and Fe to the altered rock but increases Si. Different symbols show different intensities of alteration.

Fe-Mg-Mn-Ti. Figure 9.9 shows the variations in mass exchange of the ferromagnesian minerals. The change in Fe contents in the altered rocks mirrors changes in Ti and Mg; Mg behaves in an identical way to Mn. The amount of Fe tends to increase with respect to depth and generally Fe^{2+} is higher than Fe^{3+}. This is because most Fe is accommodated in chlorite, actinolite and pyrite as Fe^{2+}. Siderite is also responsible for Fe^{2+} exceeding Fe^{3+} in the marginal area. Where smectite and illite are present, oxidation increases the amount of Fe^{3+} above Fe^{2+} (e.g. above 1200 m in well DRJ S-1 and at about 2300 m depth in well DRJ S-5). Figure 9.9 also shows that the altered rocks can lose Fe but gain either Mg (e.g. about 550 m depth in well DRJ S-1) or Mn (e.g. in the least altered rocks from well DRJ 1). This is probably reflected in the different compositions of chlorite (see Chapter 7).

Si-Ca-K-Na. Figure 9.10 shows that the formation of calc-silicates can cause the rocks to lose Si, but gain Ca and decrease K and Na. In places, K and Na will slightly increase where illite and smectite respectively form, e.g. at about 900 m depth in DRJ S-5, where illite is present, and at about 520 m in DRJ S-1, where Na-bearing smectite occurs (see Chapter 7). The occurrence of clay minerals will also increase the amounts of Si and bonded water in the altered rock.

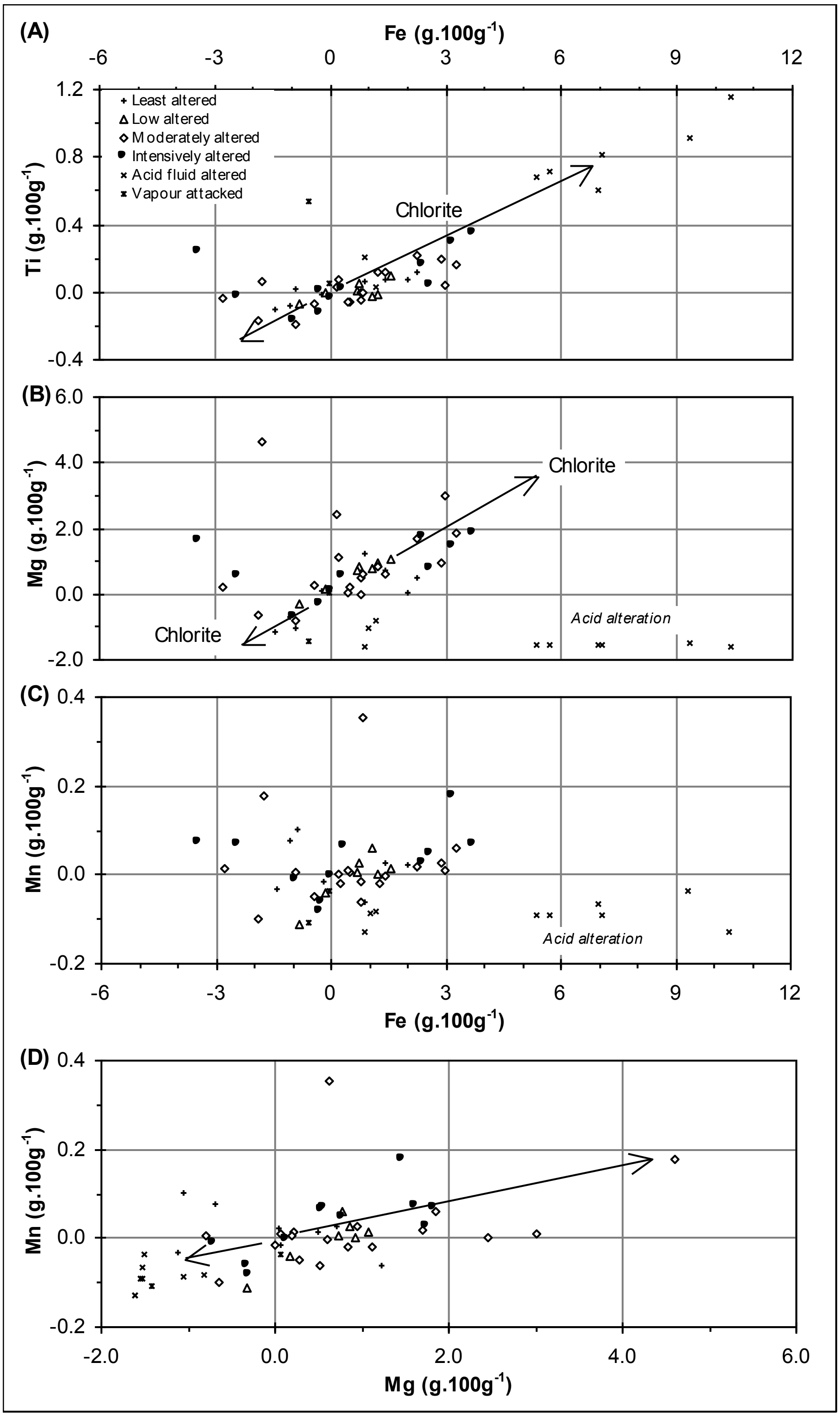

Figure 9.9. Mass exchanges between Fe and: **(A)** Ti, **(B)** Mg, **(C)** Mn and **(D)** between Mg and Mn. The trend of Fe change during alteration is identical to those of Ti and Mg; the change in Mg is likely due to variations in the compositions of chlorite. Different symbols represent different intensities of alteration.

In deeper parts, e.g. about 1300 m in DRJ S-1 and 2300 m in DRJ S-5, K and Na increase without additional water in the altered rocks due to the occurrence of adularia and albite (Figure 9.12). Silica is likely also added during the formation of secondary K feldspar.

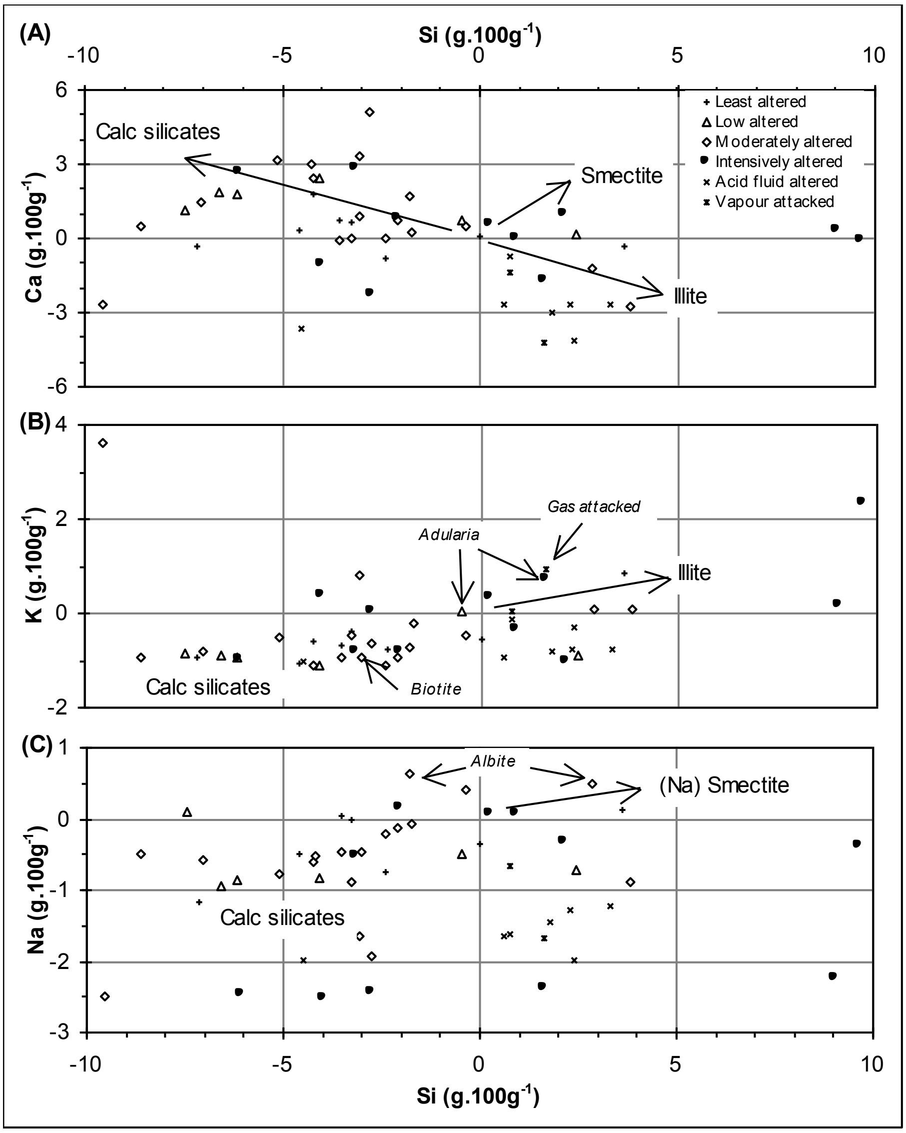

Figure 9.10. Relationship between mass exchanges of Si and: **(A)** Ca, **(B)** K and **(C)** Na with different intensities of alteration. The altered rocks tend to increase in Ca but decrease in Si, where calc-silicate minerals are present; this is accompanied by decreases in K and Na. Formation of illite and smectite is responsible for increases in K, Na and Si. Adularia, biotite and albite also affect Na and K, however, biotite does not obviously increase in K, because calc silicates are more dominant.

Ca-Fe-Mg. Figure 9.11 shows variations in mass exchange of Ca and Fe in the altered rocks. Formation of illite and smectite will cause an apparent Fe loss from the rocks. This will be followed by removal of Ca when illite forms but a slightly gain in Ca, when smectite is present. Most of the altered rocks have gained Ca and Fe as a result of calc-silicate formation. Magnesium behaviour will be associated with Fe. However, where chlorite is present, Mg tends to have increased, but Ca is likely immobile.

As shown in Figure 9.7, the gain of Ca during alteration corresponds to an increase in Al+Fe. This suggests that the occurrence of calc-silicate minerals, e.g. epidote and actinolite, has more effect on increasing Ca than calcite and anhydrite. In fact, calcite and anhydrite only increase Ca by up to 2 and 1 $g.100g^{-1}$ respectively. This obviously depends on the abundances of calcite and anhydrite. In the marginal area and at about 850 m depth in well DRJ S-5, calcite is responsible for a gain of between 3 and 5 $g.100g^{-1}$ Ca. However, addition of CO_2 and SO_4^{2-} are required to form calcite and anhydrite respectively and the abundances of calcite and anhydrite seem to decrease with depth.

9.4. WATER CHEMISTRY

As described in Chapter 3, the deep waters at Darajat are a near neutral pH, Na rich, bicarbonate-sulfate-chloride type (e.g. Amoseas Indonesia 1989a). Figure 9.13 shows that the waters were probably originally Mg rich as samples from well DRJ 1 contain about 5 $mg.kg^{-1}$ Mg. As the waters tended to be equilibrated with the reservoir rocks, the amounts of Ca in them increased from less than 25 to up to 50 $mg.kg^{-1}$, followed or accompanied by a decrease in Mg content of less than 1.6 $mg.kg^{-1}$. This had little effect on Na and K (Figure 9.13).

Water-rock equilibriation likely occurred in a rock dominated system (Giggenbach, 1988); dissolution of primary Ca-bearing minerals, e.g. plagioclase, increases the activity of Ca in the fluid, but precipitation of Mg minerals, e.g. chlorite, reduces the activity of Mg. This may explain the common replacement of plagioclase by chlorite.

The deep water from well DRJ S-1 is affected by oxidation of dissolved H_2S. It is SO_4^{2-} water with a pH of about 3.5 (Chapter 3). It contains less than 4 $mg.kg^{-1}$ Na, 2 $mg.kg^{-1}$ K, 7 $mg.kg^{-1}$Ca and 2 $mg.kg^{-1}$ Mg. Figure 9.13 shows that the deep water is far from equilibrium with the rocks, as the activity of Ca and Na decreases due to the formation of Ca- and Na-bearing minerals, e.g. calc-silicates, calcite and albite. The increase in Mg might be due to dissolution of Mg-bearing minerals, e.g. chlorite, or mixing of ascending thermal fluids with Mg-rich surface water.

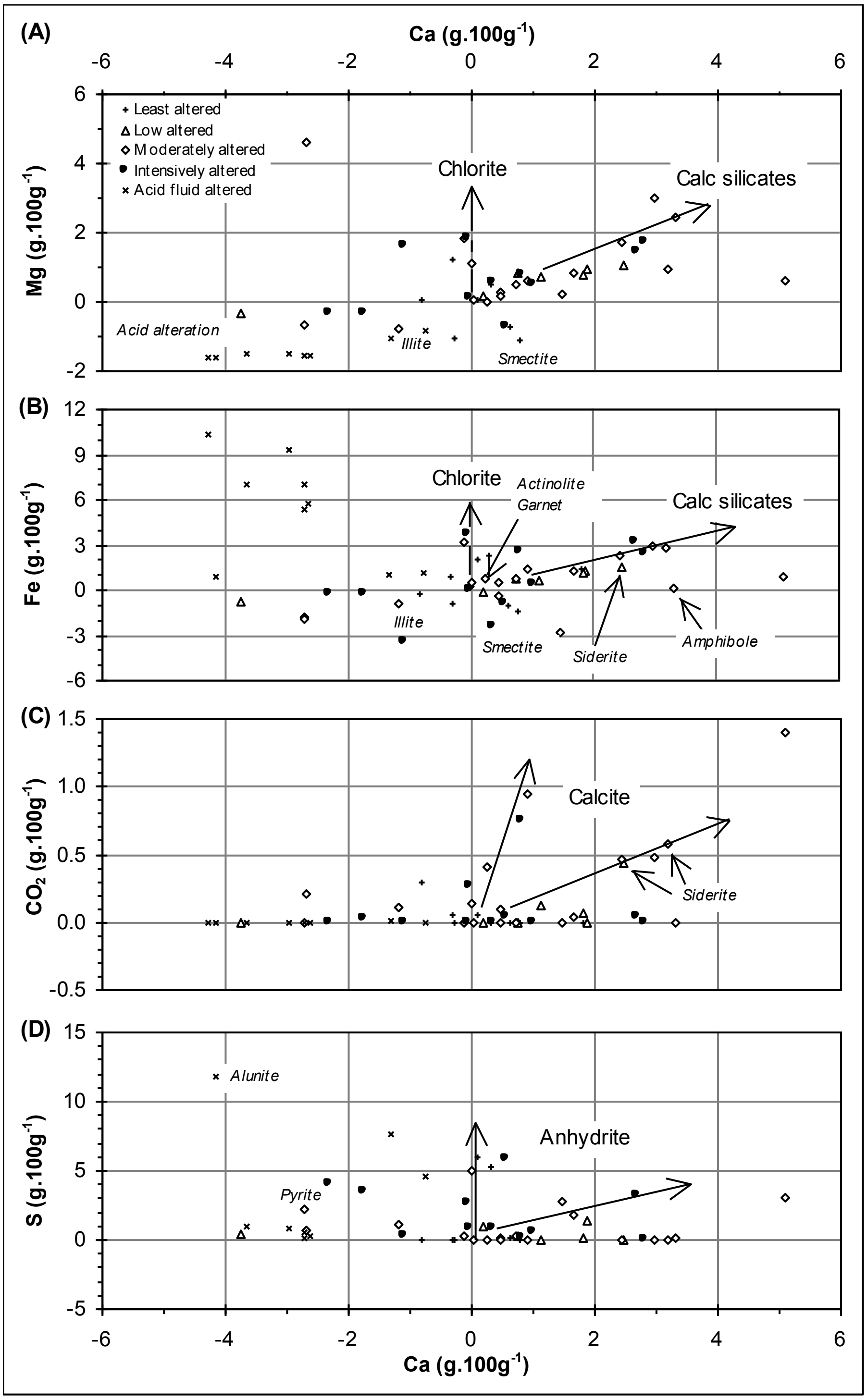

Figure 9.11. Mass exchanges of Ca and:**(A)** Mg, **(B)** Fe, **(C)** CO_2 and **(D)** S during alteration. The occurrence of calc-silicate minerals increased the amount of Ca, Fe and Mg in the altered rocks. Calcite and anhydrite are responsible for the positive correlation between Ca and CO_2 and S. Note that CO_2 and S always increase during alteration; S gains with a decrease in Ca, as it is present in pyrite and alunite. Mass exchange due to formation of siderite is also indicated. Intensity of alteration is shown in Figure (A).

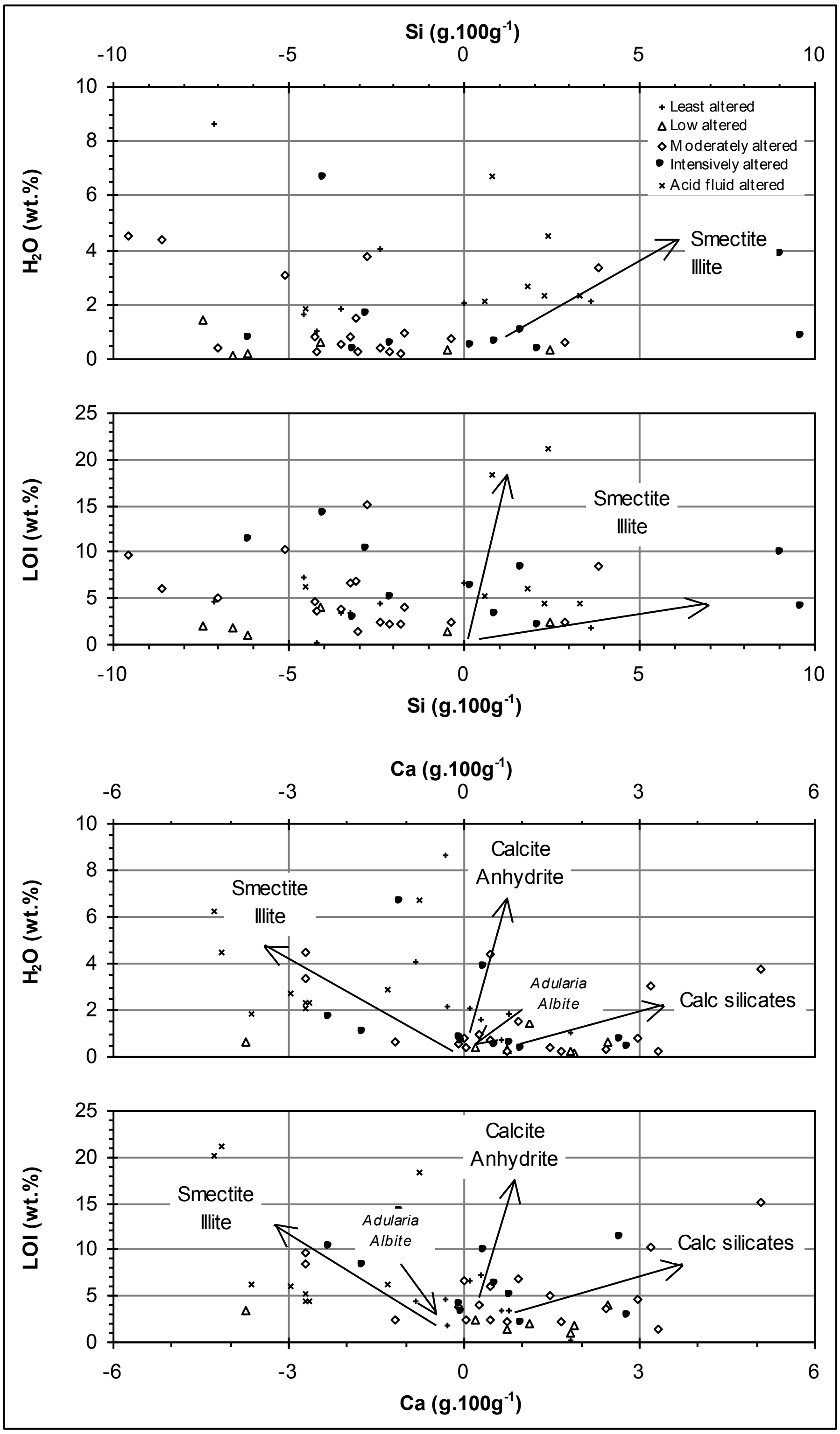

Figure 9.12. Relationships between water contents and mass exchanges of Si and Ca: **(A)** Si and H_2O, **(B)** Si and LOI, **(C)** Ca and H_2O, and **(D)** Ca and LOI. The absorbed surface water (H_2O) was measured from the weight loss of samples after heating to 110°C and the LOI (bonded surface water) is taken as identical to the weight loss after heating to 950°C. Different symbols represent different intensities of alteration.

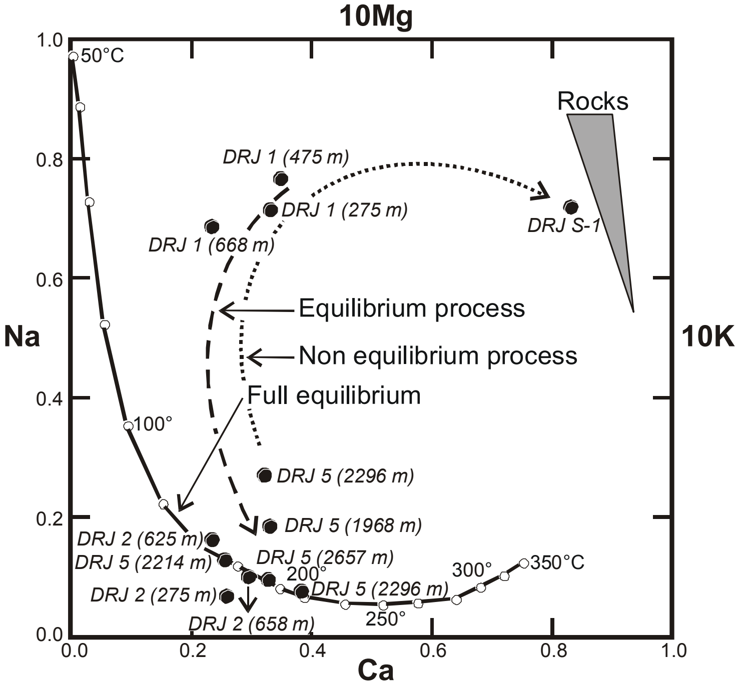

Figure 9.13. Quaternary diagram showing the proportions of Mg, Na, K and Ca in the downhole waters. The depths where the downhole water samples were collected are given. Data from Amoseas Indonesia Inc. (1989a) and the diagram follows Giggenbach (1988). As the deep waters e.g. of a composition like that from well DRJ 1 to DRJ 2 and 5) become fully equilibrated, the amount of Mg in the rock will decrease but the Ca content increase. This process has little effect on Na and K. Steam condensate may change the composition of the deep water from that in well DRJ S-1 (taken on 1998; Amoseas Indonesia Inc., written com., 1999). This creates a non equilibrium process, increasing the amounts of K and Mg, and decreasing Ca and Na in the rock which no longer dominates, but rather fluid does.

Figure 9.14 plots the activity ratios of individual Na, K, Mg and Ca. It indicates that the deep water was equilibrated with albite, Fe chlorite and calc- silicates, i.e. wairakite and epidote. At higher temperatures, garnet and actinolite could occur and at lower temperature, laumontite may be present rather than wairakite, if CO_2 is low or absent.

Boiling causes steam separation in the deep water. Figure 9.14 shows that the separated water still lies in the stability fields of albite, Fe chlorite and calc-silicates, as the composition of the separated water is similar to that of the downhole water (Chapter 3). However, during the dry steam discharge, the residual (separated) water becomes sufficiently acid and enters the stability field of kaolinite (Figure 9.14). The amounts of dissolved CO_2 in the deep and separated waters (X_{CO_2}) are less than 400 mg.kg^{-1} (up to 0.02 mol.%, Chapter 3). Therefore, calcite is rare and epidote and wairakite dominate. The ratio of H_2S to CO_2gas in the deep water is 0.02 (Chapter 3) and indicates reducing conditions (Giggenbach, 1993).

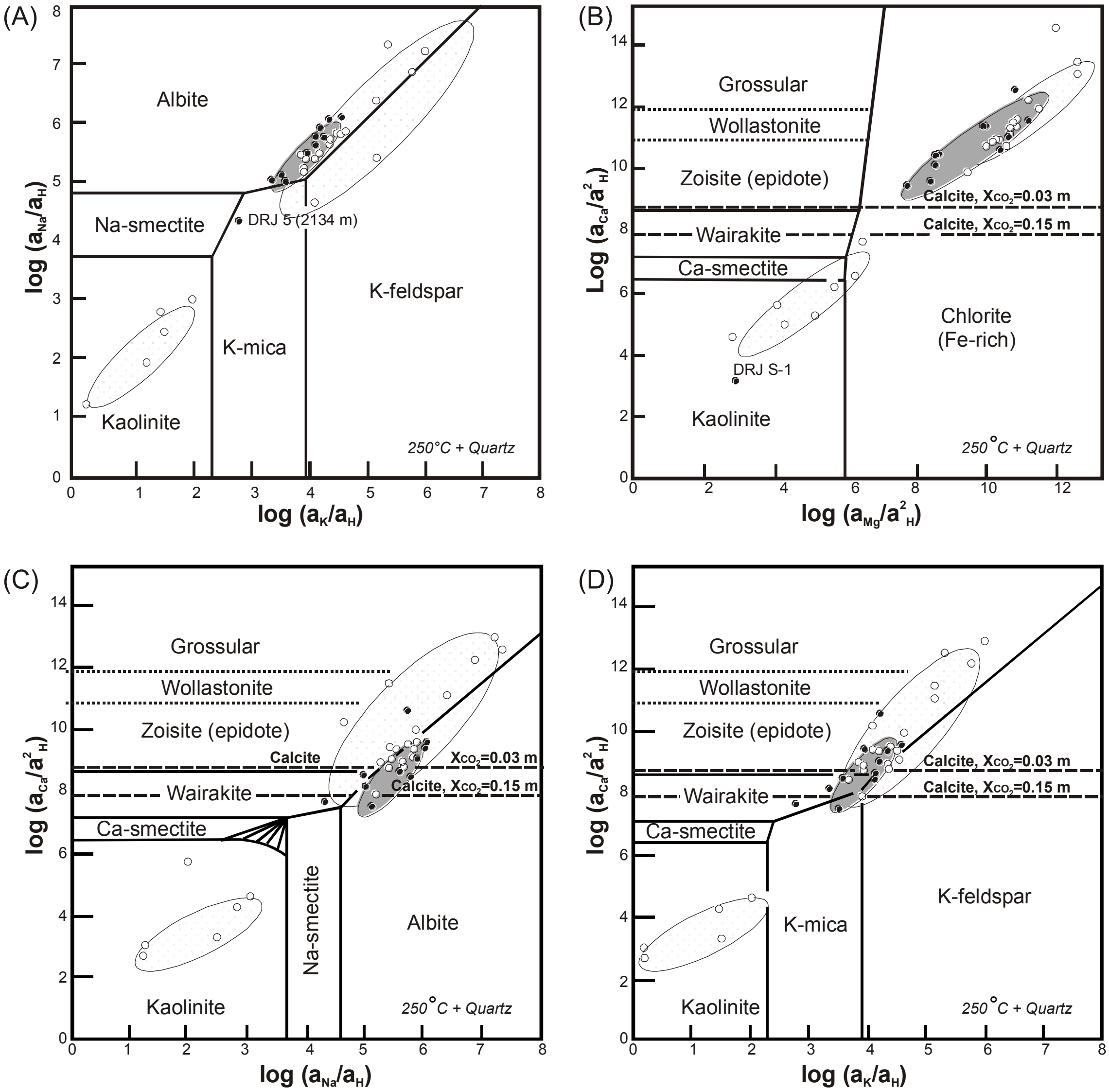

Figure 9.14. Activity diagrams for: **(A)** Na_2O-K_2O-Al_2O_3-SiO_2-H_2O, **(B)** CaO-MgO-Al_2O_3-SiO_2-$H_2O\pm CO_2$, **(C)** CaO-Na_2O-Al_2O_3-SiO_2-$H_2O\pm CO_2$ and **(D)** CaO-K_2O-Al_2O_3-SiO_2-$H_2O\pm CO_2$. Mineral phases are in equilibrium with an aqueous solution at 250°C and quartz saturation. Wollastonite and grossular are only present above 300°C. Calcite will be present depending on the amount of CO_2 dissolved in the fluids. Solid circle (●) and grey shaded area represent the deep waters and the hollow circle (○) and dotted area represents the separated waters during early discharge. Boiling changes the compositions of the deep and separated waters. Minerals presently in equilibrium with the deep and separated waters include albite, chlorite, wairakite and epidote. Below about 250°C laumontite occupies the domain of wairakite. However, the separated waters change slightly from wet to dry discharges and when dry, are in equilibrium with kaolinite. Dissolved CO_2 in the deep waters (X_{CO_2}) is less than 0.02 mol.% (about 0.01 m), so calcite is rare.

9.5. ALTERATION BY ACID WATERS

The occurrence of pyrophyllite at about 2120 m depth in well DRJ S-3 and alunite at 43 m depth in well DRJ 2 indicates that acid fluids have interacted with the surrounding rocks. The magnitude of mass exchanges of the wall rocks due to the interactions of this type of fluid were determined on

4 samples from 2118-2123 m depth in well DRJ S-3 and 4 samples, i.e. 1 core and 3 cutting samples, from 33-69 m in well DRJ 2.

9.5.1. Recognition of Immobile Elements in Acid Altered Rocks

Different type of fluids might cause alteration with different immobile elements (Appleyard, 1991). In acid altered rocks, Al is no longer an immobile element. Table 9.5 shows that the FV^0 values indicate up to 50% volume loss during alteration. The mobility of Al in acid pH waters has also been reported by Reyes (1990). The extent of mass exchange was determined by taking Zn and Pb to be immobile since they have FV^0 values from 0.8 to 1.4 (Table 9.5).

9.5.2. Rock Chemistry and Mass Exchange

Table 9.6 and Figure 9.15 represent the mass exchanges of the acid altered rocks, compared to the unaltered rocks from well DRJ 1. The chemical compositions, water contents and density values of the acid altered rocks are given in Table 9.7. The compositions of rocks from DRJ S-3 are also summarised in Figure 9.16 and compared with the surrounding rocks, which were altered by interaction with neutral pH waters.

Well DRJ S-3. Si was both gained and lost during alteration (Figures 9.15 and 9.16) but compared to the surrounding rocks, it increased (Figure 9.16). The rocks mostly also gained Al, which ranges from 16 to 23 $g.100g^{-1}$, more than in the surrounding rocks.

There were decreases of Ca and Na in the acid altered rocks; their contents are about 1.5 and 1 $g.100g^{-1}$ respectively (Figure 9.10). This indicates that plagioclase is altered as is consistent with petrography. Since calcite is absent and anhydrite can only provide up to 0.2 $g.100g^{-1}$Ca, the Ca and Na contents are hosted mainly in smectite. There is also a reduction of K, which is present below 0.5 $g.100g^{-1}$.

Iron and Ti tend to gain and Mg and Mn lost during acid alteration (Table 9.6 and Figure 9.9). The altered rocks contain 10-15 $g.100g^{-1}$ Fe, comprising 5-10 $g.100g^{-1}$ Fe^{2+} and 3-7 $g.100g^{-1}$ Fe^{3+}, and about 1.2 $g.100g^{-1}$ Ti. The Mg and Mn contents are low, i.e. less than 0.2 $g.100g^{-1}$ (Figure 9.16).

Hot acid altered rocks are likely depleted in Ca, Na and K, but are enriched in Al and Fe (Figure 9.7). There are slight decreases in Ca and Na+K and a sharp increase in Al+Fe in the acid altered rocks compared to the unaltered and less altered rocks. This may be due to dissolution of primary minerals, followed by the formation of Fe rich aluminium silicates, e.g. ferropyrophyllite (see Chapter 7).

Table 9.7 and Figure 9.16 show that the amounts of adsorbed surface water (H_2O) in the acid altered rocks is between 1.8 and 2.7 wt.% and that more bonded structure water (LOI) was adsorbed than H_2O, i.e. 4.5-6.5 wt.%. Compared to the unaltered rocks, the acid altered rocks are more hydrous (Figure 9.12). There was also a gain of S up to 1 g.100g^{-1} (Figures 9.11) that relate to the occurrence of pyrite.

Table 9.5. Zero change volume factors (FV^0) for the acid altered rocks from well DRJ S-3. The FV^0 above 1 suggests addition for the stated element, but below 1 represents depletion.

Altered Rocks	S3-6945	S3-6953	S3-6956	S3-6962	S3-6962
Depth (m)	2118	2121	2122	2123	2123
Compared to	D1-70	D1-161	D1-180	D1-397	D1-637
FV^0 for elements:					
Si	1.250	1.170	1.160	1.050	1.040
Ti	0.440	0.409	0.403	0.535	0.500
Al	0.508	0.545	0.545	0.632	0.640
Fe_{total}^{+3}	0.411	0.458	0.481	0.642	0.585
Mn	1.260	2.840	3.790	4.870	2.880
Mg	15.300	13.500	18.400	17.000	16.100
Ca	3.340	5.010	2.790	3.270	3.100
Na	2.790	4.350	3.200	2.510	2.500
K	4.760	8.530	6.060	2.820	2.730
P	1.180	1.760	0.668	2.190	2.040
S	0.015	0.020	0.020	0.108	0.087
Sc	0.40	0.45	0.49	0.77	0.75
V	0.54	0.50	0.46	0.67	0.65
Cr	0.61	0.51	0.89	0.57	0.62
Ni	0.49	0.43	0.51	0.32	0.29
Cu	28.60	0.63	2.29	11.80	10.80
Zn	1.28	0.80	1.07	1.46	1.37
Ga	0.54	0.51	0.55	0.64	0.68
Rb	5.18	8.51	6.28	2.36	2.65
Sr	2.71	4.49	3.16	2.22	2.58
Y	1.01	0.50	0.53	0.71	0.48
Zr	0.68	0.51	0.51	0.49	0.40
Nb	0.58	0.45	0.42	0.46	0.37
Ba	5.36	10.00	3.92	1.34	1.35
La	1.09	0.53	0.53	0.69	0.74
Ce	0.94	0.52	0.62	0.68	0.59
Pb	1.45	1.16	1.24	0.83	1.07
Th	0.91	0.60	0.66	0.61	0.58
U	0.99	0.47	0.58	0.61	0.88

Iron bearing minerals, e.g. pyrite and Fe rich pyrophyllite, cause a high particle density in the altered rocks, i.e. between 2.81-2.87 g.cm^{-3}. Their host rocks commonly have porosities less than 8%, except for a brecciated sample from 2118 m depth, which has a porosity of about 25% (Table 9.7 and Figure 9.16).

The mass exchange of trace elements of hot acid altered rocks is also given in Table 9.6. Compared to the unaltered rocks, there was gain of Sc, V, Ga, Y, Nb, La, Ce, Th and U. An increase in Cr and Ni might match the gain of Fe. The amounts of Sr, Rb and Ba in the acid altered rocks usually increase (e.g. Africano and Bernard, 2000; Cheynet et al., 2000), but at Darajat these elements decrease. These coincide with reductions of Ca, Na and K due to the dissolution of plagioclase by acid fluids (Aiuppa et al., 2000).

Table 9.6. Mass exchange of the acid altered rocks from wells DRJ S-3 and DRJ 2 compared with the unaltered rocks. Positive value is addition and negative value is depletion for the element.

Well	DRJ S-3				DRJ 2	
Depth (m)	2118	2121	2122	2123	33	43
Sample no.	S3-6945	S3-6953	S3-6956	S3-6962	D2-33	D2-43
Derived from	D1-70	D1-161	D1-180	D1-397	D1-70	D1-161
Elements ($g.100g^{-1}$ for major and $g.tonne^{-1}$ for trace elements)						
Si	2.77	-4.83	-0.27	1.53	-10.50	-2.24
Ti	1.01	0.62	0.83	0.57	-0.15	0.12
Al	15.30	6.97	10.20	7.06	-1.74	-6.53
Fe_{total}^{+3}	11.00	6.38	7.13	4.26	-0.50	-0.24
Mn	0.01	-0.12	-0.09	-0.12	-0.06	-0.19
Mg	-1.50	-1.68	-1.42	-1.57	-1.11	-1.79
Ca	-2.37	-3.48	-2.53	-3.33	-1.61	-4.23
Na	-1.21	-1.85	-1.57	-1.51	-1.79	-2.31
K	-1.01	-1.13	-1.08	-0.59	-0.75	-0.67
P	0.01	-0.03	0.04	-0.04	-0.03	0.01
S	0.89	0.95	0.56	0.09	2.93	7.17
Sc	47.5	24.7	28.9	12.0	1.4	-8.2
V	251.0	154.0	218.0	107.0	-26.9	-30.4
Cr	25.4	15.3	4.9	7.5	65.3	4.7
Ni	16.0	9.5	9.6	10.7	12.4	2.7
Cu	-53.7	15.7	-18.8	-39.8	-20.5	37.5
Zn	4.6	12.8	4.5	-16.2	-29.5	-54.9
Ga	26.0	15.1	19.5	13.4	-7.6	-9.0
Rb	-47.2	-49.1	-48.7	-18.6	-39.0	-53.6
Sr	-110.0	-186.0	-157.0	-134.0	-81.2	-58.9
Y	11.9	25.9	31.3	19.0	-18.8	-27.5
Zr	160.0	114.0	173.0	162.0	-75.6	-51.3
Nb	7.3	5.4	7.6	6.2	-2.7	-2.0
Ba	-200.0	-242.0	-184.0	-37.6	-133.0	-41.2
La	3.1	8.8	11.7	5.3	-5.1	0.7
Ce	17.6	26.8	26.6	15.2	-21.3	-5.4
Pb	-0.6	-1.5	-0.7	2.7	6.8	57.7
Th	3.4	3.1	4.8	2.9	-2.7	-0.3
U	0.9	2.4	2.2	1.3	-1.1	-1.0

Well DRJ 2. The Si and Al contents are mostly depleted (Figure 9.15). The Fe contents of the altered rocks are up to 6 $g.100g^{-1}$, which is mostly present as Fe^{2+}. Mg, Mn and Ti were lost during alteration (Figure 9.9) and are now present at less than 0.6 $g.100g^{-1}$.

Like the hot acid altered rocks from well DRJ S-3, the rocks here tend to have high Al+Fe but low Ca and Na+K values (Figure 9.7). There were losses of Ca, Na and K during alteration (Figure 9.10). The amounts are less than 1 $g.100g^{-1}$, but at 33 m depth, the Ca content is about 2.3 $g.100g^{-1}$. Plagioclase is dissolved by acid water, as indicated by the low Na contents of the altered rocks;

calcite is absent and anhydrite can provide Ca only up to 1 g.100g^{-1}, hence the remaining Ca is in smectite.

The altered rocks are hydrous and contain 2-7 wt.% H_2O and 6-22 wt.% LOI. Much sulfur has been added, between 2 and 8 g.100g^{-1}, and incorporated into alunite (Figure 9.11).

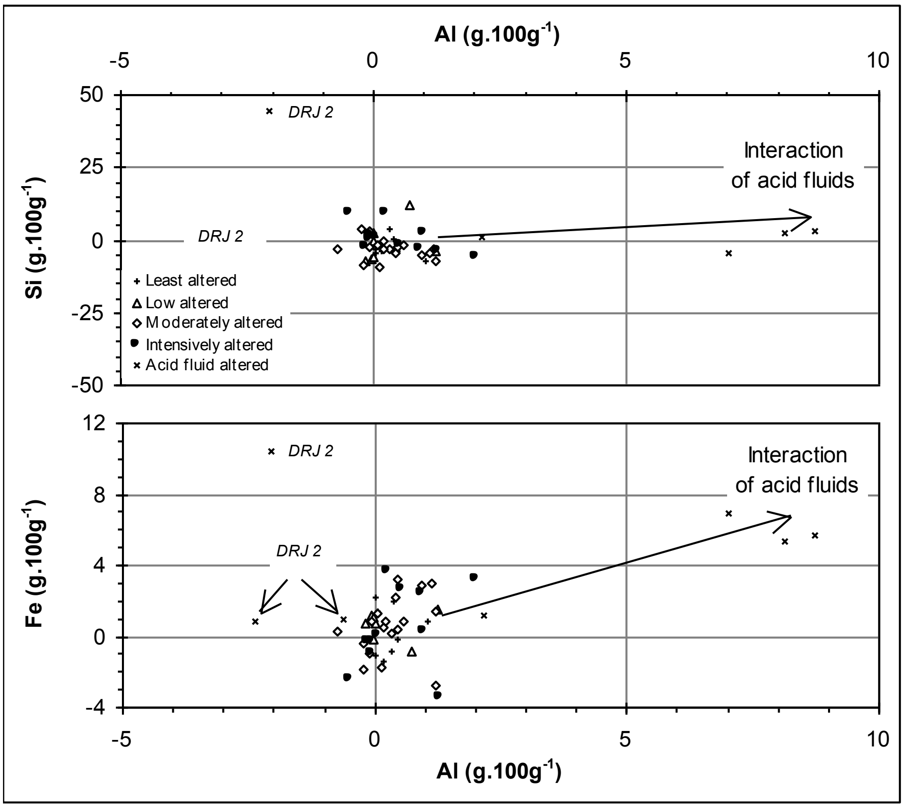

Figure 9.15. Mass exchanges of Al and: **(A)** Si and **(B)** Fe. Aluminium is immobile in the rocks with different intensities of alteration from interactions with neutral pH fluids, but tends to increase with increasing Fe and lesser in Si due to interactions with acid fluids, except for some samples from well DRJ 2. Gain of Fe is accompanied by an increase in Ti but decreases in Mg and Mn (Figure 9.9).

9.6. ALTERATION FROM VAPOUR

The style of alteration of cores from 100-130 m depth of well DRJ 1 indicates that the andesites here have been attacked by vapour (see Chapter 4). Mass exchange due to this alteration style was determined on 2 samples from well DRJ 1, i.e. D1-100 and D1-130, and calculated using immobile elements Al and Ga. Interaction between rocks and vapour was also assessed from studying 7 samples from below 1500 m the present production wells of DRJ 4, 5, 14, 17 and 24. These wells are located between well DRJ 1, where the unaltered rocks occur, and wells DRJ S-1 and S-5 (Chapter 3). Their mass exchanges and rock compositions are represented in Table 9.8.

__Above 200 m in well DRJ 1__, there is an enrichment of Si during alteration; Si is present at about 29 g.100g^{-1}. Table 9.8 shows that Ca and Na decrease below 2 g.100g^{-1}, as expected from the dissolution of plagioclase. Potassium is added (Figure 9.10) to an amount of 1-3 g.100g^{-1}. Iron, Mn and Mg were lost, whereas Ti slightly increased (Figure 9.9).

Table 9.7. Chemical composition, density and porosity of the acid altered rocks compared with the unaltered rocks.

Well	DRJ S-3				DRJ 2	
Depth (m)	2118	2121	2122	2123	33	43
Sample no.	S3-6945	S3-6953	S3-6956	S3-6962	D2-33[(i)]	D2-43
Derived from	D1-70	D1-161	D1-180	D1-397	D1-70	D1-161
Elements (g.100g^{-1} for major and g.tonne^{-1} for trace elements)						
Si	31.60	22.90	28.00	28.40	18.30	25.50
Ti	1.49	1.07	1.28	1.10	0.33	0.57
Al	24.40	16.00	19.40	16.50	7.35	2.54
Fe_{total}^{+3}	15.70	12.20	12.30	10.20	4.23	5.55
Mn	0.10	0.06	0.04	0.04	0.03	0.00
Mg	0.15	0.13	0.10	0.11	0.54	0.02
Ca	1.64	0.83	1.77	1.69	2.40	0.08
Na	1.17	0.53	0.88	1.19	0.59	0.07
K	0.41	0.14	0.25	0.38	0.67	0.60
P	0.08	0.03	0.09	0.04	0.04	0.06
Sc	67.5	46.3	50.5	40.1	21.4	13.5
V	413.0	319.0	363.0	271.0	136.0	135.0
Cr	45.6	32.4	21.8	15.4	85.5	21.9
Ni	25.0	17.1	17.2	15.1	21.4	10.3
Cu	2.7	45.3	18.9	4.1	35.9	67.1
Zn	75.7	76.4	63.4	49.9	41.6	8.7
Ga	42.9	32.2	37.4	31.7	9.4	8.1
Rb	16.9	6.3	10.9	16.4	25.1	1.7
Sr	112.0	50.8	89.4	133.0	141.0	178.0
Y	45.8	53.4	58.5	53.0	15.1	0.0
Zr	317.0	245.0	310.0	290.0	81.2	78.8
Nb	12.7	10.1	12.0	10.6	2.7	2.7
Ba	68.3	25.7	76.0	178.0	135.0	226.0
La	15.5	19.5	21.8	14.3	7.2	11.4
Ce	56.3	57.7	58.3	39.1	17.5	25.5
Pb	9.1	7.6	9.2	10.8	16.5	66.8
Th	10.1	8.1	11.4	6.6	4.1	4.8
U	3.1	4.8	4.4	2.9	1.2	1.3
H_2O (wt.%)	2.70	1.84	2.10	2.31	6.71	6.21
LOI (wt.%)	6.07	6.22	5.19	4.52	18.40	20.19
S (g.100g^{-1})	0.90	0.97	0.57	0.10	2.94	7.19
Particle Density (g.cm^{-3})	2.81	2.87	2.81	2.82	n.d	2.23
Porosity (%)	25	2-8	0-3	2-7	n.d	11

(i) Cutting sample. Particle density and porosity were not measured.

Most trace elements increased, e.g. V, Cr, Ba, Th and U. At 100 m depth in DRJ 1, where a core has been attacked mainly by gas, there is a major increase in Cu, Zn and Zr; by contrast, Sr is highly depleted here.

The altered rocks contain 2-4 wt.% absorbed water (H_2O) and about 7 wt.% bonded water (LOI). Sulfur was added and varies up to 2 g.100g^{-1}. As the gas attacked, primary minerals dissolved producing rocks with porosity ranging from 5 to 30%, depending upon the intensity of the alteration.

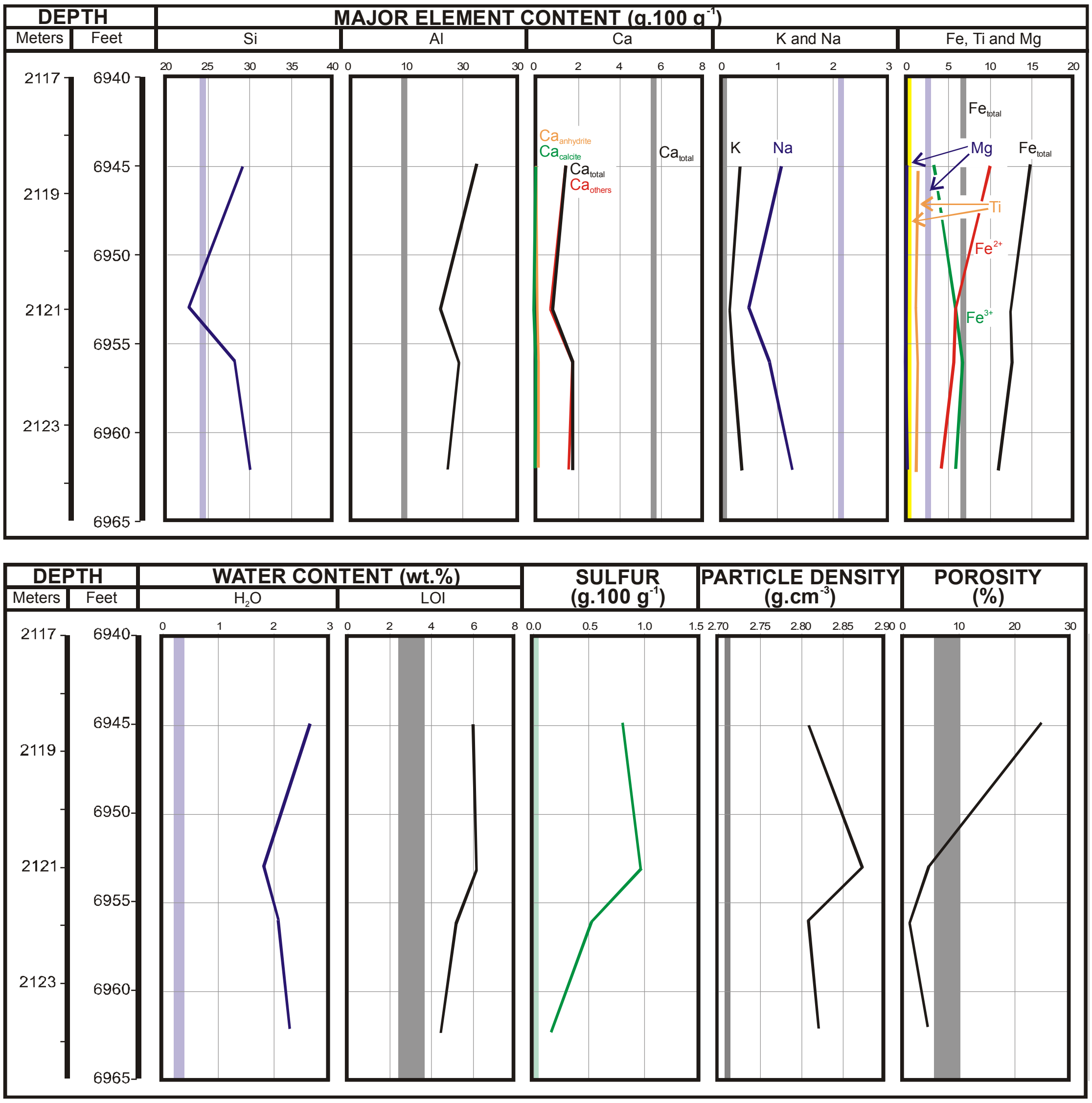

Figure 9.16. Variations in major elements, water and sulfur contents, particle density and porosity of hot acid altered rocks from well DRJ S-3. Background, shaded lines represent the range of compositions of the rocks from 2118 and 2227 m depth.

Below 1500 m present production area. Figure 9.17 shows the variations in major and trace elements in the altered rocks. During alteration, the rocks slightly gained Si. These mostly contain about 30 g.100g^{-1} Si, but at 2400-2600 m depth in well DRJ 5 and 17, Si varies between 20-25 g.100g^{-1}. There is also an increase in Ca due to the occurrence of calc silicates. Figure 9.17 also shows that Ca contents range from 4 to 8 g.100g^{-1} and the Na and K contents are about 2 and 0.3

g.100g^{-1} respectively. However, at 1575 m depth in well DRJ 14, the rock has gained K but lost Ca and Na with an increase in the intensity of alteration and the formation of illite.

Table 9.8. Mass exchange, chemical composition, density and porosity of rocks with gas or vapour attacked alteration compared with the unaltered rocks.

Well	DRJ 1				DRJ 4		DRJ 14	
Depth (m)	100		130		1501		1576	
Sample no.	D1-100		D1-130		D4-4922		D14-5166B	
Derived from	D1-70		D1-161		D1-161		D1-180	
Elements (g.100g^{-1} for major and g.tonne^{-1} for trace elements)	Mass exchange	Rock chemistry	Mass exchange	Rock chemistry	Mass exchange	Rock chemistry	Mass exchange	Rock chemistry
Si	-0.55	28.30	-0.21	27.50	-2.98	24.80	1.01	29.30
Ti	0.51	0.99	0.06	0.51	0.01	0.47	0.04	0.49
Al	-2.37	6.71	0.27	9.34	-0.17	8.90	-0.05	9.16
Fe_{total}^{+3}	-0.09	4.64	-0.62	5.17	0.20	5.98	-0.04	5.11
Mn	-0.07	0.02	-0.10	0.09	-0.12	0.07	-0.06	0.07
Mg	-1.42	0.23	-0.16	1.65	0.29	2.10	-0.19	1.33
Ca	-3.76	0.25	-1.31	3.00	0.72	5.03	-1.56	2.74
Na	-1.56	0.82	-0.58	1.80	-0.07	2.31	-2.31	0.15
K	0.64	2.06	-0.08	1.19	-1.05	0.22	0.55	1.88
P	-0.05	0.02	-0.01	0.05	0.00	0.06	0.04	0.09
Sc	-4.3	15.6	3.3	24.9	9.3	30.9	-1.3	20.4
V	53.6	216.0	5.8	171.0	39.6	205.0	-14.9	131.0
Cr	47.8	68.0	25.3	42.5	3.8	20.9	21.6	38.5
Ni	20.2	29.2	5.9	13.4	2.3	9.9	-4.9	2.8
Cu	104.0	160.0	11.0	40.6	-2.6	27.0	-9.3	28.5
Zn	91.7	163.0	1.0	64.6	-32.7	30.9	-10.3	48.5
Ga	6.0	22.9	-0.5	16.6	0.3	17.4	0.1	18.0
Rb	34.7	98.8	9.2	64.5	-48.2	7.1	13.2	72.8
Sr	-173.0	49.3	-60.2	177.0	22.9	260.0	-213.0	33.4
Y	-6.2	27.6	4.8	32.3	-4.1	23.4	7.6	34.8
Zr	78.8	236.0	0.9	131.0	-25.1	105.0	29.7	166.0
Nb	1.3	6.7	-0.8	3.9	-1.3	3.4	1.2	5.6
Ba	40.7	309.0	37.8	305.0	-187.0	80.2	116.0	376.0
La	1.4	13.8	2.3	12.9	-3.4	7.2	5.9	16.0
Ce	-13.4	25.3	6.8	37.7	-8.2	22.8	4.9	36.6
Pb	0.5	10.2	2.3	11.5	-2.4	6.8	-3.2	6.8
Th	3.9	10.6	1.4	6.4	-0.2	4.8	-1.8	4.8
U	1.8	4.1	0.8	3.1	-0.7	1.6	-0.3	2.0
H_2O (wt.%)	3.16		2.29		0.27		1.02	
LOI (wt.%)	7.41		6.72		2.26		8.29	
CO_2 (wt.%)*	n.d		n.d		n.d		0.1	
S (g.100g^{-1})	0.04		1.98		0.34		3.41	
Particle Density (g.cm^{-3})	1.80		2.55		2.80		2.66	
Porosity (%)	28		5		3		6	

* n.d = not determined.

Total Fe is about 5.6 g.100g^{-1}, consisting of 2 and 4 g.100g^{-1} Fe^{2+} and less than 2 g.100g^{-1} Fe^{3+}, and the amount of Mg varies from 1.3 to 4.2 g.100g^{-1}. However, at 2560 m depth in well DRJ 5, the amount of Fe in the altered rock is low, i.e. 2.6 g.100g^{-1} with 1.9 g.100g^{-1} Fe^{2+} and 0.5 g.100g^{-1} Fe^{3+} (Figure 9.17). Titanium and Mn contents are up to 0.5 and 0.2 g.100g^{-1} respectively.

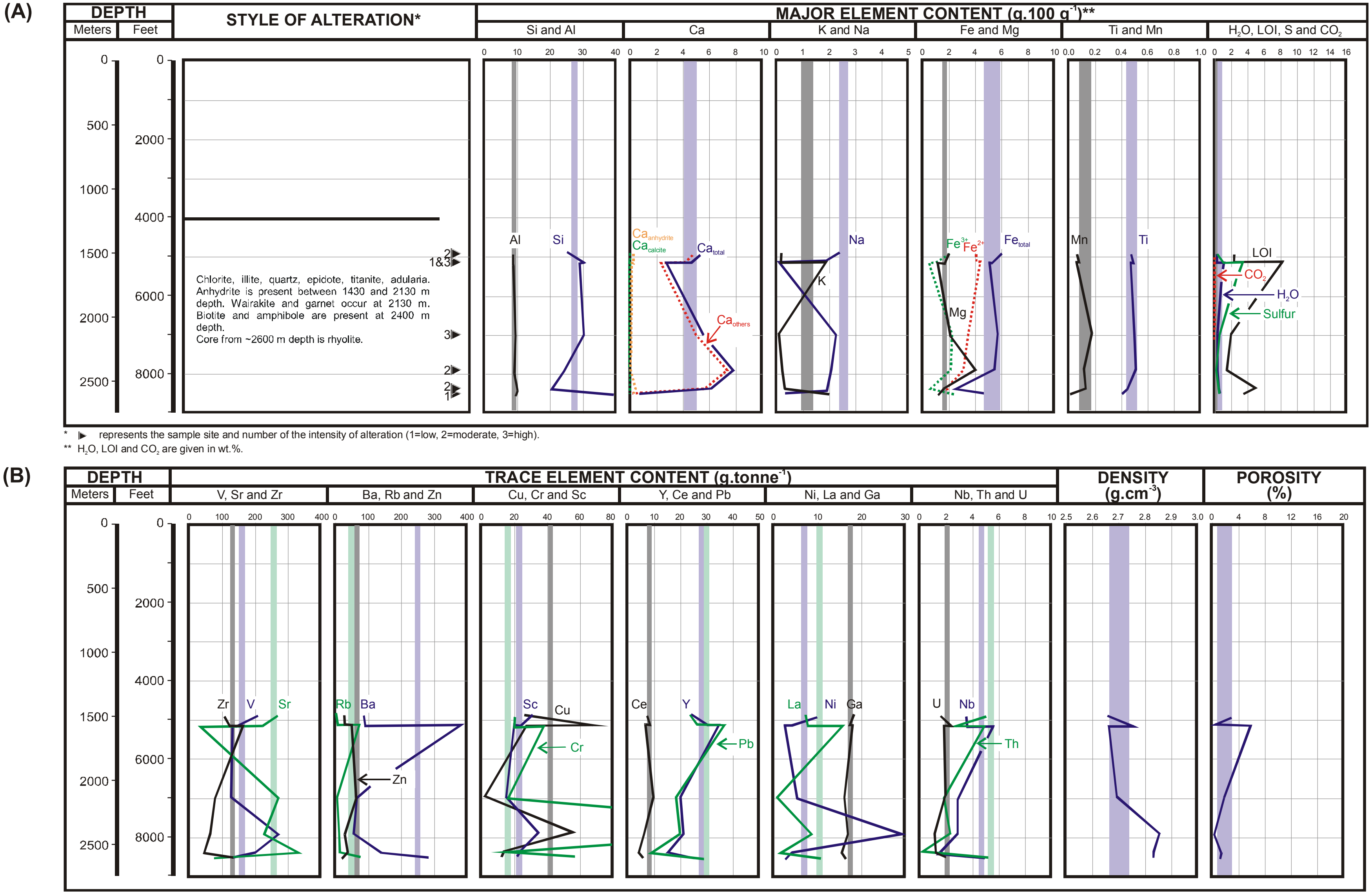

* ▶ represents the sample site and number of the intensity of alteration (1=low, 2=moderate, 3=high).

** H_2O, LOI and CO_2 are given in wt.%.

Figure 9.17. Variation in chemical composition and density of altered rocks surrounding the present production area, i.e. wells DRJ 4, 14 and 24. **(A)** Major elements. **(B)** Trace elements, particle density and porosity. The style and intensity of alteration, described from petrography, are also given. Background lines represent the average value of the element in unaltered rocks. Note that a core from about 2600 m depth is rhyolite.

Figure 9.17 also shows variations in trace elements due to alteration with respect to depth. Compared to the unaltered rocks from DRJ 1, the altered rocks from the production area seem to have gained Cu but lost Sr, Zn, Ni, Pb, Th and Y. The amounts of Cr, Ba and La vary widely and the other trace elements, e.g. V, Rb, Sc, Ce and U, remain constant.

The altered rocks have about 0.3 wt.% adsorbed water (H_2O) and less than 5 wt.% bonded (LOI) water (Figure 9.17). However, at 1575 m depth in DRJ 14, an increase in the intensity of alteration has increased H_2O to 1 wt.% and 8.3 wt.% LOI. Sulfur is mostly present at less than 1 g.100g^{-1}, but at 1575 m depth in DRJ 14 and 2560 m in DRJ 5, it is as high as 3.4 and 2.8 g.100g^{-1} respectively. There is an increase in particle density of the altered rocks here, i.e. from 2.65 to 2.90 g.cm^{-3}. Porosity is not as high as elsewhere at mostly less than 3%. However, at 1575 m depth in DRJ 14, highly altered core has a porosity of about 6%, whereas the porosity of the least altered rock is less than 1% (Figure 9.17).

9.7. WATER-ROCK INTERACTIONS

Figure 9.18 summarises the consequences of mass exchange, i.e. losses and gains, of Si, Mg, Fe and Ca during hydrothermal alteration of cores from wells DRJ S-5, through S-3 and S-1, to the marginal area with DRJ S-2 and S-6 on the northern part of the field.

Quartz commonly forms the matrix of rocks, but they tend overall to have lost Si during alteration. Figure 9.18 shows that the most depleted Si rocks occur between +700 and +1400 m in the northern part of the field, i.e. wells DRJ S-3, S-1 to S-6, and at about sea level in well DRJ S-5. This area coincides with an increase in Mg present in chlorite. Magnesium was added from waters as the deep fluids reacted with the rocks. Loss of Si from the rocks indicates that the fluids are saturated or oversaturated in silica with respect to quartz. However, in well DRJ S-5, a decrease in Si is accompanied by a slight loss of Mg, where chlorite is more Fe rich (see Chapter 7).

No changes in the Al contents of the rocks occurred, but there were increases in Ca and Fe, the latter mostly as Fe^{2+}, at elevations between sea level and +800 m. Calc-silicate minerals, e.g. epidote and prehnite, are responsible for this variation. Dissolution of plagioclase will provide Ca to form calc-silicate minerals after plagioclase. Compared to well DRJ S-5, the gain of Ca in the rocks from wells DRJ S-1 and S-3 is greater. This might be due to the different calc silicates present; laumontite is dominant in DRJ S-5, whereas wairakite and prehnite are resent in DRJ S-1. Less gain of Fe with depth in wells DRJ S-1 and S-3, as shown in Figure 9.18, might be due to the appearance of Fe rich actinolite and garnet, i.e. ferroactinolite and andradite (see Chapter 7).

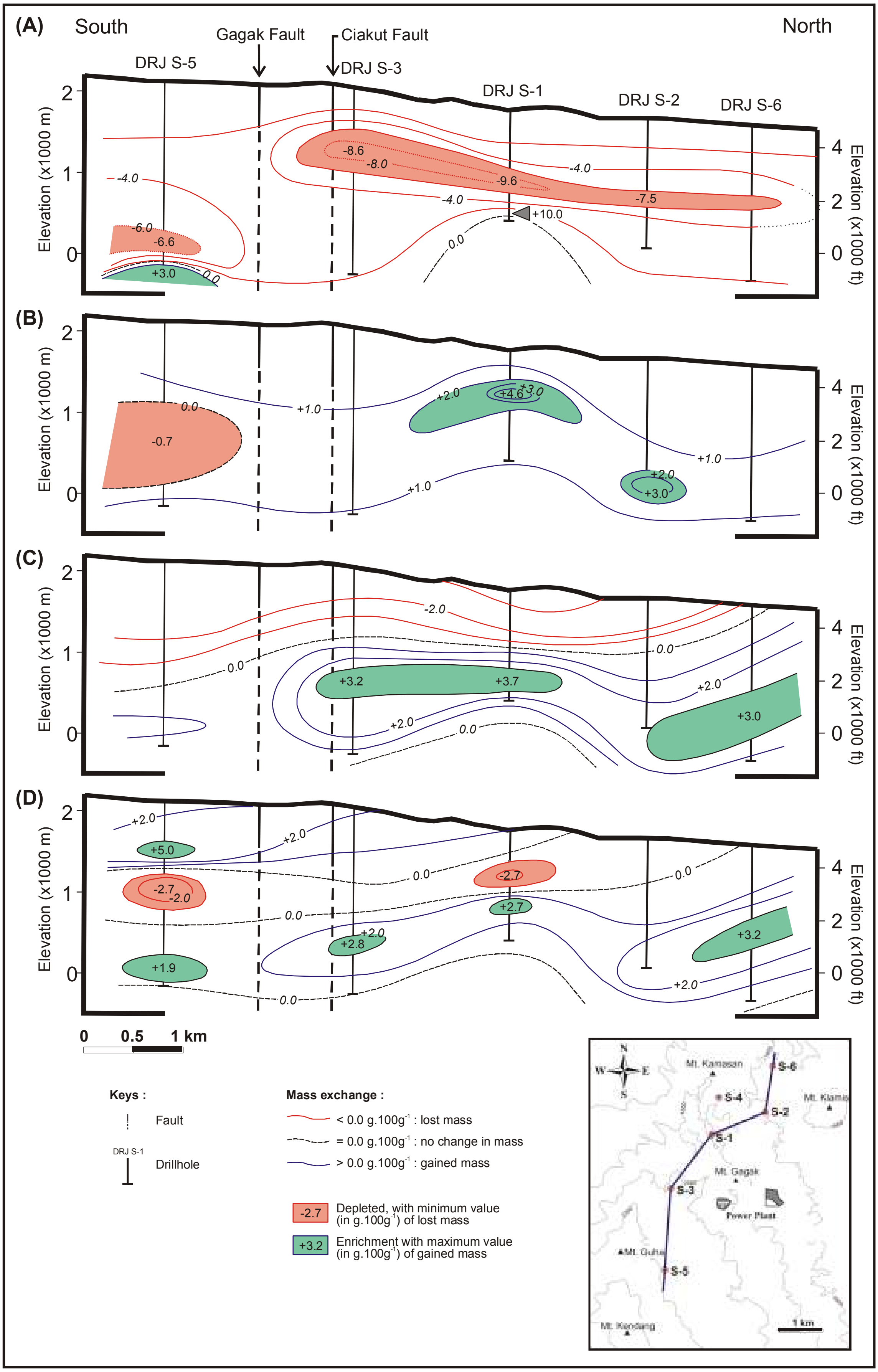

Figure 9.18. South-north cross-section, from DRJ S-5, S-3, S-1, S-2 to S-6, showing mass exchange of elements: **(A)** Si, **(B)** Mg, **(C)** Fe and **(D)** Ca (in g.100g^{-1}).

Calcite and anhydrite are also responsible for a gain of Ca, but the change is much smaller than that caused by the calc-silicates. In well DRJ S-1, there has been less gain of Ca with depth, compared to that in DRJ S-3, due to the absence of calcite in the deep part of DRJ S-1.

A gain of Mg seems to have occurred in the deeper part of well DRJ S-2, i.e. at elevations of about +150 m, due to the presence of chlorite. Here, the amount of Fe in the rocks also increases. In fact, the gain of Fe could extend into the marginal area near well DRJ S-6, where siderite is present. An increase in Ca also indicates an association of calcite and anhydrite. The occurrence of smectite is responsible to an increase in Ca above +1300 m in well DRJ S-5, since it can gain much more Ca than calcite and anhydrite.

Figure 9.18 shows a decrease in Ca at an elevation of about +1200 m in wells DRJ S-1 and S-5. It is accompanied by increases in K and Na, as illite and smectite are present. However, since Mg is high, especially in DRJ S-1, interlayered chlorite and smectite may occur. There are also increases in alkalis at about +500 m in DRJ S-1 and -100 m in DRJ S-5, corresponding to major additions of Si. Since no water is involved, this is probably due to the formation of albite and adularia. The occurrence of secondary feldspars also indicates an increase in the extent of water and rock interactions (Hedenquist and Browne, 1989).

The composition of the deep fluids changed as steam separated from them during boiling. It is likely that there were increases in K and Mg in the residual liquid as is reflected in the occurrence of phlogopite and illite in association with chlorite, overprinting the calc-silicates, e.g. actinolite. In well DRJ 2, alunite is present. However, the little exchange of K is indicated, probably due to the influence of Ca. More waters, SO_4^{2-} and, probably, CO_2were added, so calcite and anhydrite could form.

The likely influx of an acid magmatic fluid in well DRJ S-3 produced a narrow, but intense alteration zone, characterised by depletion of Ca, Na and K, but substantial increases in Al, Fe and Ti. Magnesium and Mn were lost from the rocks during alteration and enriched the fluids.

Chapter 10

EVOLUTION OF DARAJAT GEOTHERMAL SYSTEM

10.1. ORIGINAL CONDITION

The Darajat geothermal system is situated within 30 km of a Quaternary volcanic centre, which includes the active volcanoes of Papandayan and Guntur. The system itself lies within an eruptive center of the Kendang stratovolcanic complex on the northern flank of Papandayan, at elevations of 1600-2200 m above the sea level.

Darajat and its surrounds are covered by Quaternary (Pleistocene) volcanic rocks, consisting of andesitic lavas, pyroclastic breccias and tuffs. These rocks are overlain in the northeast by an obsidian flow from Mt. Kiamis, a younger than 50,000 years old dacitic-rhyolitic product of a parasitic cone in the Kendang caldera (Amoseas Indonesia Inc., 1987).

An andesite complex is the deepest unit drilled. It consists of subalkaline, Ca and Fe rich but Mg poor andesite lavas and microdiorites. It is more than 800 m thick and has an elongate dome shape with an axis trending approximately N-S (Geothermal Energy of New Zealand Ltd., 1996). The mineralogy of the andesite complex consists of labradorite-bytownite phenocrysts with mostly a labradorite groundmass, augite and hypersthene (enstatite). Other primary minerals include amphiboles, biotite, titanomagnetite and apatite. Rhyolite is locally present at depth, e.g. at about 2600 m in well DRJ 24. The original porosity of the andesites was less than 3%.

Structural features at Darajat mostly trend NE-SW and NW-SE. Those NE-SW striking include the old caldera-like Kendang fault and the younger Gagak, Cibeureum and Cipandai faults.

10.2. PRESENT CONDITIONS

10.2.1. Extent of Reservoir

The Darajat geothermal system is one of the world’s few known vapour-dominated geothermal resources. At present, it has an output of 260MWe. The Darajat reservoir fluid is dominated by steam at temperatures of 240-250°C and pressures of 36-38 bars. The present reservoir lies, in large part, beneath the main fumarolic area, trending NNW-SSE with an axis approximately parallel to the Kendang Fault. The top of the reservoir is an asymmetric dome-like shape, whereas its bottom has a bowl-like form (e.g. Amoseas Indonesia Inc., 1987 and Rejeki et al., 2010). The steam reservoir is overlain by a condensate zone.

The reservoir contains mainly steam but with about 2% non condensable gases, consisting of about 94 wt.% CO_2, 3 wt.% H_2S and 3 wt.% other gases. It also contains about 33% liquid, which is a dilute, near neutral pH, Na-SO_4^{2-}-HCO_3^--Cl water (Amoseas Indonesia Inc., 1989a). The reservoir has high permeability about 150 mD, mainly due to vertical fractures, surrounded by zones with lower permeability of up to 15 mD rocks. The porosity of the reservoir rocks varies between 5 and 20%.

10.2.2. Surface Manifestations

Surface thermal manifestations, mainly generated by the ascending steam, consist of steaming ground, steam heated acid boiling pools and fumaroles with temperatures of 50-90°C (Amoseas Indonesia Inc., 1987). Several thermal water outflows occur east of the fumarole area at lower elevations. They are the Cibeureum, Toblong and Golangsing hot springs; the first two are acid sulfate waters at 50-60°C, while the Golangsing spring has a pH of about 6 and comprises sulfate-bicarbonate water at temperatures below 30°C. No neutral pH chloride water discharges at Darajat, but a Cl water likely appears at about 12 m depth in a well, 10 km east of the fumarole area.

10.3. EVOLUTION OF THE DARAJAT SYSTEM

The Darajat geothermal system is now dry steam dominated but the occurrence of hydrothermal minerals such as epidote, wairakite and prehnite, indicates that the system was once liquid dominated. Variations in the chemical compositions of the minerals suggest that there were changes in fluid composition and/or temperature and pressure during fluid and rock interactions. The evolution of Darajat geothermal system from a liquid to vapour dominated system is represented in Figure 10.1 and summarised in Table 10.1.

10.3.1. Evolution Stage 1

Feeding thermal fluid zones were encountered at deep levels in the northern and southern parts of the field, represented in areas about wells DRJ S-1 and S-5 respectively. These parts are separated by the Gagak Fault. The fluids were of meteoric origin, deeply circulating, and likely to have been initially oversaturated in Mg; but, once, they interacted with the surrounding parent rocks of the andesitic complex, they became enriched in Ca and Fe (see Chapters 7 and 9). This allowed chlorite, mostly Si rich, calcite, probably with siderite, and rare anhydrite to deposit. The fluids also contain up to 0.4 wt.% NaCl eq. and low CO_2, and once had temperatures between 350 and 400°C (see Chapter 8, Figures 10.1A and B).

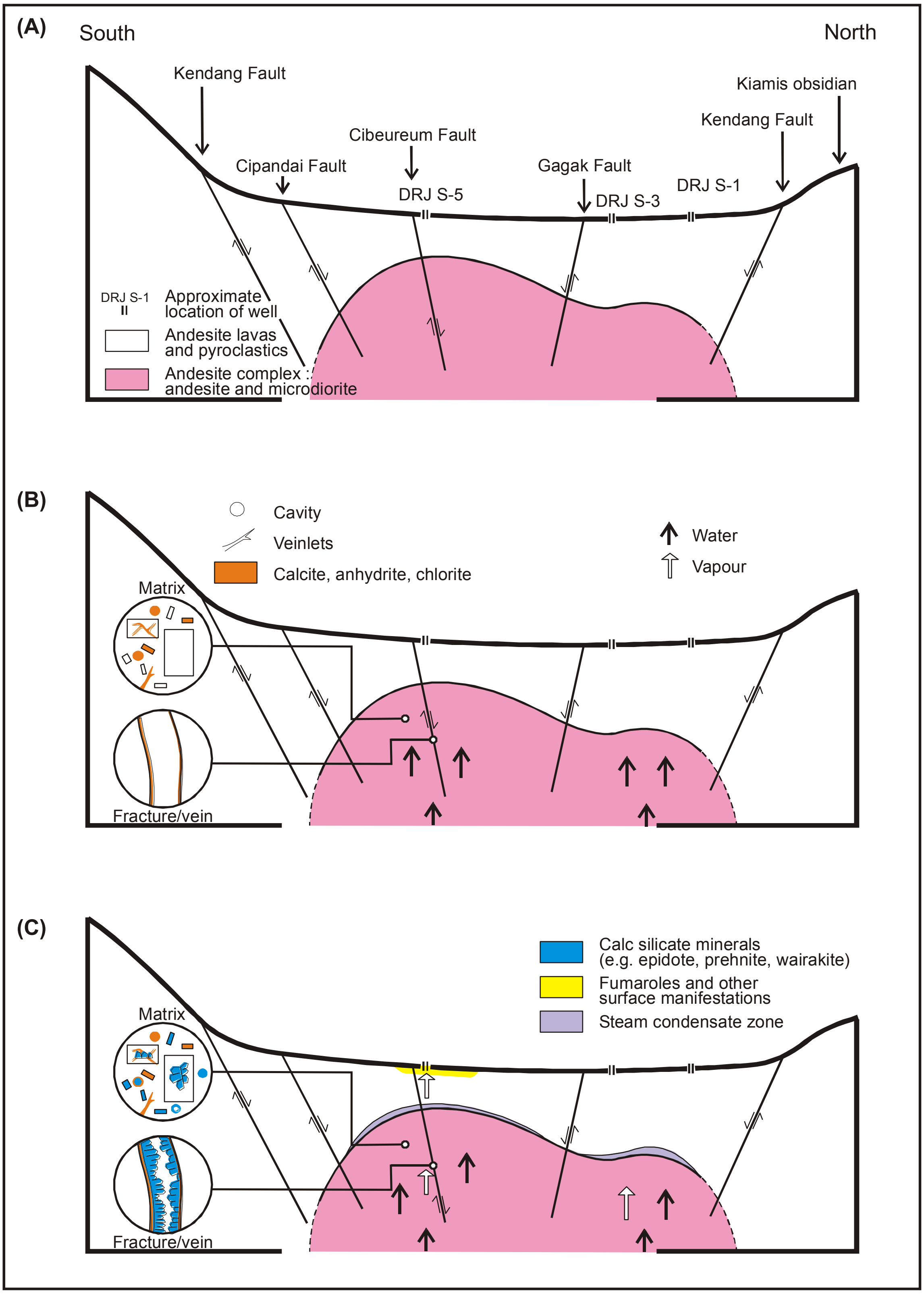

Figure 10.1.Sketch of the evolution of Darajat geothermal system, shown as a not-to-scale, south-north cross-section (across the caldera collapse structure of the Kendang Fault). See next page and Table 10.1 for explanation.

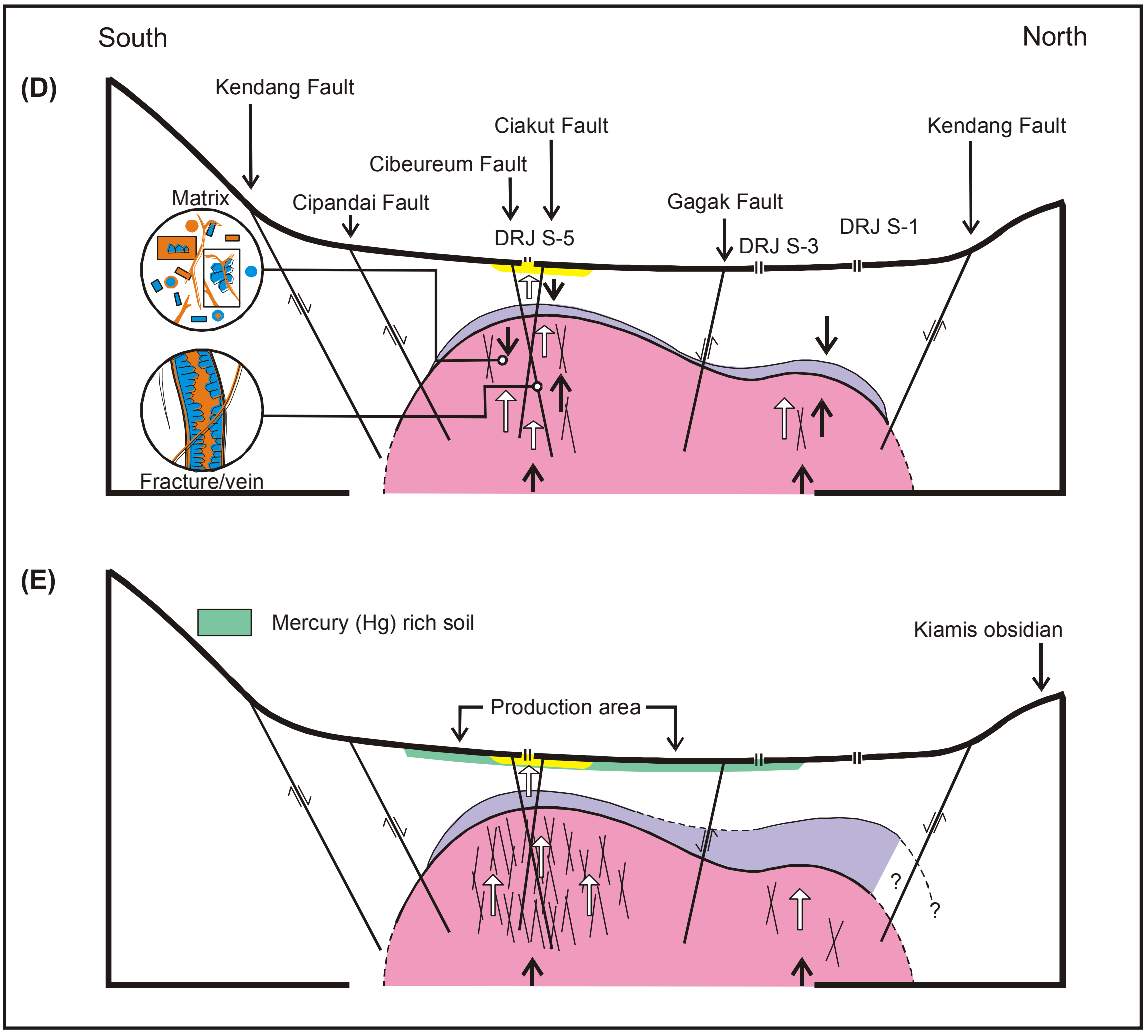

Figure 10.1.Sketch of the evolution of Darajat geothermal system, shown as a not-to-scale, south-north cross-section (across the caldera collapse structure of the Kendang Fault).

(A) Original condition. A dome shaped andesite and microdiorite bodies, intruding andesite lavas, pyroclastics and tuffs, within a caldera structure of the Kendang fault. Other fault systems, including the Gagak, Cibeureum and Cipandai Faults, are younger than the Kendang Fault. The volcanic rocks are overlain by Kiamis obsidian in the north area.

(B) Evolution stage 1. Thermal fluids ascended in the southern and northern parts of the field. The fluids interacted with the surrounding rocks and became Ca, Mg and Fe saturated. The matrix of rocks altered and the fractures and veins were filled by calcite and chlorite in association with quartz and anhydrite. Cavities filled with calcite and chlorite.

(C) Evolution stage 2. Fluids boiled as they ascended. They became Ca, Mg and Fe oversaturated and caused calc-silicates to replace primary minerals, fill cavities and veins. Vapour accumulated at the top of the reservoir, condensed and formed a steam condensate zone. Some vapour discharged to the surface through fractures as fumaroles and steaming ground.

(D) Evolution stage 3. Boiling became more intense. Vapour continued to fill the reservoir and thickened the steam condensate zone. Liquid saturation of the reservoir decreased; the residual liquids descended and were heated. Calcite and anhydrite in association with chlorite and quartz overprinted the calc-silicates, altering the matrix and filling the fractures. Self sealing allowed fracturing in the reservoir; some fractures were filled by calcite, others allowed vapour to flow. The Ciakut and other young NE-SW and NW-SE striking faults formed.

(E) Present condition. The andesite complex is highly fractured and the fractures are dominantly filled by vapour. A vapour-dominated reservoir then formed; it is capped by a steam condensate zone and surrounded by impermeable rocks that resulted from the hydrothermal alteration. The steam condensate zone is shallower in the south than in the north part of the field. Water dominated conditions likely remain below the exploited reservoir and the fluids boil intensively. At the surface, fumaroles, steaming ground, acid boiling pools and soil with high Hg contents occur. The fractures in the southern part are more intense and shallower than in the northern part of the field.

Table 10.1. Summary of the evolution of Darajat geothermal system (see also Figure 10.1).

Time	**Area**	**Fluid**					**Hydrothermal Alteration****
		Type	Phase	Characteristic*	Temperature (°C)	Geothermal Process	
A (Original)	-	-	-	-	?	None	None
B (Stage 1)	Deep	Meteoric	Liquid	Dilute, neutral pH, low CO_2	350-400	Water-rock interaction (rock dominated)	Calcite, chlorite, ± anhydrite
		Magmatic	Liquid	Acid pH (2-4). Probably CO_2, gas rich and saline.	< 450	Water-rock interaction (fluid dominated, rock dissolution, neutralisation)	Pyrophyllite
C (Stage 2)	Margin	Meteoric	Liquid	Slightly acid pH	220-250 (<150)	Boiling, mixing	Laumontite, smectite
	Deep	Meteoric	Liquid ± vapour	Neutral pH	300-250 (< 200)	Boiling, (slightly) cooling	Garnet, actinolite, epidote, prehnite, wairakite, chlorite
		Magmatic	Liquid ± vapour	Less saline, CO_2 rich, $\pm H_2S$, $\pm SO_2$, gas rich, slightly acid to near neutral pH	280-250 (200)	Boiling, mixing, cooling, neutralisation	Garnet, actinolite, epidote, ±prehnite.
D (Stage 3)	Shallow/ margin	Condensate	Liquid	HCO_3^- rich, SO_4^- rich, slightly acid to acid pH (~1.5)	200-250	Condensation	Calcite, anhydrite, ±alunite, ± kaolinite
	Deep	Meteoric	Liquid + vapour	Slightly acid (~5) to near neutral pH.	300-250 (< 200)	Boiling, mixing	Garnet, actinolite, epidote, prehnite, wairakite, chlorite, platy calcite, ± anhydrite. Illite, phlogopite.
E (Present)	Shallow/ margin	Condensate	Liquid	SO_4^{2-} and HCO_3^- rich, slightly acid to near neutral pH	~200	Condensation, mixing, neutralisation	Calcite, anhydrite, smectite, ± kaolinite
	Deep	Meteoric	Vapour ± liquid	Gas rich (mainly CO_2), Na, SO_4^{2-}, HCO_3^-, Cl rich, neutral pH	~250	Boiling, mixing, water-rock interaction (fluid dominated)	-

* CO_2 and SO_4 are present in liquid and vapour phases.
** Present as replacement mineral and filling cavities and veins. (Over) saturated with respect to quartz.

There was an influence from hot magmatic fluids. The fluids ascended the Gagak or Kendang faults and became trapped at depth midway between the northern and southern parts, i.e. at about 2000 m depth in well DRJ S-3. The magmatic fluids were acid (pH=2-4) and of andesitic origin with temperatures up to 450°C (see Chapters 5 and 7). They dissolved the surrounding rocks releasing Ca, alkalis, Mg and Mn and forming pyrophyllite (see Chapter 9). The occurrences of tourmaline and apatite are also signatures of the infiltration of magmatic fluids in the northern and southern areas of the field, i.e. in wells DRJ S-1 and S-5 respectively. Furthermore, the water and rock interactions then neutralised the acidity of the magmatic fluids (cf. Reyes, 2000).

10.3.2. Evolution Stage 2

The ascending meteoric fluids boiled below about +600 m in the northern part at 250-300°C, but were slightly cooler, at 200-250°C, when they reached about sea level in the southern part (see Chapter 8). Further interactions with the surrounding rocks caused the fluids to be fully saturated with respect to some calc-silicates and quartz. Grossular-andradite, actinolite-tremolite, high pistacite epidote, Fe-bearing prehnite and wairakite (see Chapters 5 to 7) in association with quartz formed at this stage. Magnesium was accommodated within Mg rich chlorite (see Chapter 7, Figure 10.1C).

The magmatic fluids then boiled at 250-280°C at elevations of about +100 m but were neutralised and oxidised by mixing with meteoric waters at about +600 m. The meteoric waters were derived from either the northern or the southern parts of the field or surface waters descending faults. The mixed fluids then cooled down to 230-240°C and were less saline, containing 1.2-1.8 wt.% NaCl eq., less than 3.5 mol.% CO_2 and traces of H_2S and SO_2 (see Chapter 8). The dilution of the magmatic fluids by meteoric waters, which formed the later neutral pH alkali chloride waters, might have erased evidence for the occurrence of magmatic fluids (cf. Reyes and Giggenbach, 1992). Furthermore, the meteoric waters with temperatures of 210-230°C became dominant above elevations of +800 m. These fluids were then saturated with respect to calc-silicates.

Boiling depth and temperature control the amount of CO_2. Dissolved CO_2 decreased (see Chapter 7) and the amount of CO_2 in the vapour phase varied from less than 0.3 mol.% in the northern part to about 1.4 mol.% elsewhere (see Chapter 8). Loss of $CO_2$from the liquid due to boiling is indicated by the occurrence of platy calcite in the northern area. At this time, boiling was more intense in the northern area (Chapter 8). Boiling and phase separation probably also caused differences in the pressures and compositions of fluids in the northern and the southern parts (see Chapter 7). Different boiling rates within these two areas might also cause different permeability domains as observed by Gonzáles-Partida et al. (2000) in Los Azures, Mexico. Gas rich fluids concentrated in the upper part of the boiling zone, perhaps up to 4 mol.% with up to 1 mol.% CO_2.

Boiling also occurred at the margin of the field, i.e. around wells S-2 and S-6, at temperatures of 280 to 300°C. The degassed fluids then cooled to 220-250°C and then to 130-140°C, as they ascended or flowed laterally (see Chapters 5 and 8). Cooling then occurred due to mixing between thermal water and colder, surface water, probably including steam condensate (see Chapters 7 and 8).

10.3.3. Evolution Stage 3

Evolution stage 3. A steam condensate zone, characterised by calcite and anhydrite deposited from heating downward percolating bicarbonate and sulfate rich condensate waters, was present above the boiling zone (Figure 10.1D). In the northern part of the field, this was 600 m thick, i.e. from +700 to +1300 m. The paleotemperature was 200-210°C at shallow depths, but reached boiling of about 250°C at about +800 m elevation. The southern part of the field has a thin condensate zone at an elevation of only +100 to +200 m. The condensate waters, trapped in crystals in well DRJ S-1, are very dilute, vapour rich and contain up to 0.5 mol.% CO_2 and about 0.4 mol.% HSO_4^- (see Chapter 8). Mixing between the boiled fluids and steam condensates was followed by cooling, and most likely occurred in the upper part of the boiling zone.

The deeper thermal fluids then became slightly acid, as they contain more CO_2, SO_4^{2-} and other volatiles. Where they interacted with rocks, they dissolved plagioclase and increased the activities of calcium and sodium in the liquid. The amounts of K and Mg in the fluids decreased as wormy primary plagioclase (e.g. above 200 m in DRJ 1), illite, phlogopite (e.g. in wells DRJ 13 and 17), alunite (e.g. at shallow depths in well DRJ 2) in association with kaolinite, smectite and chlorites formed (see Chapters 5, 7 and 9).

The thermal fluids continued to boil. Vapour deriving from the boiling fluids ascended continuously and rapidly through fractures and started to fill a reservoir. On the other hand, the liquid moved more slowly or even descended and accumulated below the steam reservoir. Meanwhile, the depositions of calcite and anhydrite in the steam condensate zone decreased the porosity and permeability in rocks above the reservoir. Clay minerals, such as chlorite, smectite and kaolinite, altered the rocks from the margin area of the reservoir and formed the impermeable zone minimising recharge of fluids. The self-sealing resulted from the hydrothermal alteration allowed sustained pressure differences between the reservoir and the surrounding rocks to develop. This caused hydraulic fracturing to occur in the reservoir, increasing the porosity and permeability of the reservoir rocks. At this time, the Ciakut fault and some young NW-SW trending surface lineaments likely formed. An increase in the permeability and lowering of pressure could trigger boiling to occur more intensely in the reservoir (e.g. White et al., 1971 and Truesdell and White, 1973). Consequently, the pressures and temperatures of the thermal fluids decreased. More vapour produced and became a pressure-controlling phase (White et al., 1971). Boiling and events that increased the permeability occurred several times, followed by a liquid-vapour phase separation until the maximum entalphy achieved (White et al., 1971).

Present condition. A vapour-dominated system then developed (Figure 10.1E). It has a reservoir, which comprises the highly permeable rocks and is fully filled by vapour derived from boiling fluids below it. The reservoir is capped by the steam condensate zone and surrounded by the impermeable rocks. The vapour-dominated reservoir is approximately 1 km thick (Amoseas Indonesia Inc., 1989b) and covers about 14 km^2in area (Amoseas Indonesia Inc., written com., 1998); it contains 2 wt.% dry gases, mainly CO_2, and is saturated about 33% from the neutral pH $Na\text{-}SO_4^{2-}\text{-}HCO_3^{-}\text{-}Cl$ waters (Amoseas Indonesia Inc., 1989b, see also Chapter 3). The reservoir has a stable temperature of 240-250°C and pressures of below hydrostatic at about 36 bars.

Steam ascends and some discharges to the surface through fractures and forms fumaroles, steaming ground and acid boiling pools, whose the CO_2 content may be as high as 95 mol.% (see Chapter 3). In the northern part, steam is unable to get to the surface, so no surface manifestation occurs there. Several outflows of the steam condensate water discharge at lower elevations as the Cibeureum, Toblong and Golangsing hot springs.

10.4. FLUID PROCESSES

10.4.1. Boiling

Widespread and prolonged boiling encourages the formation of a vapour reservoir. The extent and duration of boiling controls the amount of separated CO_2 gas. The amount of CO_2dissolved in the liquid decreases whereas the amount of CO_2 gas increases. Mahon et al. (1980) showed that CO_2 is a critical component in determining whether a geothermal system produces steam or a mixture of steam and water, since its concentration in the water greatly affects the boiling temperature.

Intense boiling can also cause fluid pressures to decrease in an open system. The fluid pressures in the Darajat reservoir decreased from above 100 to 36-38 bars (see Chapter 8), creating a vapour condition. A sudden decrease in the fluid pressure might cause chalcedony to deposit suddenly field wide in association with high temperature indicating minerals, e.g. epidote, in veins. Fournier (1985) showed that the precipitation of chalcedony requires either rapid cooling or depressurisation of fluids oversaturated in silica with respect to quartz. Cooling has occurred at Darajat but it is unlikely to have been rapid enough for chalcedony to form. Depressurisation causes boiling (e.g. Grant, 1982; and Gonzáles-Partida and Lavresse, 2003). The occurrence of anhydrite is also a signature of decreasing pressure (e.g. Sasada, 1986).

10.4.2. Condensation

Steam condensation is also an important process at Darajat. It occurs above the reservoir and forms a steam condensate zone. This zone can partly seal the reservoir through mineral deposition to prevent both vapour escaping and water recharging. This zone allows a vapour-dominated reservoir to develop below it from a liquid dominated deeper system. Steam condensation can occur if the rate of fluid outflow is low, otherwise steam will discharge at fumaroles (White et al., 1971). The extent of thick steam condensate zone in the northern area and the occurrence of fumaroles in the southern part of the field shows that the rate of outflow in the south is higher than elsewhere in the field. In addition, the steam condensate zone may increase in the amount of CO_2 in the deep fluids through mixing of the descending condensate with the deeper thermal water.

The occurrence of tourmaline in wells DRJ S-1 and S-5 indicates B was present in the depositing water (Deer et al., 1978). Boron favours the vapour phase during boiling but the liquid can obtain B through condensation (D'Amore et al., 1977). Where the liquid becomes oversaturated in B with respect to tourmaline this mineral deposits. Tourmaline is present at elevations +1200 to +1300 m in well DRJ S-5, i.e. more than 1000 m above the top of the reservoir. This indicates that the steam condensate zone in the southern part is deeper. In fact, there are likely two steam condensate zones in well DRJ S-5 (see Chapter 5), i.e. at the higher elevation and a deeper one at about +100 m or above the top of present reservoir. This probably consistent with the decrease in size of the present reservoir proposed by Whittome and Salveson (1990, see Chapter 3).

10.4.3. Mixing

Mixing occurs between thermal fluid and other waters, i.e. steam condensate, magmatic and surface waters.

Deep thermal fluid and steam condensate. Mixing occurs between the ascending neutral pH and downward percolating slightly acid, steam condensate waters. This takes place about sea level in the southern part (near well DRJ S-5) and at about +700 m elsewhere. Mixing increases the amount of dissolved CO_2, and probably SO_4, in the deep thermal fluid. Calcite, in places associated with anhydrite, may overprint calc-silicates.

Deep thermal water and magmatic fluid. Mixing occurs between the neutral pH alkali chloride and acid magmatic fluids about +100 m, between the northern and southern parts of the field. It results the mixed fluid to contain more CO_2. The magmatic fluid becomes less saline and neutralised by reaction with the rocks. The pH’s of the mixed fluid remains near neutral and is as hot as 300°C, allowing calc silicates, e.g. garnet and epidote, to form.

Thermal fluid and surface water. Mixing also occurs between the ascending and lateral flowing thermal waters and cold, surface waters in the marginal and near surface areas (about +1500 m). Both waters are meteoric origin and have near neutral pH. Cooling is the main result of this mixing. Hydrothermal minerals produced include smectite.

10.5. VAPOUR RESERVOIR AND PRODUCTIVITY

The shallower and higher permeability of the reservoir in the south makes this part of the field more productive than the north (Figure 10.1E). In fact, most production wells are in the south, but less than 5 are in the north.

The vapour reservoir of Darajat geothermal system is located in the fractured, highly permeable andesite complex. This complex consists of andesite and microdiorite and, like the reservoir, it has an asymmetric dome-like structure. The top of the complex, or the reservoir, in the southern part of the field is between +1200 and +1400 m, while in the north area it is deeper, i.e. between +800 and +1000 m (see Chapter 3, Figure 10.1).

The permeability of the reservoir rocks in the south is higher than in the north, since two main faults, i.e. Cibeureum and Ciakut, cross each other here. The permeability of rocks in the south is about 150 mD but is only 15 mD in the north (Amoseas Indonesia Inc., 1989, see Chapter 3). Rocks from the south area have a matrix porosity of up to 6%, whereas it is less than 2% in the north (Amoseas Indonesia Inc., 1989, see Chapter 3). In addition, the steam condensate zone is about 600 m thick in the north but only about 100 m thick in the south (see Chapter 8).

10.6. HEAT SOURCE

10.6.1. Thermal Gradient

The temperature gradient at Darajat, like in other vapour-dominated systems, is low; it increases from $0.005°C.m^{-1}$ in the vapour reservoir to $0.2°C.m^{-1}$ near the surface (see Chapter 3). Mahon et al. (1980) recorded that a thermal gradient within a geothermal system relates to the amount of gas, especially CO_2; it is generally low in the system containing CO_2.

10.6.2. Heat Source

The composition of gases present in fluid inclusions indicates that the heat source of the Darajat system is the cooling andesite intrusion, i.e. perhaps the andesite complex, including its microdiorites. However, there is also a possible minor contribution from rhyolite at shallow depth.

Temperatures of the andesitic intrusion were once likely to have been 1000-1100°C, as indicated by the augite and orthopyroxene thermometry (Lindsley, 1983, see Chapter 4).

Sibbett (1988) recorded that most geothermal systems related to Quaternary volcanism occur at between 1 and 2 km depth with the main heat source at approximately 4 to 9 km depth. A shallower heat source may be present between 1 and 3 km depth (Sibbett, 1988); if so it is generally smaller (e.g. Reyes, 1990), cooler than the main deeper heat source and of shorter duration (Sibbett, 1988 and Hochstein and Browne, 2000).

According to the topography, from the size of the vapour reservoir and the surface manifestation, the Darajat geothermal system likely belongs to the second model of vapour-dominated geothermal system of Ingebritsen and Sorey (1988, see Chapter 1). They reported that, unlike model I (see Chapter 1), the extent of the vapour system model II need not to be vertically related to a magmatic heat source but can be fed by a deeply circulating system comprised of regional heat flow over several square kilometres. It seems that the geothermal system associated with stratovolcanoes need not be associated with the volcanic activity itself (Sibbett, 1988 and Reyes, 1990). This suggests that the Darajat and nearby Kamojang geothermal systems might share the same regional heat source; this might not be the nearby Quaternary active volcanoes of Guntur or Papandayan but rather the old and dormant Guntur complex, which was active during the Pleistocene (see Chapter 2). The thermal activity itself is likely to migrate NE or SW, parallel to the major structure, the Kendang fault.

10.6.3. Heat Transfer

Conductive heating is important role in heating meteoric water recharge (Reyes et al., 1993). Thiswould not change the water salinity but could increase the amount of gases, especially CO_2, by vapour absorption (Reyes et al., 1993 and Gonzáles-Partida et al., 2000) if some component of mass transfer was involved.

The main heat transfer process at Darajat is convection. This derived from rapidly ascending steam through fractures and slow movement of liquid in intergranular pores in rocks.

10.7. TIME OF EVOLUTION

10.7.1. General

Few studies have considered the timing of hydrothermal activity, especially for vapour dominated geothermal system. Generally, there are two opinions about timing that allows a liquid dominated to evolve into a vapour dominated system, i.e. long or short.

Long evolution. A slow evolution from liquid to vapour dominated systems requires 10,000 to 30,000 years (e.g. Ingebritsen and Sorey, 1988 and Allis and Shook, 1999) but it could be as long as 500,000 years (e.g. Goguel, 1982).

Los Humeros in Mexico is a two-phase geothermal system with an excess of vapour (Prol-Ledesma, 1998); it was liquid dominated up to 500,000 years ago (Martinez-Serrano, 2002). The Geysers geothermal system needed about 300,000 years to evolve from liquid to vapour dominated (Dalrymple et al., 1999). The Larderello geothermal system was liquid dominated 2 to 3.5 x 10^6 years ago (Batini et al., 1985 and Cavarretta et al., 1982) but then evolved to vapour dominated about 41,000 years ago (Ruggieri and Gianelli, 1999). Indeed, the Geysers and Larderello needed longer to evolve, since neither is associated with active volcanic centres.

Short evolution of a geothermal system requires between 5,000 and 10,000 years (e.g. Shook, 1995). This is usually accelerated by fracturing (e.g. model III of Ingebritsen and Sorey, 1988) and catastrophic venting (Shook, 1995).

Reyes (1990) reported that, unlike other geothermal systems associated with Quaternary andesite in Philippines having ages almost a million year, Alto Peak is 6,000 year old (Reyes, 1990). The Karaha-TelagaBodas geothermal system on the Galunggung volcano and about 40 km E of Darajat (see location in Chapter 1)is a partially vapour-dominated system. Allis et al. (2000) and Moore et al. (2002b) reported that this field evolved from a liquid dominated one about 4,200 year ago. This change was triggered by the formation of Galunggung crater following a flank collapse.

10.7.2. The Darajat Geothermal System

Compared to the Karaha-TelagaBodas, Darajat lies in an older volcanic centre (see Chapter 2). Darajat also has fluid with much lower steam saturation than that of the Karaha-TelagaBodas. Therefore, the evolution of Darajat from liquid to vapour-dominated systems may have taken longer than that of Karaha-TelagaBodas.

The Darajat geothermal system is associated with the Pleistocene andesitic volcanic centre of Guntur complex. Its activity likely started as liquid dominated about 330,000 years ago, i.e. the time of the oldest fractionation of igneous rocks at the Guntur volcano recorded by Purbawinata (1988, see Chapter 2).

Obsidian from Mt. Kiamis is a product of rhyolite parasitic cone in the Kendang caldera at about 50,000 years old (Amoseas Indonesia Inc., 1987, see Chapter 3). Rhyolite rocks encountered from about 2600 m depth in well DRJ 24 altered to illite and chlorite (see Chapter 5). This suggests that

50,000 years ago, the Darajat system was still water dominated, likely in a transition to become vapour dominated; it is during the evolution stage 3, that the fluids were volatile rich (Figure 10.1 and Table 10.1).

The formation of rhyolitic rocks likely accelerated the evolution of Darajat geothermal system. Intrusion of shallow heat source may cause (rapid) boiling, as suggested by Moore et al. (2002b) for the Karaha-TelagaBodas. These processes could (suddenly) change the amount of dissolve CO_2 and temperature of the fluid affecting the concentration of SiO_2. As a result, calcite overprints calc-silicates and chalcedony is present in association with epidote (see Chapters 5 and 6).

It is therefore likely that the initially liquid-dominated Darajat geothermal system began to change to be a two-phase system about 330,000 years ago, and then further evolved to the vapour-dominated system about 50,000 years ago. A geothermal system with two different evolutionary stages, like Darajat, is also evident at Ngatamariki in New Zealand (Arehart et al., 2002), the Te Kopia also in New Zealand (Bignall and Browne, 1994), Tiwi in the Philippines (Moore et al., 2001), and Karaha-TelagaBodas (Allis et al., 2000 and Moore et al., 2002b). The later evolutionary event usually relates to magmatic and tectonic activities, e.g. fault and caldera collapse.

Chapter 11

CONCLUSIONS AND RECOMMENDATIONS

11.1. CONCLUSIONS

Geological setting. The Darajat geothermal system is located within a30 km range of Quaternary volcanic centers. It is covered by Pleistocene volcanic rocks and the subsurface geology is dominated by andesite lavas and microdiorites of an andesite complex. The youngest volcanic rock is a 50,000 year old obsidian flow. Structural features at Darajat mostly trend NE-SW and NW-SE. The NE-SW striking features, including the Kendang Fault, are the older.

Darajat at present. The Darajat geothermal system is a dry-steam resource. It has been explored since 1975 and at presenthas an output of 260 MWe. The reservoir now has an asymmetric dome-like shape, overlain by a steam condensate zone. It contains mainly steam with about 2% non-condensable gases, mainly CO_2. It also contains about 33% by volume Na-SO_4^{2-}-HCO_3^--Cl water. The temperature is about 240°C and pressure is about 36 bars.

Steaming ground and fumaroles are present above the reservoir. Warm acid sulfate and near neutral pH sulfate-bicarbonate springs are present at lower elevations. No neutral pH chloride water discharges in the field.

Host rocks are subalkaline, Ca-rich andesites. They contain 57-62 wt.% SiO_2, 17-19 wt.% Al_2O_3 and 5-7 wt.% CaO. A rhyolite occurs encountered in places at depths and contains 72 wt.% SiO_2 and 16 wt.% Al_2O_3. The primary porosity of andesites ranges from 0.9 to 3.2%; the particle density is about 2.70 g.cm^{-3}.

The mineralogy of the andesites is dominated by plagioclase (mainly labradorite-bytownite), and augite and hypersthene (enstatite) phenocrysts. Other primary minerals include amphiboles, apatite, quartz and titanomagnetite. Plagioclase alters to a variety of hydrothermal minerals, including calcite, quartz, chlorite and calc silicates. Augite behaves similarly, but hypersthene alters to chlorite, sometimes in association with smectite and illite, and opaque minerals. Volcanic glass is the most readily altered, whereas quartz is the most resistant.

Hydrothermal alteration and chemistry of minerals.The intensities of alteration in the andesite lavas range from low to moderate. Pyroclastic rocks are more intensely altered, while tuff is completely altered. The compositions of hydrothermal minerals reflect changes in fluid composition, temperature and/or pressure of fluids within the reservoir.

The most common hydrothermal minerals are quartz, calcite and anhydrite. Chlorite is the most common clay mineral; its shallowest occurrence is at about +1800 m (asl) but it is deeper to the north. Chlorite is mostly Mg rich pycnochlorite and diabantite but its composition can range from clinochlore to penninite. Other clay minerals, including smectite, illite, kaolinite, halloysite and pyrophyllite, are present locally. Illite contains up to 10 wt.% K_2O and smectite is mostly Ca rich.

Calc silicates are dominated by epidote, replacing both plagioclase and pyroxene, and disseminated in the groundmass and filling fractures and cavities. Epidote is first present at +700 to +900 m (asl) and at depth it coexists with actinolite and garnet. Epidote has pistacite values, ranging between 0.1 and 0.5. Replacement amphibole is mostly actinolite and tremolite with ratios of Mg^{2+} to $Mg^{2+}+Fe^{2+}$ above 0.5. Garnet has a grandite composition.

Other calc silicates include laumontite, wairakite, prehnite and titanite. Laumontite contains about 8 wt.% CaO and 14-18 wt.% H_2O. Titanite contains 25-37 wt.% TiO_2 and 21-29 wt.% CaO. Prehnite has up to 8 wt.% FeO.

Carbonates are mostly ferroan, manganoan and magnesian calcite. Siderite and ankerite are present locally. Secondary feldspars include adularia ($Ab_{0-15}An_{0-5}Or_{82-99}$) and albite ($Ab_{73-98}An_{1-26}Or_{0-12}$).Other minerals present include K-Na alunite, phlogopite, Cl and SO_3 bearing apatite and dravite-schorl (Mg-Fe-rich tourmaline). Opaque minerals are mostly magnetite, hematite, ilmenite, secondary rutile and pyrite.

Vein minerals. Veins and fractures are mostly almost vertical and are up to 2 cm wide. Older veins are almost horizontal, but some dip at 30-60° with respect to the core axis. Episodes of vein deposition, from the oldest to the youngest, are: chlorite + quartz + opaque minerals → calcite + anhydrite → epidote + actinolite + garnet → prehnite → wairakite + laumontite → calcite + anhydrite ± chlorite ± quartz ± platy calcite → anhydrite. Generally, the textural relations within the vein minerals record boiling and local progressive cooling, followed by condensation.

The paleohydrology of the Darajat was dominated by meteoric waters which boiled at temperatures between 240 and 300°C, followed by cooling. Descending steam condensate deposited anhydrite and calcite, as the reservoir fluids changed from water to vapour. Inputs of magmatic components also occurred locally.

Mass transfer. Interaction between water and rocks indicates both loss and gain of Si, Mg, Fe and Ca during hydrothermal alteration. Calc-silicate minerals are partly responsible for the variations in Ca and Fe.

The occurrence of chlorite could account for the loss of Si but an increase in the Mg content of the rocks. Increases in Ca and alkalis are associated with the occurrences of smectite, illite and secondary feldspars.

Evolution. It is concluded that the vapour-dominated Darajat geothermal system developed from a previously liquid dominated system. This required the formation of a highly permeable reservoir, development of impermeable barriers and intense boiling. The vapour dominated system resulted from boiling that produced steam which filled fractures in the reservoir whereas the residual liquid descended and may remain at depth.

11.2. CONSIDERATIONS

Phreatic eruptions. White et al. (1971) reported that a local accumulation of gas rich vapour could create pressures, which exceed hydrostatic, and perhaps even lithostatic, and cause rapid fracturing events. This is similar to what may happen near the surface where steam discharges through fumaroles. Indeed, if the vapour is gas rich, it could cause fracturing and be followed by explosive phreatic eruptions, including hydrothermal eruptions. However, a phreatic eruption from a vapour-dominated system is usually weaker than that from a water system (Goguel, 1982). In fact, no one has reported any evidence for the occurrence of hydrothermal eruptions at Darajat.

Drilling casing. Setting of casing can protect production wells from corrosive damage by acid fluids. The drillholes need to be cased off in at least three main zones: (i) at the surface, where the steam condenses into groundwater, (ii) within the steam condensate zone above the reservoir, and (iii) at about 2000 m depth between well DRJ S-3 and the Gagak Fault, where acid magmatic fluids are present. It is essential that the steam condensate zone be cased off. Casing of (ii) and (iii) are optimal since acid fluid may be restricted to the region of DRJ S-3. However, exploitation may induce the down flow of acid fluids along fractures to deeper level, as reported by Reyes et al. (1993).

Injection Wells. Any water in the vapour reservoir will descend quickly due to its higher density. This becomes a problem, when injection wells are needed to maintain productivity of steam. Truesdell and White (1973) suggested that a low rate of water injection into several shallow wells of small diameter would be much more effective than injecting into wide diameter, deep (originally production) wells. Fitzgerald and Woods (1995) showed that a higher rate of injection could cause condensates to descend into the reservoir. The injected water should also be of similar composition to that of the reservoir liquid (Truesdell and White, 1973) and could support the reservoir pressures (Ozeki et al., 2001). Otherwise the produced vapour will be accompanied by hot waters, as

Ozeki et al. (2001) reported to occur at Matsukawa, Japan. Temperature support also should be considered, since slow cooling might cause the deep water level to rise (Gougel, 1982).

11.3. RECOMMENDATIONS FOR FURTHER WORK

Time. The time required for Darajat to evolve from liquid-dominated system still needs to be determined. This may be possible by K-Ar dating of K bearing hydrothermal minerals, such as adularia, biotite and illite.

Evolution indicated in well DRJ S-5. Hydrothermal alteration in well DRJ S-5 records the occurrence of two steam condensate zones. A deeper steam condensate zone underlies the present vapour reservoir. The other is likely a remnant at shallower depth and occurred before the steam condensate zone deepened. However, this conclusion should be clarified.

Engineering. The evolution of the Darajat geothermal system from liquid to vapour-dominated has been revealed by analysing and interpreting the geological conditions. This should be tested from an engineering perspective by looking at the available well and borehole data. Many such studies have been done for The Geysers geothermal system.

Volcanic stratigraphy. Since not only andesitic rocks occur at depth but also rhyolites, the volcanic stratigraphy of the Darajat geothermal system needs to be studied in greater detail. Such a study could also focus on the origin of the system itself; it is truly a part of Guntur or Papandayan complex and other volcanoes nearby. A related study should also investigate the origin and source of intrusive rocks, e.g. the microdiorites. Further rock geochemistry studies and dating are recommended.

Source of fluids. The source of the Darajat fluids is meteoric waters with only minor input from magmatic fluids. The fluids then undergo boiling and condensation. Studies of stable isotopes would test this paleohydrology. It may also explain the origin of organic gases at Darajat. More chemistry also may be required. The source of magmatic fluids should be addressed, i.e. they are of andesitic or rhyolitic origin.

Lateral inflow. A chloride water discharges 10 km east of the field in a 12 m deep well (Amoseas Indonesia Inc., 1987). There are several natural spring waters at lower elevations (about +700 m), near Garut. However, the origin and composition of these waters are still unclear as is their relationship with the Darajat geothermal system.

Acid alteration. The occurrences of alunite and pyrophyllite suggest alteration due to acid fluids. They become important in a vapour-dominated system like Darajat, where they occur near the surface due the formation of acid steam condensate but are also present at depth, possibly from the contribution of hot acid magmatic fluids. Unfortunately, few studies have been made regarding this style of alteration. Therefore, a further study on the hydrothermal alteration due to their presence is suggested. This includes the determination of the chemical compositions of the acid fluid formed minerals, including alunite, diaspore and pyrophyllite.

Vapour style alteration. In Darajat, wormy plagioclase indicates the occurrence of gas attack but at Larderello, for example, some vapour-formed hydrothermal minerals, e.g. harkerite, wilkeite, cuspidine and vesuvianite (Cavarretta and Tecce, 1987), are found. A study regarding this style of alteration needs to be done. It may include a study of the surface textures of remnant minerals which have been attacked by gas or vapour.

Hydrothermal minerals. Clay minerals, especially their compositions and structures, need to be studied. The relationship between their compositions and formation conditions, e.g. temperature, is still unclear. Likewise, the occurrence of other hydrothermal minerals, such as tourmaline and apatite in geothermal systems are still not well understood and need to be further investigated.

LIST OF REFERENCES

Africano, F. and Bernard, A., 2000. Acid alteration in the fumarolic environment of Usu volcano, Hokkaido, Japan. *Journal of Volcanology and Geothermal Re*search, 97, p.475-495.

Aiuppa, A., Allard, P., D'Alessandro, W., Michel, A., Parello, F., Treuil, M. and Valenza, M., 2000. Mobility and fluxes of major, minor and trace metals during basalt weathering and groundwater transport at Mt. Etna volcano (Sicily). *Geochimica et Cosmochimica Acta*, 64, p.1827-1841.

Aja, S.U. and Dyar, M.D., 2002. The stability of Fe-Mg chlorites in hydrothermal solutions - I. Results of experimental investigations. *Applied Geochemistry*, 17, p.1219-1239.

Allis, R.G., 1981. Changes in heat flow associated with exploitation of Wairakei geothermal field, New Zealand. *New Zealand Journal of Geology and Geophysics*, 24, p.1-19.

Allis, R. and Shook, G.M., 1999. An alternative mechanism for the formation of the Geysers vapor-dominated reservoir. *Proceedings of the 24th Workshop on Geothermal Reservoir Engineering*, Stanford University, California, p.53-63.

Allis, R., Moore, J., McCulloch, J., Petty, S. and DeRocher, T., 2000. Karaha-Telaga Bodas, Indonesia: a partially vapor-dominated geothermal system. *Geothermal Resources Council Transactions*, 24, p.217-222.

Alpers, C.N., Rye, R.O., Nordstrom, D.K., White, L.D. and King, B.S., 1992. Chemical, crystallographic and stable isotopic properties of alunite and jarosite from acid-hypersaline Australian lakes. *Chemical Geology*, 96, p.203-226.

Alzwar, M., Akbar, N. and Bachri, S., 1992. *Geology of the Garut and Pameungpeuk Quadrangle, Java*. Geological Research and Development Centre, Directorate General of Geology and Mineral Resources, Department of Mines and Energy, Indonesia, 12p.

Amoseas Indonesia Inc., 1987. *Geothermal Assessment of the Darajat Contract Area, West Java, Indonesia. Phase I.* Unpublished Report, Amoseas Indonesia Inc., Indonesia, 124p.

Amoseas Indonesia Inc., 1989a. *Darajat Geothermal Project Feasibility Report. Part I. Results of Exploratory Survey and Drilling*. Unpublished Report, Amoseas Indonesia Inc., Indonesia, 113p.

Amoseas Indonesia Inc., 1989b. *Darajat Geothermal Project Feasibility Report. Part 2. Reservoir Evaluation.* Unpublished Report, Amoseas Indonesia Inc., Indonesia, 171p.

Amoseas Indonesia Inc., 1991. *Darajat Well Siting*. Unpublished Report, Amoseas Indonesia Inc., Indonesia, 151p.

Amoseas Indonesia Inc., 1998. G*eochemistry of Geothermal System with Emphasis on Vapor Dominated Systems*. Seminar for Amoseas Indonesia Inc., Darajat, West Java, Indonesia, PT Dames and Moore - Thermochem Inc., Indonesia, -p.

Appleyard, E.C., 1991. *SOMA - A Package of Fortran Programs for Calculating Mass Exchange in Metasomatic and Altered Rocks*. Unpublished Paper, Department of Earth Sciences, University of Waterloo, Canada, 38p.

Arehart, G.B., Christenson, B.W., Wood, C.P., Foland, K.A. and Browne, P.R.L., 2002. Timing of volcanic, plutonic and geothermal activity at Ngatamariki, New Zealand. *Journal of Volcanology and Geothermal Research*, 116, p.201-214.

Azam, S., Abduljauwad, S.N., Al-Shayea, N.A. and Al-Amoudi, O.S.B., 1998. Expansive characteristics of gypsiferous/anhydritic soil formation. *Engineering Geology*, 51, p.89-107.

Bargar, K.E. and Beeson, M.H., 1981. Hydrothermal alteration in research drill hole Y-2, Lower Geyser Basin, Yellowstone National Park, Wyoming. *The American Mineralogist*, 66, p.473-490.

Batini, F., Bertini, G., Gianelli, G., Pandeli, E., Puxeddu, M. and Villa, I.M., 1985. Deep structure, age and evolution of the Larderello-Travale geothermal field. *Geothermal Resource Council Transactions*, 9, Part I, p.253-259.

Beane, R.E., 1974. Biotite stability in the porphyry copper environment. *Economic Geology and the Bulletin of the Society of Economic Geologists*, 69, p.241-256.

Belkin, H.E., Cavarretta, G., De Vivo, B. and Tecce, F., 1988. Hydrothermal phlogopite and anhydrite from the SH2 well, Sabatini volcanic district, Latium, Italy: fluid inclusions and mineral chemistry. *The American Mineralogist*, 73, p.775-797.

van Bemmelen, R.W., 1949. *The Geology of Indonesia. Vol.1A*. The Hague, Goverment Printing Office, 732p.

Bignall, G. and Browne, P.R.L., 1994. Surface hydrothermal alteration and evolution of the Te Kopia thermal area, New Zealand. *Geothermics*, 23, p.645-658.

Bird, D.K. and Helgeson, H.C., 1981. Chemical interaction of aqueous solutions with epidote-feldspar mineral assemblages in geologic systems. II. Equilibrium constraints in metamorphic/geothermal processes. *American Journal of Science*, 281, p.576-614.

Bird, D.K., Schiffman, P., Elders, W.A., Williams, A.E. and McDowell, S.D., 1984. Calc-silicate mineralisation in active geothermal systems. *Economic Geology and the Bulletin of the Society of Economic Geologists*, 79, p.671-695.

Blount, C.W. and Dickson, F.W., 1969. The solubility of anhydrite ($CaSO_4$) in NaCl-H_2O from 100 to 450°C and 1 to 1000 bars. *Geochimica et Cosmochimica Acta*, 33, p.227-245.

Bowers, T.S, Jackson, K.J. and Helgeson, H.C., 1984. *Equilibrium Activity Diagrams*. Springer-Verlag, Berlin, 397p.

Bratakusuma, B.A., 1996. *Gas Distribution in Darajat Geothermal Field*. Unpublished Diploma Project Report, Geothermal Institute, the University of Auckland, New Zealand, -p.

Brindley, G.W. and Brown, G., 1980. Crystal structures of clay minerals and their X-ray identification. *Mineralogical Society Monograph*, 5, 495p.

Bronto, S., 1989. *Volcanic Geology of Galunggung, West Java, Indonesia*. Unpublished PhD Thesis, University of Canterbury, New Zealand, 490p.

Brown, E.H., 1977. Phase equilibria among pumpellyite, lawsonite, epidote and associated minerals in low grade metamorphic rocks. *Contribution to Mineralogy and Petrology*, 64, p.123-136.

Brown, K.L., Henley, R.W., Glover, R.B., Mroczek, E.K. and Plum, H., 1988. Dilution and boiling in the Wairakei Field due to exploitation 1959-1982. *Proceedings of the 10th New Zealand Geothermal Workshop*, the University of Auckland, New Zealand, p.263-267.

Browne, P.R.L., 1970. Hydrothermal alteration as an aid in investigating geothermal fields. *Geothermics*, Special issue 2, p.564-570.

Browne, P.R.L., 1978. Hydrothermal alteration in active geothermal fields. *Annual Reviews in Earth Planet Science*, 6, p.229-250.

Browne, P.R.L., 1989. Contrasting alteration styles of andesitic and rhyolitic rocks in geothermal fields of the Taupo Volcanic Zone, New Zealand. *Proceedings of the 11th New Zealand Geothermal Workshop*, the University of Auckland, New Zealand, p.111-116.

Browne, P.R.L., 1995. *Hydrothermal Alteration*. Lecture notes, Geothermal Institute, the University of Auckland, New Zealand, 68p.

Browne, P.R.L. and Ellis, A.J., 1970. The Ohaki-Broadlands hydrothermal area, New Zealand: mineralogy and related geochemistry. *American Journal of Science*, 269, p.97-131.

Browne, P.R.L. and Lawless, J.V., 2001. Characteristics of hydrothermal eruptions, with examples from New Zealand and elsewhere. *Earth-Science Reviews*, 52, p.299-331.

Browne, P.R.L., Courtney, S.F and Wood, C.P., 1989. Formation rates of calc-silicate minerals deposited inside drillhole casing, Ngatamariki geothermal field, New Zealand. *The American Mineralogist*, 74, p.759-763.

Bryndzia, L.T. and Scott, S.D., 1987. The composition of chlorite as a function of sulfur and oxygen fugacity: an experiment study. *American Journal of Science*, 287, p.50-76.

Burnham, C.W., 1997. Magmas and hydrothermal systems. In *Geochemistry of Hydrothermal Ore Deposits*., H.L. Barnes (ed.), John Wiley and Sons, Inc., New York, p.63-123.

de Caritat, P., Hutcheon. I. and Walshe, J.L., 1993. Chlorite geothermometry: a review. *Clays and Clay Minerals*, 41, p.219-239.

Cathelineau, M., 1988. Cation site occupancy in chlorites and illites as a function of temperature. *Clay Minerals*, 23, p.471-485.

Cathelineau, M. and Nieva, D., 1985. A chlorite solid solution geothermometer. The Los Azufres (Mexico) geothermal systems. *Contribution to Mineralogy and Petrology*, 91, p.235-244.

Cavarretta, G. and Tecce, F., 1987. Contact metasomatic and hydrothermal minerals in the SH2 deep well, Sabatini volcanic distric, Latium, Italy. *Geothermics*, 16, p.127-145.

Cavarretta, G., Gianelli, G. and Puxeddu, M., 1980. Hydrothermal metamorphism in the Larderello geothermal field. *Geothermics*, 9, p.297-314.

Cavarretta, G., Gianelli, G. and Puxeddu, M., 1982. Formation of authigenic minerals and their use as indicators of the physicochemical parameters of the fluid in the Larderello-Travale geothermal field. *Economic Geology and the Bulletin of the Society of Economic Geologists*, 77, p.1071-1084.

Celati, R., Noto, P., Panichi, C., Squarci, P. and Taffi, L., 1973. Interactions between the steam reservoir and the surrounding aquifers in the Larderello geothermal field. *Geothermics*, 2, p.174-185.

Cheynet, B., Dall' Aglio, M., Garavelli, A., Grasso, M.F. and Vurro, F., 2000. Trace elements from fumaroles at Vulcano Island (Italy): rates of transport and a thermochemical model. *Journal of Volcanology and Geothermal Re*search, 95, p.273-283.

Christidis, G. and Dunham, A.C., 1993. Compositional variations in smectites: Part 1. Alteration of intermediate volcanic rocks. A case study from Milos Island, Greece. *Clay Minerals*, 28, p.255-273.

Churchman, G.J., Whitton, J.S., Claridge, G.G.C. and Theng, B.K.G., 1984. Intercalation method using formamide for differentiating halloysite from kaolinite. *Clays and Clay Minerals*, 32, p.241-248.

Cox, K.G., Bell, J.D. and Pankhurst, R.J., 1979. *The interpretation of igneous rocks*. George Allen and Unwin Ltd., 450p.

Crowe, D.E., Riciputi, L.R., Bezenek, S. and Ignatiev, A., 2001. Oxygen isotope and trace element zoning in hydrothermal garnets: windows into large-scale fluid-flow behavior. *Geology (Boulder)*, 29, p.479-482.

Curtis, C.D., Hugher, C.R., Whiteman, J.A. and Whittle, C.K., 1985. Compositional variation within some sedimentary chlorites and some comments on their origin. *Mineralogy Magazine*, 49, p.375-386.

D'Amore, F. and Gianelli, G., 1984. Mineral assemblages and oxygen and sulfur fugacities in natural water-rock interaction processes. *Geochimica et Cosmochimica Acta*, 48, p.847-857.

D'Amore, F., Celati, R., Ferrara, G.C. and Panichi, C., 1977. Secondary changes in the chemical and isotopic composition of the geothermal fluids in Larderello field. *Geothermics*, 5, p.153-163.

Dalrymple, G.B., Grove, M., Lovera, O.M., Harrison, T.M., Hulen, J.B. and Lanphere, M.A., 1999. Age and thermal history of the Geysers plutonic complex (felsic unit), Geysers geothermal field, California: a $^{40}Ar/^{39}Ar$ and U-Pb study. *Earth and Planetary Science Letters*, 173, p.285-298.

Darman, H and Sidi, F.H., 2000. *An outline of the geology of Indonesia*. The Indonesian Association of Geologist, Jakarta, Indonesia, 192p.

Deer, W.A., Howie, R.A. and Zussman, J., 1962a. *Rock-Forming Minerals: Sheet Silicates*. Vol. 3, Longmans, Green and Co. Ltd., 270p.

Deer, W.A., Howie, R.A. and Zussman, J., 1962b. *Rock-Forming Minerals: Non Silicates*. Vol. 5, Longmans, Green and Co. Ltd., 371p.

Deer, W.A., Howie, R.A. and Zussman, J., 1978. *Rock-Forming Minerals: Disilicates and Ring Silicates*. Vol. 1B, 2nd edition, Longmans, Green and Co. Ltd., 629p.

Deer, W.A., Howie, R.A. and Zussman, J., 1992. *An Introduction to the Rock-forming Minerals*. 2nd ed., Longmans Group Ltd., 696p.

Dixon, J.B. and McKee, T.R., 1974. Internal and external morphology of tubular and spheroidal halloysite particles. *Clays and Clay Minerals*, 22, p.123-137.

Droop, G.T.R., 1987. A general equation for estimating Fe^{3+} concentrations in ferromagnesian silicates and oxides from microprobe analyses using stoichiometric criteria. *Mineralogical Magazine*, 51, p.431-435.

Dutrow, B.L. and Henry, D.J., 2000. Complexly zoned fibrous tourmaline, Cruzeiro Mine, Minas Gerais, Brazil: a record of evolving magmatic and hydrothermal fluids. *The Canadian Mineralogist*, 38, p.131-143.

Ebert, S.W. and Rye, R.O., 1997. Secondary precious metal enrichment by steam-heated fluids in the Crofoot-Lewis hot spring gold-silver deposit and relation to paleoclimate. *Economic Geology and the Bulletin of the Society of Economic Geologists*, 92, p.578-600.

Elders, W.A., Hoagland, J.R. and Olson, E.R., 1978. Hydrothermal mineralogy and isotopic geochemistry in the Cerro Prieto geothermal field, Mexico. III. Practical applications. *Geothermal Resources Council Transactions*, 2, p.177-180.

Elders, W.A., Hoagland, J.R., McDowell, S.D. and Cobo, J.M., 1979. Hydrothermal mineral zones in the geothermal reservoir of Cerro Prieto. *Geothermics*, 8, p.201-209.

Elder, W.A., Hoagland, J.R. and Williams, A.E., 1981. Distribution of hydrothermal mineral zones in the Cerro Prieto geothermal field of Baja California, Mexico. *Geothermics*, 10, p.245-253.

Elliott-Meadows, S.R. and Appleyard, E.C., 1991. The alteration geochemistry and petrology of the Lar Cu-Zn deposit, Lynn Lake Area, Manitoba, Canada. *Economic Geology and the Bulletin of the Society of Economic Geologists*, 86, p.486-505.

Ellis, A.J. and Golding, R.M., 1963. The solubility of carbon dioxide above 100°C in water and in sodium chloride solutions. *American Journal of Science*, 261, p.47-60.

Essene, E.J., 1983. Solid solutions and solvi among metamorphic carbonates with applications to geologic thermobarometry. In *Carbonates: Mineralogy and Chemistry*, R.J. Reeder (ed.), Reviews in Mineralogy, Vol.11, Mineralogical Society of America, p.77-96.

Evans, B.W. and Guggenheim, S., 1988. Talc, pyrophyllite, and related minerals. In *Hydrous Phyllosilicates*, S.W. Bailey (ed.), Reviews in Mineralogy, Vol. 19, Mineralogical Society of America, Washington, D.C., 725p.

Ferry, J.M. and Spear, F.S., 1978. Experimental calibration of the partitioning of Fe and Mg between biotite and garnet. *Contributions to Mineralogy and Petrology*, 66, p.113-117.

Filippo, M.D., Geri, G., Marson, I., Palmieri, F. and Perusini, P., 1985. Exploitation, subsidence and gravity changes in the Travale-Radicondoli geothermal field. *Geothermal Resources Council Transactions*, 9, p.273-278.

Fitzgerald, S.D. and Woods, A.W., 1995. Experimental and theoretical studies of liquid injection into vapour-dominated reservoir. *Proceedings of the 17th New Zealand Geothermal Workshop*, the University of Auckland, New Zealand, p.169-173.

Foster, M.D., 1961. *Interpretation on the composition of trioctahedral micas*. US Geological Survey Professional Paper, 354B, p.11-49.

Foster, M.D., 1962. *Interpretation on the composition and a classification of the chlorites*. US Geological Survey Professional Paper, 414A, 33p.

Fournier, R.O., 1985. The behaviour of silica in hydrothermal solutions. In *Geology and Geochemistry of Epithermal Systems*, B.R. Berger and P.M. Bethke (eds.), Reviews in Economic Geology, Vol. 2, p.45-59.

Fulignati, P., Malfitano, G. and Sbrana, A., 1997. The Pantelleria caldera geothermal system: data from the hydrothermal minerals. *Journal of Volcanology and Geothermal Research*, 75, p.251-270.

Gemmell, J.B., Herrmann, W. and Large, R.R., 2002. Alteration associated with volcanic-hosted massive sulfide deposits, and its exploration significance. *Auss IMM Conference 2002 Proceedings Volume*, Auckland, New Zealand, p.203-208.

Geothermal Energy of New Zealand Ltd. (GENZL), 1986. *Darajat Geochemical Survey. Final Interpretative Report.* Unpublished Report, Amoseas Indonesia Inc., Indonesia, -p.

Geothermal Energy of New Zealand Ltd. (GENZL), 1990. *Darajat Geothermal Power Plant Feasibility Study*. Unpublished Report, Amoseas Indonesia Inc., Indonesia, 415p.

Geothermal Energy of New Zealand Ltd. (GENZL), 1996. *Darajat Geothermal Project Reserves Assessment*. Unpublished Report, Amoseas Indonesia Inc., Indonesia, -p.

Ghiorso, M.S. and Sack, R.O., 1991. Fe-Ti oxide geothermometry: thermodynamic formulation and the estimation of intensive variables in silicic magmas. *Contribution to Mineralogy and Petrology*, 108, p.485-510.

Gianelli, G. and Ruggieri, G., 2002. Evidence of a contact metamorphic aureole with high-temperature metasomatism in the deepest part of the active geothermal field of Larderello, Italy. *Geothermics*, 31, p.443-474.

Giggenbach, W.F., 1981. Geothermal mineral equilibria. *Geochimica et Cosmochimica Acta*, 45, p.393-410.

Giggenbach, W.F., 1988. Geothermal solute equilibria. Derivation of Na-K-Mg-Ca geoindicators. *Geochimica et Cosmochimica Acta*, 52, p.2749-2765.

Giggenbach, W.F., 1992a. Isotopic shifts in waters from geothermal and volcanic systems along convergent plate boundaries and their origin. *Earth and Planetary Science Letters*, 113, p.495-510.

Giggenbach, W.F., 1992b. Magma degassing and mineral deposition in hydrothermal systems along convergent plate boundaries. *Economic Geology and the Bulletin of the Society of Economic Geologists*, 87, p.1927-1944.

Giggenbach, W.F., 1995. Variations in the chemical and isotopic composition of fluids discharged from the Taupo Volcanic Zone, New Zealand. *Journal of Volcanology and Geothermal Research*, 68, p.89-116.

Giggenbach, W.F., 1997a. Relative importance of thermodynamic and kinetic processes in governing the chemical and isotopic composition of carbon gases in high-heatflow sedimentary basins. *Geochimica et Cosmochimica Acta*, 61, p.3763-3785.

Giggenbach, W.F., 1997b. The origin and evolution of fluids in magmatic-hydrothermal systems. In *Geochemistry of Hydrothermal Ore Deposits*, H.L. Barnes (ed.), John Wiley and Sons, Inc., New York, p.737-796.

Giggenbach, W.F., Sano, Y. and Wakita, H., 1993. Isotopic composition of helium, and CO_2 and CH_4 contents in gases produced along the New Zealand part of a convergent plate boundary. *Geochimica et Cosmochimica Acta*, 57, p.3427-3455.

Gill, J.B., 1981. *Orogenic Andesites and Plate Tectonics*. Springer-Verlag, Berlin, 389p.

von Goerne, G. and Franz, G., 2000. Synthesis of Ca-tourmaline in the system CaO-MgO-Al_2O_3-SiO_2-B_2O_3-H_2O-HCl. *Mineralogy and Petrology*, 69, p.161-182.

von Goerne, G. and Franz, G., 2001. Synthesis of tourmaline solid solutions in the system Na_2O-MgO-Al_2O_3-SiO_2-B_2O_3-H_2O-HCl and the distribution of Na between tourmaline and fluid at 300 to 700°C and 200 MPa. *Contributions to Mineralogy and Petrology*, 141, p.160-173.

Goff, F. and Janik, C.J., 2000. Geothermal systems. In *Encyclopedia of Volcanoes*, H. Sigurdsson, B.F. Houghton, S.R. McNutt, H. Rymer and J. Stix (eds.), Academic Press, p.817-834.

Goguel, J., 1982. The behaviour of vapour-dominated reservoirs. *Geothermics*, 11, p.3-13.

Gonzáles-Partida, E. and Lavresse, G., 2003. Fluid inclusion evolution at the La Verde porphyry copper deposit, Michocan, Mexico. *Journal of Geochemical Exploration*, 78-79, p.623-626.

Gonzáles-Partida, E., Birkle, P. and Torres-Alvarado, I.S., 2000. Evolution of the hydrothermal system at Los Azures, Mexico, based on petrologic, fluid inclusion and isotopic data. *Journal of Volcanology and Geothermal Research*, 104, p.277-296.

Grant, M.A., 1979a. Interpretation of downhole pressure measurements at Baca. *Proceedings of the 5th Workshop on Geothermal Reservoir Engineering*, Stanford University, California, p.261-268.

Grant, M.A., 1979b. Water content of the Kawah Kamojang geothermal reservoir. *Geothermics*, 8, p.21-30.

Grant, M.A., 1982. On the lack of a unique relation between CO_2 partial pressure and temperature in geothermal system. Comment on "Geothermal mineral equilibria" by W.F. Giggenbach. *Geochimica et Cosmochimica Acta*, 46, p.2677-2680.

Green, T.H. and Ringwood, A.E., 1968. Origin of garnet phenocryst in calc alkaline rocks. *Contribution to Mineralogy and Petrology*, 18, p.163-174.

Green, T.H. and Ringwood, A.E., 1972. Crystallization of garnet-bearing rhyodacite under high-pressure hydrous conditions. *Journal of the Geology Society of Australia*, 19, p.203-212.

Gresens, R.L., 1967. Composition-volume relationships of metasomatism. *Chemical Geology*, 2, p.47-55.

Grey, I.E., Watts, J.A. and Bayliss, P., 1994. Mineralogical nomenclature: pseudorutile revalidated and neotype given. *Mineralogical Magazine*, 58, p.597-600.

Grim, R.E., 1968. *Clay Mineralogy*. 2nd edition, McGraw-Hill, Inc., 596p.

Groves, A.W., 1958. *Gypsum and anhydrite*. Overseas Geological Surveys, Mineral Resources Division, Her Majesty's Stationary Office, 108p.

Gudmundsson, B.T. and Arnórsson, S., 2002. Geochemical monitoring of the Krafla and Námafjall geothermal areas, N-Iceland. *Geothermics*, 31, p.195-243.

Güven, N., 1988. Smectite. In *Hydrous Phyllosilicates (Exclusive of Micas)*, S.W. Bailey (ed.), Reviews in Mineralogy, 19, Mineralogical Society of America, p.497-559.

Hadi, J., 1997. *A Hydrothermal alteration study to assess temperature and overprinting from S-1 exploration well - North Darajat field, Indonesia*. Unpublished Diploma Project Report, Geothermal Institute, the University of Auckland, New Zealand, 65p.

Hadi, J., 2001. The Darajat Geothermal Field Conceptual Model, A Vapor Dominated System. *Proceeding of the 5th Indonesian Geothermal Association (INAGA) Annual Scientific Conference and Exhibitions*. Yogyakarta, Indonesia, p.-.

Hamilton, W.B., 1979. *Tectonic of the Indonesia Region*. Geological Survey Professional Paper 1078, US Government Printing Office, Washington, 345p.

Hammarstrom, J.M. and Zen, E., 1986. Aluminium in hornblende. An empirical igneous geobarometer. *The American Mineralogist*, 71, p.1297-1313.

Haas, J.L. Jr., 1971. The effect of salinity on the maximum thermal gradient of a hydrothermal system at hydrostatic pressure. *Economic Geology and the Bulletin of the Society of Economic Geologists*, 66, p.940-946.

Hawthorne, F.C. and Ferguson, R.B., 1975. Anhydrous sulphates. II. Refinement of the crystal structure of anhydrite. *Canadian Mineralogist*, 31, p.289-292.

Healy, J., 1975. *Geology of the Kawah Manuk District, West Java*. ENEX, Geothermal Energy of New Zealand Ltd., Geothermal Project, Indonesia.

Hedenquist, J.W. and Henley, R.W., 1985. The importance of CO_2 on freezing point measurements of fluid inclusions: evidence from active geothermal systems and implications for epithermal ore depositions. *Economic Geology and the Bulletin of the Society of Economic Geologists*, 80, p.1379-1406.

Hedenquist, J.W. and Browne, P.R.L., 1989. The evolution of the Waiotapu geothermal system, New Zealand, based on the chemical and isotopic composition of its fluids, minerals and rocks. *Geochimica et Cosmochimica Acta*, 53, p.2235-2257.

Helgeson, H.C., Delany, J.M., Nesbitt, H.W. and Bird, D.K., 1978. Summary and critique of the thermodynamic properties of rock-forming minerals. *American Journal of Science*, 278A, p.1-229.

Henry, D.J. and Guidotti, C.V., 1985. Tourmaline as a petrogenetic indicator mineral: an example from the staurolite-grade metapelites of NW Maine. *The American Mineralogist*, 70, p.1-15.

Heuss-Aβbichler, S. and Fehr, K.T., 1997. Intercrystalline exchange of Al and Fe^{3+} between grossular-andradite and clinozoisite-epidote solid solutions. *Neues Jahrbuch fuer Mineralogie Abh*. 172, p.69-100.

Hey, M.H., 1954. A new review of the chlorites. *Mineralogical Magazine*, 30, p.277-292.

Hinckley, D.N., 1963. Variability in 'crystallinity' values among the kaolin deposits of the coastal plain of Georgia and South Carolina. *Clays and Clay Minerals*, 25, p.451-456.

Hoagland, J.R. and Bodell, J.M., 1991. The Tiwi geothermal reservoir: geologic characteristics and response to production. *Petromineralogy*, 20, p.28-35.

Hochstein, M.P. and Browne, P.R.L., 2000. Surface manifestation of geothermal systems with volcanic heat sources. In *Encyclopedia of Volcanoes*, H. Sigurdsson, B.F. Houghton, S.R. McNutt, H. Rymer and J. Stix (eds.), Academic Press, p.835-855.

Holaway, M.J., 1972. Thermal stability of Al-Fe epidote as a function of fO_2 and Fe content. *Contributions to Mineralogy and Petrology*, 37, p.307-340.

Honda, S., 1970. Hydrothermal alteration in core from research drill hole Y-1, Upper Geyser Basin, Yellowstone National Park, Wyoming. *The American Mineralogist*, 55, p.1714-1737.

Huertas, F.J., Cuadros, J. and Linares, J., 1995. Modelling of potassium exchange in a natural, polyionic montmorillonite under hydrothermal conditions. *Applied Geochemistry*, 10, p.347-355.

Hutcheon. I., de Caritat, P. and Abercrombie, H.J., 1974. Clay minerals – equilibrium models and temperature indicators. In *Alteration and Alteration Processes Associated with Ore-Forming Systems*, D.R. Lentz (ed.), Short Course Notes, vol, 2, Mineral Deposits Devision, Geological Association of Canada, p.43-67.

Ingebritsen, S.E. and Sorey, M.L., 1985. A quantitative analysis of the Lassen hydrothermal system, north central California. *Water Resources Research*, 21, p.853-868.

Ingebritsen, S.E. and Sorey, M.L., 1988. Vapor-dominated zones within hydrothermal systems: evolution and natural state. *Journal of Geophysical Research*, 93, p.13,635-13,655.

Jacobs, D.C. and Parry, W.T., 1976. A comparison of the geochemistry of biotite from some basin and range stocks. *Economic Geology and the Bulletin of the Society of Economic Geologists*, 71, p.1029-1035.

Jacobs, D.C. and Parry, W.T., 1979. Geochemistry of biotite in the Santa Rita porphyry copper deposit, New Mexico. *Economic Geology and the Bulletin of the Society of Economic Geologists*, 74, p.860-887.

James, R.S., 1977. Internal consistency of experimental results demonstrated by the application of Schreinemakers rules to the iron chlorite data. In *Application of Thermodynamics to Petrology and Ore Deposits*, H.J. Greenwood (ed.), Short Course Handbook, vol, 2, Mineralogical Association of Canada, p.216-231.

Ji, J. and Browne, P.R.L., 2000. Relationship between illite crystallinity and temperature in active geothermal systems of New Zealand. *Clays and Clay Minerals*, 48, p.139-144.

Jiang, S.Y., Palmer, M.R. and Slack, J.F., 1996. Mn rich ilmenite from the Sullivan Pb-Zn-Ag deposit, British Columbia. *The Canadian Mineralogist*, 34, p.29-36.

Jiang, S.Y., Palmer, M.R. and Yeats, C.J., 2002. Chemical and boron isotopic compositions of tourmaline from the Archean Big Bell and Mount Gibson gold deposits, Murchison Province, Yilgarn Craton, Western Australia. *Chemical Geology*, 188, p.229-247.

Kalinin, D.V. and Shapovalova, M.A., 1975. Kinetics of pyrophyllite formation and the stability limits of the mineral. *Geochemistry International*, 12, p.231-236.

Katili, J.A. 1975. Volcanism and plate tectonics in the Indonesian island arcs. *Tectonophysics*, 26, p.165-188.

Kawakami, T., 2001. Boron depletion controlled by the breakdown of tourmaline in the migmatite zone of the Aoyama Area, Ryoke Metamorphic Belt, Southwestern Japan. *The Canadian Mineralogist*, 39, p.1529-1546.

Keith, T.E.C., Muffler, L.J.P. and Cremer, M., 1968. Hydrothermal epidote formed in the Salton Sea geothermal system, California. *The American Mineralogist*, 53, p.1635-1644.

Keller, J.V.A., Rejeki, S., Harrison, C., 2006. Fracture Characterization and Geological Modeling of the DarajatGeothermal Field, West Java, Indonesia. *Proceeding of American Association of Petroleum Geologists (AAPG) International Conference and Exhibition*, Perth, p.-.

Keller, W.D. and Haenni, R.P., 1978. Effects of micro-sized mixtures of kaolin minerals on properties of kaolinites. *Clays and Clay Minerals*, 26, p.384-396.

Kingston Morisson Ltd., 1996. *Geochemical Review of the Darajat Geothermal Field*. Unpublished Report, Amoseas Indonesia Inc., Indonesia, p.-.

Kiyosu, Y., Asada, N. and Yoshida, Y., 1992. Origin of light hydrocarbon gases from the Matsukawa geothermal area in Japan. *Chemical Geology (Isotope Geoscience Section)*, 94, p.321-329.

Komaruddin, U. and Sujata, I.K., 1999. Kamojang geothermal field, Indonesia; evaluation and expectation after 15 years operation. *Geothermal Resources Council Transactions*, 23, p.549-555.

Lagache, M. and Weisbrod, A., 1977. The system: two alkali feldspars-KCl-NaCl-H_2O at moderate to high temperatures and low pressures. *Contributions to Mineralogy and Petrology*, 62, p.77-101.

Leake, B.E., 1978. Nomenclature of amphiboles. *The American Mineralogist*, 63, p.1023-1053.

Leitch, C.H.B. and Lentz, D.R., 1994. The Greisen approach to mass balance constraints of the alteration system: methods, pitfalls, examples. In *Alteration and Alteration Processes Associated with Ore-forming Systems*, D.R. Lentz (ed.), Short course notes volume 11, Geological Society of Canada, p.161-192.

de Ligny, D. and Navrotsky, A., 1999. Energetics of kaolin polymorphs. *The American Mineralogist*, 84, p.506-516.

Liou, J.G., 1971. Synthesis and stability relations of prehnite, $Ca_2Al_2Si_3O_{10}(OH)_2$. *The American Mineralogist*, 56, p.507-531.

Liou, J.G., 1972. Synthesis and stability relations of epidote, $Ca_2Fe^{+3}Al_2Si_3O_{13}H$. *Eos - American Geophysical Union Transactions* , 53, p.538-539.

Liou, J.G., 1973. Synthesis and stability relations of epidote, $Ca_2Al_2FeSi_3O_{12}(OH)$. *Journal of Petrology*, 14, p.381-413.

Liou, J.G., Shik, K.H. and Shigenori, M., 1983. Prehnite-epidote equilibria and their petrologic applications. *Journal of Petrology*, 24, p.321-342.

Lutz, S.J., Moore, J.M., Adams, M.C. and Norman, D.I., 1999. Tracing fluid sources in the Coso geothermal system using fluid-inclusion gas chemistry. *Proceeding 24th Workshop on Geothermal Reservoir Engineering*, Stanford University, California, p.188-195.

MacLean, W.H., 1990. Mass change calculations in altered rock series. *Mineralium Deposita*, 25, p.44-49.

MacLean, W.H. and Barrett, T.J., 1993. Lithogeochemical techniques using immobile elements. *Journal of Geochemical Exploration*, 48, p.109-133.

MacLean, W.H. and Kranidiotis, P., 1987. Immobile elements as monitors of mass transfer in hydrothermal alteration: Phelps Dodge Massive Sulfide Deposit, Matagami, Quebec. *Economic Geology and the Bulletin of the Society of Economic Geologists*, 82, p.951-962.

Mahon, W.A.J., McDowell, G.D. and Finlayson, J.B., 1980. Carbon dioxide: its role in geothermal systems. *New Zealand Journal of Science*, 23, p.133-148.

Mark,G. and Foster, D.R.W., 2000. Magmatic-hydrothermal albite-actinolite-apatite-rich rocks from the Cloncurry District, NW Queensland, Australia. *Lithos*, 51, p.223-245.

Martinez-Serrano, R.G., 2002. Chemical variations in hydrothermal minerals of the Los Humeros geothermal system, Mexico. *Geothermics*, 31, p.579-612.

Martodjojo, S., 1984. *Evolusi Cekungan Bogor, Jawa Barat*. Unpublished PhD thesis, Institut Teknologi Bandung, Indonesia, -p.

Mas, A., Patrier, P., Beaufort, D. and Genter, A., 2003. Clay-mineral signatures of fossil and active hydrothermal circulations in the geothermal system of the Lamentin Plain, Martinique. *Journal of Volcanology and Geothermal Research*, 124, p.195-218.

McDowell, S.D. and Elders, W.A., 1983. Allogenic layer silicate minerals in borehole Elmore Salton Sea geothermal field, California. *The American Mineralogist*, 68, p.1146-1159.

Miller, W.D. and Keller, W.D., 1963. Differentiation between endellite-halloysite and kaolinite by treatment with potassium acetate and ethylene glycol. *Clays and Clay Minerals*, 10, p.244-253.

Minster, J.B. and Jordan, T.H., 1978. Present day plate motion. *Journal of Geophysical Research*, 83, p.5331-5334.

Moore, D.M. and Reynolds, Jr, R.C., 1989. *X-ray Diffraction and the Identification and Analysis of Clay Minerals*. Oxford University Press, Inc., 332p.

Moore, D.M. and Reynolds, Jr, R.C., 1997. *X-ray Diffraction and the Identification and Analysis of Clay Minerals*. 2nd edition, Oxford University Press, Inc., 378p.

Moore, J.N. and Adams, M.C., 1988. Evolution of the thermal cap in two wells from the Salton Sea geothermal system, California. *Geothermics*, 17, p.695-710.

Moore, J.N., Lutz, S.J., Renner, J.L., McCulloch, J. and Petty, S., 2000a. Evolution of a volcanic-hosted vapor-dominated system: petrologic and geochemical data from corehole T-8, Karaha-Telaga Bodas, Indonesia. *Geothermal Resources Council Transactions*, 24, p.259-263.

Moore, J.N., Adams, M.C. and Anderson, A.J., 2000b. The fluid inclusion and mineralogic record of the transition from liquid- to vapor-dominated conditions in the Geyser geothermal system, California. *Economic Geology and the Bulletin of the Society of Economic Geologists*, 95, p.1719-1737.

Moore, J.N., Powell, T.S., Heizler, M.T. and Norman, D.I., 2000c. Mineralization and hydrothermal history of the Tiwi geothermal system, Philippines. *Economic Geology and the Bulletin of the Society of Economic Geologists*, 95, p.1001-1023.

Moore, J.N., Norman, D.I. and Kennedy, B.M., 2001. Fluid inclusion gas compositions from an active magmatic-hydrothermal system: a case study of the Geysers geothermal field, USA. *Chemical Geology*, 173, p.3-30.

Moore, J.N., Christensen, B., Browne, P.R.L. and Lutz, S.J., 2002a. The mineralogic consequences and behavior of descending acid-sulfate waters: an example from the Karaha-Telaga Bodas geothermal systems, Indonesia. *Proceeding 27th Workshop on Geothermal Reservoir Engineering*, Stanford University, California, p.257-265.

Moore, J.N., Norman, D.I. and Allis, R.G., 2002b. Geochemical evolution of the vapor-dominated refime at Karaha-Telaga Bodas, Indonesia: insights from fluid inclusion gas compositions. *Proceedings of the 24th New Zealand Geothermal Workshop*, the University of Auckland, New Zealand, p.243-248.

Morad, S., 1998. Carbonate cementation in sandstones: distribution patterns and geochemical evolution. In *Carbonate Cementation in Sandstones*, S. Morad (ed.), Special Publication International Association of Sedimentologists, 26, p.1-26.

Morad, S. and Aldahan, A.A., 1985. Leucoxene-calcite-quartz aggregates in sandstones and the relation to decomposition of sphene. *Neues Jahrbuch fuer Mineralogie Monatshefte*. 10, p.458-468.

Mŭcke, A. and Chaudhuri, J.N.B., 1991. The continuous alteration of ilmenite through pseudorutile to leucoxene. *Ore Geology Reviews*, 6, p.25-44.

Nakamura, H. and Sumi, K., 1961. Geothermal investigations of Matsukawa hotspring area, Iwate prefecture. *Chishitsu Chosajo Geppo. Bulletin - Japan, Geological Survey*, 12, p.73-84.

Norman, D.I. and Moore, J.N., 1999. Methane and excess N_2 and Ar in geothermal fluid inclusions. *Proceeding 24th Workshop on Geothermal Reservoir Engineering*, Stanford University, California, p.196-202.

Norman, D.I. and Musgrave, J.A., 1994. N_2-Ar-He compositions in fluid inclusions: Indicator of fluid source. *Geochimica et Cormochimica Acta*, 58, p.1119-1131.

Norman, D.I. and Sawkins, F.J., 1987. Analysis of gases in fluid inclusions by mass spectrometer. *Chemical Geology*, 61, p.10-21.

Norman, D.I., Moore, J.N., Yonaka, B. and Musgrave, J., 1996. Gaseous species in fluid inclusions: a tracer of fluids and indicator of fluid processes. *Proceeding 21st Workshop on Geothermal Reservoir Engineering*, Stanford University, California, p.233-240.

Norman, D.I., Moore, J.N. and Musgrave, J., 1997. Gaseous species as tracers in geothermal systems. *Proceeding 22nd Workshop on Geothermal Reservoir Engineering*, Stanford University, California, p.419-426.

Norman, D.I., Blamey, N.J. and Moore, J.N., 2001. Overabundance of gaseous species and the source of organic compounds in geothermal fluids. *Proceeding 26th Workshop on Geothermal Reservoir Engineering, Stanford University*, University of Stanford, California, p.390-397.

Norman, D.I., Blamey, N.J. and Moore, J.N., 2002. Interpreting geothermal processes and fluid sources from fluid inclusion organic compounds and CO_2/N_2 ratios. *Proceeding 27th Workshop on Geothermal Reservoir Engineering*, Stanford University, California, p.266-274.

Nukman, M., 1999. *Interpretation of thermal changes in well S-3B, Darajat field based on hydrothermal alteration study*. Unpublished Diploma Project Report, Geothermal Institute, the University of Auckland, New Zealand, 56p.

Ozeki, H., Fukuda, D. and Okumura, T., 2001. Historical changes of geothermal reservoir models at Matsukawa, Japan. *Chinetsu. Journal of the Japan Geothermal Energy Association*, 38/4, p.27-56.

Padmosukismo, S. and Yahya, I., 1974. The basement configuration of the northwest Java basinal area. *Proceedings of Indonesian Petroleum Association*, Jakarta, Indonesia, p.129-152.

Pattison, D.R.M., 1994. Are reversed Fe-Mg exchange and solid solution experiments really reversed? *The American Mineralogist*, 79, p.938-950.

Peacor, D.R., Bauluz, B., Dong, H., Tillick, D. and Yan, Y., 2002. Transmission and analytical electron microscopy evidence for high Mg contents of 1M illite: absence of 1M polytypism in normal prograde diagenetic sequences of pelitic rocks. *Clays and Clay Minerals*, 50, p.757-765.

Pe-Piper, G., 1988. Calcic amphiboles of mafic rocks of the Jeffers Brook plutonic complex, Nova Scotia, Canada. *The American Mineralogist*, 73, p.993-1006.

Pestov, I., 1995. Modelling studies of the evolution of vapour-dominated geothermal systems. *Proceedings of the 17th New Zealand Geothermal Workshop*, the University of Auckland, New Zealand, p.199-204.

Pollard, P.J., 2001. Sodic (-calcic) alteration in Fe-oxide-Cu-Au district: an origin via unmixing of magmatic H_2O-CO_2-NaCl±$CaCl_2$-KCl fluids. *Mineralium Deposita*, 36, p.93-100.

Porter, S., Vanko, D.A. and Ghazi, A.M., 2000. major and trace element compositions of secondary clays in basalts altered at low temperature, eastern flank of the Juan de Fuca Ridge. *Proceedings of the Ocean Drilling Program, Scientific Results*, 168, p.149-157.

Potter II, R.W., Clynne, M.A. and Brown, D.L., 1978. Freezing point depression of aqueous sodium chloride solutions. *Economic Geology and the Bulletin of the Society of Economic Geologists*, 73, p.284-285.

Pramono, B., 1999. *Hydrothermal alteration to assess temperature and the origin of deep acid fluid in well S-3B, Darajat field, Indonesia*. Unpublished Diploma Project Report, Geothermal Institute, the University of Auckland, New Zealand, 58p.

Prol-Ledesma, R.M., 1998. Pre- and post-exploitation variations in hydrothermal activity in Los Humeros geothermal field, Mexico. *Journal of Volcanology and Geothermal Research*, 83, p.313-333.

Purbawinata, M.A., 1988. Some geochemical aspects from Guntur Gandapura volcanic centre, West Java, Indonesia. Geological Society of New Zealand. Annual Conference, Programme and Abstracts. *Geological Society of New Zealand Miscellaneous Publication*, 41a, p.124.

Reed, M.H., 1974. Hydrothermal alteration in Active Continental Hydrothermal Systems. In *Alteration and Alteration Processes Associated with Ore-Forming Systems*, D.R. Lentz (ed.), Short Course Notes, vol, 2, Mineral Deposits Devision, Geological Association of Canada, p.315-337.

Reed, M.H., 1997. Hydrothermal alteration and its relationship to ore fluid composition. In *Geochemistry of Hydrothermal Ore Deposits*, H.L. Barnes (ed.), 3rd ed., John Wiley and Sons, Inc., New York, p.303-365.

Rejeki, S., Rohrs, D., Nordquist, G., Fitriyanto, A., 2010. Geologic Conceptual Model Update of the Darajat Geothermal Field, Indonesia. *Proceedings World Geothermal Congress 2010*, Bali, Indonesia, p.-.

Reyes, A.G., 1990. Petrology of Philippine geothermal systems and the application of alteration mineralogy to their assessment. *Journal of Volcanology and Geothermal Research*, 43, p.279-309.

Reyes, A.G., 2000. *Petrology and Mineral Alteration in Hydrothermal Systems: from Diagenesis to Volcanic Catastrophes*. Lecture notes, United Nations University, Geothermal Training Programme, Reykjavic, Iceland, 77p.

Reyes, A.G. and Giggenbach, W.F., 1992. Petrology and fluid chemistry of magmatic-hydrothermal systems in the Philippines. *Proceedings - International Symposium on Water-Rock Interaction*, 7, p.1341-1344.

Reyes, A.G., Giggenbach, W.F., Saleras, J.R.M., Salonga, N.D. and Vergara, M.C., 1993. Petrology and geochemistry of Alto Peak, a vapor-cored hydrothermal system, Leyte Province, Philippine. *Geothermics*, 22, p.479-519.

Rickwood, P.C., 1968. On recasting analyses of garnet into end member molecules. *Contributions to Mineralogy and Petrology*, 18, p.175-198.

Roedder, E., 1984. *Fluid Inclusions*. Reviews in Mineralogy, Vol. 12, Mineralogical Society of America, Washington, D.C., 644p.

Rosenberg, P.E., 2002. The nature, formation, and stability of end-member illite: a hypothesis. *The American Mineralogist*, 87, p.103-107.

Rosenberg, P.E and Cliff, G., 1980. The formation of pyrophyllite solid solutions. *The American Mineralogist*, 65, p.1217-1219.

Ruggieri, G and Gianelli, G., 1999. Multi-stage fluid circulation in a hydraulic fracture breccia of the Larderello geothermal field (Italy). *Journal of Volcanology and Geothermal Research*, 90, p.241-261.

Sahai, N., 2003. The effects of Mg^{2+} and H^{+} on apatite nucleation at silica surfaces. *Geochimica et Cosmochimica Acta*, 67, p.1017-1030.

Sasada, M., 1986. Anhydrite precipitation by low pressure boiling at DW-5 drill hole, Hohi geothermal area, Japan: fluid inclusion evidence and geological significance. *Geothermal Resources Council Transactions*, 10, p.149-154.

Schiffman, P. and Liou, J.G., 1983. Synthesis of Fe-pumpellyite and its stability relations with epidote. *Journal of Metamorphic Geology*, 1, p.91-101.

Schiffman, P., Elders, W.A., Williams, A.E., McDowell, S.D. and Bird, D.K., 1984. Active metasomatism in the Cerro Prieto geothermal system, Baja California, Mexico: a telescoped low-pressure, low-temperature metamorphic facies series. *Geology (Boulder)*, 12, p.12-15.

Sheets, S.A., Oreskes, N., Rhodes, A.L., Bodnar, R.J. and Szabo, C., 1997. Fluid inclusion evidence for a hydrothermal origin for magnetite-apatite mineralization at El Laco, Chile. *Geological Society of America, 1997 annual meeting, Abstracts with Programs*, 29, p.50.

Shook, G.M., 1995. Development of a vapor-dominated reservoir with a “high-temperature” component. *Geothermics*, 24, p.489-505.

Shriver, N.A. and MacLean, W.H., 1993. Mass, volume and chemical changes in the alteration zone at the Norbec mine, Noranda, Quebec. *Mineralium Deposita*, 28, p.157-166.

Sibbett, B.S., 1988. Size, depth and related structures of intrusions under stratovolcanoes and associated geothermal systems. *Earth Science Review*, 25, p.291-309.

Simmons, S.F. and Christenson, B.W., 1994. Origins of calcite in a boiling geothermal system. *American Journal of Science*, 294, p.361-400.

Simmons, S.F. and Browne, P.R.L., 2000. Hydrothermal minerals and precious metals in the Broadlands-Ohaaki geothermal system; implications for understanding low-sulfidation epithermal environments. *Economic Geology and the Bulletin of the Society of Economic Geologists*, 95, p.971-999.

Simmons, S.F., Keywood, M., Scott, B.J. and Keam, R.F., 1993. Irreversible change of the Rotomahana-Waimangu hydrothermal system (New Zealand) as a consequence of a volcanic eruption. *Geology (Boulder)*, 21, p.643-646.

Sugisaki, R. and Nagamine, K., 1995. Evolution of light hydrocarbon gases in subsurface processes: constraints from chemical equilibrium. *Earth and Planetary Science Letters*, 133, p.151-161.

Suwijanto, 1978. *Hubungan antara kegempaan dengan kelurusan structur pada citra landsat di daerah Jawa Barat: suatu tinjauan*. Unpublished Report, Lembaga Ilmu Pengetahuan Indonesia (LIPI), 1, Indonesia, p.1-8.

Swindale, L.D. and Hughes, I.R., 1968. Hydrothermal association of pyrophyllite, kaolinite, diaspore, dickite and quartz in the Coromandel Area, New Zealand. *New Zealand Journal of Geology and Geophysics*, 11, p.1163-1183.

Syahbuddin, A., Sumantri, Y.R., Kartanegara, L. and Asikin, S., 1986. Pola perkembangan tektonik Cekungan Rangkasbitung, Jawa Barat, selama Tersier sebagai akibat dari letaknya yang berada di antara Cekungan Bogor, Cekungan Jawa Baratdaya dan Cekungan Sumatra Selatan. *The 15th Annual Conference of Indonesian Association of Geology*, Yogyakarta, Indonesia, p.-.

Takagi, T., Koh, S.M., Kim, M.Y., Naito, K. and Sudo, S., 2000. Geology and hydrothermal alteration of the Milyang pyrophyllite deposit, Southeast Korea. *Resource Geology*, 50, p.243-256.

Takeno, N., 2000. Thermal and geochemical structure of the Uenotai geothermal system, Japan. *Geothermics*, 29, p.257-277.

Taverne, N.J.M., 1926. *Vulkaanstudiën op Java*. Volkanologische Mededeelingen, 7, 'S-Gravenhage-Algemeene Landsdrukkerij, 132p.

Taylor, G.F. and Appleyard, E.C., 1983. Weathering of the Zinc-Lead lode, Dugald River, Northwest Queensland: I. The gossan profile. *Journal of Geochemical Exploration*, 18, p.87-110.

Tómasson, J. and Kristmannsdóttir, H., 1972. High temperature alteration minerals and thermal brines, Reykjanes, Iceland. *Contribution to Mineralogy and Petrology*, 36, p.123-134.

Truesdell, A.H. and White, D.E, 1973. Production of superheated steam from vapor-dominated geothermal reservoirs. *Geothermics*, 2, p.154-173.

Tsuzuki, Y., 1976. Solubility diagrams for explaining zone sequences in bauxite, kaolin and pyrophyllite-diaspore deposits. *Clays and Clay Minerals*, 24, p.297-302.

Veizer, J., 1983. Trace elements and isotopes in sedimentary carbonates. In *Carbonates: Mineralogy and Chemistry*, R.J. Reeder (ed.), Reviews in Mineralogy, Vol.11, Mineralogical Society of America, p.265-299.

Velde, B., 1985. *Clay Minerals. A physico-chemical Explanation of Their Occurrence*. Elsevier, Amsterdam, 427p.

Velde, B. and Brusewitz, A.M., 1986. Composition variation in component layers in natural illite/smectite. *Clays and Clay Minerals*, 34, p.651-657.

Weast, R.C. (ed.), 1974. *Handbook of Chemistry and Physic*. CRC Press, Ohio, -p.

Wendland, R.E. and Eggler, D.H., 1980. The origin of potassic magma: 2. Stability of phlogopite in natural spinel lherzolite and in the system $KalSiO_4$-MgO-SiO_2-H_2O-CO_2 at high pressures and high temperatures. *American Journal of Science*, 280, p.421-458.

Wheeler, R.S., Browne, P.R.L. and Rodgers, K.A., 2001. Iron-rich and iron-poor prehnite from the Way Linggo epithermal Au-Ag deposit, southwest Sumatra, and the Heber geothermal field, California. *Mineralogical Magazine*, 65, p.373-382.

White, D.E., Muffler, L.J.P. and Truesdell, A.H., 1971. Vapour-dominated hydrothermal systems compared with hot-water systems. *Economic Geology and the Bulletin of the Society of Economic Geologists*, 66, p.75-97.

White, R.W., Powell, R. and Phillips, G.N., 2003. A mineral equilibria study of the hydrothermal alteration in mafic greenschist facies rocks at Kalgoorlie, Western Australia. *Journal of Metamorphic Geology*, 21, p.455-468.

Whittome, A.J. and Salveson, J.O., 1990. Exploration and evaluation of the Darajat geothermal field, West Java, Indonesia. *Geothermal Resources Council Transactions*, 14, Part II, p.999-1005.

Winchester, J.A. and Floyd, P.A., 1977. Geochemical discrimination of different magma series and their differentiation products using immobile elements. *Chemical Geology*, 20, p.325-343.

Yates, D.M. and Rosenberg, P.E., 1996. Formation and stability of endmember illite: I. Solution equilibration experiments at 100 to 250°C and $P_{v,soln}$. *Geochimica et Cosmochimica Acta*, 60, p.1873-1883.

Yoshida, Y., 1984. Origin of gases and chemical equilibrium among them in steams from Matsukawa geothermal area, Northeast Japan. *Geochemical Journal*, 18, p.195-202.

Young, R.M., 1996. A basic model for vapour-dominated geothermal reservoirs. *Proceedings of the 18th New Zealand Geothermal Workshop*, the University of Auckland, New Zealand, p.301-304.